

IntechOpen

# Smart Drug Delivery System

*Edited by Ali Demir Sezer*





---

# SMART DRUG DELIVERY SYSTEM

---

Edited by **Ali Demir Sezer**

## Smart Drug Delivery System

<http://dx.doi.org/10.5772/60475>

Edited by Ali Demir Sezer

### Contributors

Preeti Nigam Joshi, Subir Kundu, Sunil Kumar Sanghi, Alexandru Mihai Grumezescu, Alexandra Elena Oprea, Mariana Carmen Chifiriuc, Carmen Curutiu, Alina Maria Holban, Veronica Lazar, Lia-Mara Ditu, Grigore Mihaescu, Islam S. M. Khalil, Sarthak Misra, Reham M. Abdel-Kader, Iman Gomaa, Ali Demir Sezer, Kubra Elcioglu, Gaetano Lamberti, Diego Caccavo, Sara Cascone, Anna Angela Barba, Anette Larsson, Dr.Sugapriya Dhanasekaran, Sumitra Chopra, Katayoun Derakhshandeh, Dongxi Xiang, Hao-Ming Hsiao, Aichi Chien, Bor-Hann Huang, Dian-Ru Li, Hsin Chen, Chun-Yi Ko, Yuekun Lai, Remigius Agu, Tiam Feridooni, Adam Hotchkiss, Wei Li, Seyda Bucak

### © The Editor(s) and the Author(s) 2016

The moral rights of the and the author(s) have been asserted.

All rights to the book as a whole are reserved by INTECH. The book as a whole (compilation) cannot be reproduced, distributed or used for commercial or non-commercial purposes without INTECH's written permission.

Enquiries concerning the use of the book should be directed to INTECH rights and permissions department ([permissions@intechopen.com](mailto:permissions@intechopen.com)).

Violations are liable to prosecution under the governing Copyright Law.



Individual chapters of this publication are distributed under the terms of the Creative Commons Attribution 3.0 Unported License which permits commercial use, distribution and reproduction of the individual chapters, provided the original author(s) and source publication are appropriately acknowledged. If so indicated, certain images may not be included under the Creative Commons license. In such cases users will need to obtain permission from the license holder to reproduce the material. More details and guidelines concerning content reuse and adaptation can be found at <http://www.intechopen.com/copyright-policy.html>.

### Notice

Statements and opinions expressed in the chapters are these of the individual contributors and not necessarily those of the editors or publisher. No responsibility is accepted for the accuracy of information contained in the published chapters. The publisher assumes no responsibility for any damage or injury to persons or property arising out of the use of any materials, instructions, methods or ideas contained in the book.

First published in Croatia, 2016 by INTECH d.o.o.

eBook (PDF) Published by IN TECH d.o.o.

Place and year of publication of eBook (PDF): Rijeka, 2019.

IntechOpen is the global imprint of IN TECH d.o.o.

Printed in Croatia

Legal deposit, Croatia: National and University Library in Zagreb

Additional hard and PDF copies can be obtained from [orders@intechopen.com](mailto:orders@intechopen.com)

Smart Drug Delivery System

Edited by Ali Demir Sezer

p. cm.

ISBN 978-953-51-2247-0

eBook (PDF) ISBN 978-953-51-6652-8

# We are IntechOpen, the first native scientific publisher of Open Access books

**3,350+**

Open access books available

**108,000+**

International authors and editors

**114M+**

Downloads

**151**

Countries delivered to

Our authors are among the  
**Top 1%**

most cited scientists

**12.2%**

Contributors from top 500 universities



**WEB OF SCIENCE™**

Selection of our books indexed in the Book Citation Index  
in Web of Science™ Core Collection (BKCI)

Interested in publishing with us?  
Contact [book.department@intechopen.com](mailto:book.department@intechopen.com)

Numbers displayed above are based on latest data collected.  
For more information visit [www.intechopen.com](http://www.intechopen.com)





# Meet the editor



After completing his Bachelor's degree from University of Istanbul, Faculty of Pharmacy, Associate Prof. Ali Demir Sezer began working as a research assistant at the Department of Pharmaceutical Technology of the Marmara University, Faculty of Pharmacy in 1993, and completed his Masters degree in new generation controlled release systems, which was followed by the completion of his PhD in Pharmaceutical Biotechnology at the same department. Dr. Sezer, who was appointed as a Lecturer briefly after, and carried out his research at the same branch, became Associate professor in 2013. Dr. Sezer's areas of expertise are protein formulation, nanobiotechnology, pharmaceutical biotechnology and production methodologies, and the use of the new generation of drug delivery systems and biopolymers in pharmaceutical industry. He has numerous publications in the journals in international indexes, international book editions, chapter authorships, and patents. Moreover, Dr. Sezer actively took part in and mentored a variety of corporate and other institutional projects, particularly Scientific and Technological Research Council of Turkey (TÜBİTAK). He is also a peer reviewer and member of the editorial boards in international journals, and has papers at international congresses.



---

# Contents

---

## **Preface XI**

- Chapter 1 **Smart Delivery Systems with Shape Memory and Self-Folding Polymers 1**  
Sera Erkeçođlu, Ali Demir Sezer and Seyda Bucak
- Chapter 2 **Getting a Handle on Smart Drug Delivery Systems – A Comprehensive View of Therapeutic Targeting Strategies 31**  
Sugapriya Dhanasekaran and Sumitra Chopra
- Chapter 3 **Smart Drug Delivery Strategies Based on Porous Nanostructure Materials 63**  
Qun Wang, Jianying Huang and Yuekun Lai
- Chapter 4 **Active-targeted Nanotherapy as Smart Cancer Treatment 91**  
Katayoun Derakhshandeh and Abbas Hemmati Azandaryani
- Chapter 5 **Cancer Stem Cells – Perspectives and How to Target Them 117**  
Zhaopeng Tang, Qianfeng Wang, Sarah Shigdar, Wei Duan and Dongxi Xiang
- Chapter 6 **Antibody-Targeted Immunocarriers for Cancer Treatment 139**  
Mengxin Zhao, Yun Sun, Xiandi Zhu, Di Chen, Sishen Feng, Shangjing Guo and Wei Li
- Chapter 7 **Graphene Quantum Dots - From Emergence to Nanotheranostic Applications 159**  
Preeti Nigam Joshi, Subir Kundu, Sunil K. Sanghi and Dhiman Sarkar
- Chapter 8 **Noninvasive Strategies for Systemic Delivery of Therapeutic Proteins – Prospects and Challenges 197**  
Tiam Feridooni, Adam Hotchkiss and Remigius U. Agu

- Chapter 9 **Magnetic-Based Contact and Non-Contact Manipulation of Cell Mockups and MCF-7 Human Breast Cancer Cells 219**  
Islam S. M. Khalil, Iman E. O. Gomaa, Reham M. Abdel-Kader and Sarthak Misra
- Chapter 10 **Swellable Hydrogel-based Systems for Controlled Drug Delivery 237**  
Diego Caccavo, Sara Cascone, Gaetano Lamberti, Anna Angela Barba and Anette Larsson
- Chapter 11 **Antibiotic Drug Delivery Systems for the Intracellular Targeting of Bacterial Pathogens 305**  
Mariana Carmen Chifiriuc, Alina Maria Holban, Carmen Curutiu, Lia-Mara Ditu, Grigore Mihaescu, Alexandra Elena Oprea, Alexandru Mihai Grumezescu and Veronica Lazar
- Chapter 12 **Device Integrity of Drug-eluting Depot Stent for Smart Drug Delivery 345**  
Hao-Ming Hsiao, Aichi Chien, Bor-Hann Huang, Dian-Ru Li, Hsin Chen and Chun-Yi Ko
- Chapter 13 **Diabetic Neuropathy and Treatment Strategy – New Challenges and Applications 373**  
Emine Hande Bayram, Ali Demir Sezer and Hatice Kübra Elçioğlu

---

# Preface

---

Drug delivery is a method, or a process of administering a pharmaceutical compound to achieve a therapeutic effect in humans or animals. Drug delivery technologies modify drug release profile, absorption, distribution and elimination for the benefit of improving product efficacy and safety, as well as patient convenience and compliance. Drug release is from: diffusion, degradation, swelling, and affinity-based mechanisms. Most common routes of administration include the preferred non-invasive peroral, topical, transmucosal and inhalation routes. Many medications such as peptide and protein, antibody, vaccine and gene based drugs, in general may not be delivered using these routes.

However, for all these exciting new drug and vaccine candidates, it is necessary to develop suitable dosage forms or drug delivery systems to allow the effective, safe and reliable application of these bioactive compounds to the patient. In the view of most experts, pharmacology is on drugs, targets, and actions. In this context the drug as a rule is seen as an active pharmaceutical ingredient and not as a complex mixture of chemical entities of a well defined structure. Today, we are becoming more and more aware of the fact that delivery of the active compound to the target site is a key. The present volume gives a topical overview on various modern approaches to drug delivery and targeting. It covers today's options for specific carrier systems, allowing successful drug treatment at various sites of the body difficult to address, and allowing to increase the benefit-risk-ratio to the optimum possible.

On the other hand, the reader will be introduced to various aspects of the fundamentals of nanotechnology based drug delivery systems and the application of these systems for the delivery of small molecules, proteins, peptides, oligonucleotides and genes. How these systems overcome challenges offered by biological barriers to drug absorption and drug targeting will also be described.

This book offers a critical overview of therapeutically-interesting stimuli to trigger drug release and the evolution of responsive materials suitable as functional excipients, illustrated with recent examples of formulations in clinical trials or already commercially available, which can provide a perspective on the current state of the art on smart drug delivery systems.

It is critical for the field of drug delivery from a proof of concept to a pharmaceutical product at the beginning of the new millennium. A successful outcome will result in a new clinical modality that represents a revolutionary approach to medicine. One immediate benefit will be to produce a continuous level of therapeutic protein, avoiding the characteristic peak and trough behavior of intermittent administrations with drug carrier systems. Novel drug delivery carriers will have the capability to turn genes on or off on demand, producing a therapy that can treat the disease rather than the symptoms and with minimal side effects.

**Assoc. Prof. Ali Demir Sezer**

Marmara University, Faculty of Pharmacy  
Department of Pharmaceutical Biotechnology  
Istanbul, Turkey



---

# Smart Delivery Systems with Shape Memory and Self-Folding Polymers

---

Sera Erkeçođlu, Ali Demir Sezer and Seyda Bucak

Additional information is available at the end of the chapter

<http://dx.doi.org/10.5772/62199>

---

## Abstract

New generation delivery systems involve smart materials such as shape memory and self-folding polymers. Shape memory polymers revert back to their original shape above their glass transition temperatures where this temperature change can be induced conventionally, photolytically, with a laser or magnetically depending on the composition of the material. This ability to assume original shape upon a trigger can be used in delivering drugs, DNA or cells. Self folding polymers are a new class of materials which may be composed of multilayers with different thermal expansion coefficients or with hinges that allow folding upon being triggered. These new materials allow various architectural designs of smart delivery vehicles predominantly for DNA and cells. The aim of this chapter is given shape and folding polymers and their usage for drug delivery systems.

**Keywords:** Polymer, Shape memory, Self folding, Drug delivery

---

## 1. Introduction

Polymers are a group of materials that are versatile in their nature spanning from industrial materials such as synthetic plastics to biopolymers. Synthetic or naturally occurring, their properties depend on the nature of the constituent monomers, the sequence of the monomers, the length of the whole polymer, and the type of bonds they contain in their structure. In the past 20 years, a new group of polymers is recognized to exhibit interesting properties, namely shape memory and self-folding. Polymers that exhibit these properties are now the subject of intensive research for their potential applications in biomedical area and drug delivery. In this chapter, we will first introduce the principles of shape memory and then give a summary of the work done in this field. In the following section, we introduce the concept of self-folding and polymer origami, which is a subsection of self-folding. Recent research done in this

---

exciting area is then presented, and future outlook on shape memory and self-folding polymers is specified.

## 2. Shape memory materials

The main characteristics of shape memory materials (SMMs) in general are that they show a plastic deformation (temporary shape) when an external stimulus is applied and are able to recover to their original shape from the temporary shape. This is also called “shape memory effect” (SME) [1].

One of the classes of shape memory materials is shape memory polymers (SMPs), which respond to external stimulus by offering mechanical action. Network elasticity of the shape memory polymer determines if SMP remembers one or more shapes [2]. Dual-shape memory polymers, which are going to be specified later on, are the first SMPs.

Until the external (shape memory-driving) stimulus is applied to trigger the shape recovery, the temporary shape of SMP is stable.

Temperature, light, electric field, magnetic field, pH, specific ions, or enzyme can be used as stimulus in order to change the shapes of shape memory polymers. The shape change can occur rapidly from temporary shape to the permanent one [3–5]. Figure 1 summarizes the relationship between polymer composition and structure, stimulus, and shape memory function.

In late 1970s, CdF Chimie Company (France) developed the first shape memory polymer called polynorbornene [6]. One year later, it was named as Norsorex by Nippon Zeon Company (Japan) and was commercialized [7]. Other commercial shape memory polymers which are named Kurare TP-301 and Asmer were produced by Kurare Corporation (Japan) and Asahi Company (Japan), respectively [8]. Widely used polyurethane (PU)-based SMP was developed by Mitsubishi Heavy Industries [4].

Another important branch of shape memory materials is shape memory alloys (SMAs). However, shape memory alloys have disadvantages among other types of shape memory materials, such as high manufacturing cost, toxicity, limited recovery, and complicated surgical problems. Shape memory polymers, ceramics, and hydrogels are preferred recently for their advantages compared to shape memory alloys [9].

## 3. Shape memory polymers

The shape memory effect can be originated by combining polymer structure and morphology by processing and programming methods. The material properties are not related with SME [10].

The unique properties and major advantages of SMP materials are summarized below:

- SMPs are lightweight and allow substantially higher elongations, which have properties for various technical applications [11].
- SMPs have wide range of glass transition temperatures from  $-70^{\circ}\text{C}$  to  $+100^{\circ}\text{C}$ .
- Since they have a wide range of glass transition temperatures, their stiffness can be tailored. Also, SMPs can be processed easily [12].
- SMPs have shape recovery property up to 400% of plastic strain. (Shape memory alloys have 7–8%).
- Between the glassy and rubbery states of SMPs, large reversible changes of elastic modulus can be observed (as high as 500 times) [13].
- Shape memory polymers have high elastic deformation (strain up to more than 200% for most of the materials). They have low density and biodegradable materials.
- Most of the SMPs are biocompatible materials which allow them to be used in potential medical applications.
- SMPs are easy to process. They are applicable to molding or extrusion. They have low cost [13].
- Shape memory polymers have low thermal conductivity compared to shape memory alloys. This feature can be useful if shape memory foams are used as insulation materials [14,15].
- They can use many external stimuli and triggers. There are many alternative ways to actuate shape recovery such as light, magnetic field, electricity, and water [16].

As mentioned previously, shape memory polymers and their composites can recover their original shapes after large deformation when subjected to an external stimulus [17]. This external stimulus can be temperature [18,19], magnetism [20–22], moisture [23], or light [18,24].

#### *Thermally Induced Shape Memory Polymers*

Among these shape memory polymers, the thermoresponsive SMPs are the most common type [25,26]. Thermally induced shape memory polymers have a wide range of applications in biomedical fields, [27] such as drug delivery, implanting, suture, and wound healing [28].

The general thermomechanical cycle of thermoresponsive shape memory polymers consists of the following steps at a macroscopic level:

1. Programming
2. Storage
3. Recovery [29].

This cycle is depicted in Figure 1. The first step is the fabrication of the shape memory polymers into an original shape. Second, the polymer is heated above the thermal transition temperature ( $T_{\text{trans}}$ ) (this temperature can be either melting temperature  $T_m$  or glass transition temperature  $T_g$ ). When the polymer is at its  $T_{\text{trans}}$ , an applied external force deforms it, and it is cooled below

thermal transition temperature. When it is cooled, the applied force is removed in order to preserve the temporarily pre-deformed shape. In the last step, the pre-deformed shape memory polymer is heated above  $T_{trans}$  and shape recovery is observed, and SMP attains its original shape.

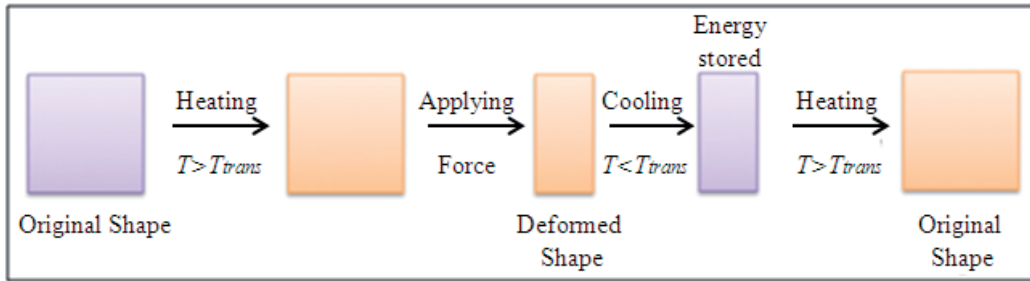


**Figure 1.** Thermomechanical cycle of thermoresponsive shape memory polymers.

At the molecular level, shape memory polymers offer shape memory effect by its two components, which are cross-links and switching segments. These SMPs can include chemically cross-linked networks or physically cross-linked copolymers. Physically cross-linked copolymers are usually made of linear block copolymers which have hard and switching segments. Their permanent shape is stabilized by hard segments, whereas temporary shape is fixed by switching segments [30]. Cross-links are formed by covalent bonds and physical interactions (i.e., molecular entanglements) [5,31]. For covalently cross-linked shape memory polymers, reshaping the materials is hard since the shape is fixed by covalent bonds. These types of polymers are called thermosets [32].

Polymer includes two separate domains in physical cross-linking case. The domain consists of two parts which are hard and reversible switching segments. The hard segment, which acts as net point, is related to the highest thermal transition temperature. Reversible switching segment or molecular switches are related to the second highest thermal transition temperature. These types of polymers are called thermoplastics [33]. Figure 2 shows the hard and soft segments during the shape memory process. The lines show the net points and square dots show the switching segments.

Rousseau et al. reported that epoxy polymers (neopentyl glycol diglycidyl ether NGDE) have tunable glass transition temperatures by changing the cross-link density and chain flexibility. Ranging up to 89°C, excellent shape fixity and recovery were observed [34].

Zhou et al. reported that PDLLA/HA (poly D,L-lactide co-glycolide/hydroxyapatite) composites have desirable shape memory effects and the amount of HA particles in composites played an important role during the shape memory recovery. Since PDLLA has remarkable properties such as shape memory effect, biodegradability, biocompatibility, easier availability, and osteoconductivity of HA, these composites have potential in biomedical applications such as minimally invasive surgery (MIS) and bone and tissue repair [35].

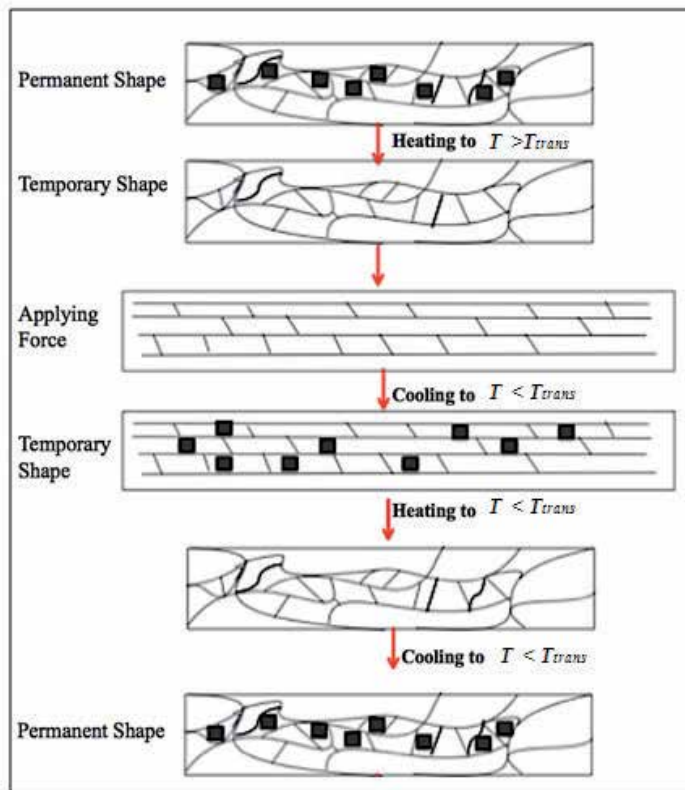


**Figure 2.** Hard and soft segments during shape memory effect.

Lendlein et al. developed a thermoresponsive shape memory polymer which consists of oligo( $\epsilon$ -caprolactone) diol (OGL) and crystallizable oligo(p-dioxanone) (ODX) as switching and hard segments, respectively. A fiber of this thermoplastic SMP was used to close the wound by loosely knotting the fiber and then when temperature increased to  $T_{trans}$ , the suture shrinks and the knot is tightened. So, they suggested that this type of material could be used in order to design new surgical devices [10].

In another study, Ashby et al. reported that poly( $\epsilon$ -caprolactone) (PCL) and poly(octylene adipate-co-meso-2,5-diazodipate) shape memory polymers were actuated by switching temperature. This new developed SMP would have potential applications in the biomedical field [36].

### 3.1. One-Way (Dual) Shape Memory Effect (1W-SME)

When an external stimulus is applied on SMP, the temporary shape becomes permanent shape. In order to obtain the temporary shape again, another external force or stress is required. This procedure shows that shape memory behavior is nonreversible or “one-way”, and it has a wide range of applications [37].

The most basic procedure of polymer shape memory effect is described in Figure 1. First, the shape memory polymer is heated to a transition temperature or deformation temperature ( $T_d$ ), which resulted in softening of the material. Second, a deformation force is applied on SMP (i.e., loading or stress). Third, the SMP is cooled down under the load. Then, load is removed and the deformed shape is fixed, which is the temporary shape. After shape fixing, shape recovery is obtained by reheating the temporarily shaped SMP to a recovery temperature ( $T_r$ ) when no stress is applied on it. Finally, the original (permanent) shape of SMP is recovered [38]. If a shape memory process follows this procedure, it is called as dual-shape memory effect.

The thermal transition temperature, which is associated with switching domains, has various types. The melting transition ( $T_{trans} = T_m$ ), liquid crystalline transition ( $T_{trans} = T_{LC}$ ), or a glass transition ( $T_{trans} = T_g$ ) can be taken as thermal transition temperature. However, mostly, melting and liquid crystalline phase transitions are designated to relatively small temperatures [39].

If we take a look at the macroscopic shape of shape memory polymer, when it has a permanent shape, its molecular chains are thermodynamically stable because of the highest entropy of SMP conformation. When SMP is heated above  $T_{trans}$ , chain mobility is triggered. Due to the lower entropy state and macroscopic shape change after applied stress, chain conformations of SMP are changed. Finally, when the SMP is cooled below  $T_{trans}$ , molecular chain segments freeze by kinetically trapping of lower entropy state. As a result of this, macroscopic shape fixity is obtained. In the last step, when heating the deformed SMP above  $T_{trans}$  when there is no stress applied, the chain mobility is activated again. So, molecular chains regain their highest entropy. The one-way shape memory effect is illustrated in Figure 3 briefly.

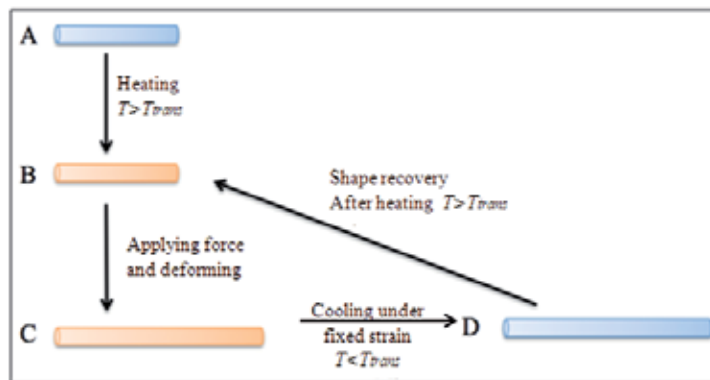


**Figure 3.** One-way shape memory effect.

Basically, shape memory polymers are able to change their shapes between original and temporary shape under applied stress which is a type of one-way shape memory effect. Another type of one-way shape memory effect is triple shape memory effect. The main difference of triple shape memory effect (TSME) is having one intermediate shape between its original and temporary shapes. If there is more than one intermediate shape, it is called multiple shape memory effect for a more complicated motion generation [40]. Polymers

blends, grafting and blocking copolymers, SMP hybrids, and polymer laminates are some of the ways of managing the triple shape memory effects [41]. Figure 4 shows the basic procedure of triple shape memory effect. As mentioned in the figure, there are two different thermal transition temperatures which are  $T_{low,1}$  and  $T_{low,2}$ . This is attributed to the two segregated crystalline domains in the original shape [42].

Kumar et al. reported that grafted polymer network contains crystallizable poly(ethylene glycol) (PEG) side chains, and poly ( $\epsilon$ -caprolactone) (PCL) shows triple shape memory effect [43]. The triple shape memory behavior of crystalline polyurethane was observed by Hu et al. [44]. Also, polyalkenamer and polyolefin-based polymer blends were used by Cuevas et al. in order to develop triple shape memory polymers which were two semicrystalline polymers (poly(cyclooctene) (PCO) and polyethylene (PE)) [42]. Xie et al. developed polymeric bilayers that consisted of two dual-shape memory polymers, and this new shape memory polymer bilayer shows triple shape memory effect [45]. Furthermore, Xie reported that perfluorosulphonic acid ionomer (PFSA) is able to show tunable shape memory effect which includes dual, triple, and quadruple without any change in the material composition [46].

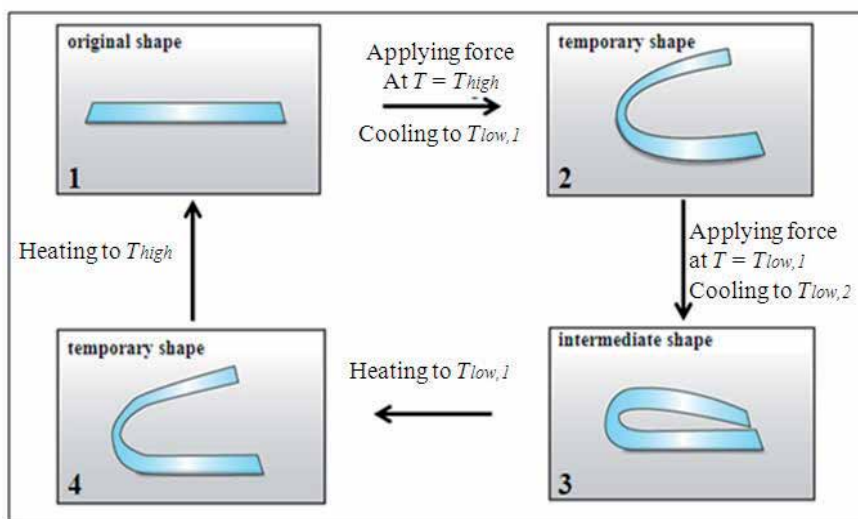


**Figure 4.** Triple shape memory effect.

### 3.2. Two-Way Shape Memory Effect (2W-SME)

Most of the typical SMPs show one-way shape memory effect. A different type of SME which is the two-way shape memory effect can be observed in liquid crystalline elastomers and photo-actuated deformation polymers [47].

2W-SME can be quite useful; however, its high cost represents an obstacle for its widespread use. In 2W-SME process, a crystallization-induced elongation and melting-induced contrac-

tion is observed during cooling and heating, respectively. This condition originated from the formation of liquid crystalline structure [48]. The comparison of 2W-SME and 1W-SME is shown in Figure 5 briefly.

Chen et al. reported that the two-way shape memory behavior of SMP laminate was observed by bending upon heating from 25°C to 60°C and reverse bending upon cooling from 60°C to 25°C. Laminated layers were prepared from shape memory exhibiting polyurethane [49].

Zhou et al. developed self-folding poly(octylene adipate) (POA). Besides showing conventional one-way irreversible shape memory, this SMP is able to form one-way reversible shape memory during heating and two-way reversible shape memory upon heating and cooling cycles. The chemical cross-links of this semicrystalline elastomer are responsible for the memorization of the original shape, whereas the physical network constructs the temporary shape [50].

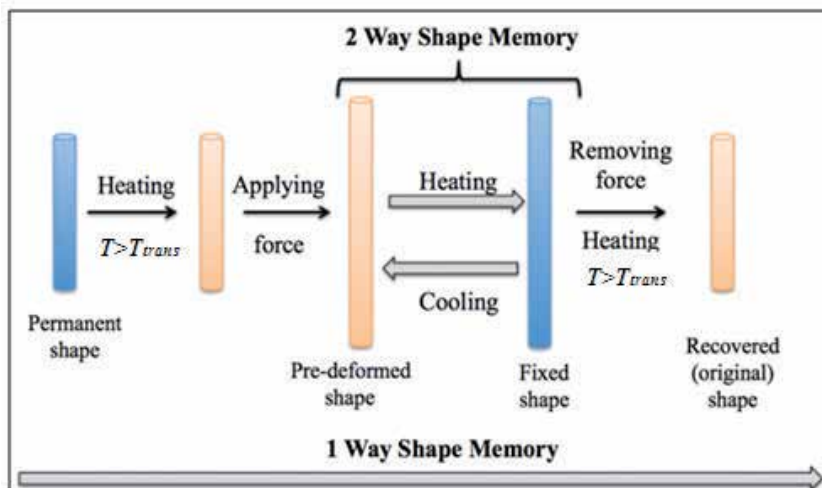


**Figure 5.** Comparison of two-way shape memory effect and one-way shape memory effect.

#### *Magnetically Induced Shape Memory Polymers*

Certain magnetic materials tend to respond to magnetic fields and are capable of maintaining their magnetic properties after the external magnetic field is removed. Such magnetic particles are called as ferrimagnetic or ferromagnetic materials which are iron, nickel, cobalt, and some of their alloys [51]. Some magnetic materials such as iron oxides ( $\text{Fe}_3\text{O}_4$ ,  $\text{Fe}_2\text{O}_3$ , etc.), when below a certain nanometer size, do not have any remaining magnetization once the external magnetic field is removed. These are superparamagnetic materials and can be preferred over ferromagnetic ones depending on the application.

Shape memory can be induced by the application of an external magnetic field due to magnetic heating. So magnetic induction is a type of thermal induction, where temperature change is driven by magnetic field due to the presence of magnetic material in the nanocomposite.

The magnetic SMP has several advantages:

1. By using magnetic heating, possible danger of overheating can be eliminated.
2. Since heat is not given to the system externally, any complex-shaped device can be actuated virtually.
3. This method is convenient for medical devices which can be actuated inside the human body, since they can be controlled in a wireless manner [52].

Hilt et al. reported that magnetic field can be used in order to heat the SMPs by remote heating. This heating method relies on magnetic nanoparticles within the polymer matrix in order to create heat via power loss when exposed to an alternating magnetic field [53].

According to the study of Razzaq et al., by changing the magnetic field parameters and amount of the  $\text{Fe}_3\text{O}_4$  in the polyurethane polymer matrix, shape recovery of the helical bended strip of polyurethane filled with 20% volume micro-sized magnetite was observed [54].

Magnetically inducing method is an indirect method. So this method can be useful if shape memory polymer cannot be actuated by direct heating methods. However, Zhou et al. reported that for cross-linked poly( $\epsilon$ -caprolactone) polymers, magnetite composite shows better reactivity to hot water than alternating magnetic field [55].

In the research study of Schmidt, polymer network composites were implemented with different contents of superparamagnetic nanoparticles ( $\text{Fe}_3\text{O}_4$ ) and butyl acrylate cross-linked with oligo( $\epsilon$ -caprolactone) dimethacrylate. As it can be seen in Figure 3, the permanent shape is deformed by heating above  $T_{\text{trans}}$ . Then by cooling the temporary shape, the crystalline phase of oligo( $\epsilon$ -caprolactone) segments makes the polymer to become stable. Induction heating of magnetic nanoparticles in electromagnetic field leads to temperature increase inside the matrix. By magnetically heating above the  $T_{\text{trans}}$ , the original (permanent) shape is recovered [56].

Zhou et al. reported that poly(D,L-lactide)/magnetite ( $\text{Fe}_3\text{O}_4$ ) nanocomposites show excellent shape memory effect when an alternating magnetic field was applied as a stimulus. Since PDLA is biocompatible, these nanocomposites show potential for application as magnetically controlled smart implants in biomedical field [57].

According to the study of Puig et al., 8 wt% oleic acid-stabilized magnetic nanoparticles exhibited a temperature increase of 25°C at its surface when exposed to an alternating magnetic field in biomedical applications. Also, this temperature was enough to actuate the shape memory of the nanocomposite [58].

#### *Electro-Active Shape Memory Polymers*

As observed, shape memory effect is usually induced by thermal stimulation by heating above the transition temperature of the polymers, such as the glass transition temperature or melting temperature. However, some other stimulating sources, such as electric field, may also be used in order to trigger polymers with shape memory [59].

Electricity can be used as a stimulus which enables resistive actuation of shape memory polymer filled with conductive fillers. By passing an electrical current, shape memory effect

can be actuated easily in these nanocomposites. To date, most of the studies regarding electroactive SMPs composite are focused on thermoplastic SMP resins [60]. As a result of these, in recent studies, most of the electroactive shape memory polymers are well-dispersed carbon nanotube (CNT)-reinforced thermoplastic polyurethane (TPU) resin nanocomposites [61–63].

According to the study of Leng et al., thermoset styrene-based shape memory polymer nanocomposite filled with different amounts of nanosized carbon powder shows that with increasing nanocarbon powder amount, electrical conductivity increases. Also, it was reported that 10 vol.% nanocarbon powder shows good electroactive shape recovery property [64].

Zhou and coworkers fabricate cross-linked poly( $\epsilon$ -caprolactone) (cPCL) and conductive multiwalled carbon nanotubes (MWNTs). These nanocomposites exhibit excellent shape memory properties under the direct thermal and electrical stimulations. Therefore it was reported that this composite might be a promising prospect in biomedical applications [65].

Jung et al. obtained electroactive shape memory polymer composites by using polyurethane and three kinds of fillers. When polyurethane-multiwalled carbon nanotube composite is lightly coated with polypyrrole (PPy), new nanocomposite shows good electroactive shape memory properties when an electric voltage is applied [66].

#### *Water-Induced Shape Memory Polymers*

As a trigger mechanism, water can be used for shape transition of shape memory polymers or shape memory polymer composites. Since solvent or water molecules can penetrate into the amorphous areas of shape memory polymers, this can result in a plasticizing effect on SMP molecules. Therefore the flexibility of the molecule increases and shape recovery is observed [67].

Chen et al. reported that water-induced poly(methacrylic acid)-grafted clay and thermoplastic polyurethane composite was developed with shape memory effect. Also, this new polymer-clay composite responds to pH changes and mechanically adaptive properties when water is exposed [68].

The polymer composite composed of carbon nanotubes and shape memory polyurethane (SMPU) was developed by Luo et al. The new and developed composite has shape memory-enhanced water-sensing property which can be used in smart polymer applications such as sensory materials [69].

Aqueous environments can be used as a trigger of shape memory effect. Nöchel et al. used different grafted copolymer networks (named CLEG) which consist of different ratios of the hydrophobic cross-linker poly( $\epsilon$ -caprolactone) diisocynoethyl methacrylate (PCLDIMA) and hydrophilic poly(ethylene glycol) monomethyl ether monomethacrylate (PEGMA). The shape memory properties of this new hydrogel were studied by bending and uniaxial elongation experiments in the aqueous environments. As a result, CLEG has dual-shape capability and degradability and could be promising materials in biomedical applications [70].

Paakinaho et al. reported that the shape memory property of orientation-programmed PDLA in an aqueous environment at 37°C was triggered by the combined effect of water molecules

and thermal activation [71]. Mendez et al. developed new water-activated biomimetic nanocomposites by adding rigid cotton cellulose nanowhiskers (CNWs) into a rubbery polyurethane matrix. At a specific concentration of CNW, aqueous swelling and shape memory behavior were observed [72].

#### 4. Self-folding polymers

Self-folding is the ability of a material to fold and unfold without the external effects. Also without any external interference, such as human control, self-folding can be attributed to the self-assembly mechanism. These mechanisms can be patterned templates or thin films which can be folded, curved, or rolled-up to become spirals, tubes, and cylindrical tubes [73,74]. Self-folding can occur spontaneously or in response to stimuli such as light, pH [75], temperature, magnetic field, or solvent [76,77]. In Figure 6, self-folding mechanism which is provided by hinges is shown briefly.

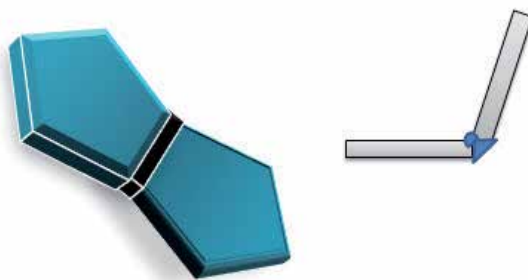


**Figure 6.** Illustration of 3D and 2D self-folding mechanism.

Self-folding films have become attractive recently since there is a variety of polymers which are sensitive to different stimuli, and they can fold by responding external signals. Many polymers are able to change their properties with pH and temperature. For biotechnological applications, biodegradable and biocompatible polymers are favorable choices and are frequently encountered. Polymers can also undergo considerable and reversible changes of volume that allow design of systems with reversible folding [78]. Thermoresponsive self-folding films can be designed using continuous thermal expansion, melting shape memory transition of polymers which demonstrate the low critical solution temperature (LCST) in solutions [79].

Luchnikov et al. reported that a polymer bilayer consisting of a polystyrene (PS) layer on top of a poly(4-vinyl pyridine) (P4VP) layer is formed on the polished surface on the silicon wafer or other substrates (e.g., a glass slide) by means of dip or spin coating. Rolling, in this system, is achieved due to the swelling of the P4VP in a water solution of an acid, due to protonation of the pyridine rings [80]. In another study of Ionov, self-rolling due to swelling was observed.

Fully biodegradable polysuccinimide shows self-rolling response with its polymer bilayers, and this results in the formation of microtubes [81].

Ionov et al. demonstrated a self-folding polymeric bilayer consisting of poly(methyl methacrylate) copolymer and poly(N-isopropylacrylamide) copolymer which can encapsulate an oily liquid. This new developed bilayer can be expressed as an anisotropic capsule, and the folding behavior is observed due to the swelling difference of the layers of the polymer film. Self-healing materials and drug delivery design are featured possible application areas of this approach [82]. A representative illustration of self-folding polymeric bilayer is shown in Figure 7.

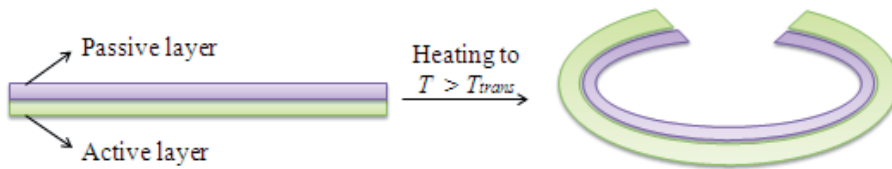


**Figure 7.** Self-folding procedure of thermoresponsive polymeric bilayer.

Ionov et al. studied two different sets of thermoresponsive polymeric bilayer behaviors to different stimuli. Polymeric bilayers were selected as one passive layer which is hydrophobic or random copolymer, and the active layer is the thermoresponsive hydrogel. Thermoresponsive hydrogels show swelling and shrink response to increased or decreased temperature, whereas passive layers prevent swelling of the active layer. In this manner, nonuniform expand/shrink behavior is achieved. In other words, folding and unfolding can be observed due to swelling [83].

Huang et al. developed a heat-responsive poly lactic acid (PLA) structure which would provide good uses for customized deployable/retractable and biodegradable implant devices for individual patients [84].

Lee et al. developed that self-folding oral delivery device which is capable of providing enhanced mucoadhesion, drug protection, and targeted multidirectional delivery. The device is composed of three layers which are backing layer, a foldable bilayer, and a mucoadhesive layer entrapped with drugs. The swelling bilayer was made of pH-sensitive hydrogel cross-linked poly(methacrylic acid) (PMAA) which swells during contact with body fluid whereas non-swelling layer is poly(hydroxyethyl methacrylate) (PHEMA), and it acts as a diffusion barrier in order to minimize drug leakage in the intestine. When mucoadhesive drug layer is attached on the bilayer, self-folding device attaches to the mucus first and then curls into the mucus due to the different swelling of the bilayered structure, leading to enhanced mucoadhesion [85].

Temperature-stimulated liquid crystal elastomer–polystyrene bilayers which can show complex shape changing behavior such as helical twisting, reversible folding, and patterned

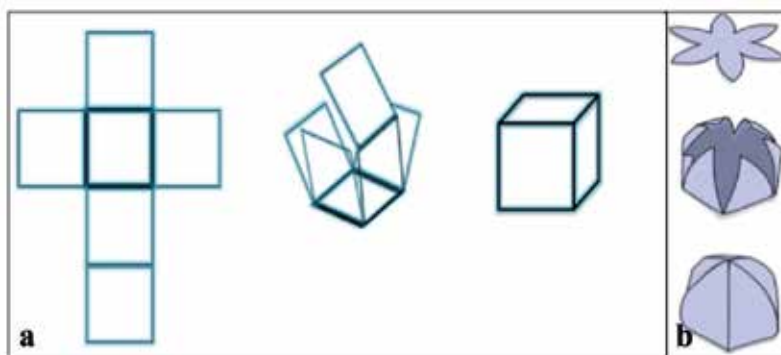


**Figure 8.** Origami folding sequence of a cubic structure (a), illustration of polymer origami self-folding (b).

wrinkles were developed by Agrawal et al. Tailoring was achieved by changing film thickness and overall aspect ratio [86].

Huck et al. reported that microscale, quasi-2D composite objects are fabricated which can respond to the addition of salt and pH changes [87].

Schenning et al. developed accordion-like striped actuators made of liquid crystal polymer films, which show response to the pH or temperature. These actuators would be used in medical systems and microrobotics [88]. Another liquid crystal shape memory actuator was developed by Park et al. which shows different swelling behavior between its UV exposed and non-UV exposed sides [89].

Visible light-induced graphene oxide/poly(vinylidene fluoride-hexafluoro propylene) (PVDF-HFP) nanocomposite films were produced by Yu et al. Tumbler movement was observed on the films due to the photothermal effect of graphene oxide and shape memory effect of PVDF-HFP. This behavior can be improved for full-plastic devices actuated by visible light [90].

Ionov et al. developed self-assembled porous scaffolds with uniaxial tubular pores. By producing rectangular polymer bilayers which include hydrophobic (poly methyl-methacrylate-co-benzophenoneacrylate) and stimuli-responding hydrophilic polymer (poly N-isopropylacrylamide-co-acrylic acid co-benzophenoneacrylate), pH-dependent rolling of bilayers was observed. Also, these bilayers are capable of controlled self-assembly [91].

## 5. Polymer origami

Origami word is originated from the Japanese words 'ori' as in to 'fold' and 'kami' as the 'paper.' It is the art of paper folding from Japan and has been known worldwide [92]. Today, origami is not only the art of paper but also can be used for technological purposes by creating three-dimensional objects. In order to obtain these objects, fold pattern sequences should be provided to develop the desired object from a flat sheet [93].

Origami enables the creation of complex structures unlike bilayers, which can only bend in one direction or fold multiple steps. The shape of self-folded structures depends on the initial shape of the film, the radius of curvature (depending on the layer thickness), and the presence of a substrate [94]. A typical origami folding structure is depicted in Figure 8(a). Space structure solar arrays, automobile airbags, shopping bags and cartons, photovoltaic cells, and biomedical are some of the uses of polymer origami structures [93].

As mentioned above, different stimuli can be used to trigger the material's self-folding behavior as well as origami folding. Gracias et al. reported that self-folding functional microgrippers that combine a swellable, photo-cross-linked N-isopropylacrylamide-co-acrylic acid soft hydrogel with a non-swellable and hard-segmented polymer (polypropylene fumarate, PPF) show thermomechanical response to hydrogel where they can be used in surgical areas [95].

In a study, Baroud et al. manually cut geometric shape of polymethylsiloxane membrane layer placed on a hydrophobic surface. When a drop of water is added on a membrane and allowed to evaporate, as water volume decreases, thin membrane sheet wraps the liquid and forms 3D shape which shows the interaction between elasticity and capillary [96]. The illustration of this procedure is shown in Figure 8(b).

Gracias et al. developed three-dimensional (3D) microfabricated nanoliter containers by thermally actuating the 2D structure to fold into a 3D structure which is analogous to polymer origami. In this case, 2D template has smart hinges. Researchers suggested that this new fabrication method would be used for developing microscale biomedical devices in the future [97].

Ryu demonstrated photo-origami which actuates both flat and curved surfaces of polymer films in order to obtain 3-dimensional objects at a macroscopic scale via "localized photo induced stress relaxation" mechanism. Photo-origami is driven with amorphous, covalently crosslinked polymer which includes pentaerythritol tetra(3-mercaptopropionate) (PETMP), 2-methylene-propane-1,3-di(thioethylvinylether) (MDTVE), and ethylene glycol di(3-mercaptopropionate) (EGDMP)). [93]. Gracias et al. developed photo-cross-linked polyethylene glycol (PEG)-based bio-origami hydrogel bilayers which can self-fold in aqueous solutions. These new developed bilayers conserve different kinds of tissues by self-folding which would be improvable considering the tissue engineering area [98].

## 6. Smart polymers as drug carriers

The most important use of shape memory polymers is as drug carriers. Some drugs due to their stability of low solubility in the blood stream become more bioavailable when delivered in a carrier system. This may also allow the sustained release of the drug which can be desired if the drug is desired to be eluted over a long period of time. There are several drug delivery systems developed such as liposomal systems of biodegradable polymeric systems. Polymers offer a wide range of adjustable properties to be tailored for the desired drug elution system.

Smart polymers are a new class of materials where novel drug delivery systems can be designed with. However, there are some criteria such as drug loading capacity, aqueous environment conditions, drug release pattern, and degradation behavior which determine the suitability of shape memory polymers as matrix materials for drug release or drug carrier applications [99].

Based on the requirements defined by a specific application, such polymer systems will allow selecting one specific polymer out of a larger number of related materials without the need to change to a totally different material chemistry. In addition to adjustable thermal properties, polymer systems can also be helpful to realize demanded mechanical properties or desired degradation rates of SMP implants [100].

For biomedical applications of SMPs, the capability to change their shape should be established at relevant conditions, i.e.,  $T_{sw}$  (switching temperature) of the SMP device should be close to or at reasonable levels above body temperature. To meet this goal, the thermal properties such as  $T_g$  or the melting temperature  $T_m$  that account for the shape memory effect need to be adjusted. Polymer systems as families of materials, in which different properties and functions can ideally be tailored over a wide range independent from each other, may allow the adjustment of  $T_{sw}$  by polymer chemistry, which make them good candidates as drug carriers [101].

About the controlled drug release ability of shape-memory polymers, Ohya et al. reported that chemically cross-linked networks of branched oligo( $\epsilon$ -caprolactone) polymer can perform sustained release of theophylline drug over a month without initial burst release in Phosphate Buffer Saline (PBS) at 37°C [102].

According to the study of Ameer et al., hydroxyl-dominant (HD) polydiolcitrates (HD polymers) can perform the subsequent release of hydrophobic dichlorofluorescein (DCF) drug. This means polydiolcitate elastomers could benefit from smart biodegradable materials for tissue engineering applications [103].

Such systems are ideal for minimally invasive surgery where implants are inserted through a small incision, and after self-anchoring, they start to release a pharmacological agent. Dobrzyński et al. developed a shape memory polymer based on L-lactide, glycolide, and trimethylene carbonate in order to obtain double layer systems for paclitaxel drug delivery that paves the way for drug eluting stents [104].

Lendlein et al. reported that oligo (caprolactone-co-glycolide) dimethacrylate was combined with drug, and its activation was obtained between 28-42°C where shape memory effect was pronounced at body temperature. In this study, diffusion-controlled drug release was observed independent from polymer degradation [105].

Gong et al. reported that biodegradable polymeric cross-linked poly( $\epsilon$ -caprolactone) (cPCL) and poly(sebacic anhydride) (PSA) were developed, and release accumulation of drug can be enhanced by adding PSA into cPCL matrix. This shape memory polymer could be used as potential drug-eluting stents in biomedical field [106].

## 7. Potential biomedical applications of smart polymers

During the past decade, biomedical applications of shape memory materials became a very active area of research [107].

As mentioned in the previous section, the progress in surgical techniques, especially in minimally invasive surgery, allows these materials to be used widely in biomedical applications of polymers.

These smart materials are enabled to insert a bulky device in the body through a small keyhole incision in a temporarily fixed shape. After a precise position by the surgeon, such smart materials gain their application-relevant shape on demand [108].

Zhang et al. demonstrated a new nanofibrous, biomimetic, shape memory, and biodegradable poly(D,L-lactide-*co*-trimethylene carbonate) by electrospinning which would be applicable for MIS implantation [109].

Nelson et al. developed hydrogel bilayers composed of N-isopropylacrylamide with polyethyleneglycol diacrylate. By using the expansion difference of these layers due to swelling, self-folding behavior was observed. These new devices are switchable and show reversible shape transition against external stimuli. These layers were designed for different purposes in order to demonstrate microstructures which can preserve magnetic alginate microbeads when they have folded structures. After exposing to NIR laser source, microbeads are capable of being released from the microstructures. So, this method offers a solution for drug and cell delivery systems [110].

Tai et al. demonstrated an origami technique by constructing 3D spherical structure from 2D parylene-C (PA-C) film for intraocular implantation application [111]. Maitland et al. developed an SMP adapter in order to reduce the hemodynamic stress which arises from impingement of dialysis needle in an arteriovenous graft [112].

The most effective areas of biomedical applications of shape memory polymers are intravascular stents, treating aneurysm occlusion and clot removal.

### 7.1. Intravascular stents

Intravascular stents are predominantly used in main arteries or peripheral arteries, in the treatment of cardiovascular diseases (CVDs) which is the number one cause of death globally: more people die annually from CVDs than from any other cause [113]. First-generation stents are metallic, whereas second-generation ones are polymer-coated drug-eluting metallic stents. New-generation stents are biodegradable polymers that are also drug eluting. The potential advantages of pure polymer stents compared to bare metal stents include increased biocompatibility, biodegradability, increased drug loading, enhanced compliance matching, reduced cost, ease of fabrication for patient-specific devices, molecular surface engineering, and the use of shape memory effect [114].

Metallic stents are effective in hindering acute occlusion and reducing late restenosis after coronary angioplasty; however, many concerns still remain. Compared with metallic stents,

poly-L-lactic acid (PLLA) stents are biodegradable and can deliver drugs locally, and these were developed by Igaki and Tamai. It was reported that feasibility, safety, and effectiveness of PLLA-biodegradable stents were verified in humans [115].

Wagner et al. reported that shape memory thermoplastic polyurethane is developed as a self-expandable stent, and it can be used as a drug delivery system [116].

A polymer system consists of *tert*-butyl acrylate, and poly(ethylene glycol) dimethylacrylate is improved which meets specific needs of minimally invasive cardiovascular devices by Gall and his coworkers. In this study, it was found that 10 wt% cross-linked polymer network can be stored unconstrained at room temperature and can be activated at body temperature which can be fabricated as a stent [117].

Chen et al. developed shape memory chitosan-based films (chitosan/PEO/glycerol) which are used to produce biodegradable stents. Chitosan cross-linked with epoxy compound stent's most remarkable property shows rapid expansion from a crimped state by using the hydration in an aqueous environment as a stimulant. By using minimally invasive surgery techniques, this stent can be placed into an artery. In another study of Chen and coworkers, genipin cross-linked chitosan-based stents were developed. The possibility of using this newly developed genipin stent as a drug delivery vehicle was also examined by loading an anti-proliferation drug, sirolimus. Findings showed that the genipin stent with enhanced mechanical strength can be used as an attractive stent platform for local drug delivery [118,119].

Maitland et al. performed the design and fabrication of an SMP stent (MM5520 thermoplastic polyurethane) which was triggered by photothermal actuation at 40–45°C [120].

Wang and coworkers developed fully biodegradable polymeric stent that can self-expand at body temperatures (37°C), using the concept of elastic memory. This self-expansion is necessary in fully polymeric stents, to overcome the problem of elastic recoil following balloon expansion in a body vessel. Bilayered biodegradable stent prototypes were produced from poly-L-lactic acid and polyglycolic acid (PLGA) polymers [121].

## 7.2. Aneurysm treatment

An aneurysm is a formation of balloon-like bulge in an artery. This bulge is formed when a part of artery wall becomes weak which results in unusual widening. Aneurysms can occur in any of the artery; however, the most common ones are aortic, cerebral (in the brain), popliteal (in the leg, behind knee), mesenteric (in the intestine), and splenic artery aneurysm (in the spleen). Almost 13,000 Americans die annually from aortic aneurysms. Surgery is the possible option for the treatment of large aortic aneurysms [122,123].

Shape memory polymer foams are the most attractive materials for aneurysm treatment by using them as a filling device in the artery [124]. Wilson and his coworkers showed that the shape memory polymer foam which includes hexamethylene diisocyanate (HDI), N,N,N',N'-tetrakis(2-hydroxypropyl)ethylenediamine (HPED), and triethanolamine (TEA) can be laser deployed in an *in vitro* aneurysm model. In this study, 10-mm aneurysm was treated with a new developed device [125].

In the study of Wong et al., shape memory polymer Calomer™ was investigated as a candidate for aneurysm coils. In this work, shape memory polymer coils spread inside a simulated aneurysm model proved that the typical hemodynamic forces do not prevent the shape recovery process [126].

Maitland et al. developed shape memory polyurethane foam with high porosity which makes it convenient for intracranial aneurysm treatments. Adding 4% tungsten into this foam improves radioopacity. Inherent radioopacity makes the material to be visualized by using conventional patient imaging modalities such as fluoroscopy in order to deliver it safely [127].

Another shape memory polymer foam based on hexamethylenediisocyanate, triethanolamine, and tetrakis(2-hydroxyl propyl)ethylenediamine was developed by Maitland et al. which is found to be suitable for aneurysm treatment [128].

Raymonda et al. developed a non-cytotoxic, non-mutagenic, and poorly thrombogenic polyurethane-based foam called cold hibernated elastic memory (CHEM) for endovascular procedures. The shape memory property and possibly modifying  $T_g$  or the size of the pores let this material for developing new tools including embolic agents that could completely replace the aneurysmal cavity, without intervening thrombus, to prevent recanalization and recurrences after the endovascular treatment of aneurysms [129].

### 7.3. Clot removal

When blood does not flow smoothly in the blood vessels, it can begin to coagulate and/or blood clots. A blood clot, or thrombus, may continue to grow, blocking the blood supply to certain parts of the body and causing damage to tissues and organs. Some medical intervention is often required to remove the clots. It is estimated that each year thrombosis affects as many as 900,000 people in the USA and kills up to 100,000 [130,131].

Maitland et al. reported that a prototype endovascular electromechanical clot extraction device was fabricated using a combination of shape memory polymer and shape memory nickel–titanium alloy (nitinol). This preliminary study suggests that SMP–nitinol device may have an application in the treatment of acute stroke or other thromboembolic diseases [132].

Also, Maitland and coworkers aimed to evaluate the feasibility of utilizing a system of SMP acrylates for a thrombectomy device by determining an optimal cross-link density that provides both adequate recovery stress for blood clot removal and sufficient strain capacity to enable catheter delivery. They have reported an acrylic SMP system with glass transitions above body temperature in the range of 65–75°C with tailorable recovery stresses that were controlled by varying the cross-link density. From the four different material compositions evaluated, devices with 15 mole% bisphenol A(BPA) gave the most favorable outcome [133].

Wilson et al. reported that coil, umbrella, and microgripper-shaped polyurethane microactuators are used to treat stroke by activating this shape memory polymer with laser to remove clots. The actuation of the devices was obtained between 65 and 85°C [134].

## 8. Conclusion and future outlook

In this chapter, novel smart polymeric materials, i.e., shape memory polymers, self-folding polymers, polymer origami structures, and their potential applications are summarized. Shape memory polymers are the class of smart materials which can fix their shape after applying a deformation by cooling below their transition temperature. Then, by reheating the above transition temperature, shape recovery to the original shape is observed. They can be produced from polymer material or blending with network-based polymers.

Due to their excellent biocompatibility, SMPs are promising building blocks of biomedical applications such as polymer vascular stents with shape memory polymers as the drug delivery system, smart surgical suture, laser-activated SMP microactuators to remove clots in a blood vessel and implants for minimally invasive surgery.

Today, SMP development continues rapidly, in the case of clinical applications. Enhancing biomedical applications beyond medical devices would be achieved by blending the shape memory polymers with compatible materials.

When minimally invasive surgery application is taken into account, implants should be able to carry out complex movements. These movements have to be performed by a material which can perform predetermined shift many times such as SMPs. Also, SMPs would be required for individual patients since they are compatible against specific conditions.

Shape memory polymers are considered to be a future strategy which may prevent undesired complications during the treatment in biomedical applications compared to shape memory alloy-based materials due to their biodegradability. Since SMPs are versatile materials, they would continue to develop as a result of their promising potential applications.

## Author details

Sera Erkeçoğlu<sup>1\*</sup>, Ali Demir Sezer<sup>2</sup> and Seyda Bucak<sup>1</sup>

\*Address all correspondence to: [seyda@yeditepe.edu.tr](mailto:seyda@yeditepe.edu.tr)

<sup>1</sup> Department of Chemical Engineering, Yeditepe University, Kayışdağı, Istanbul, Turkey

<sup>2</sup> Department of Pharmaceutical Biotechnology, Faculty of Pharmacy, Marmara University, Haydarpaşa, Istanbul, Turkey

## References

- [1] Huang W.M, Ding Z, Wang C.C, Wei J, Zhao Y, Purnawali H. Shape Memory Materials. *Materials Today*; 2010, 13(7-8): 54–61.

- [2] Mather P.T, Luo X, Rousseau I.A. Shape Memory Polymer Research. *Annual Review of Material Research*; 2009, 39: 445–471.
- [3] Konstanze K. Julich-Gruner, Löwenberg C, Neffe A.T, Behl M, Lendlein A. Recent Trends in the Chemistry of Shape Memory Polymers. *Macromolecular Chemistry and Physics*; 2013, 214(5): 527–536.
- [4] Serrano M.C, Ameer G.A. Recent Insights into the Biomedical Applications of Shape Memory Polymers. *Macromolecular Bioscience*; 2012, 12(9): 1156–1171.
- [5] Meng Q, Hu J. A Review of Shape Memory Polymer Composites and Blends. *Composites: Part A*; 2009, 40: 1661–1672.
- [6] Lendlein A, Kelch S. Shape-Memory Polymers. *Angewandte Chemie International Edition*; 2002, 41: 2034–2057.
- [7] Hiltz J.A. Shape Memory Polymers Literature Review. *Defence R&D Canada Technical Memorandum*; 2002, 127.
- [8] Liang C, Rogers C.A, Malafeew E. Investigation of Shape Memory Polymers and Their Hybrid Composites. *Journal of Intelligent Material Systems and Structures*; 1997, 8(4): 380–386.
- [9] Ahmed N, Kausar A, Muhammad B. Advances in Shape Memory Polyurethanes and Composites: A Review. *Polymer-Plastics Technology and Engineering*; 2015, 54: 1410–1423.
- [10] Lendlein A, Langer R. Biodegradable, Elastic Shape-Memory Polymers for Potential Biomedical Applications. *Science*; 2002, 296 (5573): 1673–1676.
- [11] Behl M, Zotzmann J, Lendlein A. Shape-Memory Polymers and Shape-Changing Polymers. *Advance in Polymer Science*; 2009, 226: 1–40.
- [12] Liu C, Qin H, Mather P.T. Review of Progress in Shape – Memory Polymers. *Journal of Materials Chemistry*; 2007, 17: 1543–1558.
- [13] Sokolowski W, Metcalfe A, Hayashi S, Yahia L, Raymond J. Medical Applications of Shape Memory Polymers. *Biomedical Materials*; 2007, 2: 23–27.
- [14] Monkman G.J. Advances in Shape Memory Polymer Actuation. *Mechatronics*; 2000, 10: 489–498.
- [15] Witold M, Sokolowski A, Chmielewski B, Hayashi S, Yamada T. Cold Hibernated Elastic Memory (CHEM) Self-deployable Structures. *SPIE Conference on Electroactive Polymer Actuators and Devices*; 1999.
- [16] Hu J, Zhu Y, Huang H, Lu J. Recent Advances in Shape – Memory Polymers: Structure, Mechanism, Functionality, Modeling and Applications. *Progress in Polymer Science*; 2012, 37: 1720–1763.

- [17] Leng J, Lan X, Liu Y, Dua S. Shape-Memory Polymers and Their Composites: Stimulus Methods and Applications. *Progress in Materials Science*; 2011, 56: 1077–1135.
- [18] Kumpfer J.R, Rowan S.J. Thermo-, Photo- and Chemo-Responsive Shape-Memory Properties From Photo - Crosslinked Metallo - Supramolecular Polymers. *Journal of the American Chemical Society*; 2011, 133: 12866–12874.
- [19] Leng J.S, Lan X, Liu Y.J, Du S.Y, Huang W.M, Liu N, Phee S.J, Yuan Q. Electrical Conductivity of Thermo-responsive Shape - Memory Polymer with Embedded Micron Sized Ni Powder Chains. *Applied Physics Letters*; 2008, 92 (1).
- [20] Mohr R, Kratz K, Weigel T, Lucka-Gabor M, Moneke M, Lendlein A. Initiation of Shape - Memory Effect by Inductive Heating of Magnetic Nanoparticles in Thermoplastic Polymers. *Proceedings of the National Academy of Sciences*; 2006, 103 (10): 3540–3545.
- [21] Razzaq M.Y, Behl M, Nöchel U, Lendlein A. Magnetically Controlled Shape -Memory Effects of Hybrid Nanocomposites from Oligo(*w*-pentadecalactone) and Covalently Integrated Magnetite Nanoparticles. *Polymer*; 2014, 55: 5953–5960.
- [22] Xia S, Li X, Wang Y, Pan Y, Zeng Z, Ding X, Peng Y. A Remote Activated Shape Memory Polymer Network Employing Vinyl Capped Fe<sub>3</sub>O<sub>4</sub> Nanoparticles as Netpoints for Durable Performance. *Smart Materials and Structures*; 2014, 23(8).
- [23] Huang W.M, Yang B, Zhao Y, Ding Z. Thermo-Moisture Responsive Polyurethane Shape-Memory Polymer and Composites: A Review. *Journal of Materials Chemistry*; 2010, 20: 3367–3381.
- [24] Lendlein A, Jiang H, Jünger O, Langer R. Light Induced Shape Memory Polymers. *Nature*; 2005, 434: 879–882.
- [25] Huang W.M, Zhao Y, Wang C.C, Ding Z, Purnawali H, Tang C, Zhang J.L. Thermo/Chemo - Responsive Shape Memory Effect in Polymers: A Sketch of Working Mechanisms, Fundamentals and Optimization. *Journal of Polymer Research*; 2012, 19(9952).
- [26] Chatterjee T, Dey P, Nando, Naskar K. Thermo - Responsive Shape Memory Polymer Blends Based on Alpha Olefin and Ethylene Propylene Diene Rubber, *Polymer*; 2015, 78: 180–192.
- [27] Langer R, Tirrel D.A. Designing Materials for Biology and Medicine, *Nature*; 2004, 428: 487–492.
- [28] Xue L, Dai S, Li Z. Synthesis and Characterization of Elastic Star Shape-Memory Polymers as Self Expandable Drug-Eluting Stents. *Journal of Materials Chemistry*; 2012, 22: 7403–7411.
- [29] Yakachi C.M. Shape Memory and Shape Changing Polymers. *Polymer Reviews*; 2013, 53: 1–3.

- [30] Sokolowski W, Metcalfe A, Hayashi S, Yahia L, Raymond J. *Biomedical Materials*; 2007, 2: 23–27.
- [31] Razzaq M.R, Anhalt M, Froman L, Weidenfeller B. Mechanical Spectroscopy of Magnetite Filled Polyurethane Shape Memory Polymers. *Materials Science and Engineering*; 2007, 471: 57–62.
- [32] Ebara M. Shape-Memory Surfaces for Cell Mechanobiology. *Science and Technology of Advance Materials*; 2015, 16(1).
- [33] Behl M, Lendlein A. Shape Memory Polymers. *Materials Today*; 2007, 10(4): 20–28.
- [34] Xie T, Rousseau I.A. Facile Tailoring of Thermal Transition Temperatures of Epoxy Shape Memory Polymers. *Polymer*; 2009, 50, 1852–1856.
- [35] Zheng X, Zhou S, Li X, Weng J. Shape Memory Properties of Poly(D,L-lactide)/Hydroxyapatite Composites. *Biomaterials*; 2006, 27: 4288–4295.
- [36] Brosnan S.M, Jackson A.S, Wang Y, Ashby V.S. Shape Memory Particles Capable of Controlled Geometric and Chemical Asymmetry Made from Aliphatic Polyesters. *Macromolecular Rapid Communications*; 2014, 35: 1653–1660.
- [37] Pandini S, Baldi F, Paderni K, Messori M, Toselli M, Pilati F, Gianoncelli A, Brisotto M, Bontempi E, Riccò T. One-way and Two-way Shape Memory Behavior of Semi-Crystalline Networks Based on Sol-gel Cross Linked Poly( $\epsilon$ -caprolactone). *Polymer*; 2013, 54: 4253–4265.
- [38] Xie T. Recent Advances in Polymer Shape Memory. *Polymer*; 2011, 52: 4985–5000.
- [39] Behl M, Razzaq M.R, Lendlein A. Multifunctional Shape-Memory Polymers. *Advanced Materials*; 2010, 22: 3388–3410.
- [40] Wu X, Huang W.M, Zhao Y, Ding Z, Tang C, Zhang J. Mechanisms of the Shape Memory Effect in Polymeric Materials. *Polymers*; 2013, 5: 1169–1202.
- [41] Li X, Zhu Y, Dong Y, Liu M, Ni Q, Fu Y. Epoxy Resin Composite Bilayers with Triple - Shape Memory Effect. *Hindawi Publishing Corporation Journal of Nanomaterials*; 2015.
- [42] Cuevas J.M, Rubio R, Germán L, Villas J.L, Rodriguez M, León L.M. Triple Shape Memory Effect of Covalently Crosslinked Polyalkenamer Based Semicrystalline Polymer Blends. *Soft Matter*; 2012, 8: 4928–4935.
- [43] Kumar U.N, Kratz K, Behl M, Lendlein A. Shape - Memory Properties of Magnetically Active Triple - Shape Nanocomposites Based on a Grafted Polymer Network with Two Crystallizable Switching Segments. *Express Polymer Letters*; 2012, 6(1): 26–40.
- [44] Chen S, Hu J, Yuen C, Chan L, Zhuo H. Triple Shape Memory Effect in Multiple Crystalline Polyurethanes. *Polymers for Advanced Technologies*; 2010, 21: 377–380.

- [45] Xie T, Xiao X, Cheng Y. Revealing Triple-Shape Memory Effect by Polymer Bilayers. *Macromolecular Rapid Communications*; 2009, 30: 1823–1827.
- [46] Xie T. Tunable Polymer Multi- Shape Memory Effect. *Nature*; 2010, 464: 267–270.
- [47] Basit A, L'Hostis G, Pae M.J, Durand B. Thermally Activated Composite with Two-Way and Multi-Shape Memory Effects. *Materials*; 2013, 6: 4031–4045.
- [48] Li J, Rodgers W.R, Xie T. Semicrystalline Two-Way Shape Memory Elastomer, *Polymer*; 2011, 52: 5320, 5325.
- [49] Chen S, Hu J, Zhuo H, Zhu Y. Two-way Shape Memory Effect in Polymer Laminates. *Materials Letters*; 2008, 62: 4088–4090.
- [50] Zhou J, Turner S.A, Brosnan S.M, Li Q, Cartillo J.Y, Nykypanchuk D, Gang O, Ashby V.S, Dobrynin A.V, Sheiko S.S. Shapeshifting: Reversible Shape Memory in Semicrystalline Elastomers. *Macromolecules*; 2014, 47: 1768–1776.
- [51] Madbouly S.A, Lendlein A. Shape – Memory Polymer Composites. *Advanced Polymer Science*; 2010, 226: 41–95.
- [52] Leng J, Lu H, Liu Y, Huang W.M, Du S. Shape-Memory Polymers- A Class of Novel Smart Materials. *Mrs Bulletin*; 2009, 34.
- [53] Yakachi C.M, Satarkar N.S, Gall K, Likos R, Hilt J.Z. Shape- Memory Polymer Networks with Fe<sub>3</sub>O<sub>4</sub> Nanocomposites for Remote Activation, *Journal of Applied Polymer Science*; 2002,112: 3166–3176.
- [54] Razzaq M.Y, Anhalt M, Frommann L, Weidenfeller B. Thermal, electrical and magnetic studies of magnetite filled polyurethane shape memory polymers. *Materials Science and Engineering A*; 2007, 444: 227–235.
- [55] Yu X, Zhou S, Zheng X, Guo T, Xiao Y, Song B. A Biodegradable Shape-Memory Nanocomposite with Excellent Magnetism Sensitivity. *Nanotechnology*; 2009, 20(23).
- [56] Schmidt A.M. Electromagnetic Activation of Shape Memory Polymer Networks Containing Magnetic Nanoparticles. *Macromolecules Rapid Communications*; 2006, 27: 1168–1172.
- [57] Zheng X, Zhou S, Xiao Y, Yu X, Li X, Wu P. Shape Memory Effect of Poly(D,L-lactide)/Fe<sub>3</sub>O<sub>4</sub> Nanocomposites by Inductive Heating of Magnetic Nanoparticles. *Colloids and Surfaces B: Biointerfaces*; 2009, 71: 67–72.
- [58] Puig J, Hoppe C.E, Fasce L.A, Pérez C.J, Piñeiro-Redondo Y, Bañobre-López M, López-Quintela M.A, Rivas J, Williams R.J.J. Superparamagnetic Nanocomposites Based on the Dispersion of Oleic Acid-Stabilized Magnetite Nanoparticles in a Diglycidylether of Bisphenol A-Based Epoxy Matrix: Magnetic Hyperthermia and Shape Memory. *The Journal of Physical Chemistry C*; 2012, 116: 13421–13428.

- [59] Cho J.W, Kim J.W, Jung Y.C, Goo N.S. Electroactive Shape-Memory Polyurethane Composites Incorporating Carbon Nanotubes. *Macromolecular Rapid Communications*; 2005, 26: 412–416.
- [60] Liu Y, Lv H, Lan X, Leng J, Du S. Review of Electro-Active Shape-Memory Polymer Composite, *Composites Science and Technology*; 2009, 69: 2064–2068.
- [61] Yoo H.J, Jung Y.C, Sahoo N.G, Cho J.W. Polyurethane-Carbon Nanotube Nanocomposites Prepared by In-Situ Polymerization with Electroactive Shape Memory. *Journal of Macromolecular Science, Part B: Physics*; 2006, 45: 441–451.
- [62] Jung Y.C, Yoo H.J, Kim Y.A, Cho J.W, Endo M. Electroactive Shape Memory Performance of Polyurethane Composite Having Homogenously Dispersed and Covalently Crosslinked Carbon Nanotubes, *Carbon*; 2010, 48: 1598–1603.
- [63] Sahoo N.G, Jung Y.C, Cho J.W. Electroactive Shape Memory Effect of Polyurethane Composites Filled with Carbon Nanotubes and Conducting Polymer. *Materials and Manufacturing Processes*; 2007, 22: 419–423.
- [64] Leng J, Lan X, Liu Y, Du S. Electroactive Thermoset Shape Memory Polymer Nanocomposite Filled with Nanocarbon Powders. *Smart Materials*; 2009, 18.
- [65] Xiao Y, Zhou S, Wang L, Gong T. Electro-Active Shape Memory Properties of Poly( $\epsilon$ -caprolactone)/Functionalized Multiwalled Nanotune Nanocomposite. *Applied Materials and Interfaces*; 2010, 2(12): 3506–3514.
- [66] Sahoo N.G, Yung Y.C, Yoo H.J, Cho J.W. Influence of Carbon Nanotubes and Polypyrrole on the Thermal, Mechanical and Electroactive Shape-Memory Properties of Polyurethane Nanocomposites, *Composites Science and Technology*; 2007, 67: 1920–1929.
- [67] Meng H, Li G. A review of stimuli-responsive shape memory polymer composites. *Polymer*; 2013, 54: 2199–2221.
- [68] Wu T, O’Kelly K, Chen B. Poly(methacrylic acid)-Grafted Clay–Thermoplastic Elastomer Composites with Water-Induced Shape-Memory Effects. *Journal of Polymer Science, Part B: Polymer Physics*; 2013, 51: 1513–1522
- [69] Luo H, Ma Y, Li W, Yi G, Cheng X, Ji W, Zu X, Yuan S, Li J. Shape Memory-Enhanced Water Sensing of Conductive Polymer Composites, *Materials Letters*; 2015, 161: 189–192.
- [70] Nöchel U, Reddy C.S, Uttamchand N.K, Kratz K, Behl M, Lendlein A. Shape-Memory Properties of Hydrogels Having a Poly( $\epsilon$ -caprolactone) Crosslinker and Switching Segment in an Aqueous Environment, *European Polymer Journal*; 2013, 49: 2457–2466.
- [71] Paakinaho K, Hukka T.I, Kastinen T, Kellomäki M. Demonstrating the Mechanism and Efficacy of Water-Induced Shape Memory and the Influence of Water on the

- Thermal Properties of Oriented Poly (d,l-lactide). *Journal of Applied Polymer Science*; 2013: 4209–4213.
- [72] Mendez J, Annamalai P.K, Eichhorn S.J, Rusli R, Rowan S.J, Foster E.J, Weder C. Bio-inspired Mechanically Adaptive Polymer Nanocomposites with Water-Activated Shape-Memory Effect. *Macromolecules*; 2011, 44: 6827–6835.
- [73] Hernandez E.A, Hartl D.J, Malak Jr R.J, Lagoudas D.C. Origami- Inspired Active Structures: A Synthesis and Review. *Smart Material Structures*; 2014, 23(9).
- [74] Gracias D.H. Stimuli Responsive Self-Folding Using Thin Polymer Films, *Current Opinion in Chemical Engineering*; 2013: 112–119.
- [75] Azam A, Laflin K.E, Jamal M, Fernandes R, Gracias D.H. Self - Folding Micropatterned Polymeric Containers. *Biomedical Microdevices*; 2011: 51–58.
- [76] Guan J, He H, Hansford D.J, Lee L.J. Self-Folding of Three-Dimensional Hydrogel Microstructures. *Journal of Physical Chemistry B*; 2005, 109(49): 23134–23137.
- [77] Fernandes R, Gracias D.H. Self-Folding Polymeric Containers for Encapsulation and Delivery of Drugs, *Advanced Drug Delivery Reviews*; 2012, 64: 1579–1589.
- [78] Ionov L. 3D Microfabrication Using Stimuli-Responsive Self-Folding Polymer Films. *Polymer Reviews*; 2013, 53: 92–107.
- [79] Zakharchenko S, Sperling E, Ionov L. Fully Biodegradable Self-Rolled Polymer Tubes: A Candidate for Tissue Engineering Scaffolds. *Biomacromolecules*; 2011, 12: 2211–2215.
- [80] Luchnikov V, Ionov L, Stamm M. Self-Rolled Polymer Tubes: Novel Tools for Microfluidics, Microbiology, and Drug-Delivery Systems. *Macromolecular Rapid Communications*; 2011, 32: 1943–1952.
- [81] Ionov L. Soft Microorigami: Self-Folding Polymer Films. *Soft Matter*; 2011, 7: 6786–6791.
- [82] Zakharchenko S, Ionov L. Anisotropic Liquid Microcapsules from Biomimetic Self-Folding Polymer Films. *ACS Applied Materials and Interfaces*; 2015, 7(23): 12367–12372.
- [83] Stoychev G, Zakharchenko S, Turcaud S, Dunlop J.W, Ionov L, Shape-Programmed Folding of Stimuli-Responsive Polymer Bilayers. *ACS Nano*; 2012, 6(5): 3925–3934.
- [84] Huang W.M, Lu H.B, Zhao Y, Ding Z, Wang C.C, Zhang J.L, Sun L, Fu J, Gao X.Y. Instability/Collapse of Polymeric Materials and Their Structures in Stimulus - Induced Shape/Surface Morphology Switching. *Materials and Design*; 2014, 59, 176–192.
- [85] He H, Guan J, Lee J.L. An Oral Delivery Device Based on Self-Folding Hydrogels. *Journal of Controlled Release*; 2006, 110: 339–346.

- [86] Agrawal A, Yun T, Pesek S.L, Chapman W.G, Verduzco R. Shape-Responsive Liquid Crystal Elastomer Bilayers. *Soft Matter*; 2014, 10: 1411–1415.
- [87] Kelby T.S, Wang M, Huck W.T.S. Controlled Folding of 2D Au–Polymer Brush Composites into 3D Microstructures. *Advanced Functional Materials*; 2011, 21: 652–657.
- [88] De Haan L.T, Gimenez-Pinto V, Konya A, Nguyen T, Verjans J.M.N, Sánchez-Somolinos C, Selinger J.V, Selinger R.L.B, Broer D.J, Schenning A.P.H.J. Accordion-like Actuators of Multiple 3D Patterned Liquid Crystal Polymer Films. *Advanced Functional Materials*; 2014, 24: 1251–1258.
- [89] Kamal T, Park S. Shape-Responsive Actuator from a Single Layer of a Liquid-Crystal Polymer. *Applied Material Interfaces*; 2014, 6: 18048–18054.
- [90] Yu L, Yu H. Light-Powered Tumbler Movement of Graphene Oxide/Polymer Nanocomposites. *Applied Material Interfaces*; 2015, 7(6): 3834–3839.
- [91] Zacharchenko S, Pureskiy N, Stoychev G, Waurisch C, Hickey S.G, Eychmüller A, Sommer J, Ionov L. Stimuli-Responsive Hierarchically Self-Assembled 3D Porous Polymer-Based Structures with Aligned Pores. *Journal of Material Chemistry B*; 2013, 1: 1786–1793.
- [92] Fei L.J, Sujun D. Origami Theory and Its Applications: A Literature Review. *International Scholarly and Scientific Research & Innovation*; 2013, 7(1).
- [93] Ryu J, D'Amato M, Cui X, Long K.N, Qi H.J. Photo-origami- Bending and Folding Polymers with Light. *Applied Physics Letter*; 2012, 100.
- [94] Ionov L. Polymer Origami: Programming the Folding with Shape, e-Polymers; 2014,14(2): 109–114.
- [95] Breger J.C, Yoon C, Xiao R, Kwan H.R, Wang M.O, Fisher J.P, Nguyen T.D, Gracias D.H. Self-Folding Thermo-Magnetically Responsive Soft Microgrippers. *Applied Material Interfaces*; 2015, 7: 3398–3405.
- [96] Py C, Reverdy P, Doppler L, Bico J, Roman B, Baroud C.N. Capillary Origami: Spontaneous Wrapping of a Droplet with an Elastic Sheet. *Physical Review Letters*; 2007, 98.
- [97] Randall C.L, Leong T.G, Bassik N, Gracias D.H. 3D Lithographically Fabricated Nanoliter Containers for Drug Delivery. *Advanced Drug Delivery Reviews*; 2007, 59: 1547–156.
- [98] Jamal M, Kadam S.S, Xiao R, Jivan F, Onn T, Fernandes R, Nguyen T.D, Gracias D.H. Bio-Origami Hydrogel Scaffolds Composed of Photocrosslinked PEG Bilayers. *Advanced Healthcare Materials*; 2013, 2: 1142–1150.
- [99] Wischke C, Neffe A.T, Steuer S, Lendlein A. Evaluation of a Degradable Shape-Memory Polymer Network as Matrix for Controlled Drug Release. *Journal of Controlled Release*; 2009, 138: 243–250.

- [100] Wischke C, Behl M, Lendlein A. Drug-Releasing Shape-Memory Polymers- The Role of Morphology, Processing Effects, and Matrix Degradation. *Expert Opinion on Drug Delivery*; 2013, 10(9).
- [101] Lendlein A, Wischke C. How to Accelerate Biomaterial Development? Strategies to Support the Application of Novel Polymer-Based Biomaterials in Implantable Devices. *Expert Review of Medical Devices*; 2011, 8(5): 533–537.
- [102] Nagahama K, Ueda Y, Ouchi T, Ohya Y. Biodegradable Shape-Memory Polymers Exhibiting Sharp Thermal Transitions and Controlled Drug Release. *Biomacromolecules*; 2009, 10: 1789–1794.
- [103] Serrano M.C, Carbajal L, Ameer A.G. Novel Biodegradable Shape-Memory Elastomers with Drug-Releasing Capabilities. *Advanced Materials*; 2011, 23: 2211–2215.
- [104] Musial-Kulik M, Kasperczyk J, Smola A, Dobrzyński P. Double Layer Paclitaxel Delivery Systems Based on Bioresorbable Terpolymer with Shape Memory Properties. *International Journal of Pharmaceutics*; 2014, 465: 291–298.
- [105] Wischke C, Neffe A.T, Steuer S, Lendlein A. Comparing Techniques for Drug Loading of Shape-Memory Polymer Networks – Effect on Their Functionalities. *European Journal of Pharmaceutical Sciences*; 2010, 41: 136–147.
- [106] Xiao Y, Zhou S, Wang L, Zheng X, Gong T. Crosslinked Poly( $\epsilon$ -caprolactone)/Poly(Sebacic Anhydride) Composites Combining Biodegradation. Controlled Drug Release and Shape Memory Effect. *Composites: Part B*; 2010, 41: 537–542.
- [107] Lendlein A, Behl M, Hiebl B, Wischke C. Shape-Memory Polymers as a Technology Platform for Biomedical Applications. *Expert Review of Medical Devices*; 2010, 7 (3): 357–379.
- [108] Wischke C, Lendlein A. Shape-Memory Polymers as Drug Carriers-A Multifunctional System. *Pharmaceutical Research*; 2010, 27(4).
- [109] Bao M, Lou X, Zhou Q, Dong W, Yuan H, Zhang Y. Electrospun Biomimetic Fibrous Scaffold from Shape Memory Polymer of PDLLA-*co*-TMC for Bone Tissue Engineering. *Applied Material Interfaces*; 2014, 6: 2611–2621.
- [110] Fusco S, Sakar M.S, Kennedy S, Peters C, Pene S, Mooney D, Nelson B.J. Self-Folding Mobile Microrobots for Biomedical Applications, Robotics and Automation (ICRA). *IEEE International Conference*; 2014: 3777–3782.
- [111] Liu Y, Park J, Lang R.J, Emami-Neyestanak A, Pellegrino S, Humayun M.S, Tai Y. Parylene Origami Structure for Intraocular Implantation. *Solid-State Sensors, Actuators and Microsystems*; 2013: 1549–1552
- [112] Ortega J.M, Small IV W, Wilson T.S, Bennett W.J, Loge J.M, Maitland D.J. A Shape Memory Polymer Dialysis Needle Adapter for the Reduction of Hemodynamic Stress

- within Arteriovenous Grafts. *IEEE Transactions on Biomedical Engineering*; 2007, 54(9): 1722–1724.
- [113] World Health Organization. *Global Status Report on Noncommunicable Diseases*; 2014.
- [114] Yakacki C.M, Gall K. *Shape – Memory Polymers for Biomedical Applications*. *Advanced Polymer Science*; 2010, 147–175.
- [115] Tamai H, Igaki K, Kyo E, Kosuga K, Kawashima A, Matsui S, Komori H, Tsuji T, Motohara S, Uehata H. Initial and 6-Month Results of Biodegradable Poly L-Lactic Acid Coronary Stents in Humans. *Circulation*; 2000, 102: 399–404.
- [116] Wache H.M, Tartakorska D.J, Hentrich A, Wagner M.H. Development of a Polymer Stent with Shape Memory Effect as a Drug Delivery System. *Journal of Materials Science: Materials in Medicine*; 2003, 14: 109–112.
- [117] Yakacki C.M, Shandas R, Lanning C, Rech B, Eckstein A, Gall K. Unconstrained Recovery Characterization of Shape-Memory Polymer Networks for Cardiovascular Applications. *Biomaterials*; 2007, 28: 2255–2263.
- [118] Chen M, Tsai H, Chang Y, Lai W, Mi F, Liu C, Wong H, Sung H. Rapidly Self-Expandable Polymeric Stents with a Shape-Memory Property. *Biomacromolecules*; 2007, 8: 2274–2280.
- [119] Chen M, Liu C, Tsai H, Lai W, Chang Y, Sung H. Mechanical Properties, Drug Eluting Characteristics and in Vivo Performance of a Genipin-Crosslinked Chitosan Polymeric Stent. *Biomaterials*; 2009, 30: 5560–5571.
- [120] Baer G.M, Small IV W, Wilson T.S, Benett W.J, Matthews D.L, Hartman J, Maitland D.J. Fabrication and in Vitro Deployment of a Laser-Activated Shape Memory Polymer Vascular Stent. *BioMedical Engineering OnLine*; 2007, 6(43).
- [121] Venkatraman S.S, Tan L.P, Joso J.F.D, Boey Y.C.F, Wang X. Biodegradable Stents with Elastic Memory. *Biomaterials*; 2006, 27: 1573–1578.
- [122] American Heart Association, *What Is an Aneurysm?*; 2015.
- [123] National Heart, Lung and Blood Institute (NHLBI), *What Is an Aneurysm?*; 2011.
- [124] Small IV W, Buckley P.R, Wilson T.S, Benett W.J, Hartman J, Saloner D, Maitland D.J. Shape Memory Polymer Stent with Expandable Foam: A New Concept for Endovascular Embolization of Fusiform Aneurysms. *IEEE Transactions on Biomedical Engineering*; 2007, 54(6).
- [125] Maitland D.J, Small IV W, Ortega J.M, Buckley P.R, Rodriguez J, Hartman J, Wilson T.S. Prototype Laser-Activated Shape Memory Polymer Foam Device for Embolic Treatment of Aneurysms. *Journal of Biomedical Optics*; 2007, 12(3).

- [126] Hampikian J.M, Heaton B.C, Tong F.C, Zhang Z, Wong C.P. Mechanical and Radiographic Properties of a Shape Memory Polymer Composite for Intracranial Aneurysm Coils. *Materials Science and Engineering C*; 2006, 26: 1373–1379.
- [127] Rodriguez J.N, Yu Y, Miller M.W, Wilson T.S, Hartman J, Clubb F.J, Gentry B, Maitland D.J. Opacification of Shape Memory Polymer Foam Designed for Treatment of Intracranial Aneurysms. *Annual Biomedical Engineering*; 2012, 40(4): 883–897.
- [128] Singhal P, Wilson T.S, Maitland D.J. Controlling the Physical Properties of Random Network Based Shape Memory Polymer Foams. *Materials Research Society Symposium Proceedings*; 2010, 1274.
- [129] Metcalfe A, Desfaitsa A, Salazkina I, Yahiab L, Sokolowskic W.M, Raymonda J. Cold Hibernated Elastic Memory Foams for Endovascular Interventions. *Biomaterials*; 2003, 24: 491–497.
- [130] Beckman M.G, Hooper W.C, Critchley S.E, Ortel T.L. Venous Thromboembolism: A Public Health Concern. *American Journal of Preventing Medicine*; 2010, 38(4): 494–501.
- [131] Raskob G.E, Silverstein R, Bratzler D.W, Heit J.A, White R.H. Surveillance for Deep Vein Thrombosis and Pulmonary Embolism: Recommendations from a National Workshop. *American Journal of Preventing Medicine*; 2010, 38(4): 502–109.
- [132] Hartman J, Small IV W, Wilson T.S, Brock J, Buckley P.R, Benett W.J, Loge J.M, Maitland D.J. Embolectomy in a Rabbit Acute Arterial Occlusion Model Using a Novel Electromechanical Extraction Device. *American Journal of Neuroradiol*; 2007, 28: 872–874.
- [133] Muschenborn A.D, Hearon K, Volk B.L, Conway J.W, Maitland D.J. Feasibility of Crosslinked Acrylic Shape Memory Polymer for a Thrombectomy Device. *Smart Materials Research*; 2014.
- [134] Maitland D.J, Metzger M.F, Schumann D, Lee A, Wilson T.S. Photothermal Properties of Shape Memory Polymer Micro-Actuators for Treating Stroke. *Lasers in Surgery and Medicine*; 2002, 30: 1–11.



---

# Getting a Handle on Smart Drug Delivery Systems – A Comprehensive View of Therapeutic Targeting Strategies

---

Sugapriya Dhanasekaran and Sumitra Chopra

Additional information is available at the end of the chapter

<http://dx.doi.org/10.5772/61388>

---

## Abstract

Smart drug delivery system (SDDS) is a recently emerging therapeutic approach, now turning into a conventional model to deliver drug to specific sites or target. Drug targeted (DT) delivery systems maintain the concentration of the drugs at desirable doses in the body and avoid the need for repeated doses. The DT delivery system have specific distinguishing features such as self-regulated, pre-programmed, multi-targeted, controlled by timely response, monitoring of the targeted drug delivery, responsive to pH, and spatially targeted. The DT delivery system exploits the biological membrane changes in the physiology of malignant cells to increase absorption or entry of drug-coated nanoparticles into targeted tissues. This system delivers a certain quantity of a therapeutic drug for longevity of its action to a targeted area within the human tissue, which in turn enhances efficacy of the treatment by reducing the side effects of drug administration. A new DT therapy strategy is a health improvement technique used in future generations for treatment of genetic diseases and intelligent drug delivery. The ultimate goal of SDDS is to administrate the drugs at the correct time with an exact dose in the body and with efficiency and specificity to the targeted cells that help the patients better adhere to their therapy regimen. The DT system enhances the maintenance of drug levels in targeted tissues and plasma without any destruction to the healthy tissues. This DT delivery system uses various strategies in targeting cells, drug delivery mechanisms, properties of targeted drug, organ-based targeted sites, disease, and drug-targeted vehicles. This chapter deals with all aspects of drug targeting and provides an overview of approaches in drug targeting, drug delivery vehicles, and strategies involved in successful delivery.

**Keywords:** Smart Dug Delivery System (SDDS), drug targeting strategies, nanoparticles, nanocarriers, passive and active targeting, folate receptor targeting, antibody targeting, glycoprotein targeting, drug delivery, malignant cells

## 1. Introduction

Smart drug delivery system (SDDS) is an advanced method of Drug Targeted (DT) delivery. The smart drug delivered by this system must fulfill the following criteria: 1) increase the doses of delivered drug to targeted body part of interest (tissue/cells/organs), 2) not be degraded by any of the body fluids, 3) diminish side effects by improving the efficacy of drug treatment, 4) absorption of the delivered drug must cross a biological membrane, and 5) drug is released in appropriate dosages to the body part of interest. The ultimate goal of a DT delivery system is to localize, maintain drug properties, ensure a specific route taken for the delivery of the drug, target the desired site only, reduce side effects of the drugs, and prolong drug interaction with the diseased tissue. Targeted delivery system maintains the required concentration of the drug in plasma and tissues at the targeted sites, therefore, evading damage to normal tissue/cells induced by the drug. The DT delivery system is highly complex and involves an integration of various disciplines, such as biology, chemistry, and engineering [1–3].

Nanoparticle-based drug delivery systems are framed according to specific properties of target cells, transport carrier/vehicles, nature of markers involving drug binding to specific ligands, and receptor being modulated by physical components. Superlatively, DT delivery systems should be non-immunogenic, non-toxic, chemically and physically stable in *in vitro* as well as *in vivo* conditions, have restricted drug distribution to target tissue/cells/organ, have uniform capillary distribution, have predictable and controllable rate of drug release, and have minimal drug leakage during transit [3–5]. Carriers used for targeted drug delivery should be easily bio-degradable or freely eliminated from the body without producing any side effects. The preparation of the targeted delivery system should be stress-free or reproducible, reasonably simple, and cost effective. The disadvantages of conventional drugs make attractive the reasons to concentrate our efforts on targeted delivery. Conventional drugs have less solubility of the given drug doses, poor absorption, shorter half-life, require large volume of distribution, less specificity, and less therapeutic index, all these are significantly overcome in the targeted drug delivery system [1–3].

In this chapter, we address: 1) the types of nanoparticles used internally for targeted drug delivery system based on their size, shape, and materials (metal, biological, polymers, and lipid); 2) specifically illustrate the mechanism and strategies of targeted drug delivery systems; 3) introduce the mechanism of organ-based targeted drug delivery system; 4) explain the therapeutic strategies of drug delivery and targeting action; 5) elucidate the significance and desirable properties of targeted delivery; 6) and finally, we validate a brief outlook of future challenges and trends in drug targeted delivery systems that will be established to progress their therapeutic efficiency and efficacy of drug functionality in future treatment of cancer and genetic disorders.

## 2. Strategies of Targeted Drug Delivery Systems

Drug-targeted delivery increases the therapeutic efficacy by controlling the toxic effects associated with the drug. Delivery of drugs to malignant tissue is increased and the normal

tissue remains unaltered. The approaches of targeted drug delivery systems such as passive, active, dual, combination, inverse, double, and physical targeting are being used extensively in therapy.

## 2.1. Passive Targeting System

Passive targeting refers to the accumulation of a drug-carrier system or drug targeting at a precise site; it may be attributed to chemical, physical, pharmacological, and biological aspects of the disease. The nanoparticle size and surface properties of the drug targeted system must be specially controlled to evade uptake by the reticulo-endothelial system to maximize the targeting capability and increase its circulation. Rapid vascularization assists fast-growing tumor tissue, imparting itself to a defective or leaky architecture enhancing the permeability of toxic chemotherapeutic drugs. Few drugs can be administrated as inactive drugs or prodrugs, hence, its exposure to cancerous tissue can be modified into highly active form. Passive targeting also integrates targeted drug delivery to the malignant bed through various invasive modalities.

### 2.1.1. Leaky Vasculature

Polymer nanoparticles exhibit the enhanced retention and permeability effects on targeted delivery in tumor cells [6]. Capillary endothelium in tumor tissue is disorganized and enhances the permeability towards macromolecules than normal tissues. This phenomenon allows extravasation within the tumor interstitium to the polymeric nanoparticle circulating for targeted drug delivery. The tumor bed lacks lymphatic drainage and results in drug accumulation, enhancing targeted strategies. A chemotherapeutic drug is linked with a specific nanoparticle or nanocarrier by a linker that has the potential of augmenting the concentration of therapeutic drugs within the malignant cells. These characteristic features (polymer-drug conjugates) modulates the drug concentration in malignant tissue levels 10 to 100 times more than free drug.

### 2.1.2. Tumor Microenvironment

The targeted drug is conjugated to a cancer-specific molecule and administered in an active state. When it reaches its final target, the cancerous environment modulates the drug to a volatile and active substance, the so-called malignant cell-activated prodrug therapy. Malignant tissue is characterized by vascular disorganization, intermittent basement membrane alteration that stimulates the metastasis of atypical cells to normal cells. Insufficient supply of nutrients and modulation of lymphatic networks does not remove the waste products in the cells accurately. A tumor cell retains increasing concentration of protons and leads to a decrease in the physiological pH of the cells [7]. The components of the extracellular matrix such as macrophages, fibroblasts, and collagen fibers in the cancerous tissues are also elevated. The degradation of tumor bed membranes and the extracellular matrix are enhanced by Matrix metalloproteinase-2. A recent study about a water-soluble maleimide derivative of doxorubicin incorporating a matrix metalloproteinase-2-specific peptide sequence by Mansour et al. [8] demonstrated (proved/showed) that this drug conjugate-polymer complex had a high affinity

to cysteine-34 of circulating bound form of albumin. Doxorubin was efficiently cleaved by the matrix metalloproteinase-2 from the bound form of albumin. The redox potential and modulated pH have been exposed as drug release triggers at the tumor site [9] for targeting.

### 2.1.3. Direct (Local) Drug Application

Direct application of the drug to the cancer cells permits the drug to react directly with the malignant cells without systematic blood circulation. Various methodologies have been used to improve the anticancer drug for targeted delivery for tumors such as intraperitoneal, intravesical injection, and administration of various chemotherapeutic agents. These methodologies require introducing higher concentrations of anticancer agents that is not always possible. Localized targeted drug delivery by intratumoral direction is a modified and attractive methodology, which has been used and tested [10]. Localized administration of anticancer drug mitomycin surface of the malignant tissue leads to an increased concentration of the drug and decreased toxicity at the targeted tumor site [11]. Onyx-0115 is a type 2/5 chimeric adenovirus improved by attenuation of the E1B-55 kDa gene [12]. Its complex with some other proteins binds and inactivates the p53 gene. This drug has been administered by various methods, most of which permit the drug to be applied directly into the malignant cells. Onyx-0115 is used in clinical trials through intratumoral administration to treat head and neck cancer [13], intratumoral via endoscopic ultrasound for pancreatic cancer [14], via hepatic artery for metastatic colorectal cancer [15], intraperitoneal (IP) administration in ovarian cancer [16], and intratumoral under radiographic guidance for advanced sarcomas [17]. Recently, a polymer, poly (lactic-co-glycolic acid), linked with Tacrolimus (FK506) entrapped in pH-sensitive microspheres [18] was administered rectally or orally to colitis animals. The experimental animals showed the released nanoparticles and drug concentration into the tumor environment was different from its surrounding tissues. The drug permeability level in malignant tissues was 3-fold higher than normal tissue when nanoparticles were used as drug carriers. Direct targeted delivery of antitumor drugs into the malignant tissue inhibited the drug from circulating in the blood. The drawback of direct targeted delivery of drugs into the tumor is highly invasive and localization in some type of tumors is not feasible and can be problematic.

## 2.2. Active Targeting System

“Active targeting” means specific interactions between drug/drug carrier and the target cells, commonly through specific ligand-receptor interactions [19–23]. The ligand and receptor interactions are possible only when these components are in adjacent proximity (<0.5 nm). Specific ligand-receptor interaction for intracellular localization occurs after extravasations and blood circulation. Active targeting is favored as it controls a drug carrier/drug toward a target site (e.g., cruise missile). PEGylation increased the blood circulation time by altering the surface of the drug carrier with poly (ethylene glycol) and/or improving the enhanced permeability and retention (EPR) effect to augment the drug delivery to the targeted tumor site. Earlier reports show that targeting tumor ligands does not result in augmented accumulation of the nanoparticles in targeted tumor sites. The specific molecules in tumor cells or

intracellular organelles enhance the active targeting pathways needs to active delivery of the drug into the entire tumor site [24–26]. Targeting a drug to a tumor site/specific area not only enhances the efficacy of therapeutic drugs, it also reduces the toxic effects associated with the drug and allows lower dosage of the drug for therapy. Active targeting is categorized into three approaches, these are: 1) targeting and restricting the circulation of nanoparticles to the capillary bed of a determined tumor targeted cell, site, tissue, or organ (cerebral ventricles, peritoneal cavity, compartmental targeting in lymphatics, plural cavity, joints, and eyes); 2) targeted delivery of the drug to a specific type of malignant cells/tissues and not to the normal healthy cells (specifically delivery of the nanoparticles to kupffer cells in the liver); and 3) targeting of nanoparticle delivery exactly to the intracellular site of targeted tumor cells (receptor-based ligand enters into a cell by endocytosis). The third approach is highly favored and used in guiding nanoparticles for targeted delivery through carbohydrates, receptors, and antigens.

### *2.2.1. Carbohydrate Targeted*

The cell surface of the carbohydrates disturbs the tumor cells' communication with normal healthy cells or with the extracellular matrix through metastatic growth and spread. This communication between the cells can be mediated through tumor cell binding proteins and their carbohydrates known as lectins. Endogenous lectins play an important role in the immunity to identify the “foreign patterns” of the cell surface carbohydrates on cancer cells. It clearly depict that lectins disturb the survival of malignant cells, endothelium adhesion/extracellular matrix, and tumor tissue vascularization processes that play a key role for metastatic growth and spread [27, 28]. This carbohydrate-ligand bonding communication can be made by improving the nanoparticles enclosing carbohydrate moieties focused on targeting certain lectins (direct lectin targeting Consequently, targeted drug delivery systems have been established based on this unique interaction/communication between lectins and carbohydrates targeted towards whole organs [29] and may be dangerous to normal healthy tissues. This is a major drawback of lectins, it should be rectified for the development of “smart carrier” molecules for targeted drug delivery. Lectin possesses a unique affinity for sugar moieties present on the surface of cancer tissues. Thus, unique characteristic features seem to be an attractive tool for further augmentation of nano-drug targeted delivery.

### *2.2.2. Receptor- and Antigen-directed Targeted*

Human cancer cells overexpress the receptors or antigens on their surface that enhances the efficient uptake of nanoparticles through receptor-mediated endocytosis, by which extracellular particles may enter into the intracellular environment. In general, drug-coated nanoparticles can enter into to the targeted tumor cells through ligand-receptor interactions. Once it reaches the localized area of the tumor cell surface, the targeted drug-coated nanoparticles may exert cytosolic action either after internalization or at the plasma membrane. Detachment of the drug from its carrier can occur at the cell surface, extracellular space, or more prominently, in lysosomes by lysosomal enzymes ensuing in the release of the drug alone (without carrier molecule) into the cytosol [30]. After the completion of drug delivery, the antigens or receptors should be reprocessed back to the cell surface. Therefore, this form of targeted drug

delivery contains essential molecules such as a nano-carrier to which targeted drug can be conjugated and to which ligands-antibodies are conjugated, and enhances the high affinity to the tumor cell surface, antigens, or receptors, respectively.

### **2.3. Dual Targeting System**

The targeted drug delivery system is activated by stimuli, such as temperature, pH, redox, etc., some type of malignancies possess two stimuli around the tumor targeted environment at the same time. Alteration by reduction in extracellular pH [31] and slight rise in local temperature [32] would be more favorable for guiding drug delivery carriers that resort to two or more external stimuli concurrently. However, emerging dual or multi-stimuli approachable nanocarriers for tumor targeted therapy remains a great challenge. Nowadays, smart drug targeted delivery system are drawing our attention toward thermo- and pH-sensitive activated drug targeted delivery system. Various hyper-branched polymers that have the ability of amalgamation of dual stimuli [33, 34] have been produced, and may be reasonable applications in various malignancies. Furthermore, drug targeted delivery systems retaining sensitivity for dual stimuli have also been designed. An earlier study by Wu et al. [35] examined the release of 10-hydroxycamptothecin from dual stimuli-sensitive nanoparticles. Intestine-targeted hydrogel coated with vitamin B2 accomplished by both thermo and pH stimuli-sensitive developed by Liu [36] validated that noticeable thermo and pH sensitivity are suitable for drug targeted site-specific nanocarrier in the intestine. Furthermore, thermo-sensitive hydrogels, pH-sensitive polymers [37], enzyme-degradable, redox dual responsive micelles, and high-intensity focused ultrasound (HIFU) [38], have also been designed to sustain the release of drug targeted delivery system. Thus, precise information of the dual sensitive system was not well established, but it provides an alternative for effective targeted drug delivery in biomedical applications.

### **2.4. Inverse Targeting System**

Drug targeting attempts made to evade the passive uptake of the colloidal carrier by reticuloendothelial systems are referred to as inverse targeting. The normal function of reticuloendothelial systems is blocked by pre-injecting macromolecules such as dextran sulphate or blank colloidal carriers. This targeted methodology leads to the saturation of reticuloendothelial systems and the destruction of the defense system is used as an effective approach to delivering targeted tumor drugs to non-reticuloendothelial system organs. Colloidal-carrier systems such as vesicle, micellar solutions, and liquid crystal and nanoparticle dispersions comprising of small particles demonstrate the promise of great effects for targeted drug delivery systems. The aim is to optimize the drug coating and releasing properties and longevity of self-life of the drug with less toxic effects. The amalgamated drug with the colloidal system involved in this modulation of microstructural system may impact molecular interactions of the drug, which has mesogenic and/or amphiphilic properties [39].

### **2.5. Stimuli-Responsive/Triggered Drug Release Targeting System**

Targeted tumor drug delivery systems are requisite to be biodegradable and nontoxic to normal healthy tissue/cells and lethal and incisively dangerous to destroy the malignant cells.

However, fast discharge of the drug from the nanoparticles may lead to premature release, triggering systemic side effects; whereas, slow discharge may diminish the efficacy of the drug at the targeted site of action and may enhance the action of multiple-drug resistance (MDR). Hence, discharge of the drug for targeted systems should be in a well-organized manner at the tumor targeted site. The design of stimuli-responsive drug carriers for targeted drug delivery is highly preferred to augment the efficacy and bioavailability of the drug. Characteristic features of typical stimulus include temperature (thermal), pH, light intensity, magnetic field, redox potential (i.e., enzyme), glucose (ionic strength specific stimuli such as concentration of sugar moiety), and concentrations of electrolytes are used to localize the drug-nanocarrier to the determined targeted site. Responses of nanocarriers include precipitation/dissolution, collapsing/swelling, hydrophobic/hydrophilic transition, degradation, bond cleavage, and so on. Henceforth, we clearly state that external stimuli responding system (magnetic field, light, and ultrasound) are of lesser impact, inexpedient and practically not feasible (i.e., costs, scale-up product) than those of internal stimuli-responding systems (temperature, pH, redox potential, etc.)

### **3. Organ-based Targeted Drug Delivery**

The accumulation of the drug within a target area or tissue refers to targeted drug delivery that is independent of the method for the targeted site and direction of drug administration. A successful drug target delivery involves the following steps: appropriate proposed drug coated nanoparticles must be circulated in the blood in concentration to ensure it reaches the targeted site, the site must retain the nanoparticles, the release of the drug into the cells and allowing enough time for effective mechanism of the drug. Targeted drug delivery to specific sites in the human body requires unique delivery systems depending on the route selected.

### **4. Nanoparticles Used for Targeted Drug Delivery**

Nanoparticles referred to as drug delivery vehicles or vectors are the most significant entity necessary for the efficient delivery of the coated drug. A drug vehicle delivers and retains the therapeutic drug to be transported to the site or in the locality of the targeted tissue or area. These vehicles are capable of accomplishing specific functions that can be attributed to minor modifications in its structure. An ideal vehicle must be selectively and specifically recognized by the target site and should retain the functional specificity of the surface ligand without any modification. It should be capable of crossing the barriers, stable in interstitial fluid and plasma with non-toxic, non-immunogenic and biodegradable materials. Once the target cells recognize the carrier system, it must release the therapeutic drug moiety inside the anticipated targeted site. We further discuss the properties and application of delivery vehicles in Table 1. Targeting principles of metal, polymer, lipid, and biological-based nanoparticles used in therapeutics and promising direction in therapeutic research are discussed.

Types and Description		Properties	Application	Examples	
Polymeric nanoparticles: Solid colloidal system with drug in various forms either encapsulated, adsorbed, etc. to form nanocapsules or nanospheres		Highly biocompatible and modifiable to make nanoparticle conjugates, e.g., polymeric magnetic nanoparticles, polymersomes, polyplexes, polymer hybrid system, modifiable surface properties High encapsulation of the drug and drug protection, prolonged drug delivery, and long shelf life	Wide range of targeted organs and cells, N-2(hydroxypropyl) methacrylamide (HPMA) polymer most widely used in theranostics Polymeric micelles and water soluble polymers for improved drug delivery	Synthetic polymers such as PLGA, LPLA, PCL, and natural polymers such as Chitosan, Gelatin, Albumin, Sodium Alginate	
Dendrimers: Hyperbranched macromolecules, densely packed to the periphery till they reach a "starburst effect"		Reduce viscosity of a solution, densely packed improved rheological properties, outermost dendrimeric surface can be both polar or hydrophobic capable or dissolving in different solvents	Used as contrast agents for MRI Vectors in gene therapy, soluble dendrimers able to solubilize acidic hydrophobic molecules and of fungus and bacteria	PAMAM dendrimer, PPI dendrimer, Techo dendrimer, Micellar dendrimer	
Inorganic nanoparticles	Metallic	Gold nanoparticles (GNPs): Three shapes of GNPs are rods, shells, and spheres	These have a unique interaction with light, free electrons undergo oscillations in the presence of oscillating electromagnetic field of light	Biosensors, especially colorimetric biosensors for detection of oligonucleotides immunosensors and redox enzyme biosensing	GNPs are conjugated with Silica, PEG, Chitosan, platinum tethered, gold-SPION hybrid
		Carbon-based nanotubes: Well-ordered hollow graphitic nanomaterial either single- or multi-walled	Possibility of both covalent and non-covalent bonding Site specific delivery of proteins, peptides, nucleic acids, and other drugs	Used as an imaging agent Applications in malignancies of the brain, blood, colon, breast, liver, lymph nodes, cervical, and prostate cancer	Multi-walled carbon nanotube (MWCNT) Single-walled carbon nanotube (SWCNT)
		<b>Quantum Dots (QD):</b> Uses the	Exceptional physical features applied in optical imaging,	Unique optical features for in vitro and in vivo imaging especially	Multi-spectral fluorescent Imaging –

Types and Description		Properties	Application	Examples	
		bandgap between valency and conduction electron bands, exciton is generated due to the difference in absorption energy and the spectral bandgap of the core semi-conductor	strong absorbance, bright fluorescence	biomedical fluorescent imaging, specifically used in the study of neuron and ganglia, used in photodynamic therapy especially to treat lung and gastrointestinal cancer, accurate recognition of molecular targets	Quantum Dots (MSFI-QDs), Carbon dots, carbongenic-QDs, Silica-QD's, Zinc oxide-QDs,
Metalloid	Silica based nanoparticles: Silica particles are good materials for nanoparticles because of its porosity and surface adaptability	Modifiable in size, porosity and structure Photophysical stability: does not absorb visible or uv light, biocompatibility, favorable colloidal properties, high porosity and extended surface area, relatively chemically inert, low cost of production, easily prepared and water dispersible	Application in combined therapy as they can transfer both genetic material and molecules of various sizes. Used as an optical contrast agent, can conjugate with antibodies, aptamers and polymers	Solid silica-based nanoparticles (SiNPs), Mesoporous silica nanoparticles (MSNs)	
Magnetic	Iron oxide magnetic cores with changing shells are used	Some forms of iron oxide naturally occur in the body (maghemite, magnetite), thus reducing toxicity, various bindings, and interactions between the MNP and the drug are possible such as covalent, electrostatic, encapsulation, and adsorption	Used both in diagnosis and therapy concomitantly, Liver and spleen readily imbibe the MNP and can also be used in barin malignancies and it is able to cross the blood brain barrier	Iron oxide cores with shells of gold, polymer, dendrimers, and silane	
Biological	Lipids	Homolipids, Heterolipids, complex-lipids	Increase in drug solubility, pharmokokinetics properties, reduced toxic effects	Applications in oral drug delivery, parenteral dug delivery, peptide and	Solid lipid nanoparticles (SLN), Nanostructured

Types and Description	Properties	Application	Examples
		protein drug delivery, nasal vaccination, etc.	lipid carriers (NLC), Lipid drug conjugates (LDC), Liposome, transferosomes, niosomes

**Table 1.** Types of nanoparticles, properties and applications in medicine.

#### 4.1. Lipids-based Nanoparticles

Liposomes are small, artificially designed vesicles entirely surrounded by phospholipid bilayer membranes with various size ranges (20 to 10,000 nm) [40]. Drug molecules are encapsulated or intercalated into the phospholipid bilayers that extend the location of the drug with physico-chemical nature of lipids. Recent study demonstrates that lipid DOX loaded nanoparticles have potential effects on useful therapeutic targeted drug against adriamycin-resistant breast cancer. Entrapped drug (chemical compounds) molecules inside the modified liposomes (transferring [41] or antibody [42, 43]) cause apoptosis of tumor cells [41–43]. Solid lipid nanocarriers can be commonly used for the treatment of chemotherapy resistant tumor [44] to deliver the targeted drug.

Self-assembled, hydrophobic interactions of amphiphilic block copolymers (5–50 nm) form supramolecular core-shell structures in aqueous solutions called micelles are gaining great attention in targeted drug delivery applications. Pluronic, phospholipid, polyester, and poly (L-amino acid) are the most often used micelles. Drug entrapped with block copolymer micelles and transported at high concentrations can exceed their intrinsic water-solubility. Furthermore, hydrophilic blocks form hydrogen bonds within the aqueous solution and form a compact shell that covers the micellar core protecting it against hydrolysis and enzymatic degradation with the help of hydrophobic core. Moreover, the reticuloendothelial system may prevent the recognition of the corona and eliminate the polymeric micelles from the blood circulation. The molecular weight, chemical composition, and block length ratios can be easily changed that control the size and morphology of the micelles. The cross linkable group with block copolymer can enhance the stability of the micelles and increase their temporal control. Polymeric micelles can be linked with various ligands, such as epidermal growth factors, antibody fragments,  $\alpha$ -2-glycoprotein, folic acid, and transferrin, delivering the targeted anticancer drug to the tumor tissues/cells by passive and active mechanisms. Most of the anticancer drugs are poorly water soluble in nature, polymeric micelles deliver these anti-cancer drugs to the targeted tumor sites that selectively act only on targeted cells and do not affect the normal healthy cells. However, most of the polymeric micelles have been successfully established in targeted therapeutics and some are still at preclinical trials. Future studies need to pave the way for these therapies into clinical practice to increase the survival rate of cancer patients and enhance anticipation of cancer chemotherapy [45].

Niosomes are defined as nonionic surfactant vesicles that entrap both lipophilic and hydrophilic drugs in the vesicular membrane/aqueous phase. These are made up of lipid material possessing better stability than liposomes. Niosomes may be established as useful carriers for targeting the drugs to treat tumor, viral, parasitic, and other microbial diseases more effectively. Pharmacosomes are self-assembling components consisting of a pharmocon (active component) and a carrier molecule composed of amphiphilic drugs. Drugs covalently linked to lipid molecules may be in colloidal dispersion as micelles or as ultrafine hexagonal aggregates used in targeted therapy. Ufasomes are single-chain fatty acid surfactant vesicles formed from double-chain amphiphiles and micelles. They are composed of lipid bilayer liposomes made of single-chain unsaturated fatty acids used in targeted drug delivery. Ufasome vesicles are colloidal suspensions of closed lipid bilayers consisting of ionized species (soap) and fatty acid molecules composed of more amphiphiles than micelles. These readily available fatty acids give ufasomes an advantage over liposomes. Cubosomes refer to liquid crystalline liposomes formed into cubic nanoparticles that are suitable for injection at the targeted site. Lipid droplets that allow easy penetration through the pores are called transferosomes, which are smaller than a droplet. Transferosomes is a supramolecular entity that can pass via permeability barriers and transport drug from one side to the other and is more elastic than a liposome.

#### **4.2. Biological-based Nanoparticles**

In addition to micelles, some groups of nanoparticles forming self-assembling structure are known as cell-penetrating peptides (CPPs). These molecules are applied in recognizing hydrophobic drugs and delivering biomolecules such as nucleic acids (siRNA, pDNA) intracellularly to the targeted cells. Furthermore, CPP drug delivery system is more constructive owing to its low toxicity, biocompatibility, structural stability, and easy preparation [46–49]. Addition to hydrophobic interaction, CPPs improve the nucleic acid delivery system. Both hydrophobic interactions and the electrostatic nature of CPPs contribute to its stable structure that can easily enter into the cells and deliver the siRNA.

Proteins are also important and promising agents for drug delivery that bioconjugate with drugs and deliver to the targeted sites (albumin-conjugated with paclitaxel named as abraxane). Albumin and paclitaxel linkage (abraxane) are prepared by homogenization under high pressure [50]. However abraxane is a more effective and less cytotoxic drug compared to conventional drugs. The drug is released from abraxane through the albumin receptor in blood vessels of the tumor cells [50, 51]. Bioconjugation of albumin-paclitaxel combination has been effectively used against lung cancer [50], breast cancer, [51] and gastric cancer [52].

#### **4.3. Polymeric-based Nanoparticles**

Polymers have good biocompatibility, are easily prepared, and morphologically manipulated into a variety of designs and structures. They possess bio-mimetic properties making it a widely used biomaterial. Polymers play an important role in smart drug delivery systems as they can effectively deliver chemotherapeutic drugs directly into the targeted site. The surface of polymeric nanoparticles has been functionalized by the alteration of nanoparticles through emulsification, adsorption, polymerization, functional surfactants, modulation of various

forms of bio-conjugation, and covalently-bound functional molecules. Polymers are widely used in numerous therapeutic applications for targeting cancer, disorders of the central nervous system (CNS), and other bacterial and viral infections. Zhang et al. [53] reported that more than 26 nanoparticles based on their therapeutic action have been approved for clinical trials and a few more are in the pipeline. Polymeric nanoparticles possess characteristic properties that affect its bio-distribution, efficiently enhancing the delivery of targeted drug across the blood brain barrier compared to conventional drug treatments as well as other well-known drug carriers [54].

Microspheres are biocompatible polymers either particle or soluble in nature. Polymeric backbone carriers are *N*-(2-Hydroxypropyl) methacrylamide (HPMA) prepared by ficoll, dextrans, sepharose, or poly-L-lysine as core carrier system for chemotherapeutic drugs. Microspheres (30–200  $\mu\text{m}$ ) are larger than nanoparticles (0.2–0.5  $\mu\text{m}$ ) but have a smaller area for drug loading than soluble polymers. The drug incorporation of microsphere considerably affects its release rate. Once the drug is administered or systematically transported, it rapidly dispenses into the target site and is subsequently internalized by macrophages of the phagocytic system. Moreover, microspheres and nanoparticles are mostly used for cell-selective applications of drug delivery (oral delivery peptides and peptidomimetics) [55–58].

Dendrimers play a significant role in the delivery of different compounds such as tamsulosin, primaquine phosphate, 5-fluorouracil, doxorubicin, tropicamide, indomethacin, artemether, and pilocarpine as targeted drugs [59]. Bioconjugated dendrimers can deliver the targeted drug transdermally, intravenously, orally, and through the ophthalmic route, which proves the versatility and functionality of dendrimers [60].

#### 4.4. Carbon-based Nanoparticles

The properties [61], application [62–68], and solubility nature [69] of carbon nanotubes are well-established nanocarriers for drug delivery. Jain et al. [70] reported that chemical modification of carbon nanotubes by carbohydrate D-galactose can generate a novel cascade of chemical functionalization of multi-walled carbon nanotubes (MWCNTs). Therefore, galactosylated MWCNTs are used to deliver the active ligands (such as galactose) as a bioactive(s) targeted drug to the tumor site (hepatic tissues) [70].

Carbon nanohorns related to carbon nanotubes belong to a new class of carbon materials. Single-walled carbon nanohorn (SWNH) aggregates consist of thousands of graphitic tubules (2–5 nm in diameter, similar structure to single-walled CNTs) having a spherical structure (50–100 nm in diameter). Based on the morphological features, nanohorns are divided into bud, dahlia, and seed types. SWNHs are non-metallic catalysts produced by laser ablation of a pure graphite target; however, its toxicity must be proactively investigated. Molecules completely composed of carbon are fullerene, spherical fullerenes are known as buckyballs. Fullerenes are similar to graphite structure consisting of stacked graphene sheets of connected hexagonal rings and pentagonal rings. Fullerene C60 is highly biocompatible with reduced toxicity and is used for targeted drug delivery for several diseases such as Parkinson's and HIV.

Nanoshells have a dielectric core covered with a thin metallic shell of gold-coated silica that is spherical in shape. These are used for early stages of cancer detection and treatment. Injected embedded drugs consist of cancer-targeted hydrogel polymers that are released at the tumor targeted site when exposed to laser (infrared).

#### **4.5. Metal-based Nanoparticles**

Metal-based nanoparticles are fascinating because the metal exhibits an important electronic and optical property and acts as an insulator or semiconductor [71–73]. Transition (Al, Co, Cu, Fe, Ni, Ti) and noble (Au and Ag) metal nanoparticles reveal a luminescence emission in the visible wavelength of light. Recent studies show metal linked with carbon nanotubes (Ag/CNT composites) are gaining increased attention due to their potential applications as optical limiters [74], catalyst [75], and advanced materials [76] capable of being used in bio-imaging of the cancer cells for targeted therapy [74].

Targeted drug delivery with gold nanoparticles possess a unique chemical and physical characteristic feature as they have strong binding interaction with proteins, thiols [77], aptamers [78], carboxylic acid [79], and disulfides linkages. These are widely used in tumor targeted delivery system for therapeutics. Gold particles can enter into targeted sites by phagocytosis, fluidphase endocytosis, and receptor-mediated endocytosis [80], depending upon the shape, size, surface charge, synthesis process, functionalized molecules, and surface coating toxicity of gold. Moreover, gold nanoparticles are considered to be non-toxic agents for drug delivery [81]. Gold nanoparticles possess a functional flexibility with prodrug molecules by covalent or non-covalent linkage enhancing the efficient transport of the drug into the targeted tumor sites. Gold nanoparticles can hold high drug concentration and deliver it to the specific targeted site via various routes of drug administration. Conventional drug side effects can be reduced by conjugated gold nanoparticles reducing the tumor survival rate.

## **5. Therapeutic Strategies for Drug Delivery**

### **5.1. Folate Targeting**

Folate receptors (FRs) are overexpressed in various tumors (including leukemia, endometrial, ovarian, and kidney cancer), which binds vitamin folate and folate-drug conjugates with a high affinity [82]. Folate receptors are targets of various therapeutic strategies aimed at efficient delivery of chemotherapeutic drugs. Folate receptors also play a role in the uptake of antifolate drugs that are used for therapeutic intervention in malignant disorders. The salient features of folic acid for therapeutic strategies are: i) reasonable binding affinity to both diagnostic and targeted therapeutic agents; ii) its unique and high affinity for the folate receptor, even after binding to diagnostic and therapeutic cargo; and iii) the folate receptor in normal healthy tissues have limited scattering, despite its overexpression on both type of tumors cells (FR- $\alpha$  and FR- $\beta$  isoforms) [83]. Earlier investigations [84] show that folate enter the cells through receptor-mediated endocytic process. Hence, folic acid is repeatedly used as a drug targeting

ligand coated with delivery vehicles (polymeric nanoparticles, liposomes, dendrimers, and protein toxins) to selectively deliver targeted drugs into malignant cells.

We were the first to report that curcumin enhances the up-regulation of folate receptor  $\beta$  mRNA and protein levels in KG-1 cells by modulating the uptake and cytotoxicity of methotrexate. Notably, curcumin also augmented folate receptor  $\beta$  function as a transporter for radiolabeled folic acid and methotrexate in KG-1 cells. These reports optimized curcumin dosage and reduced the concentration of methotrexate resulting in the effective destruction of tumor cells. Therefore, amalgamation of non-toxic concentrations of methotrexate and curcumin may be a viable strategy for therapeutic intervention for leukemia using a folate receptor-targeted drug delivery system [85]. Shen et al. [86] reported that folate receptor-targeted drug conjugate had less communication with the cells and easily entered through overexpressed folate receptor of malignant cells by receptor-mediated endocytosis. Later the drug was transferred into lysosomes, wherein the active form of drug poly (amido amine)] dendrimers (PAMAM) was regenerated. The PAMAM left the lysosome and released anti-cancer drug camptothecin (CPT) in the nucleus. This modulation creates PAMAM dendrimers as valuable drug carriers for in vivo tumor cell nuclear drug targeted delivery. Folate receptor-targeted (nanoparticles) delivery systems, despite showing significant promising effects in human pathologies, enhance the tumor selectivity for tumor targeting. This modulatory strategy avoids possible obstacles, and we anticipate that folic acid will act as an essential candidate for receptor-targeted therapeutics in the near future.

## 5.2. Antibodies Targeting

Specific antigens are exclusively expressed on the surface of the cancer cells. Antibodies, especially monoclonal antibodies (mAb), can be produced to identify and specially bind to the antigens associated with tumor cells. In 1981, Milstein [87] developed an mAb that binds to malignant cells, a few functional classes of antibodies that possessed more binding and destroying activity in the tumor cells. Currently, numerous mAb-based tumor tissues targeting therapeutics has been effectively translated into clinical treatment such as trastuzumab, rituximab, cetuximab, and bevacizumab [88-91]. These mAb could be used as fragments or in their native state, generally having higher affinity toward tumor-associated antigens depicting its targeting efficacy. Moreover, the whole mAb are more beneficial than fragments to develop a higher binding affinity, owing to a synergic effect of having more than one binding site. Furthermore, the full or entire antibody sequences express more EPR effects that are maintained in cancer tissues, while in small fragments express less EPR effects that can easily be eliminated from blood circulation [92].

Recent investigations have attention on multi-functionalization of the nanoparticle surface with specific mAbs and encapsulation of therapeutic drugs into nanoparticles to sustain its targeting efficacy. Recent studies by Nobs et al. [93] shows poly-(lactic acid) (PLA) nanoparticles conjugated rituximab and trastuzumab exhibit six-fold enhances affinity and uptake compared with similar particles without mAb targeting molecules. The investigation of Miyano et al. [94] shows conjugated KG6Etrastuzumab (KG6E-amino acid dendrimer with surface modified by sixth-generation lysine dendrimer with glutamate -KG6Etrastuzumab)

was expressively internalized and then transferred to lysosome for human epidermal growth factor receptor -2 (HER-2) positive cells (SKBR3), compared to HER2 – negative cells (MCF-7) indicates that KG6E-trastuzumab conjugates act as HER-2 targeting carriers in drug targeted delivery for cancer therapy. However, nanoparticles conjugated with mAbs still encounter numerous tasks and boundaries, owing to a “binding-site barrier” (decreased rate of penetration of nanocarriers due to high binding affinity) in solid tumors [95].

### 5.3. Glycoprotein Targeting

Serum glycoprotein transferrin (Tf) acts as a transporter to deliver the iron molecule into the cells via blood by binding to the transferrin receptor successfully that is being internalized through receptor-mediated endocytosis [96]. TfR is overexpressed on most of the tumor cells such as colon, pancreatic, lung, and bladder cancer cells due to increased metabolic rates. The TfR expression is 100 times greater in cancerous cells than normal healthy cells, this increase in expression is a result of a higher demand for iron in tumor cells, essential for their survival [97]. Tf has been often used as a drug targeting ligand in TfR-targeted drug delivery system for tumor cells. Direct conjugations of nanocarriers to Tf have enhanced intracellular drug delivery and efficient therapeutic outcome. Ishida et al. [98] demonstrated Tf conjugated with polyethyleneglycol (PEG)-liposomes exposed over prolonged periods in blood circulation but had reduced uptake via reticuloendothelial system (RES) in colon cancer. This proposes that Tf-conjugated nanoparticles were internalized by receptor-mediated endocytosis owing to specific ligand-receptor binding for cytoplasmic targeting to cancer cells. Tf-conjugated paclitaxel coated with poly (lactic-co-glycolic acid) (PLGA) nanoparticles showed enhanced suppression in cell growth than free paclitaxel in MCF-7 and MCF-7/Adr cells [99]. Doxorubicin (Dox)-coated, HAIYPRH (T7)-conjugated, PEG-modified polyamidoamine dendrimer (PAMAM-PEG-T7/Dox) nanoparticles was fabricated by Jiang et al. [100]. This modified targeted drug effectively accumulates in malignant cells via intravenous administration and can be internalized into cancer cells with Tf. These studies proved that Tf acts as a ligand for targeted drug delivery system in TfR overexpressed malignancies. However, TfR is also expressed in normal fast growing healthy cells (epithelial, fibroblast, and endothelial cells) that could lead to non-specific targeting and increase the cytotoxic effects reducing the efficacy of the targeted drug [101]. Furthermore, Tf with nanoparticles targeting ligands may improve drug delivery in tumor tissues and distribution in blood circulation similar to normal healthy cells expressing TfR (non-targeted systems) [102].

### 5.4. Oligonucleotide Targeting

Short, single-stranded RNA or DNA oligonucleotides designed in vitro from a huge number of random sequences around 10<sup>14</sup>–10<sup>15</sup> that can identify the specific target sites are known as aptamers [103]. Aptamers possess high affinity and specificity features enhanced to bind a wide range of intracellular molecules, such as receptors, small molecule drugs, and proteins [104] specified for aptamer-based targeted cancer therapy. Although, aptamers and mAbs have similar and specific affinity against selected molecules, aptamers possess their own unique features: they can be synthesized in vitro without laboratory animals [105] and nanoparticle-

conjugated aptamers very efficiently target the tumor tissue via active targeting pathway. Lupold et al. [106] established nanoparticle-conjugated aptamer (A10 aptamer) that target overexpressed transmembrane protein of prostate specific membrane antigen (PSMA) in various tumor tissues. Aptamers-doxorubicin (Apt-Dox) are conjugates that are also implemented (designed) for targeted delivery to malignant cells [107]. Furthermore, Huang et al. [107] demonstrated that Dox conjugated to DNA aptamer-sgc8c (sgc8c-Dox conjugate) retains its high binding affinity features increasing efficiency of internalization by tumor targeted cells. These characteristic features make targeted delivery of chemotherapeutic drugs more feasible with abundant targeting potencies. Furthermore, these therapeutic strategies give rise to a novel targeted drug delivery and provide promising approaches for future treatment.

### 5.5. Membrane Protein Targeting/Cell Surface Receptors Targeting

Integrin membrane glycoproteins are heterodimeric in nature composed of non-covalent bonding of  $\alpha$  and  $\beta$  subunits; they play a major role in tumor malignancy and angiogenesis [107]. In tumor endothelium  $\alpha_v\beta_3$  and  $\alpha_v\beta_5$ , integrins are overexpressed at the highest levels. Asparagine/glycine/arginine (NGR) and arginine/glycine/aspartic acid (RGD) are the largest number of tumor-homing peptides used to detect the corresponding receptors of integrins  $\alpha_v\beta_3$  on tumor endothelial cells. Brooks et al. [109] reported that RGD vascular homing peptides enhanced intracellular targeted drug delivery accomplished via integrin-binding RGD and suppress the tumor growth. Recent studies described Dox-coated nanoparticles with cyclic RGD peptide ligand delivered the drug to targeted integrin  $\alpha_v\beta_3$  and caused a decrease in survival rate of the tumor cells [110]. Moreover, investigations on paclitaxel entrapped liposomes with peptide consisting of specific ligand to alpha  $\nu$  integrins and specific motif to neuropilin-1 showed significant increase in paclitaxel uptake in targeted tumor cells (A549 and HUVEC) depicting the enhanced suppression of cell growth by dual targeted mechanism compared with single-targeted paclitaxel entrapped liposomes and paclitaxel injections (Taxol) alone [111]. Furthermore, investigations show that cyclic RGD peptide (cRGDyK) conjugated in PEG-b-PLGA micelles deliver the targeted hydrophobic drug into intracellular cancer cells and its neovasculature, enhancing the antiproliferative and cytotoxicity efficacy compared with cRGDyK-free non-targeted micelles [112]. However, targeted delivery to integrin glycoprotein meets many challenging tasks for therapeutic strategies. The most common are integrins receptors, which are extracellular and expressed in normal fast growing healthy epithelial cells other than tumor cells. Treatment with RGD also targets the normal functional integrin ( $\alpha_5\beta_1$  and  $\alpha_4\beta_1$ ) molecules, thus resulting in targets of nonspecific tumor cells [113].

## 6. Significant Role and Functional Properties of Targeted Drug Delivery

The application purpose of nanoparticles in nanomedicine is targeted drug delivery system [114]. In the past two decades, scientists have developed and understood the mechanism of drug delivery and drugs have been designed for targeted delivery s [3]. Most of the new and currently available therapeutic drugs (95%) have poor biopharmaceuticals and pharmacoki-

netics properties [40]. Therapeutic index of efficiently biological targeted drugs must be improved by suitable nanotechnological application for targeted delivery in tumor cells/tissues. Nanotechnological approaches [114] enhance reconsideration of failed clinical trials of chemotherapeutic drugs.

The targeted drug should be safe and effective with sufficient drug concentration in the body to deliver an effective dosage at the targeted tumor site. Chemotherapeutic targeted drugs must possess high toxicity and strong inhibition toward the targeted tumor tissue/cells proliferation. Many researchers have demonstrated that biological toxins, protein macromolecules, hydrophobic, and hydrophilic drugs are delivered through nanocarriers. Nanostructured designs are promising components that enable novel chemotherapeutic drugs for targeted delivery and explain the principles of component-targeted drug delivery systems (Figure 1). Nanomedicine has continuously released drug delivery mechanisms that enter into the cell by intracellular mechanisms and reduces its side effects. Nanoparticles have greater advantage than microparticles. They are appropriate for intravenous targeted delivery, tremendously exploited for well-controlled targeted drug release at site-specific targeting, have prolonged the time of blood circulation facilitating extravasation of drug delivery, and have favorable outcomes in site-specific drug targeting for treating cancer as well as disorders of the CNS and immunodeficiency infection [115]. Moreover, 300 pharmaceutical companies in the United States (US) mainly focus on targeted drug delivery systems. Additionally, drugs can be administrated through oral, pulmonary, ocular, transmucosal, and implantation routes of delivery.

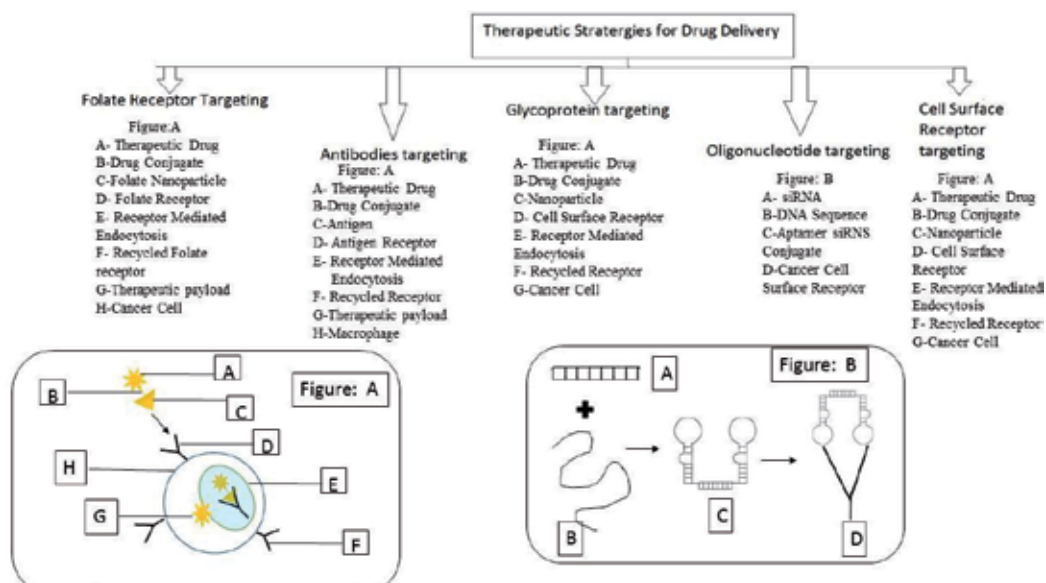


**Figure 1.** Schematic representation of components of targeted drug delivery

Nanomaterials are used in targeted drug delivery including metal-, biological-, lipid-, silicon-, carbon-, and polymer-based materials [114]. These technology-based medicines (nanomedicine platforms) can be multifunctional, also known as intelligent/smart drug system. We raise awareness of the physiological and functional challenges of therapeutic application and enlighten recent advances in our understanding and mechanism of tumor biology [116]. Nanoscale drug targeted delivery system is capable of enhancing pharmacokinetics and increasing the bio-distribution of therapeutic agents to targeted organs/tissues/cells with improved efficacy of the drug. The volume of drug distribution and toxicity is reduced, owing to drug accumulation at specific targeted sites and reduced concentration in normal healthy cells while using nanoscale carriers. It is designed to target cancer and inflammation sites through permeable vasculature. It is also biocompatible and made of biodegradable materials reported as safe replacement drug carriers than existing vehicles that may cause allergic reaction and peripheral neuropathy [40]. Few drugs have a very short half-life in blood circulation. The efficacy and stability of the drug can be increased by enclosing a drug with a nanocarrier to extend its short-half life. For example, a drug can be enclosed with a nanosized carrier (liposome).

Most of the drugs face difficulties in targeting tumor sites while crossing the blood brain barrier (BBB). Nanoparticle-coated drugs potentially penetrate BBB and are shown to potentially enhance the therapeutic concentration and index of anticancer drugs that have been delivered to the brain tumor. Its most noteworthy advantage is reduced toxicity and enhanced efficacy of the drug by guiding the drug to its target and retaining the drug concentration at the targeted site for a longer duration to increase its therapeutic action. [114]. Figure 2 explains the desirable therapeutic strategies of smart drug targeted delivery systems. Solid tumors possess vascular pores (vascular pore cut-off 380–780 nm) depending on various sizes, type of cancer, micro-environments, and proliferation rate. Thus, drug with the carrier molecules should be smaller than vascular pore cut-off size (diameter) to reach its targeted tumor sites. Normal healthy blood vessels do not permit drug-associated carrier molecules larger than 2–4 nm size compared with unassociated drug molecules. Thus, nanomedicine has paved the way to enhance drug accumulation and its concentration in targeted cells/tissues/sites by extravasation and considerably diminishing its toxicity and distribution to normal healthy cells [40]. Ideal nanocarrier materials should be without any chemical modification and must fulfill the demands of biocompatibility, biodegradability, and release dynamics of targeted drugs [117, 118].

Nanocarriers essentially need to prolong exposure time in blood circulation and allow the nanocarriers to reach the targeted site through multiple pathways. Generally, nanoparticles possess a very short half-life, owing to natural immune/defense mechanisms of the human system that eradicate them after opsonisation by phagocytic mechanisms. Thus, the nanocarrier surface must be altered to be invisible to the opsonisation process.

Nanocarriers are naturally made up of macromolecular materials or entrapped lipids, adsorbed onto the surface of the nanoparticles or dissolved within the polymeric matrix. They are categorized into two types: nanospheres (matrix systems used to dispersing drug molecules) and nanocapsules (vesicular systems drugs that are surrounded by a membrane). Nanotechnology-based polymers are designed as top-down and bottom-up processes. The top-down method is initiated by breaking down larger objects into nanostructured molecules

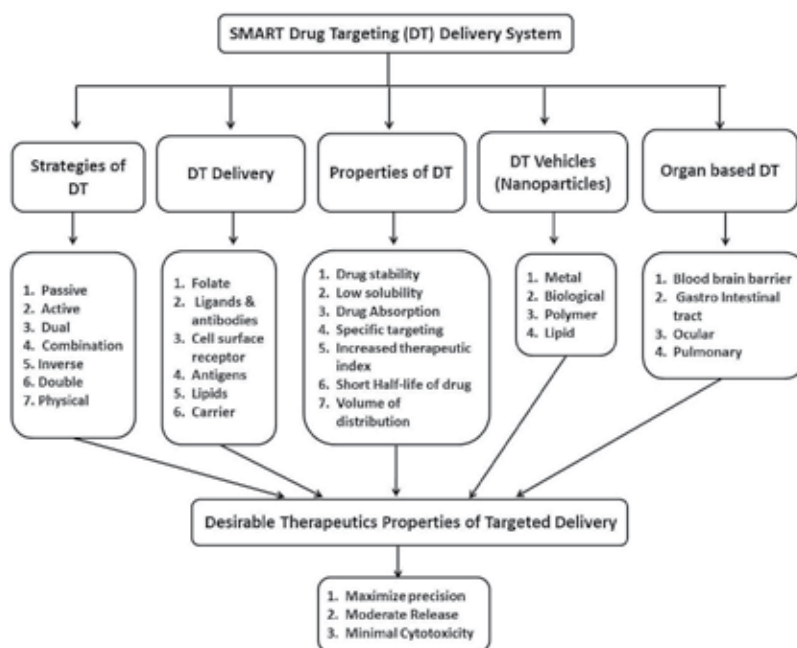


**Figure 2.** Schematic representation of SMART drug targeted strategies

by over grinding, etching, or ball milling enhanced by laser or the addition of chemicals. However, this technique is time-consuming and repeatedly produces considerably wider particle size of distribution. This type of production is based on atom-by-atom or molecule-by-molecule arrangements in a well-programmed manner, organized chemical reaction by both liquid or gas phase, ensuring in nucleation and growth of nanoparticles. The bottom-up process generates heavily clustered masses of particles that do not break up on reconstitution [119]. Particles prepared by complex coacervation, salting-out, solvent emulsification diffusion, high-pressure homogenization, nanoprecipitation, supercritical fluid, co-precipitation, rapid expansion of supercritical solutions, supercritical antisolvent precipitation, and self-assembly methods [119]. The nanoparticles used as carriers are polymeric nanoparticles, magnetic nanoparticles, metal and inorganic nanoparticles, quantum dots, polymeric micelles (PMs), solid lipid nanoparticles, and colloidal nanoliposomes.

## 7. Targeted Drug Delivery in Anticancer Therapy

A clear understanding of molecular mechanism of tumor proliferation, formation metastasis, invasion, and angiogenesis ensures a new mechanistic basis for targeted tumor drug discovery (targeted anticancer therapy). Exact blocking or altering of the molecular mechanism associated in the pathogenesis of tumor cell proliferation by targeted chemotherapeutic agents modify the natural process of the disease as well as improve therapeutic index with cytotoxic agents. Anticancer drug for targeted delivery system must meet a few requirements: a) the

targeted drug must have minimal activity loss, b) it should destroy the targeted tumor cells, c) must be well-regulated and predicate the active form of drug release [120], and d) leakage of drug during transit must be minimal. Concurrently, therapeutic drugs with less dosage should be used during targeted therapy (minimal dose than the normal chemotherapy) with minimal side effects [120, 121]. Drugs are conjugated with nanocarriers and delivered to the receptor (outside) or inside the targeted tumor cells by a selective targeting mechanism [121]. The previous traditional process of administration of chemotherapy is an aggregation of drugs inside the tumor cells/tissues through EPR [122, 123, 117] as a result of the abnormal structure of blood vessels closer to the tumor tissues. Thus, the drug discharges easily to the tissues near the cancer cells [40, 123]. Furthermore, few drugs are used in conventional treatment such as methotrexate [124], paclitaxel [125], doxorubicin [126], gemcitabine [127] hexamethylmelamine [128], and cisplatin (DDP) or carboplatin (drugs based on platinum) [129]. The drug may be delivered to: a) the capillary bed of the active site, b) specific type of cells, c) intracellular region of tumour cells absent in normal healthy cells, and d) specific organ/tissues by complexation with the nanocarrier that recognizes the target. Conventional anticancer targeted therapy is composed of ligands (receptor, antibodies, and chemotherapeutic drugs) conjugated with nanocarriers, thus, the fabricated drug enables binding affinity with particular receptors of the targeted cancer cells. Overexpression of receptors in cancer cells enhances the binding affinity of the nanocarrier conjugated ligands to the receptor [121, 123, 117]. The targeted delivery system discharges the chemotherapeutic drugs directly to tumor cells and maintains prolonged circulation of the drugs with high concentration inside the tumor cells. However, targeted drugs cannot be released back to the blood stream because of the ligand and receptor binding affinity, the same principle that is used in immunogenicity [122].

## 8. Challenges and Future Directions

Smart drug targeted delivery system is approaching optimal therapeutic strategies for malignant and other chronic diseases. Targeted drug delivery is a rather complex mechanism that has many aspects that are far-fetched; however, it is an approach that has been successfully used to treat cancer and other chronic diseases. An ideal delivery system of targeted drug molecules to its specific tissue/cells/organs is still beyond our reach in many ways and still poses a challenging task in the complex cellular network system of organisms. An ideal drug targeted delivery system is the one that delivers the drug to the exact targeted tumor site in the right dosage required [130]. The reality, however, is far away from the ideal scenario of bench-to-bedside treatment. The dosage levels of drugs delivered to targets sites is much less than 5% at most.

Our efforts must be motivated toward improving moderate drug dosages delivered to the target sites. As chronic diseases and tumors may not be eradicated by just targeting one site, it may also be necessary to concurrently aim at multiple targets. Consequently, it may be worthwhile to develop a new technology or a “magic shotgun” strategy that distributes the multiple drugs into multiple targets to achieve optimal therapy [130]. It will be a challenging task to modify our current approaches on targeted drug delivery systems through such alterations that will influence not only the strategies selected but also the approaches to identify, modify, and test the success of these methodologies.

Furthermore, clear validation for identifying new approaches and modifications, do not basically lead to an improved outcomes without theatrical changes in our current protocols on targeted drug delivery research to make significant improvements in the future. Advanced nanomedicine technology-based drug delivery to the target sites will be limited by extravasation and blood circulation. However, selective ligand targets a tumor cell marker or receptor through receptor-ligand binding that occurs only after delivery by extravasation and blood circulation. The receptor-ligand communication will be problematic for tumors as cells “over-express” targeted surface markers. The selective targeted surface marker will also be expressed on the surface of the non-cancer cells due to the gross surplus of the cancer cell burden.

Relatively, over-dependence on nanoparticles alone will be inadequate for significant clinical benefits. Improvement of targeted drug delivery systems will need better understanding of various factors involved in the regulation of distribution in the blood, temporal heterogeneity, tumor markers, energetic aspects of tumor spatial, and complexities of diffusional barriers in solid tumors. In addition, we may not depend on a sole over-expressed tumor marker for specific drug targeting therapeutic managements. Modern drug targeted delivery and its methodologies are scientifically sound rationale with limited success mainly due to the construction of nanomaterials and drugs according to biochemical and engineering principles alone. The currently available nanoparticles can improve the blood circulation time and pave the way into malignant cells by potentially modulating their ability to intermingle with tumor cell receptors. These promising nanoparticles ensure problems such as the forceful modulation of the malignant cells and cancer heterogeneity.

For malignant and other therapies, the ideal smart drug targeted delivery system delivers the drug at a targeted tumor site. In the future, efforts must focus on exploring the delivery of increased concentration of the drug to the targeted site. Malignant cells may not be eliminated by just targeting one site, it may also be important to aim at multiple targets. Furthermore, in the future, merging expertise in drug targeted delivery with technological improvements in molecular medicine will pave the way to elucidate molecular and cellular mechanism underlying diseases. New approaches under investigation should focus on "bench-to-bedside" practices to reduce delay of therapeutic stages.

## Author details

Sugapriya Dhanasekaran<sup>1\*</sup> and Sumitra Chopra<sup>2</sup>

\*Address all correspondence to: [sughaphd@gmail.com](mailto:sughaphd@gmail.com)

1 Department of Medical Laboratory Sciences (Hematology), College of Applied Medical Sciences, Prince Sattam Bin Abdulaziz University, Wadi-Ad Dawaser Campus, Riyadh Province, Kingdom of Saudi Arabia

2 Department of Medical Laboratory Sciences (Genetics), College of Applied Medical Sciences, Prince Sattam Bin Abdulaziz University, Wadi-Ad Dawaser Campus, Riyadh Province, Kingdom of Saudi Arabia

## References

- [1] Muller RH, Keck CM. Challenges and solutions for the delivery of biotech drugs—a review of drug nanocrystal technology and lipid nanoparticles. *Journal of Biotechnology*. 2004; 113(1–3):151–170.
- [2] Mark SW, Torchilin, Vladimir P. Drug delivery systems. Access Science, McGraw-Hill Companies, 2011.
- [3] Vyas SP, Khar RK. Basis of targeted drug delivery. In Targeted and controlled Drug Delivery, CBS Publishers and Distributors Reprint, 2008: 42–46, 74.
- [4] Won R. Method for delivering an active ingredient by controlled time release utilizing a novel delivery vehicle which can be prepared by a process utilizing the active ingredient as a porogen, Patent No 4690825 US: 1987.
- [5] Mastrobattista E, Koning GA, Storm G. Immunoliposomes for the targeted delivery of antitumor drugs. *Advance Drug Delivery Reviews*. 1999;10:40(1-2):103–127.
- [6] Maeda H, Matsumura Y. Tumoritropic and lymphotropic principles of macromolecular drugs. *Crit Rev Ther Drug Carrier Syst*. 1989;6:193–210.
- [7] Gref R1, Minamitake Y, Peracchia MT, Trubetskoy V, Torchilin V, Langer R. Biodegradable long-circulating polymeric nanospheres. *Science*. 1994;263(5153):1600–1603.
- [8] Mansour AM, Dreves J, Esser N, et al. A new approach for the treatment of malignant melanoma: Enhanced antitumor efficacy of an albumin binding doxorubicin prodrug that is cleaved by matrix metalloproteinase 2. *Cancer Res*. 2003;63:4062–6.
- [9] Guo X, Szoka FC, Jr. Chemical approaches to triggerable lipid vesicles for drug and gene delivery. *Acc Chem Res*. 2003;36:335–41.
- [10] Yockman JW, Maheshwari A, Han SO, Kim SW. Tumor regression by repeated intratumoral delivery of water soluble lipopolymers/p2CMVmIL-12 complexes. *J Control Release*, 2003;87:177–86.
- [11] Nomura T, Saikawa A, Morita S, et al. Pharmacokinetic characteristics and therapeutic effects of mitomycin C-dextran conjugates after intratumoural injection. *J Control Release*. 1998;52:239–52.
- [12] Barker DD, Berk AJ. Adenovirus proteins from both E1B reading frames are required for transformation of rodent cells by viral infection and DNA transfection. *Virology*. 1987;156:107–21.
- [13] Khuri FR, Nemunaitis J, Ganly I, et al. A controlled trial of intratumoral ONYX-015, a selectively-replicating adenovirus, in combination with cisplatin and 5-fluorouracil in patients with recurrent head and neck cancer. *Nat Med*. 2000;6:879–85.

- [14] Hecht JR, Bedford R, Abbruzzese JL, et al. A phase I/II trial of intratumoral endoscopic ultrasound injection of ONYX-015 with intravenous gemcitabine in unresectable pancreatic carcinoma. *Clin Cancer Res.* 2003;9:555–61.
- [15] Reid T, Galanis E, Abbruzzese J, et al. Hepatic arterial infusion of a replication-selective oncolytic adenovirus (dl1520): Phase II viral, immunologic, and clinical endpoints. *Cancer Res.* 2002;62:6070–9.
- [16] Vasey PA, Shulman LN, Campos S, et al. Phase I trial of intraperitoneal injection of the E1B-55-kd-gene-deleted adenovirus ONYX-015 (dl1520) given on days 1 through 5 every 3 weeks in patients with recurrent/refractory epithelial ovarian cancer. *J Clin Oncol.* 2002;20:1562–9.
- [17] Galanis E, Okuno SH, Nascimento AG, et al. Phase I-II trial of ONYX-015 in combination with MAP chemotherapy in patients with advanced sarcomas. *Gene Ther.* 2005;12:437–45.
- [18] Lamprecht A, Yamamoto H, Takeuchi H, Kawashima Y. Nanoparticles enhance therapeutic efficiency by selectively increased local drug dose in experimental colitis in rats. *J Pharmacol Exp Ther.* 2005;315:196–202.
- [19] Beduneau A, Saulnier P, Hindre F, Clavreul A, Leroux JC, Benoit JP. Design of targeted lipid nanocapsules by conjugation of whole antibodies and antibody Fab' fragments. *Biomaterials.* 2007;28:4978–4990.
- [20] Deckert PM. Current constructs and targets in clinical development for antibody-based cancer therapy. *Current Drug Targets.* 2009;10:158–175.
- [21] Hong M, Zhu S, Jiang Y, Tang G, Pei Y. Efficient tumor targeting of hydroxycamptothecin loaded PEGylated niosomes modified with transferrin. *J Control Release.* 2009;133:96–102.
- [22] Zensi A, Begley D, Pontikis C, Legros C, Mihoreanu L, Wagner S, Büchel C, Briesen Hv, Kreuter J. Albumin nanoparticles targeted with ApoE enter the CNS by transcytosis and are delivered to neurons. *J Control Release.* 2009;137:78–86.
- [23] Canal F, Vicent MJ, Pasut G, Schiavon O. Relevance of folic acid/polymer ratio in targeted PEGepirubicin conjugates. *J Control Release.* 2010;146:388–399.
- [24] Pirollo KF, Chang EH. Does a targeting ligand influence nanoparticle tumor localization or uptake? *Trends Biotechnol.* 2008;26:552–558.
- [25] Kirpotin DB, Drummond DC, Shao Y, Shalaby MR, Hong K, Nielsen UB, Marks JD, Benz CC, Park JW. Antibody targeting of long-circulating lipidic nanoparticles does not increase tumor localization but does increase internalization in animal models. *Cancer Res.* 2006;66:6732–6740.
- [26] Mikhail AS, Allen C. Block copolymer micelles for delivery of cancer therapy: transport at the whole body, tissue and cellular levels. *J Control Release.* 2009;138:214–223.

- [27] Raz A, Meromsky L, Lotan R. Differential expression of endogenous lectins on the surface of nontumorigenic, tumorigenic, and metastatic cells. *Cancer Res.* 1986;46:3667–72.
- [28] Gorelik E, Galili U, Raz A. On the role of cell surface carbohydrates and their binding proteins (lectins) in tumor metastasis. *Cancer Metastasis Rev.* 2001;20:245–77.
- [29] Yamazaki N, Kojima S, Bovin NV, et al. Endogenous lectins as targets for drug delivery. *Adv Drug Deliv Rev.* 2000;43:225–44. 24.
- [30] Olsnes S, Sandvig K. How protein toxins enter and kill cells. *Cancer Treat Res.* 1988;37:39–73.
- [31] Stefanadis C, Chrysochoou C, Markou D, Petraki K, Panagiotakos DB, Fasoulakis C, Kyriakidis A, Papadimitriou C, Toutouzas PK. Increased temperature of malignant urinary bladder tumors in vivo: The application of a new method based on a catheter technique. *J. Clin. Oncol.* 2001;19(3):676–681.
- [32] Gerweck LE, Seetharaman K. Cellular pH gradient in tumor versus normal tissue: Potential exploitation for the treatment of cancer. *Cancer Res.* 1996;56(6):1194–1198.
- [33] Gao M, Jia XR, Li Y, Liang DH, Wei Y. Synthesis and thermo-/pH- dual-responsive properties of poly (amidoamine) dendronized poly (2-hydroxyethyl) Methacrylate. *Macromolecules.* 2010;43:4314–4323.
- [34] Pang Y, Zhu Q, Zhou DL, Liu JY, Chen Y, Su Y, Yan DY, Zhu XY, Zhu BS. Synthesis of backbone thermo and pH dual-responsive hyperbranched poly (amine-ether)s through proton-transfer polymerization. *J. Polym. Sci. Part A: Polym. Chem.* 2011;49:966–975.
- [35] Li F, Wu H, Fan L, Zhang HT, Zhang H, Gu CH. Study of dual responsive poly[(mal-eilated dextran)-graft-(Nisopropylacrylamide)] hydrogel nanoparticles: Preparation, characterization and biological evaluation. *Polym. Int.* 2009;58:1023–1033.
- [36] Ma LW, Liu MZ, Liu HL, Chen J, Gao CM, Cui DP. Dual crosslinked pH- and temperature-sensitive hydrogel beads for intestine-targeted controlled release. *Polym. Adv. Technol.* 2010;21:348–355.
- [37] Kim IS, Oh IJ. Drug release from the enzyme-degradable and pH-sensitive hydrogel composed of glycidyl methacrylate dextran and poly (acrylic acid). *Arch. Pharm. Res.* 2005;28(8):983–987.
- [38] Li YW, Tong R, Xia HS, Zhang HJ, Xuan J. High intensity focused ultrasound and redox dual responsive polymer micelles. *Chem. Commun.* 2010;46:7739–7741.
- [39] Deol P, Khuller GK. Lung specific stealth liposomes: Stability, biodistribution and toxicity of liposomal antitubercular drugs in mice. *Biochimica Biophys Acta.* 1997;1334:161–72.

- [40] Koo OM, Rubinstein I, Onyuksel H. Role of nanotechnology in targeted drug delivery and imaging: A concise review. *Nanomedicine*. 2005 Sep;1(3):193–212.
- [41] Koren E, Apte A, Jani A, Torchilin VP. Multifunctional PEGylated 2C5-immunoliposomes containing pH-sensitive bonds and TAT peptide for enhanced tumor cell internalization and cytotoxicity. *J Control Release*. 2012 Jun 10;160(2):264–73. doi: 10.1016/j.jconrel.2011.12.002. Epub 2011 Dec 13.
- [42] Koshkaryev A, Piroyan A, Torchilin VP. Increased apoptosis in cancer cells in vitro and in vivo by ceramides in transferrin-modified liposomes. *Cancer Biol Ther*. 2012 Jan 1;13(1):50–60. doi: 10.4161/cbt.13.1.18871.
- [43] Etzerodt A, Maniecki MB, Graversen JH, Møller HJ, Torchilin VP, Moestrup SK. Efficient intracellular drug-targeting of macrophages using stealth liposomes directed to the hemoglobin scavenger receptor CD163. *J Control Release*. 2012 May 30;160(1):72–80. doi: 10.1016/j.jconrel.2012.01.034. Epub 2012 Jan 27.
- [44] Kang KW, Chun MK, Kim O, Subedi RK, Ahn SG, Yoon JH, Choi HK. Doxorubicin-loaded solid lipid nanoparticles to overcome multidrug resistance in cancer therapy. *Nanomedicine*. 2010 Apr;6(2):210–3. doi: 10.1016/j.nano.2009.12.006. Epub 2010 Jan 6.
- [45] Kedar U, Phutane P, Shidhaye S, Kadam V. Advances in polymeric micelles for drug delivery and tumor targeting. *Nanomedicine*. 2010 Dec;6(6):714–29. doi: 10.1016/j.nano.2010.05.005. Epub 2010 Jun 11.
- [46] Arukuusk P, Pärnaste L, Oskolkov N, Copolovici DM, Margus H, Padari K, Möll K, Maslovskaja J, Tegova R, Kivi G, Tover A, Pooga M, Ustav M, Langel U. New generation of efficient peptide-based vectors, NickFects, for the delivery of nucleic acids. *Biochim Biophys Acta*. 2013 May;1828(5):1365–73. doi: 10.1016/j.bbmem.2013.01.011. Epub 2013 Jan 26.
- [47] Wu Y, Sadatmousavi P, Wang R, Lu S, Yuan YF, Chen P. Self-assembling peptide-based nanoparticles enhance anticancer effect of ellipticine in vitro and in vivo. *Int J Nanomedicine*. 2012;7:3221–33. doi: 10.2147/IJN.S31858. Epub 2012 Jun 28.
- [48] Crombez L, Morris MC, Deshayes S, Heitz F, Divita G. Peptide-based nanoparticle for ex vivo and in vivo drug delivery. *Curr Pharm Des*. 2008;14(34):3656–65.
- [49] Nasrolahi Shirazi A, Tiwari R, Chhikara BS, Mandal D, Parang K. Design and biological evaluation of cell-penetrating peptide-doxorubicin conjugates as prodrugs. *Mol Pharm*. 2013 Feb 4;10(2):488–99. doi: 10.1021/mp3004034. Epub 2013 Jan 15.
- [50] Yuan DM, Lv YL, Yao YW, Miao XH, Wang Q, Xiao XW, Song Y. Efficacy and safety of Abraxane in treatment of progressive and recurrent non-small cell lung cancer patients: A retrospective clinical study. *Thoracic Cancer*. 2012;3(4):341–347.
- [51] Yan Z, Xia L, Qiu H, Chen P, Zhang B. Short-term outcomes of albumin-bound paclitaxel (abraxane)-containing chemotherapy in patients with advanced gastric cancer:

- A report of 14 cases. *The Chinese-German Journal of Clinical Oncology*. 2013;12(1):30-34.
- [52] Paik PK, James LP, Riely GJ, Azzoli CG, Miller VA, Ng KK, Sima CS, Heelan RT, Kris MG, Moore E, Rizvi NA. A phase 2 study of weekly albumin-bound paclitaxel (Abraxane®) given as a two-hour infusion. *Cancer Chemother Pharmacol*. 2011 Nov; 68(5):1331-7. doi: 10.1007/s00280-011-1621-0. Epub 2011 Apr 3.
- [53] Zhang H, Chen C, Hou L, Jin N, Shi J, Wang Z, Liu Y, Feng Q, Zhang Z. Targeting and hyperthermia of doxorubicin by the delivery of single-walled carbon nanotubes to EC-109 cells. *Journal of Drug Targeting*. 2013;21(3):312-319.
- [54] Mody N, Tekade RK, Mehra NK, Chopdey P, Jain NK. Dendrimer, liposomes, carbon nanotubes and PLGA nanoparticles: one platform assessment of drug delivery potential. *AAPS PharmSciTech*. 2014 Apr;15(2):388-99. doi: 10.1208/s12249-014-0073-3. Epub 2014 Jan 16.
- [55] Farah RA, Clinchy B, Herrera L, Vitetta ES. The development of monoclonal antibodies for the therapy of cancer. *Crit Rev Eukaryot Gene Expr*. 1998;8(3-4):321-56.
- [56] Kim GJ, Nie S. Targeted cancer nanotherapy. *Materials Today*. August 2005;8(8):28-33. ISSN: 1369-7021, [http://dx.doi.org/10.1016/S1369-7021\(05\)71034-8](http://dx.doi.org/10.1016/S1369-7021(05)71034-8).
- [57] Köhler G, Milstein C. Continuous cultures of fused cells secreting antibody of predefined specificity. *Nature*. 1975 Aug 7;256(5517):495-7.
- [58] Storm G, Daan J, Crommelin A. Liposomes: quo vadis? *Pharmaceutical Science & Technology Today*. 1 April 1998;1(1):19-31. ISSN: 1461-5347, [http://dx.doi.org/10.1016/S1461-5347\(98\)00007-8](http://dx.doi.org/10.1016/S1461-5347(98)00007-8).
- [59] Gupta U, Agashe HB, Asthana A, Jain NK. Dendrimers: Novel polymeric nanoarchitectures for solubility enhancement. *Biomacromolecules*. 2006 Mar;7(3):649-58.
- [60] 42. Wen S, Liu H, Cai H, Shen M, Shi X. Targeted and pH-responsive delivery of doxorubicin to cancer cells using multifunctional dendrimer-modified multi-walled carbon nanotubes. *Adv Healthc Mater*. 2013 Sep;2(9):1267-76. doi: 10.1002/adhm.201200389. Epub 2013 Feb 28.
- [61] Foldvari M, Bagonluri M. Carbon nanotubes as functional excipients for nanomedicines: II. Drug delivery and biocompatibility issues. *Nanomedicine*. 2008 Sep;4(3):183-200. doi: 10.1016/j.nano.2008.04.003. Epub 2008 Jun 11.
- [62] Liu Z, Chen K, Davis C, Sherlock S, Cao Q, Chen X, Dai H. Drug delivery with carbon nanotubes for in vivo cancer treatment. *Cancer Res*. 2008 Aug 15;68(16):6652-60. doi: 10.1158/0008-5472.CAN-08-1468.
- [63] Liu Z, Fan AC, Rakhra K, Sherlock S, Goodwin A, Chen X, Yang Q, Felsher DW, Dai H. Supramolecular stacking of doxorubicin on carbon nanotubes for in vivo cancer therapy. *Angew Chem Int Ed Engl*. 2009;48(41):7668-72. doi: 10.1002/anie.200902612.

- [64] Wong Shi Kam N, Dai H. Single-walled carbon nanotubes for transport and delivery of biological cargos. 2006.
- [65] Kam NW, O'Connell M, Wisdom JA, Dai H. Carbon nanotubes as multifunctional biological transporters and near-infrared agents for selective cancer cell destruction. *Proc Natl Acad Sci U S A*. 2005 Aug 16;102(33):11600–5. Epub 2005 Aug 8.
- [66] Shi Kam NW, Jessop TC, Wender PA, Dai H. Nanotube molecular transporters: Internalization of carbon nanotube-protein conjugates into Mammalian cells. *J Am Chem Soc*. 2004 Jun 9;126(22):6850–1.
- [67] Liu Z, Tabakman S, Welsher K, Dai H. Carbon nanotubes in biology and medicine: In vitro and in vivo detection, imaging and drug delivery. *Nano Res*. 2009 Feb 1;2(2):85–120.
- [68] Liu Z, Tabakman SM, Chen Z, Dai H. Preparation of carbon nanotube bioconjugates for biomedical applications. *Nat Protoc*. 2009;4(9):1372–82. doi: 10.1038/nprot.2009.146. Epub 2009 Sep 3.
- [69] Firme CP 3rd, Bandaru PR. Toxicity issues in the application of carbon nanotubes to biological systems. *Nanomedicine*. 2010 Apr;6(2):245–56. doi: 10.1016/j.nano.2009.07.003. Epub 2009 Aug 20.
- [70] Jain AK, Dubey V, Mehra NK, Lodhi N, Nahar M, Mishra DK, Jain NK. Carbohydrate-conjugated multiwalled carbon nanotubes: development and characterization. *Nanomedicine*. 2009 Dec;5(4):432–42. doi: 10.1016/j.nano.2009.03.001. Epub 2009 Mar 31.
- [71] Sandler J, Shaffer MSP, Prasse T, Bauhofer W, Schulte K, Windle A. Development of a dispersion process for carbon nanotubes in an epoxy matrix and the resulting electrical properties. *Polymer*. 1999;40(21):5967–5971. [http://dx.doi.org/10.1016/S0032-3861\(99\)00166-4](http://dx.doi.org/10.1016/S0032-3861(99)00166-4).
- [72] Silva LBD, Fagan SB, Mota R. Ab initio study of deformed carbon nanotube sensors for carbon monoxide molecules. *Nano Letters*. 2004;4(1):65–67. <http://dx.doi.org/10.1021/nl034873d>.
- [73] Guldi DM, Rahman GMA, Prato M, Jux NJ, Qin S, Ford W. Single-wall carbon nanotubes as integrative building blocks for solar energy conversion. *General & Introductory Chemistry*. 2005;44(13):2015-2018. <http://dx.doi.org/10.1002/anie.200462416>.
- [74] Chin KC, Gohel A, Chen WZ, Elim HI, Ji W, Chong GL, Sow CH, Wee ATS. Gold- and silver-coated carbon nanotubes: An improved broad-band optical limiter. *Chemical Physics Letters*. 2005;409(1-3):85–88. <http://dx.doi.org/10.1016/j.cplett.2005.04.092>.
- [75] Guo DJ, Li HL. *Carbon*. 2005;43:1259.
- [76] Wu HP, Wu XJ, Ge MY, Zhang GQ, Wang YW, Jiang J. Properties investigation on isotropical conductive adhesives filled with silver coated carbon nanotubes. *Compo*

- sites Science and Technology. 2007;67(6):1182–1186. <http://dx.doi.org/10.1016/j.compscitech.2006.05.010>.
- [77] Lee K, Lee H, Bae KH, Park TG. Heparin immobilized gold nanoparticles for targeted detection and apoptotic death of metastatic cancer cells. *Biomater*. 2010;31:6530–6536.
- [78] Tarnawski R, Ulbricht M. Amphiphilic gold nanoparticles: Synthesis, characterization and adsorption to PEGylated polymer surfaces. *Colloid Surfac A: Physicochem Engineer Aspects*. 2011;374:13–21.
- [79] Deb S, Patra HK, Lahiri P, Dasgupta AK, Chakrabarti K, Chaudhuri U. Multistability in platelets and their response to gold nanoparticles. *Nanomed: Nanotechnol Biol Med*. 2011;7376–384.
- [80] . Nalawade P, Mukherjee T, Kapoor S. High-yield synthesis of multispiked gold nanoparticles: Characterization and catalytic reactions. *Colloid Surfac A: Physicochem Engineer Aspects*. 2012;396:336–340.
- [81] Benkovicova M, Vegso K, Siffalovic P, Jergel M, Luby S, Majkova E. Preparation of gold nanoparticles for plasmonic applications. *Thin Solid Films*. 2013;543:138–141.
- [82] Leamon CP, Reddy JA. Folate-targeted chemotherapy. *Adv Drug Deliv Rev*. 2004 Apr 29;56(8):1127–41.
- [83] Low PS, Henne WA, Doorneweerd DD. Discovery and development of folic-acid-based receptor targeting for imaging and therapy of cancer and inflammatory diseases. *Acc Chem Res*. 2008 Jan;41(1):120–9. Epub 2007 Jul 27.
- [84] Kamen BA, Capdevila A. Receptor-mediated folate accumulation is regulated by the cellular folate content. *Proc Natl Acad Sci U S A*. 1986 Aug;83(16):5983–7.
- [85] Sugapriya D, Biswal BK, Sumantran VN, Verma RS. Augmented sensitivity to methotrexate by curcumin induced overexpression of folate receptor in KG-1 Cells. *Biochimie*. 2013;95:1567–1573.
- [86] Shen Y, Zhou Z, Sui M, Tang J, Xu P, Van Kirk EA, Murdoch WJ, Fan M, Radosz M. Charge-reversal polyamidoamine dendrimer for cascade nuclear drug delivery. *Nanomedicine (Lond)*. 2010 Oct;5(8):1205–17. doi: 10.2217/nmm.10.86.
- [87] Warenus HM, Galfre G, Bleehen NM, Milstein C. Attempted targeting of a monoclonal antibody in a human tumour xenograft system. *Eur J Cancer Clin Oncol*. 1981 Sep;17(9):1009–15.
- [88] James JS, Dubs G. FDA approves new kind of lymphoma treatment. *Food and Drug Administration. AIDS Treat News*. 1997 Dec 5;(284):2–3.
- [89] 160. Albanell J, Baselga J. Trastuzumab, a humanized anti-HER2 monoclonal antibody, for the treatment of breast cancer. *Drugs Today (Barc)*. 1999 Dec;35(12):931–46.
- [90] De Roock W, Piessevaux H, De Schutter J, Janssens M, De Hertogh G, Personeni N, Biesmans B, Van Laethem JL, Peeters M, Humblet Y, Van Cutsem E, Tejpar S. KRAS

- wild-type state predicts survival and is associated to early radiological response in metastatic colorectal cancer treated with cetuximab. *Ann Oncol.* 2008 Mar;19(3):508–15.
- [91] Ferrara N. VEGF as a therapeutic target in cancer. *Oncology.* 2005;69 Suppl 3:11–6. Epub 2005 Nov 21.
- [92] Matsumura Y, Kataoka K. Preclinical and clinical studies of anticancer agent-incorporating polymer micelles. *Cancer Sci.* 2009 Apr;100(4):572–9.
- [93] Nobs L, Buchegger F, Gurny R, Allemann E. Biodegradable nanoparticles for direct or two-step tumor immunotargeting. *Bioconjug Chem.* 2006 Jan-Feb;17(1):139–45.
- [94] Miyano T, Wijagkanalan W, Kawakami S, Yamashita F, Hashida M. Anionic amino acid dendrimer-trastuzumab conjugates for specific internalization in HER2-positive cancer cells. *Mol Pharm.* 2010 Aug 2;7(4):1318–27. doi: 10.1021/mp100105c.
- [95] Adams GP, Schier R, McCall AM, Simmons HH, Horak EM, Alpaugh RK, Marks JD, Weiner LM. High affinity restricts the localization and tumor penetration of single-chain fv antibody molecules. *Cancer Res.* 2001 Jun 15;61(12):4750–5.
- [96] Qian ZM, Tang PL. Mechanisms of iron uptake by mammalian cells. *Biochim. Biophys. Acta.* 1995;1269:205–214.
- [97] Prost AC, Menegaux F, Langlois P, Vidal JM, Koulibaly M, Jost JL, Duron JJ, Chigot JP, Vayre P, Aurengo A, Legrand JC, Rosselin G, Gespach C. Differential transferrin receptor density in human colorectal cancer: A potential probe for diagnosis and therapy. *Int. J. Oncol.* 1998;13(4):871–875.
- [98] Ishida O, Maruyama K, Tanahashi H, Iwatsuru M, Sasaki K, Eriguchi M, Yanagie H. Liposomes bearing polyethyleneglycol-coupled transferrin with intracellular targeting property to the solid tumors in vivo. *Pharm Res.* 2001 Jul;18(7):1042–8.
- [99] Sahoo SK, Labhasetwar V. Enhanced antiproliferative activity of transferrin-conjugated paclitaxel-loaded nanoparticles is mediated via sustained intracellular drug retention. *Mol Pharm.* 2005 Sep–Oct;2(5):373–83.
- [100] Han L, Huang R, Liu S, Huang S, Jiang C. Peptide-conjugated PAMAM for targeted doxorubicin delivery to transferrin receptor overexpressed tumors. *Mol Pharm.* 2010 Dec 6;7(6):2156–65. doi: 10.1021/mp100185f. Epub 2010 Oct 14.
- [101] Ekblom P, Thesleff I, Lehto VP, Virtanen I. Distribution of the transferrin receptor in normal human fibroblasts and fibrosarcoma cells. *Int J Cancer.* 1983 Jan 15;31(1):111–7.
- [102] Bartlett DW, Su H, Hildebrandt IJ, Weber WA, Davis ME. Impact of tumor-specific targeting on the biodistribution and efficacy of siRNA nanoparticles measured by multimodality in vivo imaging. *Proc Natl Acad Sci U S A.* 2007 Sep 25;104(39):15549–54. Epub 2007 Sep 17.

- [103] Joyce GF. Amplification, mutation and selection of catalytic RNA. *Gene*. 1989 Oct 15;82(1):83–7.
- [104] Jayasena SD. Aptamers: An emerging class of molecules that rival antibodies in diagnostics. *Clin Chem*. 1999 Sep;45(9):1628–50.
- [105] Michel F, Ellington AD, Couture S, Szostak JW. Phylogenetic and genetic evidence for base-triples in the catalytic domain of group I introns. *Nature*. 1990 Oct 11;347(6293):578–80.
- [106] Lupold SE, Hicke BJ, Lin Y, Coffey DS. Identification and characterization of nuclease-stabilized RNA molecules that bind human prostate cancer cells via the prostate-specific membrane antigen. *Cancer Res*. 2002 Jul 15;62(14):4029–33. Erratum in: *Cancer Res*. 2012 Aug 1;72(15):3887.
- [107] Bagalkot V, Farokhzad OC, Langer R, Jon S. An aptamer-doxorubicin physical conjugate as a novel targeted drug-delivery platform. *Angew Chem Int Ed Engl*. 2006 Dec 11;45(48):8149–52.
- [108] Brooks PC, Montgomery AM, Rosenfeld M, Reisfeld RA, Hu T, Klier G, Cheresh DA. Integrin alpha v beta 3 antagonists promote tumor regression by inducing apoptosis of angiogenic blood vessels. *Cell*. 1994 Dec 30;79(7):1157–64.
- [109] Erdreich-Epstein A, Shimada H, Groshen S, Liu M, Metelitsa LS, Kim KS, Stins MF, Seeger RC, Durden DL. Integrins alpha(v)beta3 and alpha(v)beta5 are expressed by endothelium of high-risk neuroblastoma and their inhibition is associated with increased endogenous ceramide. *Cancer Res*. 2000 Feb 1;60(3):712–21.
- [110] Yu MK, Park J, Jeong YY, Moon WK, Jon S. Integrin-targeting thermally cross-linked superparamagnetic iron oxide nanoparticles for combined cancer imaging and drug delivery. *Nanotechnology*. 2010 Oct 15;21(41):415102. doi: 10.1088/0957-4484/21/41/415102. Epub 2010 Sep 17.
- [111] Meng S, Su B, Li W, Ding Y, Tang L, Zhou W, Song Y, Li H, Zhou C. Enhanced anti-tumor effect of novel dual-targeted paclitaxel liposomes. *Nanotechnology*. 2010 Oct 15;21(41):415103. doi: 10.1088/0957-4484/21/41/415103. Epub 2010 Sep 17.
- [112] Yin J, Li Z, Yang T, Wang J, Zhang X, Zhang Q. Cyclic RGDyK conjugation facilitates intracellular drug delivery of polymeric micelles to integrin-overexpressing tumor cells and neovasculature. *J Drug Target*. 2011 Jan;19(1):25–36. doi: 10.3109/10611861003663531. Epub 2010 Mar 16.
- [113] Bibby DC, Talmadge JE, Dalal MK, Kurz SG, Chytil KM, Barry SE, Shand DG, Steiert M. Pharmacokinetics and biodistribution of RGD-targeted doxorubicin-loaded nanoparticles in tumor-bearing mice. *Int J Pharm*. 2005 Apr 11;293(1–2):281–90.
- [114] Cirillo G, Hampel S, Spizzirri UG, Parisi OI, Picci N, Iemma F. Carbon nanotubes hybrid hydrogels in drug delivery: A perspective review. *Biomed Res Int*. 2014;2014:825017. doi: 10.1155/2014/825017. Epub 2014 Jan 21.

- [115] Sahoo SK, Parveen S, Panda JJ. The present and future of nanotechnology in human health care. *Nanomedicine*. 2007 Mar;3(1):20–31.
- [116] Kim KY. Nanotechnology platforms and physiological challenges for cancertherapeutics. *Nanomedicine*. 2007 Jun;3(2):103–10. Epub 2007 Apr 17.
- [117] Parveen S, Misra R, Sahoo SK. Nanoparticles: A boon to drug delivery, therapeutics, diagnostics and imaging. *Nanomedicine*. 2012 Feb;8(2):147–66. doi:10.1016/j.nano.2011.05.016. Epub 2011 Jun 7.
- [118] Chouhan R, Bajpai AK. Release dynamics of ciprofloxacin from swellable nanocarriers of poly(2-hydroxyethyl methacrylate): An in vitro study. *Nanomedicine*. 2010 Jun;6(3):453–62. doi: 10.1016/j.nano.2009.11.006. Epub 2010 Jan 4.
- [119] Mishra B, Patel BB, Tiwari S. Colloidal nanocarriers: A review on formulation technology, types and applications toward targeted drug delivery. *Nanomedicine*. 2010 Feb;6(1):9–24. doi: 10.1016/j.nano.2009.04.008. Epub 2009 May 15.
- [120] Bertrand N, Wu J, Xu X, Kamaly N, Farokhzad OC. Cancer nanotechnology: The impact of passive and active targeting in the era of modern cancer biology. *Adv Drug Deliv Rev*. 2014 Feb;66:2–25. doi: 10.1016/j.addr.2013.11.009. Epub 2013 Nov 22.
- [121] Liu Y, Miyoshi H, Nakamura M. Nanomedicine for drug delivery and imaging: A promising avenue for cancer therapy and diagnosis using targeted functional nanoparticles. *Int J Cancer*. 2007 Jun 15;120(12):2527–37.
- [122] Mehra NK, Mishra V, Jain NK. A review of ligand tethered surface engineered carbon nanotubes. *Biomaterials*. 2014 Jan;35(4):1267–83. doi: 10.1016/j.biomaterials.2013.10.032. Epub 2013 Nov 7.
- [123] Torchilin VP. Multifunctional nanocarriers. *Adv Drug Deliv Rev*. 2006 Dec 1;58(14):1532–55. Epub 2006 Sep 28.
- [124] Minotti G, Menna P, Salvatorelli E, Cairo G, Gianni L. Anthracyclines: Molecular advances and pharmacologic developments in antitumor activity and cardiotoxicity. *Pharmacol Rev*. 2004 Jun;56(2):185–229.
- [125] Verweij J, Clavel M, Chevalier B. Paclitaxel (Taxol) and docetaxel (Taxotere): Not simply two of a kind. *Ann Oncol*. 1994 Jul;5(6):495–505.
- [126] Samorì C, Ali-Boucetta H, Sainz R, Guo C, Toma FM, Fabbro C, da Ros T, Prato M, Kostarelos K, Bianco A. Enhanced anticancer activity of multi-walled carbon nanotube-methotrexate conjugates using cleavable linkers. *Chem Commun (Camb)*. 2010 Mar 7;46(9):1494–6. doi: 10.1039/b923560d. Epub 2009 Dec 23.
- [127] Ren Y, Pastorin G. Incorporation of hexamethylmelamine inside capped carbon nanotubes. *Advanced Materials*. 2008;20(11):2031–2036.
- [128] Aryal S, Hu CM, Zhang L. Combinatorial drug conjugation enables nanoparticle dual-drug delivery. *Small*. 2010 Jul 5;6(13):1442–8. doi: 10.1002/smll.201000631.

- [129] Oberoi HS, Nukolova NV, Kabanov AV, Bronich TK. Nanocarriers for delivery of platinum anticancer drugs. *Adv Drug Deliv Rev.* 2013 Nov;65(13–14):1667–85. doi: 10.1016/j.addr.2013.09.014. Epub 2013 Oct 8.
- [130] Agnihotri J, Saraf S, Khale A. Targeting: New potential carriers for targeted drug delivery system. *International Journal of Pharmaceutical Sciences Review and Research.* 2011;8(2):117–123.

---

# Smart Drug Delivery Strategies Based on Porous Nanostructure Materials

---

Qun Wang, Jianying Huang and Yuekun Lai

Additional information is available at the end of the chapter

<http://dx.doi.org/10.5772/61939>

---

## Abstract

The control of drug delivery can have a great effect on its efficacy. An optimum concentration range of drugs can play a significant role in the human body, and it can cause harm to humans when it exceeds the range of the drug concentration. Recently, a variety of drug deliveries and their targeted systems have been studied to minimize drug loss and maximize the amount of drug accumulated in the required area, thus increasing drug bioavailability. In addition, we should especially consider the prevention of its harmful side-effects in the human body. Innovative drug delivery systems based on biodegradable, natural or synthetic polymers, micro- or nano-particles, lipoproteins, micelles, TiO<sub>2</sub> nanotube arrays (TNTs), nanoporous anodic aluminum oxide (AAO), and so on were developed, which combined magnetic targeting and stimulus-responsive in drug delivery systems. The composition of delivery carriers and the stimulus-responsive elements proved stimulus-responsive drug release as a smart drug delivery system.

**Keywords:** Drug delivery system, carriers, stimulus-responsive, TiO<sub>2</sub>

---

## 1. Introduction

In recent years, nanomaterials and nanotechnology have been applied in the medical field such as in disease diagnosis and therapy. Research about drug delivery and targeting systems based on nanomaterials is carried out in nanomedicine to establish systems of drug delivery [1]. Based on the systems, it is easy to find disease tissues and implement the therapy in the required location.

Drug carriers included micro- or nano-particles made of biodegradable, natural or synthetic polymers, microcapsules, lipoproteins, micelles, TNTs, nanoporous aluminum oxide, and so on. Due to its controlled size, morphology and release, and excellent biocompatibility,

---

biodegradable organic/inorganic micro/nano-particles have been studied extensively [2–5]. In fact, stimuli-responsive systems could facilitate drug release to reach a target environment. Stimuli-responsive elements have a functionality that sustains an energetic change in response to pH, temperature, magnetism, sound, and light [6–18].

Preparing particles from stimulus-responsive polymers can respond to certain pH value and temperature and so on to controllably release. The pH-responsive polymer was studied as a delivery system for therapeutic drugs [19–20] and was verified to prolong drug release circulation in vivo. Due to their special magnetic and optical properties, magnetic nanoparticles have played a great potential in drug release [21] and it has been used in disease diagnosis and therapy. Therefore, targeting drug delivery systems was built with the help of magnetic targeting. In addition, micellar solutions, vesicle and liquid crystal dispersions show great potentials as well as nanoparticle dispersions [22–23]. The drug delivery systems based on colloidal drug carriers can realize the target by obtaining systems of drug loading and release, low toxicity, and so on.

Recent progress in controlling drug release from nanotube and nanopore materials include TNT arrays, anodic aluminum oxide nanoporous, and so on [24–26]. TNT arrays have been applied in drug releases of therapies based on drug delivery because of its excellent properties, and it has been confirmed that TNT arrays change localized drug delivery therapies thoroughly. Furthermore, the method of preparing TNT arrays breaks a new nano-engineering path to propose the limitations of drug administration systems. Nanoporous materials with ordered pore structures were studied to avoid limitations of conventional drug therapies, especially for implantable drug delivery systems. In addition, porous AAOs are able to imitate dimensions of the natural bone and AAO films can be seen as promising coatings for the medical industry. Therefore, AAO has been used for new nano-platform for drug releases.

## **2. Energetic transitions of materials for drug delivery**

As is known to us, it is necessary that the chemical functionalities exhibit stimuli-responsive behavior. In some cases, the triggering stimuli are in the proximity of the internal physiological environment of the drug delivery system [27]. It is also imagined that multiple stimuli-responsive systems operating in tandem assemble into a drug delivery system [28]. For example, a temperature change in a thermo-responsive system may be induced by a magnetic system.

### **2.1. pH-sensitive drug delivery**

Polymer materials own structures with ionizable functionalities that become ionized at a specific pH where they acquire a positive or negative charge [29]. The transition of the functional group from one of water insolubility to one of water solubility under the effect of the ionization is called polyelectrolytes because of the presence of electrostatic charges in the water-soluble polymer structure.

There is a significant difference in the behavior of polymeric-charged functionalities and their uncharged counterparts in terms of their intermolecular effects on the surrounding environment and intramolecular effects within their own polymer molecules. The two types of interaction can be segregated into a polyelectrolyte and a solvent [29], and those between a polyelectrolyte and a surface [30]. In terms of the interaction between a polyelectrolyte and a solvent, there is a transition of the Gibbs free energy of mixing shifts from negative ( $-\Delta G$ ) in solubility to positive ( $+\Delta G$ ), where it is insoluble because the transition from an intermolecular hydrogen-bonded species to an intramolecular hydrogen-bonded species causes poor entropy of mixing [31]. The function is easily seen in the change in the secondary structure of polypeptides or proteins where there is a transition from an  $\alpha$ -helical to a random coil secondary structure as a result of deprotonation or protonation, as is shown in Fig. 1 [32].

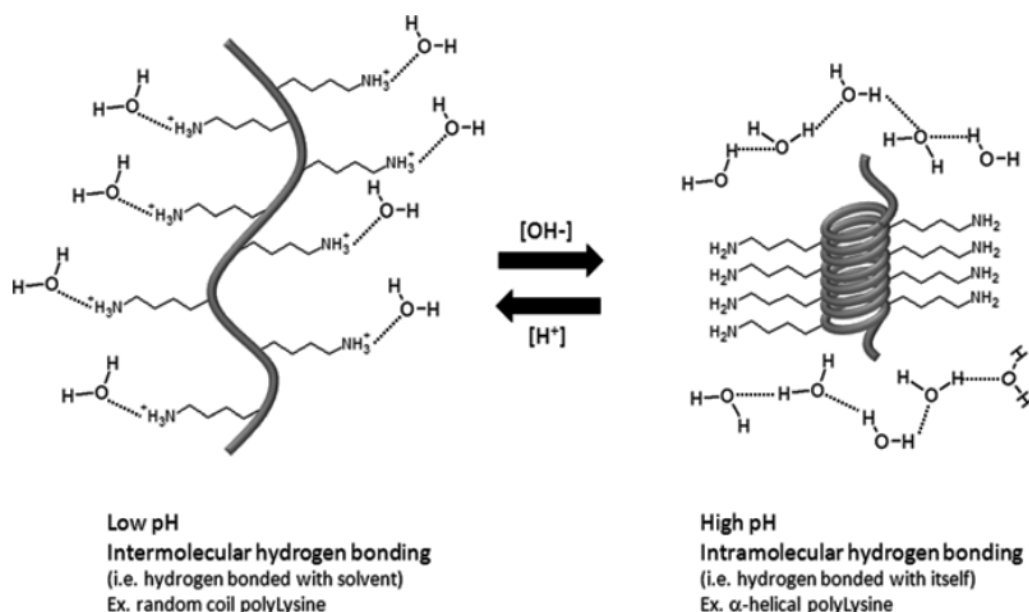


**Figure 1.** Diagram of the intramolecular versus intermolecular hydrogen bonding through the protonation–deprotonation of the pendant groups on the polymer chain [32].

In addition, several characteristic interactions between the polyelectrolyte and the surface can be seen. If a surface owns an oppositely charged energy, the polyelectrolyte is proposed to interact in a number of different ways. If there is a long-range of electrostatic interaction, it is possible that the rearrangement of the polyelectrolyte chain expresses charged functionalities at the surface [33]. This rearrangement would change based on the pH, the charge density, the composition and distribution of charges along the polymer chain and the ionic strength of the solvent and so on. For the purposes of our discussion in this section, we focus on the pH and ionic strength.

We know that the introduction of salt will screen the electrostatic forces between the polyelectrolyte and the surface, as well as reduce both the intermolecular and intramolecular electrostatic repulsions. There is also a non-electrostatic affinity under certain conditions in the case of interactions between polyelectrolytes and charged surfaces [34]. Any increase in the ionic strength under the presence of salts would decrease the electrostatic affinity of the polyelectrolyte to the charged surface when the adsorption of polyelectrolyte on a charged surface is driven by only electrostatic forces, and the adsorption increases to an upper limit when the non-electrostatic affinity is high enough.

The responsiveness of a molecule to pH presents an interesting target for stimulated drug delivery. As we know, when an encapsulated drug species is internalized by a cell, it will enter the lysosome at some point within the process. The lysosome cell has a pH of 4.5–5.0 [35], which is exclusively different from other intracellular vesicle species. Therefore, a collapse or dissociation of the self-assembled species is triggered by pH and will result in the release of the encapsulant.

We know the role of the hydrophobic domain in the self-assembly of micellar systems is to minimize the interfacial free energy between incompatible phases. The hydrophobicity could be adjusted by increasing the molecular weight into the entanglement regime, which more effectively stabilizes both the hydrophobic domain and the self-assembled species. If we begin to change the composition of the hydrophobic domain, it will destabilize the condensed, self-assembled structure [36].

The pH-responsive vesicle or micellar systems would not be orally relevant if the stimuli range is  $\sim 5$  since the premature release of drug cargo would occur in the acidic environment of the stomach (pH 1–3) [37]. The hydrogel particles are designed such that the cross-linked domains are a combination of covalent bonds and the collapse of multiple hydrophobic domains. In these cases, a change in the pH of the environment surrounding leads to a nonpolar, collapsed hydrophobic species to turn into a charged species. The change to charged groups also leads to the electrostatic repulsion of polyelectrolyte chains within close proximity to one another, which further drives the expansion of the gel network pore structure [38]. The design is typically used in drug applications where the drug needs to be delivered within the immediate proximity of a desired cell and does not require the system to facilitate the cellular internalization response. In either of these cases, systems can be designed with negative charges as well, which shifts the operable pH range to more basic stimuli. One can envision tuning their respective systems by compositionally shifting their ratios of cationic to anionic stimuli-responsive groups to allow for a specific release window (Fig. 2) [38].

## 2.2. Temperature-sensitive drug delivery

The combination of a polymer with a solvent in a binary mixture involves a series of phases of varying degrees of stability primarily in relation to its composition and temperature. Within some compositional range, a material can reach a minimum energy equilibrium state known as the binodal curve that describes a critical limit at which two phases can be either stable on one side or unstable on the other side, representing the limits of solvent interaction between two phases [39]. Plus, a curve known as the spinodal curve describes the limit of absolute

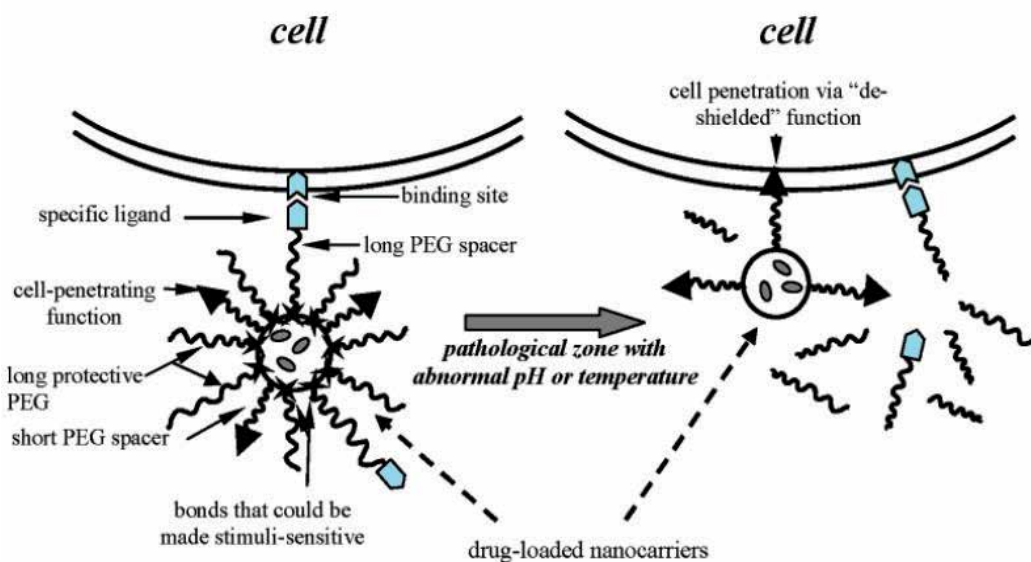


**Figure 2.** Interaction of the multifunctional pH-responsive pharmaceutical nano-carrier with the target cell. Local stimuli-dependent removal of protecting PEG chains or mAb-PEG moieties allows for the direct interaction of the CPP moiety with the cell membrane [38].

instability between phases. A complete decomposition of the system is produced when it is changed to composition within the spinodal curve [40].

The point at which the spinodal and binodal curves meet is known as the lower critical solution temperature (LCST) [41]. The LCST represents a point below which the material becomes miscible, where the Gibbs free energy of mixing is negative ( $-\Delta G$ ) and above which it is completely immiscible, and where the Gibbs free energy of mixing is positive ( $+\Delta G$ ) due to poor entropy of mixing [42]. The degree of polymerization and the polydispersity of the polymer chains can be a strong influence on the energetics of mixing and therefore can shift the values for the LCST. Typically, polymer chains with higher degrees of polymerization lead to higher values for the LCST. Polymers that exhibit an LCST behavior can have their solubility tuned based on temperature change.

We have known that the self-assembly of vesicle and micellar species is controlled by several factors, such as chemical composition, shape, charge, and so on, and species with specific size, shape, stability, and delivery efficiency are assembled under the effect of these factors [43]. For a vesicle species comprised of amphiphilic copolymers, there is much focus about their design. The chemical functionality tells us the rigidity of the system and the way hydrophobic or hydrophilic are, as well as whether a charged species is present [44].

The bond rotation of rigid species require a higher number of polymer repeats, and there are limitations in the modes of bending, so higher molecular weights is required in order to reach the entanglement regime for the more rigid systems. The closer the molecular weight is to the entanglement molecular weight, the more stable the assembled species [45]. The chemical

composition will tell us the ratio of the hydrophilic and hydrophobic components, as well as the degree of polymerization of the collapsed hydrophobic domain.

Yatvin and Weinstein pioneered the concept of temperature-triggered local drug delivery using temperature-sensitive liposomes (TSLs) [46–47]. Here, a chemotherapeutic drug is encapsulated in a heat-sensitive nanovesicle that prevents extravasation of the drug into healthy tissues at physiological temperature. The experiment about temperature-induced drug delivery was performed in small rodents with a subcutaneous tumor on the hind limb where hyperthermia was realized through putting the leg into a water bath [48]. Both tumor tissue and the whole hind limb were found with temperature-induced drug delivery phenomenon. The control of the temperature remained demanding when temperatures were monitored with thermocouples inserted into the tumor. The concept of temperature-triggered drug delivery has been extended to magnetic resonance (MR) image-guided drug delivery by the co-encapsulation of a paramagnetic magnetic resonance imaging (MRI) contrast agent in the lumen of TSLs (Fig. 3) [49].

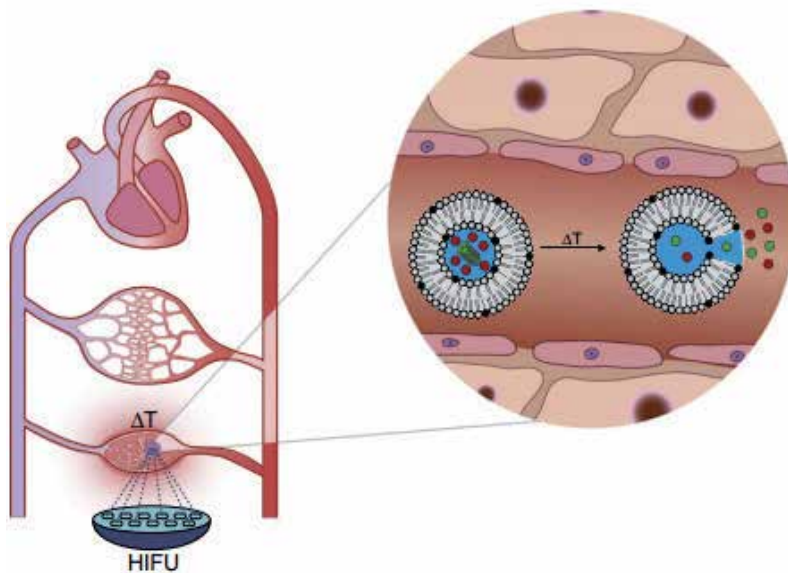


**Figure 3.** MR image-guided drug delivery illustration of the release of temperature-triggered drug using temperature-sensitive liposomes and HIFU. The co-release of MRI contrast agents from the liposome loaded with temperature-sensitive drug allows to non-invasively visualize and quantify the drug release process [49].

It has been revealed that the external aqueous medium was separated from the liposomal aqueous lumen by a single continuous bilayer of phospholipids that is from the self-assembly of phospholipids into liposomes [50]. These self-assembled structures have been investigated as molecular MRI contrast agents for drug delivery systems. Temperature-sensitive liposomes release encapsulated drugs at the melting phase transition temperature ( $T_m$ ) of the lipid bilayer (Fig. 3). Structural changes in the lipid membrane occur as it transfers from a gel to the liquid-

crystalline phase at transition temperature [51]. In comparison to the liquid-crystalline phase, liposomal membranes in the gel phase are less permeable to water and drugs.

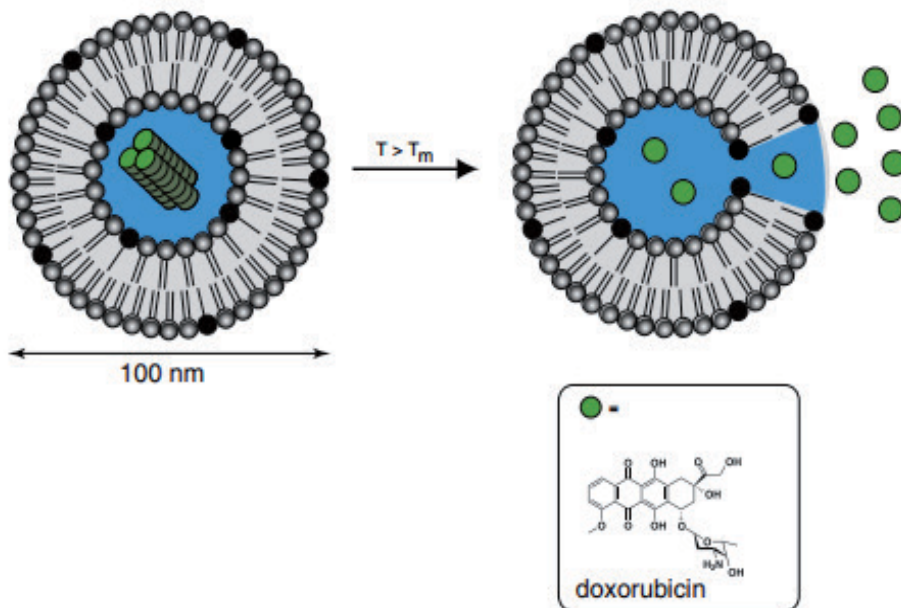


**Figure 4.** Schematic representation of heat-triggered dox release from TSLs [49].

There are several other thermo-responsive functionalities that can be incorporated within the polymer domain in order to stimulate porosity or swelling of a system in addition to NIPAAm, and each system has a different LCST, or in some cases a tunable LCST [52]. Appropriate selection of the thermo-responsive functionality for eliciting the desired behavior is critical. It is also important to keep in mind that the selection of the responsive functionality should reflect the rationalization that the system should be at the very least bioinert in order to be a candidate for a drug delivery system.

### 2.3. Magnetic-sensitive drug delivery

The stimuli-responsive behavior is dependent on the local physiological environment, such as in both cases of pH and temperature. We could direct the stimuli toward the targeted area of delivery instead of the stimuli-responsive behavior depending on a localized environment. We will adjust the chemical functionality to allow for a relevant response if there is fine control over sources that induce a direct movement including a magnetic field, light, and sound. The response is an attractive or repulsive force relative to the field direction in the case of magnetic materials. Both the material chemical functionality and the viscosity properties of the particle within a physiological system are critical in determining the extent of the response to a magnetic field (Fig. 5) [53–54]. Magnetic particles are typically divided based on size into

single-domain and multi-domain particles [55]. The single-domain particles fall in a small size regime, where decreases in size correspond to an increase in coercivity to a peak level before dropping to zero. The zero point identifies a superparamagnetic material, which is one whose magnetic moment is induced in the direction of the applied magnetic field and in the absence of a magnetic field returns to an unaligned state [56].

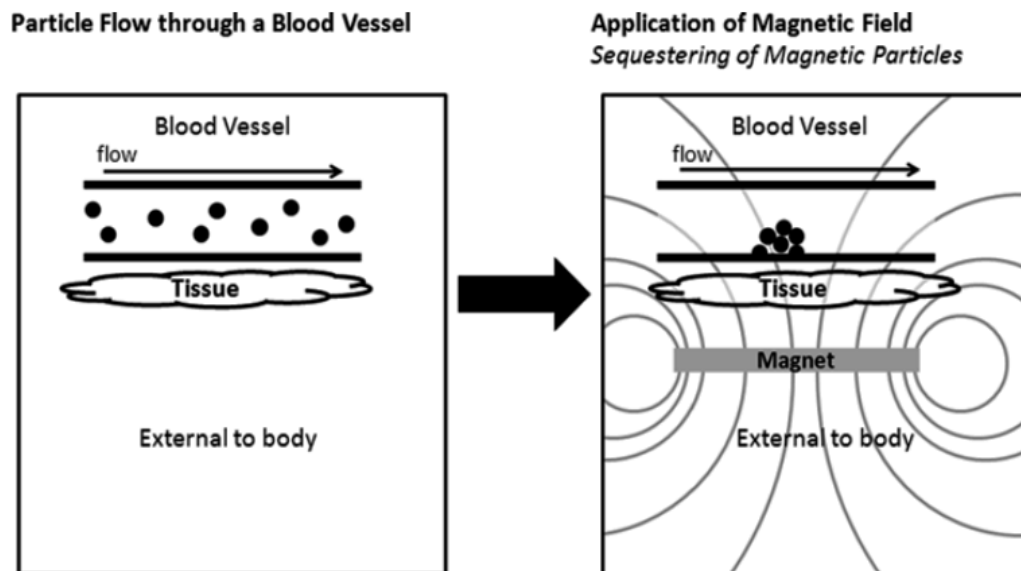


**Figure 5.** Diagram of the basic forces involved in the sequestration of magnetic nanoparticles in the bloodstream [53].

As was the case of thermo-responsive and pH-responsive systems, magneto-responsive materials represent systems that interact with an applied stimulus as opposed to an encountered stimulus. Light and sound are also suitable for responsive materials as an applied stimulus [57]. The stimulus is an externally applied magnetic field that can immobilize a particle under flow in terms of magnetic materials [58]. The design of magnetic materials involves several factors including particle size, stabilizing material, atomic identity, and so on [59]. In terms of the size of the magnetic particle, paying attention to the larger the magnetic particle size, the more susceptible it will be toward manipulation by a magnetic field. The stabilizing functionality is that the particle surface is necessary to allow for the particle to effectively function as a physiological system. The atomic identity refers to the metal atoms used in the particle composition.

In the application of a magnetic field, we should pay attention to a single-domain magnetic particle strategy for the immobilization of drug species [60]. The system depends on a small particle system in order to fall within the superparamagnetic regime. For example, systems of iron oxide ( $\text{Fe}_3\text{O}_4$ ) are used where drug species are conjugated to the surface. A larger silica particle system is used as matrix by these ferromagnetic particles, which is then surface-functionalized with chemically inert groups [60]. Fig. 6 displays the schematic illustration of

the synthesis process of the drug-loading magnetic and fluorescent chitosan nanoparticles [61]. Amino groups of chitosan consisted of cationic linear polysaccharide molecules keep positively charged under weakly acidic conditions, result in the form of a long and intertwined chain with positive charges along its backbone. The aqueous negatively charged QDs,  $\text{Fe}_3\text{O}_4$  nanoparticles, and the ionized  $\text{COO}^-$  of cefradine ( $\text{pK}_a = 2.5$  and  $7.3$ ) along the positive backbone are electrostatically attracted in weakly acidic conditions are electrostatically attracted [61].

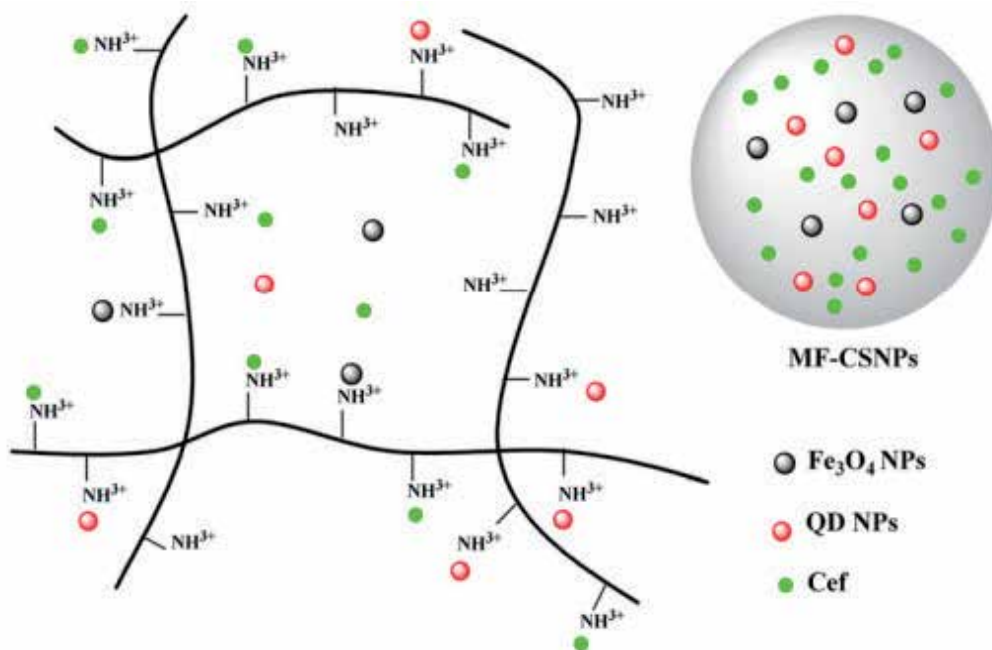


**Figure 6.** Schematic representation of the fabrication process of the drug-loading magnetic and fluorescent chitosan nanoparticles [61].

The introduction of surface-modifying groups for biocompatibility and the magnitude of the magnetic moment at the surface of the particle are reduced, which may limit its physiological application. Therefore, the design of these immobilized magnetic systems involves three basic factors: particle size ( $<10$  nm), bioinert surface functionalities, and mode of drug incorporation (conjugated or dispersed within matrix) [62]. Magnetic drug delivery systems formed using this design strategy have shown promise for clinical evaluation and treatment of brain tumor patients using a tandem approach involving acoustic and magnetic targeting of tissue across the blood–brain barrier.

The domain choices allow tunable size and magnetic susceptibility for the drug delivery system. This degree of versatility allows for a multitude of surface functionalizations in order to present a drug delivery system that is physiologically bioinert.

## 2.4. Ultrasound-sensitive drug delivery

A self-assembled species can be induced by the use of ultrasound technology to act as a nucleation site for pore formation in a membrane barrier to enhance delivery [63]. A process of acoustic droplet vaporization pushes a superheated droplet through a phase transition to yield gas micro-bubbles, which leads to membrane pore formation by a process of sonoporation [64]. For transdermal drug delivery, the permeabilizing effects of ultrasound have been applied to a number of treatments, such as for diabetes [65]. Ultrasound has been employed for targeted disruption of drug carrier vessels such as contrast or acoustically active liposomes, releasing their therapeutic payload for uptake by the target cells (Fig. 7) [66]. In addition, sonoporation has been associated with gene therapy for the introduction of nonviral plasmid DNA into target cells.

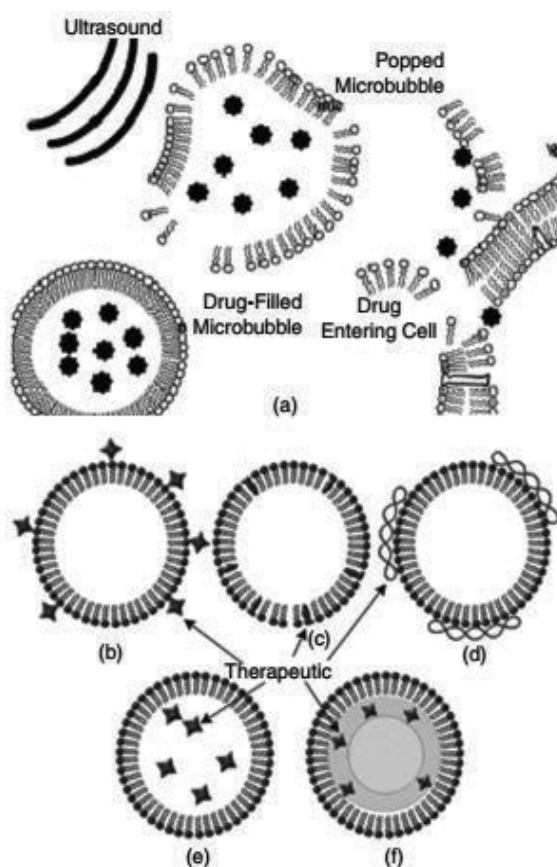


**Figure 7.** Various drug delivery strategies with micro-bubble carriers. (a) Schematic representation of drug delivery via targeted micro-bubble destruction with ultrasound. Models of different therapeutic agents loading styles, such as (b) attaching to the micro-bubble membrane, (c) imbedding in the membrane, (d) bonding noncovalently to the micro-bubble surface, (e) packing in the interior of the micro-bubble, and (f) incorporating into an oily film surrounding the micro-bubble [66].

In the case of ultrasound responsive systems, it is required for the stabilization of acoustic cavitation's gas-liquid interface and the compatibility with liquid interface to generate gas bubbles. The primary requirements of the stabilized system are extended circulation lifetime, effective size range, and efficient stimulated release of encapsulated drug via the application of ultrasound [67–68].

The circulation lifetime of the gas microbubbles is associated with the amphiphilic component that stabilizes the interface. We have known that lipid bilayer systems have a significantly short thickness, which offers little stability of microbubbles in vivo in the case of gas-liquid interfaces. Amphiphilic copolymer systems offer a significant improvement to the interfacial membrane stability, while maintaining tunability to drive membrane curvature [69].

It is known that the targeted size of allowing for tumor membrane permeability and gas microbubble stabilization is less than 750 nm. The curvature can be further tuned to form nanobubbles as a preform to merge into microbubble systems at the cell membrane interface. It is an example of improving the stability of the microbubble with no discernible effect to the biological delivery. The energy of the applied ultrasound stimulus can adjust the size regimes and stabilize the desired interfacial curvature effectively (Fig. 8) [70].

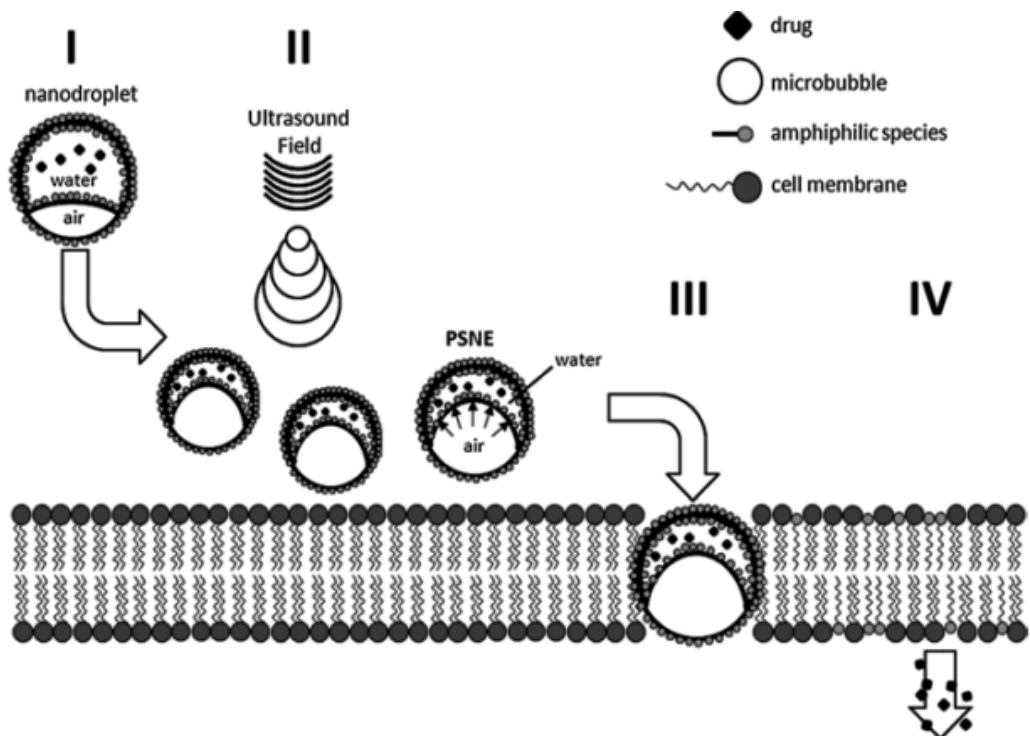


**Figure 8.** Diagram of the cavitation of PSNE (Phase-Shift Nanoemulsion) nanodroplets from ultrasound [70].

The effective delivery of the adhered drug is relevant to the echogenicity or the ability to bounce a signal base on oscillation, growth, and collapse of the microbubble system [71]. The echogenicity is affected by the choice of component mixtures such as water and PFP, the surfactant, and the size of the microbubble system. The trend appears to be that the maximization of the impedance between components and the stabilization of high-curvature systems can improve drug release profiles in vivo [72].

## 2.5. Light-sensitive drug delivery

The materials species is influenced by the presence of a specific energy wavelength of light as well as the particle species is influenced by the direction of the magnetic field in magnetic systems. The chemical structure of the drug delivery system destabilizes or changes conformation in response to the absorbed energy input when visible, ultraviolet (UV), or infrared (IR) light is directed at a desired target region.  $\text{TiO}_2$  photocatalysts have been mostly used for the purification of air and water by UV light irradiation. However, the limited photocatalytic activity of  $\text{TiO}_2$  within the UV range presents difficulties in biomedical and tissue engineering applications owing to the potential harmful effects of UV light. In this part, we focused on the extension of the photocatalytic activity of  $\text{TiO}_2$  to the visible light region by doping nitrogen into the  $\text{TiO}_2$  crystal structure, which would allow remote control of antibiotic elution by visible light irradiation [73].

A new delivery system that affords control of the time of drug elution and accurate dosing of antibiotics to the target area is required.  $\text{TiO}_2$  nanotubes have been studied predominantly in the field of photocatalysis [74–76], solar cells [77], and biomedical engineering [78–80], because of their excellent photocatalytic activity and biocompatibility. In addition, the high surface area and unique shape of  $\text{TiO}_2$  nanotubes make them a promising option for application in drug delivery systems.  $\text{TiO}_2$  nanotubes arrays fabricated by electrochemical anodization can be described as a layer of tightly packed, vertically aligned and ordered nanotube structures with hexagonal arrangement, which grow perpendicularly to the Ti surface [81]. Fig. 9A and 9B show illustrations of the chemical cell and the fabrication process of TNTs by electrochemical anodization of Ti. Typical scanning electron microscopy images of prepared TNTs are shown in Fig. 9c, with the top and the cross-sectional views showing nanotubes separated into individual entities featuring closed ends at the bottom side [82].

Kyung-Suk Moon et al. [83] immobilized Gold nanorods (GNR) at the surface of  $\text{TiO}_2$  nanotubes via a grafting technique and investigated on-off drug release triggered by near-IR laser irradiation. In addition, antimicrobial activity was monitored to assess the effectiveness of GNR-grafted  $\text{TiO}_2$  nanotubes in allowing remotely controlled drug release by IR laser irradiation. The elution concentrations of tetracycline loaded at the surface of GNR-grafted  $\text{TiO}_2$  nanotubes were evaluated after 30 s of IR light irradiation with a near-IR laser. The release concentrations of tetracycline from GNR-grafted  $\text{TiO}_2$  nanotubes with IR light irradiation ( $674.52 \pm 169.58 \mu\text{g/mL}$ ) were significantly higher than those from other experimental conditions, such as  $\text{TiO}_2$  nanotubes with or without IR light irradiation and GNR-grafted  $\text{TiO}_2$  nanotubes without IR laser irradiation (Fig. 10) [83].

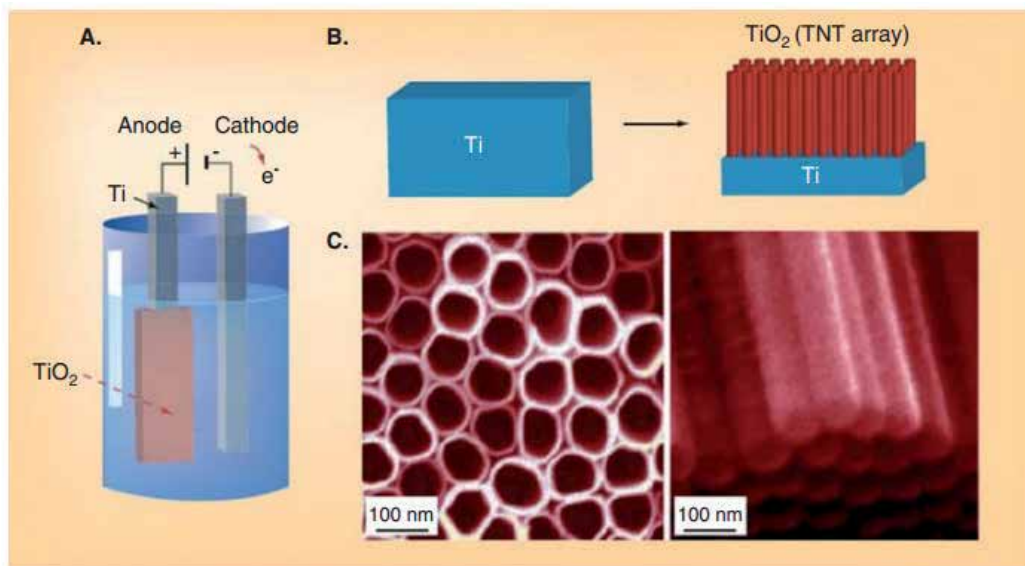


**Figure 9.** Schematic illustration of TNTs synthesis process and corresponding SEM images of typical morphology and structure. (a) Preparation of TNTs layer by electrochemical cell and anodization process. (b) Formation of self-organized and vertically aligned TNTs on Ti substrate. (c) SEM images of the typical morphology of TNT structures [82].

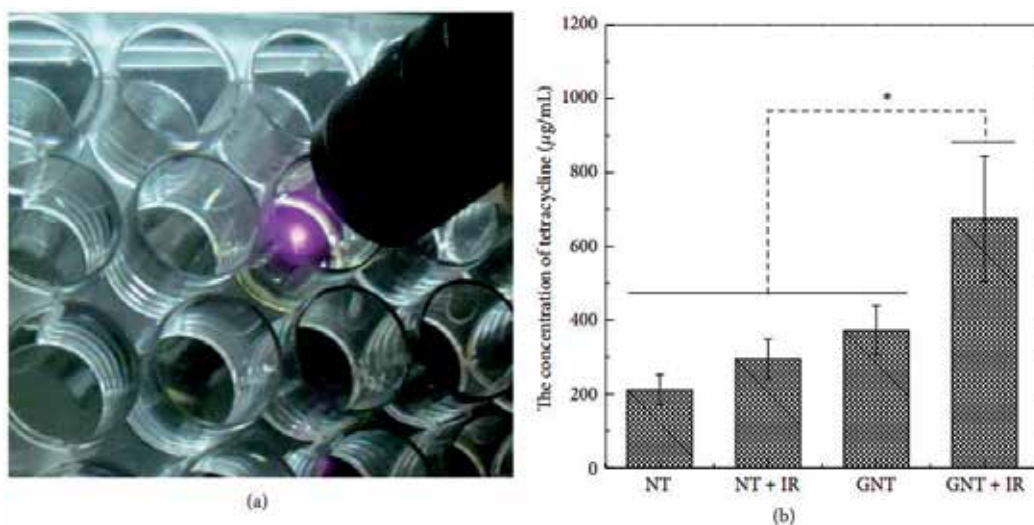


**Figure 10.** a) Near-IR laser and IR light irradiation and (b) the concentration of tetracycline released by IR light irradiation (NT, NT + IR, GNT, and GNT + IR in the graph designate TiO<sub>2</sub> nanotubes only, near-IR laser irradiated TiO<sub>2</sub> nanotubes, GNR-grafted TiO<sub>2</sub> nanotubes, and near-IR laser irradiated GNR grafted TiO<sub>2</sub> nanotubes, resp.) [83].

For photo-responsive materials, light can either induce the formation of an isomer or degrade a self-assembled component [84–85]. The photoisomerization strategy relies on the effective destabilization of a liquid crystal phase within the hydrophobic domain of micelle or vesicle

species that are formed from amphiphilic molecules or macromolecules. The aggregated region will be highly rigid and densely packed in the trans state if the hydrophobic domain consists of liquid crystal groups [86]. The visible light or heat is used to return the structure to its native initial state in photo-isomerization-induced systems that involve highly stable vesicle or micellar self-assembled systems that rapidly reform their densely packed domains.

## 2.6. Nanoporous engineered drug delivery

Recently, nanoporous anodic alumina (NAA) has become one of the most popular self-ordered periodic, porous templates. In general the highly developed, superior ordering of nanopores in NAA templates is obtained by using a two-step anodization process. NAA has been of great interest due to its outstanding material properties, including electrical insulation, optical transparency, and chemical stability, and most recently, because of its biologically inert and biologically compatibility properties [87]. The use of NAA as a drug delivery platform has been explored in several fields, such as biomedical devices for dental and bone implants, vectors, or carriers for cells transplantation. The suitability of NAA loaded with catalase, endostatin, and vitamin C as sustainable, quasi-linear drug-releasing platform for ophthalmic applications has been demonstrated by Orosz et al. [88].

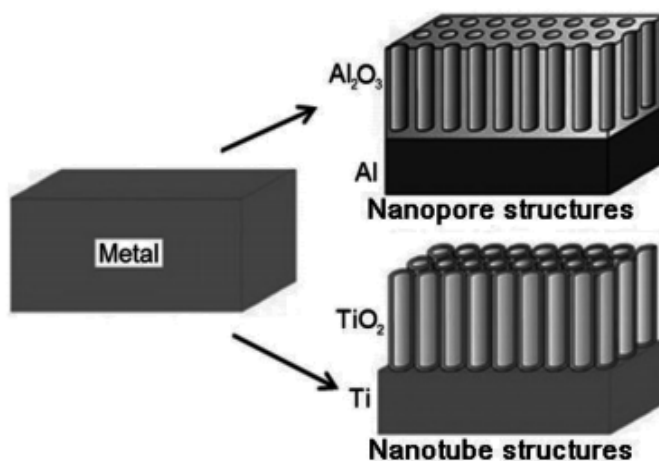


**Figure 11.** Schematic diagram showing the self-ordering anodization on selected metals (Al and Ti) to produce nanoporous and nanotube metal oxides ( $\text{Al}_2\text{O}_3$  and  $\text{TiO}_2$ ) with highly-ordered and self-aligning uniform structures. These two materials were explored as non-eroding drug-releasing implants for LDD applications [89].

Depending on the metal type, electrolyte, current, and voltage, two different oxide growth morphologies, such as nanoporous aluminum oxide ( $\text{Al}_2\text{O}_3$ ) and nanotube titanium dioxide ( $\text{TiO}_2$ ), can be obtained by a self-ordering electrochemical anodization process as shown in Fig. 11 [89]. The structural features of NAA can be controlled by the anodization parameters, so the functionalities of NAA in terms of pore geometry is an advantage for developing drug-releasing implants as the diffusion of molecules from the nanopores can be tuned by geometry

[90]. Jeonet et al. [91] developed a sophisticated system by combining NAA chips with electrically responsive polymers, in which the pore mouths of NAA were modified with polypyrrole doped with dodecylbenzenesulfonate anion (PPy/dB) by electro-polymerization on the upper surface of NAA platforms. The large volume change of that polymeric blend was used to achieve pore mouth actuation by an external electrical stimulus (Fig. 12) [90].

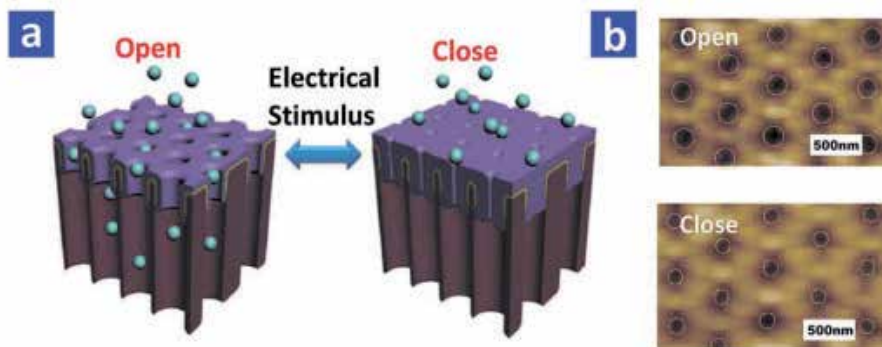


**Figure 12.** Electrically responsive drug-releasing NAA chip. (a) The mechanism of an electrically responsive drug-releasing chip based on NAA and PPy-DBS (reversible cycle). (b) AFM images of NAA chips before and after the application of electrical stimulus (pore mouth reduction) [90].

Titania nanotubes (TNTs) can be produced by anodizing metallic titanium (Ti) in different acid electrolytes as well as NAA; TNTs feature a nanotube structure during the anodization process (Fig. 13A and B) [92]. Different electrochemical approaches have made it possible to engineer the nanoporous structure of TNTs. TNT-based implants are recognized as one of the most promising nanomaterials to address the inherent drawbacks of conventional systemic drug administration due to their capability to localize the release of drugs over affected bones sites in a controllable manner [91].

In terms of the drug loading and release properties and capabilities of TNTs layers, the drug release from nanotubes is governed by a diffusion process when TNTs come into contact with the physiological milieu inside the host body, as schematically presented in Fig. 14 [90]. The release process is established by the mass transfer of drug molecules from the nanotubes, considering that the drug is completely soluble in the physiological solution without precipitation at particular concentrations. This diffusion-controlled process can be described by Fick's first law, which is governed by a number of factors such as the molecular size and charge of drugs, the diameter and length of nanotubes, their charge and surface chemistry, interfacial interaction between drug molecules and nanotube surface, dissolution rate of drugs, diffusion coefficient, pH, and so on [82].

In addition, the surface charges of TNTs can be rendered hydrophobic or hydrophilic to accommodate a variety of drug molecules should be mentioned. In vitro drug release with the aid of polymeric micelles as drug nano-carriers [93–94] and targeted drug release by means of

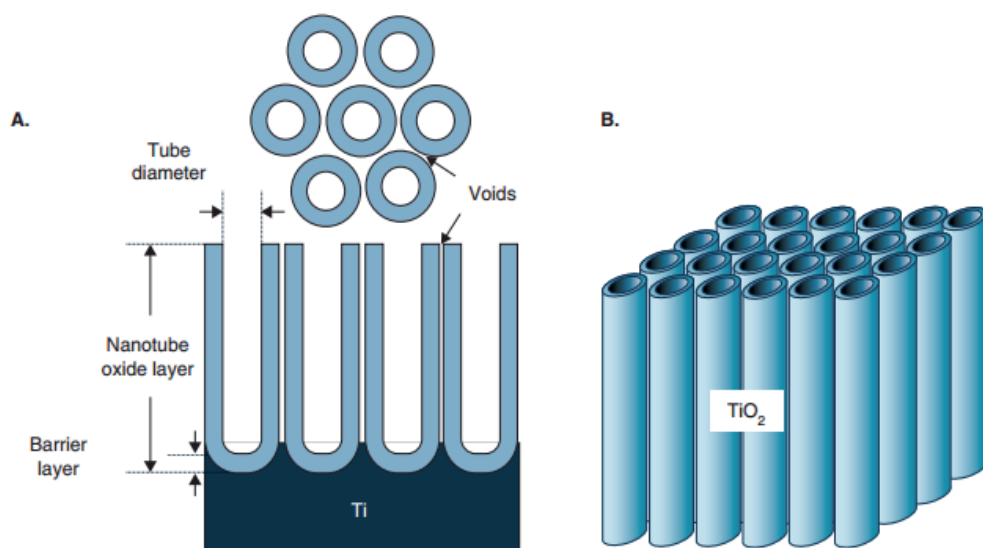


**Figure 13.** (a) Typical structures of nanotube titania fabricated by electrochemical anodization of titanium, (b) TiO<sub>2</sub> nanotube structures fabricated by electrochemical anodization in NH<sub>4</sub>F/ethylene glycol electrolyte showing the cross-sectional image of self-supporting TiO<sub>2</sub> nanotube layer and the entire structure (nanotube film) not detached from Ti substrate (inset) [92].

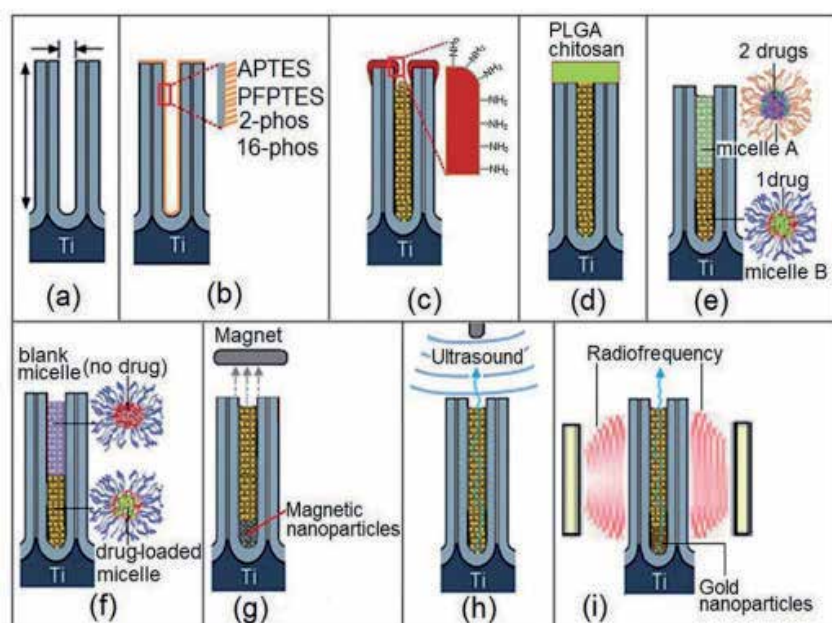


**Figure 14.** Schematic diagram showing different strategies developed by our group for controlling drug release from drug-releasing implants based on TNTs [90].

gold nanoparticles stimulated by radiofrequency field [95] and magnetic nanoparticles under the influence of a magnetic nanoparticles that are under the influence of a magnetic field [96].

Properties of NAA and TNTs that can control drug release but non-degrade in vivo are not suitable for some specific applications, such as drug-releasing implants for treating eye-related diseases [90]. Other nanostructure materials including porous silicon can also be applied to develop biodegradable drug-releasing implants with improved capabilities for definite requirement of clinical applications [91].

### 3. Applications

#### 3.1. Smart micelles for cancer

The ways of leveraging the enhanced permeability, ligand attachment, and specific receptor-ligand attachment could make micelles target to tumors. It is essential to increase drug bioavailability and the desired cytotoxic effect for the released drug from micelles carriers when micelles reach the tumor site. In order to realize the drug release triggered specifically at the tumor site, micelle structures should be designed as environmentally responsive systems, and such functionality is typically incorporated into micelles by introducing temperature/thermo-sensitive, pH sensitive, or ultrasound-activated polymers. As “smart micelles”, it is known that micelles can dynamically change their physical properties in response to environmental triggers such as pH, temperature, and chemical species.

The micelle copolymer incorporates an ionizable component and a pH-dependent stability results from the pH sensitivity to micelles. The drug is released from the micelle when it encounters an acidic environment. The pH-sensitive micelles demonstrated the long residence time and improved half-life typical of micellar nanoparticles in animal models. Comparing to non-pH-sensitive micelles, the pH-sensitive micelles achieved a satisfying effect in tumors [97]. It reveals that the potential of pH-sensitive micelles could increase drug delivery to cancerous tumors.

An alternative way of constructing environmentally responsive micelles is to build temperature sensitivity into the micelle structure. The localized hyperthermia is used clinically to treat tumors, since the vasculature of tumor is more vulnerable to hyperthermia than normal tissue [98]. Temperature-sensitive micelles could be a part of a synergistic regimen, therefore, in which the raised temperature induces local drug release and kills tumor cells directly. It is also a common technique that makes use of a thermo-sensitive polymer with LCST behavior to design temperature-responsive micelles. A temperature increase above the LCST induces the entire system to be hydrophobic and precipitate out of the solution.

An important strategy for site-specific drug release from smart micelles is ultrasound activation. A number of mechanisms could promote the drug delivery, for example, a local temperature increase in tissues, the production of highly reactive free radical species that can accelerate polymer degradation, and the cavitation that increase the permeability of cell membranes [99]. Ultrasound was used to improve the antitumor efficacy of both free doxor-

ubicin and micelle-encapsulated doxorubicin in which micelles with ultrasound broke tumor growth an additional several days over micelles without ultrasound. Bio-distribution studies revealed that ultrasound not only increased the level of drug accumulation in the tumor, but also lowered the level of drug accumulation in the kidneys and heart [100–101]. Overall, ultrasound-sensitive micelles may have the capacity to both decrease side effects and increase chemotherapeutic effectiveness during tumor treatment.

In conclusion, micelles can be triggered by modulating temperature, pH, ultrasound, and light application. Well-designed micellar biomaterials for drug delivery could decrease mortality from cancers.

### **3.2. Ultrasound-sensitive drug delivery for theranostics**

For smart therapies, ultrasound is a highly useful method that is already widely used clinically. In addition, ultrasound-triggered drug delivery vehicles can be combined with ultrasound contrast agents or microbubbles to create “theranostics” that incorporate both diagnostics via imaging and therapy via drug delivery [102]. Ultrasound-activated theranostics can improve the detection and treatment of cancerous tumors and cardiovascular pathologies such as atherosclerotic plaque [102].

It is demonstrated that ultrasound-triggered theranostics is a way of cancer treatment. For example, the mixtures of doxorubicin-loaded micelles with doxorubicin-loaded microbubbles were injected intravenously into mice bearing breast cancer tumors, and the agents were visualized at the tumor target site using ultrasound and were then degraded through ultrasound to release the doxorubicin at the tumor site. Ultrasound enhanced the intracellular uptake of doxorubicin by tumor cells and resulted in breast tumor regression in the mouse model. These results could have a significant impact on the treatment of other cancerous tumors via ultrasound-mediated visualization and drug delivery.

Ultrasound-triggered drug delivery vehicles can simultaneously detect areas requiring therapy and target drug delivery to these areas. The smart materials are in the early stages of development but hold potential for enabling rational treatment of diseases, improving clinical outcomes, and promoting a better quality of life for patients with complex chronic diseases.

### **3.3. Nanoporous implants for local drug delivery**

TNTs are an alternative technology that can address some of the problems in dentistry as this is an economically affordable technology that can be easily implemented into dental implants [82]. In addition, the scope of TNT-based delivery systems can be extended to regenerative medicine and dentistry along with preventive therapy. An overview of several aspects relevant to TNT applications in dentistry, including studies of osteoblast adhesion to TNTs surfaces and its biocompatibility, release of specific drugs and silver nanoparticles and periodontium regeneration by the delivery of multiple growth factors inducing osteogenesis (Fig. 15) [82]. TNTs can also serve as a gene and DD carrier such as growth factors and stem cells, which can further enhance osseointegration and bone regeneration relevant to tooth implants [103].

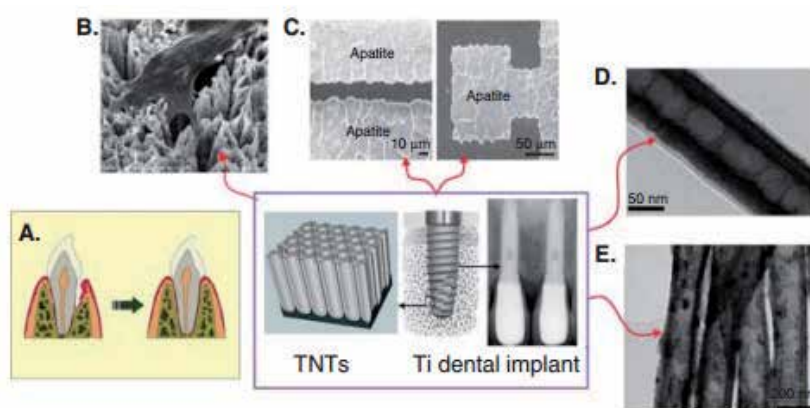


**Figure 15.** Schematic diagram summarizing the applications of TNTs in dentistry. (a) Periodontium problem and proposed regeneration by delivery of multiple growth factors inducing osteogenesis, (b) the adhesion of osteoblast cells to TNTs surface, (c) the growth of hydroxyapatite on TNTs, (d) the cross-sectional view of a single TNT revealing the drug sodium naproxen on the inside, and (e) anti-bacterial silver nanoparticles incorporated within TNT [82].

The encapsulation of sensitive drugs in nano-carriers such as polymer micelles were loaded in TNTs. Aw et al. put forward a prospective solution to both protect sensitive drugs and proteins from degradation and design TNT-based drug-releasing systems with an extended release capability [93]. Furthermore, based on the implementation of multi-drug payloads, polymeric micelles loaded with different drugs were loaded in the TNTs that are based on the formation of two or more immiscible layers of drug carriers that have opposite interfacial properties with hydrophobic and hydrophilic, which are used to generate a series of sequential release in a time controlled form [104].

Studies mentioned above in the discussion confirmed that NAAs and TNTs can be used for loading and releasing of wide range of therapeutics, with the ability to tune their drug releasing characteristics and provide multi-drug release of different drugs in different fashions. These approaches are aimed at achieving optimized drug dosage, release rate, and time needed for a broad range of specific therapies. The design of triggered drug-release from NAAs and TNTs using various external signaling sources (thermal, magnetic, electro-magnetic, ultrasonic, or mechanical activation) is an outstanding feature offering great perspectives and opportunities for combining NAAs and TNTs with sensing functions. NAAs and TNTs are shown to be very versatile in terms of their biomedical applications and can be applied as a new generation of smart implants and drug-delivery devices.

#### 4. Summary

It is a highly desirable approach for effective therapeutic treatment to use smart materials to release drugs to a specific physiological environment. We have discussed the fundamental behavior and materials design associated with five stimuli-responsive systems based on pH,

temperature, magnetism, sound, and light. The stimuli-responsive systems are classified as “smart” materials, and each system includes two major strategies for the material design.

Based on our previous knowledge of degradation, release, and self-assembly, we introduce new concepts of excitation, cavitation, and magnetophoresis for strategies for materials design. A cooperative strategy of magnetophoresis, thermal phase change, and selected concept strategies of light excitation were stated in the chapter. A variety of smart material systems are currently in various stages of clinical development, such as ultrasound and magnetic hyperthermia systems, for treating cancer. It has been proven that drug-releasing systems provide better capabilities and performances than conventional therapies, offering alternative ways to deliver therapeutics effectively over different parts of the host body and reducing the side effects associated with excessive dosages of highly toxic drugs. Despite the successes described above, more exhaustive research must be carried out in order to make drug-releasing implants feasible for clinical applications.

Finally, it is worth stressing that the combination localized drug-releasing systems with other traditional treatments such as surgery, radiation, and systemic chemotherapy could provide more efficient clinical therapies for treating the most challenging and resilient diseases, such as cancer, with minimal drawbacks. What's more, it is expected that the integration of TNT implants with sensors, microchips, and development of advanced triggered drug release can come true in the future. In conclusion, it is right that smart materials were used to study the drug delivery system, and materials design involved with several stimuli-responsive systems such as pH, temperature, magnetism, light, and sound. In addition, smart material systems are currently in various stages of clinical development based on ultrasound and magnetic hyperthermia systems for treating cancer.

## Acknowledgements

The authors thank the National Natural Science Foundation of China (21501127; 51502185), Natural Science Foundation of Jiangsu Province of China (BK20130313; BK20140400), and Priority Academic Program Development of Jiangsu Higher Education Institutions (PAPD) for financial support of this work.

## Author details

Qun Wang, Jianying Huang and Yuekun Lai\*

\*Address all correspondence to: yklai@suda.edu.cn

National Engineering Laboratory for Modern Silk, College of Textile and Clothing Engineering, Soochow University, Suzhou, China

## References

- [1] L. Li, D. Chen, Y. Zhang, Z. Deng, X. Ren, X. Meng, F. Tang, J. Ren, L. Zhang, Magnetic and fluorescent multifunctional chitosan nanoparticles as a smart drug delivery system, *Nanotechnology*, 2007, 18(40): 405012.
- [2] N. Doshi, S. Mitragotri, Designer biomaterials for nanomedicine, *Advanced Functional Materials*, 2009, 19(24): 3843–3854.
- [3] V. Thiviyanathan, A. D. Somasunderam, D. G. Gorenstein, Combinatorial selection and delivery of thioaptamers, *Biochemical Society Transactions*, 2007, 35(1): 50–52.
- [4] Y. Y. Song, F. Schmidt-Stein, S. Bauer, P. Schmuki, Amphiphilic TiO<sub>2</sub> nanotube arrays: An actively controllable drug delivery system, *Journal of the American Chemical Society*, 131(12): 4230–4232.
- [5] S. Ghosh, C. Yang, T. Cai, Z. Hu, A. Neogi, Oscillating magnetic field-actuated microvalves for micro- and nanofluidics, *Journal of Physics D: Applied Physics*, 2009, 42(13): 135501.
- [6] M. Hrubý, C. Konák, K. Ulbrich, Polymeric micellar pH-sensitive drug delivery system for doxorubicin, *Journal of Controlled Release*, 2005, 103(1): 137–148.
- [7] A. Yudina, M. de Smet, M. Lepetit-Coiffé, S. Langereis, L. Van Ruijssevelt, P. Smirnov, V. Bouchaud, P. Voisin, H. Grüll, C. T. Moonen, Ultrasound-mediated intracellular drug delivery using microbubbles and temperature-sensitive liposomes, *Journal of Controlled Release*, 2011, 155(3): 442–448.
- [8] X. Y. Li, X. L. Zheng, X. W. Wei, G. Guo, M. L. Gou, C. Y. Gong, X. Huo, D. M. Wang, L. J. Chen, Y. Q. Wei, Z. Y. Qian, A novel composite drug delivery system: Honokiol nanoparticles in thermosensitive hydrogel based on chitosan, *Journal of Nanoscience and Nanotechnology*, 2009, 9(7): 4586–4592.
- [9] J. L. Zhang, R. S. Srivastava, R. D. K. Misra, Core-shell magnetite nanoparticles surface encapsulated with smart stimuli-responsive polymer: Synthesis, characterization, and LCST of viable drug-targeting delivery system, *Langmuir*, 2007, 23(11): 6342–6351.
- [10] A. Ito, M. Shinkai, H. Honda, T. Kobayashi, Medical application of functionalized magnetic nanoparticles, *Journal of Fermentation Technology*, 2005, 100(1): 1–11.
- [11] M. Shinkai, Functional magnetic particles for medical application, *Journal of Bioscience and Bioengineering*, 2002, 94: 600–613.
- [12] A. K. Gupta, M. Gupta, Synthesis and surface engineering of iron oxide nanoparticles for biomedical applications, *Biomaterials*, 2005, 26(18): 3995–4021.

- [13] S. Mornet, S. Vasseur, F. Grasset, P. Veverka, G. Goglio, A. Demourgues, J. Portier, E. Pollert, E. Duguet, Magnetic nanoparticle design for medical applications, *Progress in Solid State Chemistry*, 2006, 34(2–4): 237–247.
- [14] J. Zhang, R. D. K. Misra, Magnetic drug-targeting carrier encapsulated with thermo-sensitive smart polymer: Core-shell nanoparticle carrier and drug release response, *Acta Biomaterialia*, 2007, 3(6): 838–850.
- [15] S. Mornet, S. Vasseur, F. Grasset, E. Duguet, Magnetic nanoparticle design for medical diagnosis and therapy, *Journal of Materials Chemistry*, 2004, 14(14): 2161–2175.
- [16] K. D. Harris, R. Cuypers, P. Scheibe, C. L. van Oosten, C. W. M. Bastiaansen, J. Lub, D. J. Broer, Large amplitude light-induced motion in high elastic modulus polymer actuators, *Journal of Materials Chemistry*, 2005, 15(47): 5043–5048.
- [17] S. Juodkazis, N. Mukai, R. Wakaki, A. Yamaguchi, S. Matsuo, H. Misawa, Reversible phase transitions in polymer gels induced by radiation forces, *Nature*, 2000, 408(6809): 178–181.
- [18] C. S. Kwok, P. D. Mourad, L. A. Crum, B. D. Ratner, Self-assembled molecular structures as ultrasonically-responsive barrier membranes for pulsatile drug delivery, *Journal of Biomedical Materials Research*, 2001, 57(2): 151–164.
- [19] R. Fernández-Urrusuno, P. Calvo, C. Remuñán-López, J. L. Vila-Jato, M. J. Alonso, Enhancement of nasal absorption of insulin using chitosan nanoparticles, *Pharmaceutical Research*, 1999, 16(10): 1576–1581.
- [20] O. Kayser, A. Lemke, N. Hernandez-Trejo, The impact of nanobiotechnology on the development of new drug delivery systems, *Current Pharmaceutical Biotechnology*, 2005, 6(1): 3–5.
- [21] V. L. Colvin, M. C. Schlamp, A. P. Alivisatos, Light-emitting diodes made from cadmium selenide nanocrystals and a semiconducting polymer, *Nature*, 1994, 370(6488): 354–357.
- [22] C. C. Müller-Goymann, Physicochemical characterization of colloidal drug delivery systems such as reverse micelles, vesicles, liquid crystals and nanoparticles for topical administration, *European Journal of Pharmaceutics & Biopharmaceutics*, 2004, 58(2): 343–356.
- [23] R. Haag, Supramolecular drug-delivery systems based on polymeric core-shell architectures, *Angewandte Chemie International Edition*, 2004, 43(3): 278–282.
- [24] D. Losic, S. Simovic, Self-ordered nanopore and nanotube platforms for drug delivery applications, *Expert Opinion on Drug Delivery*, 2009, 6(12): 1363–1381.
- [25] D. Losic, M. S. Aw, A. Santos, K. Gulati, M. Bariana, Titania nanotube arrays for local drug delivery: Recent advances and perspectives, *Expert Opinion on Drug Delivery*, 2015, 12(1): 103–127.

- [26] K. Noh, K. S. Brammer, C. Choi, S. H. Kim, C. J. Frandsen, S. Jin, A new nano-platform for drug release via nanotubular aluminum oxide, *Journal of Biomaterials and Nanobiotechnology*, 2011, 2(3): 226–233.
- [27] K. Shimizu, H. Fujita, E. Nagamori, Oxygen plasma-treated thermoresponsive polymer surfaces for cell sheet engineering, *Biotechnology and Bioengineering*, 2010, 106(2): 303–310.
- [28] J. F. Mano, Stimuli-responsive polymeric systems for biomedical applications, *Advanced Engineering Materials*, 2008, 10(6): 515–527.
- [29] J. F. Joanny, L. Leibler, Weakly charged polyelectrolytes in a poor solvent, *Journal de Physique*, 1990, 51(6): 545–557.
- [30] D. Andelman, J. F. Joanny, Polyelectrolyte adsorption, *Comptes Rendus de l'Académie des Sciences-Series IV-Physics*, 2000, 1(9): 1153–1162.
- [31] J. L. Zhang, R. S. Srivastava, R. D. K. Misra, Core-Shell Magnetite Nanoparticles Surface Encapsulated with Smart Stimuli-Responsive Polymer: Synthesis, Characterization, and LCST of Viable Drug-Targeting Delivery System, *Langmuir*, 2007, 23(11): 6342–6351.
- [32] Y. Goto, L. J. Calciano, A. L. Fink, Acid-induced folding of proteins, *Proceedings of the National Academy of Sciences*, 1990, 87(2): 573–577.
- [33] M. Schmidt (Ed.), *Polyelectrolytes with defined molecular architecture II* (Google eBook) (p. 231), Springer: Heidelberg, 2004.
- [34] M. R. Bohmer, O. A. Evers, J. M. H. M. Scheutjens, Weak polyelectrolytes between two surfaces: Adsorption and stabilization, *Macromolecules*, 1990, 23(8): 2288–2301.
- [35] G. M. Cooper, *The cell: A molecular approach* (2nd ed.), Sunderland, MA: Sinauer Associates, 2000.
- [36] E. G. Bellomo, M. D. Wyrsta, L. Pakstis, D. J. Pochan, T. J. Deming, Stimuli-responsive polypeptide vesicles by conformation-specific assembly, *Nature Materials*, 2004, 3(4): 244–248.
- [37] S. K. De, N. R. Aluru, B. Johnson, W. C. Crone, D. J. Beebe, J. Moore, Equilibrium swelling and kinetics of pH-responsive hydrogels: Models, experiments, and simulations, *Journal of Microelectromechanical Systems*, 2002, 11(5): 544–555.
- [38] R. M. Sawant, J. P. Hurley, S. Salmaso, A. Kale, E. Tolcheva, T. S. Levchenko, V. P. Torchilin, "SMART" drug delivery systems: Double-targeted pH-responsive pharmaceutical nanocarriers, *Bioconjugate Chemistry*, 2006, 17(4): 943–949.
- [39] R. H. Kaul (Ed.), *Aqueous two-phase systems: Methods and protocols*, New York: Humana Press, 2000.
- [40] J. W. Cahn, On spinodal decomposition, *Acta Metallurgica*, 1961, 9(9): 795–801.

- [41] G. Charlet, G. Delmas, Thermodynamic properties of polyolefin solutions at high temperature: 1. Lower critical solubility temperatures of polyethylene, polypropylene and ethylene-propylene copolymers in hydrocarbon solvents, *Polymer*, 1981, 22(9): 1181–1189.
- [42] N. T. Southall, K. A. Dill, A. D. J. Haymet, A view of the hydrophobic effect, *The Journal of Physical Chemistry B*, 2002, 106(3): 521–533.
- [43] K. Kita-Tokarczyk, J. Grumelard, T. Haefele, W. Meier, Block copolymer Vesicles-Using concepts from polymer chemistry to mimic biomembranes, *Polymer*, 2005, 46(11): 3540–3563.
- [44] A. Shavit, R. A. Riggleman, Influence of backbone rigidity on nanoscale confinement effects in model glass-forming polymers, *Macromolecules*, 2013, 46(12): 5044–5052.
- [45] H. Aranda-Espinoza, H. Bermudez, F. S. Bates, D. E. Discher, Electromechanical limits of polymersomes, *Physical Review Letters*, 2001, 87(20): 208301.
- [46] M. B. Yatvin, J. N. Weinstein, W. H. Dennis, R. Blumenthal, Design of liposomes for enhanced local release of drugs by hyperthermia, *Science*, 1978, 202(4374): 1290–1293.
- [47] J. N. Weinstein, R. L. Magin, M. B. Yatvin, D. S. Zaharko, Liposomes and local hyperthermia-selective delivery of methotrexate to heated tumors, *Science*, 1979, 204(4389): 188–191.
- [48] G. Kong, G. Anyarambhatla, W.P. Petros, R.D. Braun, O.M. Colvin, D. Needham, M.W. Dewhirst, Efficacy of liposomes and hyperthermia in a human tumor xenograft model: Importance of triggered drug release, *Cancer Research*, 2000, 60(24): 6950–6957.
- [49] M. de Smet, E. Heijman, S. Langereis, N. M. Hijnen, H. Grüll, Magnetic resonance imaging of high intensity focused ultrasound mediated drug delivery from temperature-sensitive liposomes: An in vivo proof-of-concept study, *Journal of Controlled Release*, 2011, 150(1): 102–110.
- [50] A. D. Bangham, R. W. Horne, Negative staining of phospholipids and their structural modifications by surface active agents as observed in electron microscope, *Journal of Molecular Biology*, 1964, 8(5): 660–668.
- [51] E. Evans, D. Needham, Physical-properties of surfactant bilayer-membranes-thermal transitions, elasticity, rigidity, cohesion, and colloidal interactions, *Journal of Physical Chemistry B*, 1987, 91(16): 4219–4228.
- [52] M. A. Ward, T. K. Georgiou, Thermoresponsive polymers for biomedical applications, *Polymers*, 2011, 3(3): 1215–1242.
- [53] Y. Zhang, N. Kohler, M. Zhang, Surface modification of superparamagnetic magnetite nanoparticles and their intracellular uptake, *Biomaterials*, 2002, 23(7): 1553–1561.

- [54] P. A. Voltairas, D. I. Fotiadis, L. K. Michalis, Hydrodynamics of magnetic drug targeting, *Journal of Biomechanics*, 2002, 35(6): 813–821.
- [55] J. Gittleman, B. Abeles, S. Bozowski, Superparamagnetism and relaxation effects in granular Ni-SiO<sub>2</sub> and Ni-Al<sub>2</sub>O<sub>3</sub> films, *Physical Review B*, 1974, 9(9): 3891–3897.
- [56] A. Aharoni, *Introduction to the theory of ferromagnetism*, Oxford: Oxford University Press, 2000.
- [57] K. Kataoka, C. Scholz, N. Rapoport, Physical stimuli-responsive polymeric micelles for anti-cancer drug delivery, *Progress in Polymer Science*, 2007, 32(8): 962–990.
- [58] A. Senyei, K. Widder, G. Czerlinski, Magnetic guidance of drug-carrying microspheres, *Journal of Applied Physics*, 1978, 49(6): 3578–3583.
- [59] G. P. Hatch, R. E. Stelter, Magnetic design considerations for devices and particles used for biological high-gradient magnetic separation (HGMS) systems, *Journal of Magnetism and Magnetic Materials*, 2001, 225(1): 262–276.
- [60] S. Gómez-Lopera, R. Plaza, A. Delgado, Synthesis and characterization of spherical magnetite/biodegradable polymer composite particles, *Journal of Colloid and Interface Science*, 2001, 240(1): 40–47.
- [61] L. Li, D. Chen, Y. Zhang, Z. Deng, X. Ren, X. Meng, F. Tang, J. Ren, L. Zhang, Magnetic and fluorescent multifunctional chitosan nanoparticles as a smart drug delivery system, *Nanotechnology*, 2007, 18(40): 405102.
- [62] M. Mitsumori, M. Hiraoka, T. Shibata, Y. Okuno, Y. Nagata, Y. Nishimura, Targeted hyperthermia using dextran magnetite complex: A new treatment modality for liver tumors, *Hepato-gastroenterology*, 1996, 43(12): 1431–1437.
- [63] C. X. Deng, F. Sieling, H. Pan, J. Cui, Ultrasound-induced cell membrane porosity, *Ultrasound in Medicine & Biology*, 2004, 30(4): 519–526.
- [64] H. Pan, Y. Zhou, F. Sieling, J. Shi, J. Cui, C. Deng, Sonoporation of cells for drug and gene delivery, In *Proceedings of the Annual International Conference of the IEEE Engineering in Medicine and Biology Society*. 2004, 5: 3531–3534.
- [65] P. Zhang, T. Porter, An in vitro study of a phase-shift nanoemulsion: A potential nucleation agent for bubble-enhanced HIFU tumor ablation, *Ultrasound in Medicine & Biology*, 2010, 36 (11): 1856–1866.
- [66] E. C. Pua, P. Zhong, Ultrasound-mediated drug delivery, *IEEE Engineering in Medicine and Biology*, 2009, 28(1): 64–75.
- [67] J. Du, R. K. O'Reilly, Advances and challenges in smart and functional polymer vesicles, *Soft Matter*, 2009, 5 (19): 3544–3550.
- [68] G. Bajic, L. Yatime, R. B. Sim, T. Vorup-Jensen, G. R. Andersen, Structural insight on the recognition of surface-bound opsonins by the integrin I domain of complement

- receptor 3, *Proceedings of the National Academy of Sciences of the United States of America*, 2013, 110(41): 16426-16431.
- [69] S. R. Sirsi, M. A. Borden, Microbubble compositions, properties and biomedical applications, *Bubble Science Engineering and Technology*, 2012, 1(1-2): 3-17.
- [70] E. Y. Lukianova-Hleb, X. Ren, J. A. Zasadzinski, X. Wu, D. O. Lapotko, Plasmonic nanobubbles enhance efficacy and selectivity of chemotherapy against drugresistant cancer cells, *Advanced Materials*, 2012, 24(28): 3831-3837.
- [71] S. D. Tiukinhoy-Laing, S. Huang, M. Klegerman, C. K. Holland, D. D. McPherson, Ultrasound-facilitated thrombolysis using tissue-plasminogen activator-loaded echogenic liposomes, *Thrombosis Research*, 2007, 119(6): 777-784.
- [72] A. Mueller, B. Bondurant, D. F. O'Brien, Visible-light-stimulated destabilization of PEG-liposomes, *Macromolecules*, 2000, 33(13): 4799-4804.
- [73] S. Oh, K. S. Moon, J. H. Moon, J. M. Bae, S. Jin, Visible light irradiation-mediated drug elution activity of nitrogen-doped TiO<sub>2</sub> nanotubes, *Journal of Nanomaterials*, 2013, 2013: 802318.
- [74] H. F. Zhuang, C. J. Lin, Y. K. Lai, L. Sun., J. Li, Some critical structure factors of titanium oxide nanotube array in its photocatalytic activity, *Environmental Science & Technology*, 2007, 41(13): 4735-4740.
- [75] M. Paulose, K. Shankar, S. Yoriya, H. E. Prakasam, O. K. Varghese, G. K. Mor, T. A. Latempa, A. Fitzgerald, C. A. Grimes, Anodic growth of highly ordered TiO<sub>2</sub> nanotube arrays to 134 $\mu$ m in length, *Journal of Physical Chemistry B*, 2006, 110(33): 16179-16184.
- [76] Y. K. Lai, J. Y. Huang, H. F. Zhang, V. P. Subramaniam, Y. X. Tang, D. G. Gong, L. Sundar, L. Sun., Z. Chen, C. J. Lin, Nitrogen-doped TiO<sub>2</sub> nanotube array films with enhanced photocatalytic activity under various light sources, *Journal of Hazardous Materials*, 2010, 184(1-3): 855-863.
- [77] M. D. Ye, J. J. Gong, Y. K. Lai, C. J. Lin, Z. Q. Lin, High-Efficiency Photoelectrocatalytic Hydrogen Generation Enabled by Palladium Quantum Dots-Sensitized TiO<sub>2</sub> Nanotube Arrays, *Journal of the American Chemical Society*, 2012, 134(38): 15720-15723.
- [78] M. Biggerelle, K. Anselme, B. Noel, I. Ruderman, P. Hardouin, A. Iost, Improvement in the morphology of Ti-based surfaces: A new process to increase in vitro human osteoblast response, *Biomaterials*, 2002, 23(7): 1563-1577.
- [79] Y. K. Lai, L. X. Lin, F. Pan, J. Y. Huang, R. Song, Y. X. Huang, C. J. Lin, H. Fuchs, L. F. Chi, Bioinspired Patterning with Extreme Wettability Contrast on TiO<sub>2</sub> Nanotube Array Surface: A Versatile Platform for Biomedical Applications, *Small*, 2013, 9(17): 2945-2953.

- [80] C. G. Galbraith, M. P. Sheetz, Forces on adhesive contacts affect cell function, *Current Opinion in Cell Biology*, 1998, 10(5): 566–571.
- [81] A. Ghicov, P. Schmuki, Self-ordering electrochemistry: A review on growth and functionality of TiO<sub>2</sub> nanotubes and other self-aligned MO<sub>x</sub> structures, *Chemical Communication*, 2009, 20(32): 2791–2808.
- [82] D. Losic, M. S. Aw, A. Santos, K. Gulati, M. Bariana, Titania nanotube arrays for local drug delivery: Recent advances and perspectives, *Expert Opinion on Drug Delivery*, 2015, 12(1): 103–127.
- [83] K. S. Moon, J. M. Bae, S. Jin, S. Oh. Infrared-Mediated Drug Elution Activity of Gold Nanorod-Grafted TiO<sub>2</sub> Nanotubes, *Journal of Nanomaterials*, 2014, 2014: 750813.
- [84] W. Brown, Thermal fluctuations of a single-domain particle. *Physical Review*, 1963, 130(5): 1677–1686.
- [85] P. Shum, J. M. Kim, D. H. Thompson, Phototriggering of liposomal drug delivery systems. *Advanced Drug Delivery Reviews*, 2001, 53(3): 273–284.
- [86] K. A. K. Musa, L. A. Eriksson, Photodegradation mechanism of the common nonsteroid anti-inflammatory drug diclofenac and its carbazole photoproduct. *Physical Chemistry Chemical Physics*, 2009, 11(22): 4601–4610.
- [87] E. Gultepe, D. Nagesha, S. Sridhar, M. Amiji, Nanoporous inorganic membranes or coatings for sustained drug delivery in implantable devices, *Advanced Drug Delivery*, 2010, 62(3): 305–315.
- [88] K. E. Orosz, S. Gupta, M. Hassink, M. Abdel-Rahman, L. Moldovan, F. H. Davidorf, N. I. Moldovan, Delivery of antiangiogenic and antioxidant drugs of ophthalmic interest through a nanoporous inorganic filter, *Molecule Vision*, 2004, 10(68): 555–565.
- [89] M. S. Aw, M. Kurian, D. Losic, Non-eroding drug-releasing implants with ordered nanoporous and nanotubular structures: Concepts for controlling drug release, *Biomaterials Science*, 2014, 2: 10–34.
- [90] A. Santos, M. S. Aw, M. Bariana, T. Kumeria, Y. Wang, D. Losic. Drug-releasing implants: Current progress, challenges and perspectives, *Journal of Materials Chemistry B*, 2014, 2: 6157–6182.
- [91] G. Jeon, S. Y. Yang, J. Byun, J. K. Kim, Electrically actuatable smart nanoporous membrane for pulsatile drug release, *Nano Letter*, 2011, 11(3): 1284–1288.
- [92] D. Losic, S. Simovic, Self-ordered nanopore and nanotube platforms for drug delivery applications, *Expert Opinion on Drug Delivery*, 2009, 6(12):1363–1381.
- [93] M. S. Aw, S. Simovic, J. Addai-Mensah, D. Losic, Polymeric micelles in porous and nanotubular implants as a new system for extended delivery of poorly soluble drugs, *Journal of Materials Chemistry*, 2011, 21 (20): 7082–7089.

- [94] M. S. Aw, K. Gulati, D. Losic, Controlling drug release from titania nanotube arrays using polymer nanocarriers and biopolymer coating, *Journal of Biomaterials & Nanobiotechnology*, 2011, 2(5): 477–484.
- [95] M. Bariana, M. S. Aw, E. Moore, N. H. Voelcker and D. Losic, Radiofrequency-triggered release for on-demand delivery of therapeutics from titania nanotube drug-eluting implants, *Nanomedicine*, 2014, 9(8): 1263–1275.
- [96] M. S. Aw, J. Addai-Mensah and D. Losic, Magnetic-responsive delivery of drug-carriers using titania nanotube arrays, *Journal of Materials Chemistry*, 2012, 22(14): 6561–6563.
- [97] D. Shenoy, S. Little, R. Langer, M. Amiji, Poly(ethylene oxide)-modified poly(beta-amino ester) nanoparticles as a pH-sensitive system for tumor-targeted delivery of hydrophobic drugs: Part 2. In vivo distribution and tumor localization studies. *Pharmaceutical Research*, 2005, 22(12): 2107–2114.
- [98] J. van der Zee, Heating the patient: A promising approach? *Annals of Oncology*, 2002, 13(8): 1173–1184.
- [99] S. Mitragotri, Healing sound: The use of ultrasound in drug delivery and other therapeutic applications, *Nature Reviews Drug Discovery*, 2005, 4(3): 255–260.
- [100] A. V. Kabanov, E. V. Batrakova, V. Y. Alakhov, Pluronic block copolymers for overcoming drug resistance in cancer, *Advanced Drug Delivery Reviews*, 2002, 54(5): 759–779.
- [101] Z. G. Gao, H. D. Fain, N. Rapoport, Controlled and targeted tumor chemotherapy by micellar-encapsulated drug and ultrasound. *Journal of Controlled Release*, 2005, 102(1): 203–222.
- [102] A. T. Nguyen, S. P. Wrenn, Acoustically active liposome-nanobubble complexes for enhanced ultrasonic imaging and ultrasound-triggered drug delivery. *Wiley Interdisciplinary Reviews in Nanomedicine and Nanobiotechnology*, 2014, 6(3): 316–325.
- [103] Y. H. Lee, G. Bhattarai, I. S. Park, G. R. Kim, G. E. Kim, M. H. Lee, H. K. Yi, Bone regeneration around N-acetyl cysteine-loaded nanotube titanium dental implant in rat mandible, *Biomaterials*, 2013, 34(38): 10199–10208.
- [104] M. S. Aw, J. Addai-Mensah, D. Losic, A multi-drug delivery system with sequential release using titania nanotube arrays, *Chemical Communications*, 2012, 48(27): 3348–3350.

---

# Active-targeted Nanotherapy as Smart Cancer Treatment

---

Katayoun Derakhshandeh and Abbas Hemmati Azandaryani

Additional information is available at the end of the chapter

<http://dx.doi.org/10.5772/61791>

---

## Abstract

Drug delivery systems (DDS) can be designed to improve the pharmacological and therapeutic properties of drugs. Targeted drug delivery, sometimes called smart drug delivery, is a method of delivering medication to a patient in a manner that increases the concentration of the medication in infective organs or cells, relative to others. Cancer is one of the major causes of mortality worldwide and innovative methods for cancer therapy are urgently required. Nanoparticles (NPs), by using active targeting strategy, can enhance the intracellular concentration of drugs in cancerous cells while avoiding toxicity in normal cells. Nanoparticles with bioscience are being actively developed for in vivo tumor imaging, bimolecular profiling of cancer biomarkers, and targeted drug delivery. The advantages of the targeted release system are the reduction in the frequency of dosages taken by the patient, having a uniform effect of the drug, reduction of drug side effects, and reduced fluctuation in circulating drug levels. In this chapter, we focus on targeted drug delivery systems integrated from nanobiotechnology.

**Keywords:** Targeted drug delivery, Nanobiotechnology, Nanocarrier, Active targeting, Cancer therapy

---

## 1. Introduction

Currently, maximizing the safety and efficacy of drug therapy is the main goal of pharmaceutical scientists and physicians. To this end, drug targeting is the best approach. This subject is critical for some diseases such as cancer treatments, which involve a balancing act between the destruction of cancerous and healthy tissues, including damage to the immune system and highly replicating cells.

---

Newly developed nanotechnological methods as active targeting carrier in the medical treatment have increased attention [1–4].

Active targeting involves attaching different ligands such as antibodies, biological proteins, peptides, sugars, and vitamins or a specific ligand to the drug or drug delivery system, which meet and form a complex with cell receptors and cause the drug to accumulate in the target cells.

Specifically, “targeting” can be categorized into three levels:

- First-order targeting: When the delivery is to a specific organ, for example, drugs may be targeted to the liver because of its leaky or fenestrated vasculature or loose junctions; the drug is not released in other tissues because of their nonleaky vasculature.
- Second-order targeting or cellular targeting: When a drug delivery system releases the drug to a particular cell within an organ or a tissue.
- Third-order or subcellular targeting: When the delivery is to distinct cell types with biological barrier transport, for example, epithelial cells or cells of the lung-associated lymphatic tissue. A good example is the delivery of genes. The delivery system carries the gene, enters specific cells and releases the gene intracellularly. This is the third order and the most sophisticated type of targeting.

Traditional targeting activities can also be grouped into passive and active targeting [5]. Drug delivery systems that have been developed to be used as targeting carriers include micelles, nanoparticles, polymeric conjugates, and liposomes. NPs protect the drug from premature degradation, prevent drugs from interacting with the biological environment, and enhance the absorption of drugs into a selected tissue. Nanoparticle technologies may improve the therapeutic index of drugs by enhancing their efficacy and/or increasing their tolerability in the body. Nanoparticles could also improve the bioavailability of water-insoluble drugs, carry large payloads, as well as enable the development of novel classes of bioactive macromolecules (e.g., DNA and siRNA) [4–8]. Thus far, over two dozen nanotechnology products have been approved by the US Food and Drug Administration (FDA) for clinical use, and many are under clinical and preclinical development [9].

In our studies, we focused on targeted drug delivery systems integrated from nanobiotechnology. Nanoparticles, by using active targeting strategies such as folate, monoclonal antibodies (mAbs) and aptamer ligands can enhance the intracellular concentration of drugs in cancerous cells while avoiding toxicity in normal cells. Nanoparticles with bioscience are being actively developed for in vivo tumor imaging, biomolecular profiling of cancer biomarkers, and targeted drug delivery. Nanoparticles remain in the blood circulation for a longer time and can passively accumulate at target sites after the systemic administration because of leaky tumor vasculature and poorly developed lymphatic drainage (the enhanced permeation and retention (EPR) effect).

In this chapter, we focus on explaining anticancer agents loaded in different nanoparticles and how they could be targeted to different tissues especially to solid tumors by attaching specific ligands [6–8].

## 2. Nano drug delivery

Drug delivery systems such as lipid-, polymer-, liposome-, dendrimeric-, or biomacromolecule-based nanoparticles can be designed to improve the pharmacological and therapeutic properties of drugs administered parenterally or by other routes of administration. There are considerable interests in exploiting the advantages of DDS for *in vivo* delivery of new drugs and for their use in targeted therapeutics. Drug targeting can improve the efficacy of therapy and reduce side effects associated with drugs and therapeutic agents [10–12]. Various carriers can be used to deliver a drug in a stable and protective form for conventional or targeted shape (Figure 1); however, it is nanotechnology that offers the most unique and intriguing approach in the field of nanomedicine.

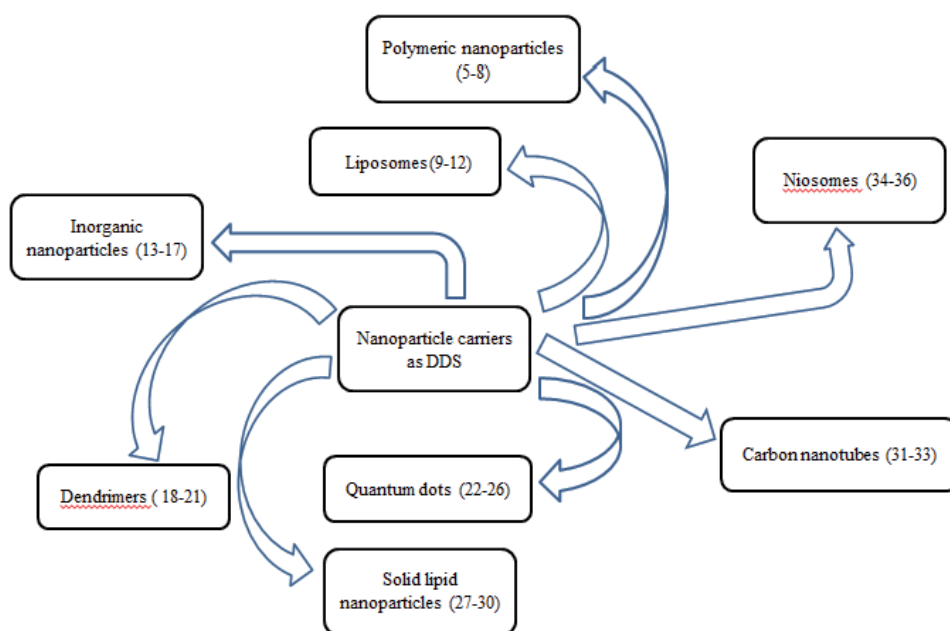


**Figure 1.** The different types of nanocarriers

Nanobiotechnology, defined as biomedical applications of nano-sized biomacromolecular systems or nano-sized materials with biomaterials, is a rapidly developing area within nanoscience. We define nanomedicines as delivery systems in the nanometer size range (preferably 1–100 nm) containing encapsulated, dispersed, adsorbed, or conjugated drugs and imaging agents. They can also facilitate the important advances in detection, diagnosis, and treatment of diseases, human cancers, vaccine delivery, etc., and have led to a new discipline of nanobiotechnology [13–16]. Nanoparticles are being actively developed for *in vivo* tumor imaging, biomolecular profiling of cancer biomarkers, and targeted drug delivery. These nanotechnology-based techniques can be applied widely in the management of different malignant diseases [17, 18].

Nanocarriers have numerous points of interest contrasted with free drugs. They protect the labile drugs from degradation in biological environments, increase uptake of the drugs into a chosen tissue such as solid tumors, facilitate modification of the pharmacokinetics and body distribution, and enhance intracellular infiltration.

Nanotechnology applications in medicine, termed as nanomedicine, have introduced a number of nanoparticles of variable chemistry and architecture in the targeted drug delivery system. Nanotechnology involves engineering multifunctional devices with dimensions on the nanoscale with similar dimensions of large biological molecules in the body, viruses, and other synthesized macromolecules. These devices can carry one or two detection signals and/or therapeutic agents for drug delivery targeting [19, 20].

Nanotechnology is well introduced in drug delivery technology for several advantages such as first passive drug delivery, increasing of drug solubility, increasing of drug half-life in the body, modification of the drug distribution pattern, and improvement of pharmacokinetics, which will result in improved efficacy. With these advantages, the future of drug delivery cannot be predicted and some problems exist such as site cytotoxicity [21–26].

Currently, the fundamental issue with cancer treatment is that they include an exercise in careful control between the destruction of malignant tissue and healthy tissues, such as damage to the immune system and profoundly replicating cells (gastrointestinal epithelia and hair follicles).

It is important to detect the revelation of malignant cells sufficiently early and in a stage that is sensible for convenient treatment. Recently, created nanotechnology drug delivery systems are promising approaches for oncologists.

The use of nanoparticles in medical treatment has increased in recent years. For example, micro- and nanoparticles, such as polymeric nanoparticles (synthetic or natural polymers), polymeric micelles, dendrimer, and solid lipid nanoparticles (SLN) have long been used as drug delivery systems to encapsulate drugs and protect them from extracellular enzymatic degradation, providing vehicles for delivering drugs to the target area, and are now being investigated as powerful platforms for vaccine delivery [27–33]. Figure 2 represents some kind of nanocarrier in drug delivery.

Being inspired by physiologically existing nanomachines, nanoparticles are designed to safely reach their target and specifically release their therapeutic agent at the site of the disease, thus increasing the drug's tissue bioavailability. Nanoparticles used in this manner for enhanced permeation and retention effect of cancerous cells that are caused by leaky angiogenetic vessels and poor lymphatic drainage has been, in turn, used to explain why macromolecules and nanoparticles are found at higher ratios in tumors compared with normal tissues [29]. Carriers are associated with the drug in a covalent or noncovalent attached mode of targeting materials, and they have been used for the delivery of drug exactly on the target tissue.

In this study, we focus on important nanoparticles such as polymeric nanoparticles and liposomes and their recent results on targeting drug delivery systems for the purpose of biomaterial.

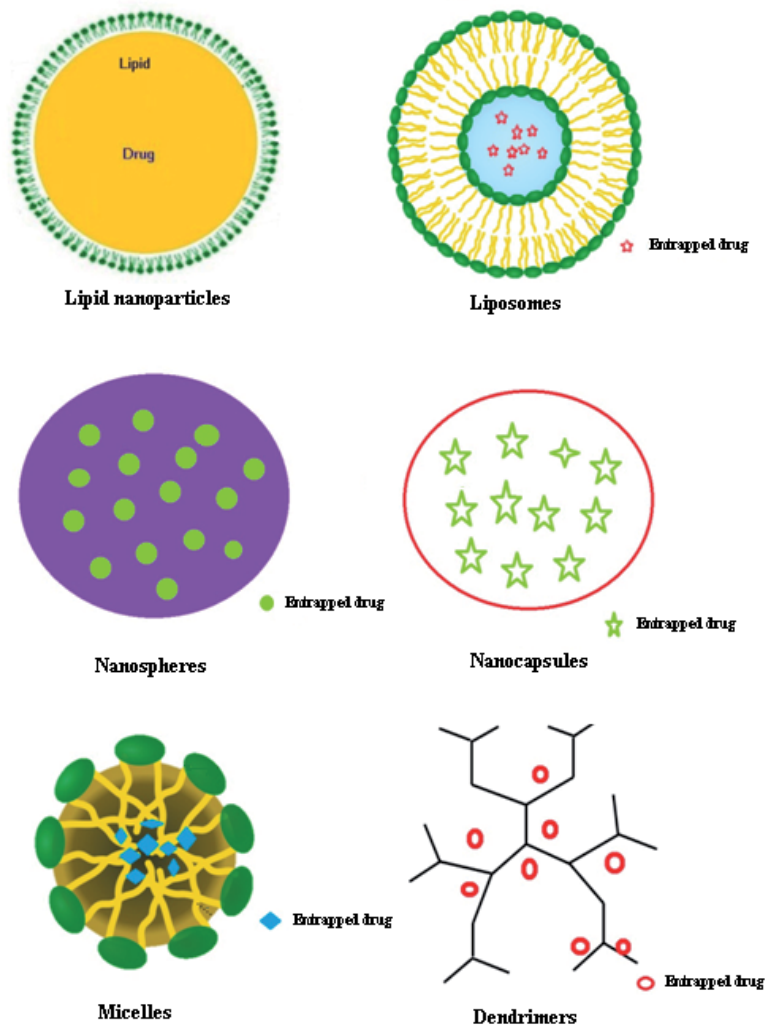


Figure 2. Basic structure of nanoparticles

### 3. Bioconjugation of nanocarriers for target therapy

The conjugation of bioagents to nanocarriers is one of the most important functions of the targeted drug delivery system. For this purpose, several methods and works have been performed until now [34–36].

One of the usual methods for attaching biomolecular ligands to nanoparticle's surface is diimide-activated amidation by direct coupling of carboxylic acid to legends using N-ethyl-N-(3-dimethyl aminopropyl) carbodiimide hydrochloride (EDAC) or N,N-dicyclohexyl

carbodiimide (DCC) as a coupling agent. The schematic perspective of the connection of proteins to carbon nanotubes (CNTs) by means of diimide-activated amidation is presented in Figure 3. Functionalization of carbon nanotubes was likewise completed using 1-pyrenebutanoic acid, succinimidyl ester for the immobilization of biomolecules, anti-fullerene IgG monoclonal antibody bound to single-wall carbon nanotubes. Proteins and DNA have also been used to modify multiwall carbon nanotubes (MWCNT) [36].

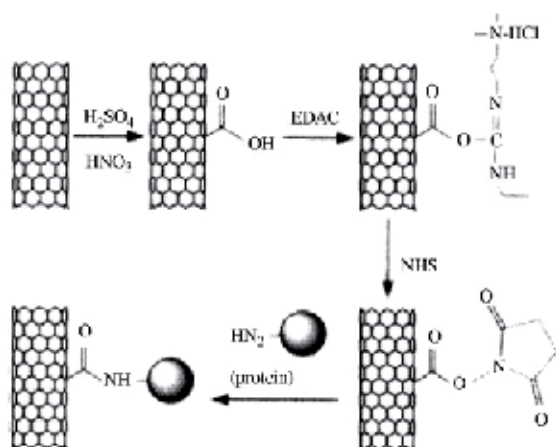


**Figure 3.** Schematic view of the attachment of proteins to CNTs via diimide activated amidation [51]

Recently, the ubiquitous alkyne–azide Huisgen “click” reaction has been used to attach proteins to NPs (Figure 4). A variety of proteins have been attached in functional form using this method, including lipase, horseradish peroxidase, and luciferase [34]. Hapuarachchige et al. [37] investigated the click reaction for specific internalization of nanotherapeutics. In this study, the pretargeting component, anti-HER2 humanized monoclonal antibody, functionalized with azide groups, labels cancer cells. This group demonstrated high efficacy for targeted nanotherapeutics using the click reaction.

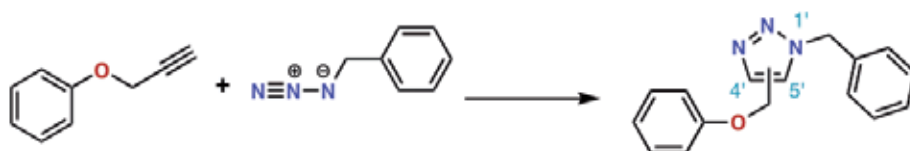


**Figure 4.** Azide–alkyne Huisgen cycloaddition “click” reaction

The biotin–streptavidin interaction (Figure 5) is widely used for the conjugation of NP systems. The formation of avidin (or streptavidin)–biotin complexes is useful in a wide variety of applications. This specific binding is largely used to immobilize enzymes, antibodies, or DNA. Biotin is a small molecule, which could bind to avidin or streptavidin binding sites with very high affinity ( $K_a = 10^{15} \text{ M}^{-1}$ ).

In addition, avidin and streptavidin are tetrameric proteins that have four known binding sites for biotin (Figure 5). Streptavidin with an isoelectric point equivalent to 5 is accordingly ideally utilized over avidin, which has a PI of 10.5, to maintain a strategic distance from nonspecific interactions [35, 38].

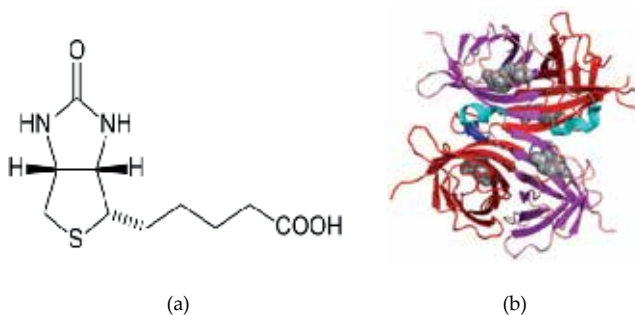


**Figure 5.** Biotin structure (a) and the simple graph for biotin–avidine binding (b)

#### 4. Active targeting using polymeric nanocarrier

Polymeric nanoparticles with specific recognition ligands bound to the surface have a good potential for site-selective delivery, and offer higher drug carrier capacity than bioconjugates, as well as improved specificity for drug targeting [1, 39–41]. The attached ligands to the surface of nanocarriers can include any molecule that specifically binds to target cells such as peptides, glycoproteins, carbohydrates and polymers, and monoclonal antibodies, which have been the most broadly studied [20, 24].

Kocbek and coworkers developed new active-targeted poly (D,L-lactic-co-glycolic acid) (PLGA) nanoparticles by attaching mAb, which have the ability to target specific antigens on breast epithelial cancer cell lines. Attempts to attach mAb to nanoparticles by covalent bonding were less successful, since the natural action of the bound mAb was inactivated. The specificity of the immunonanoparticles was shown from their selective distribution in a co-culture of MCF-10A neoT and Caco-2 cells, resulting in their final internalization by the former cells [42].

A novel, nonviral, polyethylenimine (PEI)-based, HER2-targeted gene transfer vector has been investigated. The anti-HER2 humanized antibody, trastuzumab (HerceptinR), was used as the targeting moiety to the HER2 overexpressing cancer cells. Subsequently, trastuzumab conjugation of PEI may render PEI a much more selective gene delivery carrier for anticancer gene therapy. The opinion of attaching a targeting ligand, with intrinsic antitumor activity, to a gene transfer vector may be beneficial for further investigations [43].

Recently, poly (butyl cyanoacrylate) (PBCA) NPs coated with polysorbate-80 have been proposed as suitable drug carriers for brain drug delivery. Nerve growth factor (NGF) is important for the survival of peripheral ganglion cells and central cholinergic neurons of the

basal forebrain. In spite of its inability to cross the blood–brain barrier (BBB), the NGF activity on these neuronal populaces and its adequacy in avoiding neurodegeneration recommended its potential utilization in the treatment of neurological pathologies, for example, diabetic neuropathies and Huntington’s disease. Systemic administration of NGF loaded in P80-coated PBCA NPs successfully reversed scopolamine-induced amnesia and improved recognition and memory in acute amnesia rat model [44].

Yang and coworkers synthesized doxorubicin magnetic PLGA nanoparticles conjugated with well-tailored antibodies for the detection and therapy of breast cancer. They suggested that magnetic nanocrystals embedded in polymeric nanoparticles did not inhibit the nanoparticle formulation or drug release kinetics. The multimodal nanoparticles demonstrated remarkable cancer cell affinity and ultrasensitivity via magnetic resonance imaging. However, the *in vivo* effects of the NPs were not evaluated [45].

Due to the overexpression of the folate receptor on tumor surface, the folate has been popularly used as a targeting moiety for various anticancer agents to avoid their nonspecific attacks on normal tissues and also to increase their cellular uptake within target cells [46–48]. Derakhshandeh et al. prepared the folate-decorated biodegradable PLGA nanoparticles for tumor targeting. In this study, folate-conjugated PLGA was synthesized and then PLGA-Fol nanoparticles were prepared by nanoprecipitation method, adopting PLGA as a drug carrier, folic acid (FA) as a targeting ligand, and 9-nitrocamptothecin (9-NC) as an anticancer drug model. The *in vitro* intracellular uptake of nanoparticles showed that the PLGA-Fol nanoparticles have been more efficiently taken up by MCF-7 cells compared with nonfolate-mediated carriers, and also showed greater cytotoxicity than other treated groups [49].

Active-targeted nanocarriers to the special sites and cellular uptake are especially important to therapeutics that is not taken up easily by cells, and they require facilitation by fusion, endocytosis, or other processes to access their cellular active sites. They can also enhance the penetration and distribution of nanomedicine within the tumor interstitium and resistant cancer cells. Active targeting nanocarriers have various points of interest over targeting ligand–drug conjugates [47].

Recently, Wu et al. [50] investigated polymeric nanoparticles for the treatment of metastases. This group studied the ability of micellar nanocarriers incorporating (1,2-diaminocyclohexane) platinum(II) for liver metastases of bioluminescent murine colon adenocarcinoma C-26 treatment, during overt and preangiogenic metastatic stages and thus obtained a novel approach for early diagnosis and treatment of metastases.

## 5. Inorganic nanoparticles for targeted drug delivery

Porous inorganic nanoparticles with high specific surface area have recently emerged as attractive material for the development of delivery systems, where various guest molecules could be absorbed into the pores and later released into various solutions [51, 52].

Inorganic nanoparticles, for example, gold and iron oxide, are usually conjugated with the drug, polyethylene glycol (PEG), and the targeting ligands. It gives the idea that the PEG coating and ligand design are common constituents in most types of nanoparticles for anticancer delivery. These carriers have several applications in cancer diagnosis and treatment, and large portions of them have quickly moved into clinical trials. Overall, there is still a space for optimization in the field of nanoparticle pharmacokinetics such as enhanced plasma retention time and tumor bioavailability and understanding the effectiveness of targeting ligands in the cancer treatment. The need to add to a novel and productive ligand has never been more noteworthy, and the use of proper conjugation chemistry is essential [20].

Recently, Zhou et al. prepared a surface engineered of NaGd F<sub>4</sub>:Ce/Tb hybrid nanoparticles with DNA for new type of pH-responsive therapeutic platform to enhance the therapeutic efficiency while minimizing side effects. The introduction of the layer of aptamer molecule on the surface facilitated the cellular uptake of the resulting nanocomposite into specific target cells via receptor-mediated endocytosis. This group proved that the hybrid nanocarrier may serve as a practical and multifunctional probe for cancer therapy [53].

## 6. Liposomes in targeting drug delivery

Dispersion of neutral phospholipids or amphiphilic lipids (i.e., cholesterol, glycolipids) in the aqueous solution leads to the formation of closed vesicular structures, which morphologically resemble cells. These closed vesicles have been called "Liposomes" [54] (fat bodies) and consist of hydrated bilayers. Liposomes not only have the ability to mimic structures of cell membranes but also have the potential either to encapsulate hydrophilic materials in the inner liposome water phase or to associate the lipophilic materials within the lipid bilayer region. Initial studies on the fate of liposomes and entrapped agents started in 1970 [55].

Liposomes were recommended as drug carriers in cancer chemotherapy by Gregoriadis in 1974 and later the interest in liposomes has increased and is currently being widely concentrated on as drug carriers. Three fundamental requirements need to be met if liposomes are to be fruitful in drug delivery, specifically to cancerous tissues: (i) prolonged blood circulation, (ii) adequate tumor accumulation, and (iii) controlled drug release and uptake by tumor cells with a release profile coordinating the pharmacodynamics of the drug [56–60].

Stealth liposomes are suggested to carry the drug in the aqueous core, and they are usually decorated by recognition molecules, being widely studied and applied [61]. The poor outcome of current therapies continuously stimulates the search for new treatment strategies. This includes the activation of the normal vasculature to form tumor blood vessels and the involvement of immune response elements in tumor development proliferation. The hindrance of these procedures introduces an attractive therapeutic strategy and a new class of anticancer therapeutics such as angiogenesis inhibitors and anti-inflammatory drugs [62].

Tumor-associated inflammation has been perceived as an important tumor growth propagator and, therefore, represents an attractive target for anticancer therapy. Glucocorticoids (GCs), a

potent class of anti-inflammatory drugs, showed antitumor effects at high daily doses. Unfortunately, this dose leads to severe side effects, including morbidity and mortality, attributable to severe immunosuppression. Recently, researchers have improved this unfavorable therapeutic index using long circulating liposomes as the glucocorticoid delivery nanocarrier. This vehicle could strongly inhibit tumor growth, after administration of a single weekly dose [63].

The effectiveness of the liposomal formulation was attributed to modification in drug pharmacokinetics such as increased blood circulation and glucocorticoid accumulation in the tumor, and the so-called enhanced permeability and retention effect.

Inspired by recent findings, in the tumor microenvironment, a main mechanism of the antitumor activity of GC is the inhibition of macrophage activity and downregulation of pro-angiogenic factors, which are produced by functional tumor-associated macrophages. In addition, *in vitro* information proposed a direct cytotoxic and antiproliferative activity to both endothelial and tumor cells [64].

Kluza et al. developed paramagnetic and fluorescent liposomes, encapsulating prednisolone phosphate, to evaluate its antitumor activity and therapeutic response. In this study, cytotoxicity of the new multifunctional liposomes (120 nm diameter) was tested in B16F10 melanoma subcutaneously (20 mg/kg/week) inoculated in C57BL/6 mice and compared with the free drug formulation. It was significantly found to inhibit tumor growth compared with nontreated mice and similarly to free form [63].

PEGylated liposomal doxorubicin (DOX) is approved for the treatment of refractory ovarian cancer and Kaposi sarcoma in the United States. In this carrier, the efficacy of the drug was preserved and a cardiac toxic effect was significantly decreased [18].

Albumin nanoparticle-bound paclitaxel, is also approved in the United States for the treatment of metastatic breast cancer, has greater efficacy compared with the conventional castor oil-based formulation and has lesser side effects [18].

Liposomes can also be used as a nonviral vector to deliver siRNA to target cells for gene therapy. Mokhtarieh and his coworkers developed a novel method of producing asymmetric liposome particles (ALPs) with highly efficient siRNA encapsulation. In their work, liposomes were prepared by the solvent evaporation and dialysis method, composed of ionizable cationic 1,2-dioleoyl-3-dimethyl ammonium-propane and 1,2-dioleoyl-sn-glycero-3-phosphoethanolamine (DOPE), which entrap siRNA, and the outer one is composed of 1,2-distearoyl-sn-glycero-3-phosphocholine, DOPE, polyethylene glycol-1,2-distearoyl-sn-glycero-3-phosphatidyl ethanolamine (PEG-PE), and cholesterol. Ninety percent of siRNA was entrapped in negatively charged surface liposomes. The surface-modified ALPs with a polyarginine peptide (R12) induced nonspecific cell penetration, while naked liposome has almost no uptake into cells. The modification of ALP's surface by the antihuman epidermal growth factor receptor antibody (anti-EGFR) induces an EGFR-mediated uptake into the nonsmall cell lung cancer cell lines and did not take up NIH-3T3 cell line without the receptor [65].

The triggered release of pH-sensitive liposomes is probably the most biocompatible method for releasing drugs directly in the cytoplasm of cells. When liposomes are internalized to endosomes, they enter an acidic environment. Reddy and Low prepared the pH-sensitive lipid formulation from DOPE and citraconic anhydride and used them to prepare liposomes. They observed that the resulting liposomes were stable at neutral pH but fusogenic at pH 5 [66]. Figure 6 shows the schematic diagram of the liposome in targeted drug delivery.

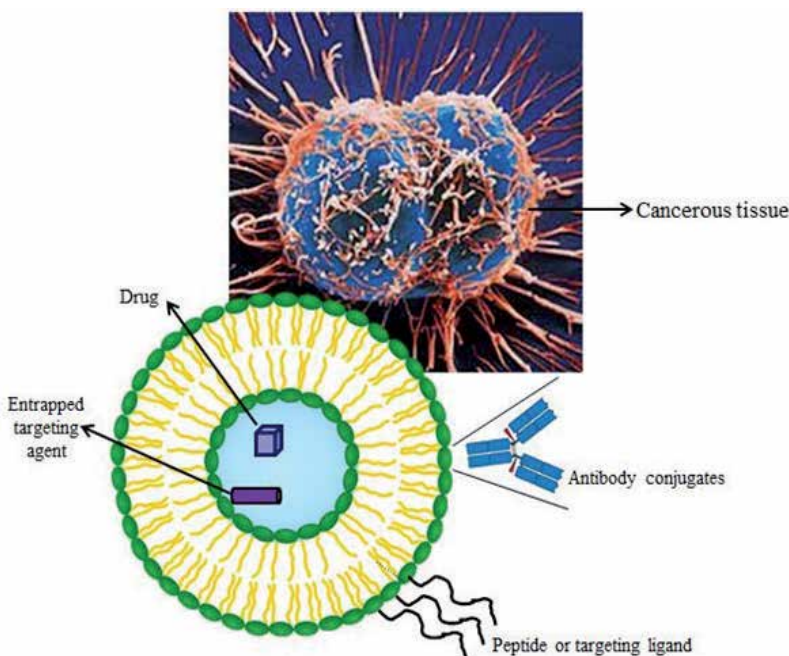


**Figure 6.** Liposome in target drug delivery

Choi and coworkers synthesized an amphiphilic DNA hybrid duplex by using Watson–Crick base pairing and DNA bioconjugation with cholesterol or tLyp-1 tumor-homing peptide. The resultant amphiphilic DNA hybrid duplexes can self-assemble in an aqueous solution into nanoliposome with the outer ligand of tLyp-1 peptides. This nanocarrier can efficiently entrap doxorubicin and also has the pH-dependent structure, which can release the drug in the acidic environment of cytosol of tumor cells [67]. These results provide an alternative approach to specifically deliver doxorubicin into targeted cells for cancer therapy as well as controlling drug release under acidic conditions such as endosomes or lysosomes.

Chiang et al. investigated the combination of polymer and liposome in carrier preparation. This group prepared pH-responsive polymer–liposome for intracellular drug transfer and targeted cancer therapy. From this work, it was obvious that the combination of carrier should be a promising for targeted drug delivery in the future, exactly when this new carrier combines with biotechnology.

## 7. Solid lipid nanoparticles as a targeted drug delivery system

In the late 1990s, SLNs were proposed for brain drug targeting application independently by two research groups, although the first proof of lipid particle transport across the BBB had already been provided. SLNs are colloidal carrier systems, which provide controlled-release profiles for many substances [68–72]. Kashanian et al. prepared aqueous dispersions of lipid nanoparticles using a modified, pH-sensitive derivative of phosphatidyl ethanolamine loaded with triamcinolone acetonide as a drug. The SLNs prepared in this study were able to control the release of drug under acidic conditions. This group showed that with increasing pH, the amount of releasing drug is increased due to the burst effect in this condition as well [30].

Studying the pharmacokinetics of two anticancer agents, namely camptothecin and doxorubicin, drug accumulation in the brain was observed after both oral and i.v. administration when loaded into SLN. As previously shown in PACA NPs, better results in brain targeting were achieved when SLN surface characteristics were modified by means of PEG derivatives or PEG-containing surfactants [73].

## 8. Gold nanoparticles in target drug delivery

Bactericidal efficacy of gold nanoparticles (GNPs) conjugated with ampicillin, streptomycin, and kanamycin was evaluated. Gold nanoparticles were conjugated with the antibiotics and drugs during the synthesis of nanoparticle utilization [74–76], by functionalizing gold particles, where amino acids, glutathione, polyethylene glycol, etc. were used as linkers [77–79]. The conjugated gold nanoparticles showed greater antibacterial effects and lower MIC compared with the free drug in three bacterial strains, *Escherichia coli* DH5a, *Micrococcus luteus*, and *Staphylococcus aureus*. In addition, nanoconjugate could increase their heat stability [80,81].

Bergen and coworkers prepared nanoparticle formulations of GNPs with varying particle size, surface charge, and surface hydrophilicity. In this study, the galactose attached to the surface of NPs by conjugation of PEG-thiol and galactose-PEG-thiol to gold colloids. This platform was applied to screen for NP formulations that demonstrate hepatocyte-targeted delivery in vivo. This group investigated that the presence of galactose ligands was found to significantly affect the targeting efficiency [82].

## 9. Niosomes

Nonionic surfactant vesicles (niosomes), are biodegradable, relatively nontoxic, more stable, and inexpensive, and therefore could be an alternative to liposomes [83]. Due to the encapsulation of a wide range of toxic drugs such as antiviral, anticancer, and anti-AIDS drugs in niosomes, this carrier is so valuable in the delivery of proteins and biological medications. Niosome is a promising carrier system in comparison with ionic drug carriers, which are relatively toxic and moderately harmful [84].

Bragagni and coworkers developed a stable and safe niosomal formulation to effectively encapsulate DOX. The developed formulation, in virtue of its relatively high efficiency of drug encapsulation and good stability, could find useful applications as an effective tool for achieving DOX brain delivery, exploiting the brain uptake properties of the glucose-targeted vesicles [85].

Preliminary *in vivo* studies involved the *i.v.* administration of a single dose of the developed niosome formulation with respect to the target tissue. This formulation gave rise to stable and nano-sized vesicles, which are able to improve doxorubicin brain delivery. Positive results of preliminary *in vivo* studies require future pharmacokinetic studies to gain more insight into the mechanism of drug transport of functionalized niosomes [86].

## 10. Quantum dots

Quantum dots (QDs), semiconductor fluorescent nanoparticles, ranging from 2 to 10 nm in size has a core of hundreds to thousands of atoms of group II and VI elements (e.g., cadmium, technetium, zinc, and selenide) or group III (e.g., tantalum) and V elements (e.g., indium). This carrier with a cadmium selenide core and a zinc sulfide shell, by a coating of an amphiphilic polymer, is ordinarily utilized for drug delivery systems [87]. QDs greatly expand the possibilities for fluorescence imaging of cells and living animals [88].

QDs have been conjugated to antibodies, allowing for simultaneous labeling and accurate quantification of these target proteins in one target section. Direct conjugation of targeted antibodies to the surface of QDs in a molar ration of four to ten, without the use of secondary antibodies, might be the best approach to achieve multiplex detection of molecular targets.

QDs can be bioconjugated to either the 3' or 5' end of an oligo sequence. Xiao and Barker have discussed the ability to control the number of attached oligonucleotides by the use of a streptavidin–biotin quantum dot system [89].

This bioconjugate has a high affinity to target cells and causes minimum nonspecific binding to normal cells. The quantum dot-based assay was developed that could quantitatively detect the estrogen receptor, progesterone receptor, and ERBB2 (e.g., MCF-7, BT474, and MDA-231 cells) in paraffin-embedded human breast cancer cells [90]. These cell lines were overexpressed by these receptors and were stained simultaneously with multiple quantum dots, which were directly bioconjugated to targeting antibodies for these three proteins [91].

Biotinylated DNA probes for labeled cells by streptavidin-coated quantum dots could identify of ERBB2, even at low levels of expression. This information recommends that the use of quantum dot-labeled oligonucleotides for detecting gene amplification especially at low levels of expression may offer points of interest over the standard fluorescence *in situ* hybridization (FISH) method [91].

## 11. Targeting drug delivery with magnetic nanoparticles

Magnetic nanoparticles (MNPs) offer several advantages when used as a drug carrier, including the large surface area, which can be properly modified to attach to drug molecules. Magnetic NPs can also be used with other carriers for drug delivery. Ensuring biocompatibility and nontoxicity, iron oxide-based particles (magnetite) with superparamagnetic characteristics are commonly used as magnetically responsive components, which can be manipulated by an external magnetic field gradient. Based on these properties, the superparamagnetic nanoparticles could be transported through the vascular system, concentrated in a specific part of the body with the aid of a magnetic field, and used as a carrier [92–94].

Iron oxide nanoparticles have found applications in the so-called magnetic drug targeting. Iron oxide nanoparticles in an external magnetic field are able to deliver particles to the desired target area [95, 96] and fix them there while the drug is released to exert a local effect [97]. Although magnetic targeting has been evaluated for a number of tumor-targeting studies, the most recent work is related to brain cancer.

It has been demonstrated that the release of drugs from magnetoliposomes could be controlled by an alternative current magnetic heating [98]. Although magnetoliposomes could be specifically heated to 42°C, the heating was mostly limited inside the thin lipid bi-layers [99].

Hsu and Su developed magnetic lipid nanoparticles with sizes ranging from 5 to 25 nm, composed of multiple drugs controlling their release in a desired pattern. The lipid matrices are solid at body temperature and melt around 45–55°C. In this study, the dissipated magnetic heat liquefied the encompassing lipid networks and resulted in an accelerated release of the encapsulated drugs.

Three accomplishments resulted: (1) Preparation of magnetic lipid nanoparticles with co-encapsulated drugs and heating components; (2) conjugation of surface-modified  $\gamma\text{-Fe}_2\text{O}_3$  particles that can be remotely energized to activate the heating and rapid drug release; and (3) designing a new nanocarrier, which can accomplish localized heating and pulsative release [99].

Zhu et al. prepared the chitosan-coated magnetic nanoparticles (CS MNPs) as carriers of 5-fluorouracil (CS–5-FuMNPs) through a reverse microemulsion method. It was found that the synthesized CS–5-Fu MNPs were spherical in shape with an average size of  $100 \pm 20$  nm, low aggregation, and good magnetic responsiveness. The result of CS–5-Fu MNPs cytotoxicity on K562 cancer cells showed that the nanoparticles have significant antitumor activities, and FITC-labeled nanoparticles could effectively enter into the cancer cells and induce cell apoptosis [74].

Gollavelli and Ling [75] investigated a novel magnetic and fluorescent graphene nanoparticles with a simple noncovalent approach. In this work, a hydrophobic silicon naphthalocyanine bis (trihexylsilyloxy) (SiNc4) photosensitizer was adopted to immobilizing onto water-dispersible magnetic and fluorescent graphene (MFG) via  $\pi$ - $\pi$  stacking to yield MFGeSiNc4 functioned as a theranostic nanocarrier. The developed MFGeSiNc4 may thus be utilized as a potential theranostic nanocarrier for phototherapy of cancer cells with a single light source for less time-consuming and cost-effective treatments with a minimal therapy dose.

## 12. Targeted delivery for vaccine

The unique properties of nanoparticles, which can be altered by planned application, make excellent approaches for immunization and treatment of different diseases. The use of nanoparticles as vaccine adjuvants and carriers has opened up an entire new field of research. Different materials in the viral (20–200 nm) or bacterial (200–5000 nm) size ranges introduced in vaccine formulations with a stable half-life prevent enzymatic degradation of antigen and increase antigen uptake by specifically targeting specialist antigen-presenting cells (APCs) [76,100]. Some nanoparticle-based vaccines are designed to include ligands that can target APC and hence help trigger immune responses. Some possess internal adjuvants, triggering toll-like receptor (TLR) ligation and local danger signals to potentiate the effective antigen presentation to T cells.

Different designs and compositions of nanoparticle-based vaccines allow for specific tailoring of antigen delivery to the target cell type or specific tissue. In addition, the size of the particles plays a major role in the mechanism of particle uptake by APCs, influencing the type of the resulting immune response [100].

More recently a synthetic nanoparticle vaccine platform that targets lymph node-resident dendritic cells (DCs) has been developed, capable of mounting an immune response to conjugated antigen. The cross-presentation by DCs was demonstrated by direct antibody staining and *in vitro* stimulation of CD8<sup>+</sup> T cells from OT-I mice and was indeed the most efficient with the reduction-sensitive conjugation.

Similarly, interferon (IFN) production by CD4<sup>+</sup> T cells from OT-II mice has been observed. Finally, immunization with OVA peptide-bearing nanoparticles resulted in *in vivo* proliferation and IFN production by adoptively transferred CD8<sup>+</sup> OT-I T cells and was also the most efficient with reduction-sensitive linking of the peptide antigen. These results demonstrate the relevance of the poly (propylene sulfide) nanoparticle vaccine platform and antigen conjugation scheme for activating both cytotoxic and helper T-cell responses [101].

## 13. Noncovalent protein–nanoparticle conjugation used for targeted drug delivery

Some of the studies have investigated the thermodynamics of binding between proteins and nanomaterials, demonstrating that properly functionalized NPs interact with proteins in an analogous fashion to protein–protein interactions. The biophysical characteristics of these interactions, such as binding affinity, residence time, binding cooperatively of NP, and the common serum proteins such as albumin, have been quantitatively described in the buffer medium to determine the behavior of proteins on NP surfaces [34,102].

Carbon nanotubes have a high surface area for chemical interactions and conjugations. The nonspecific protein–nanotube conjugates contain electrostatic interactions and hydrogen

bonding, especially when carbon nanotubes are pretreated with oxidative acids (Figure 7) [103,104].

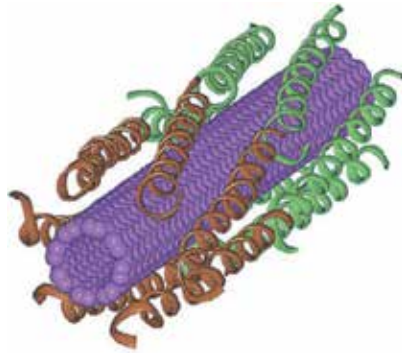


**Figure 7.** Immobilization of biomacromolecules on carbon nanotube surfaces

In this conjugation reaction, selected chemical reagents are utilized with known chemistry to link proteins to nanotubes in a more controllable manner. Protein surface amino groups of residues, such as lysine and nanotube-bound carboxylic acids, which are exposed by oxidative acid treatments, are widely involved in some of these specific conjugations and form amide linkages [35].

In another report, PEG was co-adsorbed onto single-wall nanotube (SWNT) devices with polyethylenimine. The pendant primary amine groups on PEI were available for subsequent biotin derivatization, and thus streptavidin recognition (Figure 8) [105].

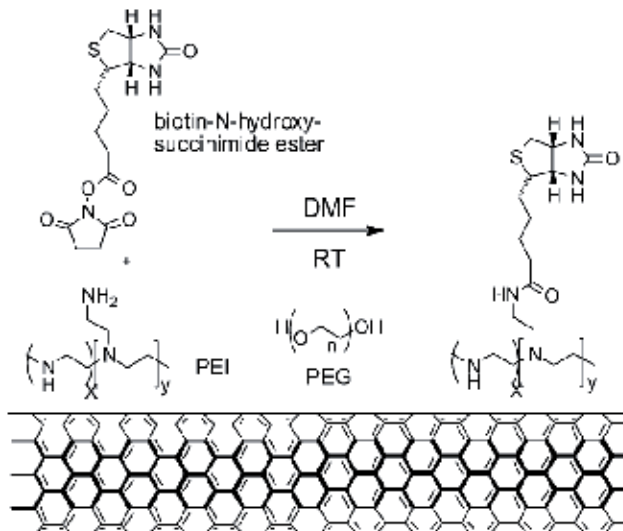


**Figure 8.** Absorption of polymer on the nanotube surface with the aid of PEG and PEI

## 14. Conclusions

Targeted drug delivery, sometimes called smart drug delivery, is a method of delivering medication to a patient in a manner that increases the concentration of the medication in infective organs or cells, relative to others. The objective of a targeted drug delivery system is to prolong, localize, and concentrate the drug in the target diseased tissue. The advantages of the targeted release system are the reduction in the frequency of the dose administration by the patient, more uniform effect of the drug, reduction of drug side effects, and reduced fluctuation in circulating drug levels. The disadvantage of the system is high cost, which makes profitability more troublesome and productivity difficult.

Nanotechnology plays an important role in therapies of the future as “nanomedicines” by enabling this situation to happen, thus lowering doses required for efficacy as well as expanding the therapeutic windows and safety profiles of new medicines.

Conventional chemotherapeutic agents are distributed nonspecifically in the body where they influence both cancerous and normal cells, thereby limiting the dose achievable within the tumor and also resulting in suboptimal treatment due to excessive toxicities. Molecularly targeted therapy has developed as one way to overcome the problem of nonspecificity of routine anticancer drugs. However, the development of resistance in cancer cells can avoid the cytotoxicity of ordinary chemotherapeutics as well as the more up-to-date targeted therapeutics [105].

Both passive- and active-targeted nanoparticles can enhance the intracellular concentration of drugs in cancer cells while avoiding toxicity in normal cells. Furthermore, when nanoparticles bind to specific receptors and then enter the cell, they are usually enveloped by endosomes via receptor-mediated endocytosis, thereby bypassing the recognition of P-glycoprotein, one of the main drug resistance mechanisms. However, although nanoparticles offer many advantages as drug carrier systems, there are still many limitations to be solved such as poor oral bioavailability, instability in circulation, inadequate tissue distribution, and toxicity.

## 15. Nomenclature

Phrase	Abbreviation
Blood brain barrier	(BBB)
1,2-dioleoyl-sn-glycero-3-phosphoethanolamine	DOPE
Antigen-presenting cell	APC
Carbon nanotubes	CNT
Dendritic cells	DC
N,N-dicyclohexyl carbodiimide	DCC
Doxorubicin	DOX

Phrase	Abbreviation
Drug delivery systems	DDS
N-ethyl-N-(3-dimethylaminopropyl) carbodiimide hydrochloride	(EDAC)
Epidermal growth factor receptor	EGFR
Enhanced permeation and retention	EPR
Fluorescein isothiocyanate	FITC
Folic acid	FA
Glucocorticoid	GC
Gold nanoparticles	GNP
Murine canin fibroblast	MCF-7
Minimum inhibition concentration	MIC
Magnetic nanoparticles	MNP
Monoclonal antibodies	mAb
Multiwall carbon nanotubes	MWCNT
Poly (D, L-lactic-co-glycolic acid)	PLGA
Quantum dots	QD
Single-wall carbon nanotubes	SWCNT
Solid lipid nanoparticles	SLN
Triggering toll-like receptor	TLR

## Author details

Katayoun Derakhshandeh<sup>1,2\*</sup> and Abbas Hemmati Azandaryani<sup>2</sup>

\*Address all correspondence to: k.derakhshandeh@umsha.ac.ir

1 Department of Pharmaceutics, School of Pharmacy, Hamadan University of Medical Sciences, Hamadan, Iran

2 Nano Drug Delivery Research Center, Kermanshah University of Medical Sciences, Kermanshah, Iran

## References

- [1] Allen TM, Cullis PR 2004 Drug delivery systems: entering the mainstream. *Science* 303: 1818–1822

- [2] Farokhzad OC, Langer R 2009 Impact of nanotechnology on drug delivery. *ACS Nano* 3(1): 16–20
- [3] Petros RA, DeSimone JM 2010. Strategies in the design of nanoparticles for therapeutic applications. *Nat Rev Drug Discov* 9(8): 615–627
- [4] Shi J, Votruba AR, Farokhzad OC, Langer R 2010 Nanotechnology in drug delivery and tissue engineering: from discovery to applications. *Nano Lett* 10(9): 3223–3236.
- [5] Dawar S, Singh N, Kanwar RK, Kennedy RL, Veedu RN, Zhou SF, Krishnakumar S, Hazra S, Sasidharan S, Duan W, Kanwar JR 2013 Multifunctional and multitargeted nanoparticles for drug delivery to overcome barriers of drug resistance in human cancers. *Drug Discov Today* 18: 1292–1300.
- [6] Derakhshandeh K, Erfan M, Dadashzadeh S 2007. Encapsulation of 9-nitrocamptothecin, a novel anticancer drug, in biodegradable nanoparticles: factorial design, characterization and release kinetics. *Euro J Pharm Biopharm* 66: 34–41.
- [7] Afshari M, Derakhshandeh K and Hosseinzadeh L 2014 Characterization, cytotoxicity and apoptosis studies of methotrexate-loaded PLGA and PLGA-PEG nanoparticles. *J Microencapsul* 31: 239–245.
- [8] Derakhshandeh K, Fathi S 2012 Role of chitosan nanoparticles in the oral absorption of Gemcitabine. *Int J Pharm.* 437(1-2): 172–177.
- [9] Davis ME, Chen Z, Shin DM 2008 Nanoparticle therapeutics: an emerging treatment modality for cancer. *Nat Rev Drug Discov* 7(9): 771–782
- [10] Xu Q, Kambhampati SP, Kannan RM 2013 Nanotechnology approaches for ocular drug delivery. *Middle East Afr J Ophthalmol* 20: 26– 37.
- [11] Prokop A, Davidson JM 2008. Nanovehicular intracellular delivery systems. *J Pharm Sci* 97: 3518–3590.
- [12] Kluza E, Yeo SY, Schmid S, van der Schaft DW.J, Boekhoven RW, Schiffelers RM, Storm G, Strijkers GJ, Nicolay K 2011 Anti-tumor activity of liposomal glucocorticoids: the relevance of liposome-mediated drug delivery, intratumoral localization and systemic activity. *J Control Release* 151: 10–17.
- [13] Ferrari M 2005 Cancer nanotechnology: opportunities and challenges. *Nat Rev Cancer* 5: 161–171.
- [14] Jain K 2005 Nanotechnology in clinical laboratory diagnostics. *Clin Chim Acta* 358: 37–54.
- [15] Sutton D, Nasongkla N, Blanco E, Gao J 2007 Functionalized micellar systems for cancer targeted drug delivery. *Pharm Res* 24: 1029–1046.

- [16] Xiang SD, Wilson K, Day S, Fuchsberger M, Plebanski M 2013 Methods of effective conjugation of antigens to nanoparticles as non-inflammatory vaccine carriers. *Methods* 60: 232–241.
- [17] Gao Z, Zhang L, Sun Y 2012 Nanotechnology applied to overcome tumor drug resistance. *J Control Release* 162: 45–55.
- [18] Yezhelyev MV, Gao X, Xing Y, Al-Hajj A, Nie S, O'Regan RM 2006 Emerging use of nanoparticles in diagnosis and treatment of breast cancer. *Lancet Oncol* 7: 657–667.
- [19] Vasir JK, Reddy MK, Labhasetwar VD 2005 Nanosystems in drug targeting: opportunities and challenges. *Curren Nanosci* 1: 47–64.
- [20] Wang M, Thanou M 2010 Targeting nanoparticles to cancer. *Pharmacol Res* 62: 90–99.
- [21] Au JL, Jang SH, Zheng J, Chen CT, Song S, Hu L 2001 Determinants of drug delivery and transport to solid tumors. *J Control Release* 74: 31–46.
- [22] Fetterly GJ, Straubinger RM 2003 Pharmacokinetics of paclitaxel containing liposomes in rats. *AAPS Pharm Sci* 5: E32.
- [23] Hoarau D, Delmas P, David S, Roux E, Leroux JC 2004 Novel long circulating lipid nanocapsules. *Pharm Res* 21: 1783–1789.
- [24] Moghimi SM, Szebeni J 2003 Stealth liposomes and long circulating nanoparticles: critical issues in pharmacokinetics, opsonization and protein-binding properties. *Prog Lipid Res* 42: 463–478.
- [25] Wang T, Kievit FM, Veiseh O, Arami H, Stephen ZR, Fang C, Liu Y, Ellenbogen RG, Zhang M 2013 Targeted cell uptake of a noninternalizing antibody through conjugation to iron oxide nanoparticles in primary central nervous system lymphoma. *World Neurosurg* 80: 134–141.
- [26] Pissuwan D, Niidome T, CortieMB 2011 The forthcoming applications of gold nanoparticles in drug and gene delivery systems. *J Control Release* 149: 65–71.
- [27] Derakhshandeh K, Soheili M, Dadashzadeh S, Saghiri R 2010 Preparation and in vitro characterization of 9-nitrocamptothecin-loaded long circulating nanoparticles for delivery in cancer patients. *Int J Nanomed* 5: 463–471.
- [28] Derakhshandeh K, Hochhaus G, Dadashzadeh S 2011 In-vitro cellular uptake and transport study of 9-nitrocamptothecin PLGA nanoparticles across caco-2 cell monolayer model. *Iran J Pharm Res* 10: 425–434.
- [29] Parveen S, Misra R, Sahoo SK 2012 Nanoparticles: a boon to drug delivery, therapeutics, diagnostics and imaging. *Nanomed Nanotechnol Biol Med* 8: 147–166.

- [30] Kashanian S, Azandaryani AH, Derakhshandeh K 2011 New surface-modified solid lipid nanoparticles using N-glutarylphosphatidylethanolamine as the outer shell. *Int J Nanomed* 6: 2393–2401.
- [31] Afshari M, Derakhshandeh K, Hosseinzadeh L 2014 Characterisation, cytotoxicity and apoptosis studies of methotrexate-loaded PLGA and PLGA-PEG nanoparticles. *J Microencapsul* 31: 239–245.
- [32] Ramana LN, Sharma S, Sethuraman S, Ranga U, Krishnan UM 2014 Evaluation of chitosan nanoformulations as potent anti-HIV therapeutic systems. *Biochimica et Biophysica Acta* 1840: 476–484.
- [33] Shi C, Guo X, Qu Q, Tang Z, Wang Y, Zhou S 2014 Actively targeted delivery of anti-cancer drug to tumor cells by redox-responsive star-shaped micelles. *Biomaterials*: 1–12.
- [34] Rana S, YehYC, Rotello VM 2010 Engineering the nanoparticle–protein interface: applications and possibilities. *Curr Opin Chem Biol* 14: 828–834.
- [35] Kumar C 2005 *Biofunctionalization of Nanomaterials*. Copyright 8. WILEY-VCH Verlag GmbH & Co. KGaA, Weinheim. ISBN: 3-527-31381-8
- [36] Daniel S, Rao TP, Rao KS, Rani SU, Naidu GRK, Lee HY, Kawai T 2007 A review of DNA functionalized/grafted carbon nanotubes and their characterization. *Sens Actuators B* 122: 672–682.
- [37] Hapuarachchige S, Zhu W, Kato Y, Artemov D 2014 Bioorthogonal, two-component delivery systems based on antibody and drug-loaded nanocarriers for enhanced internalization of nanotherapeutics. *Biomaterials* 35: 2346–2354.
- [38] Olejnik M, Krajnik B, Kowalska D, Lin G, Mackowski S 2013 Spectroscopic studies of plasmon coupling between photosynthetic complexes and metallic quantum dots. *J Phy Condens Matter* 25: 1–12.
- [39] Yokoyama M 2005 Drug targeting with nano-sized carrier systems. *J Artif Organs* 8: 77–84.
- [40] Jia H, Zhu J, Wang X, Cheng H, Chen G, Zhao Y, Zeng X, Feng J, Zhang X, Zhuo R 2014 A boronate-linked linear-hyperbranched polymeric nanovehicle for pH-dependent tumor-targeted drug delivery. *Biomaterials* 35: 5240e–5249e
- [41] Kulhari H, Pooja D, Shrivastav S, Mc Naidu VG, Sistla R 2014 Peptide conjugated polymeric nanoparticles as a carrier for targeted delivery of docetaxel. *Colloid Surf B* 117: 166–173.
- [42] Kocbek P, Obermajer N, Cegnar M, Kos J, Kristl J 2007 Targeting cancer cells using PLGA nanoparticles surface modified with monoclonal antibody. *J Control Release* 120: 18–26.

- [43] Chiu SJ, Ueno NT, Lee RJ 2004 Tumor-targeted gene delivery via anti-HER2 antibody (trastuzumab, HerceptinR) conjugated polyethylenimine. *J Control Release* 97: 357–369.
- [44] Abdel Wahab BA, Evgenivetch PV, Alyautdin RN 2005 Brain targeting of nerve growth factor using poly(butylcyanoacrylate) nanoparticles. *Internet J Pharmacol* 3.
- [45] Yang J, Lee CH, Park J, Seo S, Lim EK, Song YJ, Suh JS, Yoon HG, Huh YM, Haam S 2007 Antibody conjugated magnetic PLGA nanoparticles for diagnosis and treatment of breast cancer. *J Mater Chem* 17: 2695–2699.
- [46] Sudimack J, Lee RJ 2000 Targeted drug delivery via the folate receptor. *Adv Drug Deliv Rev* 41: 147–162.
- [47] Koo OM, Rubinstein I, Onyuksel H 2005 Role of nanotechnology in targeted drug delivery and imaging: a concise review. *Nanomedicine* 1: 193–212.
- [48] Kim JS, Oh MH, Park JY, Park TG, Nam YS 2013 Protein-resistant, reductively dissociable polyplexes for in vivo systemic delivery and tumor-targeting of siRNA. *Biomaterials* 34: 2370–2379.
- [49] Heidarian S 2012 Folate targeted nanoparticles: preparation, physicochemical characterization and in vitro cytotoxicity effect. PhD thesis. Kermanshah University of Medical Science.
- [50] Wu H, Cabral H, Toh K, Mi P, Chen YC, Matsumoto Y, Yamada N, Liu X, Kinoh H, Miura Y, Kano MR, Nishihara H, Nishiyama N, Kataoka K 2014 Polymeric micelles loaded with platinum anticancer drugs target preangiogenic micrometastatic niches associated with inflammation. *J Control Release* 189: 1–10.
- [51] Tarn D, Ashley CE, Xue M, Carnes EC, Zink JJ, Brinker CJ 2013 Mesoporous silica nanoparticle nanocarriers: biofunctionality and biocompatibility. *Acc Chem Res* 46: 792–801.
- [52] Chen C, Geng J, Pu F, Yang X, Ren J, Qu X 2011 Polyvalent nucleic acid/mesoporous silica nanoparticle conjugates: dual stimuli-responsive vehicles for intracellular drug delivery. *Angew Chem Int Ed* 50: 882–886.
- [53] Zhou L, Chen Z, Dong K, Yin M, Ren J, Qu X 2014 DNA-mediated biomineralization of rare-earth nanoparticles for simultaneous imaging and stimuli-responsive drug delivery. *Biomaterials* 35(30):8694-6702.
- [54] Hong JS, Vreeland WN, DePaoli Lacerda SH, Locascio LE, Gaitan Mi, Raghavan SR 2008 Liposome-templated supramolecular assembly of responsive alginate nanogels. *Langmuir* 24: 4092–4096.
- [55] Gregoriadis G, Ryman BE 1972 Fate of protein-containing liposomes injected into rats. An approach to the treatment of storage diseases. *Eur J Biochem* 24: 485–491.

- [56] Andresen TL, Jensen SS, Jorgensen K 2005 Advanced strategies in liposomal cancer therapy: problems and prospects of active and tumor specific drug release. *Prog Lipid Res* 44: 68–97.
- [57] Lim SB, Banerjee A, Önyüksel H 2012 Improvement of drug safety by the use of lipid-based nanocarriers. *J Control Release* 163: 34–45.
- [58] Kraft JC, Freeling JP, Wang Z, HO RJY 2014 Emerging research and clinical development trends of liposome and lipid nanoparticle drug delivery systems. *J Pharm Sci* 103: 29–52.
- [59] Howard MD, Greineder CF, Hood ED, Muzykanto VR 2014 Endothelial targeting of liposomes encapsulating SOD/catalase mimetic EUK-134 alleviates acute pulmonary inflammation. *J Control Release* 177: 34–41.
- [60] Ninomiya K, Yamashita T, Kawabata S, Shimizu N 2014 Targeted and ultrasound-triggered drug delivery using liposomes co-modified with cancer cell-targeting aptamers and a thermosensitive polymer. *Ultrason Sonochem* 21: 1482–1488
- [61] Yuan F, Leunig M, Huang SK, Berk DA, Papahadjopoulos D, Jain RK 1994 Microvascular permeability and interstitial penetration of sterically stabilized (stealth) liposomes in a human tumor xenograft. *Cancer Res* 54: 3352–3356.
- [62] Immordino ML, Dosio F, Cattel L 2006 Stealth liposomes: review of the basic science, rationale, and clinical applications, existing and potential. *Int J Nanomed* 1: 297–315.
- [63] Kluza E, Yeo SY, Schmid S, van der Schaft DWJ, Boekhoven RW, Schiffelers RM, Storm G, Strijkers GJ, Nicolay K 2011 Anti-tumor activity of liposomal glucocorticoids: the relevance of liposome-mediated drug delivery, intratumoral localization and systemic activity. *J Control Release* 151: 10–17.
- [64] Cho K, Wang X, Nie S, Chen Z, Shin DM 2008 Therapeutic nanoparticles for drug delivery in cancer. *Clinical Cancer Res* 14: 1310–1316.
- [65] Mokhtarieh AA, Cheong S, Kim S, Chung BH, Lee MK 2012 Asymmetric liposome particles with highly efficient encapsulation of siRNA and without nonspecific cell penetration suitable for target-specific delivery. *Biochim Biophys Acta* 1818: 1633–1641.
- [66] Reddy JA, Low PS 2000 Enhanced folate receptor mediated gene therapy using a novel pH-sensitive lipid formulation. *J Control Release* 64: 27–37.
- [67] Choi K, Kwon IC, Ahn HJ 2013 Self-assembled amphiphilic DNA-cholesterol/DNA-peptide hybrid duplexes with liposome-like structure for doxorubicin delivery. *Biomaterials* 34: 4183–4190
- [68] Muller RH, Mader K, Gohla S 2000 Solid lipid nanoparticles (SLN) for controlled drug delivery – a review of the state of the art. *Eur J Pharm Biopharm* 50: 161–177.

- [69] Rostami E, Kashanian S, Hemati Azandaryani A 2014 Preparation of solid lipid nanoparticles as drug carriers for levothyroxine sodium with in vitro drug delivery kinetic characterization. *Mol Biol Rep.* 41(5): 3521-3527.
- [70] Rostami E, Kashanian S, Hemati Azandaryani A, Faramarzi H, Ezzati J, Omidfar K 2014 Drug targeting using solid lipid nanoparticles. *Chemis Phys Lipids* 181: 56-61.
- [71] Bondi ML, Craparo EF 2010 Solid lipid nanoparticles for applications in gene therapy: a review of the state of the art. *Expert Opin Drug Del* 7: 7-18.
- [72] Mehnert W, Maeder K 2012 Solid lipid nanoparticles: production, characterization and applications, *Adv Drug Deliv Rev* 64: 83-101.
- [73] Jin SE, Kim CK 2012 Long-term stable cationic solid lipid nanoparticles for the enhanced intracellular delivery of SMAD3 antisense oligonucleotides in activated murine macrophages. *J Pharm Pharm Sci* 15: 467-482.
- [74] Zhu L, Ma J, Jia N, Zhao Y, Shen H 2009 Chitosan-coated magnetic nanoparticles as carriers of 5-fluorouracil: preparation, characterization and cytotoxicity studies. *Colloids Surf B Biointerfaces* 68: 1-6.
- [75] Gollavelli G, Ling YC 2014 Magnetic and fluorescent graphene for dual modal imaging and single light induced photothermal and photodynamic therapy of cancer cells. *Biomaterials* 35: 4499-4507.
- [76] Mishra D, Mishra H, Mishra PK, Nahar M, Dubey V, Jain NK 2010 Evaluation of solid lipid nanoparticles as carriers for delivery of hepatitis B surface antigen for vaccination using subcutaneous route. *J Pharm Pharm Sci* 13: 495-509.
- [77] Groneberg DA, Giersig M, Welte T, Pison U 2006 Nanoparticle-based diagnosis and therapy. *Curr Drug Targets.* 7: 643-648.
- [78] Gu YJ, Cheng J, Man CW, Wong WT, Cheng SH 2012 Gold-doxorubicin nanoconjugates for overcoming multidrug resistance. *Nanomed* 8: 204-211.
- [79] Bhattacharya D, Saha B, Mukherjee A, Ranjan Santra C, Karmakar P 2012 Gold nanoparticles conjugated antibiotics: stability and functional evaluation. *Nanosci Nanotechnol* 2: 14-21.
- [80] Paciotti GF, Kingston DGI, Tamarkin L 2006 Colloidal gold nanoparticles: a novel nanoparticle platform for developing multifunctional tumor-targeted drug delivery vectors. *Drug Develop Res* 67: 47-54.
- [81] Saha B, Bhattacharya J, Mukherjee A, Ghosh AK, Santra CR, Dasgupta AK, Karmakar P 2007 In vitro structural and functional evaluation of gold nanoparticles conjugated antibiotics. *Nanoscale Res Lett* 2: 614-622.
- [82] Bergen JM, von Recum HA, Goodman TT, Massey AP, Pun SH 2006 Gold nanoparticles as a versatile platform for optimizing physicochemical parameters for targeted drug delivery. *Macromolecular Biosci* 6: 506-516.

- [83] Uchegbu IF, Vyas SP 1998 Non-ionic surfactant based vesicles (niosomes) in drug delivery. *Int J Pharm* 172: 33–70.
- [84] Dufes C, Schatzlein AG, Tetley L, Gray AI, Watson DG, Olivier JC, Couet W, Uchegbu IF 2000 Niosomes and polymeric chitosan based vesicles bearing transferrin and glucose ligands for drug targeting. *Pharm Res* 17: 1251–1258.
- [85] Bragagni M, Mennini N, Ghelardini C, Mura P 2012 Development and characterization of niosomal formulations of doxorubicin aimed at brain targeting. *J Pharm Pharm Sci* 15: 94–102.
- [86] Bragagnia M, Menninia N, Ghelardinib C, Muraa P 2012 Development and characterization of niosomal formulations of doxorubicin aimed at brain targeting. *J Pharm Pharm Sci* 15: 184–196.
- [87] Medintz IL, Uyeda HT, Goldman ER, Mattoussi H 2005 Quantum dot bioconjugates for imaging, labelling and sensing. *Nature Mater* 4: 435–446.
- [88] Howarth M, Takao K, Hayashi Y, Ting A 2005 Targeting quantum dots to surface proteins in living cells with biotin ligase. *Proc Natl Acad Sci U S A* 102: 7583–7588.
- [89] Xiao Y, Telford WG, Ball JC, Locascio LE, Barker PE 2005 Semiconductor nanocrystal conjugates, FISH and pH. *Nature Methods* 2: 723–732.
- [90] Yezhelyev M, Morris C, Gao X 2005 Simultaneous and quantitative detection of multiple biomarkers in human breast cancers using semiconductor multicolor quantum dots breast cancer research and treatment. *Breast Cancer Res Treat* 94: 48–57.
- [91] Yezhelyev M, Gao X, Markus A 2005 Multiplex molecular diagnostic of tumor tissue using quantum dots. *Am Soc Clin Oncol* 23: 843–849.
- [92] Neuberger T, Schopf B, Hofmann H, Hofmann M, Rechenberg B 2005 Superparamagnetic nanoparticles for biomedical applications: possibilities and limitations of a new drug delivery system. *J Magn Magn Mater* 293: 483–496.
- [93] Chen JP, Yang PC, Ma YH, Wu T 2011 Characterization of chitosan magnetic nanoparticles for in situ delivery of tissue plasminogen activator. *Carbohydr Polym* 84: 364–372.
- [94] Cole AJ, Yang VC, David AE 2011 Cancer theranostics: the rise of targeted magnetic nanoparticles. *Trends Biotechnol* 29: 323–332.
- [95] Alexiou C, Jurgons R, Schmid R, Hilpert A, Bergemann C, Parak F, Iro H 2005 In vitro and in vivo investigations of targeted chemotherapy with magnetic nanoparticles. *J Magn Magn Mate* 293: 389–393.
- [96] Mahmoudi M, Sant S, Wang B, Laurent S, Sen T 2011 Superparamagnetic iron oxide nanoparticles (SPIONs): development, surface modification and applications in chemotherapy. *Adv Drug Deliv Rev* 63: 24–46.

- [97] Liu X, Guan Y, Liu H, Ma Z, Yang Y, Wu X 2005 Preparation and characterization of magnetic polymer nanospheres with high protein binding capacity. *J Magn Magn Mate* 293: 111–118.
- [98] Babincova M, Cicmanec P, Altanerova V, Altaner C, Babinec P 2002 AC-magnetic field controlled drug release from magnetoliposomes: design of a method for site-specific chemotherapy. *Bioelectro Chem* 55: 17–25.
- [99] Hsu MH, Su YC 2008 Iron-oxide embedded solid lipid nanoparticles for magnetically controlled heating and drug delivery. *Biomed Microdevices* 10: 785–793.
- [100] Xiang SD, Wilson K, Day S, Fuchsberger M, Plebanski M 2013 Methods of effective conjugation of antigens to nanoparticles as non-inflammatory vaccine carriers. *Methods* 60: 232–241.
- [101] Hirosue S, Kourtis IC, van der Vlies AJ, Hubbell JA, Swartz MA 2010 Antigen delivery to dendritic cells by poly(propylene sulfide) nanoparticles with disulfide conjugated peptides: cross-presentation and T cell activation. *Vaccine* 28: 7897–7906.
- [102] Fu K, Huang W, Lin Y, Zhang D, Hanks TW, Rao AM, Sun YP 2002 Functionalization of carbon nanotubes with bovine serum albumin in homogeneous aqueous solution. *J Nanosci Nanotechnol* 2: 457–461.
- [103] Monteiro-Riviere, NA, Nemanich RJ, Inman AO, Wang YY, Riviere JE 2005 Multi-walled carbon nanotube interactions with human epidermal keratinocytes. *Toxicol Lett* 155: 377–384.
- [104] Chengqun Chen, Huijuan Zhang, Lin Hou, Jinjin Shi, Lei Wang, Chaofeng Zhang, Mingyue Zhang, Hongling Zhang, Xiufang Shi, Huixiang Li, Zhenzhong Zhang 2013 Single-walled carbon nanotubes mediated neovascularity targeted antitumor drug delivery system. *J Pharm Pharm Sci* 16(1):40-51.
- [105] Star, A, Gabriel JCP, Bradley K, Gruner G 2003 Electronic detection of specific protein binding using nanotube FET device. *Nano Lett* 3: 459–463.
- [106] Xiao Y, Barker PE 2004 Semiconductor nanocrystal probes for human metaphase chromosomes. *Nucleic Acids Res* 32: 28–33.

---

# Cancer Stem Cells – Perspectives and How to Target Them

---

Zhaopeng Tang, Qianfeng Wang, Sarah Shigdar, Wei Duan and Dongxi Xiang

Additional information is available at the end of the chapter

<http://dx.doi.org/10.5772/61861>

---

## Abstract

Cancer stem cell is a progressive concept moving forward to interpret the hard-to-cure nature of cancer and the relevant behavior in response to clinical therapies. Despite the remaining debates regarding the existence of cancer stem cells, the cancer stem cell model provides a potential approach for advanced innovative therapies targeting the “roots” of cancer, which has enhanced treatment outcomes. This chapter summarizes advanced perspectives in the field of cancer stem cell research, including experimental strategies for targeting these cells, highlights challenges of this theory, and explores feasible therapeutic strategies for overcoming the intrinsic resistance of cancer stem cells to clinical treatment.

**Keywords:** Cancer stem cell, stemness, chemoresistance, targeted therapy

---

## 1. Introduction

Cancer remains one of the leading causes of human death, and even though extraordinary efforts and budget have been spent, clinical trials in the eradication or control of cancer progression have generally created disappointing outcomes [1, 2]. Cancer develops originally from normal cells through the accumulation of multiple genetic alterations that ultimately convert to malignant phenotypes [3, 4]. Despite a better understanding of cancer biology and evolutionary genomic characteristics, translating these achievements into feasible and successful clinical outcomes continues to be a problem [5]. One attractive theory, the concept of cancer stem cells (CSCs), being explored recently in cancer research may hold the answer [6]. This chapter summarizes the major characteristics of CSCs and highlights several key approaches used for CSC study, where they could be of help for efficient CSC-targeted therapy.

---

## 2. CSC: An involving concept moving forward

### 2.1. Cancer genetic evolution

Cancer biology and genomics have increasingly validated cancer as a complex adaptive system. This landmark perspective was introduced by Peter Nowell in 1976, who viewed cancer development as an evolutionary process driven by stepwise mutations with sequential, subclonal selection at the nuclei acid level, a theory that is similar to Darwinian natural selection [7]. This theory includes several key aspects. (1) Genetic instability: cells possess a battery of mechanisms to preserve their DNA structural integrity. Cellular genetic structural varies (deletions, duplications, and rearrangements) or DNA point mutations can initiate cell biological changes that may lead to tumor formation. Thus, the perturbation of mechanisms controlling genomic stability is responsible for the oncogenic processes [8]. (2) Error-prone repair processes and a genotoxic exposure could result in particular mutational spectra of cancer cells, including cigarette carcinogens, ultraviolet light, and chemotherapeutics. (3) Recurrent, mutation specific traits in cancer can potentially affect clonal selection [9] (Figure 1).

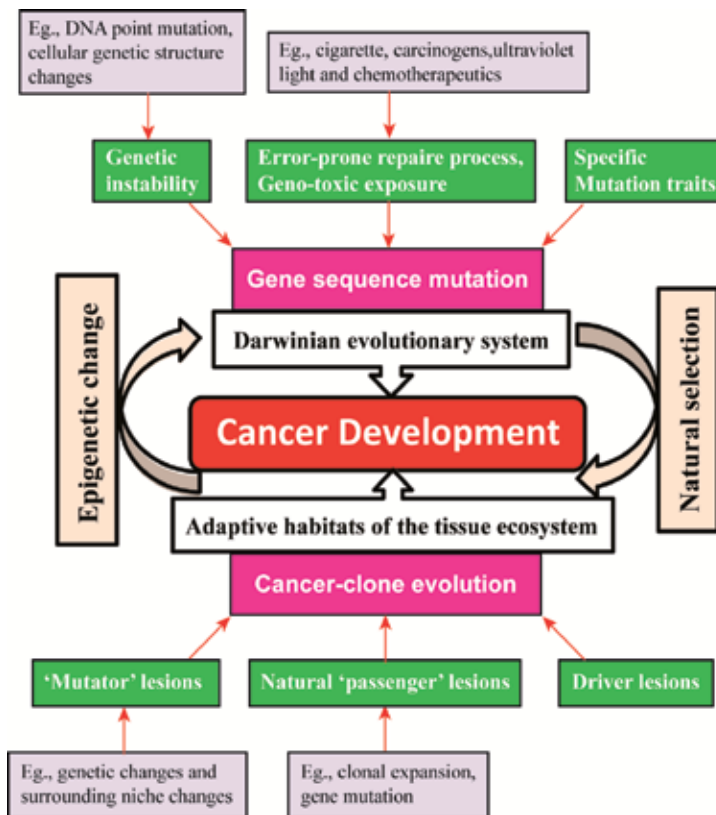
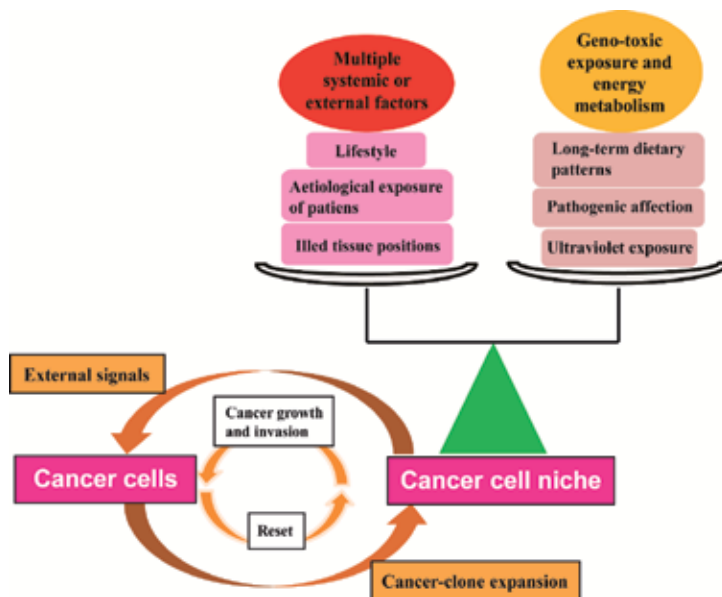


Figure 1. Genetic diversification and clonal dynamics of cancer development.

The microenvironment surrounding a tumor complexes with multiple cellular components that provide an adaptive landscape and necessary elements for natural selection of cancer growth [10]. The interaction between cancer cells and their surroundings is mutually beneficial [11]. Cancer cells can reset the extracellular environment to be specialized niches for further cancer growth and migration. The cancer niche in turn provides external signals for cancer-clone expansion and tumor cell survival and proliferation. The spatial heterogeneity is critical for evolving cancer cell to be a malignant phenotype and beneficial for cell migration and distant invasion [12]. During the process of cancer-clone expansion, migrating cells invade new habitats where they face new selective pressures, thereby increasing the rate of further cancer mutation [13].

The cancer niche is an unclosed system. In addition to the tissue positions and associated etiological environmental exposure of patients, the tissue microecosystem is manipulated by multiple systemic or external factors [14]. Genotoxic exposures, such as ultraviolet light, pathogenic infection, and long-term dietary habits, are able to modulate energy metabolism. They are speculated to be the primary etiological causes of tumor initiation and further evolution of cancer clones [14]. Cancer cell ecosystems can be altered following clinical treatment, in which most cancer cells together with healthy tissues are killed under intensive therapies. However, some specialized niches protect cells from cancer treatment, where variant or therapy-resistant cancer cells emerge [15]. On the way of cancer progression and tumor recurrence after therapy, the primary unit of selection is a specialized cell, known as CSC, which possesses extensive self-renewal potential (Figure 2).



**Figure 2.** The cancer ecosystem.

## 2.2. Cancer stem cell model

Cancer research was previously dominated by the clonal evolution model, also known as a conventional stochastic model, a concept whereby all cells within a tumor have equal potential to propagate and maintain a tumor following stepwise genetic and/or epigenetic changes, but they are hard to identify the tumorigenic subset [7, 16–19]. Recently, accumulated studies suggest cancers as hierarchical organizations, which is the basis of the hierarchical or CSC model [20]. In the CSC model, only a small subset of cancer cells possesses the ability to self-renew, differentiates, and reforms a tumor. CSCs, as “roots of cancer” operating in a hierarchical fashion, are defined by their abilities [20–24] (1) to form new tumors with high efficiency that histologically resembles the original tumors when xenotransplanted into immunodeficient mice, (2) to generate descendant cells possessing unlimited self-renewal (regeneration) potential but uncommitted differentiation options, and (3) to generate large populations of differentiated offspring and progenitor cells that exit the stem cell state and lose the ability to self-renew, thus no longer possessing tumorigenic potential. Such differentiated daughter cells can undergo limited rounds of cell division because they lack the intrinsic clonogenic characteristics that are essential for tumor initiation and long-term progression of the malignancy. The increasingly widespread attraction of the CSC model is due to the fact that it can provide a plausible account for poorly understood clinical phenomena, such as therapy resistance, as CSCs can resume growth and contribute to a new relapse after therapy suspension. It is critical to appreciate that both the stochastic and CSC models share the same conviction that only a small population of cancer cells are capable of maintaining cancer. The main difference is that CSCs within the CSC model are characterized with the help of distinct cellular phenotypes [20].

Critically, the CSC model stands on the basis that CSCs are reliable and stable over time, and their unique traits could not be obtained by differentiated descendants. It is worth to note that the persuading of CSC model has been accompanying with intense debates amongst cancer researchers. As evident from a new concept, the dynamic CSC model suggests that the CSC phenotype is much more fluid than previously predicted and can be regulated by external signals [25, 26]. Thus, not only can CSCs self-renew to create new progeny and differentiate to non-CSCs but the de-differentiation of non-CSCs to CSCs can also occur and thus return to the malignancy growth cycle [26–28]. This latest finding has significant implications for oncology in that future effective anticancer therapeutic strategies should aim at targeting both CSCs and non-CSCs (Figure 3).

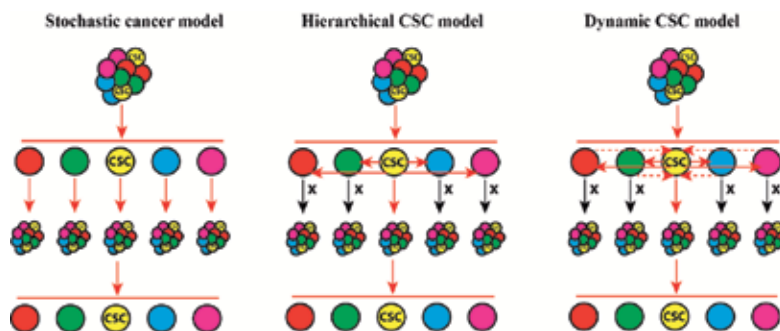


**Figure 3.** Stochastic cancer model versus hierarchical and dynamic CSC models of tumor heterogeneity.

### 3. Challenges and opportunities the CSC theory faces

Several challenges the CSC theory is now facing should be addressed before this concept can fetch benefits for the clinically relevant entity [29].

#### 3.1. Frequency of CSCs

One challenge that is intensely debated is how many CSCs exist within a tumor. Some studies suggested that the frequency of CSCs is less than 1 in every 1000 cells in a tumor, which supports the hierarchical status between CSCs and non-CSCs [30, 31]. However, recent evidences reported that the number of cells that possess intrinsic tumorigenic potential is relatively higher [32, 33]. Hepatocytes possess the potential of self-renewal and unlimited proliferation under certain conditions [34, 35]. It is shown that various colorectal cancers do not follow the same hierarchy as their CSC frequencies vary [36]. More importantly, the prediction of the number of CSCs in a particular tumor type depends on multiple manual factors, including the experimental procedure designed, the choice of cell surface markers, and the types of immunodeficient mice into which the CSCs were injected. Chiba et al. used the technique of side population (SP) analysis to detect the subpopulations that act CSC functions and revealed that SP cells possess abilities of high proliferation and antiapoptosis in both Huh7 and PLC/PRF/5 cells with a percentage of 0.25% and 0.8%, respectively [37]. Kimura et al. determined the frequency of CSCs by analyzing cell surface markers and the percentage of CD133+ cells in Huh7 and PLC/PRF/5 were 2.7% and 23.5%, which is totally different with the number obtained on the base of EpCAM-positive cells, with a proportion of 89.1% and 40.7%, respectively [38]. However, Cao et al. found the CSC frequency of PLC/PRF/5 cells was 8.8% by using the sphere-forming assay [39]. Thus, considering a tumor as a hierarchical malignancy has intrinsic limitations, as a large population of cancer cells cooperate and contribute to tumor growth, which is consistent with the conventional nonhierarchical model of malignancies [40].

#### 3.2. Therapy resistance of CSCs

The failure of cancer initial treatment is normally explained due to the presence of a subset of resistant cancer cells. CSCs are supposed to be one of such cells; they are logically resistant to traditional chemotherapies owing to their “stem-like” features, including enhanced abilities of DNA damage repair and cellular detoxification capacity via elevated aldehyde dehydrogenase (ALDH) activity, increased expression of enhancement of ATP-binding cassette (ABC) surface transporters, and their nature quiescence [41–43]. CSCs with an up-regulation of antiapoptotic molecules or a high expression of drug efflux pumps respond quite differently when exposed to drugs; they can both survive after cancer treatment [44]. The rapid relapse of the malignancy suggests that the clonogenic core of the cancer was not effectively targeted, and this might be due to the de-differentiation of non-CSCs to CSCs [45]. Even though CSCs are believed to be the most promising candidates for overcoming chemoresistance and tumor recurrence, both CSCs and non-CSCs should be targeted eventually.

### 3.3. Isolation of CSCs

The isolation and subsequent assessment of CSCs are clearly a rapidly developing area in which diverse strategies were incorporated for obtaining higher CSC purities. One continual concern after isolation assays is that whether the proposed CSCs separated from the bulk of the tumor can still possess the intrinsic cellular properties. The selected CSCs require the distinct phenotypes that can generate a similar malignancy to the parental tumor when transplanted into immunodeficient mice [46]. The subsequent challenge is to optimize experimental procedures to allow xenotransplantation of viable single suspension cells into animals.

### 3.4. Targeting “confirmed” CSCs

Due to the relevance of cancer development, CSCs are ideal targets for molecular-directed therapies. The limitation is that CSCs are typically present at very low levels. In addition, CSC markers overlap with normal stem cells or between CSCs [47]. These drawbacks indicate that the identification of CSC markers for guiding molecular therapeutics is still in its infancy. Many CSC markers are not strictly CSC antigens since they present on normal cancer cells as well, but they are molecules that support CSCs in their niche.

The characterization of CSCs has led to some experimentally “confirmed” markers or markers involved in the process of targeting or interaction with CSCs. Epithelial cell adhesion molecule (EpCAM) is one of the most highly expressed tumor-associated markers, being found in a broad range of epithelial cancers. EpCAM has been “rediscovered” as a CSC antigen in breast, colon, prostate, and pancreatic cancers [48–50]. In studies on colon cancer tumorigenicity, EpCAM<sup>high</sup>CD44<sup>+</sup> was considered as a robust marker of more “stem-like” subpopulations. Also, recruiting effector cells to tumors using an anti-EpCAM/anti-CD3 bispecific antibody has been shown to be a promising strategy in the treatment of cancer [51].

In addition to cell-surface markers that are frequently utilized to identify CSCs, the high activity of signal transduction routes can also contribute to CSCs features [52]. The self-renewal capacity of CSCs leads to a long-term clonogenicity mutation, which might be effectively therapeutically targeted. The activation of intracellular signaling pathways associated with the self-renewal of CSCs, including Wnt pathway, Hedgehog (Hh) pathway, and Notch pathway, can stimulate a more immature tumor phenotype, facilitate tumor invasion, and promote therapy resistance [53]. The interference of such pathways that promote CSC function might provide an effective therapeutic window for drugs in the war against cancer. These stem cell-associated surface marker proteins and pathways are promising targets for anticancer drug development

## 4. Approaches used for studying CSCs

The primary challenge to study CSCs is the ability to identify and investigate CSCs in laboratories using both *in vitro* and *in vivo* assays. This section addresses the methodologies that have been widely used for isolation and characterization of CSCs.

#### **4.1. In vivo xenotransplantation and limiting dilution assay: The gold standard**

Limiting dilution assays (LDAs) have been used in a broad variety of biological fields. LDA is an experimental technique that attempts to quantify the frequency of biological particles that perform a particular function within a larger mixed population [54]. The aim of LDA is to obtain highly precise data at the macro level. To achieve this goal, several conditions must be considered [55, 56]. First, the cells should be Poisson distributed. Second, the assay should be designed with maximum information containing both negative and positive cultures. Moreover, the conditions must be performed at the state that the response of a single limiting particle can be detected. Thus, the culture conditions should be uniform in all paralleled groups and wells [56].

The ability to determine the number of CSCs is a critical step for the success of in vivo transplantation. However, there has been little or no attempt to standardize this approach [57]. In all conditions tested, the statistical behavior of the system ( $E_s$ ) and changes in condition over time and statistical noise were the two major contributors to overall uncertainty [57]. However, as expected from statistical principles,  $E_s$  declines with increasing number of replicates analyzed. Also, increasing the number of replicates beyond 96 is unlikely to provide substantial decreases in error, and fewer wells can be used to obtain results with similar precision. Another requirement that arises in stem cell research is the need to accommodate small numbers of replicates in a statistically consistent and defensible manner. Operator error, mouse-to-mouse error, and other errors appear to play minor roles. These findings establish parameters that contribute to the variability of LDA and provide strategies for the optimization and interpretation of the LDA-based CSC estimates. To this end, extreme limiting dilution analysis (ELDA) has emerged as the preferred method that is based on sound statistical principle and methodologies [58]. ELDA works well when the number of replicates is small.

The CSC concept brings essential predictions of cancer research including susceptibility to chemotherapy, aggressiveness of the disease, and the pace of recurrence that may largely be influenced by the functional properties of CSCs [48, 49, 59–61]. To functionally measure CSC potential, the operational assay of evaluating CSCs has been developed. The creation of an array of genetically modified immunodeficient mice enabling analogous xenograft experiments can be used to determine and quantify cells that obtain tumor-initiating activity in human tumors [48, 49, 59–61]. These xenograft models are considered the “gold standard” in CSC research; they are able to guide the biology and therapeutic responses of human CSCs.

The enumeration of CSCs has been performed using phenotypic markers in in vitro limiting dilution transplantation assays. Some key aspects should be considered [32]: (1) inefficient engraftment in mice may result in underestimation of the actual CSC frequency; (2) phenotypic characterization of CSCs may lead to different rates depending on the antibody combinations used, and the use of specific antibodies may induce immune-mediated clearance of CSCs [48]; (3) the approach of tumor implantation (e.g., intravenously, intrafemorally) critically defines engraftment and affects the export of stem cell frequency [62]; and (4) the kind of mouse strain used as tumor recipient and the degree of mouse immunodeficiency are other factors need to be considered [32]. It is reported that the use of adjuvants/culture supplementary (e.g., Matrigel or growth factors) influences not only the measured frequency of CSCs but their phenotypes as well [30, 32].

#### 4.2. The side population assay

In addition to the isolation and identification of CSCs through a set of cell surface markers (such as CD44<sup>+</sup>/CD24<sup>low</sup>/lin<sup>-</sup>/ALDH<sup>+</sup>, CD44<sup>+</sup>/CD24<sup>low</sup>, EpCAM<sup>+</sup>/CD44<sup>+</sup>/CD24<sup>-</sup>, or CD34<sup>+</sup>/CD38<sup>-</sup>). The SP discrimination assay is another flow cytometry method used to detect stem cells based on the properties of the Hoechst dye efflux via the ABC transporters [63]. The SP assay has been used to identify stem cell and progenitor populations in various tissues [64, 65]. However, several reports have stated that dye efflux is not a universal property of all stem cells although SPs are much abundant within stem cells [66]. SPs are not just restricted to the stem cell phenotypes as ABC transporters are also expressed by specialized cells in certain organs [67]. The ABC transporters are believed to play a key role in those tissues, protecting the cytotoxic effects of toxins [68]. However, the identification of CSCs has raised interests in the SP assay, and SP subpopulations isolated from some cancers possess capabilities of drug-resistant, self-renewal, and tumorigenicity when transplanted into immunocompromised mice [63]. The SP assay can play an extremely valuable role in the primary isolation and identification of potential stem/progenitor cells, when specific cell surface markers were absent.

#### 4.3. Clonal sphere formation assay and proliferation (invasion assay) assay

The clonal sphere formation assay is another functional method used for the identification of CSCs and their purification from the rest of neighboring cells [69, 70]. This assay begins with reliable single cell suspensions originating from primary tumors or established cancer cell lines. Serial dilutions of the single cancer cell suspensions are seeded on ultra-low attachment substrata in the presence of serum-free media with growth factors [71]. CSCs can grow into 3D nonadherent structures called spheres, while non-CSCs cannot survive in such culture conditions. The results of the assay may become more reliable if the spheres are serially passaged. The self-renewal capacity of sphere-generating cells can be estimated by evaluating the sphere formation frequency through LDA and measuring sphere size [72]. The sphere formation assay has been used to identify adult stem cells or CSCs from a number of tissues, including mammary gland, brain, skin, and human melanoma [73–76].

#### 4.4. Enzymatic assay of cell-surface markers

CSCs can be isolated by the enzymatic activities (ALDH activity) [77, 78]. The measurement of ALDH activity by ALDEFLUOR staining is useful to screen tumor cells for resistance to alkylating agents and to identify heterogeneity within tumor cells [79]. The ALDH<sup>+</sup> population is consistent with CSC characteristics, generating tumors that recapitulate the phenotypic heterogeneity of the initial tumor. The measurement of ALDH populations revealed that the ALDH<sup>+</sup> cells were capable of self-renewing into both ALDH<sup>+</sup> and ALDH<sup>-</sup> cells [80]. A recent study in melanoma described both ALDH<sup>+</sup> and ALDH<sup>-</sup> cells derived from patient biopsies (100 or 2000 cells, respectively) were able to efficiently form tumors. It is also reported that ALDH cells alone may not be sufficient for CSC selection [32]. Despite this, studies in breast cancer combining other CSC surface markers with Aldefluor have improved tumorigenic enrichment and this combination may prove to be a better strategy for enrichment of CSCs [32].

#### **4.5. Slow-cycling population assay**

The slow-cycling population assay can be used to distinguish CSCs from progenitor cells, which determines the incorporation of labeled precursor of nucleotides for cellular DNA synthesis [81]. The slow-cycling cells, such as CSCs, maintaining sufficient labels allow their detection by the anti-BrdU antibody staining or radioactive label [82]. Some technical issues impede the accuracy of BrdU detection: (1) it is hard to demonstrate that cells have a similar cycling in vitro and in vivo because of the destructive nature of the BrdU detection procedure, (2) it is not expected that all the stem cells can be equally labeled because the BrdU incorporation occurs only during the S phase of cell cycle, and (3) the label retention depends on the length of the cell cycle, while the later status appears to alter as the organ matures [83]. Thus, quantification of stem cells through this assay requires further confirmation through other methods.

#### **4.6. Lineage labeling assay**

The lineage labeling assay was initially developed for understanding and tracing the biological developments of a cell, including the identification of cell origin, measuring lineage relationships, and determination of division patterns [84]. In this assay, cells are labeled (usually with a fluorescent dye or tag), followed by tracing in vitro and in vivo. There are several inherent limitations with this technique: (1) the experimental procedure can damage cells or some cells may have weak and/or transient expression of markers and unrestricted clonality [84] and (2) with whole-mount labeling, it is not possible to identify spatial relationships between stem cells and its transit amplifying progeny [85]. In this case, targeted cells are noninvasively labeled in their native environment, and the development of a progenitor cell and a composition of their lineages can be followed. It remains unclear whether the combination of these techniques can be extended to identify CSCs and metastatic initiating stem/progenitor cells.

While there has been a hot debate in recent years as to whether the CSC theory is correct, very recent lineage tracing studies have provided proof that a relatively small number of cells are capable of generating and maintaining a tumor. These studies used fluorescently labeled tumor cells and showed that the quiescent cells remained after further in vivo passages [86]. Furthermore, following treatment, these quiescent cells started to proliferate and generate proliferative progenitor cells that were capable of maintaining a tumor [87–89]. By eliminating these quiescent cells, tumor growth was impaired. These results link back to the theory that leaving a small population of CSCs after the conventional treatment lead to a recurrence of the tumor. Therefore, it is necessary to eliminate both populations of cells within a tumor to produce effective anticancer therapeutic strategies [90].

#### **4.7. CSC epigenome and next-generation sequencing**

Whole genome sequencing has made tremendous contributions to cancer research, which enables researchers to discover and understand the rules of cancer development at the nucleic acid level [91, 92]. However, the genome instability and genetic variants limit to demonstrate cancer progression. It was speculated that there exist a senior layer of information, besides

genome sequence for regulating differential gene expressions and thus determining cancer evolving. This concept was early prospected by Conrad Hal Waddington in 1942 and subsequently described as “epigenetic control system” by Nanney in 1958 [93, 94]. Epigenetics primarily refers to the study of chromosome variations that modulate gene transcription without alterations in the DNA sequences [95, 96]. Epigenome contains genetic information, not as stable as genome, representing the cellular epigenetic state varying with influence from external factors. Mechanisms produce such changes mainly include DNA methylation, histone modifications, nucleosome positioning, and chromatin remodeling [96]. These epigenetic regulation mechanisms are reported to be closely related with the gaining of stem cell-specific properties, whereby contributing to tumor inheterogeneous [97, 98]. Epigenetic alterations would offer survival benefits in CSC subpopulation which promotes the genetic expression to the self-renewal state, resulting in tumor initiation and further progression [99, 100]. The relevance of the DNA methylation and histone modifications in CSC regulation, subsequently with advancing tumor growth, were recently illustrated in various cancer models [97, 99, 101].

Next-generation sequencing (NGS), also known as high-throughput sequencing, has revolutionized the study of genomics and opened a new chapter of the epigenome research of cancer and stem cell [102, 103]. Four mainly NGS-based approaches have been developed to identify epigenome research, including methylated DNA immunoprecipitation sequencing (MeDIP-Seq), whole genome bisulfite sequencing (WGBS), reduced representation bisulfite sequencing (RRBS), and chromatin immunoprecipitation sequencing (ChIP-Seq). Compared with the previous approach, the innovative advantages of NGS have significantly accelerated the sequence of DNA and RNA and promoted the scientific sightings in CSC epigenome research.

## **5. Therapeutic strategies used for targeting CSCs**

Current failure of cancer treatment is normally due to the existence and functionalities of CSCs, which possess more chemoresistance than their non-CSC counterparts, to conventional treatments. Recently, multiple strategies have been developed for targeting and eradicating CSCs while sparing healthy tissues, thereby minimizing the patients to face therapy risks.

### **5.1. Targeting CSCs via surface markers**

Since CSCs are attractive targets for anticancer treatment, the CSC-correlated cell surface proteins have been monitored extensively for identification, probable isolation and monitoring the variation of leukemic and solid CSCs in preclinical and clinical settings [104]. Studies using certain ligands or antibodies against CSC surface maker proteins, including EpCAM, CD47, CD44, CD90, CD133, IL-3R, immunoglobulin mucin TIM-3, ALDH+, and others, have advanced the therapeutic efficacy [105–108]. Limitations, such as the expression of such cell surface makers, may vary in different stages of cancer development; only a small subpopulation of CSCs standing in the summit among bunk of cancer cells, as well as overlapping of CSC-associated marker proteins with normal stem cells, impede the effectively targeting of CSCs [47]. For bench assays, it is recommended to employ functional studies such as in vivo

LDA upon xenotransplantation to ascertain CSCs, rather than solely be dependent on the incidence of a single or a combination of multiple CSC markers. However, in case of in vivo CSC-based therapy, the CSC surface marker proteins present one of the very few feasible options for targeting CSCs in animals and patients, given the practical and ethical restrictions related with lineage tracing and xenotransplantation.

Accumulated attractions have been grasped in the development of aptamers (also known as chemical antibodies) and monoclonal antibodies for targeting CSCs via targeting surface marker proteins. Shigdar et al. have isolated two RNA aptamers using SELEX for targeting CSC surface markers, EpCAM, and CD133 [109, 110]. These CSC-targeting aptamers internalize into target cells through receptor-mediated endocytosis, which is capable of circumventing ATP-binding cassette transporters that function multiple drug resistance in CSCs [26]. In addition, this newly developed EpCAM RNA aptamer is more sensitive than counterpart antibodies for detecting the surface EpCAM proteins in formalin-fixed paraffin-embedded primary breast cancers, with no nonspecific staining or cross-reactivity with non-EpCAM-expression tissues [111]. This shows the potential of aptamers for specific targeting of cancers but with minimized side effects observation. To optimize promising approaches by targeting cell surface markers might be one of the answers for tracing CSCs and eventually eradicating CSCs, thereby preventing patients from suffering from cancer attacking.

## 5.2. Targeting ATP-driven efflux transporters

The failure of cancer chemotherapy mainly results from increased efflux of anticancer drugs from cancer cells, resulting in the impairment of drug cellular entrance and consequent reduction of chemotherapeutic sensitivity [112]. A considerable root of multidrug resistance (MDR) involves the augmented expression of the ABC transporter superfamily, many of these transmembrane proteins are responsible for effluxion of various xenobiotics (including anticancer agents) from cancer intracellular membranes [112, 113]. The well-characterized MDR transporters consist with ABCB1 (MDR1 or P-glycoprotein), ABCC1 (MRP1), and ABCG2 (BCRP or MXR) [112, 114–116]. Although projects focusing on understanding the mechanisms of these ABC transporters behind chemotherapy failure have been broadly developed, clinical outcomes in these fields have been generally unsatisfactory [113, 117]. The recurrence of primary and metastatic sites can occur following the escaped chemotherapy, in which CSCs, possessing enhanced efflux of therapeutic agents through ABC transporters, have been proven to provide major contributions [114, 118, 119].

Due to the correlation of ABC transporters with CSC phenotypes, one approach circumventing CSC-based chemoresistance involves the use of specific molecular inhibitors against certain functions of individual MDR transporters [114]. Verapamil, an agent targeting general ABC transporters, has been moved to the clinical trials, but the further study was suspended due to the dose-limiting toxicity [120]. Thus, the more specific molecules targeting individual MDR transporters are required [121]. A considerable body of evidence has shown positive outcomes of overcoming CSC drug resistance by developing physical conjugation or chemical nanoparticle-functionalized drug delivery of anticancer agents. Chou et al. indicated that the conjugation of doxorubicin (DOX) into nanodiamonds reduced efflux of DOX in MDR1 overexpressing

cancer cells and facilitated the anticancer efficacy in DOX-resistant cancer models [122]. While CSC-related chemoresistance and tumor relapse arise mainly due to the increased expression of ABC transporters, the therapeutic strategies developed for specifically disturbing actions of ABC transporter proteins would be an attractive potential for targeting and eradicating CSCs.

## 6. Conclusions

The CSC concept is still an evolving model moving forward. Recent lineage tracing strategy has proven the existence and functions of CSCs in progression of solid tumors. CSCs with intrinsic activities of chemoresistance are the culprit in tumor recurrence and the root of treatment failures. Challenges remain on how to efficiently identify and target CSCs *in vivo* and monitor CSCs posttreatment. Cancer biology has proofed that traditional clonal evolution, and CSC models are not exclusive but co-exist with each other in tumorigenesis. Therefore, future elucidation of molecular mechanisms underlying CSC biology should open a new window of efficacious novel therapy strategies that eliminate both CSCs and non-CSCs.

## Author details

Zhaopeng Tang<sup>1</sup>, Qianfeng Wang<sup>2</sup>, Sarah Shigdar<sup>3</sup>, Wei Duan<sup>3\*</sup> and Dongxi Xiang<sup>3\*</sup>

\*Address all correspondence to: wei.duan@deakin.edu.au; dxiangmedsci@gmail.com

1 Department of Orthopedics, Gansu Provincial Hospital of Traditional Chinese Medicine, Qilihe, Lanzhou, Gansu, People's Public of China

2 Department of Urology, Gansu Provincial Hospital, Chengguan, Lanzhou, Gansu, People's Public of China

3 School of Medicine, Deakin University, Waurn Ponds, Victoria, Australia

## References

- [1] Jemal A, Siegel R, Ward E, et al. Cancer statistics, 2008. *CA Cancer J Clin* 2008; 58: 71–96. DOI: 10.3322/CA.2007.0010
- [2] Herter-Sprie GS, Greulich H, Wong K-K. Activating mutations in ERBB2 and their impact on diagnostics and treatment. *Front Oncol* 2013; 3: 86. DOI: 10.3389/fonc.2013.00086.

- [3] Hanahan D, Weinberg RA. Hallmarks of cancer: the next generation. *Cell* 2011; 144: 646–674. DOI: 10.1016/j.cell.2011.02.013
- [4] Krogan NJ, Lippman S, Agard DA, Ashworth A, Ideker T. The cancer cell map initiative: defining the hallmark networks of cancer. *Mol Cell* 2015; 58: 690–698. DOI: 10.1016/j.molcel.2015.05.008
- [5] Stratton MR. Exploring the genomes of cancer cells: progress and promise. *Science* 2011; 331: 1553–1558. DOI: 10.1126/science.1204040
- [6] O'Connor ML, Xiang D, Shigdar S, et al. Cancer stem cells: a contentious hypothesis now moving forward. *Cancer Lett* 2014; 344: 180–187. DOI: doi: 10.1016/j.canlet.2013.11.012
- [7] Nowell PC. The clonal evolution of tumor cell populations. *Science* 1976; 194: 23–28.
- [8] Tsai AG, Lu H, Raghavan SC, Muschen M, Hsieh C-L, Lieber MR. Human chromosomal translocations at CpG sites and a theoretical basis for their lineage and stage specificity. *Cell* 2008; 135: 1130–1142. DOI: 10.1016/j.cell.2008.10.035
- [9] Bardelli A, Cahill DP, Lederer G, et al. Carcinogen-specific induction of genetic instability. *Proc Natl Acad Sci U S A* 2001; 98: 5770–5775. DOI: 10.1073/pnas.081082898
- [10] Gatenby RA, Gillies RJ. A microenvironmental model of carcinogenesis. *Nat Rev Cancer* 2008; 8: 56–61. DOI: 10.1038/nrc2255
- [11] Lathia JD, Heddleston JM, Venere M, Rich JN. Deadly teamwork: neural cancer stem cells and the tumor microenvironment. *Cell Stem Cell* 2011; 8: 482–485. DOI: 10.1016/j.stem.2011.04.013
- [12] Chen J, Sprouffske K, Huang Q, Maley CC. Solving the puzzle of metastasis: the evolution of cell migration in neoplasms. *PLoS One* 2011; 6: e17933. DOI: 10.1371/journal.pone.0017933
- [13] Mazzone M, Dettori D, Leite de Oliveira R, et al. Heterozygous deficiency of PHD2 restores tumor oxygenation and inhibits metastasis via endothelial normalization. *Cell* 2009; 136: 839–851. DOI: 10.1016/j.cell.2009.01.020
- [14] Greaves M, Maley CC. Clonal evolution in cancer. *Nature* 2012; 481: 306–313. DOI: 10.1038/nature10762
- [15] Gilbert LA, Hemann MT. DNA damage-mediated induction of a chemoresistant niche. *Cell* 2010; 143: 355–366. DOI: 10.1016/j.cell.2010.09.043
- [16] Cabioglu N, Ozmen V, Kaya H, et al. Increased lymph node positivity in multifocal and multicentric breast cancer. *J Am Coll Surg* 2009; 208: 67–74. DOI: 10.1016/j.jamcollsurg.2008.09.001
- [17] Nguyen-Khac F, Lesty C, Eclache V, et al. Chromosomal abnormalities in transformed Ph-negative myeloproliferative neoplasms are associated to the transforma-

- tion subtype and independent of JAK2 and the TET2 mutations. *Genes Chromosomes Cancer* 2010; 49: 919–927. DOI: 10.1002/gcc.20802
- [18] Visvader JE, Lindeman GJ. Cancer stem cells in solid tumours: accumulating evidence and unresolved questions. *Nat Rev Cancer* 2008; 8: 755–768. DOI: 10.1038/nrc2499
- [19] Nguyen-Khac F, Lesty C, Eclache V, et al. Chromosomal abnormalities in transformed Ph-negative myeloproliferative neoplasms are associated to the transformation subtype and independent of JAK2 and the TET2 mutations. *Genes Chromosomes Cancer* 2010; 49: 919–927. DOI: 10.1002/gcc.20802
- [20] Shackleton M, Quintana E, Fearon ER, Morrison SJ. Heterogeneity in cancer: cancer stem cells versus clonal evolution. *Cell* 2009; 138: 822–829. DOI: 10.1016/j.cell.2009.08.017
- [21] Lee HE, Kim JH, Kim YJ, et al. An increase in cancer stem cell population after primary systemic therapy is a poor prognostic factor in breast cancer. *Br J Cancer* 2011; 104: 1730–1738. DOI: 10.1038/bjc.2011.159
- [22] Beck B, Driessens G, Goossens S, et al. A vascular niche and a VEGF-Nrp1 loop regulate the initiation and stemness of skin tumours. *Nature* 2011; 478: 399–403. DOI: 10.1038/nature10525
- [23] Nguyen LV, Vanner R, Dirks P, Eaves CJ. Cancer stem cells: an evolving concept. *Nat Rev Cancer* 2012; 12: 133–143. DOI: 10.1038/nrc3184
- [24] Wenjing J, Jianhua P, Yue Z, Cho WCS, Kunlin J. The implications of cancer stem cells for cancer therapy. *Int J Mol Sci* 2012; 13: 16636–16657. DOI: 10.3390/ijms131216636
- [25] Vermeulen L, de Sousa e Melo F, Richel DJ, Medema JP. The developing cancer stem-cell model: clinical challenges and opportunities. *Lancet Oncol* 2012; 13: e83–e89. DOI: 10.1016/S1470-2045(11)70257-1
- [26] Xiang D, Shigdar S, Qiao G, et al. Nucleic acid aptamer-guided cancer therapeutics and diagnostics: the next generation of cancer medicine. *Theranostics* 2015; 5: 23–42. DOI: 10.7150/thno.10202
- [27] Chaffer CL, Brueckmann I, Scheel C, et al. Normal and neoplastic nonstem cells can spontaneously convert to a stem-like state. *Proc Natl Acad Sci U S A* 2011; 108: 7950–7955. DOI: 10.1073/pnas.1102454108
- [28] Scheel C, Eaton EN, Li SH-J, et al. Paracrine and autocrine signals induce and maintain mesenchymal and stem cell states in the breast. *Cell* 2011; 145: 926–940. DOI: 10.1016/j.cell.2011.04.029
- [29] O'Brien CA, Kreso A, Jamieson CHM. Cancer stem cells and self-renewal. *Clin Cancer Res* 2010; 16: 3113–3120. DOI: 10.1158/1078-0432.CCR-09-2824

- [30] Wei J, Wunderlich M, Fox C, et al. Microenvironment determines lineage fate in a human model of MLL-AF9 leukemia. *Cancer Cell* 2008; 13: 483–495. DOI: 10.1016/j.ccr.2008.04.020
- [31] Kim M, Moon HB, Spangrude GJ. Major age-related changes of mouse hematopoietic stem/progenitor cells. *Ann N Y Acad Sci* 2003; 996: 195–208. DOI: 10.1111/j.1749-6632.2003.tb03247.x
- [32] Quintana E, Shackleton M, Sabel MS, Fullen DR, Johnson TM, Morrison SJ. Efficient tumour formation by single human melanoma cells. *Nature* 2008; 456: 593–598. DOI: 10.1038/nature07567
- [33] Tan E, Ding XQ, Saadi A, Agarwal N, Naash MI, Al-Ubaidi MR. Expression of cone-photoreceptor-specific antigens in a cell line derived from retinal tumors in transgenic mice. *Invest Ophthalmol Vis Sci* 2004; 45: 764–768.
- [34] Limaye PB, Bowen WC, Orr AV, Luo J, Tseng GC, Michalopoulos GK. Mechanisms of hepatocyte growth factor-mediated and epidermal growth factor-mediated signaling in transdifferentiation of rat hepatocytes to biliary epithelium. *Hepatology* 2008; 47: 1702–1713. DOI: 10.1002/hep.22221
- [35] Michalopoulos GK, Barua L, Bowen WC. Transdifferentiation of rat hepatocytes into biliary cells after bile duct ligation and toxic biliary injury. *Hepatology* 2005; 41: 535–544. DOI: 10.1002/hep.20600
- [36] Vermeulen L, Snippert HJ. Stem cell dynamics in homeostasis and cancer of the intestine. *Nat Rev Cancer* 2014; 14: 468–480. DOI: 10.1038/nrc3744
- [37] Chiba T, Kita K, Zheng YW, et al. Side population purified from hepatocellular carcinoma cells harbors cancer stem cell-like properties. *Hepatology* 2006; 44: 240–251. DOI: 10.1002/hep.21227
- [38] Kimura O, Takahashi T, Ishii N, et al. Characterization of the epithelial cell adhesion molecule (EpCAM)+ cell population in hepatocellular carcinoma cell lines. *Cancer Sci* 2010; 101: 2145–2155. DOI: 10.1111/j.1349-7006.2010.01661.x
- [39] Cao L, Zhou Y, Zhai B, et al. Sphere-forming cell subpopulations with cancer stem cell properties in human hepatoma cell lines. *BMC Gastroenterol* 2011; 11: 71. DOI: 10.1186/1471-230X-11-71
- [40] Adams JM, Strasser A. Is tumor growth sustained by rare cancer stem cells or dominant clones? *Cancer Res* 2008; 68: 4018–4021. DOI: 10.1158/0008-5472
- [41] Resetkova E, Reis-Filho JS, Jain RK, et al. Prognostic impact of ALDH1 in breast cancer: a story of stem cells and tumor microenvironment. *Breast Cancer Res Treat* 2010; 123: 97–108. DOI: 10.1007/s10549-009-0619-3
- [42] Allikmets R, Schriml LM, Hutchinson A, Romano-Spica V, Dean M. A human placenta-specific ATP-binding cassette gene (ABCP) on chromosome 4q22 that is involved in multidrug resistance. *Cancer Res* 1998; 58: 5337–5339.

- [43] Abdullah LN, Chow EK. Mechanisms of chemoresistance in cancer stem cells. *Clin Transl Med* 2013; 2: 3. DOI: 10.1186/2001-1326-2-3
- [44] Todaro M, Francipane MG, Medema JP, Stassi G. Colon cancer stem cells: promise of targeted therapy. *Gastroenterology* 2010; 138: 2151–2162. DOI: 10.1053/j.gastro.2009.12.063
- [45] Sottoriva A, Verhoeff JJC, Borovski T, et al. Cancer stem cell tumor model reveals invasive morphology and increased phenotypical heterogeneity. *Cancer Res* 2010; 70: 46–56. DOI: 10.1158/0008-5472
- [46] Bonnet D, Dick JE. Human acute myeloid leukemia is organized as a hierarchy that originates from a primitive hematopoietic cell. *Nat Med* 1997; 3: 730–737.
- [47] Yang YM, Chang JW. Current status and issues in cancer stem cell study. *Cancer Invest* 2008; 26: 741–755. DOI: 10.1080/07357900801901856
- [48] Al-Hajj M, Wicha MS, Benito-Hernandez A, Morrison SJ, Clarke MF. Prospective identification of tumorigenic breast cancer cells. *Proc Natl Acad Sci U S A* 2003; 100: 3983–3988. DOI: 10.1073/pnas.0530291100
- [49] O'Brien CA, Pollett A, Gallinger S, Dick JE. A human colon cancer cell capable of initiating tumour growth in immunodeficient mice. *Nature* 2007; 445: 106–110. DOI: 10.1038/nature05372
- [50] Li C, Heidt DG, Dalerba P, et al. Identification of pancreatic cancer stem cells. *Cancer Res* 2007; 67: 1030–1037. DOI: 10.1158/0008-5472.CAN-06-2030
- [51] Shen J, Zhu Z. Catumaxomab, a rat/murine hybrid trifunctional bispecific monoclonal antibody for the treatment of cancer. *Curr Opin Mol Ther* 2008; 10: 273–284.
- [52] Medema JP, Vermeulen L. Microenvironmental regulation of stem cells in intestinal homeostasis and cancer. *Nature* 2011; 474: 318–326. DOI: 10.1038/nature10212
- [53] de Sousa EM, Vermeulen L, Richel D, Medema JP. Targeting Wnt signaling in colon cancer stem cells. *Clin Cancer Res* 2011; 17: 647–653. DOI: 10.1158/1078-0432.CCR-10-1204
- [54] Hu Y, Smyth GK. ELDA: extreme limiting dilution analysis for comparing depleted and enriched populations in stem cell and other assays. *J Immunol Methods* 2009; 347: 70–78. DOI: 10.1016/j.jim.2009.06.008
- [55] Parrish RS, Hazlett LJ. Design and estimation in the limiting dilution assay when concentrations vary widely among samples. *J Biopharm Stat* 2000; 10: 197–215. DOI: 10.1081/BIP-1001101022
- [56] Macken C. Design and analysis of serial limiting dilution assays with small sample sizes. *J Immunol Methods* 1999; 222: 13–29. DOI: 10.1016/S0022-1759(98)00133-1

- [57] Sieburg HB, Cho RH, Muller-Sieburg CE. Limiting dilution analysis for estimating the frequency of hematopoietic stem cells: uncertainty and significance. *Exp Hematol* 2002; 30: 1436–1443. DOI: 10.1016/S0301-472X(02)00963-3
- [58] Cheli Y, Giuliano S, Guiliano S, et al. Mitf is the key molecular switch between mouse or human melanoma initiating cells and their differentiated progeny. *Oncogene* 2011; 30: 2307–2318. DOI: 10.1038/onc.2010.598
- [59] Shultz LD, Sidman CL. Genetically determined murine models of immunodeficiency. *Ann Rev Immunol* 1987; 5: 367–403. DOI: 10.1146/annurev.iy.05.040187.002055
- [60] Ricci-Vitiani L, Lombardi DG, Pilozzi E, et al. Identification and expansion of human colon-cancer-initiating cells. *Nature* 2007; 445: 111–115. DOI: 10.1038/nature05384
- [61] Maitland NJ, Frame FM, Polson ES, Lewis JL, Collins AT. Prostate cancer stem cells: do they have a basal or luminal phenotype? *Horm Cancer* 2011; 2: 47–61. DOI: 10.1007/s12672-010-0058-y
- [62] Barabe F, Kennedy JA, Hope KJ, Dick JE. Modeling the initiation and progression of human acute leukemia in mice. *Science* 2007; 316: 600–604. DOI: 10.1126/science.1139851
- [63] Howarth KD, Blood KA, Ng BL, et al. Array painting reveals a high frequency of balanced translocations in breast cancer cell lines that break in cancer-relevant genes. *Oncogene* 2008; 27: 3345–3359. DOI: 10.1038/sj.onc.1210993
- [64] Summer R, Kotton DN, Sun X, Ma B, Fitzsimmons K, Fine A. Side population cells and Bcrp1 expression in lung. *Am J Physiol Lung Cell Mol Physiol* 2003; 285: L97–L104. DOI: 10.1152/ajplung.00009.2003
- [65] Kim M, Moon H-B, Spangrude GJ. Major age-related changes of mouse hematopoietic stem/progenitor cells. *Ann N Y Acad Sci* 2003; 996: 195–208. DOI: 10.1111/j.1749-6632.2003.tb03247.x
- [66] Triel C, Vestergaard ME, Bolund L, Jensen TG, Jensen UB. Side population cells in human and mouse epidermis lack stem cell characteristics. *Exp Cell Res* 2004; 295: 79–90. DOI: 10.1016/j.yexcr.2003.11.032
- [67] Choo CR, Danjoux C, Morton GC. Should pathological T3 and/or margin positive prostate cancer receive adjuvant therapy? A radiation oncologist's view. *Can J Urol* 2000; 7: 1043–1050.
- [68] Fromm MF, Kauffmann HM, Fritz P, et al. The effect of rifampin treatment on intestinal expression of human MRP transporters. *Am J Pathol* 2000; 157: 1575–1580. DOI: 10.1016/S0002-9440(10)64794-3
- [69] Pece S, Tosoni D, Confalonieri S, et al. Biological and molecular heterogeneity of breast cancers correlates with their cancer stem cell content. *Cell* 2010; 140: 62–73. DOI: 10.1016/j.cell.2009.12.007

- [70] Kim S, Alexander CM. Tumorsphere assay provides more accurate prediction of in vivo responses to chemotherapeutics. *Biotechnol Lett* 2014; 36: 481–488. DOI: 10.1007/s10529-013-1393-1
- [71] Willan PM, Farnie G. Application of stem cell assays for the characterization of cancer stem cells. In: *Cancer Stem Cells in Solid Tumors*. Springer; 2011. p. 259–282. DOI: 10.1007/978-1-61779-246-5\_15
- [72] Charrier C, Coronas V, Fombonne J, et al. Characterization of neural stem cells in the dorsal vagal complex of adult rat by in vivo proliferation labeling and in vitro neurosphere assay. *Neuroscience* 2006; 138: 5–16. DOI: 10.1016/j.neuroscience.2005.10.046
- [73] Ayyanan A, Civenni G, Ciarloni L, et al. Increased Wnt signaling triggers oncogenic conversion of human breast epithelial cells by a Notch-dependent mechanism. *Proc Natl Acad Sci U S A* 2006; 103: 3799–3804. DOI: 10.1073/pnas.0600065103
- [74] Singh SK, Hawkins C, Clarke ID, et al. Identification of human brain tumour initiating cells. *Nature* 2004; 432: 396–401. DOI: 10.1038/nature03128
- [75] Toma JG, McKenzie IA, Bagli D, Miller FD. Isolation and characterization of multipotent skin-derived precursors from human skin. *Stem Cells* 2005; 23: 727–737. DOI: 10.1634/stemcells.2004-0134
- [76] Fang D, Nguyen TK, Leishear K, et al. A tumorigenic subpopulation with stem cell properties in melanomas. *Cancer Res* 2005; 65: 9328–9337. DOI: 10.1158/0008-5472.CAN-05-1343
- [77] Croker AK, Goodale D, Chu J, et al. High aldehyde dehydrogenase and expression of cancer stem cell markers selects for breast cancer cells with enhanced malignant and metastatic ability. *J Cell Mol Med* 2009; 13: 2236–2252. DOI: 10.1111/j.1582-4934.2008.00455.x
- [78] Cariati M, Naderi A, Brown JP, et al. Alpha-6 integrin is necessary for the tumorigenicity of a stem cell-like subpopulation within the MCF7 breast cancer cell line. *Int J Cancer* 2008; 122: 298–304. DOI: 10.1002/ijc.23103
- [79] Chute JP, Muramoto GG, Whitesides J, et al. Inhibition of aldehyde dehydrogenase and retinoid signaling induces the expansion of human hematopoietic stem cells. *Proc Natl Acad Sci U S A* 2006; 103: 11707–11712. DOI: 10.1073/pnas.0603806103
- [80] Ginestier C, Hur MH, Charafe-Jauffret E, et al. ALDH1 is a marker of normal and malignant human mammary stem cells and a predictor of poor clinical outcome. *Cell Stem Cell* 2007; 1: 555–567. DOI: 10.1016/j.stem.2007.08.014
- [81] Braun KM, Watt FM. Epidermal label-retaining cells: background and recent applications. *J Investig Dermatol Symp Proc* 2004; 9: 196–201. DOI: 10.1111/j.1087-0024.2004.09313.x

- [82] Kase S, Yoshida K, Ohgami K, Shiratori K, Ohno S, Nakayama KI. Phosphorylation of p27(KIP1) in the mitotic cells of the corneal epithelium. *Curr Eye Res* 2006; 31: 307–312. DOI: 10.1080/02713680600584687
- [83] Oliver JA, Maarouf O, Cheema FH, Martens TP, Al-Awqati Q. The renal papilla is a niche for adult kidney stem cells. *J Clin Invest* 2004; 114: 795–804. DOI: 10.1172/JCI200420921
- [84] Bossing T, Technau GM. The fate of the CNS midline progenitors in *Drosophila* as revealed by a new method for single cell labelling. *Development* 1994; 120: 1895–1906.
- [85] Jensen UB, Lowell S, Watt FM. The spatial relationship between stem cells and their progeny in the basal layer of human epidermis: a new view based on whole-mount labelling and lineage analysis. *Development* 1999; 126: 2409–2418.
- [86] Tao L, van Bragt MPA, Laudadio E, Li Z. Lineage tracing of mammary epithelial cells using cell-type-specific cre-expressing adenoviruses. *Stem Cell Reports* 2014; 2: 770–779. DOI: 10.1016/j.stemcr.2014.04.004
- [87] Chen J, Li Y, Yu T-S, et al. A restricted cell population propagates glioblastoma growth after chemotherapy. *Nature* 2012; 488: 522–526. DOI: 10.1038/nature11287
- [88] Driessens G, Beck B, Caauwe A, Simons BD, Blanpain C. Defining the mode of tumour growth by clonal analysis. *Nature* 2012; 488: 527–530. DOI: 10.1038/nature11344
- [89] Schepers AG, Snippert HJ, Stange DE, et al. Lineage tracing reveals Lgr5+ stem cell activity in mouse intestinal adenomas. *Science* 2012; 337: 730–735. DOI: 10.1126/science.1224676
- [90] Shigdar S, Lin J, Li Y, et al. Cancer stem cell targeting: the next generation of cancer therapy and molecular imaging. *Ther Deliv* 2012; 3: 227–244.
- [91] Nater A, Burri R, Kawakami T, Smeds L, Ellegren H. Resolving evolutionary relationships in closely related species with whole-genome sequencing data. *Syst Biol* 2015; DOI: 10.1093/sysbio/syv045
- [92] Hehir-Kwa JY, Pfundt R, Veltman JA. Exome sequencing and whole genome sequencing for the detection of copy number variation. *Expert Rev Mol Diagn* 2015; 15: 1023–1032. DOI: 10.1586/14737159.2015.1053467
- [93] Li J, Wang T, Zhang X, Yang X. The contribution of next generation sequencing technologies to epigenome research of stem cell and tumorigenesis. *Hum Genet Embryol* 2011; 01: 1–10. DOI: 10.4172/2161-0436.s2-001
- [94] Nanney DL. Epigenetic control systems. *Proc Natl Acad Sci U S A* 1958; 44: 712–717.
- [95] Morales La Madrid A, Hashizume R, Kieran MW. Future clinical trials in DIPG: bringing epigenetics to the clinic. *Front Oncol* 2015; 5: 148. DOI: 10.3389/fonc.2015.00148

- [96] Busch C, Burkard M, Leischner C, Lauer UM, Frank J, Venturelli S. Epigenetic activities of flavonoids in the prevention and treatment of cancer. *Clin Epigenetics* 2015; 7: 64. DOI: 10.1186/s13148-015-0095-z
- [97] Munoz P, Iliou MS, Esteller M. Epigenetic alterations involved in cancer stem cell reprogramming. *Mol Oncol* 2012; 6: 620–636. DOI: 10.1016/j.molonc.2012.10.006
- [98] Esteller M. Epigenetics in cancer. *N Engl J Med* 2008; 358: 1148–1159. DOI: 10.1056/NEJMra072067
- [99] Volkel P, Dupret B, Le Bourhis X, Angrand P-O. Diverse involvement of EZH2 in cancer epigenetics. *Am J Transl Res* 2015; 7: 175–193.
- [100] Jeter CR, Yang T, Wang J, Chao HP, Tang DG. Concise review: NANOG in cancer stem cells and tumor development: an update and outstanding questions. *Stem Cells* 2015; 33: 2381–2390. DOI: 10.1002/stem.2007
- [101] Shukla S, Meeran SM. Epigenetics of cancer stem cells: pathways and therapeutics. *Biochim Biophys Acta* 2014; 1840: 3494–3502. DOI: 10.1016/j.bbagen.2014.09.017
- [102] Mardis ER. The impact of next-generation sequencing technology on genetics. *Trends Genet* 2008; 24: 133–141. DOI: 10.1016/j.tig.2007.12.007
- [103] Morozova O, Marra MA. Applications of next-generation sequencing technologies in functional genomics. *Genomics* 2008; 92: 255–264. DOI: 10.1016/j.ygeno.2008.07.001
- [104] Visvader JE, Lindeman GJ. Cancer stem cells in solid tumours: accumulating evidence and unresolved questions. *Nat Rev Cancer* 2008; 8: 755–768. DOI: 10.1038/nrc2499
- [105] Chen K, Huang Y-h, Chen J-l. Understanding and targeting cancer stem cells: therapeutic implications and challenges. *Acta Pharmacol Sin* 2013; 34: 732–740. DOI: 10.1038/aps.2013.27
- [106] Pollyea DA, Gutman JA, Gore L, Smith CA, Jordan CT. Targeting acute myeloid leukemia stem cells: a review and principles for the development of clinical trials. *Haematologica* 2014; 99: 1277–1284. DOI: 10.3324/haematol.2013.085209
- [107] Hoang VT, Buss EC, Wang W, et al. The rarity of ALDH(+) cells is the key to separation of normal versus leukemia stem cells by ALDH activity in AML patients. *Int J Cancer* 2015; 137: 525–536. DOI: 10.1002/ijc.29410
- [108] Fan D, Li Z, Zhang X, et al. AntiCD3Fv fused to human interleukin-3 deletion variant redirected T cells against human acute myeloid leukemic stem cells. *J Hematol Oncol* 2015; 8: 18. DOI: 10.1186/s13045-015-0109-5
- [109] Shigdar S, Qiao L, Zhou S-F, et al. RNA aptamers targeting cancer stem cell marker CD133. *Cancer Lett* 2013; 330: 84–95. DOI: 10.1016/j.canlet.2012

- [110] Shigdar S, Lin J, Yu Y, Pastuovic M, Wei M, Duan W. RNA aptamer against a cancer stem cell marker epithelial cell adhesion molecule. *Cancer Sci* 2011; 102: 991–998. DOI: 10.1111/j.1349-7006.2011.01897.x
- [111] Shigdar S, Qian C, Lv L, et al. The use of sensitive chemical antibodies for diagnosis: detection of low levels of EpCAM in breast cancer. *PLoS One* 2013; 8: e57613. DOI: 10.1371/journal.pone.0057613
- [112] Fletcher JI, Haber M, Henderson MJ, Norris MD. ABC transporters in cancer: more than just drug efflux pumps. *Nat Rev Cancer* 2010; 10: 147–156. DOI: 10.1038/nrc2789
- [113] Gottesman MM, Fojo T, Bates SE. Multidrug resistance in cancer: role of ATP-dependent transporters. *Nat Rev Cancer* 2002; 2: 48–58. DOI: 10.1038/nrc706
- [114] Abdullah LN, Chow EK-H. Mechanisms of chemoresistance in cancer stem cells. *Clin Transl Med* 2013; 2: 3. DOI: 10.1186/2001-1326-2-3
- [115] Jonker JW, Merino G, Musters S, et al. The breast cancer resistance protein BCRP (ABCG2) concentrates drugs and carcinogenic xenotoxins into milk. *Nat Med* 2005; 11: 127–129. DOI: 10.1038/nm1186
- [116] Zhou S, Schuetz JD, Bunting KD, et al. The ABC transporter Bcrp1/ABCG2 is expressed in a wide variety of stem cells and is a molecular determinant of the side-population phenotype. *Nat Med* 2001; 7: 1028–1034. DOI: 10.1038/nm0901-1028
- [117] Szakacs G, Paterson JK, Ludwig JA, Booth-Genthe C, Gottesman MM. Targeting multidrug resistance in cancer. *Nat Rev Drug Discov* 2006; 5: 219–234. DOI: 10.1038/nrd1984
- [118] Scharenberg CW, Harkey MA, Torok-Storb B. The ABCG2 transporter is an efficient Hoechst 33342 efflux pump and is preferentially expressed by immature human hematopoietic progenitors. *Blood* 2002; 99: 507–512. DOI: 10.1182/blood.V99.2.507
- [119] Chow EK-H, Fan L-l, Chen X, Bishop JM. Oncogene-specific formation of chemoresistant murine hepatic cancer stem cells. *Hepatology* 2012; 56: 1331–1341. DOI: 10.1002/hep.25776
- [120] Dalton WS, Crowley JJ, Salmon SS, et al. A phase III randomized study of oral verapamil as a chemosensitizer to reverse drug resistance in patients with refractory myeloma. A Southwest Oncology Group study. *Cancer* 1995; 75: 815–820.
- [121] Lancet JE, Baer MR, Duran GE, et al. A phase I trial of continuous infusion of the multidrug resistance inhibitor zosuquidar with daunorubicin and cytarabine in acute myeloid leukemia. *Leuk Res* 2009; 33: 1055–1061. DOI: 10.1016/j.leukres.2008.09.015
- [122] Chow EK, Zhang XQ, Chen M, et al. Nanodiamond therapeutic delivery agents mediate enhanced chemoresistant tumor treatment. *Sci Transl Med* 2011; 3: 73ra21. DOI: 10.1126/scitranslmed.3001713



---

# Antibody-Targeted Immunocarriers for Cancer Treatment

---

Mengxin Zhao, Yun Sun, Xiandi Zhu, Di Chen, Sishen Feng,  
Shangjing Guo and Wei Li

Additional information is available at the end of the chapter

<http://dx.doi.org/10.5772/61288>

---

## Abstract

Nanocarrier's engineering based on fine chemical design and novel structural tailoring can provide practical solution to solve the problems in traditional cancer immunotherapy. Nanoimmunotherapy is thus defined as the application and further development of novel nanocarriers for enhancing immunotherapy. It has become one of the most intriguing fields due to its unique power in treatment and even cure of cancer since reported in last year. Herein, this chapter illustrates the state-of-the-art development in antibody engineering and cancer immunotherapy and gives an explanation why functional nanocarriers including micelles and liposomes can be efficient for nanoimmunotherapy. We further illustrate how to promote the nanoimmunotherapy by the chemical design and carrier's engineering for the first time.

**Keywords:** Immunonanocarrier, antibody, nanoimmunotherapy, mAb engineering, drug delivery system

---

## 1. Introduction

Cancer can be caused by many elements, such as bacterial infection, radiation, and genetic abnormalities, and it is the leading cause of death all over the world. Nowadays, deaths caused by cancer are approximately one of eight of all deaths in the worldwide. Traditional cancer therapies such as chemotherapy, surgery, and radiation therapy have made a lot of progress in the treatment of cancer. However, they will still cause serious side effects or death by the damage of normal cells or organ including hepatotoxicity, cardiotoxicity, or nephrotoxicity. The application of nanotechnology in cancer treatment, monitoring, and control of cancer is

---

called “nanomedicine”, which is defined by the National Institutes of Health in USA. The cancer therapeutic index was significantly improved by the nanomedicines.

Compared with the traditional methods of therapy, newly developed cancer therapy based on the nanoparticles attracted extensive interest due to its unique advantages. However, there are still some drawbacks, such as the unfavorable *in vivo* performance for nanomedicine and the undesirable tumor escape in the immunotherapy. We know that *in vivo* performance strongly depended on the micelles structural properties; thus, the big gap between *in vitro* and *in vivo* can be overcome by micelles’ structural tailoring by chemical design and microstructural tuning. In addition, this fine micelles’ engineering can also provide practical solution to solve the problems in traditional cancer immunotherapy. In this chapter, we review the latest development in antibody engineering, nanomedicine, cancer therapy, and nanoimmunotherapy. We then give an explanation why fine micelles’ engineering with a special focus on the unique pathology of tumor microenvironments and properties of immunocells can obviously promote the *in vivo* performance and improve the therapeutic index of nanoimmunotherapy. In the chapter, we will take four parts to expound how the antibody-targeted immunomicelles play a role in cancer treatment.

## 2. Antibody engineering

Cancer-targeted therapy, aiming at targeting cancer cells and protecting normal tissue, is being developed rapidly and achieves significant improvement. One of the most significant advances in tumor-targeted therapy is nanomedicine, defined as the application and further development of nanotechnology to solve problems in medicine, specifically to diagnose, treat, and prevent diseases. [1, 2] Nanomedicines are designed to alter the pharmaceutical properties of loaded drugs (including pharmacokinetics (PK) and biodistribution (BD), or to function as drug reservoirs (i. e. , as sustained release systems), or both [3]). The adverse effects of conventional chemotherapeutics can be greatly ameliorated by nanomedicines. [4, 5] Also, the pharmacological properties of conventional drugs can be improved through the use of nanomedicines. [6, 7] On the other hand, nanomedicines can protect the drug from premature degradation and unfavorable interaction with the biological environment, improve the targeting to tumors by the “ enhanced permeability and retention (EPR) effect, ” and increase intracellular penetration. [8, 9] Recently, several nanomedicines have been approved or in clinical trials, such as Myocet (non-PEGylated doxorubicin liposomes), DaunoXome (daunorubicin liposomes), Onco TCS (vincristine liposomes), Doxil/Caelys (PEGylated doxorubicin liposomes), and Abraxane (albumin-bound paclitaxel nanoparticles).

Another significant advance in cancer-targeted therapy is the creation of monoclonal antibodies (mAbs) in cancer therapy. [10, 11] MAbs have been widely used alone or in combination with other chemotherapy agents in cancer therapy. [10-12] The use of mAbs in cancer therapy is growing rapidly due to their specific targeting to cancer cells and potent antitumor effects. [13] Until now, more than ten mAbs have been approved for cancer therapy. [14]

## 2.1. Monoclonal antibodies

MABs are monospecific antibodies which are made by identical immune cells cloning from the unique parent cell. MABs are typically made by fusing myeloma cells with spleen cells of mice immunized with antigens. The first generation of mABs of murine origins is limited in clinic use owing to their strong immunogenicity and weak activity to elicit antitumor immune response. These defects are considerably overcome by the chimeric and humanized mABs, which contain human Fc domains and retain targeting specificity by incorporating portions of the murine variable regions. Chimeric mABs are generated by grafting the entire murine regions into the human IgG framework, whereas humanized mABs are developed by grafting complementary-determining regions (CDRs) into the human IgG framework. [15-17] Recently, the fully human mABs with little immunogenicity in humans are being developed rapidly using either phage display technology or transgenic mice. [18]

MABs have achieved significant progress in cancer therapy. The most significant advances in the application of mABs to oncology have been the approval of bevacizumab (Avastin, anti-VEGF antibody), cetuximab (Erbix, anti-EGFR antibody), and trastuzumab (Herceptin, anti-HER2 antibody). Bevacizumab significantly prolongs the survival of patients with metastatic cancers of the colorectum, breast, and lungs, combined with standard chemotherapy regimens. [19] Cetuximab achieved potent antitumor responses in patients with chemotherapy-refractory colorectum cancer. [20] Herceptin has been shown to prolong the disease-free and overall survival of patients with breast cancer. [21]

## 2.2. Immunoglobulin-like antibodies

Immunoglobulin is a protein manufactured by plasma cells and lymphocytes and characteristic of these types of cells. Immunoglobulins play a key role in the body's immune system. Antibody, also known as an immunoglobulin, is a large Y-shaped protein used by the immune system to detect and neutralize foreign objects such as bacteria and viruses. The antibody recognizes a unique part of the foreign target, termed an antigen. Recent gene engineering could redesign the antibody by structure modification. After gene engineering, several antibodies still maintain their immunoglobulin-like structure but significantly enhanced the binding affinity or cytotoxic effects. Li et al. developed two genetically engineered tetravalent antibodies (TetraMcAb), respectively, derived from the anti-CD20 mABs C2B8 and 2F2. [22] TetraMcAbs were not only effective in inducing complement-dependent cytotoxicity (CDC) and antibody-dependent cellular cytotoxicity (ADCC) against B-lymphoma cells as native divalent antibodies (DiMcAbs) but also had antiproliferative and apoptosis-inducing activity markedly superior to that of DiMcAbs. Wu et al. developed dual-specific and tetravalent immunoglobulin G (IgG)-like molecule termed dual-variable-domain immunoglobulin (DVD-Ig)-that can be engineered from any two mABs while preserving activities of the parental antibodies. [23] This molecule can be efficiently produced from mammalian cells and exhibits good physicochemical and pharmacokinetic properties. In an animal disease model, preclinical studies of a DVD-Ig protein demonstrate its potential for therapeutic application in human diseases.

### 2.3. Antibody fragments

In addition to mAbs and immunoglobulin-like antibodies, antibodies could also be reduced in size, dissected into minimal binding fragments, and rebuilt into multivalent high-avidity reagents. There are many kinds of antibody fragments. (i) The scFv is a fusion protein of the variable regions of the heavy (VH) and light chains (VL) of immunoglobulins, connected with a short peptide linker consisting of 10~25 amino acids. To provide flexibility and enhance the hydrophilicity of the peptide backbone, the most commonly used linker contains a combination of glycine and serine residues. The linker is usually rich in glycine for flexibility, as well as serine or threonine for solubility, and can either connect the N-terminus of the VH with the C-terminus of the VL. Despite of the removal of the constant regions and the introduction of the linker, this engineered antibody retains the specificity of the original immunoglobulin. (ii) Multivalent antibodies are constructed by multiple Fab or scFv. [24] (iii) Domain antibodies (dAbs), derived from the "heavy chain" of the immunoglobulins from camels, are the smallest known antigen-binding fragments of antibodies, ranging from 11 kDa to 15 kDa. They are the robust variable regions of the heavy and light chains of immunoglobulins (VH and VL, respectively). Due to the small size and inherent stability, dAbs are bioactive as monomers and can be formatted into larger molecules, which could be created with prolonged serum half-lives or other pharmacological activities. [25] (iv) Qiu et al. reported that the mimetics fused by two CDRs, VHCDR1 and VLCDR3, through a cognate framework region (VHFR2) retained the antigen recognition of their parent molecules and had a superior penetration capacity. [26] The antigen-recognition abilities of these B3 kDa mimetics surpass those of comparable fragments lacking the framework region. To our knowledge, these small antibody mimetics are the smallest antibodies among all the present antibodies.

### 3. Finely assembled micelles for promoting antitumor therapy

Almost 40% of newly discovered drugs have delivery problems due to their low solubility, permeability, and stability. In comparison with the traditional small molecule therapeutic agent, nanomedicine has offered new hope for detection, prevention, and treatment in cancer therapy because it extensively improves the solubility of poorly water-soluble drugs, [27] prolongs the half-life of drug systemic circulation, [28] releases drugs at a controlled rate, [29] delivers drugs in a targeted manner with little side effects, suppresses drug resistance, and reduces the immunogenicity. [30] Nanomedicine was generally not allowed to be used for the development of nanoscale or nanostructured materials to solve the problems in medicine via its unique medical effects. With the rapid advances in nanotechnology, many cancer therapeutic agents delivering systems have been developed based on nanoparticles, such as polymeric micelles, polymer-drug conjugates, dendrimers, liposomes, nanopolymer composition, and inorganic particulates with a size range of 1-1,000 nm. Some of these products have been introduced into the pharmaceutical market. Doxil was the first liposomal drug formulation for the treatment of AIDS associated with Kaposi's sarcoma in 1995. [31] The polymer-drug conjugate, Abraxane, an albumin-bound paclitaxel drug formulation, was approved by

the Food and Drug Administration, USA (FDA) in 2005 as a second-line treatment for the breast cancer. [32-34]

However, some major challenges are raised as the clinical test of numerous ensuing nanomedicine products. The obvious drawbacks are the *in vivo* instability[35] and the fast clearance from the blood by the reticuloendothelial system (RES). [36] The most widely used strategy overcoming the instability is covering the carrier's with some hydrophilic polymers such as poly(ethylene glycol) (PEG) or poly(vinylalcohol) (PVA). Nanocarriers linked with highly hydrated flexible PEG successfully escaped from the RES. [37] The PVA coating also improved the particle's stability. However, it should be a commonsense that introducing too much adjuvant into the body resulted in the undesirable toxicity. Moreover, the size, structure, and surface electronic properties of the formulations were changed resulting in unfavorable therapy index. On the contrary, the micellar system mainly including the polymeric micelle and phospholipid micelle has successfully overcome the above drawbacks because these spherical nanoparticles have simple structure and no adjuvant. The lipid based micelles show high potential in the doxorubicin entrapping. [38] However, its intrinsic phospholipid structure resulted in the untunable micellar structure with  $D > 100$  nm, which considerably limited the intratumor accumulation. Additionally, drug release from conventional liposome formulations is quite limited once these particles reach the tumor. [39]

Fortunately, the nanosized polymeric micelles (10-100 nm in diameter) self-assembled from amphiphilic block copolymers can significantly improve the hydrophobic drug solubility in the core via the similar-to-similar interaction. The micelle possesses well-defined hydrophobic core and hydrophilic corona structure in aqueous media. [40] On the other hand, the densely packed corona forming hydrophilic polymer chain can protect micellar system from the RES by reducing the interaction with serum proteins and renal filtration. [41] In comparison with lipid-based micelles, block copolymeric micelles provide a unique and powerful nanoplatform for anticancer drug delivery. The size of polymeric micelles can be easily tuned by varying the block lengths of the amphiphilic copolymer. It is also easy to modify micellar surface via the functional shell forming polymer. Both the tunable size range and the tailorable structure successfully reduce the renal filtration and obviously enhance tumor penetration. Some nanosized micelles such as PEG-PLA/PCL or PEG-PPO-PEG have significantly improved the *in vitro* /*vivo* application. Several polymeric micellar formulations are currently undergoing phase I/II clinical trials, which have shown significant antitumor efficacy and reduced systemic toxicity. [40, 41]

It is known that the endothelial cells of the tumor blood vessels proliferate at a 30- to 40-fold higher rate than those in normal tissues, which results in the larger endothelial cells gaps (200-700 nm, or sometimes even larger, up to 1.2  $\mu\text{m}$ ) than 7 nm in the normal tissue. [42] Additionally, the high metabolism of tumor cells requires much more oxygen, nutrients, gas exchange, and waste removal. However, the heterogeneity structure and distribution of the tumor blood vessels as well as the blood capillaries slow down the energy exchange between intra- and extratumor. All these result in unique characteristics of tumor, that is, the unnormal tumor blood vessels with gap in 200-700 nm, [43] the relative high temperature of tumor ( $T > 37^\circ\text{C}$ ), [44] and the relative low pH (5~6). In order to further improve micellar delivering

profile, including the lesion's accumulating, cellular uptake, and intracellular release, many new stimulate-responsive micelles were extensively investigated with special focus on the tumor microenvironment. Utilizing the lower pH value in solid tumors and endosomes (5.5), Kataoka's group explored the novel multifunctional pH-sensitive doxorubicin-conjugated PEG-p(Asp-Hyd-DOX) copolymer micelles. The pH linker broke as pH < 6.0 ensued a sustained release. [46] An enhanced accumulation in lung and colon tumors of the micelle-forming PEO-PAsp (ADR) conjugates after 24 h (ca. 10% dose per g tumor) was much higher than the free ADR (ca. 0.90% dose per g tumor). Later, they further investigated the pH triggered intracellular release profile of poly(ethyleneglycol)-poly(aspartate hydrazone adriamycin) micelles and observed that the micelles can stably circulate in physiological conditions (pH 7.4) and selectively release drug by sensing the intracellular low pH (pH 5-6). In vitro and in vivo studies show that the micelles had a good pH-triggered drug release capability, tumor-infiltrating permeability, and effective antitumor activity with extremely low toxicity. [45, 46] Okano's group used the temperature-sensitive poly(*N*-isopropylacrylamide) (PNIPAM) to investigate the cellular uptake of bovine carotid endothelial cells. As  $T > LCST$ , the cell uptake was significantly enhanced. In addition, the LCST of such PNIPAM can be tuned to  $\sim 39^\circ C$  by introducing some hydrophilic monomer into the chain backbone. Thus, the system can stably circulate at  $37^\circ C$  but be disassociated as  $T$  approaching to  $39^\circ C$ . This PNIPAM was designed to enhance the intracellular release because the cargo structure was disrupted as phase transition. [47, 48] The oxidative condition in the extracellular medium and reductive conditions in the tumor was used to enhance intracellular release. For example, the bioreducible PEG-SS-P[Asp(DET)] micelles bearing the disulfide bridge showed both 1-3 orders of magnitude higher gene transfection efficiency and a more rapid onset of plasmid DNA release than micelles without disulfide linkages. [49] Feng's group recently developed a micellar system containing a functional polymer of *D*- $\alpha$ -tocopheryl polyethylene glycol succinate (Vitamin E TPGS or TPGS), which stabilized the micelle and further promotes synergistic effects with the encapsulated drug. [50] This is a novel micellar system. The formulation formed by folic acid-conjugated *D*- $\alpha$ -tocopheryl polyethylene glycol succinate 2000 (Vitamin E TPGS2k) micelles successfully suppress the tumor cell growth. [51] For improving the therapeutic effect, some other intelligent micellar systems such as light responsive poly(methacrylate) and poly(acrylic acid) (PAzoMA-PAA) micelle were developed. This trans-cis photoisomerization of the azobenzene group improved drug release. [52] In addition, the polymeric micelles conjugated tumor targeting V3lig-and cyclic-(arginine-glycine-aspartic acid-D-phenylalanine-lysine) (cRGDfK) to DOXO-loaded polyethylene glycol-polycaprolactone (PEG-PCL) micelles greatly enhanced internalization of the micelles through receptor-mediated endocytosis. [53]

These significant advances in intelligent block copolymer micelles have dawned upon a new era for nanomedicine. However, for translating an optimal micelle to clinical practice, there is still a big gap between in vitro and in vivo for lacking of understanding of the correlation between tumor unique characteristics (needs) and micellar physical chemistry properties (seeds). It is helpful to know that the micellar in vitro/vivo performance is strongly affected by its physical chemistry properties such as composition, dimension, microstructure, and the intelligent properties. The driving force for self-assembly is the strict solubility difference

between the hydrophobic and the hydrophilic blocks as described by the Flory-Huggins parameter.

## 4. Immunoliposome

Although liposomes have already achieved significant advance, antitumor activity could be further enhanced for liposomes through ligand-mediated targeting. For liposomes, the ligands would promote the selective binding and facilitate the intracellular delivery. The most commonly used ligands include mAbs or antibody fragments, folic acid, or receptor ligands. [54-59] MABs or their derivatives (e. g., Fab fragments, single-chain variable fragments (scFv)) are often adopted as the targeted ligands in LTLs. LTLs decorated with mAbs or their derivatives are termed as immunoliposomes. Immunoliposomes can be used to deliver various drugs, like chemotherapeutics, gene, or protein drugs, and significantly improve the therapeutic efficacy of conventional strategies in cancer. [60-64] When conjugated with antibodies as targeting ligands, immunoliposomes can target tumor cells with high specificity and affinity, resulting in significantly improved antitumor activity over untargeted liposomes. [65] The development of immunoliposomes, which perfectly combine antibody engineering and liposomes, is becoming a possible state-of-the-art in liposome research. This review discusses the recent development and therapeutic effect of immunoliposomes in cancer therapy. This review includes the following sections: antibody engineering, antibody conjugation strategies, therapeutic potential of immunoliposomes in cancer, challenges, and future perspectives of immunoliposomes.

### 4.1. Conjugation of thiolated antibody with liposomes

The most common conjugation strategy employs the reaction between thiol functions and maleimide groups, which form thioether bonds. This strategy consists of two steps. First, after reaction with Traut's reagent (2-iminothiolane), the antibodies modified with free sulfhydryl are obtained. [66] Alternately, antibodies react with the heterobifunctional crosslinking agents such as *N*-succinimidyl 3-(2-pyridyldithio) propionate (SPDP) or succinimidyl- $\alpha$ -methyl- $\alpha$ -(2-pyridyldithio) toluene (SMPT). Once modified with SPDP or SMPT, antibodies are treated with dithiothreitol (DTT) and form the free sulfhydryl. [67, 68] Also, antibodies react with the heterobifunctional crosslinking agents such as *N*-succinimidyl *S*-acetylthioacetate (SATA), *S*-acetylmercaptosuccinic anhydride (SAMSA), or succinimidyl acetylthiopropionate (SATP). [69-71] Once modified with SATA, SAMSA, or SATP, antibodies are treated with hydroxylamine and form free sulfhydryl. Second, thiolated antibody bearing the free sulfhydryl reacted with maleimide groups on the liposomes, and the resultant liposomes conjugated with antibodies were obtained. Attachment of antibodies to liposomes via a disulfide linkage A disulfide bond formed by two thiols is easily obtained. However, the disulfide bond is relatively unstable under reductive conditions. Thiolated antibodies could react with the pyridyldithio moiety of the anchor (PE-PDP) to form a disulfide linkage. This coupling strategy achieved efficient conjugation of antibodies to liposomes without denaturation of antibodies. [72-74]

#### **4.2. Crosslinking between carboxylic acid on liposomes and the ligand**

Antibodies could be conjugated to the liposomes by an amide bond using the membrane-anchored lipid functionalized with carboxylic acid end groups. This conjugation commonly used distearoyl-*N*-(3-carboxypropionoyl poly(ethylene glycol) succinyl) phosphatidylethanolamine (DSPE-PEG-COOH) offering carboxylic acid groups at the distant end of surface-grafted PEG chains as the membrane-anchored lipid. [75, 76] In the coupling reaction, 1-ethyl-3-(3-dimethylaminopropyl) carbodiimide (EDAC) and *N*-hydroxysulfosuccinimide (NHS) are usually used to form an acyl amino ester, which subsequently react with the primary amine of the ligand, yielding an amide bond. Suzuki et al. prepared liposomes conjugated with transferrin specific for transferrin receptor overexpressing solid colon 26 tumor cells, and the results indicated that the immunoliposomes recognized and bound specifically to target cells *in vivo*.

#### **4.3. Antibody conjugation with Liposomes via a hydrazone bond**

Antibodies can be covalently bound to hydrazide groups of the liposomes through their carbohydrate moieties to form a hydrazone bond. In the conjugation strategy, the carbohydrates groups on the constant region of the heavy chain of the antibody are oxidized by sodium periodate to produce reactive aldehydes, which form hydrazone linkages with the hydrazide groups on the PEG-terminus. [77, 78] It has to be noted that the oxidation reaction should be performed in mild conditions to avoid the loss of antibody activity. The antibodies are correctly orientated on the surface of the liposomes because only the Fc region is involved in the conjugation reaction and the antigen binding site are protected. Furthermore, this conjugation strategy avoids the recognition of the immunoliposomes by the macrophages, resulting in longer circulation time of immunoliposomes.

#### **4.4. Crosslinking between primary amines on liposomes with the antibody**

Direct amine-amine crosslinking has also been investigated in antibody conjugation. [79] In the conjugation, two homobifunctional crosslinkers including glutaraldehyde and suberimide are used, and no prior modification is required to add functional groups to the antibody. Briefly, the primary amine of phosphatidylethanolamine of the liposomes is firstly activated using the crosslinkers and subsequently conjugated to the antibody. It is reported that almost 60% of the antibodies were coupled to the liposomes, and these conjugated antibodies still retained their binding affinity. However, this conjugation strategy was rarely applied because the uncontrollable homopolymerization of antibodies or liposomes would happen during the crosslinking reaction.

#### **4.5. Noncovalent methods for antibodies conjugated with liposomes**

A noncovalent technique is an alternative means to for antibody conjugation to liposomes. The unique advantage of a noncovalent technique is easy and rapid performance without the need of aggressive reagents. For example, simply mixing antibodies and phospholipids during the preparation of the liposomes would achieve the binding of antibodies to the liposomes. [80]

However, the disadvantages of the noncovalent technique are obvious. The conjugation efficiency of antibodies is relatively low and liposome aggregation would happen. Furthermore, the amount of antibody conjugated to the liposome is not easily controllable, and the correct orientation of the antibodies is not guaranteed. Finally, conjugated antibodies are not stable and may detach easily. Thus, due to the weak interaction between the liposome and the antibodies, the noncovalent technique has not been widely used. However, it is noteworthy that one noncovalent technique, which uses the binding between streptavidin and biotin for attachment of antibodies to liposomes, is an exception. The binding of streptavidin to biotin is simple, highly stable, and reproducible; thus, the attachment of antibodies to liposomes using such a strategy is rather favorable and promising. [81] Generally, two strategies of antibody conjugation use the streptavidin-biotin interaction.

First, the streptavidin-modified antibodies were conjugated to the anchor lipid DSPE-PEG-biotin. The immunoliposomes redirected the biodistribution of entrapped drugs and showed specific targeting to the targeted organ overexpressing specific antigens, leading to significant accumulation in the targeted organ. [82] Second, the biotinylated antibodies were incubated with the targeted cells overexpressing specific antigens. Then streptavidin was added, followed by biotinylated liposomes. The results showed that the liposomes specifically bound to the targeted cells coated with antibodies but not to the control cells, which do not express the specific antigen. [83]

## 5. Well-defined nanocarrier's engineering for immunotherapy

Various immune cells such as B cells, T-lymphocytes (TL), and dendritic cells (DCs) are retained to the tumor. The modification of host immune system and/or the utilization of components of the immune system for cancer treatment are called immunotherapy, which mainly contains the active and passive form. Passive immunotherapy is to supply high amounts of effector molecules such as tumor-specific monoclonal antibodies (mAbs) to complement the immune system. Active immunotherapy is the utilization of humoral and/or cytotoxic T-cell effector mechanisms of the immune system following vaccination, namely, the cancer vaccines. This method can simultaneously activate antigen presenting cells (APCs), CD4<sup>+</sup> T cells, CD8<sup>+</sup> T cells, B cells, and innate immune cells, for example, granulocytes and NK cells. DCs are the most specialized and important APCs, which are responsible for an adaptive immune response. [84] Vaccines based on lipid-based nanocarriers can not only promote the accumulation in DCs in tumor-bearing hosts but also has a profound effect on DC function. [85] Poly(D, L-lactic acid-co-glycolic acid) (PLGA) nanoparticles carrying cancer-associated antigen (MUC1 mucin peptide: BLP25) and mouse-specific peripheral lymphocyte antigen (MPLA) obviously promoted native T-cell activation in normal and MUC1-transgenic mice. [86] The efficiency of vaccination strongly depends on tumor-specific antigens (TSAs) and vaccine delivery system. Polymeric nanoparticles attract extensive interest due to their facilely tunable composition, tailorable structure, unique intelligent properties, and high potential in cancer immunotherapy (i. e. , the nanoimmunotherapy).

Immunotherapy cannot only kill tumor cells in a specific manner but also alert the immune system to eradicate the disseminated tumor cells in blood circulation and micrometastases in distant organs. [87, 88] However, tumor cells can survive when they either maintain chronically or immunologically sculpt by immune “editors.” This well-known “immunoediting” refers to the elimination, equilibrium, and escape. [88] The new populations of tumor variants may eventually evade the immune system and escape from host immune surveillance by a variety of mechanisms including loss of MHC-I, adhesion molecules, tumor-associated antigens (TAAs), generation of regulatory T-(Treg-) lymphocyte, expansion of myeloid-derived suppressor cells (CD11b<sup>+</sup> Gr-1<sup>+</sup> cells, MDSCs), immunosuppression, blocking of NKG2D-mediated activation, and apoptosis induction of antitumor effector cells. [89, 90] Tumor-specific immune activation and nonspecific immune activation have been applied for overcoming such tumor escape. The tumor-specific immune responses are teaching the immune cells to recognize tumor cells specifically. B cells secrete antigen-specific antibodies that recognize, bind, and help to destroy the targets with the help of the CD4<sup>+</sup>T cells. CD4<sup>+</sup> T cells recognize the antigens presented by MHC-II molecules and then stimulate B cells to produce antibodies to that specific antigen. Such antibody-coated cancer cells recognized and killed by NK cells, macrophage, and activated monocytes are called antibody-dependent cell-mediated cytotoxicity (ADCC). The nonspecific immune activation strategy mainly utilizes the cytokines (IL2 and IL8), the interferons (IFN- $\alpha$ ,  $\beta$ , and IFN- $\gamma$ ), and the Toll-like receptors (TLRs) for triggering DC maturation, stimulating proliferation of CD4<sup>+</sup> and CD8<sup>+</sup> T cells and modulating the suppressive function of regulatory T cells (Treg cells). [91] Treg cells suppress TAA-specific immunity by inhibiting TAA-specific priming in tumor draining lymph nodes and further recruiting into the tumor microenvironment. [92] Thus, depletion, blocking, and tracking Treg cells in tumors or reducing their differentiation and suppressive mechanisms represent new strategies for cancer treatment. It was known that the knockdown of transcription factor Foxp3 gene in mature Treg cells resulted in the loss of their suppressive function. [93] However, the transfection efficiency is very low. The newly developed novel carbon nanotubes (CNTs) can enhance the transfection of Treg cells. [92] The PLGA nanoparticle (PLGA-NP) carrying murine melanoma antigenic peptides hgp100<sub>25-33</sub> and TRP2<sub>180-188</sub> can also induce cytotoxic T lymphocyte responses against tumor-associated self-antigens in C57BL/6 mouse. [94]

Thus, finely engineering nanocarriers from homopolymers, copolymers, and lipids with high loading and transferring efficiency, site-specific targeting to immune cells, high in vitro/vivo stability, and intelligent responsive to tumor microenvironment show high potential in nanoimmunotherapy. [95, 96] Tumor microenvironment is the main battlefield for tumor escape and immune system activation. As shown in Figure, the high proliferation and metabolism of tumor endothelial cells resulted in the unique properties of tumor microenvironment, including large endothelial cells gaps (200-1000 nm), the relative high temperature ( $T > 37^{\circ}\text{C}$ ), low pH (5~6), lacking lymphatic nodes, and lymph vessels. [97] This unique pathological condition of microenvironment offers challenges for novel nanocarrier's engineering. Based on the self-assembly mechanism, well-defined micelle and vesicle with surface targeting decorating were finely engineered. [98] We found that the temperature-regulated passive and mAb-tuned active dual targeting immunomicelles significantly enhanced

intratumor accumulation and cellular uptake. The nanostructure and the dimension were also tailored to match the large endothelial cells gaps in tumors with enhanced permeability and retention (EPR). [86] The extracellular pH is  $\sim 7.4$ , but the pH in the endosome and microenvironment is  $\sim 6.0$ . This value is still lowered to  $\sim 5.0$  in the lysosome. The hydrolysis rates of polyester such as polylactic acid, polyglycolic acid, and their copolymers can thus be tuned for endosomal and/or lysosomal delivery. [99] Additionally, the endosome is reductive, but the lysosomal is oxidative. This difference is very important for spatial delivery antigens for MHC presentation. The antigens for MHC class I pathways must be available in cytosol, whereas those for MHC class II molecules must be present in endolysosome. The finely engineered lipids with protein antigens in nanovesicle core and lipid-based immunostimulatory molecules in the walls successfully elicits endogenous T cell and antibody responses, which showed rapid release adjuvants in the presence of endolysosomal lipases. [100] Some danger signals (adjuvants) for APC activation are present on the plasma membrane. So nanocarriers engineered from polycations such as polyethyleneimine (PEI) or its graft copolymers (Figure) hold favorable effect on membrane destabilization by the "proton-sponge" effect, which can also control the endosomal release. [101] Both structural defects and fibrosis of the interstitial matrix result in poor/dysfunctional T-cell priming in tumor microenvironment. However, the forced expression of the tumor necrosis factor (TNF) can induce naive T-cell priming. Thus, delivery stimulator such as CD80, interleukin-4 (IL-4), and cytokines by intelligent nanocarriers to tumor microenvironment can produce T-cell priming with the microenvironment reversion. [102]

DCs appear in most peripheral tissues where antigens typically first encounter the immune system. Immature DCs phagocytose the encountered antigens followed by the activation, maturation, and migration to draining lymph nodes. They present antigens to their cognate naive T-cell partners and instruct the anergy, tolerance, or immunity. Then the antigen-specific T-cell immunity is initiated. Noted here is the timing at which antigen and adjuvant reach DCs is crucial. If the maturation stimulus is too late, tolerance will be induced. If the antigens reach mature DCs, they will not be efficiently presented. The intelligent responsive polymer carriers can be finely designed to regulate the antigen's communication with DCs. Some lipids had successfully been used to promote the lymphatic trafficking and endue the DCs mutation. [103] The DCs preferentially take up smaller particles with size similar to viral ( $\sim 20$  nm), whereas macrophages ingest the large particles with size around bacterial. It is also worth mentioning that PLGA-NPs (500 nm) are more effective than microparticles ( $\sim 2$  nm) in stimulating CTL responses. The DC's phagocytosis is also affected by nanoparticle's surface charge. [104] Cationic particles are particularly effective for uptake by DCs and macrophages due to that the ionic attraction increases the particle binding and internalization. Above-mentioned nanocarrier's size, microstructure, charge, and intelligent properties can be facilely engineered by tuning polymer composition and particle formation process. In addition, specific DC-specific antibodies such as anti-CD11c and anti-DEC205 can enhance nanocarrier's accumulation in DCs. The PLA nanoparticles loaded dacarbazine (DTIC) decorated with TRAIL-receptor2 (DR5) mAb (DTIC-NPs-DR5) showed high internalization by DR5-overexpressing metastatic melanoma and chemo-immunocooperative therapeutic effects. [105] Based on our understanding of the molecular mechanism of immunoescape and the physiologic

conditions of tumor, the nanocarriers in nanoimmunotherapy should be further finely engineered with well-defined dimension, intelligent properties, specific targeting, advance lymphatic imaging, and precisely intracellular release for optimizing the therapeutic index.

## Acknowledgements

This work was financially supported by the Ministry of Science and Technology of China (2012CB934002, 2012AA02A304) and the National Natural Science Foundation of China, including the projects 31470964 and 81171450.

## Author details

Mengxin Zhao<sup>1,2</sup>, Yun Sun<sup>1</sup>, Xiandi Zhu<sup>1</sup>, Di Chen<sup>1</sup>, Sishen Feng<sup>1,3</sup>, Shangjing Guo<sup>2</sup> and Wei Li<sup>1,2\*</sup>

\*Address all correspondence to: liwei@smmu.edu.cn

1 International Joint Cancer Institute, The Second Military Medical University, Shanghai, PR China

2 College of Pharmacy, Liaocheng University, Liaochaneg, Shangdong, China

3 Department of Chemical and Biomolecular Engineering, National University of Singapore, Singapore

## References

- [1] Archakov A. I. 2010. Nanobiotechnologies in medicine: nanodiagnostics and nano-drugs. *Biochemistry (Moscow)* 4:2-14.
- [2] Feng S. S. 2006. New-concept chemotherapy by nanoparticles of biodegradable polymers: where are we now? *Nanomedicine (Lond)* 1:297-309.
- [3] Allen T. M. , Cullis P. R. 2004. Drug delivery systems: entering the mainstream. *Science* 303:1818-22.
- [4] Moghimi S. M. , Hunter A. C. , Murray J. C. 2005. Nanomedicine: current status and future prospects. *FASEB Journal* 19:311-30.
- [5] Bawarski W. E. , Chidlowsky E. , Bharali D. J. , Mousa S. A. 2008. Emerging nanopharmaceuticals. *Nanomedicine* 4:273-82.

- [6] Duncan R. Polymer conjugates as anticancer nanomedicines. 2006. *Nature. Review Cancer* 6:688-701.
- [7] Gao J. , Feng S. S. , Guo Y. 2012. Nanomedicine against multidrug resistance in cancer treatment. *Nanomedicine (Lond. )* 7:465-8.
- [8] Matsumura Y. , Maeda H. 1986. A new concept of macromolecular therapies in cancer chemotherapy: mechanism of tumortropic accumulation of proteins and the tumor agent. *SMANCS. Cancer Research* 6:6387-92.
- [9] Davis M. E. , Chen Z. G. , Shin D. M. 2008. Nanoparticle therapeutics: an emerging treatment modality for cancer. *Nature Reviews. Drug Discovery* 2:771-82.
- [10] Torchilin V. P. 2005. Recent advances with liposomes as pharmaceutical carriers. *Nature Reviews. Drug Discovery* 2:145-60.
- [11] Schrama D. , Reisfeld R. A. , Becker J. C. 2006. Antibody targeted drugs as cancer therapeutics. *Nature. Reviews. Drug Discovery* 5(2):147-59.
- [12] Adams G. P. , Weiner L. M. 2005. Monoclonal antibody therapy of cancer. *Nature. Biotechnol* 23:1147-57.
- [13] Zhang T. , Herlyn D. 2009. Combination of active specific immunotherapy or adoptive antibody or lymphocyte immunotherapy with chemotherapy in the treatment of cancer. *Cancer Immunol. Immunother* 58 : 475-92.
- [14] Beckman R. A. , Weiner L. M. , Davis H. M. 2007. Antibody constructs in cancer therapy: protein engineering strategies to improve exposure in solid tumors. *Cancer* 109:170-79.
- [15] Kolkman J. A. , Law D. A. 2010. Nanobodies—from llamas to therapeutic proteins. *Drug Discovery Today: Technologies* 2:139-46.
- [16] Dai J. , Jin J. , Li B. , Wang H. , Hou S. , Qian W. , Kou G. , Zhang D. , Li J. , Tan M. , Ma J. , Guo Y. 2007. A chimeric SM5-1 antibody inhibits hepatocellular carcinoma cell growth and induces caspase-dependent apoptosis. *Cancer Letters* 258 : 208-14.
- [17] Wu L. , Wang C. , Zhang D. , Zhang X. , Qian W. , Zhao L. , Wang H. , Li B. , Guo Y. 2010. Characterization of a humanized anti-CD20 antibody with potent antitumor activity against B-cell lymphoma. *Cancer Letters* 292 :208-14.
- [18] Li B. , Wang H. , Zhang D. , Qian W. , Hou S. , Shi S. , Zhao L. , Kou G. , Cao Z. , Dai J. , Guo Y. 2007. Construction and characterization of a high-affinity humanized SM5-1 monoclonal antibody. *Biochemical Biophysical Research Communications* 357:951-56.
- [19] Lonberg, N. 2005. Human antibodies from transgenic animals. *Nature Biotechnol* 23:1117-25.

- [20] Jain R. K. , Duda D. G. , Clark J. W. , Loeffler J. S. 2006. Lessons from phase III clinical trials on anti-VEGF therapy for cancer. *Nature Clinical Practice Oncology* 3:24-40.
- [21] Cunningham D. , Humblet Y. , Siena S. , Khayat D. , Bleiberg H. , Santoro A. , Bets D. , Mueser M. , Harstrick A. , Verslype C. , Chau I. , Van Cutsem E. 2004. Cetuximab monotherapy and cetuximab plus irinotecan in irinotecan-refractory metastatic colorectal cancer. *New England Journal of Medicine* 351:337-45.
- [22] Hortobagyi G. N. 1998. Treatment of breast cancer. *New England Journal of Medicine* 339:974-84.
- [23] Li B. , Shi S. , Qian W. , Zhao L. , Zhang D. , Hou S. , Zheng L. , Dai J. , Zhao J. , Wang. H. , Guo Y. , 2008. Development of novel tetravalent anti-CD20 antibodies with potent antitumor activity. *Cancer Research* 68 :2400-08.
- [24] Wu C. , Ying H. , Grinnell C. , Bryant S. , Miller R. , Clabbers A. , Bose S. , McCarthy D. , Zhu R. R. , Santora L. , Davis-Taber R. , Kunes Y. , Fung E. , Schwartz A. , Sakorafas P. , Gu J. , Tarcsa E. , Murtaza A. , Ghayur T. 2007. Simultaneous targeting of multiple disease mediators by a dual-variable domain immunoglobulin. *Nature Biotechnol* 25:1290-97.
- [25] Hudson P. J. , Kortt A. A. 1999. High avidity scFv multimers; diabodies and triabodies. *Journal of Immunological Methods* 231:177-189.
- [26] Holt L. J. , Herring C. , Jespers L. S. , Woolven B. P. , Tomlinson I. M. 2003. Tomlinson domain antibodies: proteins for therapy. *Trends Biotechnol* 21:484-90.
- [27] Lin J. H. , Lu A. Y. H. 1997. Role of pharmacokinetics and metabolism in drug discovery and development. *Pharmacological Reviews* 49:403-449
- [28] Lukyanov A. N. , Torchilin V. P. 2004. Micelles from lipid derivatives of water-soluble polymers as delivery systems for poorly soluble drugs. *Advanced Drug Delivery Reviews* 56:1273-1289
- [29] Kwon G. S. , Kataoka K. 1995. Block copolymer micelles as long-circulating drug vehicles. *Advanced Drug Delivery Reviews* 16:295-309,
- [30] Jeong B. , Bae Y. H. , Kim S. W. 2000. Drug release from biodegradable injectable thermosensitive hydrogel of PEG-PLGA-PEG triblock copolymers. *Journal of Controlled Release* 63:155-163
- [31] Barenholz Y. 2012. Doxil<sup>®</sup>—the first FDA-approved nano-drug: lessons learned. *Journal of Controlled Release* 160:117-134.
- [32] Wagner V. , Dullaart A. , Bock A-K. , Zweck A. 2006. The emerging nanomedicine landscape. *Nature Biotechnology* 24:1211-1217
- [33] Ferrari, M. 2005. Cancer nanotechnology: opportunities and challenges. *Nature Reviews Cancer* 5:161-171.

- [34] He L. , Wang G. L. , Zhang Q. 2003. An alternative paclitaxel microemulsion formulation: hypersensitivity evaluation and pharmacokinetic profile. *International Journal of Pharmaceutics* 250:45-50.
- [35] Feng Z. , Zhao G. , Yu L. , Gough D. , Howell S. B. 2010. Preclinical efficacy studies of a novel nanoparticle-based formulation of paclitaxel that out-performs Abraxane. *Cancer Chemotherapy and Pharmacology* 65:923-930.
- [36] Alexis F. , Pridgen E. , Molnar L. K. , Farokhzad O. C. 2008. Factors affecting the clearance and biodistribution of polymeric nanoparticles. *Molecular Pharmaceutics* 5:505-515.
- [37] Matsumura Y. , Maeda H. 1986. A new concept for macro-molecular therapeutics in cancer chemotherapy: mechanism of tumoritropic accumulation of proteins and the antitumor agent smancs. *Cancer Research* 46:6387-6392.
- [38] Talelli M. , Iman M. , Varkouhi A. K. 2010. Core-crosslinked polymeric micelles with controlled release of covalently entrapped, doxorubicin. *Biomaterials* 31:7797-7804,
- [39] Lukyanov A. N. , Torchilin V. P. 2004. Micelles from lipid derivatives of water-soluble polymers as delivery systems for poorly soluble drugs. *Advanced Drug Delivery Reviews* 56:1273-1289.
- [40] Kakizawa Y. , Kataoka K. 2002. Block copolymer micelles for delivery of gene and related compounds. *Advanced Drug Delivery Reviews* 4:203-222.
- [41] Kabanov A. V. , Nazarova I. R. , Astaieva I. V. 1995. Micelle formation and solubilization of fluorescent probes in poly (oxyethylene-b-oxypropylene-b-oxyethylene) solutions. *Macromolecules* 28:2303-2314.
- [42] Brown J. M. , Giaccia A. J. 1998. The unique physiology of solid tumors: opportunities (and problems) for cancer therapy. *Cancer Research* 58:1408-1416.
- [43] Yahara T. , Koga T. , Yoshida S. , Nakagawa S. , Deguchi H. , Shirouzo K. 2003. Relationship between microvessel density and thermographic hot areas in breast cancer. *Surgery Today* 33:243-248,
- [44] Bae Y. , Nishiyama N. , Fukushima S. , Koyama H. , Yasuhiro M. , Kataoka K. 2005. Preparation and biological characterization of polymeric micelle drug carriers with intracellular pH-triggered drug release property: tumor permeability, controlled sub-cellular drug distribution, and enhanced in vivo antitumor efficacy. *Bioconjugate Chemistry* 16:122-130,
- [45] Kwon G. , Suwa, S. , Yokoyama M. , Okano T. , Sakurai Y. , Kataoka K. , 1994. Enhanced tumor accumulation and prolonged circulation times of micelle-forming poly(ethylene oxide-aspartate)block copolymer-adriamycin conjugates. *Journal of Controlled Release* 29:17-23,

- [46] Nakayama, M. Okano, T. Miyazaki, T. Kohori, F. Sakai, K. Yokoyama, M. 2006. Molecular design of biodegradable polymeric micelles for temperature-responsive drug release. *Journal of Controlled Release* 115:46-56,
- [47] Akimoto J. , Nakayama M. , Sakai K. , Okano T. , 2009. Temperature-induced intracellular uptake of thermoresponsive polymeric micelles. *Biomacromolecules* 10:1331-1336.
- [48] Takae S. , Miyata K. , Oba M. 2008. PEG-detachable poly-plex micelles based on disulfide-linked block cationomers as bioresponsive nonviral gene vectors. *Journal of the American Chemical Society* 130:6001-6009.
- [49] Zhang Z. Z. , Tan S. W. , Feng, S. S. 2012. Vitamin E TPGS as a molecular biomaterial for drug delivery. *Biomaterials* 33: 4889-4906.
- [50] Mi Y. , Liu Y. , Feng S. S. 2011. Formulation of Docetaxel by folic acid-conjugated D-tocopheryl polyethylene glycol succinate 2000 (Vitamin E TPGS2k) micelles for targeted and synergistic chemotherapy. *Biomaterials* 32:. 4058-4066,
- [51] Lee H. I. , Wu W. , Oh J. K. 2007. Light-induced reversible formation of polymeric micelles. *Angewandte Chemie* 46:2453-2457.
- [52] Nasongkla N. , Bey E. , Ren J. 2006. Multifunctional polymeric micelles as cancer-targeted, MRI-ultrasensitive drug delivery systems. *Nano Letters* 6:. 2427-2430.
- [53] Li W. , Li J. 2011. The fine-tuning of thermosensitive and degradable polymer micelles for enhancing intracellular uptake and drug release in tumors. *Biomaterials* 32:3832-3844,
- [54] Lee R. J. , Low P. S. 1994. Delivery of liposomes to cultured KB cells via folate receptor-mediated endocytosis. *Journal of Biological Chemistry* 269:3198-3204.
- [55] Lopes de Menezes D. E. , Pilarski L. M. , Allen T. M. 1998. In vitro and in vivo targeting of immunoliposomal doxorubicin to human B-cell lymphoma. *Cancer Research* 58:3320-30.
- [56] Lopes de Menezes D. E. , Kirchmeier M. J. , Gagne J. F. , Pilarski L. M. , Allen T. M. 1999. Cellular trafficking and cytotoxicity of anti-CD19-targeted liposomal doxorubicin in B lymphoma cells. *Journal of Liposome Research* 9:199-228.
- [57] Singh M. 1999. Transferrin As A targeting ligand for liposomes and anticancer drugs. *Current Pharmaceutical Design* 5:443-51.
- [58] Sugano M. , Egilmez N. K. , Yokota, S. J. , et al. 2000. Antibody targeting of doxorubicin-loaded liposomes suppresses the growth and metastatic spread of established human lung tumor xenografts in severe combined immunodeficient mice. *Cancer Research* 60:6942-49.

- [59] Abra R. M. , Bankert R. B. , Chen F. , et al 2002. The next generation of liposome delivery systems: recent experience with tumor-targeted, sterically-stabilized immunoliposomes and active-loading gradients. *Journal of Liposome Research* 12:1-3.
- [60] Gao J. , Kou G. , Wang H. , et al. 2009. PE38KDELloaded anti-HER2 nanoparticles inhibit breast tumor progression with reduced toxicity and immunogenicity. *Breast Cancer Research and Treatment* 115:29-41.
- [61] Gao J. , Kou G. , Chen H. W. , et al. 2008. Treatment of hepatocellular carcinoma in mice with PE38KDEL type I mutant-loaded poly(lactic-co-glycolic acid) nanoparticles conjugated with humanized SM5-1 F(ab') fragments. *Molecular Cancer Therapeutics* 7:3399-407.
- [62] Gao J. , Sun J. , Guo Y. , et al. 2010. Lyophilized HER2-specific PEGylated immunoliposomes for active siRNA gene silencing. *Biomaterials* 31:2655-64.
- [63] Gao J. , Feng S. S. , Guo Y. 2010. Antibody engineering promotes nanomedicine for cancer treatment. *Nanomedicine (Lond)* 5:1141-5.
- [64] Kou G. , Gao J. , Wang H. , et al. 2007. Preparation and characterization of paclitaxel-loaded PLGA nanoparticles coated with cationic SM5-1 single-chain antibody. *Journal of Biochemistry Molecular Biology* 40:731-39.
- [65] Sapra P. , Tyagi P. , Allen T. M. 2005. Ligand-targeted liposomes for cancer treatment. *Current Drug Delivery* 2 :369-381
- [66] Traut R. R. , Bollen A. , Sun R. R. , et al. 1973. Methyl 4-mercaptobutyrimidate as a cleavable cross-linking reagent and its application to the Escherichia coli 30s ribosome. *Biochemistry* 12:3266-73.
- [67] Carlsson J. , Drevin H. , Axen R. 1978. Protein thiolation and reversible protein-protein conjugation. *N-succinimidyl 3(2-pyridyldithio) propionate*, a new heterobifunctional reagent. *Biochemical Journal* 173:723-37.
- [68] Thorpe P. E. , Wallace P. M. , Knowles P. P. , et al. 1987. New coupling agents for the synthesis of immunotoxins containing a hindered disulfide bond with improved stability in vivo. *Cancer Research* 47:5924-31.
- [69] Duncan R. J. , Weston P. D. , Wrigglesworth, R. 1983. A new reagent which may be used to introduce sulfhydryl groups into proteins, and its use in the preparation of conjugates for immunoassay. *Analytical Biochemistry* 132:68-73.
- [70] Klotz I. M. , Heiney R. E. 1962. Introduction of sulfhydryl groups into proteins using acetylmercaptosuccinic anhydride. *Archives Biochemistry Biophysics* 96:605-12.
- [71] Wegner G. J. , Lee H. J. , Marriott G. , et al. 2005. Fabrication of histidine-tagged fusion protein arrays for surface plasmon resonance imaging studies of protein-protein and protein-DNA interactions. *Analytical Chemistry* 75:4740-6.

- [72] Martin F. J. , Hubbell W. L. , Papahadjopoulos D. 1981. Immunospecific targeting of liposomes to cells: a novel and efficient method for covalent attachment of Fab fragments via disulfide bonds. *Biochemistry* 20:4229-38.
- [73] Ivanov V. O. , Preobrazhensky S. N. , Tsubulsky V. P. , et al. 1985. Liposome uptake by cultured macrophages mediated by modified low-density lipoproteins. *Biochimica Biophysica. Acta* 846:76-84.
- [74] Leserman L. D. , Barbet J. , Kourilsky F. , et al. 1980. Targeting to cells of fluorescent liposomes covalently coupled with monoclonal antibody or protein A. *Nature* 288:6024.
- [75] Suzuki R. , Takizawa T. , Kuwata Y. , et al. 2008. Effective anti-tumor activity of oxaliplatin encapsulated in transferrin-PEG-liposome. *International Journal of Pharmaceutics* 346:43-50.
- [76] Ying X. , Wen H. , Lu W. L. , et al. 2010. Dual-targeting daunorubicin liposomes improve the therapeutic efficacy of brain glioma in animals. *Journal of Control Release* 141:183-92.
- [77] Koning G. A. , Kamps J. A. , Scherphof G. L. 2002. Efficient intracellular delivery of 5-fluorodeoxyuridine into colon cancer cells by targeted immunoliposomes. *Cancer Detection Prevention* 26:299-307.
- [78] Harding J. A. , Engbers C. M. , Newman M. S. , et al. 1997. Immunogenicity and pharmacokinetic attributes of poly(ethylene glycol)-grafted immunoliposomes. *Biochimica Biophysica. Acta* 1327:181-92.
- [79] Torchilin V. P. , Khaw B. A. , Smirnov V. N. , et al. 1979. Preservation of antimyosin antibody activity after covalent coupling to liposomes. *Biochemical and Biophysical. Research Communications* 89:1114-9.
- [80] Torchilin V. P. , Goldmacher V. S. , Smirnov V. N. 1978. Comparative studies on covalent and noncovalent immobilization of protein molecules on the surface of liposomes. *Biochemical and Biophysical. Research Communications* 85:983-90.
- [81] Huang L. , Kennel S. J. 1979. Binding of immunoglobulin G to phospholipid vesicles by sonication. *Biochemistry* 18:1702-7.
- [82] Ko Y. T. , Bhattacharya R. , Bickel U. 2009. Liposome encapsulated polyethylenimine/ODN polyplexes for brain targeting. *Journal of Control Release* 133:230-7.
- [83] Xiao Z. , McQuarrie S. A. , Suresh M. R. , et al. 2002. A three-step strategy for targeting drug carriers to human ovarian carcinoma cells in vitro. *Journal of Biotechnology* 94:171-84.
- [84] Feldmann M. , Steinman L. 2005. Design of effective immunotherapy for human autoimmunity. *Nature* 435:612-619

- [85] Herber D. L. , Cao W. , Nefedova Y. , et al. 2010. Lipid accumulation and dendritic cell dysfunction in cancer. *Nature Medicine* 16:880-886
- [86] Elamanchili P. , Diwan M. , Cao M. , et al. 2004. Characterization of poly(D, L-lactico-glycolic acid) based nanoparticulate system for enhanced delivery of antigens to dendritic cells. *Vaccine* 22:2406-2412,
- [87] Schietinger A. , Philip M. , Liu R. B. , et al. 2010. By stander killing of cancer requires the cooperation of CD4+ and CD8+ T cells during the effect or phase. *Journal of Experimental Medicine* 207:2469-2477.
- [88] Schuster M. , Nechansky A. , Kircheis R. 2006. Cancer immunotherapy. *Biotechnology Journal* 1:138-147
- [89] Ganss R. , Hanahan D. 1998. Tumor microenvironment can restrict the effectiveness of activated antitumor lymphocytes. *Cancer Research* 58: 4673-4681,
- [90] Kim R. , Emi M. , Tanabe K. 2007. Cancer immunoediting from immune surveillance to immune escape. *Immunology* 121:1365-2567.
- [91] Dunn G. P. , Old L. J. , Schreiber R. D. 2004. The immunobiology of cancer immunosurveillance and immunoediting. *Immunity* 21:137-148
- [92] Liu Z. , Winters M. , Holodniy M. M. , et al. 2007. siRNA delivery into human T cells and primary cells with carbon-nanotube transporters. *Angewandte Chemie* 46:2023-2027
- [93] Williams L. M. , Rudensky A. Y. 2007. Maintenance of the Foxp3-dependent developmental program in mature regulatory T cells requires continued expression of Foxp3. *Nature Immunology* 8:277-284,
- [94] Zhang Z. , Tongchusak S. , Mizukami Y. , et al. 2011. Induction of anti-tumor cytotoxic T cell responses through PLGA-nanoparticle mediated antigen delivery. *Biomaterials* 32:3666-3678,
- [95] Li W. , Zhang L. , Zhang G. , et al. 2013. The finely regulating well-defined functional polymer nanocarriers for anti-tumor immunotherapy. *Mini-Reviews in Medicinal Chemistry* 13:643-652,
- [96] Li W. , Guo Q. , Zhao H. , et al. 2012. Novel dual-control poly (N-isopropylacrylamide-chlorophyllin) nanogels for improving drug release. *Nanomedicine* 7:383-392,
- [97] Li W. , Feng S. S. , Guo Y. 2013. Nanocarrier's engineering for immunotherapy. *Nanomedicine* 8: 643-52.
- [98] Li W. , Li J. , Li H. , et al. 2012. Self-assembled supramolecular nano vesicles for safe and highly efficient gene delivery to solid tumors. *International Journal of Nanomedicine* 7:4661-4677,

- [99] Ayano E. , Karaki M. , Ishihara T. , Kanazawa H. , Okano T. 2012. Poly (N-isopropylacrylamide)-PLA and PLA blend nanoparticles for temperature-controllable drug release and intracellular uptake. *Colloids and Surfaces B* 99:4661-4677
- [100] Moon J. J. , Suh H. , Bershteyn A. et al. 2011. Interbilayer-crosslinked multilamellar vesicles as synthetic vaccines for potent humoral and cellular immune responses. *Nature Materials* 10:243-251.
- [101] Fischer D. , Li Y. , Ahlemeyer B. J. , et al. 2003. In vitro cytotoxicity testing of polycations: influence of polymer structure on cell viability and hemolysis. *Biomaterials* 24:1121-1131
- [102] Zou W. 2005. Immunosuppressive networks in the tumour environment and their therapeutic relevance. *Nature Reviews Cancer* 5:263-274
- [103] Zhuang Y. , Ma Y. , Wang C. , et al. 2012. PEGylated cationic liposomes robustly augment vaccine-induced immune responses: role of lymphatic tracking and biodistribution. *Journal of Controlled Release* 159:135-142.
- [104] Champion J. A. , Mitragotri S. 2006. Role of target geometry in phagocytosis. *Proceedings of the National Academy of Sciences of the United States of America* 103:4930-4934,
- [105] Ding B, Wu X. , Fan W. , et al. 2011. Anti-DR5 monoclonal antibody-mediated DTIC-loaded nanoparticles combining chemotherapy and immunotherapy for malignant melanoma: target formulation development and in vitro anticancer activity. *International Journal of Nanomedicine* 6:1991-2005

---

# Graphene Quantum Dots - From Emergence to Nanotheranostic Applications

---

Preeti Nigam Joshi, Subir Kundu, Sunil K. Sanghi and Dhiman Sarkar

Additional information is available at the end of the chapter

<http://dx.doi.org/10.5772/61932>

---

## Abstract

Quantum dots are at the cutting edge of nanotechnology development. Due to their unique optical and physical properties, they have potential applications in many avenues of medicine and biotechnology. With the advancements in nano-sciences, novel applications of quantum dots are constantly being explored for drug delivery and bioimaging. Graphene quantum dots (GQDs) are nanoparticles of graphene with properties of quantum dots as well as graphene. GQDs have ignited remarkable research interest in the field of medicine and biology and are considered as well-suited candidates for nanotheranostic applications due to their excellent biocompatibility and tunable physicochemical properties. The promising emerging implications of GQD platforms for diagnostics and therapeutics advances are the basis of this chapter.

**Keywords:** Graphene quantum dots, Nanotheranostics, Bioimaging, Smart Materials

---

## 1. Introduction

Nanotechnology is undoubtedly the most promising research arena that has deeply influenced biotechnology and medicinal fields and can be considered as the prime technology of the 21st century. Not only biological endeavors, nanotechnology facilitates innovative techniques and applications in electronics, computer science, and aerospace technology also. In the present socioeconomical scenario, nanotechnology can play a significant role in solving many health and environmental issues. "Nano" is a Latin word meaning "dwarf" and technically, an object having one dimension in nano size is considered a nanomaterial. At nanoscale, the physicochemical properties of a substance change drastically like surface area enhancement; changes in thermal and optical properties and dominance of quantum effect are associated with the conversion of a substance to nanoscale. The concept of nanotechnology was first described by

---

physicist Richard P. Feynman in 1959 and the term nanotechnology itself was coined by Norio Taniguchi in 1974.

From its evolution, to date, nanotechnology has marked its significant presence in diverse areas of medicines, biology, electronics, space research, and agriculture.

In the field of medical science and health care sector, nanotechnology intervention has created a new field called “nanomedicine.” The most prominent areas of nanotechnology application in pharmaceutical industry include drug delivery, biosensors, and diagnostic imaging. Different nanoparticles (metal, polymeric, liposomes, and dendrimers) already have well-established applications in drug delivery and disease diagnostics, but in this chapter we will mainly focus on the applications of graphene quantum dots (GQDs) in drug delivery and bioimaging.

### 1.1. History and evolution of graphene quantum dots

In general, a quantum dot (QD) is a semiconductor crystal in the size range of 1–10 nm. Due to their specific size range, QD exhibits quantum phenomena that yield significant benefits in optical properties. It is a well-known fact that on excitation, smaller the size of QD higher will be the energy and intensity of emitted light. QDs can be derived from metals (gold), semiconductors (e.g., selenium, cadmium, etc.), or carbon-based materials (carbon dots and graphene). Due to their specific properties, QDs are used as photodiodes and have a wide range of applications in analytical chemistry but the potential toxicity associated with semiconductor quantum dots prevents their applicability in biology and medicine. This limitation of QDs was the prime driving source for finding out new alternatives, and with the advancement in nanotechnology, quantum dots fabricated from graphene evolved as a more biocompatible source for biomedical applications. Graphene is a carbon-allotrope, zero-band-gap, two-dimensional (2D) sheet of a single layer  $sp^2$ -hybridized carbon with excellent thermoelectric properties [1, 2]. First, its properties were studied by R. Wallace in 1947 [3], and Hoffman et al. isolated pure graphene from graphene oxide via hydrazine reduction in 1963 [4]. The name “graphene” was given by Mouras et al. in 1987 [5]. Though initial discoveries on graphene were mostly unnoticed, it is only after the groundbreaking work by Geim and Novoselov in isolating graphene from highly oriented pyrolytic graphite (HOPG) that huge interest in research was ignited exploring the properties of graphene [2].

GQDs, first reported by Peng et al., are zero-dimensional graphene segments that are small enough to exhibit quantum confinement and size effect. Unlike graphene sheets, they exhibit band gap that is responsible for their unique electrical and optoelectronic properties. Moreover, GQDs also possess size-dependent strong photoluminescence properties [6–9]. These are relatively new nano-dimension entities with a size range between 1 and 10 nm, having a “molecule-like structure,” nontoxic, and can be easily handled compared with colloidal QDs. GQDs are gradually attaining significance due to their potential applications in sensors, electronics, and biology from the standpoint of less health concerns than their traditional semiconductor counterparts due to their less toxicity, ease of functionalization, and favorable electro-optic properties [10–12].

## 2. Synthesis methodologies for graphene quantum dots

To date, remarkable progress has been made in developing new synthesis methodology for graphene quantum dots. There are two broad synthesis approaches for GQDs that can be classified as top-down and bottom-up methods. The first route is based on the cleavage and exfoliation of bulk graphene-based material (graphite) under harsh conditions. In the bottom-up approach, GQDs are mostly prepared from polycyclic aromatic compounds or molecules with aromatic structures.

Though the top-down method is more cost effective having multiple synthesis steps, harsh reaction conditions and lack of morphological control are the major shortcomings associated with this method. However, the prime advantage with this approach is that GQDs obtained by this method have oxygen-containing functional groups influencing the solubility and functionalization of GQDs. Bottom-up approaches give precise control on morphology, size, and shape but still suffer from disadvantages like need for expensive precursors and complex synthesis steps. GQDs synthesized by this method have a strong tendency of aggregation that limits the applicability of this approach. In this segment, a brief overview of recent approaches for GQD synthesis will be given.

### 2.1. Top-down approaches

The basic route of implementing top-down methods is either chemical reactions or physical methods. Based on their mechanism, these approaches can be described as “defect-mediated fragmentation processes.” Mostly, chemical approaches are applied due to some distinguished benefits. Generally, graphene oxide (GO) is cleaved to generate GQDs, and chemical methods generate defects due to the presence of oxygen-containing reactive epoxy and hydroxyl groups. The reactive groups generate a cleavage site, thus allowing GO sheets to be cut into smaller sheets [13]. During the oxidation procedure of graphene, epoxy groups appear linearly on the carbon lattice and this alignment causes the cleavage of C–C bond. The emergence of epoxy groups on GO makes it energetically favorable to convert these groups into stable carbonyl pairs at room temperature. Graphene sheets become fragile due to these chemical transformation and defects and can be readily attacked by chemicals to generate GQDs. The presence of aromatic  $sp^2$  domains having epoxy groups on graphene, GO, carbon black, and carbon nanotubes makes them excellent starting candidates for GQD synthesis.

#### 2.1.1. Hydrothermal and solvothermal synthesis

Particle size of GQDs and formation mechanisms are deeply influenced by hydrothermal synthesis. Water, as a green solvent used in this procedure, is a key player in atom-economical reactions [14]. These methods generally require a high amount of strong alkali (NaOH and ammonia) for cutting carbon precursors into GQDs. First, Pan et al. reported this method to synthesize water-soluble blue luminescent quantum dots. The diameter of QDs was 5–13 nm and they exhibited strong fluorescence in alkali conditions, while in acidic conditions the fluorescence got quenched. The basic synthesis step involved was the oxidation of graphite to GO that produces epoxy groups, which cause the rupture of C–C bonds. Further, these epoxy

groups are oxidized into stable carbonyl groups responsible for the water dispersibility of GQDs as shown in Figure 1. Later, Pan et al. put forth a modified high-temperature synthesis procedure to synthesize fine crystalline GQDs with green fluorescence [14, 15].

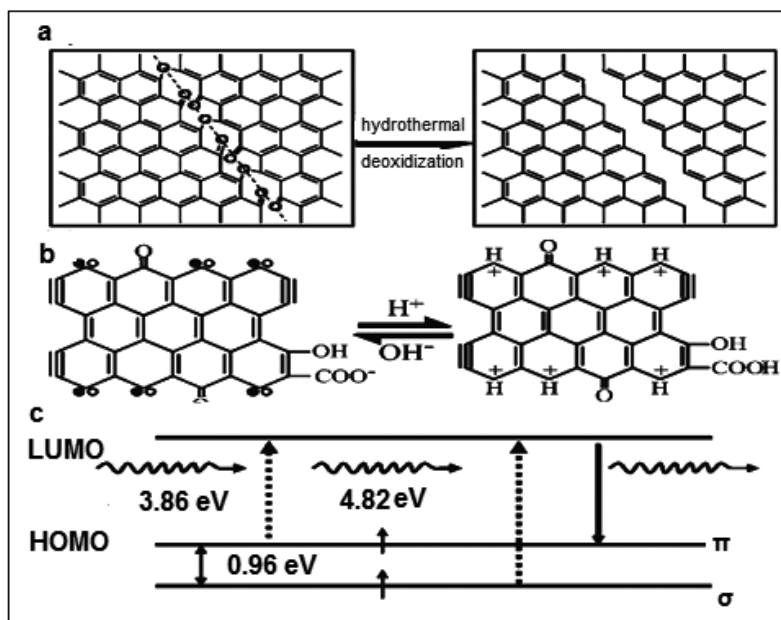


**Figure 1.** Synthesis mechanism of GQDs via cutting of graphite sheets. This was a multistep process and GQDs were prepared by the reduction of epoxy groups generated in oxidation and cutting step. (Ref [14]: Pan et al.)

In recent years, graphene-based materials have seen extensive applications in the field of electronics, pollution treatment, solar cells, Li-ion batteries, and sensing. The modification of graphene by nitrogen or boron doping significantly amends its optical and electronic properties. Similarly, a change in photoluminescence and electric properties can be attained by tuning the band gap of GQDs [16].

Hydrothermal approach deeply influences the size and morphology of GQDs. In one report, Tetsuka et al. [17] synthesized amine-functionalized graphene quantum dots (NH<sub>2</sub>-GQDs) using oxidized graphene sheets and ammonia using this method by bond-scission reaction. Concentration variation of ammonia played a key role in controlling the luminescence of GQDs from violet to yellow. The nucleophilic substitution upon ammonia addition to graphene triggered the reaction of ring-opening epoxide, and sp<sup>2</sup> domains were cut out to generate amino-functionalized GQDs of 2.5 nm size and 1.1 nm thickness (Figure 2). In this series, few researchers have reported altered optical properties of GQDs after functionalization with polymers or small molecules. Feng et al. have put forth their idea of fluorinated GQDs (F-GQDs) prepared by hydrothermal procedure. Xenon difluoride was utilized for fluorinated graphene synthesis at high temperatures and then F-GQDs were obtained by hydrothermal procedure [18].

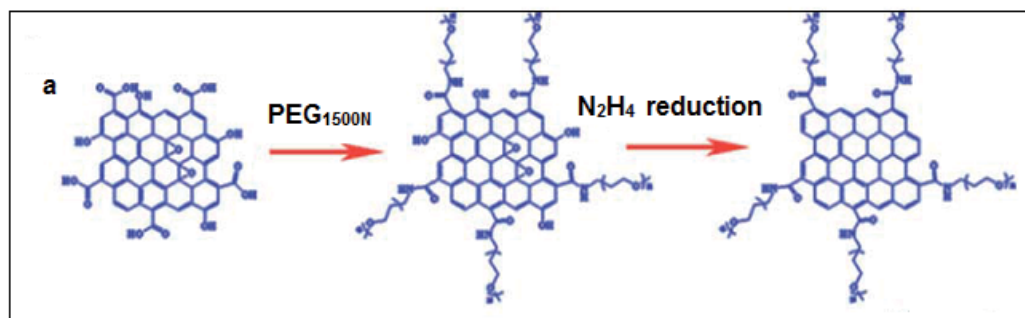


**Figure 3.** Synthesis of surface-passivated GQDs with hydrazine hydrate reduction and surface passivation by PEG<sub>1500N</sub>. (Ref. [23]; Shen et al.)

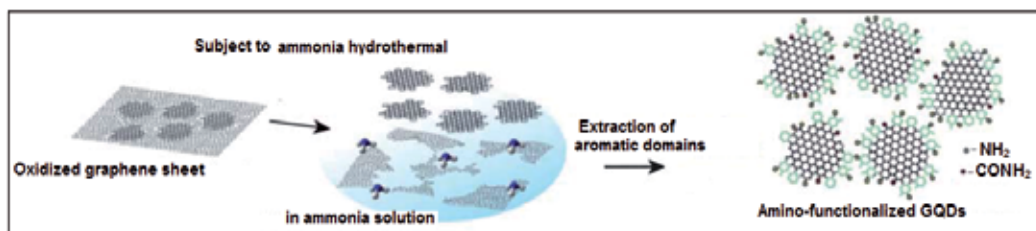


**Figure 2.** Illustration of hydrothermal synthesis of amino-functionalized GQDs. (Ref [17]; Tetsuka et al.)

Hu et al. [19] came up with a new methodology by synthesizing nitrogen-doped GQDs (N-GQDs) from oxidized debris (ODs) on graphene oxide by the hydrothermal treatment of GO at 180°C in the presence of ammonia without any strong acid treatment. The as-prepared N-GQDs were highly blue luminescent, 2–6 nm in size, with a quantum yield (QY) of 24.6. Aqueous route and novel application of ODs for the synthesis of N-GQDs were the major highlights of their work. The prime advantage associated with this approach was its cost effectiveness due to aqueous reaction conditions in the absence of any surface-passivation agent or strong acids. Liu et al. and Zhang and coworkers also reported similar procedures for the synthesis of functionalized GQDs [20, 21]. Recently, Nigam et al. have reported a novel reducing agent Lawsone for hydrothermal synthesis of GQDs of 3–6 nm size and green fluorescence from graphene oxide reduction. The GQDs were stable and showed good biocompatibility at higher concentrations [22]. In another approach, Shen et al. prepared surface-passivated GQDs from hydrazine hydrate reduction of GO that were further passivated by poly(ethylene glycol) diamine (PEG<sub>1500N</sub>) as depicted in Figure 3. By this method, they obtained GQDs of broad diameter in the range of 5–19 nm with blue fluorescence; hence, they further modified the procedure, and the GQDs were synthesized via one-pot hydrothermal synthesis route using GO and PEG as starting materials. The basic advantage of PEG-surface passivation was high photoluminescence (PL) quantum yield, better photon-to-electron conversion, and improved unconverted PL properties than native GQDs [23].

In solvothermal reaction, organic solvents (dimethyl sulfoxide (DMSO), dimethylformamide (DMF), and benzene) are utilized instead of water to obtain GQDs. The size and morphology of the GQDs are greatly influenced by the physicochemical properties of solvents. In a recent approach reported by Zhu et al. [24], DMF was used as a solvent to split graphene oxide into green fluorescent GQDs under ultrasonication followed by heating at 200°C in a Teflon autoclave. Column chromatography on silica gel was performed to obtain GQDs instead of dialysis treatment with water as eluent. As an improvisation, they later increased the reaction time to 8 h using methanol/methylene chloride and water as mobile phase for GQD synthesis [25]. Shin et al. put forth a new solvothermal approach based on novel acid-free and oxone-oxidant-assisted synthesis of GQDs using various natural carbon resources, including graphite, multiwall carbon nanotubes (MWCNTs), carbon fibers (CFs), and charcoal (C) [26].

### *2.1.2. Microwave-assisted cutting and ultrasonic approach*

Hydrothermal/solvothermal techniques are the most applied processes for GQD synthesis, but due to their tedious synthesis protocols, researchers have reported a few procedures based on microwave-assisted synthesis as this technique has the advantage of both hydrothermal and microwave processes. In a recent work by Luk et al., nitrogen-doped GQDs (N-GQDs) were prepared by mixing 3 wt% of glucose dissolved in aqueous ammonia (25%) at room temperature. The homogeneous solution was heated in a microwave reactor (300 W power) for 5 min at 180°C. Using this method, GQDs with 6 nm size and excitation-dependent luminescence spectra were obtained. Upconversion emission spectrum was another important feature of their work. According to their findings, nitrogen doping played the key role in two-photon luminescence [27]. Recently, a one-step-microwave-assisted solvothermal method for fabricating sulfur- and nitrogen-doped GQDs (S-, N-GQDs) has been reported based on the reaction of GO and reduced glutathione in N,N-dimethylformamide (DMF) at 200°C under microwave irradiation [28].

Tang et al. have reported glucose-derived GQDs through a microwave-assisted hydrothermal (MAH) approach. The basic advantage of this method was uniform heating that produced particles of small sizes. The authors have synthesized GQDs of average size of 4 nm. Based on the microwave heating time, GQDs of varying sizes were obtained [29].

In another approach, Li et al. [30] have developed a method for facile microwave-assisted synthesis of two-color GQDs in acidic conditions. Figure 4 shows the schematic of basic steps involved in the synthesis procedure. Greenish yellow luminescent GQDs (gGQDs) of average size 4–5 nm were obtained. The as-synthesized GQDs were further moderately reduced with NaBH<sub>4</sub>, and blue GQDs were produced with the same dimensions. The quantum yield of blue and green GQDs was 23% and 12%, respectively.

Ultrasonication is a simpler procedure to prepare GQDs, because of the fact that ultrasound can generate alternating low-pressure and high-pressure waves in liquid that can be useful for shearing the carbon layer materials into GQDs. Zhu et al. [31] have reported one-step synthesis using ultrasonication with only graphene oxide and KMnO<sub>4</sub>, and luminescent graphene quantum dots of 3 nm in high quantum yield were prepared.

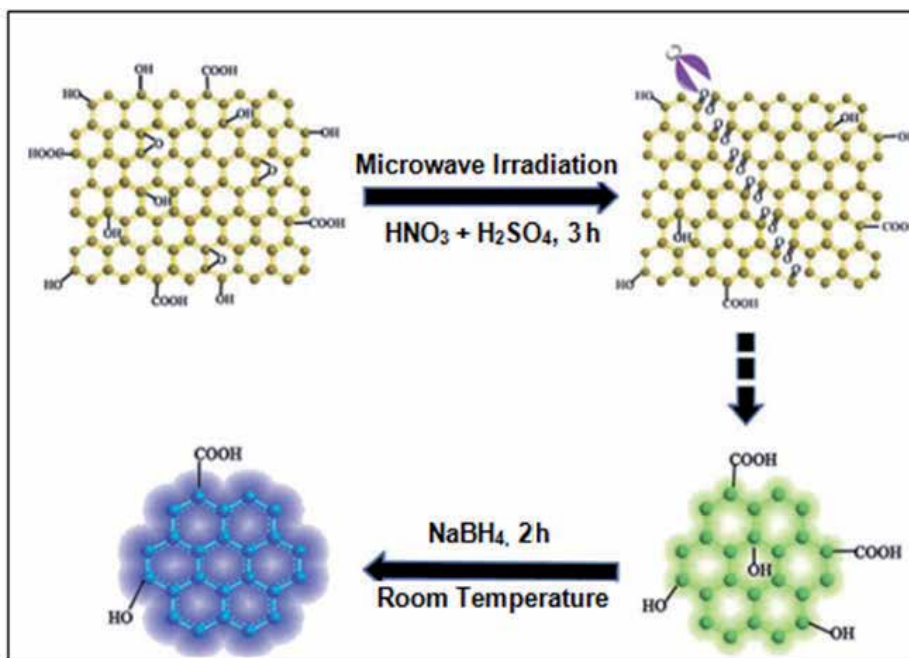


**Figure 4.** Schematic of synthesis of green and blue GQDs. (Ref [30]: Li et al.)

### 2.1.3. Electrochemical exfoliation approaches

Electrochemical approaches were already established for the synthesis of carbon dots at a potential of 1.5–3 V, where electrochemical exfoliation and intercalation are the basic steps to obtain the desired product by generating hydroxyl and oxygen radicals that play the role of electrochemical “scissors” in an oxidative cleavage reaction [32, 33].

Li et al. [34] extended this strategy further to synthesize GQDs of 3–5 nm size through an electrochemical method that involved the breaking up of a graphene film that has been treated with oxygen plasma to increase hydrophilicity. The as-synthesized GQDs exhibited green luminescence and enhanced stability in water dispersion. Zhang et al. [35] put forth another approach for synthesizing water-soluble GQDs by electrochemical exfoliation of graphite and further reducing the as-synthesized nanoscale GQDs with hydrazine at room temperature in contrast to earlier reported high-temperature reductions. It was the first report of strong yellow fluorescence in high yield and uniform sizes. The yellow fluorescence can be attributed to hydrazide groups on the surface of GQDs, produced during the low-temperature hydrazine reduction step. Though carbon nanotubes are not very suitable materials for GQD synthesis due to their potential toxicity, recently Pillai and Shinde have described an electrochemical procedure for GQDs based on multiwalled nanotubes. Figure 5 illustrates the mechanism of GQD synthesis. This method is a new procedure to synthesize size-tunable quantum dots by the oxidation time [36]. Due to the toxic base material, applicability of GQDs prepared by such methods is limited and it involves extra efforts to coat the GQDs with any polymer or com-

pound to enhance their biocompatibility. However, in another report, Shinde et al. put forth a two-step electrochemical strategy of synthesizing nitrogen-doped GQDs (N-GQDs) from multiwall CNTs. The presence of nitrogen dopants in the carbon framework caused faster unzipping of N-MWCNTs, and also provided lower activation energy site that was beneficial for enhanced electrocatalytic activity for oxygen reduction reaction [37].

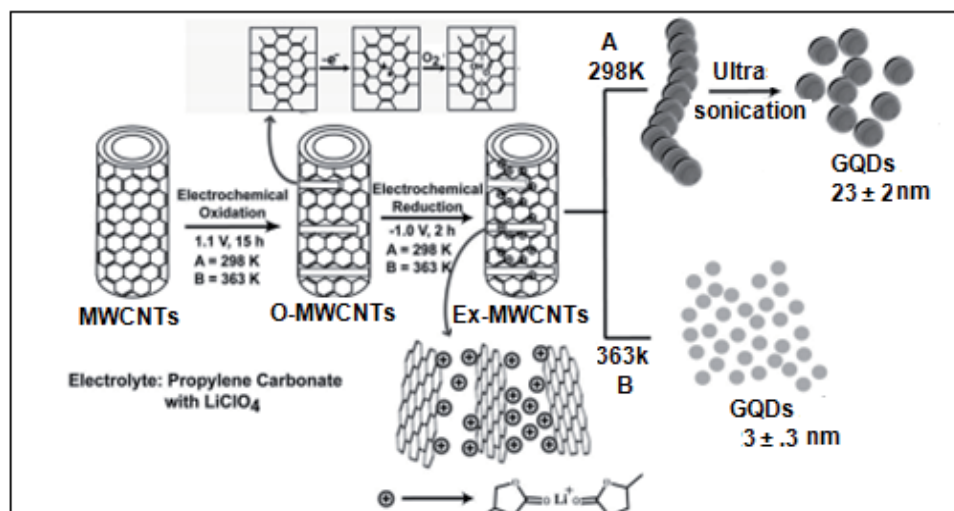


**Figure 5.** Synthesis stages involved in electrochemical synthesis of GQDs from MWCNTs. (Ref [36]: Shinde et al.)

Recently, a facile electrochemical exfoliation of graphite in  $K_2S_2O_8$  solution for the synthesis of uniform small-sized red fluorescent GQDs (RF-GQDs) was demonstrated by Tan et al. with no chemical modification. This method was relatively simple, and water-soluble GQDs of uniform size (3 nm diameter) with excellent PL properties and less cytotoxicity were obtained with in vivo applicability in bioimaging applications.

#### 2.1.4. Nanolithography

Nanolithography is a high-precision technique but gives low yield, and expensive instrumentation is required, which is the prime reason for very few reports being available on this methodology. Ponomarenko et al. [39] used ultrahigh-resolution electron beam lithography to cut graphene to desired sizes. In another work by Lee and coworkers [40], chemical vapor deposition method was used to generate GQDs of uniform size from self-assembled block copolymers (BCP) as an etch mask on graphene films. Although this was a low-yielding method, uniform particles were synthesized for probing effects of size and functionalization.

## 2.2. Bottom-up approaches

As compared to top-down approaches, very few bottom-up procedures have been reported.

### 2.2.1. Pyrolysis

Pyrolysis is one of the simplest methods of synthesizing graphene quantum dots. In this method, GQDs are formed via carbonization of small organic molecules. However, apart from its simplicity, GQDs of low quantum yield are produced in most of the cases. Few recent reports based on this method are described here. GQDs from hexa-peri-hexabenzocoronene (HBC) were reported by Liu et al. [41]. HBC is a polycyclic aromatic hydrocarbon that resembles nanoscaled fragments of graphene that stack via  $\pi$ - $\pi$  interactions. This method produced monodisperse disk-like GQDs of  $\approx 60$  nm and 2–3 nm thickness. Pyrolysis, unfunctionalization, and oxidation processes are shown in Figure 6. Further, GQDs from citric acid (CA) and glutathione (GSH) as starting materials were also prepared. Glutathione is a tripeptide containing glutamate, cysteine, and glycine. The core advantage of glutathione is enhanced biocompatibility and high quantum yield. In this method, a 33.6% QY was obtained that can be attributed to the amination reaction between the amine group of GSH and the epoxy and carboxylic groups of GQDs [42]. It has been reported earlier that carboxylic and epoxy groups act like non-radiative electron-hole combination centers [18], and during amination reaction, reduction in number of these centers leads to better emission properties.

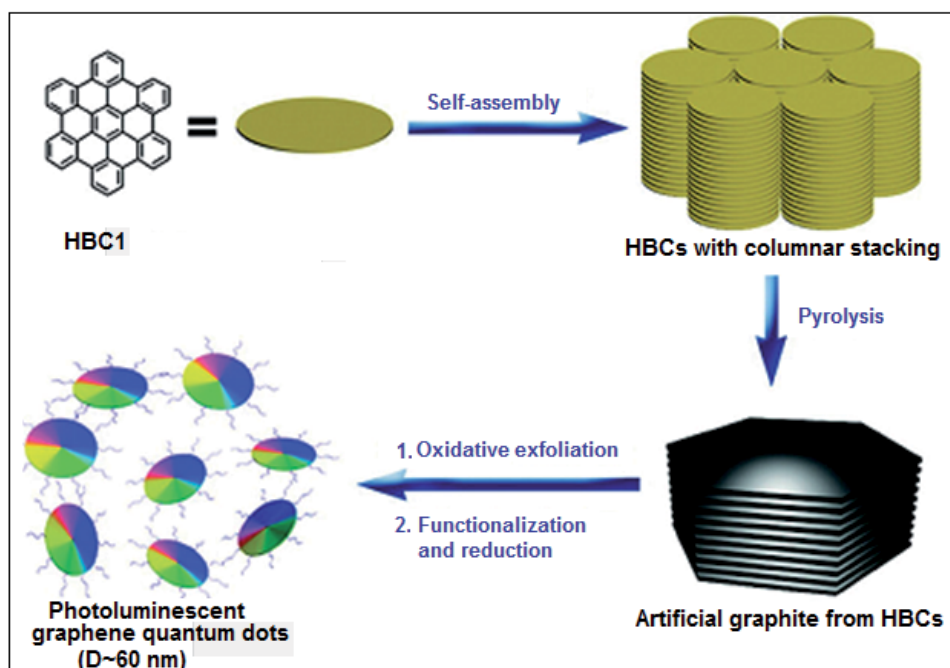


**Figure 6.** Illustration of pyrolysis procedure of HBC for synthesis of GQDs. Monodisperse disk like GQDs with 2–3 nm thickness and 60 nm diameters were obtained. (Ref [41]: Liu et al.)

In another approach, Wu and coworkers synthesized GQDs via a simple one-step pyrolysis of L-glutamic acid in a heating mantle. With this method, GQDs with a broad emission range

(from visible to near infrared (NIR)) with excellent quantum yield of 55% were obtained. Figure 7a illustrates the basic steps of pyrolysis procedure, while Figure 7b, c depicts the characteristic features of GQDs. These quantum dots exhibited tremendous bioimaging potential, and as shown in Figure 7d they can be successfully utilized for *in vitro* and *in vivo* cell imaging [43].

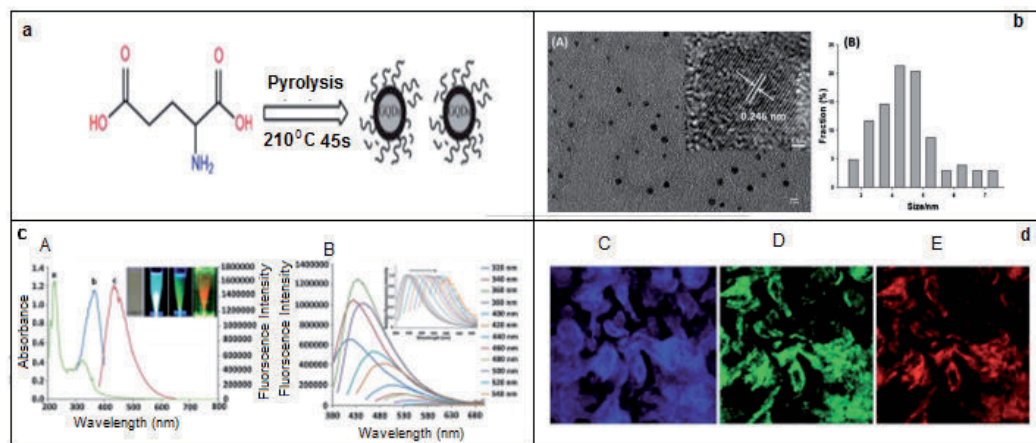


**Figure 7.** (a) Schematic of pyrolysis of L-glutamic acid; (b) HRTEM image of GQDs and size distribution; (c) Absorption spectra (A) and fluorescence emission spectra (B); (d) Confocal fluorescence images (C–E) under different excitation wavelengths from 359 nm, 488 nm, and 514 nm. (Ref [43]: Wu et al.)

Citric acid was also explored as the starting material to synthesize blue luminescent GQDs by tuning its carbonization degree. The as-synthesized GQDs were 15 nm in width and 0.5–2.0 nm in thickness. GQDs obtained by this method were self-passivated due to incomplete carbonization of citric acid [13]. Gram-scale synthesis of functionalized GQDs from pyrene via facile molecular fusion route was described by Wang et al. [44]. The single-crystalline GQDs were having excellent optical properties such as bright excitonic fluorescence, strong excitonic absorption bands extending to the visible region, large molar extinction coefficients, and long-term photostability.

Recently, a facile bottom-up method producing fluorescent nitrogen-doped graphene quantum dots (N-GQDs) based on one-step pyrolysis of citric acid and tris(hydroxymethyl)aminomethane was reported. These nitrogen-doped GQDs emitted strong blue fluorescence under 365 nm ultraviolet (UV) light excitation with the highest reported quantum yield of 59.2% [45].

### 2.2.2. From fullerene

Lu et al. [46] reported a mechanistic approach for the synthesis of geometrically well-defined GQDs on a ruthenium surface using  $C_{60}$  molecules as a precursor. Ruthenium (Ru) catalyzed the cage opening reaction of  $C_{60}$ . The strong  $C_{60}$ –Ru interaction initiated the formation of surface vacancies in the Ru single crystal and a subsequent embedding of  $C_{60}$  molecules in the surface. At high temperatures, embedded molecules get fragmented and form carbon clusters that undergo diffusion and aggregation to form GQDs.

### 3. Physicochemical properties of graphene quantum dots

GQDs are nanosized graphene sheets. In this chapter, we will deal with Bohr radius and quantum confinement effect to explain the optical properties of GQDs. It is believed that the variations in photoluminescence, electronic, and physical characteristics of GQDs are related with these two important terminologies. Therefore, let us briefly look at these terms that will enhance our basic understanding on the properties of GQDs.

#### Bohr radius

Quantum dots possess the structural features of parent molecule but exhibit unique electrical and optical properties as a function of their size. The quantum size effect occurs when these nanostructures attain a size smaller than a fundamental unit of exciton Bohr radius. An exciton is a bound state of an electron and an electron hole, which are attracted to each other by the electrostatic Coulomb force that is formed when a photon is absorbed by a semiconductor that excites an electron from the valence band into the conduction band.

In Gaussian unit, a Bohr radius is given by:

$$a_0 = \hbar^2 / m_e e^2 \quad (1)$$

where  $a_0$  is the Bohr radius,  $\hbar$  is the reduced Plank's constant, and  $m_e$  is the electron rest mass. Bohr radius has an approximate value of 0.53 Å [47].

#### Quantum confinement effect

When the size of quantum dot becomes smaller and approaches toward the Bohr radius of bulk exciton, the quantum confinement effect becomes apparent. Depending on the dimension of the confinement, three kinds of structures can be defined: quantum well (QW), quantum wire (QWR), and quantum dot (QD) based on the reduced dimension. Material size is reduced in one direction in a QW and the exciton is free to move in other two directions, while in a QWR the material size is reduced in both the directions leaving only a single direction for the movement of exciton. In a QD, all directions are reduced restricting the free movement of exciton in any direction [48].

Due to this confinement effect exciton nature gets modified, which leads to distinguished optical and electrical properties of quantum dots.

#### 3.1. Electrochemical properties

The 2010 Nobel Prize was awarded to Geim and Novoselov for their remarkable work in graphene. This not only validated the importance of graphene but also paved the way for their applications in different research areas of electronics and optics as well as commercial applications. GQDs are so closely related to graphene that a discussion on GQD would be incomplete without describing the basics of graphene. With technological advancements in different fields, demand for carbon and carbon-related materials like graphene, carbon

nanotubes is increasing rapidly for electrical, mechanical, and biomedical applications due to their tremendous thermal, electrical, mechanical, optical, and other unique properties [49–51]. Although graphene has an upper hand in comparison to CNTs due to low toxicity, it has the disadvantages of aggregation and low dispersity. The nanoparticles of GQDs are more advantageous due to their better physicochemical properties.

Graphene is known as a zero-band-gap material having infinite exciton Bohr radius, because of the linear energy dispersion of the charge carriers [52, 53]. Quantum confinement is a phenomenon that evolves in a finite-size graphene sheet and GQDs are best examples of this prominent effect. GQDs exhibit non-zero, tunable band gap than graphene and luminescence on excitation. Moreover, GQDs provide the flexibility of tuning the band gap by size and surface chemistry amendments. Eda et al. have reported that electrical properties of GQDs are size tunable. According to their findings of density functional theory (DTF), the band gap of GQDs consisting of 20 aromatic rings is approximately 2 eV, while for a benzene ring the value is 7 eV [54]. GQDs are a very new addition to the family of quantum dots and a great deal is left to explore their electronic and electrochemical properties. Graphene has been widely explored in field-effect transistors but GQDs are applied in single electron transistor (SET)-based charge sensors [55–57]. SETs are newer switching devices that use controlled electron tunneling to amplify a current [58]. Apart from charge variation detection, GQDs are applied for electronic sensors for humidity detection based on the modulation of electron tunneling distances caused by humidity and pressure.

### 3.2. Absorption and photoluminescence properties

GQDs are widely explored for their photoluminescence properties. They generally show a strong absorbance in UV region. The basic absorption spectra of GQDs show a prominent peak at about 230 nm, which is assigned to the  $\pi \rightarrow \pi^*$  excitation of the  $\pi$  bonds of aromatic C=C, and a shoulder peak at 300 nm is assigned to the  $n-\pi^*$  transition of C=O bonds [59]. GQDs also exhibit size-dependent UV–Vis absorption spectrum due to quantum confinement effect. Peng et al. [60] analyzed that the absorbance peak red shifted from 270 nm to 330 nm, with increase in the size from 1–4 nm to 7–11 nm (Figure 8a). It was also observed that varying the average size of GQDs from 5 nm to 35 nm, the peak energy of the absorption spectra monotonously decreases from 6.2 eV to 4.6 eV (Figure 8b) [61]. According to the findings of Fuyuno et al., the absorption spectra of GQDs showed increases in absorbance with decreasing wavelength for each sample. GQD samples were collected via high-performance liquid chromatography (HPLC) at different intervals. A gradual change in the absorption spectra of HPLC-GQDs was observed depending on the retention time (i.e., with the size of the GQDs). For the GQD samples collected at 4 h, no distinct energy gap and peak structure were obtained, while for the GQDs of 7 h and 10 h, peak structures were observed at  $\sim 300$  nm, which corresponds to  $n-\pi^*$  transitions of nonbonding electrons in the C=O bonds (Figure 8c). However, the size dependency was not visible and the absorbance peaks were independent of size variation from 1.7 nm to 21 nm with GQDs prepared via glucose carbonization [62]. Moreover, absorption spectra also vary with difference in the method of synthesis [63, 64]. The presence of oxygen-containing groups also plays a governing role in the absorption peak position of

GQDs, as illustrated in Figure 8d. The two electronic transitions at 300 nm (3.81 eV) in the absorption spectra of the GQDs can be attributed to electronic transitions from s and p orbitals or from highest occupied molecular orbital (HOMO) to lowest unoccupied molecular orbital (LUMO) [65].

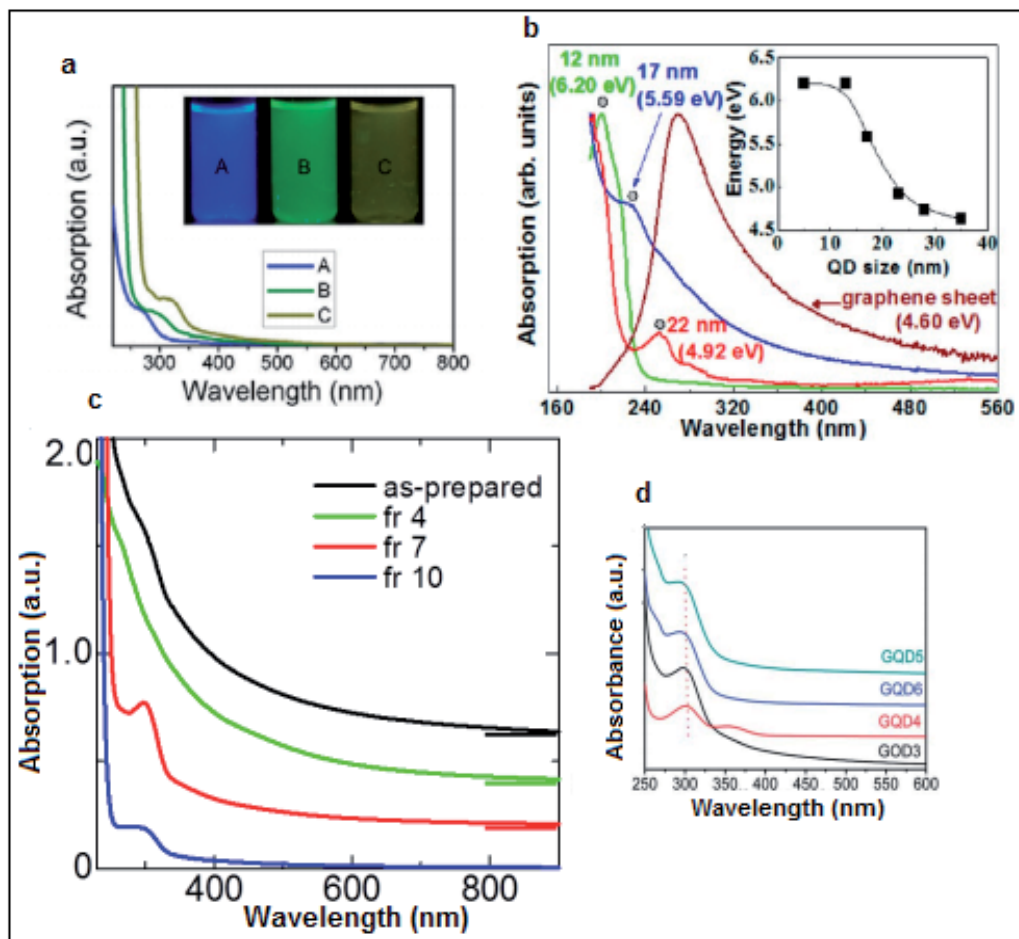


**Figure 8.** Variation in absorption spectra of GQDs with synthesis parameters (a) UV-Vis spectra of GQDs A, B, and C correspond to synthesized reaction temperature at 120, 100, and 80°C, respectively (Ref [60]: Peng et al.); (b) Absorption spectra for three typical GQDs of 12, 17, and 22 nm average sizes dispersed in DI water and a graphene sheet. Inset: absorption peak energy as a function of average GQD size (Ref [61]: Kim et al.); (c) Spectra of different sizes of GQDs at different collection times (4, 7, 10 h) (Ref [62]: Fuyuno et al.); (d) Presence of oxygen functional groups variation and its effect on UV spectra (Ref [65]: Yang et al.)

Another attractive feature of GQDs is their photoluminescence profile. Though the exact mechanism of PL is still not completely validated, researchers have revealed that the possible causes can be quantum confinement effect, aromatic structures, presence of functional groups and oxygen-containing groups, free zigzag sites, and edge defects, due to which GQDs show

new absorption features that affect the photoluminescence profile of QDs [66–69]. It is a well-known fact that QDs exhibit quantum confinement and edge effects, the key players of PL properties. Researchers have identified that the band gap is a function of size of QDs and decreases with an increase in size. Eda et al. [55] in their hypothesis proposed that the radiative recombination of e–h pairs generated within localized states can be the possible cause of blue PL spectra. The energy gap between the  $\pi$  and  $\pi^*$  states generally depends on the size of  $sp^2$  clusters [27] or conjugation length [18]. According to their findings, it is the interaction between the nanometer-sized  $sp^2$  clusters and the finite-sized molecular  $sp^2$  domains which is the key in optimizing the blue emission. Moreover, the synthesis procedure of QDs in top-down approaches and cutting of large graphene fragments in different crystallographic directions generates edges (zigzag and arm chair). These edges are *prima facie* responsible for diverse emission properties, as suggested by Kim et al. [61]. Zigzag sites are either carbene like with a triplet ground state or carbyne-like with a singlet ground state, and the irradiation decay of activated electrons from LUMO to HOMO is the most probable cause of blue emission [14].

In this segment, we will discuss some aspects of QDs and their effect on PL spectra. Size dependency of PL of QDs was reported by Alam et al. [70]. In their analysis, emission wavelengths of pristine zigzag-edged QDs of different diameters were calculated. On varying the size from 0.46 nm to 2.31 nm, QDs exhibited PL spectra from deep UV to near infrared as shown in Figure 9a. The smallest QD (benzene) showed an emission peak at 235.2 nm while a peak at 999.5 nm was exhibited by QDs of size 2.31 nm. They reported a linear and steep size dependence and concluded that emission covers the entire visible-light spectrum (400–770 nm) on varying the diameter of QD from 0.89 nm to 1.80 nm [70].

Depending on the method of synthesis, QDs possess oxygen-containing groups, that is, hydroxyl, carboxy, carbonyl, and epoxy ether groups; the difference in energy levels of surface groups and emission traps on QDs governs the difference in emission spectra and PL with different colors including red, green, blue, and yellow [52, 71].

As reported by Zhu et al., surface defects on QDs that arise from oxidation of surface groups also result in red-shifted PL spectra [72]. In addition, not only the surface defects and functional groups but also the synthesis parameters (pH and solvent), size, and excitation wavelength have marked their impact on the PL spectra of QDs. As described above, quantum confinement effect is a major phenomenon of QDs that arises when the size of QDs is less than the Bohr exciton radius. This size dependency of band gap of QDs is responsible for their unique optical and spectroscopic characteristics. It is reported that by decreasing the size of QDs, emission spectra show blue or high energy shift [73–76]. Figure 9 illustrates various effects of physiological parameters on emission spectrum of QDs.

In an interesting finding, few reports deal with the upconversion luminescence properties exhibited by QDs. As reported by Shen et al., surface-passivated QDs showed strong upconversion PL when illuminated with 980 nm. An unconverted PL spectrum at 525 nm was obtained (Figure 10a). The upconversion emissions also showed peak shifts from 390 nm to 460 nm when excited with wavelengths of 600–800 nm. They further demonstrated that the PL spectrum was a transition from the lowest unoccupied molecular orbital to the highest occupied molecular orbital [23]. Similar phenomena were also observed by Zhu et al., and

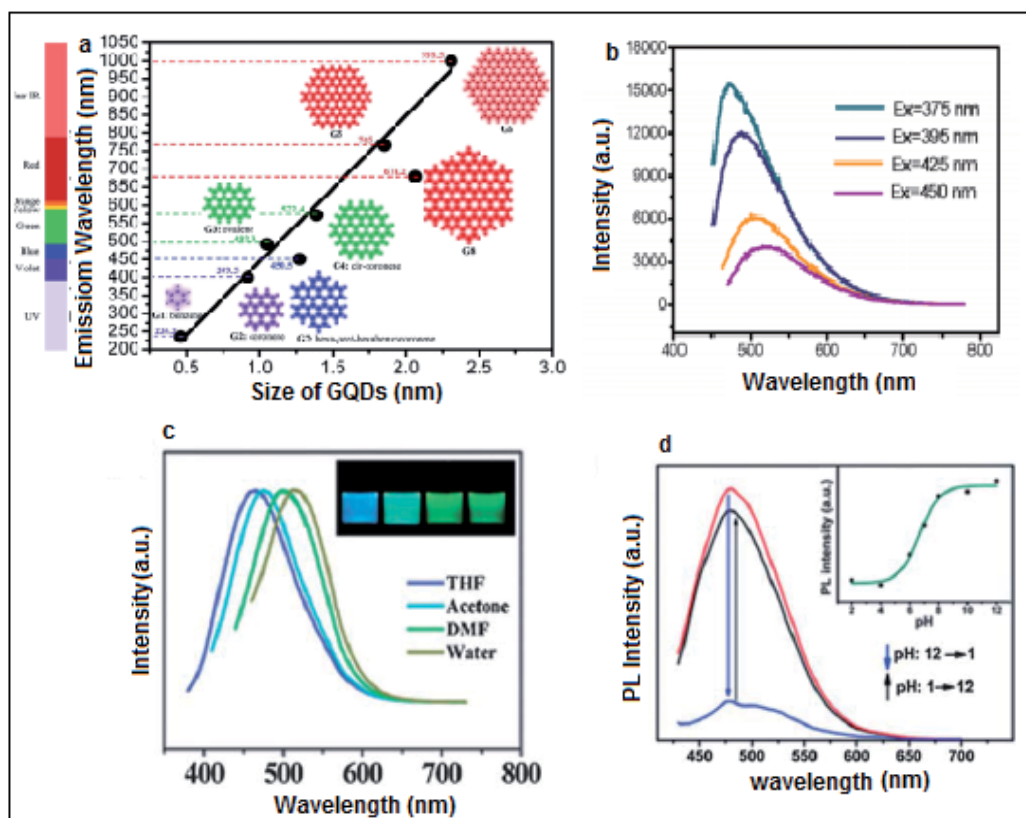


**Figure 9.** Illustrating the change in emission spectra of GQDs based on (a) size (Ref [70]: Alam et al.); (b) Excitation dependent (Ref [71]: Tang et al.); (c) in different solvents (Ref [75], Zhu et al.); (d) with pH of the GQD solution (Ref [15]: Pan et al.)

when their GQDs were illuminated with 600–900 nm wavelengths, a significant red shift was obtained. The possible cause for this can be explained by the multi-photon active process as reported for carbon dots earlier [77, 78]. The possible cause of upconversion effect was depicted by anti-Stokes transition, as shown in Figure 10c. In comparison to excitation-dependent upconversion effect, Zhou et al. observed an excitation-independent upconversion effect with GQDs synthesized via ultrasonication as illustrated in Figure 10d [79].

### 3.3. Quantum yield

Quantum yield is another important aspect associated with the PL of GQDs. The highest value reported was 28%. However, Wu et al. have reported a high QY of ~55% by the pyrolysis method of GQD synthesis [43]. In general, the QY depends on the fabrication methods and surface chemistry. It was reported by Liu et al. and Loh and coworkers that the removal of oxygen-containing groups and surface passivation can drastically enhance the QY of GQDs [80–82]. The possible reasons for this can be the non-radiative electron–hole recombination

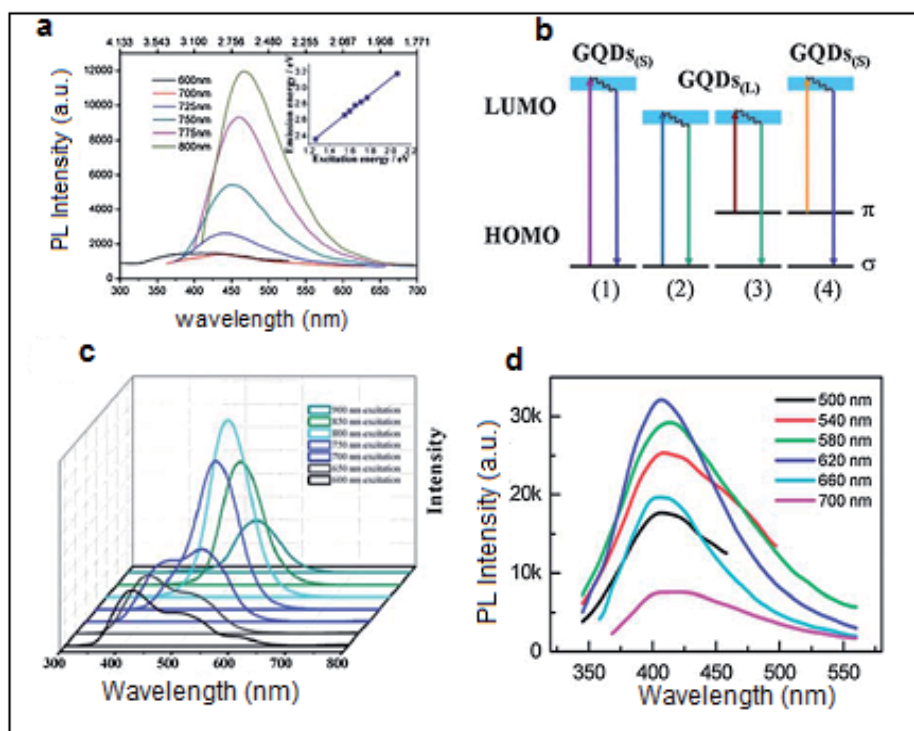


**Figure 10.** (a) Upconversion luminescence properties exhibited by GQDs; (b) A schematic illustration of various typical electronic transitions processes of GQDs (Ref [23]: Shen et al.) (c) PL spectra of GQDs upconversion GQDs on illumination of 600–900 nm (Ref [78]: Zhu et al.); (d) Upconverted excitation-independent PL spectra of the ultrasonically synthesized GQDs at different excitation (Ref [79]: Zhou et al.)

tendency of oxygen-containing groups. Though GQDs have optical properties similar to semiconductor QDs, few basic differences in PL spectra in terms of bandwidth (GQDs have broad bandwidth) and spectral shift toward red that decreases with increasing excitation clearly distinguish them from the semiconductor QDs [82].

### 3.4. Electrochemiluminescence

Another unique characteristic of GQDs is electrochemiluminescence (ECL), a phenomenon of showing luminescence during electrochemical reactions. GQDs are electro-active species and few reports deal with their ECL properties [83, 84]. Figure 11 is an illustration of ECL and PL spectra of GQDs synthesized by hydrothermal method. GQDs exhibited bright blue emission under ultraviolet irradiation ( $\sim 365$  nm) in a water solution of neutral pH, an excitation-independent photoluminescence feature, and interestingly, it also exhibited a novel anodic ECL by using  $\text{H}_2\text{O}_2$  as a co-reactant [83]. The possible mechanism can be the formation of excited-state GQDs<sup>\*</sup> through electron transfer (ET) annihilation of negatively and positively radical species.

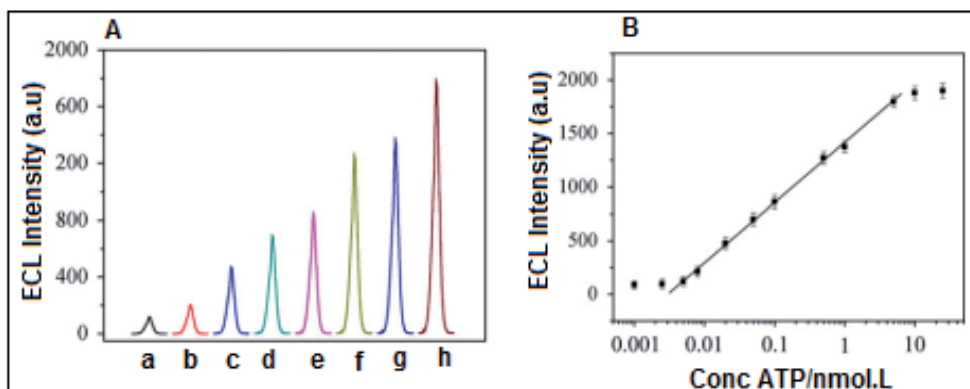


**Figure 11.** ECL intensity curves at different ECL intensities and ATP concentration. (Ref [83]: Lu et al.)

### 3.5. Biocompatibility of GQDs

GQDs are basically carbon materials and show low toxicity. As graphene and related materials have shown great potential in disease diagnosis and bioimaging, the potential toxicity of GQDs in biological systems has become a cause of concern. It is previously reported that graphene or graphene oxide can cause pulmonary inflammation upon inhalation [55], and graphene family materials were found to be toxic to bacteria [85–87]. In vitro studies on animal cell lines were also conducted and it was reported that the cytotoxicity of graphene and GQDs is also dependent on the method of synthesis and starting material. GQDs synthesized from carbon nanotubes are more toxic than those synthesized from graphene oxide and amino acids. Few reports have shown that GQDs can be well tolerated at low concentrations (50  $\mu\text{g/ml}$ ) but at higher concentrations (1  $\text{mg/ml}$ ), they show acute toxicity. In this regard, it is imperative to find out new strategies for less-toxic graphene materials for their practical biological applications with enhanced bioavailability. Surface functionalization of GQDs and graphene material can play an important role in mitigating the cytotoxicity of GQDs. These are the materials of future with potential biomedical applications, and surface modification of GQDs is an important criterion for their wide applicability. Many researchers have reported the emergence of unique properties with variations in surface properties. Production of reactive oxygen species (ROS) from GQDs by blue laser ablation and surface passivation by polyethylene glycol was reported by Christensen et al. in cell-free conditions [88] In another study by Yuan and coworkers, on functionalized GQDs, very encouraging results of cytotoxicity were observed; even at higher concentrations (200  $\mu\text{g/ml}$ ), quantum dots showed good biocompatibility as depicted in Figure 12 a, b. Their analysis proved that surface functionalization can be a better alternative to reduce the cytotoxicity of GQDs [89]. Jastrzębska et al. have summarized the toxicological analysis of graphene-related materials in a recent review [90]. As an interesting fact, many researchers have reported that GQDs are less toxic than GO and the possible cause may be less damage to cell membrane owing to their smaller size and their fast clearance [91].

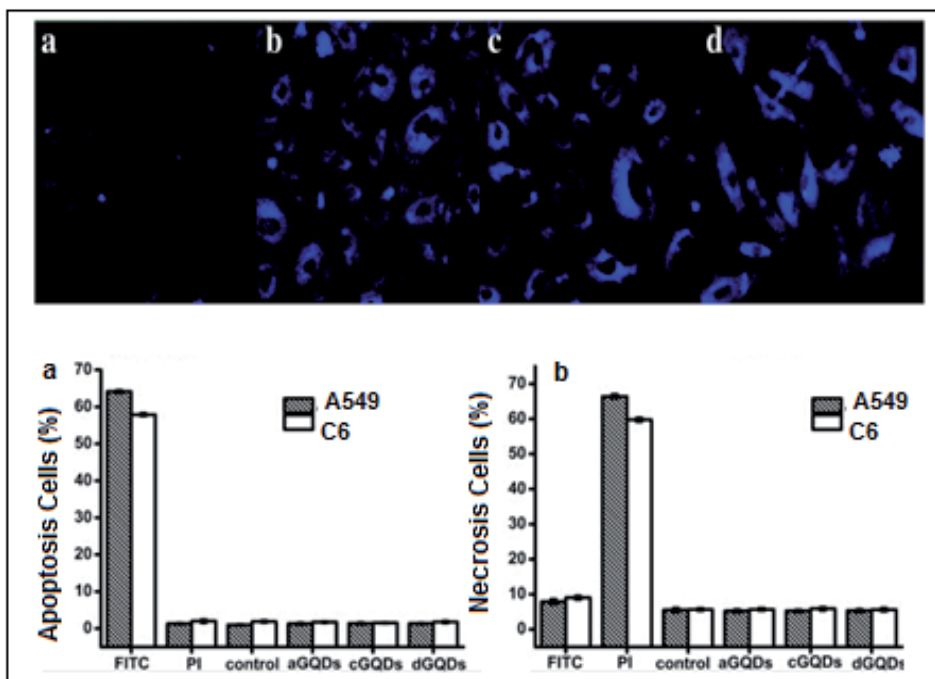


Figure 12. Biocompatibility analysis of GQDs in vitro. (Ref [89]: Yuan et al.)

Moreover, due to increasing biological applications of GQDs and graphene materials, in vivo toxic effects should also be considered. Wang et al. have reported that high doses (0.4 mg) of graphene oxide caused chronic toxicity in animals [91, 92]. In another study, PEGylated GQDs showed no toxicity to mice while PEG-GO was toxic due to its accumulation in liver and spleen. They observed dark spots of micrometer size, much larger than the size of GO in animal organs. That was a clear indication of aggregation of PEG-GO in organs, responsible for organ damage and even deaths [93].

Based on the data available, it can be concluded that GQDs are less toxic than other graphene family materials and that is the prime reason for newer applications of GQDs in the field of biology and medicine.

#### 4. Nanotheranostic applications of GQDs

Due to the excellent optical and physical properties of GQDs, they have wide biological applications as a sensitive probe for disease marker screening in fluids, precise marker for tissue biopsy classification, and high-resolution contrast agent for biomedical cell/tissue imaging that can be applied for detecting tiny tumors. Moreover, the most distinctive feature of GQDs is their precise detection from macroscale visualization, down to atomic resolution using electron microscopy. Though many reports are there dealing with the wide applications

of QDs in energy-related [94, 95] biosensing [96, 97] and light-emitting diodes [98, 99], in this section we will only emphasize the role of QDs in drug delivery and bioimaging or specifically nanotheranostic application of QDs in medical biology. "Theranostics" is a new term coined by Funkhouser in 2002 that describes any "material that combines the modalities of therapy and diagnostic imaging" into a single package [100].

With the advancement in the field of nanotechnology, the field of nanotheranostics has emerged that not only provides a platform for simultaneous drug distribution and release monitoring but also enables us to evaluate the therapeutic efficacy of a noninvasive treatment in real time that will guide toward personalized therapy based on patients' individual responses and needs, minimizing the chances of the adverse side effects due to over- or under-dosing [101, 102].

In this segment, recent advances in the application of graphene quantum dots in drug delivery and bioimaging will be discussed.

#### 4.1. Drug delivery applications

QDs are emerging as an effective drug carrier for nanotheranostics application due to their unique properties as quantum dots as well as goodness of graphene. To date, many reports deal with QDs as drug carrier and bioimaging. Recently, Wang et al. [103] synthesized PEGylated green fluorescent QDs for carrying doxorubicin (Dox) for cancer treatment. Surface passivation by PEG enhanced the fluorescence and improved the solubility of QDs. Moreover, QDs were synthesized via reduction of GO by L-ascorbic acid so they adopted the green route for better biocompatibility. Figure 13a represents the schematic of Dox-loaded QDs. QD-PEG showed distinctly different loading capacities toward Dox at different pH values. The maximum loading capacity of Dox on QD-PEG is 0.9 mg/mg at pH 5.5; 2.5 mg/mg at pH 7.4; and 1.1 mg/mg at pH 9 (Figure 13b, c).

In another similar application, Zhu et al. [104] fabricated paclitaxel-loaded multifunctional core-shell structure capsules composed of olive oil, dual-layer porous TiO<sub>2</sub> shell, Fe<sub>3</sub>O<sub>4</sub>, and QDs. The olive oil core for hydrophobic drug loading was the novel aspect of this formulation. The TiO<sub>2</sub> shell suppressed the initial burst release, while Fe<sub>3</sub>O<sub>4</sub> and QDs were utilized for magnetic targeting and fluorescence imaging, respectively. In two different interesting applications, DNA cleavage activity with drug delivery of QDs was reported. Wang et al. [105] prepared QD-Dox complex for enhanced nucleus accumulation and DNA cleavage efficiency. They achieved efficient delivery of doxorubicin to the nucleus through Dox/QD conjugates, as the conjugates assumed different cellular and nuclear internalization pathways compared to free Dox. Furthermore, with drug-resistant cancer cells, the Dox/QD conjugates increased the nuclear uptake and cytotoxicity of Dox, capable of increasing the chemotherapy efficacy of anticancer drugs that are suboptimal due to the drug resistance. Figure 14 shows the DNA cleavage activity and cellular internalization of QD-Dox complex via diffusion and the release of drug in nucleus after interaction with DNA. In another approach, Zhou et al. [106] have reported QDs in DNA cleavage system. According to their findings, by using QDs and Cu<sup>2+</sup>, about 90% supercoiled DNA was converted into nicked DNA, while only about 59% supercoiled DNA was cleaved with the same amount of large-sized GO and Cu<sup>2+</sup>.

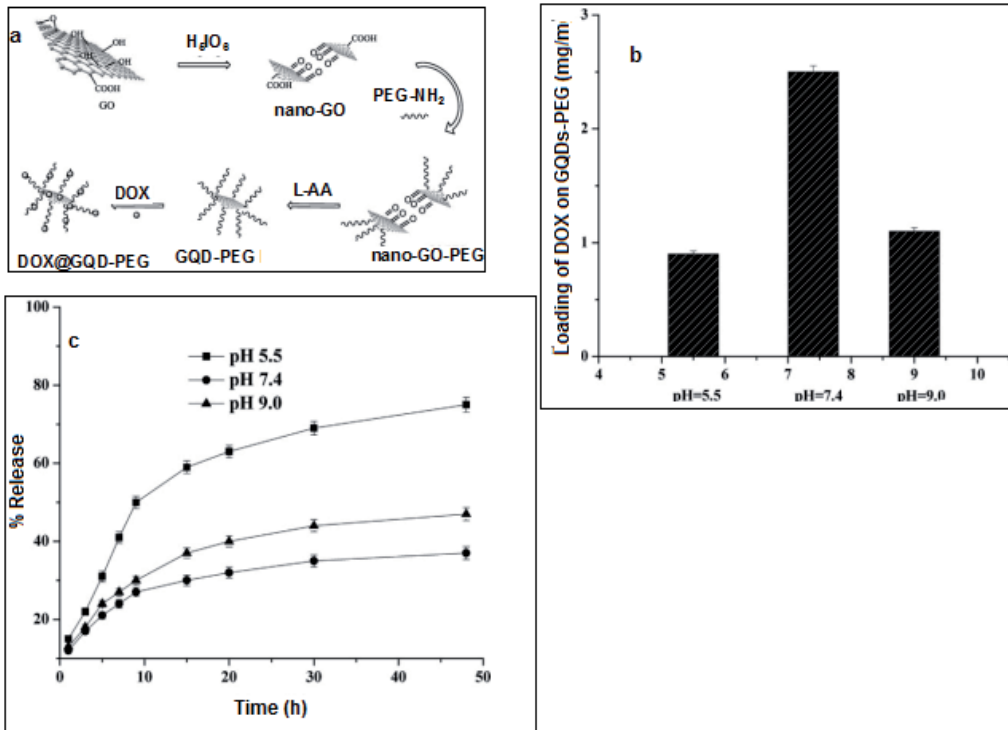


**Figure 13.** (a) Illustration of drug loading on QGDs; (b) Drug loading capacity of QGDs; (c) Percentage release profile of drugs at different pH. (Ref [103]: Wang et al.).

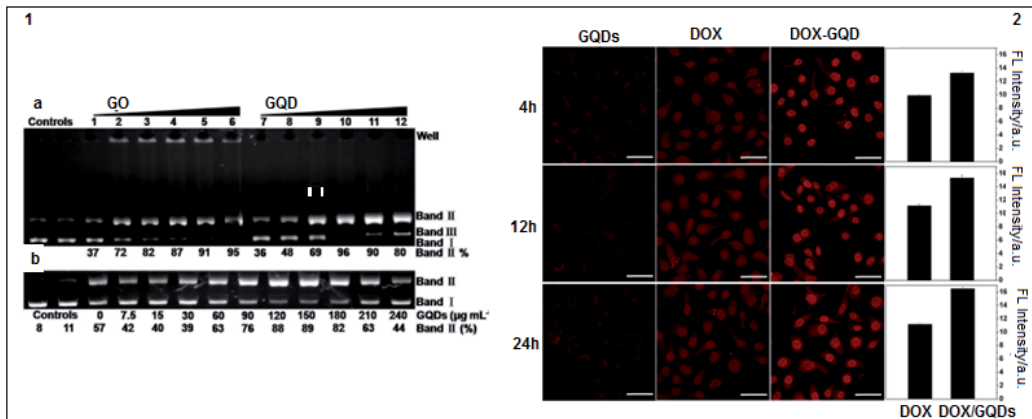


**Figure 14.** (a) Illustrating DNA (38  $\mu$ M) cleavage with  $Cu(Phen)_2$  (di-1,10-phenanthroline-copper) with GO and GQDs; 1(b) Cleavage with different concentrations of GQDs and DOX. 2: CLSM images of MCF-7 cells incubated with GQDs, DOX and DOX-GQD. (Ref [105]: Wang et al.).

According to their hypothesis, the as-prepared GQD sheets with smaller lateral size performed as a better intercalator to DNA molecules than micron GO sheets and therefore, under the same conditions, GQDs exhibited better efficiency than GO for DNA cleavage.

A nanocomposite based on conglomeration of Au-Fe<sub>3</sub>O<sub>4</sub> core-shell with GQDs is reported by Oza et al. [107]. This modular design enabled Au-Fe<sub>3</sub>O<sub>4</sub>-GQD-based magnetic combined therapeutic nanoplatform to perform multiple functions simultaneously, such as in multimodal imaging, drug delivery, and real-time monitoring. Dox was loaded by cystamine linker and the drug release was a temperature-dependent phenomenon. With folic acid (FA) as the targeted moiety, this formulation showed potential to be developed as an efficient drug delivery system. Another FA-mediated Dox-loaded GQD-based targeted delivery system was reported by Wang et al. [108]. Due to the inherent fluorescence of GQDs, cell movement in real time can be easily monitored without employing external dyes, and simultaneous localization of the drug carrier and the loaded drug can be possible. The nanoassembly was internalized by the target cells via receptor-mediated endocytosis with prolonged Dox release and accumulation. Though there are many reports utilizing folic acid as targeting moieties for cancer-cell-specific drug delivery, the major constraint is that folic acid receptor is overexpressed on healthy cells as well that restricts the applicability of FA-functionalized delivery system. Nahain et al. [109] put forth a new targeting strategy by functionalizing GQDs with hyaluronic acid (HA). HA is a natural polysaccharide and a targeting receptor for CD44 cells. CD44 are cancer stem cells responsible for drug resistance and reoccurrence of pancreatic cancer. Hence, by targeting CD44 by HA, an effective targeting strategy was developed. Figure 15 illustrates Dox-loaded green fluorescent GQD nanoformulation. The authors also evaluated the *in vivo* efficacy of GQDs in bioimaging and therapy. Figure 15b shows the *in vivo* imaging of mice model studies performed. HA-functionalized GQDs showed enhanced stability and stable fluorescence *in vivo* that could pave the way for future applications of GQDs in targeted drug delivery for cancer, the most fatal disease of human history (Figure 16b).

#### 4.2. Bioimaging applications

Traditional semiconductor quantum dots like CdSe or CdS and their core-shell nanoparticles have been exploited for applications in *in vitro* and *in vivo* cell imaging [110, 111], but the toxicity and potential health and environmental hazards associated with them restrict their applicability in live systems. In this regard, GQDs with their tunable PL, ecofriendly nature, and emergence of GQDs to date have shown remarkable potential for their successful application in the field of biotechnology and medicine owing to their excellent optical properties and low cytotoxicity up to very high concentrations of 400 µg/ml [112]. The authors also noted good uptake of GQDs by cells, as shown by the bright PL observed. Another example of bioimaging potential of GQDs, made from CX-72 carbon black, was reported by Dong et al. [113] in human breast cancer MCF-7 cells. They obtained effective luminescence inside the cell nucleus along with the cell membrane and cytoplasm. It was the first example that illustrated that GQDs have the ability to penetrate the cell nucleus and is another promising feature of GQDs to prove their strong candidature in nanotheranostic applications (Figure 16a). Sun et al. [114] compared the cytotoxicity and bioimaging capabilities of chemically reduced and

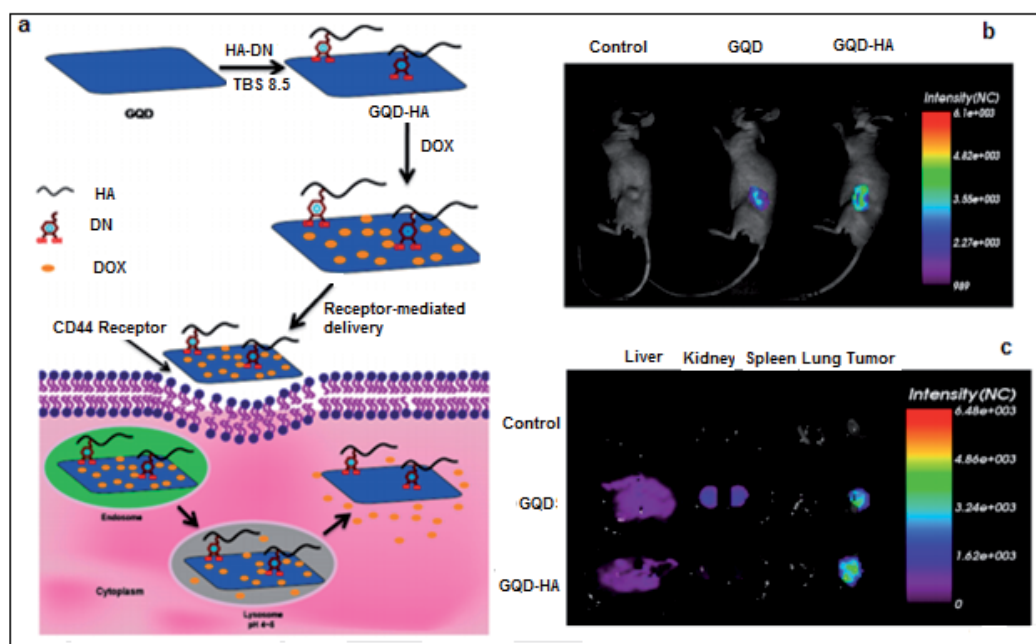


**Figure 15.** (a) Schematic of target delivery of GQDs using hyaluronic acid and subsequent release of the drug from the surfaces of GQD in a tumor-cell environment; (b) In vivo fluorescence images of GQD-HA in mice after tail vein injection; (c) Ex vivo images of liver, kidney, spleen, heart, and tumor after dissection. (Ref [109]: Nahin et al.)

photoreduced brightly blue luminescent GQDs in A549 cells using the MTT (3-(4,5-dimethylthiazol-2-yl)-2,5-diphenyltetrazolium bromide) assay. According to their findings, the cytotoxicity of the chemically reduced GQDs (cGQDs) was significantly greater than that of the photoreduced GQDs (pGQDs). The possible reason for this was the use of toxic reagents ( $\text{NaBH}_4$  and  $\text{N}_2\text{H}_4 \times \text{H}_2\text{O}$ ) during the chemical reduction. Photoreduced GQDs also exhibited stronger fluorescence indicating better cellular uptake due to the presence of less negative charge on the GQD surface. A very interesting approach was presented by Zhang et al. [35] by utilizing GQDs to label stem cells. The ability of GQDs to penetrate stem cell without reducing cell viability was exploited. Three different types of stem cells (neurosphere cells (NSCs), pancreas progenitor cells (PPCs), and cardiac progenitor cells (CPCs)) with GQDs at a final concentration of  $25 \mu\text{g/ml}$  were labeled and strong fluorescence was observed in the cytoplasm of the stem cells, but not in the nuclei. They obtained good penetration into cytoplasmic areas but not inside the cell nucleus. The authors also found that the GQDs were able to easily penetrate tumor cells (human lung cancer (A549) and human breast cells (MCF-7) and showed little cytotoxicity (Figure 16b). In most of the cases, downconversion PL imaging is reported, but Zhu et al. came up with upconversion GQDs. In downconversion, mainly UV or blue excitations are involved that are considered unsafe for living systems. In this scenario, Zhu et al. could attain more biocompatibility with their upconversion GQDs excited at near-infrared light of wavelength 808 nm for illuminating mouse osteoblast precursor cell line

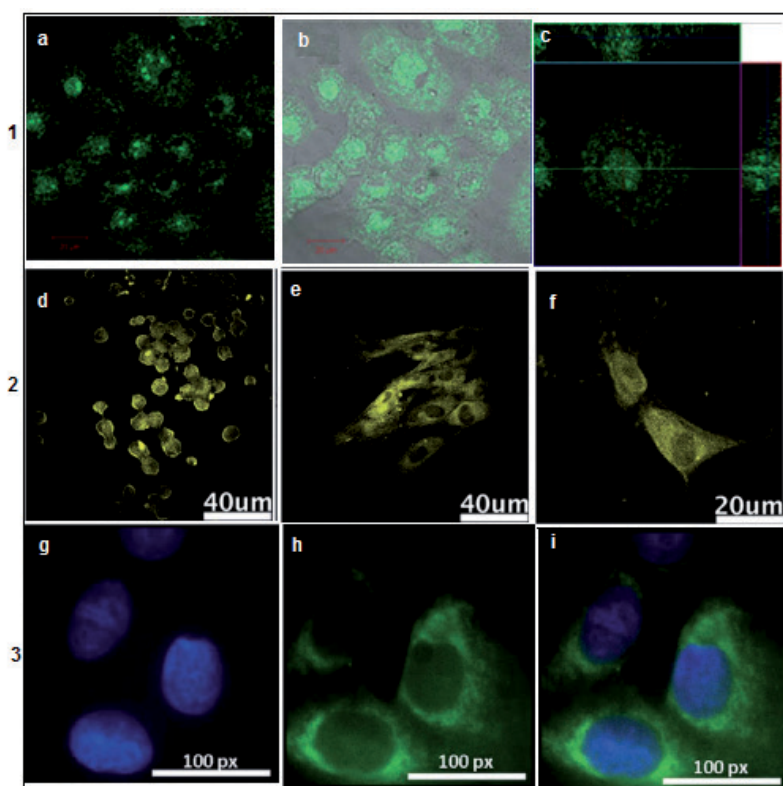


**Figure 16.** Confocal Images of MCF-7 cells labeled with GQDs 1 (a) Fluorescent image; (b) Bright field; (c) Merged fluorescent and bright field; (d) Section analysis (Ref [114]: Dong et al.); 2. Stem cells images of (d) Neurospheres cells (NSCs); (e) Pancreas progenitor cells (PPCs); (f) Cardiac progenitor cells (CPCs) (Ref [35] Zhang et al.); 3. High-contrast bioimaging via GQDs for breast cancer cell line (T47D). (Ref [9]: Peng et al.)

(MT3T3) cells. A blue or bright green fluorescence was observed inside the cells even after 20 min of continuous excitation. This indicated the successful internalization of GQDs inside the cells and photostability of GQDs as well [115].

Recently, Nigam et al. [20] have also reported the excellent bioimaging potential in a human serum-albumin-based multifunctional drug delivery system for pancreatic cancer. A strong and stable green fluorescence with good biocompatibility was observed in their analysis. In another report, Peng et al. [9] incubated breast cancer cell line T47D. The cell nucleus was stained with DAPI (blue color). Figure 16c illustrates the images of T47D cells treated with green GQDs with a 4-h incubation time, which clearly visualized the phase contrast image of T47D cells with nucleus stained with blue DAPI and green fluorescence from the cytoplasm. This bioimaging data proved that GQDs can be utilized in high-contrast bioimaging applications. Recently, GQDs synthesized by polycyclic aromatic compound via bottom-up approach by Zhou et al. were applied for illuminating MCF-7 (breast cancer cell lines). A stable green fluorescence inside the cytoplasm was obtained [116].

Zheng et al. have demonstrated a novel application of QDs for insulin receptor dynamics, using total internal reflection fluorescence microscopy (TIRFM), by functionalizing insulin with QDs [117]. According to their observation, small discrete clusters of QDs after pre-incubating adipocytes with insulin QDs were detected. The steady lateral movement of QD-enlightened clusters to the cell membrane and vertical movement between the inner cytosol and the plasmalemmal region were also tracked by following the QD fluorescence (Figure 17). This application is a good example of the potential of the edge-functionalized QDs for investigating dynamic cellular processes.

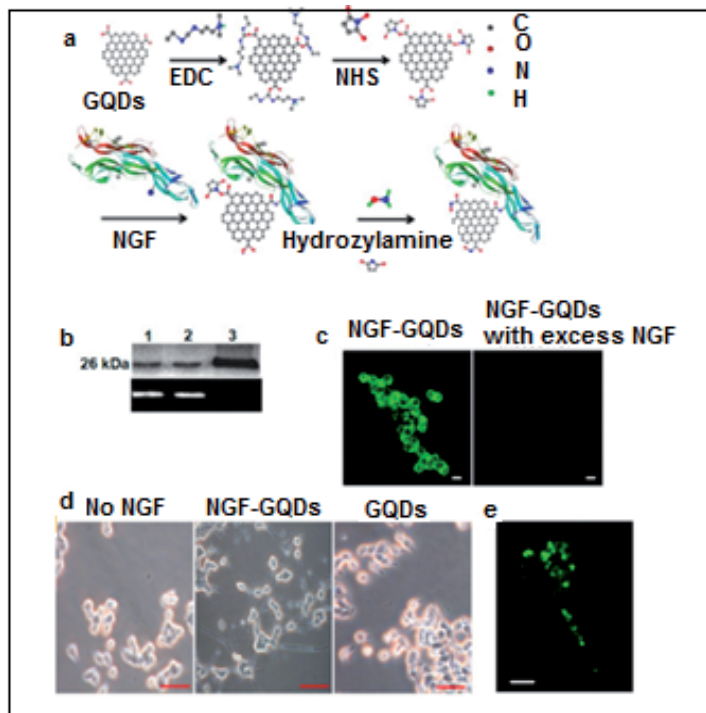


**Figure 17.** (a) Schematic illustration of conjugating a QD with NGF; (b) Gel electrophoresis of NGF-QD (lane 1), FITC-NGF (lane 2), and NGF (lane 3); (c) Fluorescence images of living PC12 cells incubated with 200 ng/mL NGF-QDs (left) or NGF-QDs together with 20 µg/mL free NGF (right) for 15 min; (d) Representative phase-contrast images of PC12 cells after 2-day incubation; (e) Distribution of NGF-QDs in PC12 cells differentiated by 200 ng/mL NGF-QDs for 24 h. (Ref [117]: Zheng et al.)

QDs are gradually attaining popularity for their *in vivo* applications also. The basic flaw related with *in vivo* imaging is background signal associated with autofluorescence of animal tissues. Moreover, the Rayleigh scattering of short wavelength light absorbed by water is another undesirable effect that is to be considered. It was reported by Nurunnabi et al. that carboxylated QDs can be efficiently explored for superficial tissue imaging but short-wavelength excitation limits their use for deep tissue bioimaging [118]. However, With QDs of near-infrared photoluminescence, after 8 h of QD injection, fluorescent signals were

obtained near heart, spleen, and kidney [119]. In another approach, Ge and coworkers synthesized GQDs with polythiophene derivatives via hydrothermal approach and they observed an emission wavelength of 680 nm that enables these GQDs for in vivo applications. Another important finding of their work was the application of as-synthesized GQD in photodynamic therapy as it was observed that GQDs could produce  $^1\text{O}_2$  via multistate sensitization process (Figure 18) with a quantum yield of about 1.3, the highest yield reported for photodynamic therapy (PDT) agents to date [120].

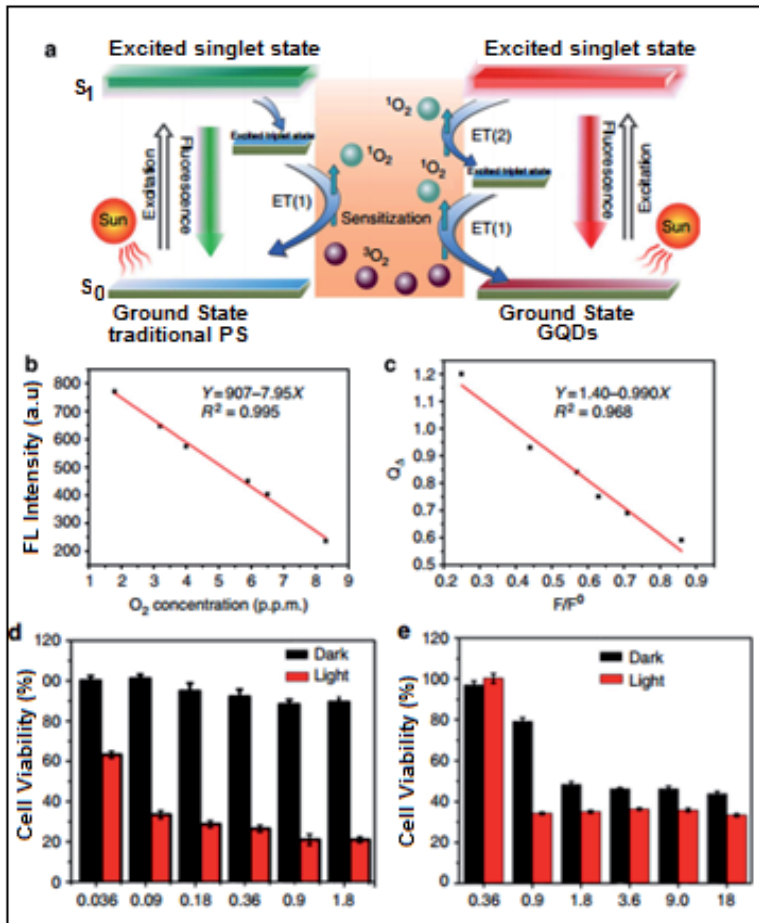


**Figure 18.** (a) Schematic illustration of the  $^1\text{O}_2$  generation mechanisms by conventional PDT agents (left) and GQDs (right); (b) Fluorescence intensity of GQDs at 680 nm versus the  $\text{O}_2$  concentration in solution; (c) The dependence of the  $^1\text{O}_2$  quantum yield ( $Q_1$ ) on the fluorescence intensity ratio at 680 nm ( $F/F^0$ ); (d) GQDs in the concentration range 0.036–1.8  $\mu\text{M}$ ; (e) Protoporphyrin (PpIX) in the concentration range 0.36–18  $\mu\text{M}$ . (Ref [120]: Ge et al.)

Although the cytotoxicity of GQDs in cells has been reported to be relatively low, contradictory findings were reported by Markovic et al. [121]. According to their observation, GQDs could be cytotoxic to U251 human glioma cells. They postulate that the GQDs can induce oxidative

stress and activate apoptosis and autophagy-type cell deaths by generating reactive oxygen species (ROS).

## 5. Conclusion and future prospects

GQDs have attracted tremendous interest in various fields like biotechnology, electronics, and medicine due to their excellent optical and physical properties, biocompatibility, and chemical stability. However, the research on GQDs is still in nascent state and there is huge scope to further explore the applicability of GQDs. The major issues related with GQDs are low quantum yield, low productivity, surface chemistry, and size tunability, and lack of control over PL and optical properties. However, irrespective of these drawbacks, GQDs represent an optimistic future for carbon materials. In our speculation, the future research on GQDs will be based on the following aspects.

### Advancement in synthesis approaches

Low production yield is the major problem associated with GQDs. Hence, the development of better synthesis strategies by solvent selection, reaction conditions, and appropriate cutting methodology in top-down approaches and better size and solubility control in bottom-up methods should be explored.

### Multifunctionality of GQDs

To extend the applicability of GQDs in bioimaging and drug delivery, novel approaches are to be developed. Still there are very few reports dealing with in vivo imaging and drug delivery mediated with multifunctional GQDs. Based on their application potential, it is imperative to explore the newer techniques for generating functionalized GQDs for their application in MRI and CT scan.

### Quantum yield enhancement

To date, the GQDs with QY ranging from 10% to 55% have been reported. To increase the QY and PL efficiency of GQDs, new surface-passivation strategies are needed so that GQDs with better bioimaging and stable fluorescence can be obtained.

### Applicability in newer areas

There is no report to date on application of GQDs in brain. A great deal can be done by tuning the excitation and emission properties of GQDs and they can be potentially exploited for blood–brain barrier penetration and brain gene therapy for neurodegenerative diseases.

### Toxicological evaluation

Toxicity of nanoparticles is an area of growing research. GQDs are a new addition in the family of nanoparticles and there are concerns about the possible side effects associated with GQDs. So biodistribution, organ accumulation, and genotoxicity of GQDs synthesized via different methods, shapes, sizes, and surface groups should be evaluated.

Graphene quantum dots have shown a high potential in such a short span of time. The ongoing research in this field will open new vistas that will revolutionize the future of medical and biotechnology applications.

## Acknowledgements

Author Dr Preeti Nigam Joshi is thankful to the Department of Science and Technology, Government of India, for providing financial support as INSPIRE Faculty Award grant.

## Author details

Preeti Nigam Joshi<sup>1\*</sup>, Subir Kundu<sup>2</sup>, Sunil K. Sanghi<sup>3</sup> and Dhiman Sarkar<sup>1</sup>

\*Address all correspondence to: [ph.joshi@ncl.res.in](mailto:ph.joshi@ncl.res.in); [nigampreeti@gmail.com](mailto:nigampreeti@gmail.com)

1 Combichem Bioresource Center, National Chemical Laboratory, Pune, India

2 School of Biochemical Engineering, Indian Institute of Technology, Varanasi, India

3 Microfluidics and MEMS Center, Advance Materials and Process Research Institute, Bhopal, India

## References

- [1] Novoselov KS, Geim AK, Morozov SV, Jiang D, Zhang Y, Dubonos SV, Grigorieva V, Firsov A. Electric field effect in atomically thin carbon films. *Science*. 2004; 306: 666–669. DOI:10.1126/science.1102896.
- [2] Novoselov KS, Geim AK, Morozov SV, Jiang D, Katsnelson MI, Grigorieva IV, Dubonos SV, Firsov AA. Two-dimensional gas of massless Dirac fermions in graphene. *Nature*. 2005; 438: 197–200. DOI:10.1038/nature04233.
- [3] Wallace PR. The band theory of graphite. *Phu. Rev.* 1947; 71: 622. DOI:[http://dx.DOI.org/10.1103/PhysRev.71.622](http://dx.doi.org/10.1103/PhysRev.71.622).
- [4] Boehm HP, Clauss A, Fischer GO, Hofmann U, *Anorg Z. Das Adsorptionsverhalten sehr dünner Kohlenstoff-Folien.* *Allg. Chem.* 1962; 316: 119–127. DOI:10.1002/zaac.19623160303.
- [5] Mouras S, Hamwi A, Djurado D, Cousseins JC. Synthesis of first stage graphite intercalation compounds from fluoride. *Rev. Chim. Miner.* 1987; 24: 572–582.

- [6] Li LS, Yan X. Colloidal quantum dots. *J. Phys. Chem. Lett.* 2010; 1: 2572–2576. DOI: 10.1021/jz100862f.
- [7] Ye R, Peng Z, Metzger A, Lin J, Mann JA, Huang K, Xiang C, Fan X, Samuel ELG, Alemany LB, Marti AA, Tour JM. Bandgap engineering of coal-derived graphene quantum dots. *ACS Appl. Mater. Interface.* 2015; 7: 7041–7048. DOI:10.1021/acsami.5b01419.
- [8] Mueller, X Yan, JA McGuire, L Li. Triplet states and electronic relaxation in photoexcited graphene quantum dots. *Nano Lett.* 2010; 10: 2679–2682. DOI:10.1021/nl101474d.
- [9] Peng J, Gao W, Gupta BK, Liu K, Romero-Aburto R, Ge L, Song L, Alemany LB, Zhan X, Gao G, Vithayathil SA, Kaiparettu B, Marti AA, Hayashi T, Zhu TT, Ajayan PM. Graphene quantum dots derived from carbon fibers. *Nano Lett.* 2012; 12: 844–849. DOI:10.1021/nl2038979.
- [10] Yan X, Cui X, Li B, Li L. Large, solution-processable graphene quantum dots as light absorbers for photovoltaics. *Nano Lett.* 2010; 10: 1869–1873. DOI:10.1021/nl101060h.
- [11] Dutta M, Sarkar S, Ghosh T, Basak D. ZnO/Graphene quantum dot solid-state solar C \ cell. *J. Phys. Chem. C.* 2012; 116: 20127–20131. DOI:10.1021/jp302992k.
- [12] Gupta V, Chaudhary N, Srivastava R, Sharma GD, Bhardwaj R, Chand S. Luminescent graphene quantum dots for organic photovoltaic devices. *J. Am. Chem. Soc.* 2011; 133: 9960–9963. DOI:10.1021/ja2036749.
- [13] Dong Y, Shao J, Chen C, Li H, Wang R, Chi Y, Lin X, Chen G. Blue luminescent graphene quantum dots and graphene oxide prepared by tuning the carbonization degree of citric acid. *Carbon.* 2012; 50: 4738–4743. DOI:10.1016/j.carbon.2012.06.002.
- [14] Pan DY, Zhang JC, Li Z, Wu MH. Hydrothermal route for cutting graphene sheets into blue-Luminescent graphene quantum dots. *Adv Mater.* 2010; 22: 734–738. DOI: 10.1002/adma.200902825.
- [15] Pan D, Guo L, Zhang L, Xi C, Xue Q, Huang H, Li J, Zhang Z, Yu W, Chen Z, Zu M. Cutting sp<sup>2</sup> clusters in graphene sheets into colloidal graphene quantum dots with strong green fluorescence. *J. Mater. Chem.* 2012; 22: 3314–3318. DOI:10.1039/C2JM16005F.
- [16] Yan X, Li B, Cui X, Wei Q, Tajima K, LS Li. Independent tuning of the band gap and redox potential of graphene quantum dots. *J. Phys. Chem. Lett.* 2011 ; 2: 1119–1124. DOI:10.1021/jz200450r.
- [17] Tetsuka H, Asahi R, Nagoya A, Okamoto K, Tajima I, Ohta R, Okamoto A. Optically tunable amino-functionalized graphene quantum dots. *Adv. Mater.* 2012; 24: 5333–5338. DOI:10.1002/adma.201201930.

- [18] Feng Q, Cao QQ, Li M, Liu FC, Tang NJ, Du YW. Synthesis and photoluminescence of fluorinated graphene quantum dots. *Appl. Phys. Lett.* 2013; 102: 013111–013114. DOI:10.1063/1.4774264.
- [19] Hu CF, Liu YL, Yang YH, Cui JH, Huang ZR, Wang YL, Yang LF, Wang HB, Xiao Y, Rong JH. One-step preparation of nitrogen-doped graphene quantum dots from oxidized debris of graphene oxide. *J. Mater. Chem. B.* 2013; 1: 39–42. DOI:10.1039/C2TB00189F.
- [20] Zhang ZH, Wu PY. Hydrothermal aggregation induced crystallization: a facial route towards polycrystalline graphite quantum dots with blue photoluminescence. *Cryst. Eng. Comm.* 2012; 14: 7149–7152. DOI:10.1039/C2CE26117K.
- [21] Liu Y, Wu PY. Graphene quantum dot hybrids as efficient metal-free electrocatalyst for the oxygen reduction reaction. *ACS Appl. Mater. Interface.* 2013; 5: 3362–3369. DOI:10.1021/am400415t.
- [22] Nigam P, Waghmode S, Louis M, Wangnoo S, Chavan P, Sarkar D. Graphene quantum dots conjugated albumin nanoparticles for targeted drug delivery and imaging of pancreatic cancer. *J. Mater. Chem. B.* 2014; 2: 3190–3195. DOI:10.1039/C4TB00015C.
- [23] Shen J, Zhu Y, Chen C, Yang X, Li C. Facile preparation and upconversion luminescence of graphene quantum dots. *Chem. Commun.* 2011; 47: 2580–2582. DOI:10.1039/C0CC04812G.
- [24] Zhu SJ, Zhang JH, Qiao CY, Tang SJ, Li YF, Yuan WJ, Li B, Tian L, Liu F, Hu R, Gao HN, Wei HT, Zhang H, Sun HC, Yang B. Strongly green-photoluminescent graphene quantum dots for bioimaging applications. *Chem. Commun.* 2011; 47: 6858–6860. DOI:10.1039/C1CC11122A.
- [25] Zhu SJ, Zhang JH, Liu X, Li B, Wang XF, Tang SJ, Meng QN, Li YF, Shi C, Hu R, Yang B. Graphene quantum dots with controllable surface oxidation, tunable fluorescence and up-conversion emission. *RSC Adv.* 2012; 2: 2717–2720. DOI:10.1039/C2RA20182H.
- [26] Shin Y, Park J, Hyun D, Yang J, Lee J, Kim J, Lee H. Acid-free and oxone oxidant-assisted solvothermal synthesis of graphene quantum dots using various natural carbon materials as resources. *Nanoscale.* 2015; 7: 6533–6537. DOI:10.1039/C5NR00814J.
- [27] Chan CF, Lau SP, Luk CM, Tsang MK. Two-photon fluorescence in N-doped graphene quantum dots. *Int. J. Chem. Nucl. Mater. Metall. Eng.* 2014; 8: 1313–1316.
- [28] Luo Z, Yang D, Qi G, Shang J, Yang H, Wang Y, Yuwen L, Yu T, Huang W, Wang L. Microwave-assisted solvothermal preparation of nitrogen and sulfur co-doped reduced graphene oxide and graphene quantum dots hybrids for highly efficient oxygen reduction. *J. Mat. Chem. A.* 2014; 2: 20605–20611. DOI:10.1039/C4TA05096G.

- [29] Tang L, Ji R, X C, Lin L, Jiang H, Li X, Teng KS, Luk CM, Zeng S, Hao J, Lau SP. Deep ultraviolet photoluminescence of water-soluble self-passivated graphene quantum dots. *ACS Nano*. 2012; 6: 5102–3110. DOI:10.1021/nn300760g
- [30] Li LL, Ji J, Fei R, Wang CZ, Lu Q, Zhang JR, Jiang LP, Zhu JJ. A facile microwave avenue to electrochemiluminescent two-color graphene quantum dots. *Adv. Funct. Mater.* 2012; 22: 2971–2979. DOI:10.1002/adfm.201200166.
- [31] Zhu Y, Wang G, Jiang H, Chen L, Zhang X. One-step ultrasonic synthesis of graphene quantum dots with high quantum yield and their application in sensing alkaline phosphatase. *Chem. Commun. (Camb)*. 2015; 5: 948–951. DOI:10.1039/c4cc07449a.
- [32] Lu J, Yang JX, Wang J, Lim A, Wang S, Loh KP. One-pot synthesis of fluorescent carbon nanoribbons, nanoparticles, and graphene by the exfoliation of graphite in ionic liquids. *ACS Nano*. 2009; 3: 2367–2375. DOI:10.1021/nn900546b.
- [33] Zheng L, Chi Y, Dong Y, Lin J, Wang B. Electrochemiluminescence of water-soluble carbon nanocrystals released electrochemically from graphite. *J. Am. Chem. Soc.* 2009; 131: 4564–4565. DOI:10.1021/ja809073f.
- [34] Li Y, Hu Y, Zhao Y, Shi G, Deng L, Hou Y, Qu L. An Electrochemical avenue to green-luminescent graphene quantum dots as potential electron-acceptors for photovoltaics. *Adv. Mater.* 2011; 23: 776–780. DOI:10.1002/adma.201003819.
- [35] Zhang M, Bai L, Shang W, Xie W, Ma H, Fu Y, Fang D, Sun H, Fan L, Han M, Liu C, Yang S. Facile synthesis of water-soluble, highly fluorescent graphene quantum dots as a robust biological label for stem cells. *J. Mater. Chem.* 2012; 22: 7461–7467. DOI: 10.1039/C2JM16835A.
- [36] Shinde DB, Pillai VK. Electrochemical preparation of luminescent graphene quantum dots from multiwalled carbon nanotubes. *Chem. Eur. J.* 2012; 18: 12522–12528. DOI: 10.1002/chem.201201043.
- [37] Shinde DB, Dhavle VM, Kurungot S, Pillai VM. Electrochemical preparation of nitrogen-doped graphene quantum dots and their size-dependent electrocatalytic activity for oxygen reduction. *Bull. Mater. Sci.* 2015; 38: 435–442. DOI:10.1007/s12034-014-0834-3.
- [38] Tan X, Li Y, Li X, Zhou S, Fan L, Yang S. Electrochemical synthesis of small-sized red fluorescent graphene quantum dots as a bioimaging platform. *Chem. Comm.* 2015; 51: 2544–2546. DOI:10.1039/C4CC09332A.
- [39] Ponomarenko LA, Schedin F, Katsnelson MI, Yang R, Hill EW, Novoselov KS, Geim AK. Chaotic dirac billiard in graphene quantum dots. *Science*. 2008; 320: 356–358. DOI:10.1126/science.1154663.

- [40] Lee J, Kim K, Park WI, Kim BH, Park JH, Kim TH, Bong S, Kim CH, Chae G, Jun M, Hwang Y, Jung YS, Jeon S. Uniform graphene quantum dots patterned from self-assembled silica nanodots. *Nano Lett.* 2012; 12: 6078–6083. DOI:10.1021/nl302520m.
- [41] Liu R, Wu D, Feng X, Müllen K. Bottom-up fabrication of photoluminescent graphene quantum dots with uniform morphology. *J. Am. Chem. Soc.* 2011; 133: 15221–15223. DOI:10.1021/ja204953k.
- [42] Liu JJ, Zhang XL, Cong ZX, Chen ZT, Yang HH, Chen GN. Glutathione-functionalized graphene quantum dots as selective fluorescent probes for phosphate-containing metabolites. *Nanoscale.* 2013; 5: 1810–1815. DOI:10.1039/C3NR33794D.
- [43] Wu X, Tian F, Wang W, Chen J, Wub M, Zha JX. Fabrication of highly fluorescent graphene quantum dots using L-glutamic acid for in vitro/in vivo imaging and sensing. *J. Mat. Chem. C.* 2013; 1: 4676–4684. DOI:10.1039/C3TC30820K.
- [44] Wang L, Wang Y, Xu T, Yao C, Liu Y, Li Z, Chen Z, Pan D, Sun L, Wu M. Gram-scale synthesis of single-crystalline graphene quantum dots with superior optical properties. *Nat. Commun.* 2014; 5: 1–9. DOI:10.1038/ncomms6357.
- [45] Lin L, Rong M, Lu S, Song X, Zhong Y, Yan J, Wang Y, Chen Xi. A facile synthesis of highly luminescent nitrogen-doped graphene quantum dots for the detection of 2,4,6-trinitrophenol in aqueous solution. *Nanoscale.* 2015; 7: 1872–1878. DOI:10.1039/C4NR06365A.
- [46] Lu J, Yeo PSE, Gan CK, Wu P, Loh KP. Transforming C<sub>60</sub> molecules into graphene quantum dots. *Nat. Nanotechnol.* 2011; 6: 247–252. DOI:10.1038/nnano.2011.30.
- [47] Sinclair J, Dr. Dagotto, “An introduction to quantum dots: confinement, synthesis, artificial atoms and applications,” Solid State II Lecture Notes, University of Tennessee, Knoxville, 2009.
- [48] Chukwuocha EO, Onyeaju MC, Harry TST. Theoretical studies on the effect of confinement on quantum dots using the Brus Equation. *World J. Condens. Matter. Phys.* 2012; 2: 96–100. DOI:10.4236/wjcmp.2012.22017.
- [49] Dinadayalane TC, Leszczynski J. Remarkable diversity of carbon–carbon bonds: structures and properties of fullerenes, carbon nanotubes, and graphene. *Struct. Chem.* 2010; 21: 1155–1169. DOI:10.1007/s11224-010-9670-2.
- [50] Geim A. Graphene: status and prospects. *Science.* 2009; 324: 1530–1534. DOI:10.1126/science.1158877.
- [51] Allen MJ, Tung VC, Kaner RB. Honeycomb carbon: a review of graphene. *Chem. Rev.* 2010; 110: 132–145. DOI:10.1021/cr900070d.
- [52] Li L, Wu G, Yang G, Peng J, Zhao J, Zhu JJ. Focusing on luminescent graphene quantum dots: current status and future perspectives. *Nanoscale.* 2013; 5: 4015–4039. DOI: 10.1039/C3NR33849E.

- [53] Baker SN, Baker GA. Luminescent carbon nanodots: emergent nanolights. *Angew. Chem. Int. Ed.* 2010; 49: 6726–6744. DOI:10.1002/anie.200906623.
- [54] Eda G, Lin YY, Mattevi C, Yamaguchi H, Chen HA, Chen IS, Chen CW, Chhowalla M. Blue photoluminescence from chemically derived graphene oxide. *Adv. Mater.* 2010; 22: 505–509. DOI:10.1002/adma.200901996.
- [55] Güttinger J, Seif J, Stampfer C, Capelli A, Ensslin K, Ihn T. Time-resolved charge detection in graphene quantum dots. *Phys. Rev. B.* 2011; 83: 165445–165452. DOI:http://dx.doi.org/10.1103/PhysRevB.83.165445.
- [56] Li HO, Tu T, Cao G, Wang LJ, Guo GC, Guo GP. Quantum transport in graphene quantum dots. *Nanotechnology and nanomaterials: new progress on graphene research* DOI:10.5772/52873.
- [57] González JW, Delgado F, Fernández-Rossier J. Graphene single-electron transistor as a spin sensor for magnetic adsorbates. *Phys. Rev. B.* 2012; 87: 085433. DOI:http://dx.Doi.org/10.1103/PhysRevB.87.085433.
- [58] Ihn T, Güttinger J, Molitor F, Schnez S, Schurtenberger E, Jacobsen A, Hellmüller S, Fery T, Ensslin K. Graphene single-electron transistors. *Mater. Today.* 2010; 13: 44–50. DOI:10.1016/S1369-7021(10)70033-X.
- [59] Luo Z, Lu Y, Somers LA, Johnson ATC. High yield preparation of macroscopic graphene oxide membranes. *J. Am. Chem. Soc.* 2009; 131: 898–899. DOI:10.1021/ja807934n.
- [60] Peng J, Gao W, Gupta BK, Liu Z, Ge RRL, Song L, Alemany LB, Zhan X, Gao G, Vithayathil SA, Kaipparattu BA, Marti AA, Hayashi T, Zhu JJ, Ajayan PM. Graphene quantum dots derived from carbon fibers. *Nano Lett.* 2012; 12: 844–849. DOI:10.1021/nl2038979.
- [61] Kim S, Hwang SW, Kim MK, Shin DY, Shin DH, Kim CO, Yang SB, Park JH, Hwang E, Choi SH, Ko G, Sim S, Sone S, Choi HJ, Bae S, Hong BH. Anomalous behaviors of visible luminescence from graphene quantum dots: interplay between size and shape. *ACS Nano.* 2012; 6: 8203–8208. DOI:10.1021/nn302878r.
- [62] Fuyuno N, Kozawa D, Miyauchi Y, Mouri S, Kitaura R, Shinohara H, Yasuda T, Komatsu N, Matsuda K. Size-dependent luminescence properties of chromatographically-separated graphene quantum dots. <https://scirate.com/arxiv/1311.1684>.
- [63] Liu R, Wu D, Feng X, Muellen K. Bottom-Up Fabrication of photoluminescent graphene quantum dots with uniform morphology. *J. Am. Chem. Soc.* 2011; 133: 15221–15223. DOI:10.1021/ja204953k.
- [64] Qu D, Zheng M, Zhang L, Zhao H, Xie Z, Jing X, Haddad RE, Fan H, Sun Z. Formation mechanism and optimization of highly luminescent N-doped graphene quantum dots. *Sci. Rep.* 2014; 4: 1–9. DOI:10.1038/srep05294.

- [65] Yang F, Zhao M, Zheng B, Xiao D, Wu L, Guo Y. Influence of pH on the fluorescence properties of graphene quantum dots using ozonation pre-oxide hydrothermal synthesis. *J. Mater. Chem.* 2012; 22: 25471–25479. DOI:10.1039/C2JM35471C.
- [66] Li H, He X, Liu Y, Huang H, Lian S, Lee ST, Kang Z. One-step ultrasonic synthesis of water-soluble carbon nanoparticles with excellent photoluminescent properties. *Carbon.* 2011; 49: 605–609. DOI:10.1016/j.carbon.2010.10.004.
- [67] Li H, He X, Kang Z, Huang H, Liu Y, Liu J, Lian S, Tsang CHA, Yang X, Lee ST. Water-soluble fluorescent carbon quantum dots and photocatalyst design. *Angew. Chem. Int. Ed.* 2010; 49: 4430–4434. DOI:10.1002/anie.200906154.
- [68] Qiao ZA, Wang Y, Gao Y, Li H, Dai T, Liu Y, Huo Q. Commercially activated carbon as the source for producing multicolor photoluminescent carbon dots by chemical oxidation. *Chem. Commun.* 2010; 46: 8812–8814. DOI:10.1039/C0CC02724C.
- [69] Li H, Kang Z, Liu Y, Lee ST. Carbon nanodots: synthesis, properties and applications. *J. Mater. Chem.* 2012; 22: 24230–24253. DOI:10.1039/C2JM34690G.
- [70] Mahasin Alam SK, Ananthanarayanan A, Huang L, Lim KH, Chen P. Revealing the tunable photoluminescence properties of graphene quantum dots. *J. Mater. Chem. C.* 2014; 2: 6954–6960. DOI:10.1039/C4TC01191K.
- [71] Tang L, Ji R, Cao X, Lin J, Jiang H, Li X, Teng KS, Luk CM, Zeng S, Hao J, Lau SP. Deep ultraviolet photoluminescence of water-soluble self-passivated graphene quantum dots. *ACS Nano.* 2012 ; 6: 5102–5110. DOI:10.1021/nn300760g.
- [72] Zhu S, Zhang J, Liu X, Li B, Wang X, Tang S, Meng Q, Li Y, Shi C, Hu R, Yang B. Graphene quantum dots with controllable surface oxidation, tunable fluorescence and up-conversion emission. *RSC Adv.* 2012; 2: 2717–2720. DOI:10.1039/C2RA20182H.
- [73] Michalet X, Pinaud FF, Bentolila LA, Tsay JM, Doose S, Li JJ, Sundaresan G, Wu AM, Gambhir SS, Weiss S. Quantum dots for live cells, in vivo imaging, and diagnostics. *Science.* 2005; 307: 538–544. DOI:10.1126/science.1104274.
- [74] Smith AM, Nie S. Semiconductor nanocrystals: structure, properties, and band gap engineering. *Acc. Chem. Res.* 2010; 43: 190–200. DOI:10.1021/ar9001069.
- [75] Fan T, Zeng W, Tang W, Yuan C, Tong S, Cai K, Liu Y, Huang W, Min Y, Epstein AJ. Controllable size-selective method to prepare graphene quantum dots from graphene oxide. *Nanoscale Res. Lett.* 2015; 10: 55. DOI:10.1186/s11671-015-0783-9.
- [76] Tian L, Liu F, Hu R, Gao H, Wei H, Zhang H, Sun H, Yang B. Strongly green-photoluminescent graphene quantum dots for bioimaging applications. *Chem. Commun.* 2011; 47: 6858–6860. DOI:10.1039/C1CC11122A.
- [77] Zhu S, Zhang J, Tang S, Qiao C, Wang L, Wang H, Liu X, Li B, Li Y, Yu W, Wang A, Sun H, Yang B. Surface chemistry routes to modulate the photoluminescence of gra-

- phene quantum dots: From fluorescence mechanism to up-conversion bioimaging applications. *Adv. Funct. Mater.* 2012; 22: 4732–4740. DOI:10.1002/adfm.201201499.
- [78] Shen WJ, Zhu Y, Chen C, Yang X, Li C. Facile preparation and upconversion luminescence of graphene quantum dots. *Chem. Comm.* 2011; 47: 2580–2582. DOI: 10.1039/C0CC04812G.
- [79] Zhuo S, Shao M, Lee S. Upconversion and downconversion fluorescent graphene quantum dots: ultrasonic preparation and photocatalysis. *ACS Nano.* 2012; 6: 1059–1064. DOI:10.1021/nn2040395.
- [80] Liu R, Wu D, Feng X, Muellen K. Bottom-up fabrication of photoluminescent graphene quantum dots with uniform morphology. *J. Am. Chem. Soc.* 2011; 133: 15221–15223. DOI:10.1021/ja204953k.
- [81] Loh KP, Bao Q, Eda G, Chhowalla M. Graphene oxide as a chemically tunable platform for optical applications. *Nat. Chem.* 2010; 2: 1015–1024. DOI:10.1038/nchem.907.
- [82] Pan D, Zhang J, Li Z, Wu M. Hydrothermal route for cutting graphene sheets into blue-luminescent graphene quantum dots. *Adv. Mater.* 2010; 22: 734–738. DOI: 10.1002/adma.200902825.
- [83] Lu J, Yan M, Ge L, Ge S, Wang S, Yan J, Yu J. Electrochemiluminescence of blue-luminescent graphene quantum dots and its application in ultrasensitive aptasensor for adenosine triphosphate detection. *Biosens. Bioelect.* 2013; 47: 271–277. DOI:10.1016/j.bios.2013.03.039.
- [84] Li LL, Ji J, Fei R, Wang CZ, Lu Q, Zhang JR, Jiang LP, Zhu JJ. A Facile microwave avenue to electrochemiluminescent two-color graphene quantum dots. *Adv. Funct. Mater.* 2012; 22: 2971–2979. DOI:10.1002/adfm.201200166.
- [85] Hu W, Peng C, Luo W, Lv M, Li X, Li D, Huang Q, Fan C. Graphene-based antibacterial paper. *ACS Nano.* 2010; 4: 4317–4323. DOI:10.1021/nn101097v.
- [86] Ruiz OR, Fernando KAS, Wang B, Brown NA, Luo PG, McNamara ND, Vangsness M, Sun Y, Bunker CE. Graphene oxide: a nonspecific enhancer of cellular growth. *ACS Nano.* 2011; 5: 8100–8107. DOI:10.1021/nn202699t.
- [87] Zhang D, Liu X, Wang X. Green synthesis of graphene oxide sheets decorated by silver nanoprisms and their anti-bacterial properties. *J. Inorg. Biochem.* 2011; 105: 1181–1186. DOI:10.1016/j.jinorgbio.
- [88] Christensen IL, Sun YP, Juzenas P. Carbon dots as antioxidants and prooxidants. *J. Biomed. Nanotechnol.* 2011; 7: 667–676. DOI:10.1007/s11434-013-6058.
- [89] Yuan X, Liu Z, Guo Z, Ji Y, Jin M, Wang X. Cellular distribution and cytotoxicity of graphene quantum dots with different functional groups. *Nanoscale Res. Lett.* 2014; 9: 108. DOI:10.1186/1556-276X-9-108.

- [90] Jastrzębska AM, Kurtycz P, Olszyna AR. Recent advances in graphene family materials toxicity investigations. *J. Nanopart. Res.* 2012; 14: 1320–1327. DOI:10.1007/s11051-012-1320-8.
- [91] Wang A, Pu K, Dong B, Liu Y, Zhang L, Zhang Z, Duan W, Zhu Y. Role of surface charge and oxidative stress in cytotoxicity and genotoxicity of graphene oxide towards human lung fibroblast cells. *J. Appl. Toxicol.* 2013; 33: 1156–1164. DOI:10.1002/jat.2877.
- [92] Wang K, Ruan J, Song H, Zhang J, Wo Y, Guo S, Cui D. Biocompatibility of graphene oxide. *Nanoscale Res. Lett.* 2011; 6: 1–8. DOI:10.1007/s11671-010-9751-6.
- [93] Chong Y, Ma Y, Shen H, Tu X, Zhou X, Xu J, Dai J, Fan F, Zhang Z. The in vitro and in vivo toxicity of graphene quantum dots. *Biomaterials.* 2014; 35: 5041–5048. DOI: 10.1016/j.biomaterials.2014.03.021.
- [94] Pan D, Xi C, Li Z, Wang L, Chen Z, Lu B, Wu M. Electrophoretic fabrication of highly robust, efficient, and benign heterojunction photoelectrocatalysts based on graphene-quantum-dot sensitized TiO<sub>2</sub> nanotube arrays. *J. Mater. Chem. A.* 2013; 1: 3551–3555. DOI:10.1039/C3TA00059A.
- [95] Hamilton IP, Li B, Yan X, Li L. Alignment of colloidal graphene quantum dots on polar surfaces. *Nano Lett.* 2011; 11: 1524–1529. DOI:10.1021/nl200298c.
- [96] Li X, Zhu S, Xu B, Ma K, Zhang J, Yang B, Tian W. Self-assembled graphene quantum dots induced by cytochrome c: a novel biosensor for trypsin with remarkable fluorescence enhancement. *Nanoscale.* 2013; 5: 7776–7779.
- [97] Shi J, Chan C, Pang Y, Ye W, Tian F, Lyu J, Zhang Y, Yang Mo. A fluorescence resonance energy transfer (FRET) biosensor based on graphene quantum dots (GQDs) and gold nanoparticles (AuNPs) for the detection of mecA gene sequence of *Staphylococcus aureus*. *Biosens Bioelectron.* 2015; 67: 595–600. DOI:10.1016/j.bios.2014.09.059.
- [98] Gupta V, Chaudhary N, Srivastava R, Sharma GD, Bhardwaj R, Chand S. Luminescent graphene quantum dots for organic photovoltaic devices. *J. Am. Chem. Soc.* 2011; 133: 9960–9963. DOI:10.1021/ja2036749.
- [99] Luk CM, Tang LB, Zhang WF, Yu SF, Teng KS, Lau SP. An efficient and stable fluorescent graphene quantum dot–agar composite as a converting material in white light emitting diodes. *J. Mater. Chem.* 2012; 22: 22378–22381. DOI:10.1039/C2JM35305A.
- [100] Funkhouser J. Reinventing pharma: the theranostic revolution. *Curr. Drug Discov.* 2002; 2: 17–25.
- [101] Luk BT, Zhang L. Current advances in polymer-based nanotheranostics for cancer treatment and diagnosis. *ACS Appl. Mater. Interface.* 2014; 6: 21859–21873. DOI: 10.1021/am5036225.

- [102] Lammers T, Kiessling F, Hennink WE, Storm G. Nanotheranostics and image-guided drug delivery: current concepts and future directions. *Mol. Pharm.* 2010; 7: 1899–1912. DOI:10.1021/mp100228v.
- [103] Wang Z, Xia J, Zhou C, Via B, Xia Y, Zhanga F, Lia Y, Xia L, Tang J. Synthesis of strongly green-photoluminescent graphene quantum dots for drug carrier. *Colloid Surf B Biointerface.* 2013; 112: 192–196. DOI:10.1016/j.colsurfb.2013.07.025.
- [104] Jing Y, Zhu Y, Yang X, Shen J, Li C. Ultrasound-triggered smart drug release from multifunctional core-shell capsules one-step fabricated by coaxial electro-spray method. *Langmuir.* 2010; 27: 1175–1180. DOI:10.1021/la1042734.
- [105] Wang C, Wu C, Zhou X, Han T, Xin X, Wu J, Zhang J, Guo S. Enhancing cell nucleus accumulation and DNA cleavage activity of anti-cancer drug via graphene quantum dots. *Sci. Rep.* 2013; 3: 2852. DOI:10.1038/srep02852.
- [106] Zhou X, Zhang Y, Wang, Wu X, Yang Y, Zheng B, Wu H, Guo S, Zhang J. Photo-fenton reaction of graphene oxide: a new strategy to prepare graphene quantum dots for DNA cleavage. *ACS Nano.* 2012; 6: 6592–6599. DOI:10.1021/nn301629v.
- [107] Oza G, Ravichandran OM, Velumani S, Ramirez JT, Garcia-Sierra F, Asomoza R. Designing a drug-delivery vehicle with Au-Fe<sub>3</sub>O<sub>4</sub>-graphene quantum dots: a tri-pronged mechanism for bioimaging, synaptic delivery and apoptosis induction in cancer cells. *J. Nanomed. Nanotechnol.* 2014; 5: 5. DOI.org/10.4172/2157-7439.S1.018.
- [108] Wang X, Sun X, Lao J, He H, Cheng T, Wang M, Wang S, Huang F. Multifunctional graphene quantum dots for simultaneous targeted cellular imaging and drug delivery. *Colloid Surf. B Biointerface.* 2014; 122: 638–644. DOI:10.1016/j.colsurfb.2014.07.043.
- [109] Nahain AA, Lee JE, In I, Lee H, Lee KD, Jeong JH, Park SY. Target delivery and cell imaging using hyaluronic acid-functionalized graphene quantum dots. *Mol. Pharm.* 2013; 10: 3736–3744. DOI:10.1021/mp4003283.
- [110] Vibin M, Vinayakan R, John A, Raji V, Rejiya CS, Vinesh NS, Abraham A. Cytotoxicity and fluorescence studies of silica-coated CdSe quantum dots for bioimaging applications. *J. Nanopart. Res.* 2011; 13: 2587–2596. DOI:10.1007/s11051-010-0151-8.
- [111] Liu LW, Hu S, Pan Y, Zhang J, Feng Y, Zhang X. Optimizing the synthesis of CdS/ZnS core/shell semiconductor nanocrystals for bioimaging applications. *Beilstein J. Nanotechnol.* 2014; 5: 919–926. DOI:10.3762/bjnano.
- [112] Zhu S, Zhang J, Qiao C, Tang S, Li Y, Yuan W, Li B, Tian L, Liu F, Hu R, Gao H, Wei H, Zhang H, Sun H, Yang B. Strongly green-photoluminescent graphene quantum dots for bioimaging applications. *Chem. Commun.* 2011; 47: 6858–6560. DOI:10.1039/C1CC11122A.
- [113] Dong Y, Chen C, Zheng X, Gao L, Cui Z, Yang H, Guo C, Chi Y, Li CM. One-step and high yield simultaneous preparation of single- and multi-layer graphene quantum

- dots from CX-72 carbon black. *J. Mater. Chem.* 2012; 22: 8764–8766. DOI:10.1039/C2JM30658A.
- [114] Sun H, Wu L, Gao N, Ren J, Qu X. Improvement of photoluminescence of graphene quantum dots with a biocompatible photochemical reduction pathway and its bioimaging application. *ACS Appl. Mater. Interface.* 2013; 5: 1174–1179. DOI:10.1021/am3030849.
- [115] Zhu S, Zhang J, Tang S, Qiao C, Wang L, Wang H, Liu X, Li B, Li Y, Yu W, Wang X, Sun H, Yang B. Surface chemistry routes to modulate the photoluminescence of graphene quantum dots: from fluorescence mechanism to up-conversion bioimaging applications. *Adv. Funct. Mater.* 2012; 22: 4732–4740. DOI:10.1002/adfm.201201499.
- [116] Zhou L, Geng J, Liu B. Graphene quantum dots from polycyclic aromatic hydrocarbon for bioimaging and sensing of Fe<sup>3+</sup> and hydrogen peroxide. *Part. Part. Syst. Charact.* 2013; 30: 1086–1092. DOI:10.1002/ppsc.201300170.
- [117] Zheng XT, Than A, Ananthanaraya A, Kim DH, Chen P. Graphene quantum dots as universal fluorophores and their use in revealing regulated trafficking of insulin receptors in adipocytes. *ACS Nano.* 2013; 7: 6278–6286. DOI:10.1021/nn4023137.
- [118] Nurunnabi M, Khatun Z, Huh KM, Park SY, Lee DY, Cho KJ, Lee Y. In vivo biodistribution and toxicology of carboxylated graphene quantum dots. *ACS Nano.* 2013; 7: 6858–6867. DOI 10.1021/nn402043c.
- [119] Nurunnabi M, Khatun J, Reeck GR, Lee DY, Lee YK. Near infra-red photoluminescent graphene nanoparticles greatly expand their use in noninvasive biomedical imaging. *Chem. Commun.* 2013; 49: 5079–5081. DOI:10.1039/C3CC42334D.
- [120] Ge J, Lan M, Zhou B, Liu W, Guo L, Wang H, Jia Q, Niu G, Huang X, Zhou, Meng X, Wang P, Lee CS, Zhang W, Han X. A graphene quantum dot photodynamic therapy agent with high singlet oxygen generation. *Nat. Commun.* 2014; 5 : 4596. DOI: 10.1038/ncomms5596.
- [121] Markovic ZM, Ristic BZ, Arsikin KM, Klisic DG, Harhaji-Trajkovic LM, Todorovic-Markovic BM, Kepic DP, Kravic-Stevovic TK, Jovanovic SP, Milenkovic MM, Milivojevic DD, Bumbasirevic VZ, Dramicanin MD, Trajkovic VS. Graphene quantum dots as autophagy-inducing photodynamic agents. *Biomaterials.* 2012; 33: 7084–7092. DOI:10.1016/j.biomaterials.2012.06.060.



---

# Noninvasive Strategies for Systemic Delivery of Therapeutic Proteins — Prospects and Challenges

---

Tiam Feridooni, Adam Hotchkiss and Remigius U. Agu

Additional information is available at the end of the chapter

<http://dx.doi.org/10.5772/61266>

---

## Abstract

It is well established that proteins have great physiological importance, thus possessing great potential for therapeutic use. There is increased interest in protein/peptide pharmaceuticals delivery due to recent improvements in analytical methods, advancements in molecular biology and genetic engineering, and a better understanding of regulatory roles of proteins and peptides. There are however major challenges that need to be overcome for systemic delivery of these biological molecules. The major hurdles that contribute to low biological activity are low stability, immunogenicity, and toxicity. A combination of strategies can be used to overcome these challenges and improve the bioavailability of protein drugs. Alternative delivery routes (e.g., nasal and pulmonary) and the development of new methods for overcoming delivery challenges (e.g., nanomedicine, and PEGylation), along with the development of innovative formulation strategies (e.g., spray-freeze drying, supercritical fluid methods, fluidized-bed spray coating, lyophilization, jet milling and spray drying), have resulted in improved pharmacokinetics of protein drugs and in some cases increased patient compliance.

**Keywords:** Protein drugs, peptides, protein stability, bioavailability, systemic delivery

---

## 1. Introduction

Proteins and peptides are polymers of amino acids that differ in chain size. These compounds are an assorted class of biological macromolecules with amino acid sequence characterized by a unique three-dimensional structure [1]. The three-dimensional structure is not only responsible for the biochemical reactions but also useful in feedback mechanism, transport, and solubility in physiological solutions. Proteins have a variety of important physiological roles, which are due to their ability to specifically bind to respective biological counterparts.

---

Enzymes, hormones, antibodies, globulins, hemoglobin, myoglobin, and numerous lipoproteins are all proteins and peptides involved in catalysis and transport of substances within the body [2].

In 2010, it was reported that around 20 antibody products and 150 protein-based products were approved for use in the US market alone [3]. In that same year, it was reported that >100 approved protein drugs were in use, and ~800 were being developed to treat numerous conditions, including cancer, Alzheimer's, Huntington's, and Parkinson's diseases [4], with worldwide sales figures estimated to be around \$70 billion [5]. It is clear that the protein drug class is continuing its strong economic growth, with the global market for bioengineered protein drugs being valued at \$151.9 billion in 2013 and expectations that the market could reach \$222.7 billion by 2019 ([http://www.bccresearch.com/pressroom/bio/global-market-for-bioengineered-protein-drugs-to-reach-\\$222.7-billion-in-2019](http://www.bccresearch.com/pressroom/bio/global-market-for-bioengineered-protein-drugs-to-reach-$222.7-billion-in-2019)). Most of these protein and peptide-based products are still administered by daily or weekly injections [5]. Besides administration route, shelf life imposes a major challenge to the pharmaceutical industry as there are no general rules on how to stabilize protein products and guarantee its safety and activity during the time it is supposed to be marketable [6].

Protein drugs are biopharmaceuticals, which include other biological drugs such as nucleic acid-based drugs, monoclonal antibodies, and recombinant proteins. Although recent advancements in genomics and proteomics have created a large number of protein drug candidates, most fail to be biologically promising *in vivo* [5]. Proteins by nature are prone to denaturation and structural modifications by heat and agitation once in aqueous environments or organic solvent [5].

Major obstacles that contribute to low biological activity are low stability, immunogenicity, and toxicity [7]. A combination of these factors results in low plasma half-life, ranging from minutes to several hours, which necessitates repeated administrations, which in turn leads to higher costs and lower patient compliance [7]. To overcome the challenges that protein drugs present, the development of strategies that focus on improving the bioavailability of the drugs by alternative routes of delivery (parenteral, oral, nasal, pulmonary, etc.) and innovative formulation strategies (spray-freeze drying, supercritical fluid methods, fluidized-bed spray coating, lyophilization, jet milling and spray drying) are trending topics in the protein delivery sphere. The aim of these strategies is to improve protein stability during manufacturing, storage and *in vivo*, following drug administration, allowing the drug to reach the intended biological target. Furthermore, the development of new strategies for overcoming drug delivery challenges such as the use of Nanomedicine and PEGylation can eventually lead to improved pharmacokinetics of some protein drug candidates. In this chapter, we will examine the major challenges facing noninvasive protein drug delivery and strategies for overcoming these problems.

## 2. Major protein delivery challenges

The use of proteins as therapeutic agents is hampered by their chemical/physical instabilities, low oral bioavailability due to enzymatic degradation in the gastrointestinal tract, low

permeability across the epithelial cells lining of the small intestine, and rapid elimination from the circulation. In this section, major obstacles to be overcome in order to successfully deliver protein drugs are examined.

## 2.1. Chemical and physical instabilities

Peptide and protein drugs although generally formulated in solid state still undergo multiple degradative reactions [6]. Chemical degradation involves covalent modification of the primary protein structure via bond cleavage or formation, while physical degradation refers to changes in higher-order structure by denaturation and noncovalent aggregation or precipitation. Physical and chemical types of reactions do not necessarily occur in isolation, but rather one may cause or facilitate the other [7]. Prominent mechanisms of chemical degradation in the solid state include deamidation, oxidation, and the Maillard reaction. Chemical instability due to deamidation has been observed for a number of important proteins, including human growth hormone, recombinant human interleukin-1 receptor antagonists, and recombinant bovine somatotropin [8]. A common deamidation reaction in peptides and proteins in drug formulations is the nonenzymatic intramolecular deamidation reaction of Asn residues. The use of peptide model VYPNGA has led to a better understanding of the Asn deamidation degradative process [8]. By examining the amino acid sequence of a particular peptide or protein with therapeutic potential, residues, which may be susceptible to deamidation, can be identified and formulation decisions made to minimize this type of degradation. The potential for degradative oxidation reactions can be found at various stages of production, packaging, and storage. For instance, peroxide contamination has been found in formulation excipients such as polyethylene glycols and surfactants leading to oxidation of these products [9]. The activation of molecular oxygen to more reactive species requires light or presence of a reducing agent and trace levels of transition metal ions, which can then convert molecular oxygen into more reactive oxidizing species such as superoxide radicals ( $O_2^{\cdot-}$ ), hydroxyl radical ( $\cdot OH$ ), or hydrogen peroxide ( $H_2O_2$ ) [9]. Transition metal ions are often present in excipients, and processing in stainless steel equipment can lead to significant iron contamination [9] and thus represent potential sources, which may contribute to degradative oxidation of peptide or protein drugs. After formulation, the final packaging decision can also have an effect on drug stability. It was demonstrated that even low levels of oxygen (1%) in the vial headspace can result in complete oxidation of a particular product [9]. By understanding the potential sources of contaminants leading to oxidation at all stages of drug production, and the mechanisms by which oxidation reactions take place, formulation strategies can be adopted to minimize these events. For instance, in the process of developing the PTH (1-34) microprojection patch for transdermal delivery, oxidation was identified as the major chemical degradation pathway [10]. It was determined that the addition of 0.03% EDTA to the drug formulation could effectively delay oxidation, which was measured using RP-HPLC. Further, stability testing in the presence and absence of antioxidizing agents and other excipients was performed to assess the compatibility of the patch with packaging components. Indeed, several of the patch components were shown to contribute to volatile compounds, which were chemically and/or physically incompatible with the coated PTH (1-34) formulation. Overall, the selection of appropriate packaging materials and the use of a desiccant sachet in the package appeared to

make it possible to achieve the target of 95% PTH (1-34) purity at the end of a two-year shelf life at ambient storage temperature [11]. In some protein formulations, reducing sugars (e.g., fructose, maltose, lactose, glucose, and xylose) react with basic protein residues such as lysine, arginine, asparagine, and glutamine [9]. In a stability study of recombinant human relaxin, it was discovered that the use of glucose as an excipient in a lyophilized formulation resulted in covalent adducts of glucose with amino groups on the side chains of the protein formed by Maillard reaction [12]. In this case, switching to the nonreducing sugar (trehalose), or a polyhydric alcohol (mannitol), resulted in greater relaxin stability.

Protein drugs very often undergo physical changes that may result in change of pharmacological effect and potency. Physical instability involves changes in the three-dimensional conformational integrity of the protein and does not necessarily involve covalent modification. These physical processes include denaturation, aggregation, precipitation, and adsorption to surfaces [8]. Protein drugs may undergo these changes during manufacturing, shipping, storage, and administration. Earlier concerns focused on denaturation (unfolding), oxidation, and deamination of protein drugs. Recently, aggregation has emerged as the main problem with protein therapeutics [11]. Protein aggregation is a multistage process that involves unfolding or misfolding of monomeric units of protein along with one or more assembly steps of monomeric protein to form soluble or insoluble oligomers or higher-molecular-weight aggregates [13]. Protein aggregates are often considered ordered if they occur as long, rigid fibrils or filaments. The most characterized aggregation state is the amyloid fibril, associated with neurodegenerative diseases such as Alzheimer's disease, Parkinson's disease, and Huntington's disease [14, 15]. Protein aggregation can be problematic during drug manufacturing, especially if it is insoluble and tends to precipitate, and typically reduces drug stability and shelf life [15]. In worst-case scenarios, aggregation might have an undesirable impact on drug potency, pharmacokinetics, and immunogenicity [16]. Protein aggregation can be triggered by many factors such as shear stress, high temperatures, changes in pH, and high protein concentration [16]. Unfortunately, it is very difficult to predict if the protein drug will undergo aggregation because of the complexity of the mechanism involved in the aggregate formation.

## 2.2. Biopharmaceutical challenges

Therapeutic activity of proteins is highly dependent on their conformational structure, which is flexible and sensitive to external conditions such as pH, temperature, and impurities in the excipients [15]. The detection of structural changes in protein is complex in pharmaceutical formulations and is a major challenge for the development and quality of protein drugs [16]. In addition, protein-based drugs have been shown to be immunogenic and in some cases the production of neutralizing antibodies have led to the inhibition of the therapeutic effect [16].

Until recently, injections (i.e., intravenous, intramuscular, or subcutaneous routes) remained the most common means for administering protein drugs. However, the bioavailability of protein drugs using these routes are low due to their rapid elimination from the circulation through renal filtration, enzymatic degradation and uptake by the reticuloendothelial system [17]. Oral dosage is the most attractive route of administration because of the accompanying

decreased medical costs and improved patient compliance. However, oral administration of protein drugs results in even lower bioavailability [2]. The main reasons for the low oral bioavailability are the instability of these drugs in the low pH environment of the gastrointestinal tract as well as inactivation and digestion by proteolytic enzymes in the intestinal lumen. In addition, protein drugs have high molecular masses and are hydrophilic, with logP values <0. This means that these drugs are more difficult to transport via the paracellular route across the epithelial cells lining of the small intestine [2, 16].

### 3. Strategies for mitigating delivery challenges

#### 3.1. Processing strategies for improving protein stability

Despite their many attractive features, protein drugs come with many complications with regards to formulation. Unlike their small molecule drug counterparts, they are often complex molecules with secondary, tertiary, and quaternary structures and generally contain side chains with various chemical properties. The disruption of this complexity can lead to loss of function of the drug. Thus, the formulation of these biological compounds for therapeutic use must maintain their shape and form thus maintaining their activity [2].

##### 3.1.1. *Spray-freeze drying*

Spray-freeze drying was first introduced in 1994, and it was at first classified as a variant of dry milling [18]. Since pharmacological therapeutics have limited stability in liquid solutions, several methods, such as spray-freeze drying and spray drying, have been developed for proper removal of liquids such as water. Spray-freezing involves spraying a solution containing the macromolecule of interest into a vessel containing cryogenic liquid such as oxygen, nitrogen, or argon, which results in freezing of the droplets due to the low boiling point of the cryogenic fluids used [19]. Spray-freeze drying is the sublimation of solid water (ice) following freezing of the solution, and despite its disadvantages, it has become quite an established method in the pharmaceutical industry [20]. The reason for this is quite clear, spray-freeze drying significantly increases the shelf life of pharmaceuticals, it is an extremely sterile process (compared to spray drying), and the product can be readily reconstituted at the time of use. Spray-freeze drying entails three major steps: (1) freezing, the crystallization of water; (2) primary drying, the removal of ice via sublimation; and finally (3) secondary drying, the desorption of residual water from product [19].

Even though this method is used for obtaining protein particles, stresses involved with freezing and drying have been shown to cause irreversible damage to the protein due to degradation, aggregation, and eventual loss of biological activity [19]. Similar to spray drying the majority of the damage occurs in the atomization and freezing of the droplets in the cold vapor phase of the lyophilization process [21].

### 3.1.2. Supercritical fluid methods

Supercritical fluids (SCF) are used in variety of extraction and analytical methods. They can also be used for the production of pharmaceutical powders, mainly those intended for inhalation such as inhalation steroids dexamethasone, flunisolide, and triamcinolone acetonide [22]. SCFs have properties of gases and liquids at temperatures and pressures above their critical point. Advantages of SCFs include density values resulting in high dissolving power, lower viscosity levels compared to other liquids, and higher diffusivity allowing high mass transfer [19]. Among present SCFs, CO<sub>2</sub> is the most commonly used due to its low critical temperature (31.2°C) and pressure (7.4 MPa); other advantages include nonflammability, nontoxicity, and cost-effectiveness [19].

There are two major principles for particle precipitation when using SCFs. SCFs can be used as (1) solvents (rapid expansion of supercritical solution (RESS) and particles from gas saturated solutions (PGSS)) and (2) antisolvents (gas antisolvent (GAS), aerosol solvent extraction system (ASES), supercritical fluid antisolvent (SAS), precipitation with compressed antisolvent (PCA), and solution enhanced dispersion by supercritical fluids (SEDS)). Since the early 2000s, solutions consisting of proteins along with a cosolvent, such as ethanol, have been precipitated using CO<sub>2</sub> [23]. The integrity of such proteins depends on the operating conditions such as temperature, pressure, flow rates, and the concentration of the ingredients used, and by properly optimizing such conditions, the precipitation of proteins using the SCFs, such as CO<sub>2</sub>, has become a promising method for particle precipitation [24].

### 3.1.3. Fluidized-bed spray coating

Fluidized-bed spray coating is a commonly used method in the pharmaceutical industry for coating of small particles [25]. Coating of particles has several advantages, such as providing acid resistance [24], modifying the release of the particles [26], protecting the therapeutic agent from light, and moisture and masking the taste of a substance [27]. In this process, particles to be coated come in contact with droplets of coating solution after being fluidized via air currents and are then dried using heated air; thus, after several loops through the spraying and drying zones, a uniform coat is achieved [28]. Further, the uniformity and success of the coating is dependent on the spreading of the droplet on the surface of the particle [29].

As a result of recent advancements in fluidized-bed spray coating systems, particles as small as 50 µm can be coated. For instance, fluidized-bed spray coating was applied to recombinant human deoxyribonuclease (rhDNase), and the coating was examined via scanning electron microscopy [30]. The coating demonstrated strong integrity when introduced to mechanical force; however, the process resulted in aggregation of the proteins,, which may be mainly due to the thermal stress involved with the process [29]. Aggregation was significantly reduced however, when rhDNase was formulated with calcium ions, thus suggesting in presence of proper stabilizers fluidized-bed spray coating is a feasible method for coating and preparing dried pharmaceutical proteins [31].

### 3.1.4. Lyophilization

Protein instability is one of the major reasons protein drugs are still administered via injections and not orally. Therefore, in order to overcome this hurdle, proteins must be made into solid forms to achieve an acceptable shelf life [32]. Lyophilization has become one of the most commonly used methods for generating solid protein drugs [33]. Lyophilization consists of three steps beginning with (1) freezing, where the solution that is to be dried is frozen at a controlled rate thus removing water from the protein as ice crystals, at this point ~20% of water remains in a unfrozen phase known as maximal freeze concentrate [31]. Freezing is followed by (2) primary drying, where frozen water is removed via sublimation resulting in significant desorption of water (~10%). The remaining water is removed at higher temperatures in the final stage, (3) secondary drying, via desorption which lowers the fluid moisture content to few tenth of a percent [34].

A variety of stresses caused by lyophilization, such as low temperatures, formation of dendritic ice crystals, pH changes, phase separations, increase in ionic strengths, and removal of protein hydration shell, can result in reversible [33] and irreversible [34] structural changes in the protein [33]. Thus, for proteins that are sensitive to the listed stresses, specific cryo-/lyo-protectants can be used, such as commonly used sugars/polyols, nonaqueous solvents, polymers, protein itself, surfactants, and amino acids [33]. Further, extra effort is made to fully customize the lyophilization cycles in order to avoid lyophilization cycle-related stresses such as freezing rate and temperature, thermal treatment conditions, drying rate and temperature, and final moisture content [33].

### 3.1.5. Jet milling

Jet milling is a method used for particle size reduction using interparticle collisions and abrasion to produce particles ranging between 1 and 20  $\mu\text{m}$  [19]. Although Jet milling is a great method for particles size reduction (1–20  $\mu\text{m}$ ), it does come with some drawbacks, such as lack of control over size, shape, surface properties, and morphology. Furthermore, the high energy input can be detrimental to proteins as it can lead to protein degradation [19]. In a study where horseradish peroxidase was coprecipitated with carbomer and jet milled for two different time points, it was demonstrated that the longer the jet milling process, the more significant the reduction in protein activity [35]. In fact, grinding the power for 10 min in a mortar almost completely eliminated the activity of peroxidase [36]. However, pulmonary activity of salmon calcitonin along with a variety of absorption enhancers (oleic acid, lecithin, citric acid, taurocholic acid, dimethyl-beta-cyclodextrin, and octyl-beta-D-glucoside) micronized after freeze drying with lactose showed significant blood levels of calcitonin in rats [37]. Further, it has been suggested that microparticle preparation is possible via melting, pregrinding, and a final jet milling step for particle size reduction [36]. Lastly, as peptides fed into the machine have to be coarse enough to allow for free flow and fine enough not to block the hopper and pipe work, they are at times required to be lyophilized which can result in protein degradation if no lyoprotectant is used [36].

### 3.1.6. *Spray drying*

Spray drying is a method used for forming protein particles in lower molecular range [38]. The solution is automatically fed into droplets that rapidly dry due to high surface area and large amount of air–water interfacial area. During the drying process, which can range from 100 milliseconds to seconds, the critical increase in temperature is prevented by the evaporation of the solvent, which results in the temperature of particles remaining significantly lower than the temperature of the gas and drying powder is quickly removed from the drying zone to prevent overheating [25]. Spray drying allows control over a variety of particle design features, including particle size and distribution, surface energy and rugoses, particle density, surface area, porosity, and microviscosity [39]. Since the average radius of particles obtained ranges between 2 and 6  $\mu\text{m}$ , spray drying is generally used for pulmonary particle delivery [40] such as the protein insulin [41].

Although the air-drying process of spray drying prevents thermal degradation of proteins, the atomization process may present a different obstacle. The high shear rate required for the atomization process can lead to degradation of macromolecules. For instance, a study demonstrated degradation of human growth hormone (hGH) during the air–liquid interface following atomization, while the tissue-type plasminogen activator (t-PA) remained intact [42]. There have been several proteins that have been successfully air-dried. Niven et al. spray dried formulations of recombinant human granulocyte colony-stimulating factor (rhG-CSF) [43], and Dalby et al. produced fine protein particles in a process where they combined nebulization, air drying, and electrostatic collection [44].

## 4. Formulation strategies for overcoming protein delivery challenges

### 4.1. Nanotechnology approaches

Another promising approach to enhance the stability of therapeutic peptides and proteins is encapsulation into a micro- or nanoparticle, with the aim of protecting the drug from the hostile environments in the body [45]. At their target location, biodrugs typically are released from the particle by diffusion, swelling, erosion, or degradation [46]. Biological systems are usually protected by nanometer-sized barriers, which are extremely specific with regards to transport of biological molecules. Permeation through such barriers and their access to specific biological compartments is dictated by chemical properties, size, and shape of biological molecules [47]. Nanotechnology, defined as development and application of materials, structures, devices, and systems by modeling and manufacturing of the matter in the nanoscale range (1–100 nm), can be used to provide protection against the degradation of biological agents [48]. As nanoparticles are similar in scale to biological molecules, nanoparticles can have many medical applications and be engineered to have various functions. As their properties allow them to cross biological barriers, nanoparticles can be used to transport therapeutic molecules to sites of interest, providing access to molecules of interest and thus modulation of molecular interactions [48, 49].

One of the main issues for lack of efficacy for some current therapeutics is the inability to be fully delivered to the required sites, which can be due to their low solubility. Low efficacy may result in increasing dosage, thus correlating with increased side effects [50]. The use of nanocarriers can aid in overcoming some of these obstacles. The surface of nanocarriers usually consists of polymers or biodegradable molecules that are customized to ensure biocompatibility and selective targeting [48]. In fact, nanocarriers may offer numerous advantages over free drugs, such as protecting the drug from premature interaction with unwanted biological entities and degradation, enhancing the absorption of the drug into a specific tissue of interest (cancers or tumors), increasing the pharmacokinetics of the drug, and improving the intracellular penetration of the drug [51].

Nanoparticles and nanocarriers can be used for delivery of peptide drugs to specific sites of interest, avoiding degradation in the GIT and first-pass metabolism via the hepatic route. In fact, peptides have been transported using nanocarriers. Hyaluronic acid-Fe<sub>2</sub>O<sub>3</sub> hybrid magnetic nanoparticles were designed to deliver peptides to HEK293 and A529 cells at a 100% level [52]. Further, functionalized gold nanoparticles consisting of a drug peptide ligand and a targeting peptide were shown to be both effective and enhance the activity and selectivity of such peptide multifunctionalized conjugates [53]. Furthermore, carrier molecules have been shown to increase membrane permeability of protein therapeutics such as insulin, interferon  $\alpha$ 2b, and human growth hormone through epithelial membrane of small intestine thus increasing the bioavailability of listed protein therapeutics [54].

#### 4.2. PEGylation

Proposed in 1970s [55], PEGylation is the attachment of polyethylene glycol to drug molecules as a method of transforming proteins, peptides, small molecules, and oligonucleotides into more potent drugs [56]. PEGylated molecules tend to be more clinically useful compared to their unmodified counterparts as they tend to have higher stability and solubility, longer half-life in the systemic circulation, reduced renal clearance, reduced immunogenicity and antigenicity [57], and higher potency [58].

Protein drugs, such as enzymes, cytokines, and antibodies, have been shown to be significantly improved as a result of PEGylation [59]. Although it is common to see improvements in retention within circulation and reduction of immune response and degradation, the loss of biological activity due to PEGylation is quite common [60]. The loss of biological activity is however compensated with improved pharmacokinetics as seen in  $\alpha$ -interferon Pegasys® [61]. Currently, there are several PEGylated drugs available for public use, including PEG-adenosine deaminase (Adagen®) [62], PEG-asparaginase (Oncaspar®) [63], PEG-interferon  $\alpha$ 2b (PEG-Intron®) [64], PEG-interferon  $\alpha$ 2a (Pegasys®) [63], and PEG-growth hormone receptor antagonist (Pegvisomant, Somavert®) [65]. Before PEGylated drugs are made available to public use, they must undergo biological tests to ensure that the advantage of PEGylation does not result in increased toxicity [62].

## 5. Approaches for decreasing protein aggregation and enhancing bioavailability

Numerous strategies have been developed and applied to control or prevent protein aggregation. Protein aggregation can be reduced by introducing disulphide bonds, salt bridges, and metal ions to stabilize and rigidify regions involved in local unfolding. However, extensive clinical trials will be required to confirm if there are any adverse effects associated with these modifications [15, 16]. A more direct approach is to alter the formulation of the protein. One approach to reduce aggregation is to work with protein solutions at lower concentrations and correspondingly larger volumes. A number of excipients have been used with varying success to reduce protein aggregation; however, each has its own limitations [14]. Nonionic detergents can be used to reduce aggregation induced by shear and heat. Cyclodextrins can also be used to reduce aggregation. For example, cyclodextrins suppress the aggregation of insulin. Another approach to reduce aggregation is to use lyophilized dosage forms [16]. Lyophilization is generally regarded as an effective means to stabilize proteins [13, 14]. However, proteins can undergo reversible conformational changes in the lyophilized state, which makes them more susceptible to undesirable side reactions. For example, the aggregation of lyophilized insulin can be ameliorated by the presence of trace moisture [15, 16].

To improve the oral bioavailability of protein drugs, many strategies have been developed. One strategy involves the modulation of the physicochemical properties of the gastrointestinal tract. This could be achieved by the use of protease inhibitors as an additive to reduce the rate of enzymatic degradation [18]. For example, the enzymatic degradation of insulin in the intestine is known to be mediated by the serine proteases trypsin,  $\alpha$ -chymotrypsin, and thiol metalloproteinase insulin degrading enzymes. The use of additives that inhibit these enzymes was found to increase the intestinal absorption of insulin by 10% in rats [66]. Also, the modulation of the tight-junction permeability to increase paracellular transport of protein molecules has been studied. However, this approach requires further investigations before it can be applied [18].

Another strategy to improve protein drug bioavailability involves chemical modification of the protein. This includes the synthesis of a protein analog with an improved enzymatic stability and/or membrane penetration. For example, insulin tends to self-associate to form hexamers. The absorption of hexameric insulin is lower than that of the monomeric insulin analog [2]. Mutation of the amino acids that are involved in self-association results in the formation of the monomeric insulin analog known as insulin lispro (Humalog®, Eli Lilly), which is characterized by rapid onset of action following subcutaneous injection [16]. Chemical modification could also be used to produce a prodrug, which could be useful to protect the drugs against enzymatic degradation [18]. The introduction of novel functional groups to protein drugs that are recognized by transporters can also aid in their absorption. For example, adding a dipeptide that is recognized by peptide-influx transporters in the gastrointestinal tract to a protein drug results in significant improvement in its oral bioavailability [16, 18]. Another way to improve protein stability is acylation of the protein drug, which involves the attachment of fatty acids to the exposed residues on the protein surface. This kind of modifi-

cation increases the affinity of the protein to the serum albumin resulting in an increase in its half-life. Acetylation of insulin led to the development of insulin detemir (Levemir®, Nova Nordisk), which is a long-acting insulin analog [16]. The conjugation of protein drugs with polymers is one of the approaches used to improve the bioavailability of protein drugs. Currently, poly (ethylene glycol) (PEG) is the most widely used polymer. Protein conjugation with PEG reduces the plasma clearance rate by reducing the metabolic degradation [67].

It is also possible to increase the bioavailability of protein drugs by using pharmaceutical technologies. For example, the use of the mucoadhesive delivery system was found to prolong the residence time of protein drug at the local site of absorption and to increase the concentration gradient between delivery system and intestinal membrane, which ultimately results in a higher rate of drug absorption [18]. In addition, protein delivery systems represent an effective method to effectively deliver protein drugs. The most often used delivery systems include liposomes, micelles, microspheres, and hydrogels. The use of carriers provides a higher degree of protection against enzymatic degradation and other destructive factors because the carrier wall completely isolates drug molecules from the environment [18]. Liposomes possess the most suitable characteristics for protein encapsulation. Encapsulating insulin in liposomes results in enhanced oral absorption of insulin [16], [18]. A combination of these approaches can also be used for the development of a successful [16], [18] approach for the delivery of protein drugs, for example, the multifunctional smart polymer that is equipped with a pH-dependent drug release, Ca<sup>2+</sup> deprivation ability, and mucoadhesive characteristic. The use of this system to deliver insulin by the oral route results in 10% bioavailability [18].

## 6. Exploration of various delivery routes

Currently, the most accepted method of delivery of protein/peptide compounds is the parenteral administration of liquid formulations [68]. This method has become widely accepted by the pharmaceutical companies as it is the fastest way toward achieving commercialization [69]. However, as the therapeutic range of protein/peptide compounds increases, so does the demand for improved formulations. Even though designing novel drug delivery systems is not essential for the success of such compounds, they are important for increased efficacy, patient compliance, and reduced errors in drug administration [20]. Thus, along with parenteral administration of protein/peptide compounds, other routes of delivery such as oral, nasal, pulmonary, ocular, and transdermal delivery have been explored [69].

### 6.1. Parenteral delivery

Parenterally administered protein drugs are most likely to be commercially successful since most animal studies and early clinical trials are performed via direct injections, thus making parenteral drug delivery one of the most popular forms of delivery assuming that injections meet the desired safety and efficacy targets [17]. Drugs delivered parenterally, whether intravenously or intramuscularly, gain full access to the systemic circulation due to rapid drug

absorption. The short half-life of peptide drugs within the bloodstream results in repeat doses which correlate with oscillating drug concentrations within the blood [69].

There are numerous injection devices available for patients. For patients with daily injection requirements such as insulin, there are small diameter needle and syringes available. In fact, to improve patients' quality of life, the patient is now provided with prefilled syringes, syringe injectors, injectors, and pen devices, which may be preloaded with the drug of interest, and autoinjectors are regularly utilized as patients require more flexible and convenient injection devices moving away from the traditional syringe and vial [70]. For instance, insulin is now available in a variety of syringe injectable forms, infusion pumps, jet injectors (a needleless system that transports insulin transcutaneously), and reusable and prefilled pens [70]. All injectable devices must undergo stringent testing to ensure that the patient receives the proper dose of the drug in its expected form. For instance, in needleless systems that depend on high velocity liquid injection, which is dependent on compressed gas, the sheer stress can compromise the configuration of the protein [71, 72].

The rapid absorption of parenterally delivered drug is quickly followed by a rapid decline in the drug levels in the systemic circulation, which can be problematic in cases of chronic conditions where daily or weekly injections may be required for years. The requirement for numerous injections can result in decreased patient compliance, thus resulting in the development of prolonged release parenteral drug delivery systems [71]. These drug delivery systems include use of implants, which are biodegradable drug delivery systems mainly composed of either polylactic acid (PLA) or polyglycolic acid (PLGA) to control the release of the therapeutic drug [73]. However, since implants often require surgery and have been shown to have poor content uniformity in lower drug doses, *in situ* microparticle systems have been shown to be more advantageous due to the presence of an external oil phase [74]. ISM showed comparable drug release profile to drug release of microparticles prepared by solvent evaporation method, thus potentially becoming an alternative to more complicated microencapsulation methods [75].

## 6.2. Oral delivery

One of the major challenges for protein drug delivery via the oral route is the susceptibility of the protein drug to proteolytic degradation in the gastrointestinal tract (GIT), which is at its highest in the stomach and the duodenum of the small intestines and is significantly lower in the mouth, pharynx, esophagus, ileum, and the colon. Another challenge is the bioavailability of the drug, which is dependent on two major factors, the molecular weight (MW) of the drug and its solubility. Bioavailability is essentially independent of MW for drugs less than 700 Da; however, with increasing MW passed this threshold, there is a decrease in the bioavailability of the drug. Drug compounds also need to meet a certain level of hydrophobicity criteria as they are required cross biological membranes. However, most biological drug compounds considered for therapeutic use are frequently greater than 700 Da and are hydrophilic [76]. Thus, degradation and poor absorption are the main bioavailability barriers. There are however suggested methods for increasing the survival of the peptides as it moves through the GIT [75].

There are current methods for increasing the bioavailability of peptidic drugs such as (1) modifying the N- or C-terminus to increase half-life (encephalin, conversion of C-terminal methionine to methioniol group [77]); (2) altering the terminal amino acids from L-amino acid to a D-amino acid (arginine-vasopressin analog 1-deamino-8-D-arginine [77, 78]); (3) converting the linear peptide into a cyclic analog to avoid degradation by carboxy- and amino-peptidases (successfully performed in a model hexapeptide [77]); (4) use of peptidomimetics, which are molecules that mimic the action of peptides but are no longer peptidic in nature and prodrugs, which can be metabolized in the body releasing the therapeutic agent in return; and (5) coadministration of the peptide drug with digestive enzyme inhibitors [79]. The GIT presents both physical and chemical challenges for oral delivery of protein drugs; however, recent developments have made progress in facing each of those challenges and obstacles. Even though the development of new formulation methods, which have shown to improve bioavailability of protein drugs, are still costly, the progress in this field is still quite promising [20].

### 6.3. Nasal delivery

The use of the nasal cavity as a site for systemic peptide drug delivery has several benefits, such as (1) rapid absorption rate, which in some cases have been shown to be as effective as intravenous injections and require lower doses; (2) high permeability due to the nasal epithelium (up to 1 kDa) [80]; along with (3) high total blood flow; (4) avoidance of first-pass metabolism; and (5) accessibility. The combination of such characteristics allows for a faster onset of pharmacological activity and lower side effects [81]. The olfactory nerves also allow for the direct transport of drug to the brain as the blood–brain barrier provides a challenging obstacle for numerous drugs such as antibiotics, antineoplastic agents, and other drugs that are active in the central nervous system [82].

There are a variety of formulation factors that can affect the absorption of drugs within the nasal cavity. Such factors include dose and volume, pH, osmolarity of the solution which the drug is dissolved in, viscosity, excipients used (such as absorption enhancers), dosage form (spray, powder, or drops), administration techniques (inhalation or mechanically assisted), and devices used to administer the drug [83]. Further, despite the fact that nasally administered drugs are able to avoid first-metabolism, bioavailability of peptide drugs is still limited due to the presence of broad range of metabolic enzymes that reside in the nasal mucosal cavity and the epithelial cell lining [84].

Currently, drugs ranging from small to large macromolecules such as protein drugs, hormones, and vaccines are delivered through the nasal cavity [85]. For instance, in the presence of absorption enhancers, which aid in modulating the nasal epithelium permeability, insulin can be effectively administered through the nasal cavity [84].

### 6.4. Pulmonary delivery

The large surface area of the lung along with its well vascularized thin epithelial lining provides a noninvasive method for drug delivery, direct access to systemic circulation, and

allows for avoidance of first pass metabolism and GIT degradation [86]. It has been suggested that to achieve successful pulmonary delivery of drug, the drug must reach the alveoli or deep lung; thus, the particle size must range within 1–2  $\mu\text{m}$  for optimum absorption [87]. The inhalation of therapeutics is an effective means for providing therapies for respiratory [88] and a wide range of other disorders [89].

Even though animal studies have shown the bioavailability of drugs delivered via the pulmonary route ranging from ~10% to 50% depending on the type of protein, similar success rates have not been seen in human studies [70]. For instance, pulmonary insulin delivery demonstrated just below 50% bioavailability in animals [90]; bioavailability in humans is merely 10–15% [70]. These findings suggest that the bioavailability of a drug in animals is not necessarily predictive of that of a human. Another obstacle associated with pulmonary delivery is the clinical toxicology of the lungs, particularly when dealing with cytokines and growth factors that may have a local effect on the tissue [70]. The particle size of the drug also plays a critical role in its bioavailability in the lungs [91]. As previously stated, the smaller the particle size, the deeper it will penetrate the lung thus the higher the bioavailability. However, for larger molecular drugs, patients may need to use different dosages and multiple administrations to achieve the desired therapeutic effect [70]. Another challenge for pulmonary delivery of protein drugs is the rapid increase in levels of the drug in the serum, which may not be problematic in cases where the drug has a large margin of safety [89]. Although, this may be desirable for instances where fast delivery of a drug is required, such as insulin preceding a meal, it can result in unwanted side effects and will require more doses to achieve and maintain the required serum levels. However, new technologies, such as rapid-acting, slow-release analogs of drugs, such as insulin, have been developed to allow for an improved pulmonary peptide drug delivery [91].

## 7. Concluding remarks

In order to develop an analog of a protein drug, which can be deemed, therapeutically viable there are a variety of factors that need to be considered. A logical first step would be to gain a full understanding of physiological and chemical barriers, which the protein drug will encounter. Although this field is only a few decades old, significant progress has been made in many areas. There has been an increase in understanding of the advantages and disadvantages of different routes of protein drug delivery. Thus, with proper modifications, such as modifications of the N- or C- terminus, alteration of terminal amino acids, converting the conformation of protein from linear to a circular form, use of peptidomimetics, enzyme inhibitors, or PEGylation, protein drugs can be engineered based on the existing knowledge of proteolytic enzymes, which the protein drug will face once within the systemic circulation. Furthermore, recent advancements in the field of nanomedicine has allowed for the encapsulation of proteins resulting in increased bioavailability. Modifications and new developments in formulation technologies have also allowed for the potential production of protein drugs, which were originally thought to be uneconomical for large-scale production. Proper formulation of the drug product is dependent on choosing the most stable form of the protein drug

and fully understanding the chemical and physical properties and the stability of the compound in varying conditions in short and long-term studies.

## Author details

Tiam Feridooni, Adam Hotchkiss and Remigius U. Agu\*

\*Address all correspondence to: [Remigius.agu@dal.ca](mailto:Remigius.agu@dal.ca)

College of Pharmacy and Department of Pharmacology, Dalhousie University, Halifax, NS, Canada

## References

- [1] M. S. Chang and B. Yeung, Eds., *Formulation and Process Development Strategies for Manufacturing Biopharmaceuticals*. Hoboken, NJ, USA: John Wiley & Sons, Inc., 2010.
- [2] J. Shaji and V. Patole, "Protein and peptide drug delivery: oral approaches," *Indian J. Pharm. Sci.*, vol. 70, no. 3, pp. 269–77, Jan. 2008.
- [3] M. C. Manning, D. K. Chou, B. M. Murphy, R. W. Payne, and D. S. Katayama, "Stability of protein pharmaceuticals: an update," *Pharm. Res.*, vol. 27, no. 4, pp. 544–75, Apr. 2010.
- [4] G. Hu, "Understanding the basics of peptide and protein production," *Bioprocess Int.*, vol. 8, pp. 22–25, 2010.
- [5] L. R. Brown, "Commercial challenges of protein drug delivery," *Expert Opin. Drug Deliv.*, vol. 2, no. 1, pp. 29–42, Jan. 2005.
- [6] M. A. H. Capelle, R. Gurny, and T. Arvinte, "High throughput screening of protein formulation stability: practical considerations," *Eur. J. Pharm. Biopharm.*, vol. 65, no. 2, pp. 131–48, Feb. 2007.
- [7] M. Werle and A. Bernkop-Schnürch, "Strategies to improve plasma half life time of peptide and protein drugs," *Amino Acids*, vol. 30, no. 4, pp. 351–67, Jun. 2006.
- [8] M. C. Lai and E. M. Topp, "Solid-state chemical stability of proteins and peptides," *J. Pharm. Sci.*, vol. 88, no. 5, pp. 489–500, May 1999.
- [9] L. (Lucy) Chang and M. J. Pikal, "Mechanisms of protein stabilization in the solid state," *J. Pharm. Sci.*, vol. 98, no. 9, pp. 2886–2908, Sep. 2009.

- [10] A. A. Wakankar and R. T. Borchardt, "Formulation considerations for proteins susceptible to asparagine deamidation and aspartate isomerization," *J. Pharm. Sci.*, vol. 95, no. 11, pp. 2321–36, Nov. 2006.
- [11] M. Ameri, P. E. Daddona, and Y.-F. Maa, "Demonstrated solid-state stability of parathyroid hormone PTH(1-34) coated on a novel transdermal microprojection delivery system," *Pharm. Res.*, vol. 26, no. 11, pp. 2454–63, Nov. 2009.
- [12] R. Hamburger, E. Azaz, and M. Donbrow, "Autoxidation of polyoxyethylenic non-ionic surfactants and of polyethylene glycols," *Pharm. Acta Helv.*, vol. 50, no. 1–2, pp. 10–7, Jan. 1975.
- [13] S. Li, T. W. Patapoff, D. Overcashier, C. Hsu, T. H. Nguyen, and R. T. Borchardt, "Effects of reducing sugars on the chemical stability of human relaxin in the lyophilized state," *J. Pharm. Sci.*, vol. 85, no. 8, pp. 873–7, Aug. 1996.
- [14] E. T. Maggio, "Novel excipients prevent aggregation in manufacturing and formulation of protein and peptide therapeutics," *Bioprocess Int.*, vol. 6, no. 10, pp. 58–65, Nov. 2008.
- [15] W. F. Weiss, T. M. Young, and C. J. Roberts, "Principles, approaches, and challenges for predicting protein aggregation rates and shelf life," *J. Pharm. Sci.*, vol. 98, no. 4, pp. 1246–77, Apr. 2009.
- [16] S. Frokjaer and D. E. Otzen, "Protein drug stability: a formulation challenge," *Nat. Rev. Drug Discov.*, vol. 4, no. 4, pp. 298–306, Apr. 2005.
- [17] V. P. Torchilin and A. N. Lukyanov, "Peptide and protein drug delivery to and into tumors: challenges and solutions," *Drug Discov. Today*, vol. 8, no. 6, pp. 259–66, Mar. 2003.
- [18] M. Morishita and N. A. Peppas, "Is the oral route possible for peptide and protein drug delivery?," *Drug Discov. Today*, vol. 11, no. 19–20, pp. 905–10, Oct. 2006.
- [19] S. A. Shoyele, "Engineering protein particles for pulmonary drug delivery," *Methods Mol. Biol.*, vol. 437, pp. 149–60, Jan. 2008.
- [20] R. Singh, S. Singh, and J. W. Lillard, "Past, present, and future technologies for oral delivery of therapeutic proteins," *J. Pharm. Sci.*, vol. 97, no. 7, pp. 2497–523, Jul. 2008.
- [21] S. D. Allison, T. W. Randolph, M. C. Manning, K. Middleton, A. Davis, and J. F. Carpenter, "Effects of drying methods and additives on structure and function of actin: mechanisms of dehydration-induced damage and its inhibition," *Arch. Biochem. Biophys.*, vol. 358, no. 1, pp. 171–81, Oct. 1998.
- [22] M. C. Heller, J. F. Carpenter, and T. W. Randolph, "Protein formulation and lyophilization cycle design: prevention of damage due to freeze-concentration induced phase separation," *Biotechnol. Bioeng.*, vol. 63, no. 2, pp. 166–74, Apr. 1999.

- [23] W. Han, W. Bao, Z. Wang, and S. Nattel, "Comparison of ion-channel subunit expression in canine cardiac Purkinje fibers and ventricular muscle," *Circ. Res.*, vol. 91, no. 9, pp. 790–7, Nov. 2002.
- [24] H. Okamoto and K. Danjo, "Application of supercritical fluid to preparation of powders of high-molecular weight drugs for inhalation," *Adv. Drug Deliv. Rev.*, vol. 60, no. 3, pp. 433–46, Feb. 2008.
- [25] K. Johnson, "Preparation of peptide and protein powders for inhalation," *Adv. Drug Deliv. Rev.*, vol. 26, no. 1, pp. 3–15, Jun. 1997.
- [26] M. Luštrik, R. Dreu, R. Šibanc, and S. Srčič, "Comparative study of the uniformity of coating thickness of pellets coated with a conventional Wurster chamber and a swirl generator-equipped Wurster chamber," *Pharm. Dev. Technol.*, vol. 17, no. 3, pp. 268–76, Jan..
- [27] M. A. Rahman and J. Ali, "Development and in vitro Evaluation of Enteric Coated Multiparticulate System for Resistant Tuberculosis," *Indian J. Pharm. Sci.*, vol. 70, no. 4, pp. 477–81, Jan..
- [28] A. Dashevsky, K. Wagner, K. Kolter, and R. Bodmeier, "Physicochemical and release properties of pellets coated with Kollicoat SR 30 D, a new aqueous polyvinyl acetate dispersion for extended release," *Int. J. Pharm.*, vol. 290, no. 1–2, pp. 15–23, Feb. 2005.
- [29] E. Teunou and D. Poncet, "Batch and continuous fluid bed coating—review and state of the art," *J. Food Eng.*, vol. 53, no. 4, pp. 325–340, Aug. 2002.
- [30] N. Pearnchob, J. Siepmann, and R. Bodmeier, "Pharmaceutical applications of shellac: moisture-protective and taste-masking coatings and extended-release matrix tablets," *Drug Dev. Ind. Pharm.*, vol. 29, no. 8, pp. 925–38, Sep. 2003.
- [31] Y. F. Maa and C. C. Hsu, "Feasibility of protein spray coating using a fluid-bed Wurster processor," *Biotechnol. Bioeng.*, vol. 53, no. 6, pp. 560–6, Mar. 1997.
- [32] Y. Fukumori, H. Ichikawa, K. Jono, Y. Takeuchi, and T. Fukuda, "Computer simulation of agglomeration in the Wurster process," *Chem. Pharm. Bull. (Tokyo)*, vol. 40, no. 8, pp. 2159–63, Aug. 1992.
- [33] W. Wang, "Lyophilization and development of solid protein pharmaceuticals," *Int. J. Pharm.*, vol. 203, no. 1–2, pp. 1–60, Aug. 2000.
- [34] S. Luthra, J.-P. Obert, D. S. Kalonia, and M. J. Pikal, "Investigation of drying stresses on proteins during lyophilization: differentiation between primary and secondary-drying stresses on lactate dehydrogenase using a humidity controlled mini freeze-dryer," *J. Pharm. Sci.*, vol. 96, no. 1, pp. 61–70, Jan. 2007.
- [35] K. Griebenow and A. M. Klibanov, "Lyophilization-induced reversible changes in the secondary structure of proteins," *Proc. Natl. Acad. Sci. U. S. A.*, vol. 92, no. 24, pp. 10969–76, Nov. 1995.

- [36] W. Schlocker, S. Gschliesser, and A. Bernkop-Schnürch, "Evaluation of the potential of air jet milling of solid protein-poly(acrylate) complexes for microparticle preparation," *Eur. J. Pharm. Biopharm.*, vol. 62, no. 3, pp. 260–6, Apr. 2006.
- [37] D. B. Volkin and A. M. Klibanov, "Alterations in the structure of proteins that cause their irreversible inactivation," *Dev. Biol. Stand.*, vol. 74, pp. 73–80; discussion 80–1, Jan. 1992.
- [38] S. Kobayashi, S. Kondo, and K. Juni, "Pulmonary delivery of salmon calcitonin dry powders containing absorption enhancers in rats," *Pharm. Res.*, vol. 13, no. 1, pp. 80–3, Jan. 1996.
- [39] G. Nykamp, U. Carstensen, and B. W. Müller, "Jet milling—a new technique for microparticle preparation," *Int. J. Pharm.*, vol. 242, no. 1–2, pp. 79–86, Aug. 2002.
- [40] R. Vehring, "Pharmaceutical particle engineering via spray drying," *Pharm. Res.*, vol. 25, no. 5, pp. 999–1022, May 2008.
- [41] J. G. Weers, T. E. Tarara, and A. R. Clark, "Design of fine particles for pulmonary drug delivery," *Expert Opin. Drug Deliv.*, vol. 4, no. 3, pp. 297–313, May 2007.
- [42] M. Sakagami and P. R. Byron, "Respirable microspheres for inhalation: the potential of manipulating pulmonary disposition for improved therapeutic efficacy," *Clin. Pharmacokinet.*, vol. 44, no. 3, pp. 263–77, Jan. 2005.
- [43] A. X. C. N. Valente, R. Langer, H. A. Stone, and D. A. Edwards, "Recent advances in the development of an inhaled insulin product," *BioDrugs*, vol. 17, no. 1, pp. 9–17, Jan. 2003.
- [44] M. Mumenthaler, C. C. Hsu, and R. Pearlman, "Feasibility study on spray-drying protein pharmaceuticals: recombinant human growth hormone and tissue-type plasminogen activator," *Pharm. Res.*, vol. 11, no. 1, pp. 12–20, Jan. 1994.
- [45] R. W. Niven, F. D. Lott, A. Y. Ip, and J. M. Cribbs, "Pulmonary delivery of powders and solutions containing recombinant human granulocyte colony-stimulating factor (rhG-CSF) to the rabbit," *Pharm. Res.*, vol. 11, no. 8, pp. 1101–9, Aug. 1994.
- [46] R. Dalby, V. Naini, and P. Byron, "Droplets drying and electrostatic collection a novel alternative to conventional comminution techniques," *J. Biopharm. Sci.*, 1992.
- [47] U. Bilati, E. Allémann, and E. Doelker, "Strategic approaches for overcoming peptide and protein instability within biodegradable nano- and microparticles," *Eur. J. Pharm. Biopharm.*, vol. 59, no. 3, pp. 375–88, Apr. 2005.
- [48] B. Y. S. Kim, J. T. Rutka, and W. C. W. Chan, "Nanomedicine," *N. Engl. J. Med.*, vol. 363, no. 25, pp. 2434–43, Dec. 2010.
- [49] K. Uekama, F. Hirayama, and T. Irie, "Cyclodextrin Drug Carrier Systems," *Chem. Rev.*, vol. 98, no. 5, pp. 2045–2076, Jul. 1998.

- [50] D. Peer, J. M. Karp, S. Hong, O. C. Farokhzad, R. Margalit, and R. Langer, "Nanocarriers as an emerging platform for cancer therapy," *Nat. Nanotechnol.*, vol. 2, no. 12, pp. 751–60, Dec. 2007.
- [51] Y. Xia, Y. Xiong, B. Lim, and S. E. Skrabalak, "Shape-controlled synthesis of metal nanocrystals: simple chemistry meets complex physics?," *Angew. Chem. Int. Ed. Engl.*, vol. 48, no. 1, pp. 60–103, Jan. 2009.
- [52] M. Cavadas, Á. González-Fernández, and R. Franco, "Pathogen-mimetic stealth nanocarriers for drug delivery: a future possibility," *Nanomedicine Nanotechnology, Biol. Med.*, vol. 7, no. 6, pp. 730–743, Dec. 2011.
- [53] K. K. Jain, "Nanomedicine: application of nanobiotechnology in medical practice," *Med. Princ. Pract.*, vol. 17, no. 2, pp. 89–101, Jan. 2008.
- [54] A. Kumar, B. Sahoo, A. Montpetit, S. Behera, R. F. Lockey, and S. S. Mohapatra, "Development of hyaluronic acid-Fe<sub>2</sub>O<sub>3</sub> hybrid magnetic nanoparticles for targeted delivery of peptides," *Nanomedicine*, vol. 3, no. 2, pp. 132–7, Jun. 2007.
- [55] L. Hosta-Rigau, I. Olmedo, J. Arbiol, L. J. Cruz, M. J. Kogan, and F. Albericio, "Multi-functionalized gold nanoparticles with peptides targeted to gastrin-releasing peptide receptor of a tumor cell line," *Bioconjug. Chem.*, vol. 21, no. 6, pp. 1070–1078, Jun. 2010.
- [56] B. R. Stoll, H. R. Leipold, S. Milstein, and D. A. Edwards, "A mechanistic analysis of carrier-mediated oral delivery of protein therapeutics," *J. Control. Release*, vol. 64, no. 1–3, pp. 217–28, Feb. 2000.
- [57] F. Davis, A. Abuchowski, and T. Van Es. Enzyme-polyethylene glycol adducts: modified enzymes with unique properties. In: Broun G, Manecke G, Wingard L Jr, editors. *Enzyme Engineering*. New York: Springer, 1978. pp. 169–7.
- [58] M. Hamidi, A. Azadi, and P. Rafiei, "Pharmacokinetic consequences of pegylation," *Drug Deliv.*, vol. 13, no. 6, pp. 399–409, Jan. 2006.
- [59] A. Abuchowski, J. R. McCoy, N. C. Palczuk, T. van Es, and F. F. Davis, "Effect of covalent attachment of polyethylene glycol on immunogenicity and circulating life of bovine liver catalase," *J. Biol. Chem.*, vol. 252, no. 11, pp. 3582–6, Jun. 1977.
- [60] P. Bailon and C.-Y. Won, "PEG-modified biopharmaceuticals," *Expert Opin. Drug Deliv.*, vol. 6, no. 1, pp. 1–16, Jan. 2009.
- [61] G. Pasut, A. Guiotto, and FM Veronese, "Protein, peptide and non-peptide drug PEGylation for therapeutic application," *Expert Opin. Drug Deliv.*, vol. 14, no. 6, pp. 859–894, Jun. 2004.
- [62] F. M. Veronese and G. Pasut, "PEGylation, successful approach to drug delivery," *Drug Discov. Today*, vol. 10, no. 21, pp. 1451–8, Nov. 2005.
- [63] P. Bailon, A. Palleroni, C. A. Schaffer, C. L. Spence, W. J. Fung, J. E. Porter, G. K. Ehrlich, W. Pan, Z. X. Xu, M. W. Modi, A. Farid, W. Berthold, and M. Graves, "Rational

- design of a potent, long-lasting form of interferon: a 40 kDa branched polyethylene glycol-conjugated interferon alpha-2a for the treatment of hepatitis C," *Bioconjug. Chem.*, vol. 12, no. 2, pp. 195–202, Jan. 2001.
- [64] Y.-S. Wang, S. Youngster, M. Grace, J. Bausch, R. Bordens, and D. F. Wyss, "Structural and biological characterization of pegylated recombinant interferon alpha-2b and its therapeutic implications," *Adv. Drug Deliv. Rev.*, vol. 54, no. 4, pp. 547–70, Jun. 2002.
- [65] Y. Levy, M. S. Hershfield, C. Fernandez-Mejia, S. H. Polmar, D. Scudiery, M. Berger, and R. U. Sorensen, "Adenosine deaminase deficiency with late onset of recurrent infections: response to treatment with polyethylene glycol-modified adenosine deaminase," *J. Pediatr.*, vol. 113, no. 2, pp. 312–7, Aug. 1988.
- [66] M. L. Graham, "Pegaspargase: a review of clinical studies," *Adv. Drug Deliv. Rev.*, vol. 55, no. 10, pp. 1293–302, Sep. 2003.
- [67] P. J. Trainer, W. M. Drake, L. Katznelson, P. U. Freda, V. Herman-Bonert, A. J. van der Lely, E. V Dimaraki, P. M. Stewart, K. E. Friend, M. L. Vance, G. M. Besser, J. A. Scarlett, M. O. Thorner, C. Parkinson, A. Klibanski, J. S. Powell, A. L. Barkan, M. C. Sheppard, M. Malsonado, D. R. Rose, D. R. Clemmons, G. Johannsson, B. A. Bengtsson, S. Stavrou, D. L. Kleinberg, D. M. Cook, L. S. Phillips, M. Bidlingmaier, C. J. Strasburger, S. Hackett, K. Zib, W. F. Bennett, and R. J. Davis, "Treatment of acromegaly with the growth hormone-receptor antagonist pegvisomant," *N. Engl. J. Med.*, vol. 342, no. 16, pp. 1171–7, Apr. 2000.
- [68] R. B. Shah, F. Ahsan, and M. A. Khan, "Oral delivery of proteins: progress and prognostication," *Crit. Rev. Ther. Drug Carrier Syst.*, vol. 19, no. 2, pp. 135–69, Jan. 2002.
- [69] S. Stolnik and K. Shakesheff, "Formulations for delivery of therapeutic proteins," *Biotechnol. Lett.*, vol. 31, no. 1, pp. 1–11, Jan. 2009.
- [70] J. L. Cleland, A. Daugherty, and R. Mrsny, "Emerging protein delivery methods," *Curr. Opin. Biotechnol.*, vol. 12, no. 2, pp. 212–9, Apr. 2001.
- [71] H. Bari, "A prolonged release parenteral drug delivery system-an overview," *Int J Pharm Sci Rev Res*, vol. 3, no. 1, pp.1-11, Jul. 2010.
- [72] K. E. Robertson, N. B. Glazer, and R. K. Campbell, "The latest developments in insulin injection devices," *Diabetes Educ.*, vol. 26, no. 1, pp. 135–8, 141–6, 149–52, Jan. 2000.
- [73] J. Oberyé, B. Mannaerts, J. Huisman, and C. Timmer, "Local tolerance, pharmacokinetics, and dynamics of ganirelix (Orgalutran) administration by Medi-Jector compared to conventional needle injections," *Hum. Reprod.*, vol. 15, no. 2, pp. 245–9, Feb. 2000.
- [74] P. Mikkelsen Lynch, J. Butler, D. Huerta, I. Tsals, D. Davidson, and S. Hamm, "A pharmacokinetic and tolerability evaluation of two continuous subcutaneous infu-

- sion systems compared to an oral controlled-release morphine," *J. Pain Symptom Manage.*, vol. 19, no. 5, pp. 348–56, May 2000.
- [75] H. Kranz and R. Bodmeier, "A novel in situ forming drug delivery system for controlled parenteral drug delivery," *Int. J. Pharm.*, 2007.
- [76] L. Brannon-Peppas, "Recent advances on the use of biodegradable microparticles and nanoparticles in controlled drug delivery," *Int. J. Pharm.*, 1995.
- [77] G. Pauletti, S. Gangwar, and G. Knipp, "Structural requirements for intestinal absorption of peptide drugs," *J. Control....*, 1996.
- [78] S. J. Shire, "Formulation and manufacturability of biologics," *Curr. Opin. Biotechnol.*, vol. 20, no. 6, pp. 708–14, Dec. 2009.
- [79] A. Fjellestad-Paulsen, C. Söderberg-Ahlm, and S. Lundin, "Metabolism of vasopressin, oxytocin, and their analogues in the human gastrointestinal tract," *Peptides*, vol. 16, no. 6, pp. 1141–7, Jan. 1995.
- [80] S. Lundin, N. Pantzar, A. Broeders, M. Ohlin, and B. R. Weström, "Differences in transport rate of oxytocin and vasopressin analogues across proximal and distal isolated segments of the small intestine of the rat," *Pharm. Res.*, vol. 8, no. 10, pp. 1274–80, Oct. 1991.
- [81] A. Bernkop-Schnürch, "The use of inhibitory agents to overcome the enzymatic barrier to perorally administered therapeutic peptides and proteins," *J. Control. Release*, vol. 52, no. 1–2, pp. 1–16, Mar. 1998.
- [82] M. I. Ugwoke, N. Verbeke, and R. Kinget, "The biopharmaceutical aspects of nasal mucoadhesive drug delivery," *J. Pharm. Pharmacol.*, vol. 53, no. 1, pp. 3–21, Jan. 2001.
- [83] S. Türker, E. Onur, and Y. Ozer, "Nasal route and drug delivery systems," *Pharm. World Sci.*, vol. 26, no. 3, pp. 137–42, Jun. 2004.
- [84] Z. Antosova, M. Mackova, V. Kral, and T. Macek, "Therapeutic application of peptides and proteins: parenteral forever?," *Trends Biotechnol.*, vol. 27, no. 11, pp. 628–35, Nov. 2009.
- [85] M. I. Ugwoke, R. U. Agu, N. Verbeke, and R. Kinget, "Nasal mucoadhesive drug delivery: background, applications, trends and future perspectives," *Adv. Drug Deliv. Rev.*, vol. 57, no. 11, pp. 1640–65, Nov. 2005.
- [86] C. Ehrhardt and K.-J. Kim, Eds., *Drug Absorption Studies*, vol. VII. Boston, MA: Springer US, 2008.
- [87] M. Hinchcliffe and L. Illum, "Intranasal insulin delivery and therapy," *Adv. Drug Deliv. Rev.*, vol. 35, no. 2–3, pp. 199–234, Feb. 1999.
- [88] A. Martini, L. Muggetti, and M. P. Warchol, "Nasal and pulmonary drug delivery systems," *Expert Opin. Ther. Pat.*, vol. 10, no. 3, pp. 315–323, Mar. 2000.

- [89] J. Patton, J. Bukar, and S. Nagarajan, "Inhaled insulin," *Adv. Drug Deliv. Rev.*, vol. 35, no. 2–3, pp. 235–247, Feb. 1999.
- [90] P. Dames, B. Gleich, A. Flemmer, K. Hajek, N. Seidl, F. Wiekhorst, D. Eberbeck, I. Bittmann, C. Bergemann, T. Weyh, L. Trahms, J. Rosenecker, and C. Rudolph, "Targeted delivery of magnetic aerosol droplets to the lung," *Nat. Nanotechnol.*, vol. 2, no. 8, pp. 495–9, Aug. 2007.
- [91] C. Friebel and H. Steckel, "Single-use disposable dry powder inhalers for pulmonary drug delivery," *Expert Opin. Drug Deliv.*, vol. 7, no. 12, pp. 1359–72, Dec. 2010.

---

# Magnetic-Based Contact and Non-Contact Manipulation of Cell Mockups and MCF-7 Human Breast Cancer Cells

---

Islam S. M. Khalil, Iman E. O. Gomaa,  
Reham M. Abdel-Kader and Sarthak Misra

Additional information is available at the end of the chapter

<http://dx.doi.org/10.5772/61686>

---

## Abstract

The use of wireless magnetic control to transport and deliver chemotherapeutic agents selectively to tumor cells has become a promising strategy to mitigate the negative side effects associated with conventional treatment. It is necessary to manipulate and penetrate biological cells using magnetic agent to achieve this targeted drug delivery. Contact and non-contact micromanipulation of cell mockups and biological cells (human astrocytoma cell line U-373 MG and human breast adenocarcinoma cell line MCF-7) is achieved using magnetic agents (paramagnetic microparticles and iron oxide nanoparticles). The contact manipulation is accomplished under the influence of the controlled magnetic field gradients exerted on the magnetic agent, whereas the non-contact manipulation is done under the influence of the magnetic field and pressure gradients exerted on the agent and biological cells, respectively. We develop a magnetic-based teleoperation system that allows us to control the motion of the magnetic agents using microscopic feedback. This teleoperation is used to manipulate cell mockups toward reference positions in the presence and absence of contact between the cells and the magnetic agents. In addition, we demonstrate that iron oxide nanoparticles selectively move toward an MCF-7 cell and penetrate its walls without permanently damaging the membrane. This penetration is achieved in 28 seconds using controlled external magnetic fields and under microscopic vision guidance. The precise non-contact manipulation of biological cells using microparticles provides broad possibilities in targeted therapy and biomedical applications that require successful releases and selective penetration of cells without causing a permanent damage to the membrane.

**Keywords:** Magnetic, Breast cancer cells, motion control, wireless, magnetic forces, manipulation, non-contact, drug delivery

## 1. Introduction

Manipulation at microscale can be used in diverse biomedical, e.g., manipulation and positioning of biological cells in an aqueous environment and targeted drug delivery (Fig. 1), and nanotechnology applications [1, 2, 8]. One of the main challenges that prevent the automation of manipulation at microscale is the difficulty to make successful releases at the desired position due to the adhesive forces [9]. These adhesive forces result in stickiness between the tips of the manipulator and the manipulated object and thus prevent the release of the object in the desired position. Several techniques have been introduced to overcome the effect of the dominant adhesive forces. Saito et al. have proposed the utilization of voltage between the end effector and the substrate to produce an electric field that assists the sample release [10]. Kim et al. have reduced the adhesion between biological cells and microgripper tips by dip coating the tips with 10% SurfaSil siliconizing fluid and 90% histological-grade xylenes for 10 seconds before use [11]. Magnetic microrobotic systems have been also used in micromanipulation to push and pull the microobject toward the desired positions [2, 12]. Khalil et al. have demonstrated contact micromanipulation of nonmagnetic (SU-8) microobjects using clusters of paramagnetic microparticles using an orthogonal array of electromagnetic coils [5]. It has also been shown that these microparticles can be used to achieve a microassembly of microobjects. However, it is difficult to achieve successful releases and decrease the completion time of the microassembly tasks.

Manipulation using magnetic agents can be classified into two categories, i.e., contact [13] and non-contact manipulation [14, 29]. In contact manipulation, the presence of adhesive forces prevents the release of the microobjects, whereas in non-contact manipulation, it is relatively easy to break free from the adhesive force and achieve successful releases.

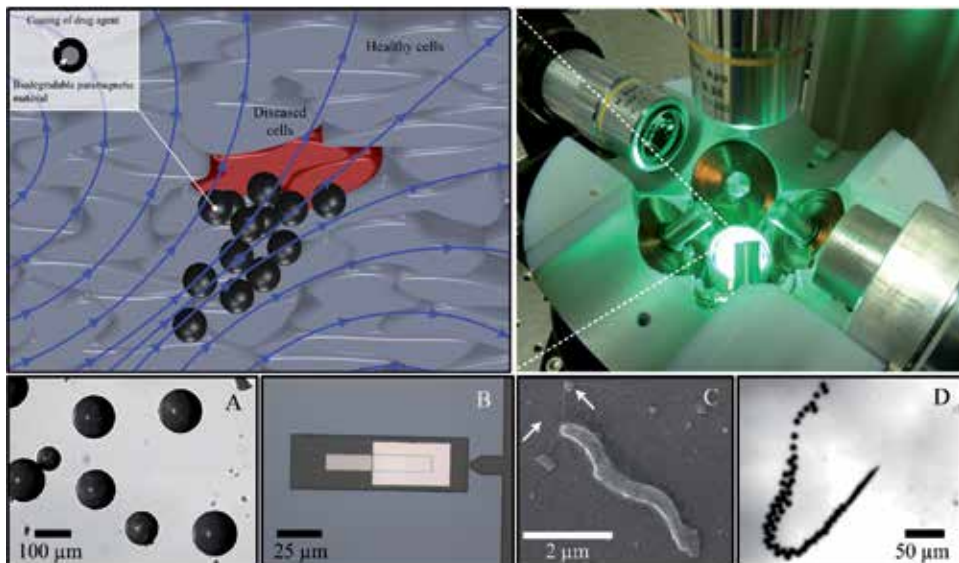


**Figure 1.** A schematic representation of targeted drug delivery using magnetic microparticles. The microparticles move toward the diseased cells (red) without affecting the healthy cells (gray). This level of control is achieved under the influence of the controlled magnetic forces (emanating from the electromagnetic system [15]) exerted on the magnetic dipole of the microparticles. The following magnetic agents can also be used to achieve targeted drug delivery: (a) microparticles, (b) magnetic microrobots, (c) magnetotactic bacteria [16], and (d) self-propelled microrobots [31].

Gazzar et al. have demonstrated that non-contact micromanipulation of nonmagnetic beads can be achieved using a transition between low and high Reynolds numbers [29]. First, the magnetic agents achieve non-contact pushing or pulling at low Reynolds number (by moving slowly). Second, the control system increases the speed of the magnetic agent once the nonmagnetic bead is positioned at the reference position to break free from the adhesive forces. Two-dimensional contact and non-contact micromanipulation of microspheres using a mobile microrobot has been achieved by Floyd et al. [14]. In the contact mode, the microrobot has been used to push the microspheres, whereas in the non-contact mode, the fluid flow caused by the translation of the microrobot generates enough force to push the microspheres. However, this non-contact manipulation has not been implemented using multiple microrobotic agents (microparticles) to control the non-contact driving forces (by changing the number of microparticles within the cluster) on the microobjects and to allow for coarse and fine non-contact positioning.

In this study, we achieve the following:

1. Development of a magnetic-based teleoperation system for the contact and non-contact manipulation of cell mockups and MCF-7 human breast cancer cells
2. Characterization of the motion control specifications of the contact and non-contact manipulation in the transient and steady states
3. Analyzing the relation between the speed of non-contact manipulation for different numbers of microparticles within the cluster during pushing and pulling

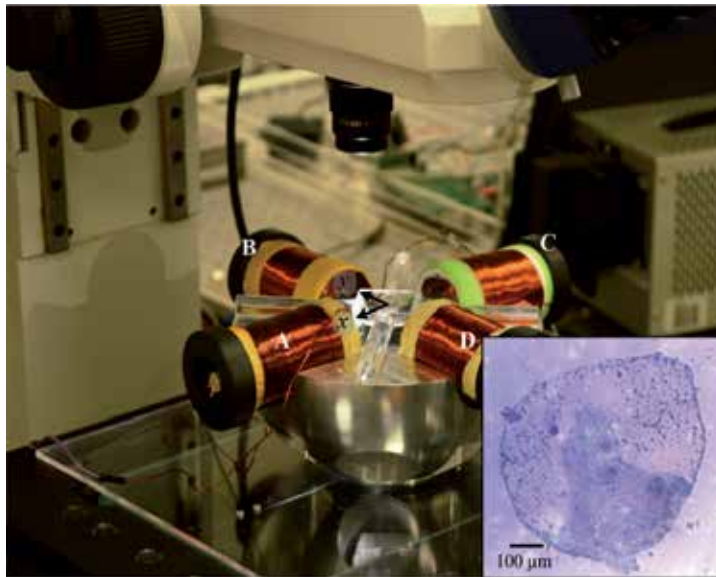


**Figure 2.** An electromagnetic system for the contact and non-contact manipulation and penetration of U-373 MG cells and MCF-7 cells. The system consists of an orthogonal array of electromagnetic coils with iron cores. The electromagnetic configuration surrounds a reservoir that contains the cells (or the cell mockups) and the magnetic agents. Position of the cells and magnetic agents is determined using a microscopic unit (MF Series 176 Measuring Microscopes, Mitutoyo, Kawasaki, Japan) and a high-speed camera (avA1000-120kc, Basler Area Scan Camera, Basler AG, Ahrensburg, Germany). The letters A, B, C, and D indicate the electromagnetic coils. The inset shows a human astrocytoma cell line U-373 MG.

#### 4. Selective penetration of MCF-7 cells using clusters of iron oxide nanoparticles.

We present a magnetic-based manipulation technique that allows for the contact and non-contact positioning of biological cells and penetration of the cells without causing damage to its walls. This manipulation is done using an electromagnetic configuration, cell mockups, and human astrocytoma cell line U-373 MG (Fig. 2) and human breast adenocarcinoma cell line MCF-7. The non-contact manipulation of the cell mockups is modeled, and experiments are done for Reynolds number regimes of less and greater than 0.1. In addition, the effect of the distance between the cluster of microparticles and the cell mockup and the number of microparticles within the clusters are investigated. We also fabricate iron oxide nanoparticles and use them in the penetration of the MCF-7 cells under the influence of the controlled magnetic field and using microscopic vision guidance.

The remainder of this chapter is organized as follows: Section 2 provides theoretical and experimental analysis pertaining to the non-contact manipulation of cell mockups using paramagnetic microparticles. The difference between contact and non-contact manipulation is explained and verified experimentally for Reynolds number less and greater than 0.1, in Section 2. The fabrication of iron oxide nanoparticles and the preparation of the U-373 MG and MCF-7 cells are included in Section 3. In addition, this section also includes a proof-of-concept experimental trial on the penetration of an MCF-7 cell using a cluster of nanoparticles, under the influence of the controlled magnetic field gradients. Finally, Section 4 concludes and provides directions for future work.

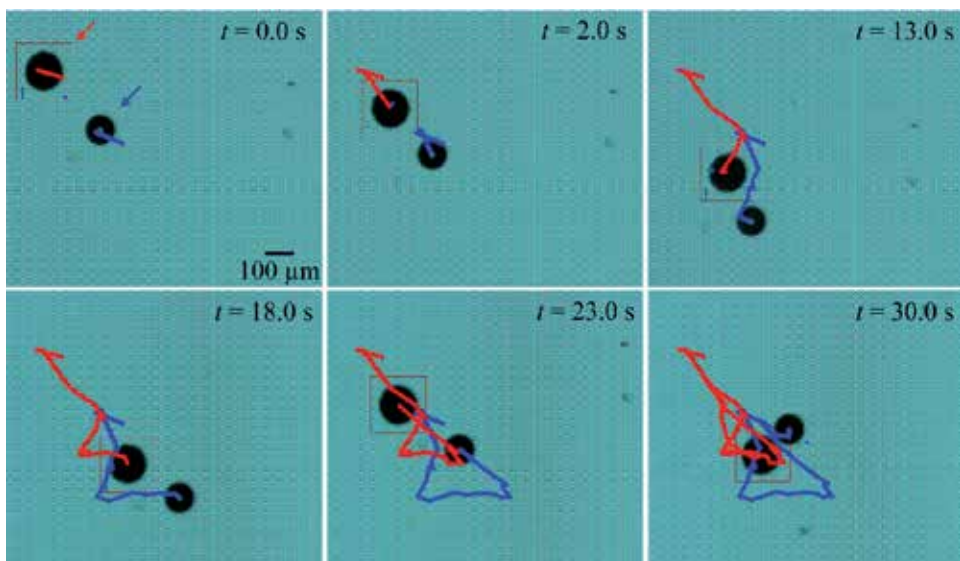


**Figure 3.** A representative teleoperation experiment of a cell mockup (blue polystyrene particles, Micromod Partikeltechnologie GmbH, Rostock-Warnemunde, Germany) with average diameter of  $100\ \mu\text{m}$  using a paramagnetic microparticle (PLAParticles-M-redF-plain, Micromod Partikeltechnologie GmbH, Rostock-Warnemunde, Germany) with average diameter of  $100\ \mu\text{m}$ . The teleoperation is achieved without contact between the cell mockup and the microparticle. The red and blue arrows indicate the paramagnetic microparticle and the cell mockup, respectively. At time,  $t=0.0$  seconds, magnetic field gradient is exerted on the paramagnetic microparticle, and non-contact manipulation of the cell mockup is achieved.

## 2. Modeling and control of the contact and non-contact manipulation

Cell mockups and biological cells can be manipulated, sorted, and fixed for diverse biomedical applications. The motion of the cells is studied under the influence of a moving fluid that is carried by controlled magnetic microparticles at low Reynolds number regime. We also study the effect of the inertia when clusters of microparticles are used to control the position of the cell mockups or biological cells.

### 2.1. Modeling and characterization of the manipulation

Clusters of magnetic microparticles are subjected to magnetic force ( $\mathbf{F}(\mathbf{P})$ ) and magnetic torque ( $\mathbf{T}(\mathbf{P})$ ) under the influence of an external magnetic field ( $\mathbf{B}(\mathbf{P})$ ), at point ( $\mathbf{P}$ ). The magnetic force exerted on the dipole of the cluster is given by [25]

$$\mathbf{F}(\mathbf{P}) = (\mathbf{m} \cdot \nabla)\mathbf{B}(\mathbf{P}) = (\mathbf{m} \cdot \nabla)\tilde{\mathbf{B}}(\mathbf{P})\mathbf{I} = \Lambda(\mathbf{m}, \mathbf{P})\mathbf{I}, \quad (1)$$

where  $\mathbf{m} \in \mathbb{R}^{3 \times 1}$  and  $\mathbf{B}(\mathbf{P}) \in \mathbb{R}^{3 \times 1}$  are the magnetic dipole moment of the cluster of microparticle and the induced magnetic field, respectively [18, 19]. Further,  $\mathbf{I}$  is the current input to the electromagnetic coils (Fig. 2) and  $\tilde{\mathbf{B}}(\mathbf{P})$  is the magnetic field-current map.  $\Lambda(\mathbf{m}, \mathbf{P})$  is the magnetic force-current map [2]. The position of the cluster of microparticles is controlled using (1) by pulling using the field gradient, whereas the orientation of the cluster is controlled using the magnetic torque that is given by

$$\mathbf{T}(\mathbf{P}) = \mathbf{m} \times \mathbf{B}(\mathbf{P}) = \mathbf{m} \times \tilde{\mathbf{B}}(\mathbf{P})\mathbf{I}. \quad (2)$$

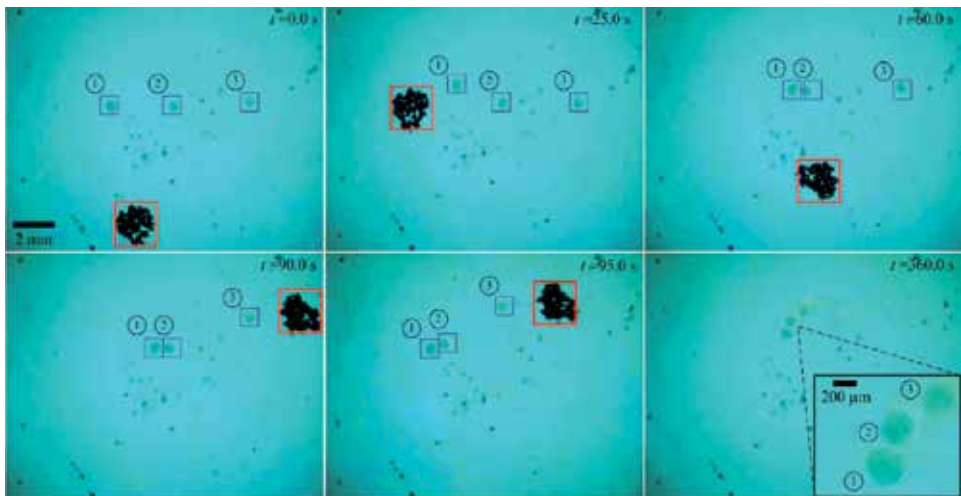


**Figure 4.** A representative teleoperation experiment of non-contact microassembly of three cell mockups using a cluster of microparticles at different time instants ( $t$ ). The cluster pushes and pulls the cell mockups without contact under the influence of the controlled magnetic fields to form a row of three cell mockups connected together (at time,  $t=360$  seconds). In this microassembly experiment, the average speed of the cluster is  $300 \mu\text{m/s}$ . The cluster consists of 15 microparticles. Paramagnetic microparticles with average diameter of  $100 \mu\text{m}$  are used in this experiment.

Fig. 3 shows a representative non-contact manipulation using pushing and pulling between a paramagnetic microparticle (PLAParticles-M-redF-plain, Micromod Partikeltechnologie GmbH, Rostock-Warnemunde, Germany) and a nonmagnetic cell mockup (blue polystyrene particles, Micromod Partikeltechnologie GmbH, Rostock-Warnemunde, Germany). At time,  $t=0.0$  seconds, the paramagnetic microparticle is pulled toward the cell mockup. The traces of the paramagnetic microparticle (red) and the cell mockup (blue) indicate that a non-contact force exists. This force allows us to manipulate the cell mockup without contact. At time,  $t=30$  seconds, the adhesive force between the microparticle and the cell mockup dominates, and at this instance, contact manipulation can be used to move the cell mockup. We calculate Reynolds number to understand the non-contact manipulation that is shown in Fig. 3. Reynolds number ( $R_e$ ) is given by

$$R_e = \frac{2\rho_f v r_p}{\eta}, \quad (3)$$

where  $v$  and  $\eta$  are the speed of the microparticle and fluid dynamic viscosity (1 mPa.s), respectively. Further,  $r_p$  is the radius of the particle (100  $\mu\text{m}$ ) and  $\rho_f$  is the density of the fluid. Using (3), Reynolds number is calculated to be less than 0.01 for velocity of 30  $\mu\text{m}/\text{s}$  of the paramagnetic microparticle. Therefore, the motion of the microparticle results in

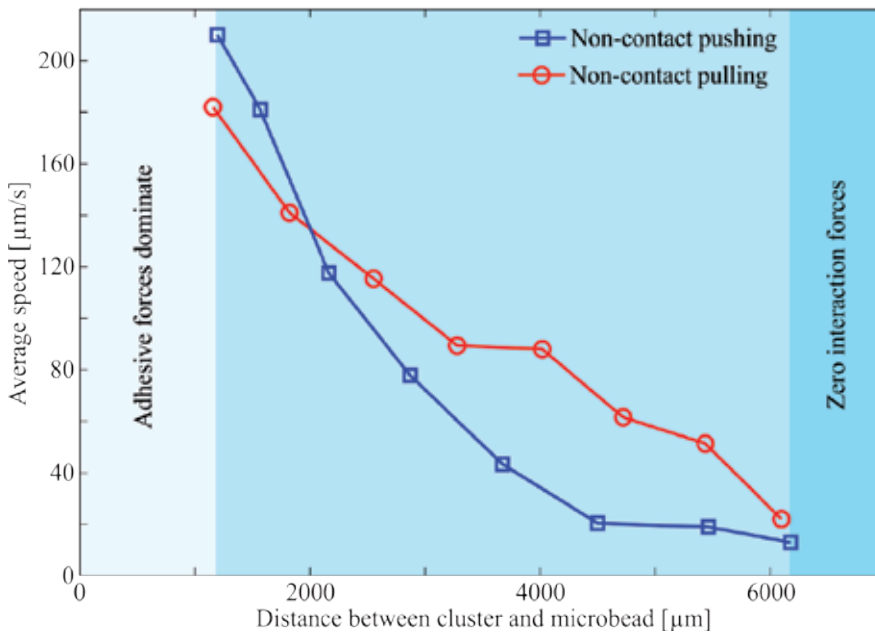


**Figure 5.** Average speed of the cell mockup versus the distance between the centers of the cluster of microparticles and the cell mockup. A cluster of 10 microparticles is used during pushing and pulling. The speed of the cell mockup is inversely proportional to the distance between the cluster and the cell mockup for the pushing and pulling. The adhesive force dominates for  $d < 1200 \mu\text{m}$ , and non-contact pushing and pulling cannot be achieved. Non-contact manipulation can be done within  $1200 \mu\text{m} < d < 6200 \mu\text{m}$ . Zero interaction force is observed for  $d > 6200 \mu\text{m}$ . The paramagnetic microparticles have an average diameter of 100  $\mu\text{m}$  [29].

shear and the fluid at the surface of the microparticle moves with the microparticle [20] and hence moves the cell mockup without contact. At time,  $t=18$  seconds, the direction of the microparticle is reversed by the magnetic field gradient. We observe that the cell mockup also reverses its direction and moves with the paramagnetic microparticle. This behavior is attributed to the motion of the fluid within the vicinity of the paramagnetic microparticle, as the fluid is carried with the microparticle. This behavior is only observed at low Reynolds number due to the absence of inertia.

We also investigate the non-contact manipulation of cell mockups for a Reynolds number larger than 0.1. For a cluster of less than 4 microparticles, the Reynolds number is calculated to be 0.024 (at average speed of  $120 \mu\text{m/s}$ ). For a cluster of eight microparticles, the Reynolds number is calculated to be 0.19 (at average speed of  $494 \mu\text{m/s}$ ). The Reynolds number at these two representative numbers of microparticles indicates that the inertial effect in the fluid could influence the non-contact manipulation of the nonmagnetic cell mockup based on the number of microparticles in the cluster. Fig. 4 shows a representative control of a cluster of microparticles (indicated using the red square) under the influence of the controlled magnetic force and torque using (1) and (2), respectively. The input current to the electromagnetic coils is controlled by the operator using a teleoperation system [26–28]. The blue squares indicate the positions of cell mockups that are used to test the magnetic-based motion control system. At time, instant  $t = 0$  seconds, the cluster starts to move toward the cell mockups. The cell mockups are subjected to the following non-contact force  $F_{nc}(\mathbf{P}_c)$  due to the pressure gradient that is caused by the motion of the cluster:

$$F_{nc}(\mathbf{P}_c) = m \left( \frac{P_h - P_l}{\rho_f d} \right) \hat{\mathbf{n}}, \tag{4}$$

where  $P_h$  and  $P_l$  are the high and low pressures on the cell mockup due to the motion of the cluster and  $\hat{\mathbf{n}}$  and  $m$  are a unit vector of the velocity of the cell mockup and the mass of the

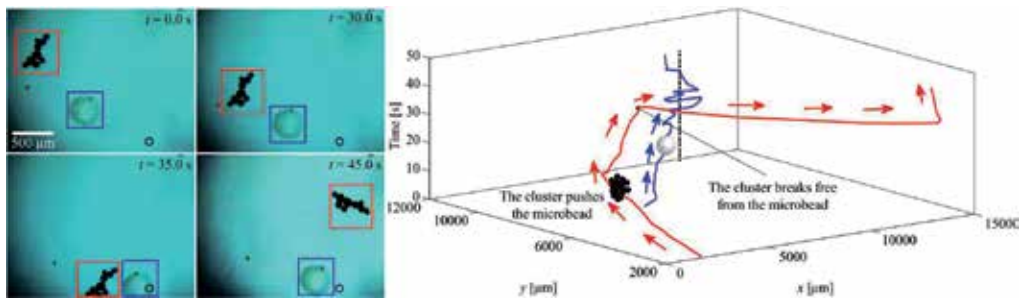


**Figure 6.** A representative teleoperation experiment of non-contact pushing of a cell mockup towards a reference position using a cluster of microparticles at different time instants ( $t$ ). The cluster pushes the cell mockup under the influence of the controlled magnetic fields. In this micromanipulation experiment, the velocity of the cluster is  $494 \mu\text{m/s}$  and  $2129 \mu\text{m/s}$  before and after the positioning of the cell mockup, respectively. The average velocity of the bead is  $219 \mu\text{m/s}$ . The red and blue rectangles represent the position of the cluster and the cell mockup, respectively. The cross hair indicates the reference position. The graph (right) plots the trajectory of both the cluster and the cell mockup throughout the experiment. Paramagnetic microparticles with average diameter of  $100 \mu\text{m}$  are used in this experiment [29].

fluid, respectively. Further,  $d$  is the distance between the cluster and the cell mockup and  $P_c$  is the position of the cell mockup. The distance ( $d$ ) affects the wireless manipulation.

The distance between the cluster of microparticles and the cell mockup influences the non-contact force (4). We calculate the average speed of the cell mockup versus its distance with the cluster, as shown in Fig. 5. We observe the following cases for a cluster of ten microparticles and a cell mockup with average diameter of  $100\ \mu\text{m}$ :

- Adhesive force is dominant ( $d < 1200\ \mu\text{m}$ ): The adhesive forces attract the cell mockup to the cluster of microparticles for distance of approximately  $1200\ \mu\text{m}$ . In this case, the cluster can be controlled to achieve contact manipulation of the cell mockup. However, it is difficult to break free from the adhesive forces to achieve successful release at a reference position.
- Non-contact force exists ( $1200\ \mu\text{m} < d < 6200\ \mu\text{m}$ ): In this range, the cluster generates enough non-contact force to overcome the drag force on the cell mockup, and hence, non-contact pushing and pulling can be achieved.
- Zero interaction forces ( $d > 6200\ \mu\text{m}$ ): At this distance, the cluster of microparticles cannot exert a non-contact force to pull or push the cell mockup.

## 2.2. Non-contact manipulation of cell mockups

The non-contact manipulation of the cell mockups is done using an electromagnetic system with closed configuration [22]. This system consists of four orthogonal electromagnetic coils that are controlled independently (Fig. 2). The electromagnetic coils surround a reservoir that contains the paramagnetic microparticles and the cell mockups. A microscopic system and a feature tracking algorithm are used to provide visual feedback to the control system [21]. The feature tracking algorithm determines the positions of the paramagnetic microparticle and the cell mockup, as shown in Fig. 6.

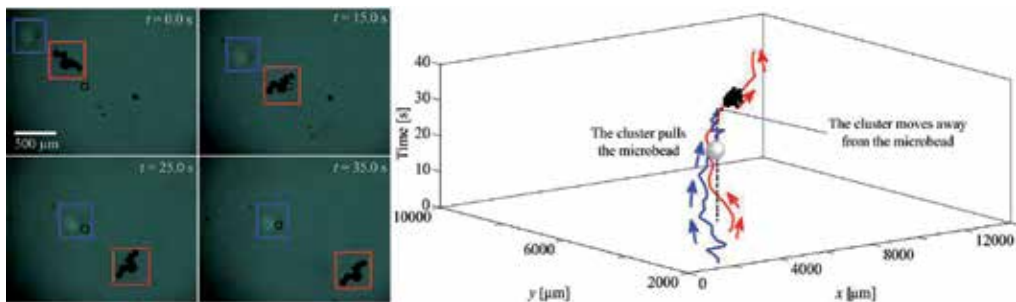


**Figure 7.** A representative teleoperation experiment of non-contact pulling of a cell mockup toward a reference position using a cluster of microparticles at different time instants ( $t$ ). The cluster pulls the cell mockup under the influence of the controlled magnetic fields. In this micromanipulation experiment, the average velocity of the cluster is  $298\ \mu\text{m/s}$  and  $854\ \mu\text{m/s}$  before and after the positioning of the cell mockup at the reference position, respectively. The average speed of the cell mockup is  $258\ \mu\text{m/s}$ . The red and blue rectangles represent the position of the cluster and the cell mockup, respectively. The cross hair indicates the reference position. The graph (right) plots the trajectory of both the cluster and the cell mockup throughout the experiment. Paramagnetic microparticles with average diameter of  $100\ \mu\text{m}$  are used in this experiment [29].

Non-contact micromanipulation of cell mockups within the vicinity of the reference positions is done, as shown in the representative experiment in Fig. 6. In this experiment, a cluster of nine microparticles is used to drive a cell mockup with a diameter of  $300\ \mu\text{m}$ . The average speed of the cluster is calculated to be  $494\ \mu\text{m/s}$  and  $2129\ \mu\text{m/s}$  before and after the positioning of the cell mockup at the reference position, respectively. The average speed of the cell mockup is calculated to be  $219\ \mu\text{m/s}$ . The time taken to drive the cell mockup from the initial position to the reference position (vertical black line) is 35 seconds. This experiment shows that the cluster achieves successful positioning and release of the cell mockup within the vicinity if the reference position has an error of  $259\ \mu\text{m}$  along  $x$ -axis and  $66\ \mu\text{m}$  along  $y$ -axis. We repeat the non-contact micromanipulation using pushing three times, and the average positioning time is calculated to be 30 seconds, whereas the average position errors are  $190\ \mu\text{m}$  along  $x$ -axis and  $70\ \mu\text{m}$  along  $y$ -axis. We observe that it is easier to release the cell mockup precisely at the reference position using non-contact pushing. However, this accuracy is affected when the cluster moves away from vicinity of the reference position and cell mockup (as shown in Fig. 6 at times,  $t=35$  seconds and  $t=45$  seconds).

Non-contact pulling of cell mockups is achieved, as shown in Fig. 7. A cluster of five microparticles are controlled under the influence of the magnetic field gradient and positioned between the reference position and the cell mockup. Motion of the cluster generates a pressure gradient in the fluid and achieves pulling of the cell mockup toward the reference position. The average speeds of the cluster and cell mockup are calculated to be  $75\ \mu\text{m/s}$  and  $30\ \mu\text{m/s}$ , respectively. The time taken to pull the cell mockup from its initial position to the reference position is 30 s. The cluster localizes the cell mockup within the vicinity of the reference position and also achieves successful release with an error of  $300\ \mu\text{m}$  along  $x$ -axis and  $200\ \mu\text{m}$  along  $y$ -axis. The non-contact micromanipulation using pulling is repeated three times, and the average positioning time is calculated to be 25 seconds. The average positioning time of micromanipulation using pulling is less than that using

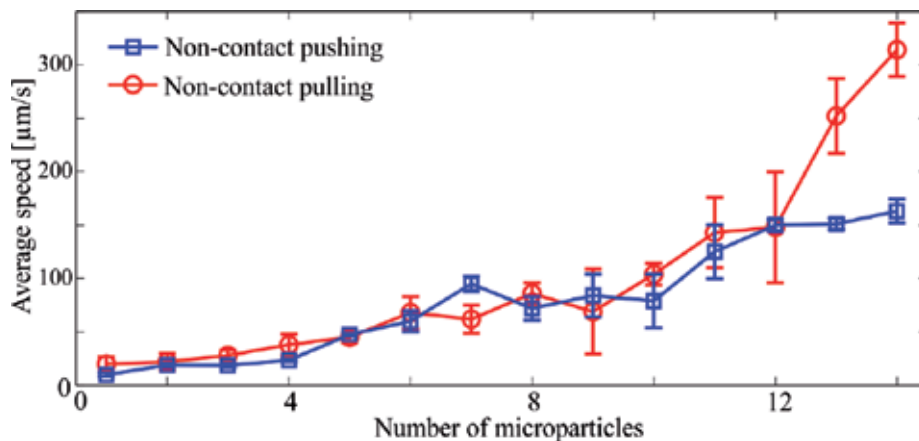


**Figure 8.** Average speed of the cell mockup versus the number of microparticles within the clusters. The electromagnet coil B is used to pull the cluster by the field gradients during pushing, whereas electromagnetic coil D is used during pulling. These gradients are generated by applying 1.4 A to the electromagnetic coils. The paramagnetic microparticles have an average diameter of  $100\ \mu\text{m}$  (PLAParticles-M-redF-plain from Micromod Partikeltechnologie GmbH, Rostock-Warnemuende, Germany) [29].

pushing since the average speed of pulling is greater than the average speed of pushing. We also observe that the non-contact micromanipulation via pulling achieves successful releases easily as in the non-contact pushing. The average position errors are calculated to be  $110\ \mu\text{m}$  along  $x$ -axis and  $45\ \mu\text{m}$  along  $y$ -axis.

The speed of the cluster of microparticles during non-contact pushing and pulling affects the release of the cell mockup and the positioning accuracy. During the micromanipulation, our control system maintains a steady speed of the cluster of microparticles. Once the cell mockup reaches the reference position, the speed of the cluster increases to break free from the non-contact forces between the cluster and the cell mockup. In the representative non-contact micromanipulation via pushing (Fig. 6), the speed of the cluster before and after the positioning of the cell mockup are  $494\ \mu\text{m/s}$  and  $2129\ \mu\text{m/s}$ , respectively. In the non-contact micromanipulation via pulling the (Fig. 7), the speeds of the cluster before and after the positioning of the cell mockup at the reference position are calculated to be  $298\ \mu\text{m/s}$  and  $894\ \mu\text{m/s}$ , respectively.

The effect of the number of microparticles within the cluster on the velocity of the cell mockup during pushing and pulling is analyzed. This analysis is done by pulling the cluster by the field gradients and measuring the linear velocity of the cell mockup for different numbers of microparticles. The number of microparticles per cluster is varied from 2 to 16 microparticles. The average speed is calculated from five pushing and pulling trials. One electromagnet is used in pushing and pulling to drive the cluster along  $x$ -axis. In these experiments, cell mockups with similar size are used, and the non-contact pulling and pushing are done between similar initial and final positions within the workspace of our magnetic system for all trails. In addition, the distance between the cluster of microparticles and the center of the cell mockup is kept constant during the calculation of the data provided in Fig. 8.

### 3. Manipulation and penetration of MCF-7 cells

Targeted drug delivery can be achieved by coating magnetic microparticles and nanoparticles with chemotherapeutic agents and localizing these particles within the vicinity of diseased cells. Two strategies have been proposed to release the drugs once the carriers are

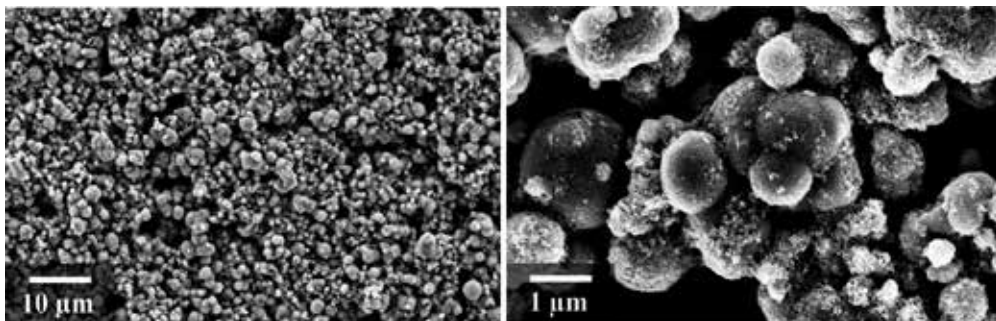


**Figure 9.** Scanning Electron Microscopy images of iron oxide nanoparticles. The nanoparticles ranges from  $250\ \text{nm}$  to  $1\ \mu\text{m}$  in diameter. These nanoparticles are pulled under the influence of the magnetic field gradient toward the MCF-7 cells.

concentrated at the diseased cell, namely, enzymatic activity-based approach and change of the physiological conditions approach [23]. Under certain physiological conditions, nanoparticles start releasing drug molecules in approximately 45 min and finish in 3 h [24]. Therefore, we control the motion of the nanoparticles toward MCF-7 cell to penetrate its walls or to be taken up by the cell.

### 3.1. Fabrication of the magnetic nanoparticles

First, a mixture of 0.675 g of iron chloride hexahydrate ( $\text{FeCl}_3 \cdot \text{H}_2\text{O}$ ), 19 ml of ethylene glycol, 1.8 g of sodium acetate (NaAc), and 1.0 g of polyethylene glycol is stirred for 30 min. Second, the mixture is sealed in a teflon-lined stainless-steel autoclave. The autoclave is heated to a temperature of  $200^\circ\text{C}$  for 8 h and then cooled to room temperature. Finally, the particles are washed several times with ethanol and dried at  $60^\circ\text{C}$ . Fig. 9 provides scanning electron microscopy images of the fabricated iron oxide nanoparticles. These nanoparticles are controlled using (1) and (2) toward the MCF-7 cells.

### 3.2. Preparation of the MCF-7 cells

MCF-7 cells are cultured in RPMI 1640 media (Lonza, 12-702F) containing 10% fetal bovine serum (FBS) (Lonza, 14-802F) and 1% penicillin-streptomycin (Lonza, 17-602E). The cells

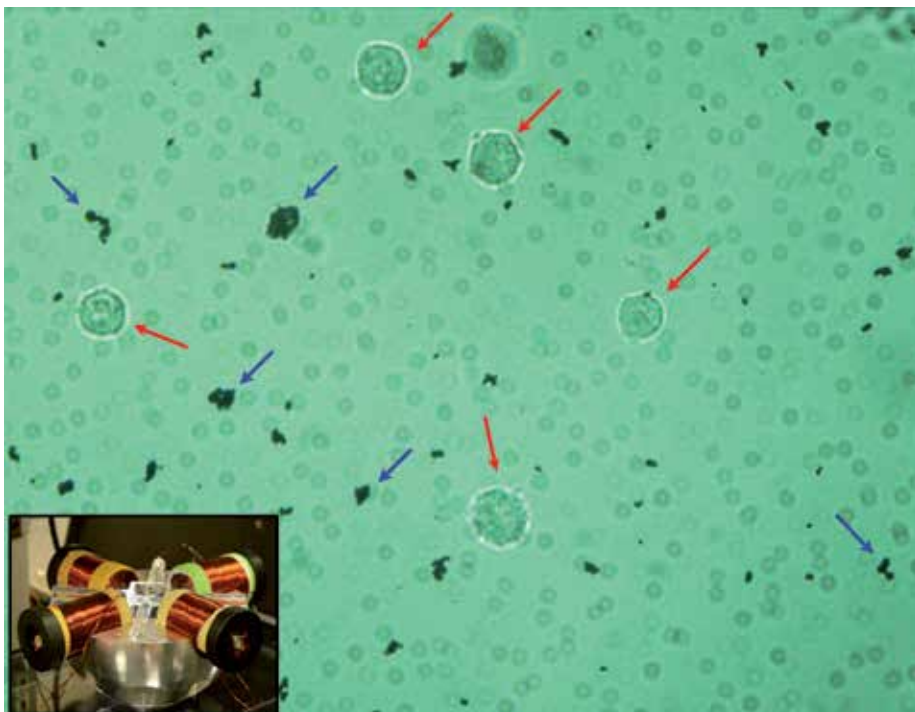


**Figure 10.** Microscopic image of MCF-7 cells (red arrows) and clusters of iron oxide nanoparticles (blue arrows). The nanoparticles are controlled under the influence of the magnetic field gradients. These gradients are generated using the electromagnetic system in the inset.

are incubated at 5% CO<sub>2</sub> and 37°C (Galaxy 170R) until they reach 80–90% confluency. Cells are washed twice using phosphate-buffered saline (PBS) (Lonza, 17-516F), followed by trypsinization (Lonza, CC-5002) and re-suspension in 10 ml RPMI. The cell suspension is then centrifuged (MIKRO, 22R) at 121xg for 5 min at 18°C. The supernatant is aspirated, and the cell pellet is re-suspended in fresh medium. Approximately  $0.25 \times 10^6$  cells are mounted as cell suspension together with the nanoparticles in a ratio of 1:10 on a microscopic slide for further processing.

### 3.3. Cell Penetration using nanoparticles

The iron oxide nanoparticles and the MCF-7 cells are contained in a Petri dish, and the motion of the nanoparticles is controlled using the magnetic field gradient. Fig. 10 provides a microscopic image of the MCF-7 cells (red arrows) and the clusters of nanoparticles (blue arrows). Our magnetic-based control system allows us to selectively target any of the cells using a cluster of nanoparticles. The cluster is pulled toward one of MCF-7 cells using the controlled magnetic force (1), as shown in Fig. 11. At time,  $t=4$  seconds, contact is achieved between the cluster and the cell. At this instant, our electromagnetic system exerts larger magnetic force on the dipole moment of the cluster to penetrate the wall of the cell. We observe that the cluster is taken up by the cell at time,  $t=22$  seconds. Once the nanoparticles are ingested by the cell, they stop moving since the exerted magnetic force is not large enough to move them inside the cell.

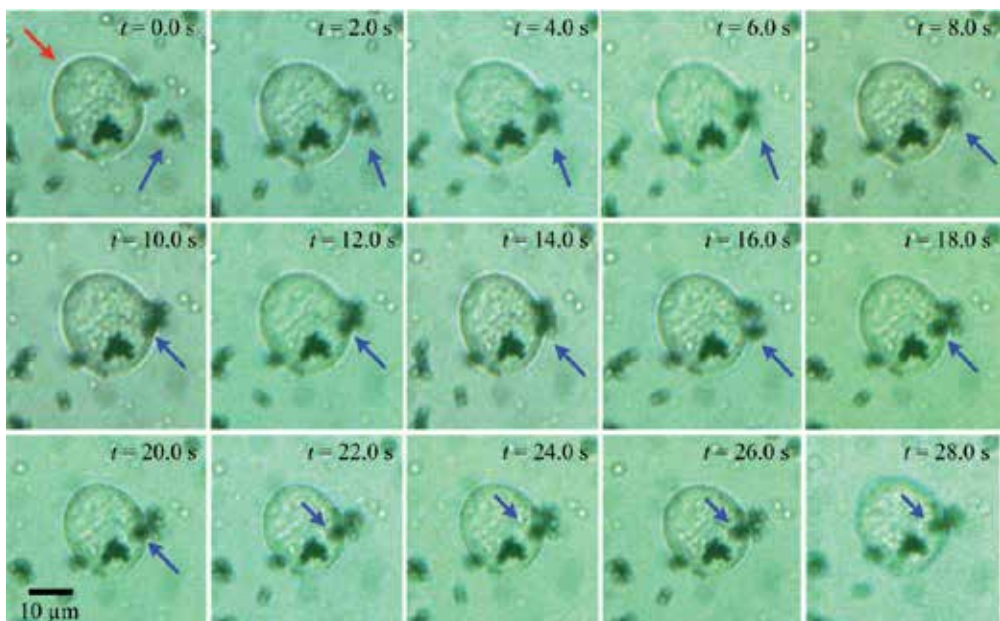


**Figure 11.** Penetration of MCF-7 cell (red arrow) using a cluster (blue arrow) of iron oxide nanoparticles is achieved. The cluster is pulled toward the cell under the influence of the magnetic field gradient and penetration (initial contact) of the cell is achieved at time,  $t=6.0$  seconds. The cluster of nanoparticles is partially taken up by the cell at time,  $t=28$  seconds.

The ability to move the nanoparticles toward the living MCF-7 cell and penetrate its wall holds promise for medicine. These nanoparticles can be coated with a chemotherapeutic agent and selectively controlled to target and destroy the diseased cells that engulf them. Despite the progress in fabrication of drug carriers and penetration of the MCF-7 cells, numerous challenges remain for translating this work into in vivo applications. It is necessary to achieve the motion control of the nanoparticles using feedback provided by an imaging modality, for instance, [33–35]. Fig. 12 provides a proof-of-concept result of the imaging of paramagnetic microparticles using an ultrasound system (Siemens ACUSON S2000, Siemens Healthcare, Mountain View, California, USA). We observe that the motion of the microparticles with average diameter of  $100\ \mu\text{m}$  and clusters of nanoparticles can be detected as artifact. Therefore, an ultrasound system can be used to achieve motion control of the nanoparticles and selective penetration of the living MCF-7 cells [32].

#### 4. Conclusions and future work

We demonstrate experimentally the non-contact manipulation of cell mockups using paramagnetic microparticles under the influence of the controlled magnetic field gradients. At  $Re < 0.1$ , the non-contact manipulation is achieved by the fluid that is carried by the controlled paramagnetic microparticle. This strategy allows us to achieve non-contact pulling and non-contact pushing of the cell mockup at average speeds of  $20\ \mu\text{m/s}$  and  $10\ \mu\text{m/s}$ , respectively. At  $Re > 0.1$ , clusters of microparticles cause pressure gradient within their vicinity. This pressure is also used to move the cell mockup without contact. We observe that a cluster of 14 microparticles achieves non-contact pulling and non-contact pushing of a cell mockup at average speeds of  $310\ \mu\text{m/s}$  and  $160\ \mu\text{m/s}$ , respectively. We also demonstrate that iron oxide nanoparticles (with maximum diameter of approximately  $1\ \mu\text{m}$ ) can penetrate a living MCF-7 cell under the influence of the magnetic field gradient exerted on the dipole moment of the nanoparticles. The nanoparticles are taken up by the MCF-7 cell in approximately 28 s.

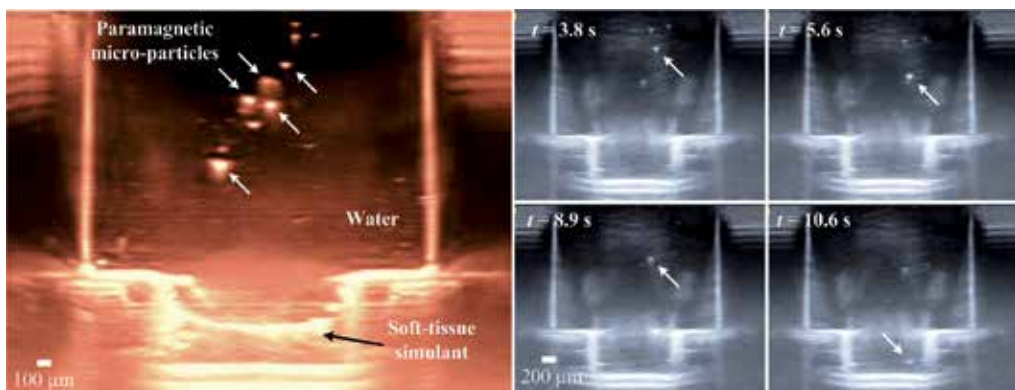


**Figure 12.** Ultrasound imaging of paramagnetic microparticles (PLAParticles-M-redF-plain from Micromod Partikeltechnologie GmbH, Rostock-Warnemunde, Germany). The microparticles moves under the influence of the gravitational forces inside a reservoir of water and soft-tissue simulant. This representative experiment is done using an ultrasound system (Siemens ACUSON S2000, Siemens Healthcare, Mountain View, California, USA). The insets show the motion (in real-time) of microparticles at different time instants ( $t$ ).

As part of future studies, the iron oxide nanoparticles will be coated with chemotherapeutic agents and controlled toward MCF-7 and U-373 MG cells. In addition, our control system will be adapted to allow for selective targeting of certain MCF-7 and U-373 MG cells. The electromagnetic system will also be redesigned to incorporate an ultrasound imaging modality to provide feedback to the system.

## 5. Acknowledgements

The authors acknowledge the funding from the German University in Cairo. The research leading to these results has also received funding from the DAAD-BMBF funding project.

The authors thank Dr. Rasha M. El-Nashar and Ms. Mariam Ayoub for preparing the iron oxide nanoparticles used in Fig. 9. They would also like to thank Mr. Hazem Salah and Ms. Aya Sameh for collecting the data used in Figs. 10 and 11.

## Author details

Islam S. M. Khalil<sup>1\*</sup>, Iman E. O. Gomaa<sup>1</sup>, Reham M. Abdel-Kader<sup>1</sup> and Sarthak Misra<sup>2,3</sup>

\*Address all correspondence to: islam.shoukry@guc.edu.eg

1 The German University in Cairo, Egypt

2 University of Twente, The Netherlands

3 University of Groningen and University Medical Centre Groningen, The Netherlands

## References

- [1] Q. A. Pankhurst, J. Connolly, S. K. Jones, and J. Dobson, "Applications of magnetic nanoparticles in biomedicine," *Journal of Physics*, vol. 36, no. 13, pp. 167–181, June 2003.
- [2] M. P. Kummer, J. J. Abbott, B. E. Kartochovil, R. Borer, A. Sengul, and B. J. Nelson, "OctoMag: an electromagnetic system for 5-DOF wireless micromanipulation," *IEEE Transactions on Robotics*, vol. 26, no. 6, pp. 1006–1017, December 2010.
- [3] S. Martel, O. Felfoul, J.-B. Mathieu, A. Chanu, S. Tamaz, M. Mohammadi, M. Mankiewicz, and N. Tabatabaei, "MRI-Based medical nanorobotic platform for the control of magnetic nanoparticles and flagellated bacteria for target interventions in human capillaries," *The International Journal of Robotics Research*, vol. 28, no. 9, pp. 1169–1182, September 2009.
- [4] D. Popa and E. Stephanou, "Micro and meso scale robotic assembly," *Journal of Manufacturing Processes*, vol. 6, no. 1, pp. 52–71, September 2004.
- [5] I. S. M. Khalil, F. van den Brink, O. S. Sukas, and S. Misra, "Microassembly using a cluster of paramagnetic microparticles," in *Proceedings of the IEEE International Conference on Robotics and Automation (ICRA)*, pp. 5507–5512, Karlsruhe, Germany, May 2013.

- [6] S. Martel and M. Mohammadi, "Towards mass-scale micro-assembly systems using magnetotactic bacteria," *International Manufacturing Science and Engineering Conference (ASME)*, vol. 2, no. 6, pp. 487–492, Oregon, USA, June 2011.
- [7] S. Martel, C. C. Tremblay, S. Ngakeng, and G. Langlois, "Controlled manipulation and actuation of micro-objects with magnetotactic bacteria," *Applied Physics Letters*, vol. 89, no. 23, pp. 1–3, January 2007.
- [8] S. Martel and M. Mohammadi, "Using a swarm of self-propelled natural microrobots in the form of flagellated bacteria to perform complex micro-assembly tasks," in *Proceedings of The IEEE International Conference on Robotics and Automation (ICRA)*, pp. 500–505, Alaska, USA, May 2010.
- [9] B. K. Chen, Y. Zhang, Y. Sun, "Active release of microobjects using a MEMS microgripper to overcome adhesion forces," *Journal of Microelectromechanical Systems*, vol. 18, no. 3, pp. 652–659, May 2009.
- [10] S. Saito, H. Himeno, and K. Takahashi, "Electrostatic detachment of an adhering particle from a micromanipulated probe," *Applied Physics Journal*, vol. 93, no. 4, 2219, January 2003.
- [11] K. Kim, X. Liu, Y. Zhang, and Y. Sun, "Nanonewton force-controlled manipulation of biological cells using a monolithic MEMS microgripper with two-axis force feedback," *Journal of Micromechanics and Microengineering*, vol. 18, no.5, pp. 055013, May 2008.
- [12] B. E. Kratochvil, M. P. Kummer, S. Erni, R. Borer, D. R. Frutiger, S. Schüürle, and B. J. Nelson, "MiniMag: a hemispherical electromagnetic system for 5-DOF wireless micromanipulation," *Proceeding of the 12th International Symposium on Experimental Robotics*, New Delhi, India, December 2010.
- [13] E. Avci, H. Yabugaki, T. Hattori, K. Kamiyama, M. Kojima, Y. Mae, and T. Arai, "Dynamic releasing of biological cells at high speed using parallel mechanism to control adhesion forces," in *Proceedings of The IEEE International Conference on Robotics and Automation (ICRA)*, Hong Kong, China, May 2014.
- [14] S. Floyd, C. Pawashe, and M. Sitti, "Two-dimensional contact and noncontact micromanipulation in liquid using an untethered mobile magnetic microrobot," *IEEE Transactions on Robotics*, vol. 25, no. 6, pp. 1332–1342, December 2009.
- [15] I. S. M. Khalil, R. M. P. Metz, B. A. Reefman, and S. Misra, "Magnetic-Based minimum input motion control of paramagnetic microparticles in three-dimensional space," in *Proceedings of the IEEE/RSJ International Conference of Robotics and Systems (IROS)*, pp. 2053–2058, Tokyo, Japan, November 2013.
- [16] I. S. M. Khalil, M. P. Pichel, L. Zondervan, L. Abelmann, and S. Misra, "Characterization and control of biological microrobots," in *Proceedings of the 13th International Symposium on Experimental Robotics-Springer Tracts in Advanced Robotics*, Quebec City, Canada, June 2012.

- [17] D. Li and Y. Xia. "Electrospinning of nanofibers: reinventing the wheel?" *Advanced Materials*, vol. 16, no. 14, pp. 1151–1170, July 2004.
- [18] T. H. Boyer, "The force on a magnetic dipole," *American Journal of Physics*, vol. 56, no. 8, pp. 688–692, August 1988.
- [19] S. S. Shevkoplyas, A. C. Siegel, R. M. Westervelt, M. G. Prentiss, and G. M. Whitesides, "The force acting on a superparamagnetic bead due to an applied magnetic field," *Lab on a Chip*, vol. 7, no. 6, pp. 1294–1302, July 2007.
- [20] H. C. Berg, "Random Walks in Biology," *Princeton University Press*, 1993.
- [21] I. S. M. Khalil, V. Magdanz, S. Sanchez, O. G. Schmidt, and S. Misra, "The control of self-propelled microjets inside a microchannel with time-varying flow rates," *IEEE Transactions on Robotics*, vol. 30, no. 1, pp. 49–58, February 2013.
- [22] I. S. M. Khalil, L. Abelmann, and S. Misra, "Magnetic-based motion control of paramagnetic microparticles with disturbance compensation," *IEEE Transactions on Magnetics*, vol. 50, no. 10, pp. 5400110, October 2014.
- [23] C. Alexiou, W. Arnold, R. J. Klein, F. G. Parak, P. Hulin, C. Bergemann, W. Erhardt, S. Wagenpfeil, and A. S. Lübke, "Locoregional cancer treatment with magnetic drug targeting," *Cancer Research*, vol. 60, pp. 6641–6648, December 2000.
- [24] S. R. Rudge, T. L. Kurtz, C. R. Vessely, L. G. Catterall, and D. L. Williamson, "Preparation, characterization, and performance of magnetic iron-carbon composite microparticles for chemotherapy," *Biomaterials*, vol. 21, no. 14, pp. 1411–1420, July 1999.
- [25] S. S. Shevkoplyas, A. C. Siegel, R. M. Westervelt, M. G. Prentiss, and G. M. Whitesides, "The force acting on a superparamagnetic bead due to an applied magnetic field," *Royal Society of Chemistry*, vol. 7, no. 6, pp. 1294–1302, July 2007.
- [26] Y. Xie, D. Sun, C. Liu, H. Y. Tse and S. H. Cheng, "A force control approach to a robot-assisted cell microinjection system," in *The International Journal of Robotics Research*, vol. 29, no. 9, pp. 322–331, November 2009.
- [27] K. Takeo and K. Kosuge, "Implementation of the micro-macro teleoperation system without using slave-side force sensors," in *Proceedings of the IEEE International Conference on Robotics and Automation (ICRA)*, pp. 1600–1605, Albuquerque, USA, April 1997.
- [28] A. Bolopion, H. Xie, D. S. Haliyo, and Stéphane Régnier, "Haptic teleoperation for 3-D microassembly of spherical objects," in *IEEE/ASME Transactions on Mechatronics*, vol. 17, no. 1, pp. 116–127, December 2010.
- [29] A. G. El-Gazzar, L. E. Al-Khouly, A. Klingner, S. Misra and I. S. M. Khalil, "Non-Contact manipulation of microbeads via pushing and pulling using magnetically controlled clusters of paramagnetic microparticles," in *Proceedings of the IEEE/RSJ International Conference of Robotics and Systems (IROS)*, pp. 778–783, Hamburg, Germany, September 2015.

- [30] A. Hosney, A. Klingner, S. Misra, and I. S. M. Khalil, "Propulsion and steering of helical magnetic microrobots using two synchronized rotating dipole fields in three-dimensional space," in *Proceedings of the IEEE/RSJ International Conference of Robotics and Systems (IROS)*, pp. 1988–1993, Hamburg, Germany, September 2015.
- [31] I. S. M. Khalil, V. Magdanz, S. Sanchez, O. G. Schmidt and S. Misra, "Magnetotactic bacteria and microjets: a comparative study," in *Proceedings of the IEEE/RSJ International Conference of Robotics and Systems (IROS)*, pp. 2035–2040, Tokyo, Japan, November 2013.
- [32] I. S. M. Khalil, P. Ferreira, R. Eleutério, C. L. de Korte, and S. Misra, "Magnetic-based closed-loop control of paramagnetic microparticles using ultrasound feedback," in *Proceedings of the IEEE International Conference on Robotics and Automation (ICRA)*, pp. 3807–3812, Hong Kong, June 2014.
- [33] S. Martel, O. Felfoul, J.-B. Mathieu, A. Chanu, S. Tamaz, M. Mohammadi, M. Mankiewicz, and N. Tabatabaei, "MRI-based medical nanorobotic platform for the control of magnetic nanoparticles and flagellated bacteria for target interventions in human capillaries," *International Journal of Robotics Research*, vol. 28, no. 9, pp. 1169–1182, September 2009.
- [34] J.-B. Mathieu and S. Martel, "Steering of aggregating magnetic microparticles using propulsion gradients coils in an MRI scanner," *Magnetic Resonance in Medicine*, vol. 63, no. 5, pp. 1336–1345, May 2010.
- [35] M. Evertsson, M. Cinthio, S. Fredriksson, F. Olsson, H. W. Persson, and T. Jansson, "Frequency- and phase-sensitive magnetomotive ultrasound imaging of superparamagnetic iron oxide nanoparticles," in *IEEE Transactions on Ultrasonics, Ferroelectrics, and Frequency Control*, vol. 60, no. 3, pp. 481–491, March 2013.



---

# **Swellable Hydrogel-based Systems for Controlled Drug Delivery**

---

Diego Caccavo, Sara Cascone, Gaetano Lamberti, Anna Angela Barba and Anette Larsson

Additional information is available at the end of the chapter

<http://dx.doi.org/10.5772/61792>

---

## **Abstract**

The controlled delivery of drugs can be effectively obtained using systems based on hydrogels. Tablets, to be orally administered, represent the simplest and the most traditional dosage systems based on hydrogel. Their formulation and preparation require to mix and to compress, in proper ratios, various excipients, including a swellable polymer and a drug. Carriers for controlled release systems are usually cross-linked polymers able to form hydrogels that show peculiar release mechanisms, where both diffusion and tablet swelling play important roles.

When a dry swellable hydrogel-based matrix is immersed in a physiological fluid, this starts to penetrate inside the polymeric hydrophilic matrix. When a certain solvent concentration is reached, the polymeric chains unfold due to a glass–rubber transition, and a gel-like layer is formed. In the swollen region, the drug molecules can easily diffuse toward the outer dissolution medium, once they are dissolved. The polymer network became extremely hydrated where the swollen matrix is in contact with the outer medium, and processes like chain disentanglement take place, “eroding” the matrix.

This chapter is focused on the analysis of the state of the art about the uses of carriers for controlled release systems composed by hydrogel-based matrices. This analysis has been performed studying in deep both the experimental and the modeling techniques which have been investigated over the years to characterize all the phenomena involved during the drug release.

**Keywords:** Hydrogels, Controlled drug delivery, Modeling, Characterization

## 1. Introduction

Hydrogels are hydrophilic polymer networks, able to absorb large amounts of water, increasing their volume (i.e., they are able “to swell,” giving rise to a phenomenon known as swelling) [1-3]. Networks can be composed of homopolymers or copolymers, and their network structure and physical integrity are due to the presence of cross-links, of chemical (tie-points, junctions) or physical (entanglements, crystallites) nature. Based on the stability of these cross-links, the hydrogel can withstand exposure to water; otherwise, it can degrade and dissolve in water, after a given exposure time.

The first known mention to potential use of hydrogels in medical science is probably due to Wichterle and Lim in 1960 [4], which proposed the use of methacrylate polymers for biomedical applications (i.e., the filling of eyes after enucleation). Since then, countless applications of hydrogels in pharmacy and medicine have been proposed, tested, and in several cases implemented as in common uses. Of course, during these (more than) 50 years, several very valuable reviews and reference books have been published on the work done too. A comprehensive list of these reviews/book today could be really huge, and it is beyond the scope of this work. Just a few examples are given in the following. With reference to the medical applications of hydrogels, the reader can refer to the handbook by Peppas [5], as well as to the reviews by Hoffman [1], by Peppas et al. [3], and by Cabral and Moratti [6]. With reference to the applications of hydrogels in drug delivery, the reader can refer to the reviews by Kamath and Park [7], by Peppas [8], by Peppas et al. [2], and by Hoare and Kohane [9]. It is worth to note that the scientific interest on the hydrogels and their applications is really large, witnessed not only by the large amount of papers published on the topic but also by the fact that several papers related to hydrogels are “most cited” in bibliographic databases. In 2012, the journal *Advanced in Drug Delivery Reviews* has devoted a special issue to the most cited papers (over than 1 thousand citations each) published on the journal in its 25-year lifetime, and four of the 32 papers were specifically devoted to hydrogels [1, 10-12].

### 1.1. Swelling hydrogels: Nature and classification

Hydrogels are interesting candidates for pharmaceutical and biomedical applications because of their characteristics such as:

- a. Biocompatibility and bioabsorbable nature
- b. Mechanical properties
- c. Degradation properties
- d. Compliance with sterilization protocols [7]

In particular, the balance between mechanical and degradation properties plays a relevant role in the design of a pharmaceuticals as well as a scaffold made of hydrogel to allow the desired release profile from the pharmaceutical in the time interval needed by the drug to perform the desired effect on the body or to ensure the structural function of the scaffold over the necessary time interval for the body to reconstruct the damaged part.

Several hydrophilic polymers can be used to produce hydrogels [1]:

- a. Natural polymers, for example, alginate and carrageenan (anionic polymers); chitosan (cationic polymer); dextran, agarose, cellulose, and derivatives (neutral polymers); and pectin
- b. Synthetic polymers, for example, PEG and PLA (polyesters), acrylates, and PVA
- c. Combinations of natural and synthetic polymers, for example, alginate and Pluronic<sup>®</sup> (block copolymers PPO-PEO-PPO)

Hydrogels can be classified according to several criteria. The most widespread and used one is based on the nature (physical or chemical) of the gel [1, 7, 9]:

- a. Physical or “reversible” hydrogels:
  1. Simple entanglement systems, in which the network is held together by molecular entanglements or crystallites
  2. Ion-mediated or “ionotropic” networks, in which the network is stabilized by interaction between polyelectrolyte and multivalent ions of opposite charges (e.g., alginate)
  3. Thermally induced networks, in which the heating (or the cooling) induces the structure formation (e.g., Pluronic<sup>®</sup> micelles which require heat to be formed)
- b. Chemical or “permanent” hydrogels, mainly covalently bounded
  1. Cross-linked polymers (by radiation, by chemical cross-linkers, and by multifunctional reactive compounds)
  2. Copolymers obtained from monomer + cross-linkers or monomer + multifunctional macromer
  3. Conversion of hydrophobic polymer in a hydrophilic polymer
  4. Polymerization of a monomer in the presence of a solid polymer to obtain an interpenetrating network (IPN)

Other possible classifications are based on the following:

Macromolecular structure [1]:

- a. Cross-linked or entangled networks of linear homopolymers, linear copolymers, and block or graft copolymers
- b. Polyion–multivalent ion and polyion–polyion or H-bonded complexes
- c. Hydrophilic networks stabilized by hydrophobic domains
- d. Interpenetrating networks (IPNs) or physical blends

Final form of the system [1]:

- a. Solid molded forms (e.g., soft contact lenses)

- b. Pressed powder matrices (e.g., tablets for oral delivery)
- c. Microparticles (e.g., bioadhesive carriers)
- d. Coatings (e.g., on pills and capsules)
- e. Membranes (e.g., in transdermal drug delivery patches)
- f. Encapsulated solids (e.g., in osmotic pumps)
- g. Liquids (e.g., solutions that form gels on heating or on cooling)

## 1.2. Swelling hydrogels: Nanostructure characterization

The three most important parameters, useful in order to characterize the nanostructure of the hydrogel network, are [2, 3]:

- a. The polymer volume fraction in swollen state,  $\phi_{2,s}$
- b. The number-average molecular weight of the polymer chain between two neighboring cross-linking points,  $\bar{M}_C$
- c. The corresponding mesh size,  $\xi$

In this paper, the notation convention will be 1, solvent (water); 2, polymer; 3, solute (drug); and higher numbers for other components (e.g., ions).

### 1.2.1. Polymer volume fraction in swollen state

The polymer volume fraction in swollen state,  $\phi_{2,s}$ , is a measure of the amount of water which can be retained in hydrogel, and it is given by the ratio between the dry polymer volume,  $V_p$ , and the swollen gel volume,  $V_G$ . It can be seen also as the reciprocal of the volumetric swelling ratio [13],  $Q$  :

$$\phi_{2,s} = \frac{V_p}{V_G} = \frac{1}{Q} \quad (1)$$

### 1.2.2. Molecular weight between two consecutive cross-links

The molecular weight between two consecutive cross-links (of chemical or physical nature),  $\bar{M}_C$ , is an average measure of the degree of polymer cross-linking. In order to estimate its value, the Gibbs free energy of the system has to be evaluated in terms of the elastic and the polymer/water mixing contributions ( $\Delta G_{total} = \Delta G_{elastic} + \Delta G_{mixing}$ ). The equilibrium condition is achieved once the change of chemical potential due to the polymer/water mixing,  $\Delta\mu_{mixing}$  (expressed on the basis of entropy and heat of mixing), and the change of chemical potential due to the elastic forces,  $\Delta\mu_{elastic}$ , are equal. The change of chemical potential due to the elastic forces can be estimated on the basis of the theory of rubber elasticity [14, 15]. Equating these two terms, an

expression for determining the molecular weight between two consecutive cross-links has been derived by Flory and Rehner [16] for a polymer network swollen by absorption of solvent:

$$\frac{1}{\bar{M}_C} = \frac{2}{\bar{M}_n} - \frac{\bar{v}}{V_1} \frac{[\ln(1 - \phi_{2,s}) + \phi_{2,s} + \chi_{12}\phi_{2,s}^2]}{[\phi_{2,s}^{1/3} - \phi_{2,s}/2]} \quad (2)$$

where  $\bar{M}_n$  is the number-average molecular weight of the polymer,  $\bar{v}$  is the polymer-specific volume,  $V_1$  is the molar volume of the solvent, and  $\chi_{12}$  is the Flory polymer-solvent interaction parameter. For a network obtained starting from a polymer in solution, in a “relaxed” state, with a volume fraction  $\phi_{2,r}$ , by swelling with further solvent molecules, Flory [17] and Bray and Merrill [18] derived another equation able to estimate the molecular weight between two consecutive cross-links:

$$\frac{1}{\bar{M}_C} = \frac{2}{\bar{M}_n} - \frac{\bar{v}}{V_1} \frac{[\ln(1 - \phi_{2,s}) + \phi_{2,s} + \chi_{12}\phi_{2,s}^2]}{\phi_{2,r} \left[ \left( \frac{\phi_{2,s}}{\phi_{2,r}} \right)^{1/3} - \left( \frac{\phi_{2,s}}{2\phi_{2,r}} \right) \right]} \quad (3)$$

The relaxed state is the state of the polymer immediately after the cross-linking but before the swelling. The use of equation 3 has been assessed by Merrill and Peppas [19, 20] working with PVA hydrogels, and it has been used to estimate the interaction parameter,  $\chi_{12}$ , and its dependence upon polymer concentration and temperature [21]. For ionic hydrogels, i.e., hydrogels in which ionic moieties are present, the theoretical treatment has to take into account the Gibbs free energy change due to the ionic nature of the network. Therefore, the change of chemical potential due to the ionic character of the hydrogel has to be taken into account. The problem has been faced out and solved by Brannon-Peppas and Peppas [22], who had derived the following two equations, to describe the swelling of anionic and cationic hydrogels, respectively, prepared in the presence of the solvent:

$$\frac{V_1}{4IM_r} \left( \frac{\phi_{2,s}}{\bar{v}} \right)^2 \left( \frac{K_a}{10^{-pH} + K_a} \right)^2 = [\ln(1 - \phi_{2,s}) + \phi_{2,s} + \chi_{12}\phi_{2,s}^2]_{1/3} + \left( \frac{V_1}{\bar{v}\bar{M}_C} \right) \left( 1 - \frac{2\bar{M}_C}{\bar{M}_n} \right) \phi_{2,r} \left[ \left( \frac{\phi_{2,s}}{\phi_{2,r}} \right)^{1/3} - \left( \frac{\phi_{2,s}}{2\phi_{2,r}} \right) \right] \quad (4)$$

$$\frac{V_1}{4IM_r} \left( \frac{\phi_{2,s}}{\bar{v}} \right)^2 \left( \frac{K_b}{10^{pH-14} + K_b} \right)^2 = [\ln(1 - \phi_{2,s}) + \phi_{2,s} + \chi_{12}\phi_{2,s}^2]_{1/3} + \left( \frac{V_1}{\bar{v}\bar{M}_C} \right) \left( 1 - \frac{2\bar{M}_C}{\bar{M}_n} \right) \phi_{2,r} \left[ \left( \frac{\phi_{2,s}}{\phi_{2,r}} \right)^{1/3} - \left( \frac{\phi_{2,s}}{2\phi_{2,r}} \right) \right] \quad (5)$$

where  $I$  is the ionic strength;  $K_a$  and  $K_b$  are the dissociation constants for the acid and the base, respectively; and  $M_r$  is the molecular weight of the repeating unit. The molecular weight between two consecutive cross-links  $\bar{M}_c$  can be obtained for the two cases solving the suitable equation for the given value of pH.

### 1.2.3. Mesh size

The mesh size,  $\xi$ , also known as the correlation length between two cross-links, is a measure of the space available between the macromolecular chains. Therefore, it is related to the ability of a drug molecule to diffuse through the network to be released. It can be calculated by [23]:

$$\xi = \alpha (\bar{r}_0^2)^{1/2} \quad (6)$$

where  $\alpha$  is the elongation ratio (which for isotropically swollen hydrogels is given by  $\alpha = \phi_{2,s}^{-1/3}$ ) and  $(\bar{r}_0^2)^{1/2}$  is the unperturbed root-mean-square of the end-to-end distance for polymer chains between two neighboring cross-links. The last one can be evaluated as follows:

$$(\bar{r}_0^2)^{1/2} = l(C_n N)^{1/2} = l \left( C_n \frac{2\bar{M}_c}{M_r} \right)^{1/2} \quad (7)$$

where  $l$  is the length of the bond along the polymer backbone (for vinyl polymers is 0.154 nm),  $C_n$  is the Flory characteristic ratio (actually, eq. 7 is the definition of Flory's characteristic ratio:  $C_n = \bar{r}_0^2 / Nl^2$ ), and  $N = (2\bar{M}_c / M_r)$  is the number of links for the chain. Therefore, the mesh size for isotropically swollen hydrogels can be calculated as follows:

$$\xi = l \phi_{2,s}^{-1/3} \left( C_n \frac{2\bar{M}_c}{M_r} \right)^{1/2} \quad (8)$$

All these three parameters  $\{\phi_{2,s}, \bar{M}_c, \xi\}$  are important for the drug delivery processes, since they determine the kinetics of drug diffusion and release. They, which are related to one another, can be determined theoretically or by means of experimental techniques. The ability to tailor the molecular structure of hydrogels (i.e., to design hydrogels with desired values of the three parameters) allows to tailor the hydrogels' mechanical and diffusive properties.

### 1.2.4. Structure-properties relationships: Mechanical behavior

From the mechanical point of view, the rubber elasticity theory [24], applicable also to hydrogels for relatively small deformation (less than 20 %), allows to evaluate the tensile stress

$\tau$ , expressed as the force per unit area of an unstretched sample, swollen by absorption of solvent (analogous to eq. 2):

$$\tau = \frac{RT}{\bar{v}\bar{M}_C} \left( \alpha - \frac{1}{\alpha^2} \right) \left( 1 - \frac{2\bar{M}_C}{\bar{M}_n} \right) \phi_{2,s}^{1/3} \quad (9)$$

For the case in which the polymer is initially in solution at mass concentration  $\rho_{2,r}$ , the tensile stress can be calculated as follows [19]:

$$\tau = \rho_{2,r} \frac{RT}{\bar{M}_C} \left( \alpha - \frac{1}{\alpha^2} \right) \left( 1 - \frac{2\bar{M}_C}{\bar{M}_n} \right) \left( \frac{\phi_{2,s}}{\phi_{2,r}} \right)^{1/3} \quad (10)$$

To characterize the hydrogel, the cross-linking concentration,  $c_x$  (sometimes defined as cross-linking density), can be used. The cross-linking concentration is defined as the mole of cross-links for unit volume, and thus, it can be calculated as follows [19]:

$$c_x = \frac{1}{\bar{v}\bar{M}_C} = \frac{\rho}{\bar{M}_C} \quad (11)$$

where  $\rho$  is the polymer density (the inverse of polymer-specific volume). Using the cross-linking concentration and the rubber elasticity theory, the elastic shear modulus at rest,  $G_0$ , can be evaluated (e.g., equation 4.9c in [15]), in which  $\bar{M}_C$  can be calculated by eq. 2, 3, 4, or 5:

$$G_0 = c_x RT = \frac{\rho}{\bar{M}_C} RT \quad (12)$$

It is worth noticing that, according to the “equivalent network theory,” in which the network is represented as a collection of spherical “blobs,” whose diameters represent the network mesh size  $\xi$  of the entangled structure, it is possible to relate the cross-linking concentration,  $c_x$ , with the mesh size:

$$\xi = \left( \frac{1}{N_A} \frac{6}{\pi c_x} \right)^{1/3} = \left( \frac{1}{N_A} \frac{6}{\pi \rho} \bar{M}_C \right)^{1/3} \quad (13)$$

A comparison between eq. 8 and eq. 13 is not straightforward, since eq. 13 predicts a one-third power dependence of  $\xi$  from  $\bar{M}_C$ , whereas eq. 8 requires the knowledge of  $\phi_{2,s}$  (plus, if

necessary, of  $\phi_{2,r}$  and of pH) dependence upon  $\bar{M}_c$  (given by eq. 2, 3, 4, or 5), and thus, it is not possible to clearly identify the dependence of  $\xi$  from  $\bar{M}_c$ . Generally, the equivalent network theory (eq. 13) predicts mesh size smaller than the swelling theory (eq. 8).

### 1.2.5. Structure-properties relationships: Mass-transport behavior

The release of an active ingredient (AI, a drug molecule) from a hydrogel-based system takes place mainly by diffusion. These systems are prepared by dissolution or dispersion of the drug within the polymer matrix, which is initially dry. Under this condition, the mass transport of the drug through the matrix is negligible; therefore, no release kinetics is observable. When the matrix comes into contact with water (or biological fluids mainly composed of water), the polymer gives origin to a swollen hydrogel network, within which the drug can diffuse and then it can be released (see also section 1.3). The diffusion in hydrogel networks can be concentration gradient-driven (Fickian diffusion) or polymer relaxation-driven (non-Fickian, or viscoelastic, diffusion). The non-Fickian diffusion is known as *anomalous transport*, and its limiting case has been defined by Alfrey et al. [25] as *Case-II transport*. The Case-II transport is characterized by a sharp front between the rubbery and the glassy region of the network (see also section 1.3), advancing at a constant velocity, and the rubbery region is a swollen network at equilibrium with the solvent. Because of the constant-velocity advancement of the front, in principle the Case-II diffusion can give rise to a constant mass-flow-rate release of the drug, i.e., a zero-order release kinetics [26].

Vrentas et al. [27, 28] have suggested a simple way to establish the regions in which Fickian and non-Fickian transports take place, on the basis of the *diffusional Deborah number*,  $N_{De.D}$ , defined according to eq. 14, in which  $\lambda_m$  is the characteristic stress-relaxation time of the polymer-solvent system and  $\theta_D$  is the characteristic time for the diffusion of the solvent in the polymer:

$$N_{De.D} = \frac{\lambda_m}{\theta_D} = \frac{\int_0^\infty sG(s)ds / \int_0^\infty G(s)ds}{L_{Ch}^2 / D_{1,s}} \quad (14)$$

The stress-relaxation time,  $\lambda_m$ , can be evaluated by integrals of the shear relaxation modulus,  $G(t)$ , over the entire relaxation time spectrum; the diffusion time,  $\theta_D$ , is given by the ratio between the second power of a characteristic diffusional path length (for the solvent),  $L_{Ch}$ , and the diffusion coefficient of the solvent in the swollen network,  $D_{1,s}$  [29]. If the change in solvent concentration during the swelling process is limited, average values for each characteristic time have to be used, and then the full process can be characterized by a single value of the Deborah number. If the change in solvent concentration is large, the Deborah number have to be calculated for both the initial and final stages, and their order of magnitude will be used to characterize the behavior of the system.

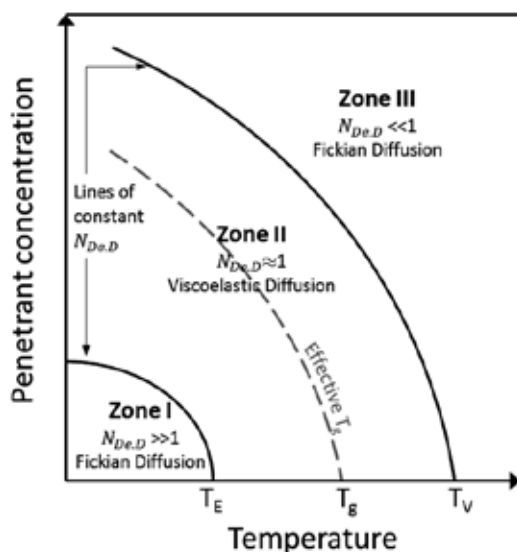


**Figure 1.** Schematic illustrating the different zones of diffusion, function of the temperature, and penetrant concentration. The solid lines represent lines at constant diffusional Deborah number,  $N_{De,D}$ ; the dashed gray line represents the effective glass transition temperature,  $T_g$ . The temperatures  $T_E$  and  $T_V$  represent the temperatures at which the polymer behaves like an elastic solid and viscous fluid, respectively. Figure redrawn on the basis of the suggestions in [27, 29].

The value of the diffusional Deborah number,  $N_{De,D}$ , discriminates the nature of the diffusive phenomena, as schematized in Figure 1:

- a. Large values of the Deborah number ( $N_{De,D} \gg 1$ ) identify **Zone I**, where the characteristic relaxation time,  $\lambda_m$ , is long with respect to characteristic diffusion time,  $\theta_D$ : the polymer structure does not change during the water diffusion process, i.e., the polymer remains in its glassy state. The diffusion phenomenon is usually described by the conventional Fick's law, using coefficients of diffusion constant and independent from water/polymer concentrations.
- b. Small values of the Deborah number ( $N_{De,D} \ll 1$ ) identify **Zone III**, where the relaxation phenomenon is much faster than the diffusion phenomenon. Practically, it is a diffusion through a viscous mixture (the swollen, rubbery hydrogel), a process which can be described by again the conventional Fick's law, using coefficients of diffusion which are a strong function of water/polymer concentrations.
- c. Intermediate values of the Deborah number ( $N_{De,D} \approx 1$ ) identify **Zone II**, when the two characteristic times are of the same order of magnitude, i.e., the relaxation and the diffusion phenomena take place on the same time scale. This is the transition zone in which the polymer experiences its glass-rubber phase change, the mixture has a viscoelastic nature, and the diffusion is an *anomalous* transport (and its limit, the *Case-II* transport), which is non-Fickian.

Several models have been proposed to describe the deviation from the Fickian behavior, among which is the Camera-Roda and Sarti equation [30] that was proven [31] to be able to catch the *Case-II* and the *anomalous* transport behaviors with a minimum number of additional parameters. However, despite some experimental evidences of *Case II/anomalous* transport in polymers used for swellable hydrogel-based delivery systems [32-34], none of the mechanistic models developed to describe drug release have included this feature, considering an instantaneous rearrangement of the polymer chains and therefore limiting their attention to the Zone III (Figure 1) behavior.

Another way to characterize the behavior of the hydrogel network, with particular reference to drug diffusion, requires to consider the so-called swelling interface number,  $N_{Sw.I}$ , defined [35] by eq. 15, as the ratio between the velocity of the solvent penetration,  $v$ , and the rate of diffusion, i.e., the ratio between the diffusivity of the solute (the drug) in the swollen network,  $D_{3,s}$ , and the thickness of the swollen region through which the solute diffusion occurs,  $\delta$  :

$$N_{Sw.I} = \frac{v}{D_{3,s} / \delta} \quad (15)$$

The analysis of diffusional Deborah number,  $N_{De,D}$ , and of swelling interface number,  $N_{Sw.I}$ , allows to identify the nature of the mass transport. In order to get a zero-order release kinetics, two conditions are expected to be satisfied [29]:

- a. The movement of the solvent has to be controlled by polymer relaxation, i.e.,  $N_{De,D}$  has to be close to unity.
- b. The solute diffusion has to be faster than the front movement (solvent movement), i.e.,  $N_{Sw.I}$  has to be lower than unity.

### 1.2.6. Modeling of the diffusion behavior

In order to model the diffusive phenomena which take place in hydrogel networks, several models have been proposed and they have been thoroughly reviewed [36-39], and the reader should refer to these reviews in order to have a better view of the problem. Generally, the models useful to predict the diffusivity of a solute "3" in a swollen network "s,"  $D_{3,s}$ , with respect to the diffusivity of the same solute in the solvent "1," have the following general form [13] (the ratio  $D_{3,s} / D_{3,1}$  is sometimes called "the retardation effect"):

$$\frac{D_{3,s}}{D_{3,1}} = f(\xi, \phi_2, r_s) \quad (16)$$

where  $\xi$  and  $\phi_2$  have been already defined and they are, respectively, the network mesh size and the polymer volume fraction, while the parameter  $r_s$  is the size of the diffusing solute. The

mechanistic theories which are used in order to build the left-hand side of eq. 16 are known as hydrodynamic theories, obstruction theories, and theories based on free volume. In the following, the basics of each approach are reported along with the most common models.

### Hydrodynamic theories

The hydrodynamic theory assumes that the solute molecules, depicted as hard spheres, move through the liquid phase of the network, the diffusion coefficient being dependent upon the drag force exerted by the liquid molecules on the spheres. The binary diffusive coefficient is given by the Stokes–Einstein equation, i.e.,  $D_{3,1} = k_B T / f$ , where  $f$  is the frictional drag coefficient (for hard spheres of radius  $R$  in a liquid of viscosity  $\eta$ , the frictional drag coefficient is  $f = 6\pi\eta R$ ), and the focus of the hydrodynamic theories is on the estimation of the frictional drag coefficient. Cukier [40] proposed eq. 17 for strongly cross-linked networks (rigid polymeric chains, chemical gels) and eq. 18 for weakly cross-linked networks (flexible polymeric chains, physical gels):

$$\frac{D_{3,s}}{D_{3,1}} = \exp \left[ - \left( \frac{3\pi L_c N_A}{M_f \ln(L_c / 2r_f)} \right) r_s \phi_2^{0.5} \right] \quad (17)$$

$$\frac{D_{3,s}}{D_{3,1}} = \exp \left[ -k_c r_s \phi_2^{0.75} \right] \quad (18)$$

In eq. 17,  $L_c$  is the length of the polymeric chain,  $N_A$  is the Avogadro number,  $M_f$  is the molecular weight of the polymeric chain, and  $r_f$  is the polymer fiber radius. In eq. 18,  $k_c$  is a parameter depending on the polymer–solvent system. On the basis of the flow through a porous network, Phillips et al. [41] have obtained eq. 19:

$$\frac{D_{3,s}}{D_{3,1}} = \left[ 1 + \left( \frac{r_s^2}{k} \right)^{0.5} + \frac{1}{3} \frac{r_s^2}{k} \right]^{-1} \quad (19)$$

$$k = (0.31) r_s^2 \phi_2^{-1.17}$$

where  $k$  is the hydraulic permeability of the medium, considered to be made of straight and rigid fibers oriented in a random three-dimensional way.

### Obstruction theories

The obstruction theories are based on the sieve effect due to the presence of an impenetrable polymer network. The diffusion takes place through the holes in the network; therefore, the path length is increased with respect to the diffusion in pure solvent. The retardation effect is thus calculated on the basis of the sieve effect. Different equations are obtained on the basis of

the different model for the polymer network. A useful parameter is given by eq. 20, in which  $r_f$  is the polymer fiber radius:

$$\alpha = \left( \frac{r_s + r_f}{r_f} \right)^2 \phi_2 \quad (20)$$

Most of the models based on obstruction theories have the same mathematical structure, given by eq. 21. The two parameters  $\{a, b\}$  are listed in Table 1 for different models (for Amsden's model,  $k_1$  is a further parameter depending from the polymer-solvent system).

$$\frac{D_{3,s}}{D_{3,1}} = \exp[-a \cdot \alpha^b] \quad (21)$$

Model		$a$	$b$
Ogston et al.	[42]	1.00	0.50
Johansson et al.	[43]	0.84	1.09
Amsden	[38]	$\frac{\pi}{(k_1 + 2\phi_2^{0.5})^2}$	1.00

**Table 1.** Obstruction theory-based models

By analogy with electrical conduction, Tsai and Strieder [44] proposed a different model, given by eq. 22:

$$\frac{D_{3,s}}{D_{3,1}} = \left( 1 + \frac{2}{3} \alpha \right)^{-1} \quad (22)$$

Obstruction theories are better applicable to heterogeneous networks made of rigid polymeric chains.

### Combined (hydrodynamic and obstruction) theories

To improve the predictive capability of hydrodynamic and obstruction models, their retardation effects can be multiplied with each other. For example, Johansson et al. [45] combined their obstruction model [43] with the hydrodynamic model by Phillips et al. [41], obtaining eq. 23 which is a better predictor than the two parent models:

$$\frac{D_{3,s}}{D_{3,1}} = \frac{\exp(-0.84\alpha^{1.09})}{\left[ 1 + \left( \frac{r_s^2}{k} \right)^{0.5} + \frac{1}{3} \frac{r_s^2}{k} \right]} \quad (23)$$

Another example is given by Clague and Phillips [46], who proposed a structure for the hydrodynamic term, and then they coupled this last with the obstruction model proposed by Tsai and Streider [44]. The resulting model is given here as eq. 24:

$$\frac{D_{3,s}}{D_{3,1}} = \left(1 + \frac{2}{3}\alpha\right)^{-1} \exp\left[-\pi\phi_2^{(0.174)\ln(59.6r_f/r_s)}(r_f/r_s)\right] \quad (24)$$

### Free volume theory

According to the free volume theory, a molecule of solute diffuses through the hydrogel by “jumping” into void which is present in the network. The free volume is the volume of the holes, formed on statistical bases due to random thermal motions. The total free volume is due to the water (solvent, index “w” or “1”) and to the polymer (index “p” or “2”), neglecting the presence of the drug, i.e.,  $v_f = \phi_1 v_{f,w} + \phi_2 v_{f,p}$ . Assuming that the free volume in the polymer,  $v_{f,p}$  is negligible,  $v_f \approx (1 - \phi_2)v_{f,w}$ . The retardation effect can be evaluated on the basis of statistical reasoning, accounting for the probabilities of finding holes in the water free volume,  $v_{f,w}$ , close enough to the molecule which is moving, accounting that such holes are big enough and accounting for the sieving effects by the polymeric chains. Different estimations for these probabilities give different results for the retardation effect; however, the general structure of models for retardation effect, based on free volume theory, is always given by eq. 25. The two parameters {a, b} are listed in Table 2 for the most common models. The parameter “a” plays the role of a sieving factor of the polymer network on the solute molecule, and for drug size smaller than the mesh size ( $r_s \ll \xi$ ), a is unity.

$$\frac{D_{3,s}}{D_{3,1}} = a \cdot \exp\left[-b\left(\frac{\phi_2}{1 - \phi_2}\right)\right] \quad (25)$$

Model		a	b
Yasuda et al.	[47]	$P_0$	$\frac{Ba^*}{v_{f,w}}$
Peppas and Reinhart	[48]	$k_1 \left(\frac{\bar{M}_c - \bar{M}_c^*}{\bar{M}_n - \bar{M}_c^*}\right)$	$k_2 r_s^2$
Lustig and Peppas	[49]	$\left(1 - \frac{r_s}{\xi}\right)$	$\frac{\gamma\pi\lambda}{v_{f,w}} r_s^2 \cong 1$
Hennink et al.	[50]	$\Psi$	$k_2 r_s^2$

**Table 2.** Free volume theory-based models

In Table 2, the meanings of the parameters are  $P_0$  is the probability of finding an opening between the polymer chains (sieve effect);  $a^*$  is the effective cross-sectional area of the solute

molecule;  $B$  is a model parameter;  $k_1$  and  $k_2$  are two structural constants, different for each polymer–solvent system;  $\bar{M}_c^*$  is a critical molecular weight between cross-links to allow solute passage;  $\gamma$  is a numerical factor ( $0.5 \leq \gamma \leq 1.0$ ) used to correct overlapping of free volume between more than one solute molecule;  $\lambda$  is the jump length, which is roughly equivalent to the solute diameter ( $\lambda \approx 2r_s$ ); and  $\Psi$  is the sieving factor.

All the models listed in equations 17 to 25 are useful to have an idea of the retardation effect, but still there is not a single approach able to describe the behavior of all the hydrogels. Therefore, for modeling purposes, a phenomenological approach, based on simple equations, with a limited number of fitting parameters, is highly desirable. As a result of the free-volume approach, a simple equation useful to predict the diffusive coefficient for a given molecule specie “ $i$ ” in hydrogel, with respect to the diffusive coefficient of the same molecule in the swollen network (at equilibrium conditions),  $D_{i,H} / D_{i,s}$ , has been proposed by Fujita [51], used firstly by Korsmeyer et al. [52], to describe the transport of both the solvent ( $i=1$ ) and the solute ( $i=3$ ) within the polymeric network:

$$\frac{D_{i,H}}{D_{i,s}} = \exp \left[ -\beta_i \left( 1 - \frac{\phi_1}{\phi_{1,s}} \right) \right] \quad (26)$$

where  $\beta_i$  is the single parameter of the equation, and the effect of this parameter on the predictions has been extensively tested by Korsmeyer et al. [53].

### 1.3. Phenomenology of drug release from swelling hydrogels

In controlled drug delivery, the main goal is to design systems able to give tailored release profiles, as function of the time as well as in response to external stimuli (sensitive systems) and/or in a certain environment (targeted delivery systems). One of the main goals of controlled drug delivery is a system able to give a zero-order release kinetics, i.e., a constant-rate release, for which the mass flow rate of drug released is designed to be equal to the rate of consumption of the drug by the body (by metabolism, excretion, and reactions with its targets), causing a constant plasma concentration of the active principle. Graham and McNeill [54] were the first to prove that by combination of the device geometry, nature of hydrogel, and initial concentration profile of the drug, a zero-order release kinetics is possible working with hydrogel-based systems (morphine release from pessaries shaped as hollow cylinders made of PEO, with a U-shaped initial concentration of the drug through the cylinder wall). This was the starting point for several studies, development, and applications of hydrogel-based pharmaceutical systems for drug delivery. Several pharmaceuticals based on this approach have made their way up to the market.

A full understanding of the phenomena involved, and their detailed mathematical description (modeling), is an objective still unfulfilled. The detailed knowledge of the transport phenomena involved is the key prerequisite in developing a reliable mathematical model useful for

the prediction of the release kinetics as function of the formulation parameters or of the external conditions [55]; on the other hand, the availability of a reliable mathematical model of the drug release process could allow to theoretically predict the drug release profile for a given, newly designed, pharmaceutical product, reducing the number of necessary experiments and facilitating the development of new pharmaceuticals [11].

The basics of release mechanisms from swellable hydrogel-based pharmaceuticals are summarized in the following and they are schematized in Figure 2.

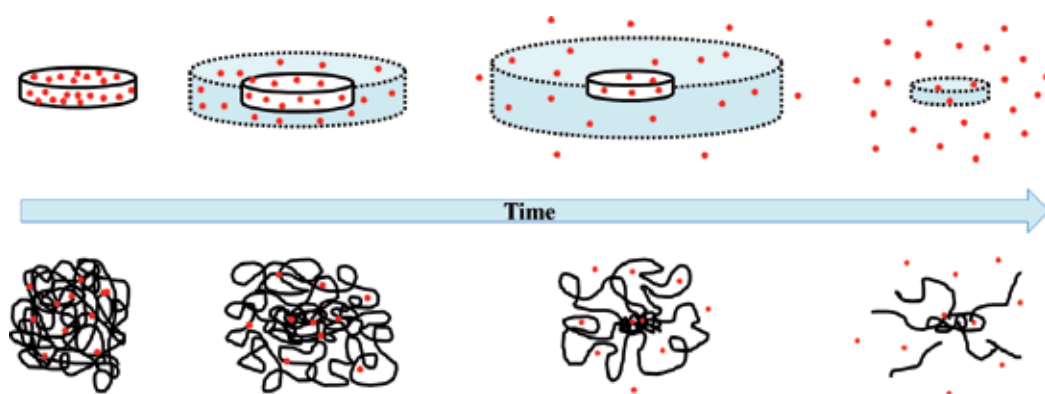


**Figure 2.** Drug release from a matrix (tablet) made of swellable hydrogel. The phenomena (described in the text) of water uptake, swelling, polymer chain relaxation, drug diffusion, polymer chain disentanglement, and polymer erosion are graphically depicted.

When swellable hydrogel-based matrix comes into contact with water, the following are observed:

1. The water diffuses into the matrix.
2. The water acts as a plasticizer, lowering the polymer glass transition temperature,  $T_g$ , thus causing the glass–rubber transition, the gel formation, and polymer swelling (polymer chain relaxation).
3. The (soluble) drug dissolves and diffuses through the gel layer.
4. The drug can be released in the dissolution medium.
5. Finally, the polymer dissolves (erodes) at the matrix surface. In case of insoluble drugs, erosion is the main mechanism which allows drug release in the external medium.

This sequence of steps, suggested by Siepmann et al. [56], is coherent with a space distribution of the polymer chains as described by Ju et al. [57, 58], who identified several regions in a hydrogel-based matrix exposed to a water-based dissolution medium:

1. An inner *dry glassy core*, in which the polymer is practically un-hydrated

2. A *glassy gel layer*, in which the polymeric chains have very strong entanglements
3. A *rubbery gel layer*, with highly swollen hydrogels and strong entanglement
4. A *diffusion layer*, with weak entanglements within the few polymeric chains present
5. The external, or *bulk*, medium, in which the dissolved polymeric chains are found

These layers, which are not rigidly defined and thus not clearly identifiable, are characterized by a polymer concentration decreasing from the inner regions toward the outer regions, a water concentration decreasing from the outer regions toward the inner regions. Furthermore, they allow to identify several “fronts,” i.e., interfaces which roughly locate the place in which most of the phenomena take place [59]. In particular, the interface between the diffusion layer and the bulk medium is known as the *erosion front* (because it is the surface on which most of the polymer erosion takes place), the interface between the rubbery gel layer and the diffusion layer is known as the *diffusion front* (because it is the place in which most of the drug diffusion takes place), and the interface between the glassy gel layer and the rubbery gel layer is known as the *swelling front* (because it is the place in which the polymer swells, experiencing the glass–rubber transition).

#### 1.4. Swellable hydrogels in drug delivery: A path to understanding

Once the general framework of the phenomena which take place during the drug release from a hydrogel-based pharmaceutical system has been clarified, there are still two needs:

1. The single phenomenon (e.g., the water uptake, the drug diffusion, the polymer dissolution, the shape deformation due to the swelling) has to be quantified, i.e., one or more experimental method(s) have to be pointed out, applied, and validated in order to gather quantitative data useful to confirm the hypothesized phenomenon and to know its extent.
2. Each single observed and quantified phenomenon has to be described by a mathematical sub-model, and all of them together should be collected in a comprehensive mathematical model, able to reproduce quantitatively all the observed phenomena: at this level, the model can be seen as a *descriptive* tool. Once all the sub-models have been properly tuned using experimental data, the model could become *predictive*, i.e., able to describe the behavior of a novel system before it is tested or to describe the behavior of an existing system working outside the range of operative conditions within which it has been tested.

The road to the goal of a predictive model is pictorially depicted in Figure 3: on the right of the arrow, several experimental approaches published in literature have been listed (grouped by the main technique adopted in each paper); on the left of the arrow, the succession of modeling approaches proposed in literature is listed (grouped by similarity between the approaches). Of course, the lists are not exhaustive, since a huge number of papers on the topic have been published in the last years. In the remainder of the chapter, the experimental approaches (section 2) and the modeling approaches (section 3) will be reviewed in better details.

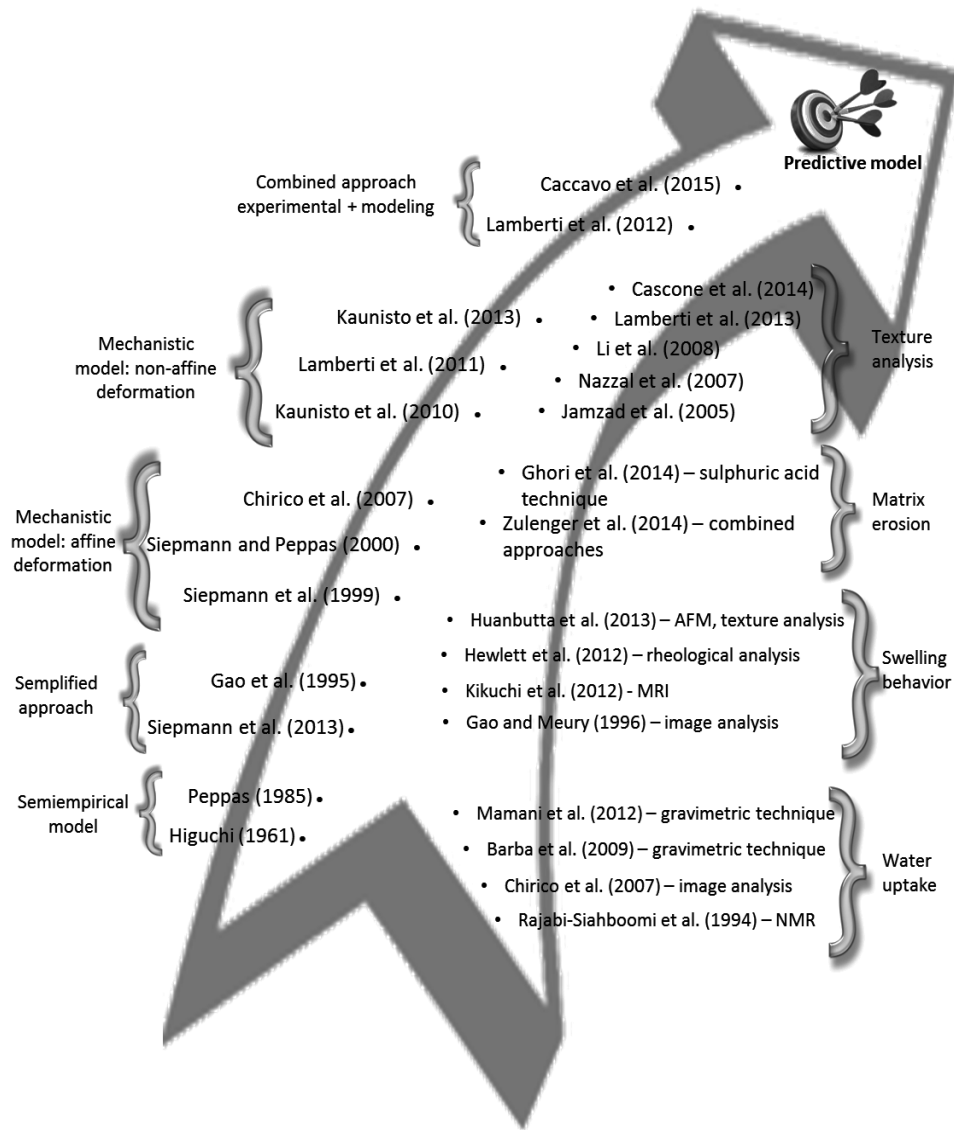


**Figure 3.** The evolution of experimental approaches (on the right of the arrow) and of theoretical approaches (on the left of the arrow) reported in literature with reference to the study of drug release from matrix made of swellable hydrogels.

## 2. Experimental approaches

The study of hydrogel-based systems started on simplified systems (simple geometries such as cylinders or sheets, in which only 1D – for example, lateral – water uptake is allowed) and

has been continued on more complicated systems (i.e., pharmaceutical forms composed of several units, each with a specific behavior). The complexity of the whole process which takes place during the drug release from hydrogel-based matrices has led to the development of several experimental techniques to deeply understand the behavior of these polymers.

## 2.1. Factors influencing the drug release

The factors influencing the drug release from hydrogel matrices have been studied for a long time to create a pharmaceutical form with the desired release profile both theoretically and experimentally. In fact, it has to be taken into account that, in addition to the phenomena which take place during a hydrogel hydration, the presence of a local drug concentration influences the polymer behavior [60]. As described in section 1.3, during the water uptake, the polymer chains are subjected to a relaxation, and the presence of an additional component (the drug) changes both the swelling osmotic pressure and the time-dependent relaxation process. Of course, not only the drug has an impact on the release rate from a hydrogel based matrix, but the entire formulation and its constituents influence the matrix behavior.

### 2.1.1. Influence of the formulation composition

Among these variables, the polymer concentration and its viscosity grade are the most used to control and modulate the drug release [61] due to the fact that the drug release profile is affected both kinetically and mechanistically by these two variables. For example, changes in HPMC (hydroxypropyl methylcellulose) percentages in the formulation can result in a wide range of release rate, but usually, faster drug release rate is obtained with lower HPMC content, as well as faster polymer release is obtained in these conditions. In the analysis of the influence of the HPMC viscosity grade on the drug release, it was demonstrated that the release rate decreases with the increase of the viscosity of the used polymer, but there is a “limiting HPMC viscosity grade” and beyond its value, no further decrease in the release rate is detected; usually, this value is 15000 cP [61]. These analyses can be performed only by evaluating the drug release in the dissolution medium; instead, more complex experimental methods are necessary to evaluate the microscopic variation in surface topography during the swelling such as the cryogenic SEM [62].

In the optimization of the matrix formulation, it is important to evaluate not only the composition of the matrix but even the micrometric properties such as the bulk density of the powders used. The true density of the powders can be measured using a pycnometer. The bulk density can be calculated pouring a pre-weighted amount of powder into a graduated cylinder and measuring the occupied volume. The tapped bulk density can be calculated by measuring the powder volume after tapping the cylinder three times from a defined height and with a constant frequency (i.e., from 2.5 cm height every 2 s); the ultimate tapped density can be calculated after continued tapping till no further volume decrease is observed [62]. The compressibility index was calculated using the bulk and ultimate tapped bulk density.

### 2.1.2. Influence of the polymer properties

In addition to the type of formulation, the drug release profile from a pharmaceutical form is affected by factors closely related to the polymer, such as its particle size distribution [63]. Studying the release rate of propranolol hydrochloride from HPMC K15M tablet, it was found that the release rate decreased as the particle size of polymer was reduced till about 180  $\mu\text{m}$ . Further reduction caused no further decrease in dissolution rate. The different particle size fractions are usually obtained by sieving. This behavior is probably due to the fact that the larger-sized fraction of HPMC absorbs water faster than the smaller one [63]. These water uptake studies were performed by using DSC (differential scanning calorimetry). Of course, the behavior of the matrix strongly depends on the polymer chosen to constitute the pharmaceutical form. For example, Zuleger et al. [64] found that neither viscosity grade nor the particle size or the compaction pressure of methyl hydroxyethyl cellulose (MHEC) has a strong impact on the release rate of the drug embedded in these matrices. Thus, there is not a general rule from the matrix behavior; it depends on the formulation and drug used. Moreover, even the dissolution medium can influence the release kinetics, both in the case in which the polymer is sensitive to the medium pH and to the ionic strength of the medium.

A recent review on the factors affecting the drug release from hydrophilic matrices was published by Maderuelo et al. [65]. The authors analyzed the effect of different variables, which depend on drug (such as its solubility, particle size, and initial dose), on polymer (such as its particle size, viscosity, and the influence of the dissolution medium), or on formulation (such as manufacturing process) on the drug release kinetics.

## 2.2. Evaluation of the water uptake, matrix erosion, and drug release

The water uptake is a key parameter to determine the swelling phenomenon of a hydrogel and, as a consequence, the drug release from a matrix. For this reason, several scientists have developed different methods to quantify the water diffusion into the polymeric matrix.

The simplest technique used to evaluate the weight gain after a certain dissolution time, which is directly connected to the water uptake, is the gravimetric method. According to this method, the weighted pharmaceutical form is immersed in the dissolution medium and, at predetermined time intervals, it is withdrawn from the medium, lightly patted, and weighted, and then it is dried until constant weight is reached [66]. The percent weight gain and the mass loss can be calculated according to the following equations:

$$\text{Weight gain (\%)} = \frac{\text{wet weight} - \text{dry weight}}{\text{dry weight}} \cdot 100 \quad (27)$$

$$\text{Mass loss (\%)} = \frac{\text{initial weight} - \text{dry weight}}{\text{initial weight}} \cdot 100 \quad (28)$$

The percent of mass loss is directly connected to the matrix erosion and drug release (if drug is contained in the polymer matrix) due to the fact that, after drying, only the polymer and drug remain in the matrix, meaning that all the weight loss during the dissolution is imputable to the dissolution of drug and polymer in the external medium. Investigation of matrix hydration and erosion is a fundamental approach to understand the mechanisms involved during the drug release and the parameters which influence the matrix behavior [67]. For example, if the mass loss follows an increasing kinetics with the dissolution time, probably the controlling mechanism in the pharmaceuticals is the erosion of the matrix; on the contrary, if the weight gain continuously increases, the controlling mechanism can be attributed to the swelling. On these bases, Mamani et al. [68] evaluated the influence of components ratio on the release kinetics varying the composition and pH of the dissolution medium.

Thus, the information which can be obtained by the estimation of the mass determination via gravimetric analysis is the concentration profiles of water and polymer. If the matrix analyzed is composed also of a drug, with the aid of an analytical technique to determine the amount of drug released (i.e., the spectrometric method), all the macroscopic profiles can be measured [69]. Indeed, during the dissolution, the drug leaves the pharmaceutical form and dissolves in the dissolution medium. A typical dissolution test is performed using the standardized apparatuses approved by the USP (United States Pharmacopeia), which are numbered from 1 to 7 [70]. Withdrawing samples of the medium at certain time intervals, it is possible to know the amount of drug released and then, by the difference with the initial drug content, which is usually known by the manufacturer, the amount of drug still contained in the tablet. Repeating these tests for several dissolution times, the drug concentration profile can be evaluated. Usually, the percentage of drug release is evaluated according to the following expression:

$$\text{Drug release(\%)} = \frac{\text{drug released in the dissolution medium}}{\text{initial drug content}} \cdot 100 \quad (29)$$

The typical drug release profile from a matrix composed of a hydrogel (HPMC) and a drug (theophylline) is shown in Figure 4, red circles on the right axis [34]. As could be expected, the release kinetics is higher at the beginning of the dissolution (after 3 h of dissolution, about 30 % of the drug is released) and tends to decrease with time, till all of the drug contained into the matrix reaches the dissolution medium. On the contrary, the mass of the drug still contained in the matrix is shown in Figure 4 as green stars, on the left axis. It can be measured by the difference between the drug released and the initial amount of drug in the tablet or by a more direct measure. According to this method, after the chosen dissolution time, the tablet is removed from the medium, weighted, and dried. Then, the tablet is immersed into a medium till complete dissolution, and another spectrometric analysis can be performed on the medium to evaluate the concentration of the drug. Usually this technique is used to perform a check on the total amount of drug in the matrix, which can be different with respect to the theoretical one, i.e., due to manufacture errors.

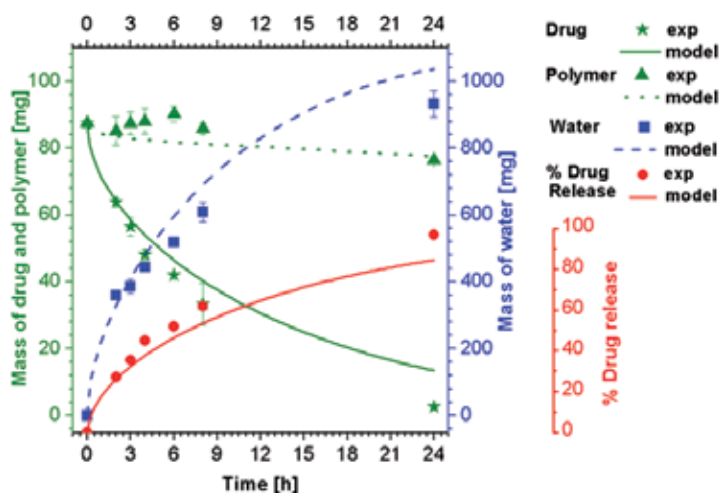


**Figure 4.** Mass evolution inside a swelling matrix during a dissolution test. Drug and polymer mass evolutions (in green) are reported on the left axis and water mass evolution (in blue) on the right axis. On the red axis, the percentage of drug released is shown.

Using the gravimetric technique to evaluate the total amount of water absorbed by the matrix, the method previously described to evaluate the weight gained by the pharmaceutical form can be used. After a certain dissolution time, the matrix can be removed from the dissolution medium, weighted, dried, and weighted again. By the difference between the wet and dry weights, the amount of water taken during the dissolution (after the predetermined time) can be evaluated. In Figure 4, the mass of water absorbed by the tablet is shown as blue squares, on the right axis. As could be seen from the graph, the amount of water which can be absorbed by a hydrogel is well beyond the initial amount of polymer, reaching ten times its value during the time interval shown. The last component which has to be quantified is the polymer. This can be done by a simple technique which provides that once the wet weight of the matrix after a certain dissolution time is known and once the drug and water amounts are quantified, the polymer mass can be calculated by the difference between these masses, according to the following expression:

$$\text{Polymer mass} = \text{wet weight (after dissolution)} - (\text{water} + \text{drug}) \text{ masses inside the matrix} \quad (30)$$

Another technique which allows to directly evaluate the amount of polymer dissolved in the dissolution medium and then of the polymer into the tablet is the sulfuric acid technique, recently re-proposed by Ghori et al. [71]. This method consists of taking from the dissolution medium samples of 1 mL at predetermined dissolution times and, after filtration, adding 1 mL of a solution of 5 % phenol in 0.1 M hydrochloric acid, followed by 5 mL of concentrated sulfuric acid. After 10 min of shaking, the solution is cooled (the reaction taking place is strongly exothermic), and a spectrometric analysis can be performed, at 490 nm of wavelength, due to

the fact that the solution assumes an intense colored aspect. Besides, this method is more complicated than the measurement of the difference between components; it is a direct measurement of the polymer mass, which means a more reliable matrix characterization.

### 2.3. Mass evolution inside the matrix

The described gravimetric technique has the practical advantage to be a very simple technique to determine the macroscopic behavior of a pharmaceutical matrix (i.e., the total water uptake, the total mass of polymer eroded by the dissolution medium) or films [72]. On the other hand, it is a destructive technique (different samples have to be removed from the dissolution medium and dried, one for each dissolution time) which gives no information about the concentration profiles inside the matrix and about how they vary with time. For this reason, it is clear that the macroscopic analyses described above are not sufficient to characterize the matrix behavior. Over the years, several experimental techniques have been developed to evaluate the mass evolution inside pharmaceutical matrices.

#### 2.3.1. Image analysis technique

To evaluate the polymer concentration across the gel layer during the tablet hydration, a semiquantitative in situ technique based on the image analysis was developed [73]. According to this method, a HPMC matrix tablet was mounted on a weighted pin and inserted in a vessel filled with the dissolution medium. This stirred vessel was placed on top of a light box. Depending on the orientation of the tablet, the swelling along the radial or axial position can be observed and recorded by a black-and-white camera equipped with a macroscopic zoom lens mounted above the tablet. The light source was represented by a light box containing two fluorescent light tubes. The whole apparatus was closed to avoid the entrance of external sources of light. Each digitalized image had a gray level from 0 (black) to 255 (white) representing the relative scattered light intensity. To understand and explain the results obtained, it was necessary to correlate the scattered light intensity with the concentration of HPMC in the gel layer. This has been done in preparing a series of polymer solutions at known concentrations and evaluating their scattered light intensity, and, by the fitting of these data, a calibration curve to interpret the data was obtained. Due to the complexity involved in the simultaneous evaluation of what happens during the polymer matrix swelling, Bettini et al. [59] used the image analysis to evaluate the movement of the swelling front (as defined in section 1.3) of a tablet during the dissolution in a simplified system which allows the water penetration only in the lateral surface of the tablet. This system was obtained confining the tablet between two transparent Plexiglass disks; in this way, only the radial swelling is allowed, making the system simpler to analyze. Recording the swelling of the matrix during dissolution through the transparent disks, the obtained images were analyzed with image analysis software. Once more, this technique gives no information about the mass fraction evolutions inside the matrix.

On these bases, a nondestructive test to determine the water mass fraction along the radial profile of a pure HPMC tablet was developed by Chirico et al. [55]. Being the tablet composed only by the polymer, this work was focused only on the water penetration inside the matrix, and the tablet was confined between two glass slides to limit the water uptake only in the radial

surface. The system composed of the tablet, confined between the glass slides was immersed in the dissolution medium, colored by adding trypan blue to enhance the visibility of the water penetration, and recorded with a camera. Both the camera and the dissolution chamber were closed in a dark room to avoid exposure to external light. Light intensity profiles were evaluated starting from the pictures by the image analysis technique. The analyses were performed, considering the picture as a matrix composed of pixels with intensity values ranging from 0 (white) to 255 (black). To relate the water mass fraction to the light intensity, a relation was adopted:

$$\left( \frac{I - I_0}{I_{max} - I_0} \right)^\gamma = \frac{\omega_1 - \omega_{10}}{\omega_{1eq} - \omega_{10}} \quad (31)$$

where  $\omega_{10}$  and  $\omega_{1eq}$  are the initial water mass fraction in the tablet (in case of a dry tablet, it is equal to 0) and the equilibrium water mass fraction in the hydrogel, respectively. Concerning the light intensity, it was varied between  $I_0$ , which is a plateau value observed at the matrix core, corresponding to the brightest image, and  $I_{max}$ , which is the maximum value observed at the fully hydrated gel, corresponding to the darkest image. Since both the variables ( $I$  and  $\omega_1$ ) vary from 0 to 1, the authors chose to apply the simplest relation between them, a linear one, which is realized when parameter  $\gamma$  is equal to 1.

A typical water mass fraction profile obtained via image analysis is reported in Figure 5, a) as gray dotted lines. Moreover, an image of the hydrate tablet after 1 day of dissolution is shown as an inset. Comparing the evolution of the water mass fraction calculated via image analysis and the appearance of the tablet, the correspondence is clear. In fact, in the picture, still visible is the glassy core, in which only a small amount of water is penetrated and the water fraction is the smallest; then it starts to increase due to the fact that the image becomes darker. Then, the swelling front (as defined in section 1.3) becomes visible with a decrease of the light intensity, which leads to an apparently inconsistent decrease of the water mass fraction; actually, this decrease is due to the presence of the swelling front. Then, the light intensity increases gradually, due to the fact that the gel is more hydrated as the radius increases, until the erosion radius is reached, which indicates the final dimension of the swollen tablet, corresponding to a light intensity and water fraction equal to 1. The main drawback of the described technique is the fact that only the water uptake inside the matrix can be evaluated due to the fact that the tablet is composed only of the hydrogel. In fact, the presence of the drug could disturb the image analysis, leading to mistakes in the evaluation of water concentration inside the pharmaceutical form. For this reason, a more complete method taking into account also the drug presence has to be developed.

### 2.3.2. Gravimetric technique

In 2009, Barba et al. [69] proposed a method to quantify all the components inside a matrix at a given dissolution time. This approach, based on the gravimetric technique, was applied

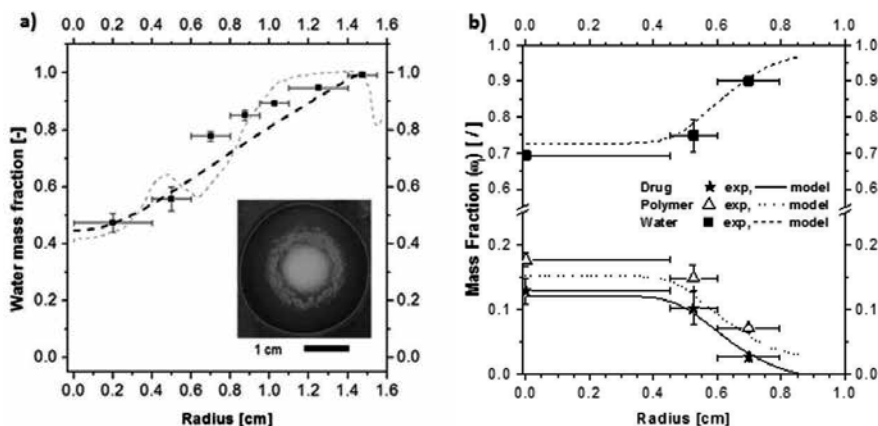


**Figure 5.** a) Water mass fraction along the radial direction after 48 h of dissolution of a radial system. The full squares are the experimental data obtained by the gravimetric analysis; the dotted gray curve is the result of the image analysis; the dashed black curve is the model prediction. In the inset, the real photo of the matrix used for the image analysis. b) Mass fraction evolutions along the radial direction for semioverall system after 6 h of dissolution (the values are averaged along the thickness direction). The scatters are the experimental data; the curves are the model predictions. In both the graphs, the vertical bars represent the standard deviation between the experimental runs, and the horizontal bars represent the extension of the section cut by the punch.

firstly on a simplified system, which allows the water uptake only from the lateral surface (the so-called radial system), and then to a more complex system in which the water can penetrate along the whole exchange area (the so-called semioverall system) [34]. The experimental procedure used to evaluate the mass evolutions (polymer, HPMC; drug, theophylline; and water) inside a swollen matrix is illustrated in Figure 6. In the case of the radial systems, the first step was to confine the matrix, containing a polymer, a drug, and eventually an initial water content, between two glass disks. Instead, in the case of the semioverall systems, the matrix was glued at the center of one glass slide, which represents the symmetry plane for the experiment; in fact, the tablet weighted the half part with respect to that used in the radial system. Then, the system was immersed in the dissolution medium until a predetermined time; at the end of this time, the swollen matrix was removed from the dissolution medium (step 2 in Figure 6) and the excess water was removed; in the case of the radial system, the superior slab was carefully removed. The swollen matrix was cut by a series of punches characterized by a thin wall centered in the matrix center (step 3 in Figure 6). The punches had a decreasing diameter: chosen the first punch and centered, all the matrix material external at the punch is recovered on a watch glass (step 4 in Figure 6) and weighted (step 5 in Figure 6). This material contained all the polymer, drug, and water in the wet tablet at greater radii than the punch one. Then, a punch with a small diameter was used for a second cut and, once more, the material recovered in another watch glass. These operations were repeated since a central core was reached, recovered, and weighted. All the samples collected were dried in oven at 45 °C (step 6 in Figure 6) until a constant weight was reached, meaning that all the water initially contained in the wet material was removed (step 7 in Figure 6). These last three phases can

be combined together using an infrared moisture meter, as suggested by Tahara et al. [74]. Using this device, the wet material was weighted and dried simultaneously at a temperature of 120 °C, until the ratio of decreasing sample weights becomes less than 0.5 % for 5 min. In the last step of the gravimetric analysis, each glass was immersed into a vessel containing distilled water till complete dissolution with the aim of quantifying, spectrometrically, the amount of drug still in the matrix.

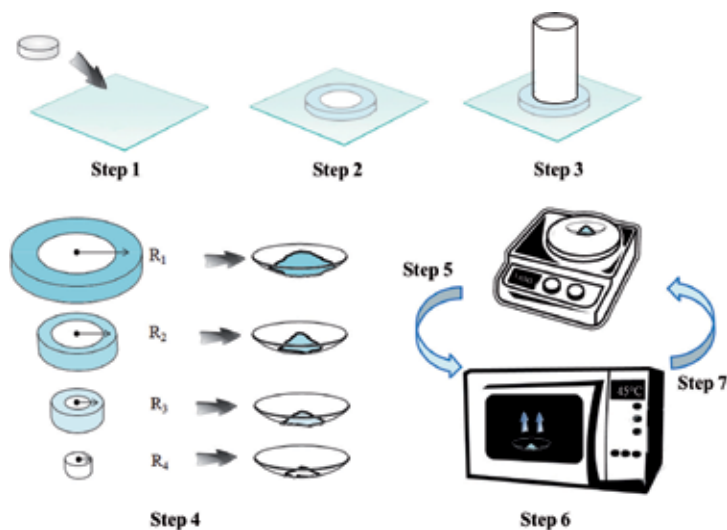


**Figure 6.** Experimental procedure used to evaluate the mass evolutions inside a swollen matrix by gravimetric technique.

Using this method, it is possible to evaluate how the amounts of drug, polymer, and water vary not only with the dissolution time but even with the matrix radius. A typical behavior of a matrix composed initially of 50 % wt of polymer and drug after 6 h of dissolution is reported in Figure 5, b). In this graph, the vertical bars represent the standard deviation between the experimental runs, and the horizontal bars represent the extension of the section cut by the punch. In fact, if the external section is considered, it ranges from 0.6 to 0.8 cm, which means that the punch used had a diameter of 0.6 cm and the wet matrix material recovered had a diameter greater than 0.6 cm and lower than 0.8 cm, which is the maximum radius reached by the swollen matrix. The experimental data were represented at the mean radius of the section of interest, as an average value of mass amount in that section. In Figure 5, the matrix was divided into three sections, two annuli and a central core, and the internal drug and polymer profiles are illustrated as full stars and empty triangles, respectively. As could be seen, both the polymer and drug tend to decrease with the radius; this is easily predictable because, due to the water penetration into the matrix, this tends to unfold the polymeric chains and the drug can easily diffuse outward in the dissolution medium. On the other hand, in the central glassy core, the water is not penetrated yet, and the fractions of the drug and polymer are higher. Concerning the polymer behavior, its fraction decreases with the matrix radius; this is due to

the swelling phenomenon which takes place from the interface of the dissolution medium (the erosion front, as defined in section 1.3) toward the inner regions. Concerning the water profile in the swollen matrix, it is shown as full squares in Figure 5, b). The water mass fraction increases with the matrix radius, till it reaches a fraction equal to 1 at the interface with the dissolution medium, which is completely composed of water.

With the aid of this technique, the swollen tablet is completely characterized not only from a macroscopic point of view but also microscopically, because even the internal concentration profiles are known. As previously mentioned, the main drawback of this experimental method is that it is destructive for the sample analyzed.

The water profiles inside the matrix obtained via image analysis are compared with the gravimetric ones in Figure 5, a). To make comparable the results obtained by the gravimetric and the image analysis techniques, the  $\gamma$  value in eq. 31 was optimized to minimize the distance between the two sets of data for a system composed only of polymer and water. The found value is 0.425; thus, it is far from the unity [75], and it depends on the experimental setup. The gravimetric data are the full squares, and the image analysis results are reported as gray dotted line. As could be seen, in the most part of the profile, the data are in good agreement, even if they originate from very different techniques.

### 2.3.3. Magnetic resonance imaging

Nuclear magnetic resonance imaging (NMRI) is a technique used to produce a two-dimensional map of the density of nuclei inside a thin slice of a more complex object. Besides, the NMRI technique has been extensively used in various fields, such as medical diagnostic and polymer science; in recent years, it has been applied as a noninvasive method to study the behavior of hydrophilic matrices [76]. Usually the nucleus of interest is  $^1\text{H}$  in water molecules; thus, the images show the spatial variation of the local water concentration inside the sample; for this reason, this technique is of great aid to characterize the water content inside a swollen matrix during the dissolution. Moreover, the NMRI technique provides an excellent method to evaluate the self-diffusion coefficients, a measure of transport due to the Brownian motion of molecules in the absence of a chemical concentration gradient [77]. The image experiments were usually carried out to measure the water diffusion inside a polymeric matrix and to observe the changing diameter of a tablet during the swelling [78].

Nuclear magnetic resonance imaging (NMRI) is a branch of NMR spectroscopy, usually used to study the swelling and diffusion phenomena of pharmaceutical forms under static conditions (without stirring). The extent of the swelling can be identified by this technique, identifying the position of the interface between the dry core of the tablet and the swollen region. On the other hand, the erosion front can be identified at the interface between the dissolution medium and the swollen region. A great improvement in the use of the MRI technique had been the development of a release cell where the images could be recorded directly at different times during the dissolution, happening in a stirred device [79]. The stirring of the medium was realized in a small release cell, which was equipped with a rotating disk. Gluing the tablet under the rotating disk, the relative movement of the tablet and the dissolution medium ensured the stirring. During the test, the MRI probe was placed at 1 mm below the rotating

disk to optimize the tablet position. The release cell is connected to a vessel containing the dissolution medium, kept at constant temperature, which is continuously pumped in the cell by a peristaltic pump. The described setup was used to describe the water uptake into polyethylenoxide (PEO) matrices during a dissolution test [79]. The disk rotation was switched off 2 min before the start of imaging sequences, both in axial and radial directions, and samples of the dissolution medium were collected. The study of the water uptake in the tablet was performed using a multi-spin pulse sequence, in which the signal intensity is weighted on the bases of the proton spin-spin and spin-lattice relaxation times. Due to the very short proton spin-spin relaxation time, differences on the image intensity were mainly dependent on the properties of the dissolution medium. Once the experimental setup was built, it was possible to use this device to better understand the swelling and erosion phenomena happening during the dissolution of a complex matrix. For example, extended release tablets of HPMC were studied via this NMR microimaging technique, and the influence of additives solubility on the matrix behavior was analyzed [80]. By the use of this technique, the authors found that the rate of matrix erosion depends not only on the polymer fraction but even on the solubility of the additives used in the formulation and on the HPMC substituent heterogeneity [81].

In Figure 7, a), a typical example of the use of the NMRI technique to evaluate the water content of a matrix during dissolution is shown. The real picture was taken after 2.7 h of dissolution. At each pixel of the image (128x128) is associated a numerical value that, with the proper scaling factor (given by the instrument), can be related to the proton T2 relaxation. The proton T2 relaxation in turn is mainly attributed to water protons; therefore, it can be related to the amount of water through specific calibration curves. These calibration curves were obtained by analyzing water solutions with known concentrations of solutes. The calibration curve equation obtained with an exponential decay function of the second order was

$$\text{H}_2\text{O}\%_{(w/w)} = a_1 - a_2 \exp\left(-\frac{\text{T2}}{a_3}\right) - a_4 \exp\left(-\frac{\text{T2}}{a_5}\right) \quad (32)$$

where  $a_1 \div a_5$  are specific parameters. The range of confidence of the calibration curve is 60–100 % w/w of water content [34]. The experimental results were shown using different colors to indicate different hydration levels. For example, the blue color was used to indicate the layer of the matrix which showed a percentage of water, included between 60 and 65 %. The results showed a water concentration profile along the “*r*” and “*z*” axes with the 97 % w/w of water content on the erosion boundaries and with a decreasing trend going toward the tablet core. It is worth noting that in this system, the most hydrated layer, 90–97 % w/w, is extremely thin, due to the high system erosion.

#### 2.3.4. Texture analysis

A recent approach in pharmaceutical research and development consists of the study of the correlation between drug release and polymer hydration via texture analysis. In general, variation in the textural and physic-mechanical properties could be associated with changes

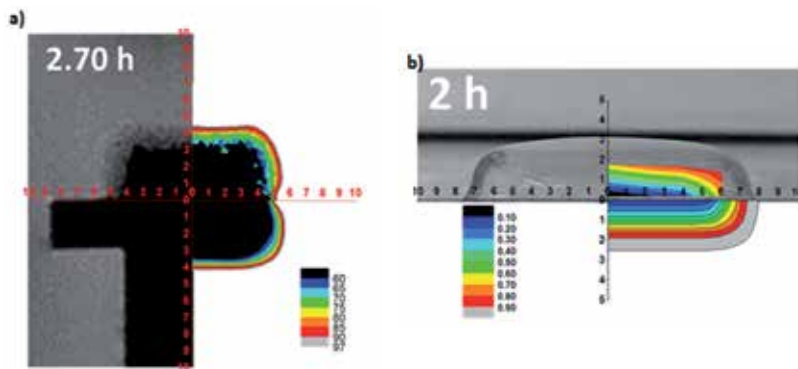


**Figure 7.** a) On the left, NMR image of a swollen matrix composed of HPMC after 2.7 h of dissolution. At the top, experimental water fraction distribution; at the bottom, calculated water fraction distribution. b) On the left top, photo of a semioverall system after 2 h of dissolution (the matrix was cut along its diameter). On the right top, experimental water mass fraction obtained by texture analysis; on the bottom right, model predictions. In both images, the dimensions are in mm; the color scale is referred to the water content fraction (black = lower water content; gray = fully hydrated matrix).

in gel layer and glassy core [82]. One of the first approaches in using the texture analysis to correlate the mechanical properties of the polymeric gels and the water content was that of Yang et al. [82]. They proposed the use of a texture analyzer to evaluate the stress–strain behavior of the polymeric matrix. A matrix composed of HPMC and PEO at different compositions was subjected to dissolution tests. After predetermined time intervals, they were removed from the dissolution medium and subjected to a texture analysis. A probe of 2 mm in diameter was forced to penetrate inside the matrix and a transducer measured the resistance force opposed by the material to the probe penetration. The penetration was ended when a trigger force was reached (0.7 g), the value chosen in a manner in which it was possible to distinguish the glassy polymer from the polymer gel. From the slope of the force–displacement diagrams obtained, it was possible to establish the position of the gel layer; in fact, the resistance encountered by the texture probe is dependent on the gel strength; thus, in the inner part of the tablet, where the water was not penetrated and the gel was strong, the slope of the diagram was very high. On the contrary, in the external parts of the matrix, where the water was penetrated, the resistance encountered by the probe is lower, due to the fact that the gel was hydrated and the slope of the diagrams results to be less pronounced. Based on these considerations, the glassy core and rubbery gel interface can be determined, as well as the overall gel strength. To validate the reliability of these evaluations, the texture experimental data were compared with the position of the gel fronts measured by the NMRI technique. The main drawback of this method is the fact that it is not quantitative: in fact, only the position of the gel front can be quantified, not the water content in the matrix.

In addition to the determination of gel layer thickness and the movement of the erosion and swelling fronts, the texture analysis could be used to determine the total work of probe penetration inside the swollen matrix [66]. Using a method similar to that described previously, swollen thickness was determined by measuring the total probe displacement value (given by

the instrument), the axial swelling can be determined by the force–displacement diagrams, and, finally, the work of penetration can be determined by the integration of the force–displacement curve (the area under the curve). The total work of penetration indicates the matrix stiffness or rigidity, and its evaluation can be helpful to understand the effect of an additive on a matrix formulation and how it affects its properties. Moreover, it has to be considered that the gel strength of a matrix system has a great relevance *in vivo* due to exposure to destructive forces in the gastrointestinal tract.

In 2008, a novel nondestructive probe equipped with a texture analyzer was developed [83], which can be used directly in the dissolution medium during the run. With the use of this probe, the swelling, the erosion, and the positions of the rubbery region and of the glassy core can be simultaneously measured. The probe is constituted by a body through which two supports can move. A circular plate with a central hole contains a fixed probe, which can be exposed outside when the plate is pushed upward. The plate is connected to the movable supports in the probe body. During the analysis, the body of the probe and the plate move downward in the dissolving tablet direction. The loading cell is calibrated in a manner that does not trigger the cell with the movement of the plate in the dissolution medium (the resistance is too low). On the contrary, when the plate reaches the surface of the swollen tablet, it is forced to stop its movement or to move upward if the tablet continues its expansion (due to the swelling). This movement forces the supports connected with the plate to slide into the probe body; this action triggers the load cell which starts to record the resistance force. This movement continues till the probe passes through the hole in the plate and reaches the swollen tablet. The probe is stopped when it reaches a maximum force of 150 g and returns in its original position. This procedure is repeated at preset time intervals and allows the evaluation of the relationship between the thickness of the glassy core and the swollen rubbery region with time. Using the texture analysis technique, various mathematical correlations can be obtained, such as the correlation between the drug dissolution and the polymer hydration obtained by Li and Gu [84]. Modified release tablets were subjected to a conventional dissolution test after their snapping into cylindrical caps, which had a diameter equal to the tablet time. The sample prepared allows the water penetration only along one direction (from the surface exposed to the dissolution medium); in this way, the analysis was significantly simplified. Then, these samples were subjected to a conventional dissolution test and then removed from the dissolution medium and subjected to a texture analysis. The relationship between polymer hydration and drug dissolution was obtained, correlating texture analysis parameters (such as the area under the force–displacement graph), drug release rate, and PEO proportion in the matrix by a mathematical fitting based on both linear and multiple regressions.

With the aim to quantify the amount of water penetrating into a hydrogel-based matrix, using a fast and simple technique, such as the texture analysis, a correlation between the percentage of water content and the penetration work resulting from an indentation test was developed [85]. In this case, matrices composed of HPMC and a model drug were confined between two glass slides, to allow the water uptake only by the radial direction and then immersed in the dissolution medium. After predefined times, the system (composed by the swollen matrix and the slabs) was withdrawn from the medium and the superior slab removed. Due to this sample

preparation, the water amount in the matrix changes along the radius (at different radii, there is a different hydration level), but axially, the water content is the same. In particular, at the same radius, the water content is the same in all the matrix thickness. A texture analysis, in particular an indentation test, was performed on these swollen samples. A needle was used to penetrate, at a constant rate, into the matrix, and a diagram force–displacement was obtained. This procedure was repeated at several distances from the center of the matrix, to evaluate how the resistance force changes with the radius of the tablet. For each radius value, a force–displacement diagram was obtained, and, by the calculation of the area under the curve, the work of penetration of the needle to penetrate into the tablet was calculated. In parallel, a gravimetric analysis (described in section 2.3.2) was performed on samples hydrated with the same procedure to obtain the water profiles inside the swollen matrix. The gravimetric data obtained were fitted using a Boltzmann-type equation to obtain a continuous trend of the water mass fraction inside the swollen matrix. Then, the results obtained in terms of water content (evaluated by the gravimetric technique) and the work of penetration (evaluated by the texture analysis) were compared to find a relation between them. A simple relation was obtained:

$$\omega_1(W_p) = \frac{b_1}{1 + (b_2 W_p)^{b_3}} \quad (33)$$

where  $b_1$ ,  $b_2$ ,  $b_3$  are equation parameters,  $\omega_1$  is the water mass fraction, and  $W_p$  is the penetration work. As expected, the penetration work decreases, increasing the water content; this is due to the fact that more hydrated is the matrix, more gel is formed, and less force is necessary to penetrate into the sample. The main drawback of this technique is the fact that this relation between the work and the water content is possible and reliable only if the water content along the matrix thickness is constant (the force–displacement curves are linear); in the cases where the matrix swells both in axial and radial directions, this relation is not so immediate.

Thus, this technique was improved to correlate the water content to the slope of the force–displacement diagrams [86]. This technique was calibrated firstly on the matrix which swells only in the radial direction, since the force increases linearly with the penetration of the matrix. The correlation obtained is

$$\omega_1(dF / ds) = c_1 \text{Log} \left( \frac{dF}{ds} \right) + c_2 \quad (34)$$

where  $c_1$  and  $c_2$  are equation parameters,  $\omega_1$  is the water percentage into the matrix, and  $dF / ds$  is the slope of the force–penetration curves. In this way, a calibration relation was obtained and, in each radius of the matrix, it is possible to know the water percentage. At this point, the method was extended to the matrix swollen both in the radial and in the axial direction, the so-called “semioverall” system. Concerning the texture analysis of these systems, the shape of the force–penetration curves was very different with respect to the previous one. In fact, being

the water content variable even along the thickness (the water penetration happens both in the radial and axial directions), the measured force increases with the penetration of the needle in a nonlinear behavior. In fact, at the beginning of the test, the needle meets the gel layer formed on the top of the swollen tablet; thus, the force necessary to penetrate this layer is very low. Approaching the core of the tablet, where the water is not penetrated enough, the probe needs a higher force to penetrate the tablet, and the values measured by the texture analyzer increase exponentially. This test was repeated for several radii of the swollen matrix, to evaluate how the force necessary to penetrate varies not only with the thickness but even with the radius of the tablet. This behavior is characteristic of all the curves; the force magnitude varies depending on the radius where the penetration is carried on, since the hydration of the matrix occurs also along the radial direction, thus leaving the matrix center the water content increases; that means that the force necessary to penetrate the matrix decreases. Moreover, it has to be considered that also the thickness of the swollen matrix changes at the changing of the radius position. The experimental data are very well fitted by simple exponential curves. It is thus easy to obtain  $dF/ds$  which is, in this case, a function of the penetration distance rather than a single value for each test. Once it is evaluated how the  $dF/ds$  varies, for each radius, along the matrix thickness, it is possible to calculate the respective water content using eq. 34.

The measurement of water content in the axial direction can be repeated for each penetration point for all the hydration times considered. Thus, a contour plot can be drawn and compared with a real picture of the semioverall swollen tablet; in Figure 7, b) is shown a matrix after 2 h of dissolution. The picture taken is of a swollen tablet cut along a diameter, in such a way that the glassy core and the swollen gel are clearly distinguishable. The contour plot represents the water content in the tablet evaluated by the described technique, and it is shown in Figure 7, in the first quarter of the picture. Areas containing the same water amount are colored with the same filling, and, in general, the water content decreases while approaching the glass slide of the tablet. It can be noted that there are zones where it is not possible to evaluate the water content, due to both a water content higher than the limit imposed by the obtained relationship applicability (relationship between the force/displacement derivative and the water content) and the hydration in the more external zones, so high that the force opposed by the gel to the penetration is negligible and not easily detectable by the instrument. The legend of the color used and of the water percentage at which they correspond is shown in the third quarter of the picture.

## 2.4. Characterization of the swelling behavior

In the description of the performances of delivery systems for controlled release, the swelling phenomenon has a central role. For this reason, over the years, several scientists tried to quantify and predict the capability of the matrices to swell and thus release the drug eventually contained inside, usually quantifying the so-called swelling ratio, which corresponds to the weight gain defined in section 2.2. One of the first attempts to describe the swelling phenomenon was that followed by Colombo and his coworkers [87]. The goal of their work was to quantify the matrix relaxation measuring the surface exposed during polymer swelling. To evaluate the influence of the swelling phenomenon on drug release, the amount of drug

released was plotted versus the area of the system, at the same time, obtaining a linear relationship. This result indicates a direct dependence between the drug release and the tablet surface. Moreover, the authors proposed a new dimensionless number in order to correlate the matrix expansion during dissolution to the increase of the releasing area. This number is called the swelling area number,  $N_{Sw.A}$  and it is defined as

$$N_{Sw.A} = \frac{1}{D_{3,s}} \cdot \frac{dA}{dt} \quad (35)$$

where  $dA/dt$  is the rate of the area change during the dissolution and  $D_{3,s}$  is the drug diffusion coefficient in the swollen phase. Thus, this number represents the ratio between the matrix surface area expansion rate and the drug diffusion, weighting the contribution of the swelling and the diffusion phenomena on the drug release. The matrix swelling was determined by a measure of the releasing area from pictures of the matrix taken during the dissolution. By this technique, the influence of the presence of a hydrogel matrix coating on the swelling kinetics can be evaluated [88].

Later, the behavior of gel layer thickness in swellable matrices loaded with drugs was studied using a colorimetric technique [89]. This method was based on the dissolution of a radial system for predetermined intervals and the use of the image analysis technique to evaluate the position of the swelling, the diffusion, and the erosion fronts. This method is based on the fact that the used drug was light yellow in the dry state and became orange in solution, with a color intensity dependent on its concentration. These measures are able only to evaluate the radial position of the fronts, being a 1D analysis. Moreover, the water concentration at the glassy-rubber interface ( $c^*$ ) (thus at the swelling front, as defined in section 1.3) was calculated starting from the glass transition temperature of the polymer ( $T_g$ ) to the experimental temperature ( $T_{exp}$ ), according to the following expression [29]:

$$c^* = \frac{T_g - T_{exp}}{\beta / \alpha_f} \quad (36)$$

where  $\beta$  is the contribution of water to the expansion of the polymer and  $\alpha_f$  is the thermal linear expansion coefficient of the polymer. This equation is usually used in terms of volume fraction of the components because, due to the swelling of the polymer, the volume changes in the swollen tablet. Thus, the water volume fraction can be expressed as water volume per volume of polymer. Thus, from the image analysis, the position of the swelling front can be evaluated and by theoretical consideration, the water concentration at the interface calculated.

As seen in the previous paragraph, the NMRI technique is very useful to monitor the swelling and the erosion phenomena. Proton density- and diffusion-weighted images of the hydrating tablets can be acquired at different intervals, and apparent self-diffusion coefficient maps can

be generated from the diffusion-weighted images [90]. The image intensities characteristic of the swollen tablets obtained from the NMRI analysis are usually evaluated by software, i.e., ImageJ.

During the swelling of a hydrogel, the mechanical properties of the gel, and then of the release formulation, change continuously. Thus, one of the analyses which can be performed to evaluate how the swelling influences the matrix behavior is the rheological characterization of the polymer. The effective elastic modulus and gel thickness during the swelling can be evaluated by indentation tests [91]. In a standard indentation test, the needle moves till it enters in contact with the sample and reaches a specified load target. The results in terms of load and displacement are used to compare the effective elastic modulus and gel thickness during the swelling. In particular, Hewlett et al. defined the effective modulus from the slope of the stress–displacement curve at a stress of 10 kPa at which corresponds the effective thickness, that is, the displacement at the point where the effective modulus was calculated. The definition of the effective elastic modulus allows to compare the behavior of different polymers. On the other hand, the viscoelastic materials are usually characterized in terms of dynamic mechanical behavior, when they are subjected to an oscillatory test. The authors performed an oscillatory indentation test to a swollen matrix. The indenter was advanced in contact with the sample. Once a specific load was reached, the indenter velocity was oscillated sinusoidally and the response of the material recorded. Higher loads were used at shorter hydration times and lower loads at longer hydration times because, dependent on the amount of water penetrated inside the matrix, the sample changes its characteristic, becoming harder or softer, respectively. Thus, the oscillatory indentation experiments can be used as a small-scale measure of the rheological behavior of polymers to evaluate the viscoelastic nature of the gel layer as it swells.

In general, for a full description of the swelling phenomenon, a single experimental approach cannot be sufficient to consider all the aspects involved. For this reason, a combined approach of four different methods was proposed [92]. In particular, four different methods can be used: determination of the expansion factor, texture analysis, visual swelling observation, and photomicroscopy. The determination of the expansion factor was performed by positioning the sample into a flat-bottomed test tube and adding a small volume of swelling medium. After the medium was penetrated into the sample, the axial expansion was calculated as the ratio between the measured heights of the swollen and dry tablet. Then, the expansion of the tablets and the development of the gel layer thickness were evaluated using a texture analysis. To evaluate visually the swelling phenomena and thus the water uptake, samples were confined between two disks (as in the radial system) and photographed after predetermined dissolution times using a digital camera to obtain the final dimensions of the tablets. Finally, the swelling of polymer slabs was analyzed by photomicrography with a microscope connected to a digital camera. The combination of all these methods allows a deep analysis of the swelling phenomenon.

As described in this section, a lot of experimental techniques which can be used to clearly understand the swelling kinetics of a polymer and the mobility of the water inside the matrix were developed over the years. Each technique described has its advantages and can be a valid aid for a study purpose. A complete review of all the techniques used to monitor the swelling–

erosion behavior was proposed by Huanbutta et al. [93], and the pros and cons of each of them were elucidated.

### 3. Modeling approaches

#### 3.1. Introduction

The knowledge of the mechanisms that affect drug release, in order to obtain a tailored drug release, has been already pointed out to be essential. A considerable aid in the path of understanding can be given by the mathematical modeling of these physical phenomena, which could highlight the main features of drug release from hydrogel-based delivery systems. The modeling of the physical phenomena involved could help in the development and optimization of these systems, sensibly reducing the time and costs required by trial-and-error procedures. The modeling is rather complex because of the presence of several, synergistic and competing, transport phenomena. Several mathematical models have been proposed in literature, from the simple empirical models to the more sophisticated mechanistic models; the most important are reported in Figure 3 and some of them are discussed in the following.

#### 3.2. Empirical models

The first modeling attempt can be traced back to the semiempirical model of Higuchi [94], where the fractional drug release from an ointment (thin film) was related to the square root of the time:

$$\frac{M_t}{M_\infty} = k\sqrt{t} \quad (37)$$

$M_t$  is the cumulative amount of drug released at time  $t$ .  $M_\infty$  is the mass of drug released at infinite time (equal to the initial drug loading), and  $k$  is a constant reflecting the design variables of the system.

In 1985, Peppas and coworkers [95] proposed a generalization of the Higuchi equation, in which the fractional drug release was related to the  $n$ th power of the time. The index “ $n$ ” is an index function of the drug transport regime and of the shape of the delivery system.

$$\frac{M_t}{M_\infty} = k t^n \quad (38)$$

For example, for a thin film, the exponent “ $n$ ” in eq. 38 is equal to 0.5 for Fickian diffusive process (Higuchi’s equation), “ $n$ ” is equal to 1 for the Case-II transport (swelling-controlled drug release), and it takes intermediate values for intermediate behaviors (anomalous transport).

To distinguish between the relative importance of the Fickian release and the swelling-controlled release, Peppas and Sahlin [96] proposed the model

$$\frac{M_t}{M_\infty} = k_1 t^m + k_2 t^{2m} \quad (39)$$

where  $k_1$ ,  $k_2$ , and  $m$  are constants. The first term on the RHS represents the Fickian diffusional contribution,  $F$ , whereas the second term the swelling-controlled (case II) contribution,  $R$ . The relative importance of the two transport mechanisms can be highlighted by the ratio:

$$\frac{R}{F} = \frac{k_2 t^m}{k_1} \quad (40)$$

Bettini et al. [88] used this equation to investigate the effect of the HPMC molecular weight on the kinetics of drug release. No significant difference was found within the different grades of HPMC and the value of the ratio  $R/F$  was smaller than 0.1, suggesting that the drug transport is mainly Fickian diffusion driven.

Due to their simplicity, these equations have been used countless times to analyze the experimental results, often without taking into account that these equations are empirical in nature, and thus, they are useful only under some restrictions: constant diffusivities and negligible swelling (which is not the case of swellable systems [11, 97]). Thus, these equations should be used as simple fitting tools, giving limited information about the release mechanisms, in particular for complex systems such as the hydrogel-based ones.

### 3.3. The basics of the mechanistic modeling of the hydrogel-based systems

Let us consider a hydrogel-based system loaded with drug, submerged in a dissolution medium. The hydrogel "H" will be formed by the solvent ( $i=1$ ), the polymer matrix ( $i=2$ ), the drug ( $i=3$ ), and the ions ( $i=4 \dots N_c$ ). To describe the movements of these species along with the hydrogel deformation, proper mass balance equations, coupled with the momentum conservation equation, are needed. Two different approaches can be used to describe this system: the multiphasic model and the multicomponent mixture model. With the first, the hydrogel is seen as constituted by different phases, each characterized by their own mass and momentum conservation equations. With the second approach, instead, the system is considered as made of one phase composed of several components. In Table 3 is depicted a general framework useful for the mechanistic modeling of hydrogel-based systems. Most of the literature works dealing with both the drug release from hydrogels and the hydrogel mechanics could be traced back to this scheme, as shown in the following. In the formulation of the multiphasic approach, it has been considered that the drug is already dissolved. The transient and the inertial terms in the momentum balance equations (Table 3 equations (G-I)) have been neglected.

3.3.1. Free energy of a hydrogel network

In Table 3, eq. (K), it is indicated that the stress tensor and the osmotic pressure of the hydrogel are functions of the Helmholtz free energy that in turn is divided in three terms: elastic, mixing, and ionic free energy. The Helmholtz and the Gibbs free energy for these systems are interchangeable since  $dG=dA+d(pV)$  and, at constant pressure, the pressure–volume product does not change significantly in swelling [98].

Multiphasic approach	Multicomponent approach
<b>Mass conservation:</b>	
$\frac{\partial \rho_i}{\partial t} = -\nabla \cdot (\rho_i v_i) i=1...N_C$ (A)	
$\left\{ \begin{array}{l} \frac{\partial \phi_i}{\partial t} = -\nabla \cdot (\phi_i v_i) i=1, 2 \\ \frac{\partial \phi_1 c_i}{\partial t} = -\nabla \cdot (\phi_1 c_i v_i) i=3...N_C \end{array} \right. \quad (B)$	$\frac{\partial \rho_i}{\partial t} = -\nabla \cdot (\rho_i v_{\text{mix}}) - \nabla \cdot j_i i=1...N_C$ (D) or $\rho \frac{\partial \omega_i}{\partial t} = -\rho v_{\text{mix}} \cdot \nabla \omega_i - \nabla \cdot j_i i=1...N_C$ (E)
$\phi_1 + \phi_2 \cong 1$ (C)	$\sum_{i=1}^{N_C} \omega_i = 1$ (F)
<b>Momentum conservation:</b>	
$\nabla \cdot (\sigma_H - p\delta) = 0$ (G)	
$\left\{ \begin{array}{l} \mathbf{0} = \nabla \cdot (-\phi_1 p\delta + \mu_1 \dot{\gamma}) + \phi_1 RT \sum_{i=3}^{N_C} \nabla c_i + f_{12} + \sum_{i=3}^{N_C} f_{1i} \quad i=1 \\ \mathbf{0} = \nabla \cdot (-\phi_2 p\delta + \sigma_2) - \phi_1 (z_F c_F F) \nabla \psi + f_{21} i=2 \\ \mathbf{0} = -\phi_1 RT \nabla c_i - \phi_1 (z_i c_i F) \nabla \psi + f_{i1} i=3...N_C \end{array} \right. \quad (H)$	$\nabla \cdot (\sigma_{\text{mix}} - p\delta) = 0$ (I)
<b>Distribution of the ionic species:</b>	
$\nabla^2 \psi = -\frac{F}{\epsilon \epsilon_0} \left( \sum_{i=4}^{N_C} z_i c_i - z_F c_F \right), \quad \text{electroneutrality} \quad \nabla^2 \psi = 0$ (J)	
<b>Constitutive equations:</b>	
$\{p_{\text{osm}}, \sigma_H\} = g(A_{\text{el}}, A_{\text{mix}}, A_{\text{ion}})$ (K)	
$p = p' + p^{\text{osm}}$ (L)	
$f_{ij} = -f_{ji} = f_{ij}(\zeta, v_i, v_j)$ (M)	$j_i = -\rho_i (v_i - v_{\text{mix}}) \propto -$ $-\rho D_i g(\mu_i, x_i, \omega_i, M, p_{\text{osm}}, \psi, \dots)$ $D_i = g(\rho_1 \text{ or } \rho_2)$ (N)
<b>Unknowns to solve for:</b>	
$\phi_1, \phi_2, c_3...c_{N_C}, v_1...v_{N_C}$	$\omega_i, v_{\text{mix}}$
*Hydrogel (H) = Solvent (i=1) + Polymer (i=2) + Drug (i=3) + Ions (i=4...N <sub>C</sub> )	

**Table 3.** A general framework for the mechanistic modeling of hydrogel-based systems

The hydrogel can be viewed as formed by an elastomeric network with solvent molecules and ions, and the overall free energy of the system will have to consider the presence and the interactions of these species.

Let us consider a dry elastomeric network in which the stress–strain relation is based on the concept of the finite elasticity theory. This theory relates the deformations of the material to the stresses needed to obtain that deformation through the so-called strain energy density function:  $W = W(\lambda_1, \lambda_2, \lambda_3)$  where  $\lambda_i$  represents the stretch ratio in each direction (a material for which the stress–strain relationship derives from a strain energy density function is defined hyperelastic). The strain energy density function corresponds to the Helmholtz free energy per unit volume [99], and it can be derived from statistical theories of the elastomeric network. The aim of statistical models is to provide predictive relationships between the molecular structure and topology of the network and its macroscopic behavior.

Several molecular models for rubber networks have been proposed [98, 100], and the two limiting cases are the “affine” and the “phantom” models. Both these simplified network models give a strain energy density function of neo-Hookean type, i.e., in the following is reported the expression derived from the affine network:

$$W^{aff}(\lambda_1, \lambda_2, \lambda_3) = A_{el}^{aff}(\lambda_1, \lambda_2, \lambda_3) = \frac{1}{2} k_b T \left[ \frac{v_{el}}{V_0} (\lambda_1^2 + \lambda_2^2 + \lambda_3^2 - 3) - 2 \frac{\mu_{el}}{V_0} \ln(\lambda_1 \lambda_2 \lambda_3) \right] \quad (41)$$

where  $k_b$  is the Boltzmann constant,  $T$  is the temperature,  $V_0$  is the volume of the dry polymer,  $v_{el}$  is the number of elastic chains, and  $\mu_{el}$  is the number of junctions in the network. Equation 41 can be reformulated in terms of Finger deformation tensor  $\mathbf{B} = \mathbf{F}\mathbf{F}^T$ , where  $\mathbf{F} = d\mathbf{x}/d\mathbf{X}$  is the deformation gradient (in which  $\mathbf{x}$  and  $\mathbf{X}$  are the vectors representing a generic point P in the current and in the reference configuration, respectively):

$$A_{el}^{aff}(\mathbf{B}) = \frac{1}{2} k_b T \left[ \frac{v_{el}}{V_0} (I_B - 3) - \frac{\mu_{el}}{V_0} \ln(III_B) \right] \quad (42)$$

where  $I_B = tr(\mathbf{B})$  and  $III_B = \det(\mathbf{B})$  are the first and the third invariants of  $\mathbf{B}$ .

Since the hydrogel is characterized by the solvent present, the mixing contribution to the free energy has to be considered. As there is no explicit molecular model for the energy of mixing in gel (cross-linked polymer plus solvent), the functional dependence of the free energy of the mixing is generally assumed to be the same as in a polymer solution (linear polymer plus solvent). The classical treatment is based on the Flory–Huggins model, which is built on a lattice model with the assumption of uniform polymer segment concentration throughout the entire system. The free energy of mixing is given by

$$A_{mix} = \frac{RT}{V} \left[ n_1 \ln(\phi_1) + n_2 \ln(\phi_2) + n_1 \phi_2 \chi_{12} \right] \quad (43)$$

where  $R$  is the gas constant,  $n_1$  and  $\phi_1$  are the number of moles and the volume fraction of the solvent,  $n_2$  and  $\phi_2$  are the number of moles and the volume fraction of the polymer, and  $\chi_{12}$  is the Flory–Huggins interaction parameter.

When the network chains contain ionic groups (polyelectrolyte gels), there will be additional forces that affect their swelling properties, like the translational entropy of counterions, Coulomb interactions, and ion pair multiplets. It is evident that the mobile and fixed ions present contribute to the system free energy. Several expressions, based on different assumptions, have been used [101-104]. Quite commonly, the free energy due to ionic charges is divided into mobile ion contribution and fixed charge contribution:

$$A_{ion} = A_{ion}^{mob} + A_{ion}^{fix} \quad (44)$$

Following the Frenkel–Flory–Rehner approach, the free energy of a swelling cross-linked polymer is separable and additive, so that

$$A = A_{el} + A_{mix} + A_{ion} \quad (45)$$

This allows to consider singularly the free energy contributions and to derive constitutive equations for polymeric gels. It is quite common to relate the network stress only to the elastic Helmholtz free energy:

$$\sigma_2 = 2J^{-1} \mathbf{B} \frac{\partial A_{el}(\mathbf{B})}{\partial \mathbf{B}} \quad (46)$$

where  $J = \det(\mathbf{F})$ . The mixing and ionic free energy terms instead are often considered as contributing factors to the osmotic pressure ( $p^{osm}$ ), despite some other approaches that are possible [105].

### 3.3.2. Multicomponent approach: Mass transfer

In 1999, Siepmann et al. [106] developed a mechanistic model based on purely diffusive mass transport equations (Table 3 equations (D) with  $(\rho_i v_{mix}) \rightarrow 0$  and  $j_i = -D_i \nabla \rho_i$ ) to calculate the drug release from HPMC-based matrices. The modeled system was made of three species, water “1”, polymer “2”, and drug “3”, and the domain was the 2D axisymmetric representation of a cylindrical tablet (Figure 8). The water and drug transport equations were solved under the assumptions of:

- No volume contraction upon mixing
- Fast drug dissolution compared to drug diffusion
- Perfect sink condition for the drug
- Strong dependence of the diffusivities (of water and drug) on the hydration level
- Affine deformations

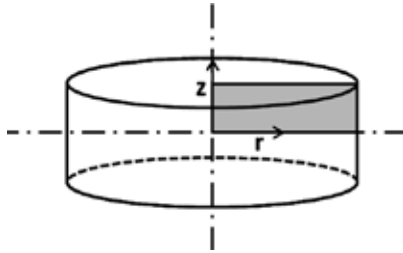


**Figure 8.** Schematic of the matrix, in light gray, the mathematical domain on which the transport equations were solved.

The mass transport equations (PDEs: partial differential equations) for water and drug in cylindrical coordinates were numerically (finite difference) solved along with the proper initial and boundary conditions:

$$\left\{ \begin{array}{l} \frac{\partial \rho_i}{\partial t} = \frac{1}{r} \frac{\partial}{\partial r} \left( D_i \frac{\partial \rho_i}{\partial r} \right) + \frac{\partial}{\partial z} \left( D_i \frac{\partial \rho_i}{\partial z} \right) \quad i = 1, 3 \\ @t = 0, \forall r, \forall z, \rho_i = \rho_{i,0} \\ @r = R(t), \forall t, \forall z, \rho_i = \rho_{i,eq} \\ @z = Z(t), \forall t, \forall r, \rho_i = \rho_{i,eq} \\ @r = 0, \forall t, \forall z, \frac{\partial \rho_i}{\partial r} = 0 \\ @r = 0, \forall t, \forall z, \frac{\partial \rho_i}{\partial r} = 0 \end{array} \right. \quad (47)$$

where  $\rho_i$  is the mass concentration of the  $i^{\text{th}}$  species,  $\rho_{i,eq}$  is the interface mass concentration of the  $i^{\text{th}}$  species, and  $D_i$  is the diffusion coefficient of the  $i^{\text{th}}$  species, described by a Fujita-type equation [51] (the general form given by eq. 26):

$$D_i = D_{i,eq} \exp \left[ -\beta_i \left( 1 - \frac{\rho_1}{\rho_{1,eq}} \right) \right] \quad (48)$$

where  $D_{i,eq} / \exp(\beta_i)$  are the values of the effective diffusion coefficients in the dry matrix ( $\rho_1 = 0$ ) and  $D_{i,eq}$  are the values of the effective diffusion coefficients in the fully swollen matrix

( $\rho_1 = \rho_{1,eq}$ ). The polymer erosion/release was described with the following ordinary differential equation (ODE):

$$\begin{cases} \frac{dm_2}{dt} = -k_{er} A_{er}(t) \\ @ t = 0 m_2 = m_{2,0} \end{cases} \quad (49)$$

where  $m_2$  and  $m_{2,0}$  are the polymer mass and the initial polymer mass,  $k_{er}$  is an erosion constant, and  $A_{er}$  is the erosion surface, that is, the surface exposed to the external medium. The system deformation was obtained, calculating at each time step the amount of water absorbed in the matrix and the released amount of drug and polymer. Considering affine deformations (the shape is conserved), the swelling and shrinking in the axial and the radial directions were obtained. The model parameters,  $D_{i,eq}$ ,  $\beta_{ir}$ ,  $k_{er}$  were found from the fitting of a wide set of experimental data. The so-tuned model was able to describe the evolution of the global masses of drug, water, and polymer in the system at several dissolution times.

In 2003, Kiil and Dam-Johansen [107] proposed a 1D model able to describe the radial movements of swelling, diffusion, and erosion fronts along with the hydration and drug release, under the (main) assumptions of drug release only in the radial direction, negligible matrix erosion, and constant diffusivities. Even in this case, the system description was based on the mass transport equation (Table 3 equations (D) with  $(\rho_i v_{mix}) \rightarrow 0$  and  $j_i = -D_i \nabla \rho_i$ ) with the addition of physical constraints to model the deformation. In particular, the domain was divided radially in three zones individuated by the front radii: zone 1 (solid part) characterized by the swelling radius, zone 2 (gel plus solid drug) between the diffusion and swelling radii, and zone 3 (gel plus dissolved drug) between the erosion and the diffusion radii. The model was made of one ODE, one algebraic equation, and four PDEs to describe, respectively, the movement of the swelling radius, the erosion front, the diffusion front, the dissolved drug concentration, and the water concentration in zones 3 and 2. Most of the model parameters were taken from literature; others, i.e., diffusivities and dissolution kinetic constants, were adjusted by fitting the experimental data. Despite such a complete approach, the model was not able to describe the swelling that occurs when there is no more solid part (zone 1) and its complexity has downhearted from developing a 2D axisymmetric version.

Inspired by Siepmann's work, in the 2007, Chirico et al. [55] developed a 1D model to describe the hydration of pure HPMC tablets confined between two glass slabs (Figure 9).

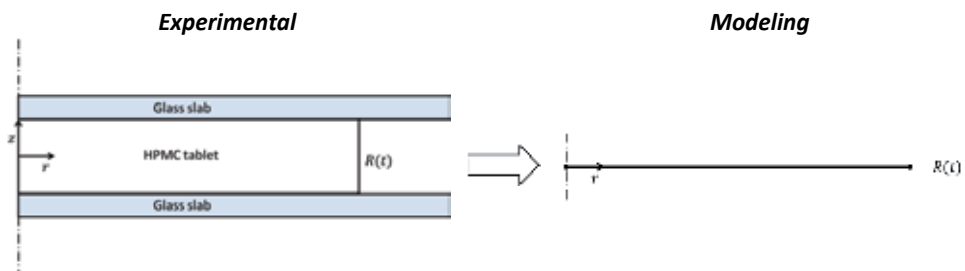


Figure 9. Experimental tablet dissolution scheme (left) and modeling domain (right)

Considering that the main transport phenomenon is the pseudo-diffusion of water from the medium ( $r > R(t)$ ) into the tablet through the radial direction (Table 3 equations (E) with  $(v_{\text{mix}}) \rightarrow 0$ ), the water mass balance in cylindrical coordinates was solved numerically (with a finite difference method):

$$\left\{ \begin{array}{l} \rho \frac{\partial \omega_1}{\partial t} = \frac{1}{r} \frac{\partial}{\partial r} \left( r \rho D_1 \frac{\partial \omega_1}{\partial r} \right) \\ @t = 0, \forall r, \omega_1 = \omega_{1,0} \\ @r = 0, \forall t, \frac{\partial \omega_1}{\partial r} = 0 \\ @r = R(t), \forall t, \omega_1 = \omega_{1,eq} \end{array} \right. \quad (50)$$

where  $\omega_1$  is the water mass fraction,  $\omega_{1,eq}$  is the equilibrium water mass fraction in the gel (0.97 [55]), and  $D_1$  is the diffusion coefficient of water in HPMC, modeled with a Fujita-type equation (the general form given by eq. 26) to account for the dependency of diffusivity on the water content:

$$D_1 = D_{1,eq} \exp \left[ -\beta_1 \left( 1 - \frac{\omega_1}{\omega_{1,eq}} \right) \right] \quad (51)$$

where  $D_{1,eq}$  is the diffusivity in the fully swollen gel ( $@\omega_1 = \omega_{1,eq}$ ), and  $\beta_1$  is a parameter that tunes the degree of dependency of  $D_1$  on the water content.

The system swelling was described, considering the variation of the total mass due to the water inlet and the polymer erosion.

$$\left\{ \begin{array}{l} m_1 = \int_{\rho(\omega_1)} \omega_1 dV \\ \frac{dm_2}{dt} = -k_{er} A_{er}(t) \\ @t = 0 m_2 = m_{2,0} \end{array} \right. \quad (52)$$

$$V(t) = \pi R^2 H = \frac{m_1 + m_2}{\langle \rho_{(\omega_1)} \rangle}$$

where  $m_1$  and  $m_2$  are the water and polymer masses in the system at a given time,  $k_{er}$  and  $A_{er}$  are the erosion constant and the erosion surface (surface exposed to the external medium),  $V(t)$  and  $H$  are the system volume and the tablet thickness, and  $\langle \rho_{(\omega_1)} \rangle$  is the averaged system density.

With this approach, after an initial tuning of the model parameters ( $D_{1,eq}$ ,  $\beta_1$ ,  $k_{er}$ ), the macroscopic system swelling, the amount of water uptake, and the polymer dissolved were correctly described. In their work, the authors compared, satisfactorily, the model results with an extra experimental data: the water mass fraction profile along the radial direction obtained by analyzing the normalized light intensity of swollen tablet pictures; an example of this model application is shown in Figure 5a. The model abilities were later on improved [108] to describe the drug release kinetics from different shaped matrices, bringing back everything to a 1D model valid for slabs, spheres, infinite cylinders, and finite cylinders (where the approach proposed by Coviello et al. [109] was used).

Despite that these transport models were validated against a wide set of experimental data, they were limited by the strong assumption of affine deformation that impedes the use of such models in more geometrically complex systems where the non-affine deformation can sensibly affect the drug release.

In 2011, Lamberti et al. [110] proposed a 2D axisymmetric model, in some ways similar to the Siepmann's model but with a big step forward: the assumption of affine deformation was no longer needed.

The transport equations for water and drug were solved for the respective mass fraction with a finite element method (FEM), along with the proper initial and boundary conditions (Table 3 equations (E) with ( $v_{\text{mix}} \rightarrow 0$ ):

$$\left\{ \begin{array}{l} \rho \frac{\partial \omega_i}{\partial t} = \nabla \cdot (\rho D_i \nabla \omega_i) \quad i = 1, 3 \\ @t = 0, \forall r, \forall z, \omega_i = \omega_{i,0} \\ @r = R(t), \forall t, \forall z \omega_i = \omega_{i,eq} \\ @z = Z(t), \forall t, \forall r \omega_i = \omega_{i,eq} \\ @r = 0, \forall t, \forall z \frac{\partial \omega_i}{\partial r} = 0 \\ @z = 0, \forall t, \forall r \frac{\partial \omega_i}{\partial z} = 0 \end{array} \right. \quad (53)$$

where  $\omega_i$  is the mass fraction of the  $i^{\text{th}}$  species,  $\omega_{i,eq}$  are the interface mass fraction of the  $i^{\text{th}}$  species, and  $D_i$  is the diffusion coefficient of the  $i^{\text{th}}$  species, described by a Fujita-type equation (see eqs. 48 and 51). The constitutive equation for the system density was obtained considering the summability of the specific volume of the single species:

$$\frac{1}{\rho} = \frac{\omega_1}{\rho_{10}} + \frac{(1 - \omega_1 - \omega_3)}{\rho_{20}} + \frac{\omega_3}{\rho_{30}} \quad (54)$$

where  $\rho_{10}$ ,  $\rho_{20}$ ,  $\rho_{30}$  are the pure species densities.

The peculiarity of this approach was the decomposition of the inlet water flux to describe the system swelling. In particular, it was considered that part of the total inlet water mass flux was responsible for the tablet swelling,  $j_{1,swe}$ , whereas the rest ( $j_{1,diff}$ ) was responsible for the inner layer hydration. Assuming that

$$\begin{aligned}
 j_{1,swe} &= k_{swe} j_{1,diff} \\
 \text{and} \\
 j_1 &= j_{1,diff} + j_{1,swe} = (1 + k_{swe}) \rho D_1 \nabla \omega_1
 \end{aligned}
 \tag{55}$$

where  $k_{swe}$  is a new fitting parameter.

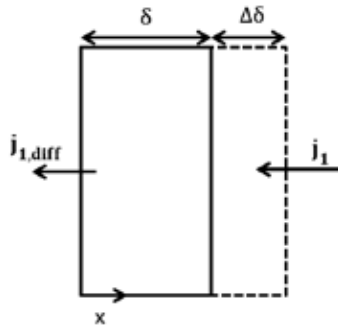


**Figure 10.** Representation of the water mass balance on a boundary element

The rate of deformation was obtained performing a water mass balance on a boundary element (Figure 10):

$$\begin{aligned}
 \rho \frac{d}{dt} (A \delta \omega_{1,eq}) &= A \cdot j_{1,diff} - A \cdot j_1 \\
 v_{swe} &= \frac{d\delta}{dt} = - \frac{j_{1,swe}}{\rho \omega_{1,eq}} = - \frac{k_{swe} j_{1,diff}}{\rho \omega_{1,eq}}
 \end{aligned}
 \tag{56}$$

where  $v_{swe}$  is the swelling velocity of the boundary element. On the other hand, the polymer erosion could lead to a volume decrease; therefore, an opposite constant velocity (the erosion velocity  $v_{eros} = -k_{eros}$ ) was considered, so that the effective velocity of the boundary element was given by

$$v = v_{swe} + v_{eros}
 \tag{57}$$

The application of this boundary velocity through an ALE (Arbitrary Lagrangian–Eulerian) moving mesh method was proved to describe the matrix non-affine swelling. The model, after an initial tuning of the parameters, was successfully compared to macroscopic results in terms of overall water, drug, and polymer masses, erosion radius, and semi-thickness as well as a picture of swollen tablets.

The approach used in this model overcame the affine deformation at the cost of an additional parameter: the  $k_{swe}$  (1° drawback). Moreover, the mass fraction constraint (Table 3 equation (F)) was not implemented along with the PDEs (as well as in Siepmann’s model), possibly leading to unrealistic results in some domain points (2° drawback).

Kaunisto et al. developed a mechanistic model (in 2010 for the dissolution of pure poly(ethylene oxide) tablets [111], extended in 2013 [112] to HPMC matrices loaded with a poorly soluble drug) to analyze the drug release behavior in swellable systems. In this model (considered at constant density), the polymer mass fraction description was coupled with the transport equations for drug and water through the mass fraction constraint (Table 3 equations (E-F) with  $(v_{mix}) \rightarrow 0$ ), therefore overcoming the Lamberti model 2° drawback. The transport equations were based on a simplified version of the generalized Fick equation [113]. Despite the elegant approach, all the multicomponent interactions, except those with the solvent, were assumed to be zero, and the multicomponent Fick diffusivities were interpreted as “pseudo-binary.” For the water–polymer diffusivity, a “Fujita-type” form was used (eqs. 48 and 51). Even in this case, like in Lamberti’s model, the swelling was described through an ALE moving mesh method, but the swelling velocity was derived from a polymer/solid drug mass balance on the erosion boundaries, with zero additional parameters, therefore overcoming also the 1° Lamberti model drawback.

Recently, in 2015, Caccavo et al. [114, 115] developed a mechanistic model based on the diffusion of water and drug in a concentrate system, accounting for the molar mass gradient, coupled with an ALE method.

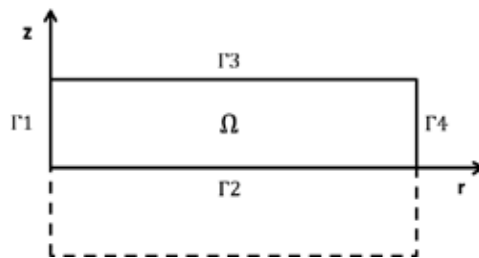


**Figure 11.** Computational domain for the model of Caccavo et al. [114, 115]

Under the assumption of:

- No volume change upon mixing.
- The drug dissolution within the matrix is fast compared to drug diffusion.

- Perfect sink conditions for drug and constant critical solvent concentration on the erosion front are maintained.
- The water convection contribution to mass transfer is negligible.
- The swelling is due to the water uptake and to the translocation of polymer. The polymer flow at the interface between the tablet and the external medium causes the swelling and the shape change, without polymer release.
- The erosion is due to external fluid dynamics and thus to interactions between the tablet surface and external fluid, which remains constant during the dissolution runs.

The water and drug balances (transport equations) (Table 3 equations (E-F) with  $(v_{\text{mix}}) \rightarrow 0$ ) in cylindrical coordinates (Figure 11) were:

$$\left\{ \begin{array}{l} \rho \frac{\partial \omega_i}{\partial t} = \nabla \cdot \left( \rho D_i \nabla \omega_i + \rho \frac{\omega_i}{M} D_i \nabla M \right) \\ \omega_2 = 1 - (\omega_1 + \omega_3) \\ @t = 0 \forall \mathbf{x} \in \Omega \quad \omega_i = \omega_{i,0} \\ @x \in \Gamma 1 \forall t > 0 \quad \mathbf{j}_i = 0 \\ @x \in \Gamma 2 \forall t > 0 \quad \mathbf{j}_i = 0 \\ @x \in \Gamma 3 \forall t > 0 \quad \omega_i = \omega_{i,eq} \\ @x \in \Gamma 4 \forall t > 0 \quad \omega_i = \omega_{i,eq} \end{array} \right. \quad (58)$$

where  $M$  is the average molar mass. The ideal mixing rule (like in Lamberti's model) was used for the system density, and the diffusion coefficients were described with Fujita-type equations (eqs. 48 and 51). The domain deformation was described with the ALE method imposing the swelling and the erosion velocities on the erosion boundaries:

$$\left\{ \begin{array}{l} \frac{\partial^2}{\partial R^2} \left( \frac{\partial r}{\partial t} \right) + \frac{\partial^2}{\partial Z^2} \left( \frac{\partial r}{\partial t} \right) = 0 \\ \frac{\partial^2}{\partial R^2} \left( \frac{\partial z}{\partial t} \right) + \frac{\partial^2}{\partial Z^2} \left( \frac{\partial z}{\partial t} \right) = 0 \\ @t = 0 \quad r = r_0; z = z_0 \\ @x \in \Gamma 1 \forall t > 0 \quad dr = 0 \\ @x \in \Gamma 2 \forall t > 0 \quad dz = 0 \\ @x \in \Gamma 3 \forall t > 0 \quad \frac{\partial z}{\partial t} = (v_{swe} + v_{er})|_z \\ @x \in \Gamma 4 \forall t > 0 \quad \frac{\partial r}{\partial t} = (v_{swe} + v_{er})|_r \end{array} \right. \quad (59)$$

where the uppercase and the lowercase indicate the domain coordinates in the reference and current configuration, respectively. The swelling velocity was derived through a polymer mass balance on the erosion front [114]. The polymer flow toward the erosion front was intended to be used to form new layers of gel, contributing in this way to the swelling phenomena.

$$v_{swe} = -\frac{(j_1 + j_3)}{\rho \omega_2} \quad (60)$$

whereas the erosion velocity was accounted using a constant value  $|v_{er}| = -k_{er}$ .

Thanks to this approach, the evolution of the water, drug, and polymer masses was described, along with the mass fraction profiles inside the swollen tablets (Figure 5b) and the tablet shape evolution (Figure 12).

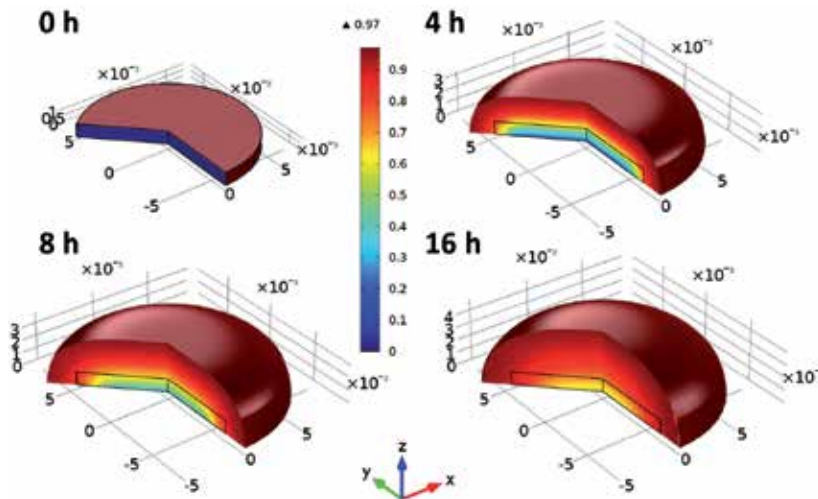


**Figure 12.** Calculated hydration level, in terms of water mass fraction, and swelling at several dissolution times. In the pictures is represented the half portion of the tablet.

Moreover, the model was successfully compared to experimental data of water mass fraction distribution obtained with the texture analysis (Figure 7b) [115]. A modified version of the model [34], with the inclusion of an excipient (lactose), was compared to hydration and swelling data obtained from an MRI technique, proving that in case of Fickian transport, the model is still reliable (Figure 7a) with some discrepancy at higher dissolution times where the fluid dynamic forces, in the specific testing tool, take over and deform the weak gel.

### 3.3.3. Multicomponent approach: Mass and momentum transfer

Achilleos et al. [101, 116] proposed a modified transport model for a polyelectrolyte gel made of four components (water "1", polymer "2", Na<sup>+</sup> "4", Cl<sup>-</sup> "5"), where the volume transition of

the hydrogel was still considered to be driven by the ionic diffusion, but the osmotic pressure is contributed by the mixing, elastic, and electrostatic free energies. Since the system is considered monophasic, with the presence of several species, this kind of formulation can be considered, according to the scheme of Table 3, a multicomponent approach.

Following the mixture theory approach, the mass and momentum balance equations can be written for the mixture, considering a mass average velocity ( $v_{\text{mix}}$ ). The system is considered in isothermal conditions so that there is no need for an energy balance. Along with the momentum and mass balance for the mixture, the species mass balance has to be satisfied. All these equations were nondimensionalized and written in terms of polymer velocity (and not the mass average velocity), since it is the one that enters in the stress constitutive expression:

$$\left\{ \begin{array}{l} \rho^* \frac{D^{(2)}\omega_i}{Dt} - \rho^* \frac{\omega_i}{\omega_2} \frac{D^{(2)}\omega_2}{Dt} + \nabla \cdot \left( j_i^* - \frac{\omega_i}{\omega_2} j_2^* \right) = 0, i \neq 2 \\ \nabla \cdot v_2^* + \frac{1}{\rho^*} \frac{D^{(2)}\rho^*}{Dt} + \frac{1}{\omega_2} \frac{D^{(2)}\omega_2}{Dt} = 0 \\ \nabla \cdot \sigma_2^* - \nabla p^* = 0 \\ \nabla^2 \psi^* \propto - \left( \sum_{i=4}^{N_c} \frac{z_i \omega_i M_1}{M_i} - \frac{z_2 \omega_2 a M_1}{M_{2,m}} \right) = 0 \end{array} \right. \quad (61)$$

where  $\rho^*$ ,  $v_2^*$ ,  $p^*$ , and  $\psi^*$  are the dimensionless mixture density, polymer velocity, hydrostatic pressure, and electrical potential, respectively.  $\omega_i$ ,  $j_i^*$ ,  $M_i$ , and  $z_i$  are the weight fraction, the dimensionless diffusive flux, the molecular weight, and the charge of the  $i^{\text{th}}$  species, respectively. The variable  $a$  and  $M_{2,m}$  represent the polymer network ionization ( $0 \leq a \leq 1$ ) and the molecular weight of a monomer.  $D^{(2)}/Dt$  is the substantial derivative following the polymer velocity.

Equation 61 represents (in order) the species mass balances ( $N_c - 1$ ) (Table 3 eq. (E)), the continuity equation (Table 3 sum on  $N_c$  of eq. (D)), the momentum balance (Table 3 eq. (I)), and the electroneutrality condition (Table 3 eq. (J)). These equations solve for  $\omega_i$ ,  $p^*$ ,  $v_2^*$ ,  $\psi^*$ , respectively. It is worth to specify that the mixture stress tensor, with this approach, is equal to the polymer network stress tensor:  $\sigma_{\text{mix}} = \sigma_2$ .

### 3.3.3.1. Constitutive equations

The diffusive flux of the  $i^{\text{th}}$  components is given by (Table 3 eq. (N)):

$$j_i^* = -D_i^* \omega_i \left( \nabla p_i^{\text{osm}*} + \frac{M_i}{M_1} \nabla \cdot \sigma_2^* + z_i \nabla \psi^* \right) \quad (62)$$

where  $p_i^{osm*}$  and  $D_i^*$  are the dimensionless osmotic pressure and diffusion coefficient ( $D_1$  was considered function of the water concentration) of the  $i^{\text{th}}$  components. The Helmholtz free energy of the mixture, consisting of mixing ( $A_{mix}$ ), elastic ( $A_{el}$ ), and electrostatic ( $A_{ion}$ ) contributions, can be used to obtain the osmotic pressure and the network stress (Table 3 eq. (K)). The mixture and the electrostatic contribution were accounted in the osmotic pressure:

$$p_i^{osm*} = \left( \ln(\omega_i) + \chi_{i,2}\omega_2 + 1 \right) - \omega_2 \sum_{\substack{\beta=1 \\ \beta \neq 2}}^{N_c} \frac{\chi_{\beta,2}\omega_\beta M_i}{M_\beta} - \sum_{\substack{\beta=1 \\ \beta \neq 2}}^{N_c} \frac{\omega_\beta M_i}{M_\beta} + C_{DH} \left( I_s^{1.5} \frac{M_i}{M_1} - 3 Z_i I_s^{0.5} \right) + C_{mf} a^2 \omega_2 \left( -\frac{z_i^2 M_1}{I_s M_i} + 1 \right) \quad (63)$$

where  $\chi_{i,2}$  is the Flory–Huggins interaction parameter and  $C_{DH}$  and  $C_{mf}$  are two determined constants. The osmotic pressure is therefore composed of a solvent–polymer mixing contribution, a mobile ions contribution, and fixed charges contribution. The elastic contribution of the Helmholtz free energy was used, according to eq. 46, to derive the network stress tensor:

$$\boldsymbol{\sigma}_2 = 2 J^{-1} \mathbf{B} \frac{\partial A_{el}(\mathbf{B})}{\partial \mathbf{B}} = G_0 \frac{\phi_2}{\phi_{20}} (\mathbf{B} - \boldsymbol{\delta}) = G (\mathbf{B} - \boldsymbol{\delta}) \quad (64)$$

where  $G_0$  is the hydrogel modulus and  $\phi_2$  and  $\phi_{20}$  are the volume fraction of the polymer and the volume fraction of polymer at the gelation (stress-free state) so that the shear modulus is  $G = G_0 \phi_2 / \phi_{20}$ . The network stress was related to the polymer velocity  $v_2$ :

$$\frac{D^{(2)} \boldsymbol{\sigma}_2}{Dt} - \boldsymbol{\sigma}_2 \cdot \nabla v_2 - \nabla v_2^T \cdot \boldsymbol{\sigma}_2 + \boldsymbol{\sigma}_2 \nabla \cdot v_2 = G_0 \frac{\phi_2}{\phi_{20}} (\nabla v_2 + \nabla v_2^T) \quad (65)$$

These last equations, coupled with the momentum balance, allow to solve for  $\boldsymbol{\sigma}_2$ .

Applying the proper initial and boundary conditions, this model solution (obtained with a FEM method) provided the hydrogel water concentration, deformation, stress, and potential fields as functions of external and gel parameters: solution molarity, degree of polymerization, shear modulus, and problem geometry.

### 3.3.4. Multicomponent approach: Monophasic theory

On the basis of the poroelastic theory, Suo and his group developed a framework (the monophasic theory) for modeling the mass transport of small molecular species in a three-dimensional polymeric network coupled with large deformations [105, 117]. Once again, the

model can be classified, according to the scheme of Table 3, as a multicomponent approach. Indeed, the system is monophasic and the solvent transport is modeled with a diffusive mass transport equation.

The basic idea is that because of its microstructure, a gel is capable of two basic modes of deformation. First, the stretching of polymer chains accompanied by local rearrangement of small molecules allows a gel to change its shape rapidly but maintain a constant volume. The gel behaves just like an incompressible elastomer in this mode, showing a viscoelastic nature. The second mode, which involves long-range transportation of the small molecules, is usually slow and size dependent. The deformation in the second mode allows the gel to swell or shrink in volume, emphasizing the poroelastic nature.

The first mode of deformation was neglected in the earliest publication [117], considering an instantaneous rearrangement of the polymer chain, therefore not considering the viscoelastic nature of the hydrogel. In the wake of this framework, several other works have been published [105, 118-122]. Later on, in seek of completeness, the viscoelastic nature of hydrogel has been then added to the framework [123].

In the following the viscoporoelastic model [123] will be reported, using the “index notation” and the summation convention (with the uppercase and with the lowercase are denoted the variables in the reference and current state, respectively). Let  $\Omega$  be the volume of each solvent molecule in the gel. Taking the dry state of the polymer network to be the reference, it is possible to relate the nominal solvent concentration  $C$  to the volumetric expansion  $\det F$  as

$$\det F := \frac{V_{tot}}{V_{dry}} = 1 + \frac{V_{solv}}{V_{dry}} = 1 + \frac{V_{solv}}{N_{solv\ molecules}} \frac{N_{solv\ molecules}}{V_{dry}} = 1 + \Omega C \quad (66)$$

As usual, the gel Helmholtz free energy is considered as the sum of the elastic (affine network) contribution and the polymer–solvent mixing contribution. A peculiarity of this approach is the reformulation of the Flory–Huggins  $A_{mix}(C)$  as  $A_{mix}(F)$ , using eq. 66, therefore considering the strain energy density function given by the sum of the elastic and mixing free energy.

### 3.3.4.1. Nonequilibrium thermodynamics

The second law of thermodynamics dictates that the total free energy of a closed system keeps constant or decreases in any physical process. Assuming that the energy is dissipated mainly through two processes, solvent migration  $\dot{W}_s$  and viscous deformation  $\dot{W}_v$  ( $\dot{W}_s$  being dependent on the true solvent flux  $j_1$  and  $\dot{W}_v$  being dependent on the deviatoric part of the strain rate tensor), it is possible to write

$$\frac{\partial \Phi}{\partial t} - \frac{\partial W}{\partial t} + \int_V \dot{W}_s dV + \int_V \dot{W}_v dV = 0 \quad (67)$$

where the first term is the rate of variation of the total free energy ( $\Phi$ ) of the hydrogel  $\partial\Phi/\partial t = \int_V \partial A/\partial t dV$ . The second term is the total work ( $W$ ) done to the hydrogel, including the mechanical work by the surface traction and the chemical work via absorption of solvent molecules  $\partial W/\partial t = \int_{\partial V} t_i \partial x/\partial t dS + \int_{\partial V} \bar{\mu} IdS$ , where  $t_i$  is the stress acting on the gel surface,  $\bar{\mu}$  is the chemical potential of the solvent in the external medium, and  $I$  is the molecular flux. The third and fourth terms represent the free energy dissipation due to solvent migration ( $\dot{W}_s$ ) and viscous deformation ( $\dot{W}_V$ ).

Moreover, the system has to respect the solvent molecule conservation  $\partial C/\partial t = -(\partial J_K)/(\partial X_K)$  that rewritten in terms of  $C=C(F)$  can be added (using a Lagrange multiplier ( $\mu$ )) to eq. 67:

$$\int_V \frac{\partial A}{\partial F_{iK}} \frac{\partial v_i}{\partial X_K} dV - \int_V t_i \frac{\partial x}{\partial t} dS - \int_V \bar{\mu} IdS + \int_V \dot{W}_s dV + \int_V \dot{W}_V dV + \int_V \mu \left[ \frac{det\mathbf{F}}{\Omega} H_{Ki} \frac{\partial v_i}{\partial X_K} + \frac{\partial J_L}{\partial X_L} \right] dV = 0 \tag{68}$$

where the tensor  $\mathbf{H}=\mathbf{F}^{-1}$ . With the aid of integration by parts and the divergence theorem, it can be shown that to satisfy eq. 68,

$$\left\{ \begin{array}{l} \frac{\partial P_{iK}}{\partial X_K} = 0 \\ P_{iK} N_K = t_i \\ \frac{\partial C}{\partial t} + \frac{\partial J_L}{\partial X_L} = \frac{det\mathbf{F}}{\Omega} H_{Ki} \frac{\partial v_i}{\partial X_K} + \frac{\partial J_L}{\partial X_L} = 0 \\ J_K = -\frac{D}{k_b T} \frac{det\mathbf{F} - 1}{\Omega det\mathbf{F}} H_{Ki} H_{Li} \frac{\partial \mu}{\partial X_L} \\ \mu = \bar{\mu} \end{array} \right. \tag{69}$$

where  $P_{iK}$  is the nominal stress (first Piola–Kirchhoff stress that relates to the Cauchy stress by  $\sigma_{mix} = \mathbf{P}\mathbf{F}^T$ .) defined as

$$P_{iK} = N k_b T (F_{iK} - H_{iK}) + \frac{k_b T}{\Omega} \left[ \ln \left( 1 - \frac{1}{det\mathbf{F}} \right) det\mathbf{F} + 1 + \frac{\chi}{det\mathbf{F}} \right] H_{Ki} + \eta det\mathbf{F} H_{Lj} \left( \frac{1}{2} H_{Kj} \frac{\partial v_i}{\partial X_L} + \frac{1}{2} H_{Ki} \frac{\partial v_i}{\partial X_L} - \frac{1}{3} H_{Ki} \frac{\partial v_i}{\partial X_L} \right) - \mu \frac{det\mathbf{F}}{\Omega} H_{Ki} \tag{70}$$

Equation 70 represents the momentum (Table 3 eq. (I) in terms of nominal stress) and the solvent mass conservation equations (Table 3 eq. (D) in the reference configuration) in the hydrogel, derived from nonequilibrium thermodynamics considerations, along with their natural boundary conditions rising from the transformation from the strong to the weak form. The expression of the stress tensor in eq. 70 results in a more complex equation, i.e., with respect to Achilles's model, since this accounts for the network elasticity, the polymer–solvent mixing, and the energy dissipations.

### 3.3.5. Multiphasic models

With the “multiphasic models,” the hydrogel is divided into two (biphasic) or three (triphasic) phases, including a solid polymer network phase, a fluidic solvent phase, and a mobile ion phase for polyelectrolyte hydrogels. In the following will be analyzed the biphasic (polymer plus water) model of Birgersson and Kurnia [124–126]. It has to be said that with the multiphasic approach, unlike the multicomponent approach, some attempts have been made in coupling the drug release and the hydrogel mechanics [127], treating the drug as a diffusant species, according to Table 3.

In 2008, an interesting work aiming to describe the transient analysis of temperature-sensitive neutral hydrogels was published [126] and improved in the years [128] until the last publication in 2012 [125]. The starting point was the mass and the momentum conservation of the phases, coupled with the energy conservation. It was demonstrated [126] that the energy transport is considerably quicker than the deformation; therefore, the system can be accurately described through an isothermal deformation based on the new equilibrium temperature [125].

Considering the conservation of the mass for the two phases (Table 3 equations (B)):

$$\begin{aligned} \frac{\partial \phi_1}{\partial t} &= -\nabla \cdot (\phi_1 v_1) \\ \frac{\partial \phi_2}{\partial t} &= -\nabla \cdot (\phi_2 v_2) \end{aligned} \quad (71)$$

where  $\phi_2$  and  $\phi_1$  are the polymer and the fluid volume fractions and  $v_2$  and  $v_1$  the polymer and fluid velocities. Summing these equations, the mixture mass conservation expression was derived:

$$0 = -\nabla \cdot (\phi_2 v_2 + (1 - \phi_2) v_1) = -\nabla \cdot v_{vol} \quad (72)$$

where  $v_{vol}$  is the system volume average velocity. After some manipulations, it is possible to reformulate the polymer mass conservation in terms of the relative velocity ( $v_R = v_1 - v_2$ ):

$$\nabla \cdot v_2 = -\frac{\nabla \cdot q}{\rho_{1,0}} \quad (73)$$

where  $\mathbf{q} = \phi_1 \rho_{1,0} \mathbf{v}_R$  is the relative flow vector of the fluid phase with respect to the polymer phase.

Considering the momentum conservation for the polymer and fluid phases (Table 3 equations (H) for nonionic system and with  $(\mu_1 \dot{\gamma}) \rightarrow 0$ ):

$$\begin{aligned} \mathbf{0} &= \nabla \cdot (-\phi_1 p \boldsymbol{\delta}) + \mathbf{f}_{12} \\ \mathbf{0} &= \nabla \cdot (-\phi_2 p \boldsymbol{\delta} + \boldsymbol{\sigma}_2) + \mathbf{f}_{21} \end{aligned} \quad (74)$$

In eq. 74,  $p$  is the fluid pressure inside the hydrogel,  $\boldsymbol{\sigma}_2$  is the polymer stress tensor, and  $\mathbf{f}_{12}$  and  $\mathbf{f}_{21}$  are the reaction couple of the drag force between the two phases:  $\mathbf{f}_{12} = -\mathbf{f}_{21} = p \nabla \phi_p + \zeta \mathbf{v}_R$ , where  $\zeta$  is the friction coefficient defined as  $\zeta = \mu_1 \phi_1^2 / \kappa$ , function of the fluid viscosity  $\mu_1$ , of the fluid volume fraction, and of the hydrogel permeability  $\kappa$ . From the momentum balance on the fluid phase, the pressure gradient can be related to  $\mathbf{q}$ :

$$\nabla p = -\frac{\mu_1}{\kappa} \frac{\mathbf{q}}{\rho_{1,0}} \quad (75)$$

While summing both eq. 71, the mixture moment conservation can be obtained:

$$\mathbf{0} = \nabla \cdot (-p \mathbf{I} + \boldsymbol{\sigma}_2) \quad (76)$$

Equation 76 highlights that in the multiphasic approach, due to the preliminary assumptions, the stress tensor is the one of the polymer network, while the solvent–polymer interaction – and eventually the ion effect – influences the momentum of the hydrogel through the pressure term.

### 3.3.5.1. Constitutive equations

The Helmholtz free energy of a hydrogel is constituted by the elasticity-related term and by the polymer–solvent mixing-related term. As usual, the elastic contribution is attributed to the polymer chain through the Cauchy stress, and the mixing term is considered through the osmotic pressure.

The mixing term of the Helmholtz free energy was considered through the presence of an osmotic pressure with the expression [129]

$$p^{osm} = -\frac{k_b T}{V_m} \left[ \phi_p + \chi \phi_p^2 + \ln(1 - \phi_p) \right] \quad (77)$$

where  $\chi$  is the polymer–solvent interaction parameter,  $k_b$  is the Boltzmann constant,  $T$  is the temperature, and  $V_m$  is the volume occupied by one monomer.

The Cauchy stress tensor for the polymer  $\boldsymbol{\sigma}_2$  was derived using eq. 46 and an affine elastic free energy:

$$\sigma_2 = G \left( \mathbf{B} - \frac{1}{2} \boldsymbol{\delta} \right) \quad (78)$$

Equation 78 is similar to eq. 64, a part from the factor 0.5 that multiplies the unit tensor. It is worth highlighting that in some cases, it might be useful to separate the concept of reference configuration (state of polymerization of the hydrogel) from the initial configuration to avoid singular behavior (i.e., for polymerization in gas where  $\phi_2 \approx 1$ , the osmotic pressure goes to infinity). However, this is not the case, and the reader is referred to [105, 119, 129] for further information.

At this point with the proper initial and boundary conditions, knowing the constitutive equations, the partial differential eqs. 73, 75, and 76 could be simultaneously solved for  $q$ ,  $p$ , and  $v_2$  that in conjunction with a moving mesh and the other algebraic equations previously defined, allow to completely characterize the hydrogel deformation due to a temperature variation. The authors, to avoid the use of a moving mesh, recast the equations in Lagrangian configuration; however, since this last step is not indispensable for the modeling approach comprehension, it will not show here, and the interested readers are referred to [125, 126].

## 4. Nomenclature

$A$	Generic area	$[m^2]$
$A$	Helmholtz free energy per unit volume	$[J / m^3]$
$A_{el}$	Elastic contribution to the Helmholtz free energy	$[J / m^3]$
$A_{ion}$	Ionic contribution to the Helmholtz free energy	$[J / m^3]$
$A_{mix}$	Mixing contribution to the Helmholtz free energy	$[J / m^3]$
$\mathbf{B}$	Finger tensor (left Cauchy–Green)	$[-]$
$C$	Solvent concentration in the reference configuration (see 3.3.4)	$[1 / m^3]$
$C_n$	Flory’s characteristic ratio	$[-]$
$c^*$	Solvent concentration at the glass–rubber interface (see 2.4)	$[k g_{solvent} / k g_{dry\ Polymer}]$
$c_i$	Concentration of the $i^{th}$ species	$[mol / m^3]$
$c_x$	Cross-linking concentration	$[mol / m^3]$
$D_i$	Diffusion coefficient of the $i^{th}$ species	$[m^2 / s]$
$D^{(i)} / Dt$	Substantial derivative following the $i^{th}$ species velocity	$[1 / s]$
$dF / ds$	Slope of the force–penetration curve	$[N / m]$
$F$	Faraday’s constant	$[C / mol]$

$F$	Fickian contribution to drug release	$[-]$
$F$	Deformation gradient tensor	$[-]$
$f$	Frictional draw coefficient	$[(J \cdot s)/m^2]$
$f_{ij}$	Drag force per unit volume of the phase $i$ on the phase $j$	$[N/m^3]$
$G$	Hydrogel shear modulus	$[Pa]$
$G_0$	Hydrogel initial shear modulus at the stress-free state (gelation condition)	$[Pa]$
$H$	Tablet height	$[m]$
$H$	Inverse of the deformation gradient tensor	$[-]$
$I$	Light intensity	$[-]$
$I$	Ionic strength	$[mol/m^3]$
$I_0$	Light intensity of the dry tablet	$[-]$
$I_B$	First invariant of the Finger tensor	$[-]$
$III_B$	Third invariant of the Finger tensor	$[-]$
$I_{max}$	Light intensity of the fully hydrated gel	$[-]$
$J$	Solvent flux in the reference configuration (see 3.3.4)	$[1/(m^2s)]$
$j_i$	Mass flux of the $i^{\text{th}}$ species	$[kg/(m^2s)]$
$K_a$	Acid dissociation constant	
$K_b$	Basic dissociation constant	
$k$	Hydraulic permeability	$[m^2]$
$k$	Generic constant	
$k_b$	Boltzmann's constant	$[J/K]$
$k_{er}$	Erosion constant	$[kg/(m^2s)]$
$k_{eros}$	Erosion constant velocity	$[m/s]$
$k_{swell}$	Constant of swelling	$[-]$
$L_{Ch}$	Characteristic diffusion path length	$[m]$
$L_c$	Length of the polymeric chain	$[m]$
$l$	Length of the bond along the polymer backbone	$[m]$
$M$	Average molecular weight	$[kg/mol]$
$M_\infty$	Amount of drug released at infinite time	$[kg]$
$M_f$	Weight of the polymeric chain	$[kg]$
$M_i$	Molecular weight of the $i^{\text{th}}$ species	$[kg/mol]$
$M_r$	Molecular weight of the repeating unit	$[kg/mol]$

$M_t$	Cumulative amount of drug released at time $t$	[kg]
$\overline{M}_c$	Molecular weight between two consecutive cross-links	[kg / mol]
$\overline{M}_n$	Number-average molecular weight of the polymer	[kg / mol]
$m_i$	Mass of the $i^{\text{th}}$ species	[kg]
$N$	Number of links for chain	[-]
$N_A$	Avogadro constant	[1 / mol]
$N_{De.D}$	Diffusional Deborah number	[-]
$N_{Sw.A}$	Swelling area number	[-]
$N_{Sw.I}$	Swelling interface number	[-]
$N_c$	Number of species	[-]
$n_i$	Mole of the $i^{\text{th}}$ species	[mol]
$\mathbf{P}$	First Piola–Kirchhoff stress tensor	[Pa]
$p$	Total intrinsic fluid pressure	[Pa]
$p'$	Total intrinsic fluid pressure minus osmotic pressure (eq. L)	[Pa]
$p^{osm}$	Osmotic pressure	[Pa]
$Q$	Volumetric swelling ratio	[-]
$\mathbf{q}$	Relative flow vector of fluid phase with respect to the polymer phase	[kg / (m <sup>2</sup> s)]
$R$	Gas constant	[J / (K mol)]
$R$	Swelling contribution to drug release	
$r_f$	Polymer fiber radius	[m]
$r_s$	Size of the diffusing solute	[m]
$(\overline{r}_0^2)^{1/2}$	Unperturbed root-mean-square of the end-to-end distance for polymer chains between two neighboring cross-links	[m]
$T$	Temperature	[K]
$T_2$	Spin–spin relaxation time	[s]
$T_{exp}$	Experimental temperature	[K]
$T_g$	Glass transition temperature	[K]
$t_i$	Stress acting on the gel surface	[Pa]
$V$	System volume	[m <sup>3</sup> ]
$V_0$	Volume of the dry polymer	[m <sup>3</sup> ]
$V_1$	Molar volume of the solvent	[m <sup>3</sup> / mol]
$V_G$	Volume of the swollen gel	[m <sup>3</sup> ]

$V_p$	Volume of the dry polymer	$[m^3]$
$v$	Velocity of the solvent penetration	$[m/s]$
$v_f$	Total free volume	$[m^3]$
$v_{f.p}$	Polymer free volume	$[m^3]$
$v_{f.w}$	Water free volume	$[m^3]$
$v_R$	Relative velocity of the fluid phase with respect to the polymer phase	$[m/s]$
$v_{eros}$	Erosion velocity	$[m/s]$
$v_i$	Velocity of the $i^{\text{th}}$ species	$[m/s]$
$v_{mix}$	Mass average velocity of the mixture	$[m/s]$
$v_{swe}$	Swelling velocity	$[m/s]$
$v_{vol}$	System volume average velocity	$[m/s]$
$W$	Total work done to the hydrogel	$[J]$
$W_p$	Penetration work	$[J]$
$W^{aff}$	Strain energy density function from affine network theory	$[J/m^3]$
$\dot{W}_V$	Energy dissipation due to viscous deformation	$[W/m^3]$
$\dot{W}_s$	Energy dissipation due to solvent migration	$[W/m^3]$
$x_i$	Molar fraction of the $i^{\text{th}}$ species	$[-]$
$z_i$	$i^{\text{th}}$ species charge	$[-]$

---

**Greek symbols**

$\alpha$	Elongation ratio	$[-]$
$\alpha$	Obstruction theory parameter	$[-]$
$\alpha_f$	Thermal linear expansion coefficient of the polymer	$[1/K]$
$\beta$	Contribution of the water to the expansion of the polymer	$[k_{g,dry\ Polymer} / k_{g,solvent}]$
$\beta_i$	Diffusivity parameter for the $i^{\text{th}}$ species	$[-]$
$\gamma$	Parameters used to relate the light intensity to the weight fraction	$[-]$
$\dot{\gamma}$	Rate of strain tensor	$[1/s]$
$\delta$	Thickness of the swollen region through which the solute diffuses (see 1.2.5)	$[m]$
$\delta$	infinitesimal thickness of the boundary element (see 3.3.2)	$[m]$
$\delta$	Identity tensor	$[-]$
$\varepsilon$	Relative permittivity	$[-]$
$\varepsilon_0$	Vacuum permittivity	$[F/m]$
$\zeta$	Friction coefficient	$[(Pa \cdot s)/m^2]$

$\theta_D$	Characteristic time for the diffusion of the solvent in the polymer	[s]
$\lambda_m$	Characteristic stress-relaxation time	[s]
$\bar{\mu}$	Chemical potential of the solvent in the external medium	[J]
$\mu_{el}$	Number of junctions in the network	[-]
$\mu_1$	Fluid viscosity	[Pa · s]
$\nu_{el}$	Number of elastic chains	[-]
$\xi$	Gel mesh size	[m]
$\eta$	Viscosity	[Pa · s]
$\pi$	Pi	
$\rho_i$	Density of the $i^{\text{th}}$ species	[kg / m <sup>3</sup> ]
$\sigma$	Cauchy stress tensor	[Pa]
$\tau$	Tensile stress	[Pa]
$\bar{v}$	Polymer-specific volume	[m <sup>3</sup> / kg]
$\Phi$	Total Helmholtz free energy	[J]
$\phi_i$	Volume fraction of the $i^{\text{th}}$ species	[-]
$\chi_{12}$	Flory–Huggins solvent–polymer interaction parameter	[-]
$\psi$	Electric potential	[V]
$\Omega$	Volume of each solvent molecule in the gel	[m <sup>3</sup> ]
$\omega_i$	Mass fraction of the $i^{\text{th}}$ species	[-]

## Author details

Diego Caccavo<sup>1</sup>, Sara Cascone<sup>1</sup>, Gaetano Lamberti<sup>1\*</sup>, Anna Angela Barba<sup>2</sup> and Anette Larsson<sup>3,4</sup>

\*Address all correspondence to: [glamberti@unisa.it](mailto:glamberti@unisa.it)

1 Dipartimento di Ingegneria Industriale, University of Salerno, Fisciano (SA), Italy

2 Dipartimento di Farmacia, University of Salerno, Fisciano (SA), Italy

3 SuMo Biomaterials, A Vinnova VINN Excellence Center at Chalmers University of Technology, Gotenburg, Sweden

4 Pharmaceutical Technology, Department of Chemical Engineering, Chalmers University of Technology, Gotenburg, Sweden

## References

- [1] A.S. Hoffman, Hydrogels for biomedical applications, *Advanced Drug Delivery Reviews*, 64 (2012) 18-23.
- [2] N. Peppas, P. Bures, W. Leobandung, H. Ichikawa, Hydrogels in pharmaceutical formulations, *European Journal of Pharmaceutics and Biopharmaceutics*, 50 (2000) 27-46.
- [3] N.A. Peppas, J.Z. Hilt, A. Khademhosseini, R. Langer, Hydrogels in biology and medicine: from molecular principles to bionanotechnology, *Advanced Materials*, 18 (2006) 1345.
- [4] O. Wichterle, D. Lim, Hydrophilic gels for biological use, *Nature*, 185 (1960) 117-118.
- [5] N.A. Peppas, *Hydrogels in Medicine and Pharmacy*, CRC Press, Boca Raton, 1987.
- [6] J. Cabral, S.C. Moratti, Hydrogels for biomedical applications, *Future Medicinal Chemistry*, 3 (2011) 1877-1888.
- [7] K.R. Kamath, K. Park, Biodegradable hydrogels in drug delivery, *Advanced Drug Delivery Reviews*, 11 (1993) 59-84.
- [8] N.A. Peppas, Hydrogels and drug delivery, *Current Opinion in Colloid & Interface Science*, 2 (1997) 531-537.
- [9] T.R. Hoare, D.S. Kohane, Hydrogels in drug delivery: progress and challenges, *Polymer*, 49 (2008) 1993-2007.
- [10] Y. Qiu, K. Park, Environment-sensitive hydrogels for drug delivery, *Advanced Drug Delivery Reviews*, 53 (2001) 321-339.
- [11] J. Siepmann, N.A. Peppas, Modeling of drug release from delivery systems based on hydroxypropyl methylcellulose (HPMC), *Advanced Drug Delivery Reviews*, 48 (2001) 139-157.
- [12] W.E. Hennink, C.F. van Nostrum, Novel crosslinking methods to design hydrogels, *Advanced Drug Delivery Reviews*, 54 (2002) 13-36.
- [13] C.-C. Lin, A.T. Metters, Hydrogels in controlled release formulations: network design and mathematical modeling, *Advanced Drug Delivery Reviews*, 58 (2006) 1379-1408.
- [14] P.J. Flory, *Principles of Polymer Chemistry*, Cornell University Press, Ithaca, 1953.
- [15] L.R.G. Treloar, *The Physics of Rubber Elasticity*, Oxford University Press, 1975.
- [16] P.J. Flory, J. Rehner Jr, Statistical mechanics of cross-linked polymer networks II. Swelling, *The Journal of Chemical Physics*, 11 (1943) 521-526.

- [17] P.J. Flory, Statistical mechanics of swelling of network structures, *The Journal of Chemical Physics*, 18 (1950) 108-111.
- [18] J.C. Bray, E.W. Merrill, Poly (vinyl alcohol) hydrogels. Formation by electron beam irradiation of aqueous solutions and subsequent crystallization, *Journal of Applied Polymer Science*, 17 (1973) 3779-3794.
- [19] N.A. Peppas, E.W. Merrill, Crosslinked poly (vinyl alcohol) hydrogels as swollen elastic networks, *Journal of Applied Polymer Science*, 21 (1977) 1763-1770.
- [20] N.A. Peppas, E.W. Merrill, Poly (vinyl alcohol) hydrogels: reinforcement of radiation-crosslinked networks by crystallization, *Journal of Polymer Science: Polymer Chemistry Edition*, 14 (1976) 441-457.
- [21] N.A. Peppas, E.W. Merrill, Determination of interaction parameter  $\chi_1$ , for poly (vinyl alcohol) and water in gels crosslinked from solutions, *Journal of Polymer Science: Polymer Chemistry Edition*, 14 (1976) 459-464.
- [22] L. Brannon-Peppas, N.A. Peppas, Equilibrium swelling behavior of pH-sensitive hydrogels, *Chemical Engineering Science*, 46 (1991) 715-722.
- [23] T. Canal, N.A. Peppas, Correlation between mesh size and equilibrium degree of swelling of polymeric networks, *Journal of Biomedical Materials Research*, 23 (1989) 1183-1193.
- [24] P.J. Flory, N. Rabjohn, M.C. Shaffer, Dependence of elastic properties of vulcanized rubber on the degree of cross linking, *Journal of Polymer Science*, 4 (1949) 225-245.
- [25] T. Alfrey, E. Gurnee, W. Lloyd, Diffusion in glassy polymers, *Journal of Polymer Science Part C: Polymer Symposia*, Wiley Online Library, 1966, pp. 249-261.
- [26] G.R. Davidson, N.A. Peppas, Solute and penetrant diffusion in swellable polymers: V. Relaxation-controlled transport in P (HEMA-co-MMA) copolymers, *Journal of Controlled Release*, 3 (1986) 243-258.
- [27] J. Vrentas, C. Jarzebski, J. Duda, A Deborah number for diffusion in polymer-solvent systems, *AIChE Journal*, 21 (1975) 894-901.
- [28] J. Vrentas, J. Duda, Diffusion in polymer-solvent systems. III. Construction of Deborah number diagrams, *Journal of Polymer Science: Polymer Physics Edition*, 15 (1977) 441-453.
- [29] G.R. Davidson, N.A. Peppas, Solute and penetrant diffusion in swellable polymers: VI. The Deborah and swelling interface numbers as indicators of the order of biomolecular release, *Journal of Controlled Release*, 3 (1986) 259-271.
- [30] G. Camera-Roda, G.C. Sarti, Mass transport with relaxation in polymers, *AIChE Journal*, 36 (1990) 851-860.

- [31] J. Wilmers, S. Bargmann, Simulation of non-classical diffusion in polymers, *Heat and Mass Transfer*, 50 (2014) 1543-1552.
- [32] J. Tritt-Goc, J. Kowalczyk, N. Piślewski, MRI study of Fickian, case II and anomalous diffusion of solvents into hydroxypropylmethylcellulose, *Applied Magnetic Resonance*, 29 (2005) 605-615.
- [33] J. Tritt-Goc, J. Kowalczyk, N. Piślewski, Hydration of hydroxypropylmethyl cellulose: effects of pH and molecular mass, *Acta Physica Polonica-Series A General Physics*, 108 (2005) 197-206.
- [34] D. Caccavo, G. Lamberti, A.A. Barba, S. Abrahmsén-Alami, A. Viridén, A. Larsson, Modeling of extended release matrix tablet performance: water up-take, polymer and drug release, and shape deformation, (in preparation).
- [35] N.A. Peppas, N.M. Franson, The swelling interface number as a criterion for prediction of diffusional solute release mechanisms in swellable polymers, *Journal of Polymer Science: Polymer Physics Edition*, 21 (1983) 983-997.
- [36] G. Grassi, R. Lapasin, M. Grassi, I. Colombo, *Understanding Drug Release and Absorption Mechanisms A Physical and Mathematical Approach*, 2007.
- [37] B. Amsden, Solute diffusion within hydrogels. Mechanisms and models, *Macromolecules*, 31 (1998) 8382-8395.
- [38] B. Amsden, Solute diffusion in hydrogels: an examination of the retardation effect, *Polymer Gels and Networks*, 6 (1998) 13-43.
- [39] L. Masaro, X. Zhu, Physical models of diffusion for polymer solutions, gels and solids, *Progress in Polymer Science*, 24 (1999) 731-775.
- [40] R. Cukier, Diffusion of Brownian spheres in semidilute polymer solutions, *Macromolecules*, 17 (1984) 252-255.
- [41] R. Phillips, W. Deen, J. Brady, Hindered transport of spherical macromolecules in fibrous membranes and gels, *AIChE Journal*, 35 (1989) 1761-1769.
- [42] A. Ogston, B. Preston, J. Wells, On the transport of compact particles through solutions of chain-polymers, in: *Proceedings of the Royal Society of London A: Mathematical, Physical and Engineering Sciences*, The Royal Society, 1973, pp. 297-316.
- [43] L. Johansson, C. Elvingson, J.E. Lofroth, Diffusion and interaction in gels and solutions. 3. Theoretical results on the obstruction effect, *Macromolecules*, 24 (1991) 6024-6029.
- [44] D.S. Tsai, W. Strieder, Effective conductivities of random fiber beds, *Chemical Engineering Communications*, 40 (1986) 207-218.

- [45] L. Johansson, J.E. Löfroth, Diffusion and interaction in gels and solutions. 4. Hard sphere Brownian dynamics simulations, *The Journal of Chemical Physics*, 98 (1993) 7471-7479.
- [46] D.S. Clague, R.J. Phillips, Hindered diffusion of spherical macromolecules through dilute fibrous media, *Physics of Fluids (1994-present)*, 8 (1996) 1720-1731.
- [47] H. Yasuda, A. Peterlin, C.K. Colton, K.A. Smith, E.W. Merrill, Permeability of solutes through hydrated polymer membranes. Part III. Theoretical background for the selectivity of dialysis membranes, *Die Makromolekulare Chemie*, 126 (1969) 177-186.
- [48] N.A. Peppas, C.T. Reinhart, Solute diffusion in swollen membranes. Part I. A new theory, *Journal of Membrane Science*, 15 (1983) 275-287.
- [49] S.R. Lustig, N.A. Peppas, Solute diffusion in swollen membranes. IX. Scaling laws for solute diffusion in gels, *Journal of Applied Polymer Science*, 36 (1988) 735-747.
- [50] W. Hennink, H. Talsma, J. Borchert, S. De Smedt, J. Demeester, Controlled release of proteins from dextran hydrogels, *Journal of Controlled Release*, 39 (1996) 47-55.
- [51] H. Fujita, Diffusion in polymer-diluent systems, in: *Fortschritte Der Hochpolymeren-Forschung*, Springer, Berlin, Heidelberg, 1961, pp. 1-47.
- [52] R.W. Korsmeyer, S.R. Lustig, N.A. Peppas, Solute and penetrant diffusion in swellable polymers. I. Mathematical modeling, *Journal of Polymer Science Part B: Polymer Physics*, 24 (1986) 395-408.
- [53] R.W. Korsmeyer, E. Von Meerwall, N.A. Peppas, Solute and penetrant diffusion in swellable polymers. II. Verification of theoretical models, *Journal of Polymer Science Part B: Polymer Physics*, 24 (1986) 409-434.
- [54] N. Graham, M. McNeill, Hydrogels for controlled drug delivery, *Biomaterials*, 5 (1984) 27-36.
- [55] S. Chirico, A. Dalmoro, G. Lamberti, G. Russo, G. Titomanlio, Analysis and modeling of swelling and erosion behavior for pure HPMC tablet, *Journal of Controlled Release*, 122 (2007) 181-188.
- [56] J. Siepmann, H. Kranz, R. Bodmeier, N. Peppas, HPMC-matrices for controlled drug delivery: a new model combining diffusion, swelling, and dissolution mechanisms and predicting the release kinetics, *Pharmaceutical Research*, 16 (1999) 1748-1756.
- [57] R.T. Ju, P.R. Nixon, M.V. Patel, Drug release from hydrophilic matrices. 1. New scaling laws for predicting polymer and drug release based on the polymer disentanglement concentration and the diffusion layer, *Journal of Pharmaceutical Sciences*, 84 (1995) 1455-1463.
- [58] R.T. Ju, P.R. Nixon, M.V. Patel, D.M. Tong, Drug release from hydrophilic matrices. 2. A mathematical model based on the polymer disentanglement concentration and the diffusion layer, *Journal of Pharmaceutical Sciences*, 84 (1995) 1464-1477.

- [59] R. Bettini, P. Catellani, P. Santi, G. Massimo, N. Peppas, P. Colombo, Translocation of drug particles in HPMC matrix gel layer: effect of drug solubility and influence on release rate, *Journal of Controlled Release*, 70 (2001) 383-391.
- [60] P.I. Lee, Kinetics of drug release from hydrogel matrices, *Journal of Controlled Release*, 2 (1985) 277-288.
- [61] K. Sung, P.R. Nixon, J.W. Skoug, T.R. Ju, P. Gao, E. Topp, M. Patel, Effect of formulation variables on drug and polymer release from HPMC-based matrix tablets, *International Journal of Pharmaceutics*, 142 (1996) 53-60.
- [62] J. Nerurkar, H. Jun, J. Price, M. Park, Controlled-release matrix tablets of ibuprofen using cellulose ethers and carrageenans: effect of formulation factors on dissolution rates, *European Journal of Pharmaceutics and Biopharmaceutics*, 61 (2005) 56-68.
- [63] K. Mitchell, J. Ford, D. Armstrong, P. Elliott, J. Hogan, C. Rostron, The influence of the particle size of hydroxypropylmethylcellulose K15M on its hydration and performance in matrix tablets, *International Journal of Pharmaceutics*, 100 (1993) 175-179.
- [64] S. Zuleger, B.C. Lippold, Polymer particle erosion controlling drug release. I. Factors influencing drug release and characterization of the release mechanism, *International Journal of Pharmaceutics*, 217 (2001) 139-152.
- [65] C. Maderuelo, A. Zarzuelo, J.M. Lanao, Critical factors in the release of drugs from sustained release hydrophilic matrices, *Journal of Controlled Release*, 154 (2011) 2-19.
- [66] S. Jamzad, L. Tutunji, R. Fassihi, Analysis of macromolecular changes and drug release from hydrophilic matrix systems, *International Journal of Pharmaceutics*, 292 (2005) 75-85.
- [67] S. Jamzad, R. Fassihi, Development of a controlled release low dose class II drug-Glipizide, *International Journal of Pharmaceutics*, 312 (2006) 24-32.
- [68] P.L. Mamani, R. Ruiz-Caro, M.D. Veiga, Matrix tablets: the effect of hydroxypropyl methylcellulose/anhydrous dibasic calcium phosphate ratio on the release rate of a water-soluble drug through the gastrointestinal tract I. In vitro tests, *AAPS PharmSciTech*, 13 (2012) 1073-1083.
- [69] A.A. Barba, M. d'Amore, S. Cascone, S. Chirico, G. Lamberti, G. Titomanlio, On the behavior of HPMC/theophylline matrices for controlled drug delivery, *Journal of Pharmaceutical Sciences*, 98 (2009) 4100-4110.
- [70] U.P. XXIII, The United States Pharmacopoeia Convention Inc, Rockville, 1995, pp 557.
- [71] M.U. Ghorji, G. Ginting, A.M. Smith, B.R. Conway, Simultaneous quantification of drug release and erosion from hypromellose hydrophilic matrices, *International Journal of Pharmaceutics*, 465 (2014) 405-412.

- [72] C. Remunan-Lopez, R. Bodmeier, Mechanical, water uptake and permeability properties of crosslinked chitosan glutamate and alginate films, *Journal of Controlled Release*, 44 (1997) 215-225.
- [73] P. Gao, R.H. Meury, Swelling of hydroxypropyl methylcellulose matrix tablets. 1. Characterization of swelling using a novel optical imaging method, *Journal of Pharmaceutical Sciences*, 85 (1996) 725-731.
- [74] K. Tahara, K. Yamamoto, T. Nishihata, Overall mechanism behind matrix sustained release (SR) tablets prepared with hydroxypropyl methylcellulose 2910, *Journal of Controlled Release*, 35 (1995) 59-66.
- [75] A.A. Barba, M. d'Amore, S. Chirico, G. Lamberti, G. Titomanlio, Swelling of cellulose derivative (HPMC) matrix systems for drug delivery, *Carbohydrate Polymers*, 78 (2009) 469-474.
- [76] A. Rajabi-Siahboomi, R. Bowtell, P. Mansfield, A. Henderson, M. Davies, C. Melia, Structure and behaviour in hydrophilic matrix sustained release dosage forms: 2. NMR-imaging studies of dimensional changes in the gel layer and core of HPMC tablets undergoing hydration, *Journal of Controlled Release*, 31 (1994) 121-128.
- [77] P. Gao, P.E. Fagerness, Diffusion in HPMC gels. I. Determination of drug and water diffusivity by pulsed-field-gradient spin-echo NMR, *Pharmaceutical Research*, 12 (1995) 955-964.
- [78] W.E. Baille, C. Malveau, X.X. Zhu, R.H. Marchessault, NMR imaging of high-amylose starch tablets. 1. Swelling and water uptake, *Biomacromolecules*, 3 (2002) 214-218.
- [79] S. Abrahmsén-Alami, A. Körner, I. Nilsson, A. Larsson, New release cell for NMR microimaging of tablets: swelling and erosion of poly (ethylene oxide), *International Journal of Pharmaceutics*, 342 (2007) 105-114.
- [80] F. Tajarobi, S. Abrahmsén-Alami, A.S. Carlsson, A. Larsson, Simultaneous probing of swelling, erosion and dissolution by NMR-microimaging—effect of solubility of additives on HPMC matrix tablets, *European Journal of Pharmaceutical Sciences*, 37 (2009) 89-97.
- [81] A. Viridén, S. Abrahmsén-Alami, B. Wittgren, A. Larsson, Release of theophylline and carbamazepine from matrix tablets—consequences of HPMC chemical heterogeneity, *European Journal of Pharmaceutics and Biopharmaceutics*, 78 (2011) 470-479.
- [82] L. Yang, B. Johnson, R. Fassihi, Determination of continuous changes in the gel layer thickness of poly (ethylene oxide) and HPMC tablets undergoing hydration: a texture analysis study, *Pharmaceutical Research*, 15 (1998) 1902-1906.
- [83] S. Nazzal, M. Nazzal, Y. El-Malah, A novel texture-probe for the simultaneous and real-time measurement of swelling and erosion rates of matrix tablets, *International Journal of Pharmaceutics*, 330 (2007) 195-198.

- [84] H. Li, X. Gu, Correlation between drug dissolution and polymer hydration: a study using texture analysis, *International Journal of Pharmaceutics*, 342 (2007) 18-25.
- [85] G. Lamberti, S. Cascone, M.M. Cafaro, G. Titomanlio, M. d'Amore, A.A. Barba, Measurements of water content in hydroxypropyl-methyl-cellulose based hydrogels via texture analysis, *Carbohydrate Polymers*, 92 (2013) 765-768.
- [86] S. Cascone, G. Lamberti, G. Titomanlio, M. d'Amore, A.A. Barba, Measurements of non-uniform water content in hydroxypropyl-methyl-cellulose based matrices via texture analysis, *Carbohydrate Polymers*, 103 (2014) 348-354.
- [87] P. Colombo, P. Catellani, N. Peppas, L. Maggi, U. Conte, Swelling characteristics of hydrophilic matrices for controlled release new dimensionless number to describe the swelling and release behavior, *International Journal of Pharmaceutics*, 88 (1992) 99-109.
- [88] R. Bettini, P. Colombo, G. Massimo, P.L. Catellani, T. Vitali, Swelling and drug release in hydrogel matrices: polymer viscosity and matrix porosity effects, *European Journal of Pharmaceutical Sciences*, 2 (1994) 213-219.
- [89] P. Colombo, R. Bettini, N.A. Peppas, Observation of swelling process and diffusion front position during swelling in hydroxypropyl methyl cellulose (HPMC) matrices containing a soluble drug, *Journal of Controlled Release*, 61 (1999) 83-91.
- [90] S. Kikuchi, Y. Onuki, H. Kuribayashi, K. Takayama, Relationship between diffusivity of water molecules inside hydrating tablets and their drug release behavior elucidated by magnetic resonance imaging, *Chemical and Pharmaceutical Bulletin*, 60 (2012) 536-542.
- [91] K.O. Hewlett, J. L'Hote-Gaston, M. Radler, K.R. Shull, Direct measurement of the time-dependent mechanical response of HPMC and PEO compacts during swelling, *International Journal of Pharmaceutics*, 434 (2012) 494-501.
- [92] S. Zuleger, R. Fassihi, B.C. Lippold, Polymer particle erosion controlling drug release. II. Swelling investigations to clarify the release mechanism, *International Journal of Pharmaceutics*, 247 (2002) 23-37.
- [93] K. Huanbutta, K. Terada, P. Sriamornsak, J. Nunthanid, Advanced technologies for assessment of polymer swelling and erosion behaviors in pharmaceutical aspect, *European Journal of Pharmaceutics and Biopharmaceutics*, 83 (2013) 315-321.
- [94] T. Higuchi, Rate of release of medicaments from ointment bases containing drugs in suspension, *Journal of Pharmaceutical Sciences*, 50 (1961) 874-875.
- [95] N.A. Peppas, Analysis of Fickian and non-Fickian drug release from polymers, *Pharmaceutica Acta Helvetiae*, 60 (1985) 110-111.

- [96] N.A. Peppas, J.J. Sahlin, A simple equation for the description of solute release. III. Coupling of diffusion and relaxation, *International Journal of Pharmaceutics*, 57 (1989) 169-172.
- [97] C.-C. Lin, A.T. Metters, Hydrogels in controlled release formulations: network design and mathematical modeling, *Advanced Drug Delivery Reviews*, 58 (2006) 1379-1408.
- [98] J.E. Mark, B. Erman, *Rubberlike Elasticity: A Molecular Primer*, Cambridge University Press, Cambridge, UK, 2007.
- [99] G.A. Holzapfel, *Nonlinear Solid Mechanics*, Wiley, Chichester, 2000.
- [100] F. Horkay, G. McKenna, Polymer networks and gels, in: J. Mark (Ed.) *Physical Properties of Polymers Handbook*, Springer, New York, 2007, pp. 497-523.
- [101] E.C. Achilleos, K.N. Christodoulou, I.G. Kevrekidis, A transport model for swelling of polyelectrolyte gels in simple and complex geometries, *Computational and Theoretical Polymer Science*, 11 (2001) 63-80.
- [102] J. Ricka, T. Tanaka, Swelling of ionic gels: quantitative performance of the Donnan theory, *Macromolecules*, 17 (1984) 2916-2921.
- [103] P. Chiarelli, D. De Rossi, Polyelectrolyte intelligent gels: design and applications, in: *Ionic Interactions in Natural and Synthetic Macromolecules*, Wiley, Hoboken, 2012, pp. 581-620.
- [104] T. Wallmersperger, Modelling and simulation of the chemo-electro-mechanical behaviour, in: G. Gerlach, K.-F. Arndt (Eds.) *Hydrogel Sensors and Actuators*, Springer, Berlin, Heidelberg, 2010, pp. 137-163.
- [105] W. Hong, Z. Liu, Z. Suo, Inhomogeneous swelling of a gel in equilibrium with a solvent and mechanical load, *International Journal of Solids and Structures*, 46 (2009) 3282-3289.
- [106] J. Siepmann, H. Kranz, R. Bodmeier, N.A. Peppas, HPMC-matrices for controlled drug delivery: a new model combining diffusion, swelling, and dissolution mechanisms and predicting the release kinetics, *Pharmaceutical Research*, 16 (1999) 1748-1756.
- [107] S. Kiil, K. Dam-Johansen, Controlled drug delivery from swellable hydroxypropyl-methylcellulose matrices: model-based analysis of observed radial front movements, *Journal of Controlled Release*, 90 (2003) 1-21.
- [108] A.A. Barba, M. d'Amore, S. Chirico, G. Lamberti, G. Titomanlio, A general code to predict the drug release kinetics from different shaped matrices, *European Journal of Pharmaceutical Sciences*, 36 (2009) 359-368.

- [109] T. Coviello, M. Grassi, R. Lapasin, A. Marino, F. Alhaique, Scleroglucan/borax: characterization of a novel hydrogel system suitable for drug delivery, *Biomaterials*, 24 (2003) 2789-2798.
- [110] G. Lamberti, I. Galdi, A.A. Barba, Controlled release from hydrogel-based solid matrices. A model accounting for water up-take, swelling and erosion, *International Journal of Pharmaceutics*, 407 (2011) 78-86.
- [111] E. Kaunisto, S. Abrahmsen-Alami, P. Borgquist, A. Larsson, B. Nilsson, A. Axelsson, A mechanistic modelling approach to polymer dissolution using magnetic resonance microimaging, *Journal of Controlled Release : Official Journal of the Controlled Release Society*, 147 (2010) 232-241.
- [112] E. Kaunisto, F. Tajarobi, S. Abrahmsen-Alami, A. Larsson, B. Nilsson, A. Axelsson, Mechanistic modelling of drug release from a polymer matrix using magnetic resonance microimaging, *European Journal of Pharmaceutical Sciences*, 48 (2013) 698-708.
- [113] B.R. Bird, W.E. Stewart, E.N. Lightfoot, *Transport Phenomena*, Wiley, New York, 2007.
- [114] D. Caccavo, S. Cascone, G. Lamberti, A.A. Barba, Modeling the drug release from hydrogel-based matrices, *Molecular Pharmaceutics*, 12 (2015) 474-483.
- [115] D. Caccavo, S. Cascone, G. Lamberti, A.A. Barba, Controlled drug release from hydrogel-based matrices: experiments and modeling, *International Journal of Pharmaceutics*, 486 (2015) 144-152.
- [116] E.C. Achilleos, R.K. Prud'homme, I.G. Kevrekidis, K.N. Christodoulou, K.R. Gee, Quantifying deformation in gel swelling: Experiments and simulations, *AIChE Journal*, 46 (2000) 2128-2139.
- [117] W. Hong, X. Zhao, J. Zhou, Z. Suo, A theory of coupled diffusion and large deformation in polymeric gels, *Journal of the Mechanics and Physics of Solids*, 56 (2008) 1779-1793.
- [118] W. Hong, X. Zhao, Z. Suo, Large deformation and electrochemistry of polyelectrolyte gels, *Journal of the Mechanics and Physics of Solids*, 58 (2010) 558-577.
- [119] A. Lucantonio, P. Nardinocchi, L. Teresi, Transient analysis of swelling-induced large deformations in polymer gels, *Journal of the Mechanics and Physics of Solids*, 61 (2013) 205-218.
- [120] S.A. Chester, L. Anand, A coupled theory of fluid permeation and large deformations for elastomeric materials, *Journal of the Mechanics and Physics of Solids*, 58 (2010) 1879-1906.

- [121] F.P. Duda, A.C. Souza, E. Fried, A theory for species migration in a finitely strained solid with application to polymer network swelling, *Journal of the Mechanics and Physics of Solids*, 58 (2010) 515-529.
- [122] M.K. Kang, R. Huang, A variational approach and finite element implementation for swelling of polymeric hydrogels under geometric constraints, *Journal of Applied Mechanics*, 77 (2010) 061004.
- [123] X. Wang, W. Hong, A visco-poroelastic theory for polymeric gels, *Proceedings of the Royal Society A: Mathematical, Physical and Engineering Sciences*, 468 (2012) 3824-3841.
- [124] J.C. Kurnia, E. Birgersson, A.S. Mujumdar, Computational study of pH-sensitive hydrogel-based microfluidic flow controllers, *Journal of Functional Biomaterials*, 2 (2011) 195-212.
- [125] J.C. Kurnia, E. Birgersson, A.S. Mujumdar, Finite deformation of fast-response thermo-sensitive hydrogels – a computational study, *Polymer*, 53 (2012) 2500-2508.
- [126] E. Birgersson, H. Li, S. Wu, Transient analysis of temperature-sensitive neutral hydrogels, *Journal of the Mechanics and Physics of Solids*, 56 (2008) 444-466.
- [127] Y. Xu, Y. Jia, Z. Wang, Z. Wang, Mathematical modeling and finite element simulation of slow release of drugs using hydrogels as carriers with various drug concentration distributions, *Journal of Pharmaceutical Sciences*, 102 (2013) 1532-1543.
- [128] J.C. Kurnia, *Computational Study of Transport Phenomena and Deformation Behavior of Stimuli Sensitive Hydrogels*, Department of Mechanical Engineering, National University of Singapore, 2011.
- [129] H. Li, *Smart Hydrogel Modelling*, Springer, Heidelberg, New York, 2009.



---

# Antibiotic Drug Delivery Systems for the Intracellular Targeting of Bacterial Pathogens

---

Mariana Carmen Chifiriuc, Alina Maria Holban, Carmen Curutiu, Lia-Mara Ditu, Grigore Mihaescu, Alexandra Elena Oprea, Alexandru Mihai Grumezescu and Veronica Lazar

Additional information is available at the end of the chapter

<http://dx.doi.org/10.5772/61327>

---

## Abstract

Intracellular bacterial pathogens are hard to treat because of the inability of conventional antimicrobial agents belonging to widely used classes, like aminoglycosides and  $\beta$ -lactams, fluoroquinolones, or macrolides to penetrate, accumulate, or be retained in the mammalian cells. The increasing problem of antibiotic resistance complicates more the treatment of the diseases caused by these agents. In many cases, the increase in therapeutic doses and treatment duration is accompanied by the occurrence of severe side effects. Taking into account the huge financial investment associated with bringing a new antibiotic to the market and the limited lifetime of antibiotics, the design of drug delivery systems to enable the targeting of antibiotics inside the cells, to improve their activity in different intracellular niches at different pH and oxygen concentrations, and to achieve a reduced dosage and frequency of administration could represent a prudent choice. An ideal drug delivery system should possess several properties, such as antimicrobial activity, biodegradability, and biocompatibility, making it suitable for use in biomedical and pharmaceutical formulations. This approach will allow reviving old antibiotics rendered useless by resistance or toxicity, rescuing the last line therapy antibiotics by increasing the therapeutic index, widening the antimicrobial spectrum of antibiotics scaffolds that failed due to membrane permeability problems, and thus reducing the gap between increasingly drug-resistant pathogens and the development of new antibiotics. Different improved drug carriers have been developed for treating intracellular pathogens, including antibiotics loaded into liposomes, microspheres, polymeric carriers, and nanoplexes. The purpose of this chapter is to present the limitations of each class of antibiotics in targeting intracellular pathogens and the main research directions for the development of drug delivery systems for the intracellular release of antibiotics.

**Keywords:** Intracellular bacterial pathogens, drug delivery systems, drug carriers, liposomes, polymeric carriers, nanoplexes

## 1. Introduction

Infections with intracellular bacterial pathogens are hard to treat due to the inability of conventional antimicrobial agents to penetrate, accumulate, or be retained in the mammalian cells [1]. The increasing problem of antibiotic resistance complicates more the treatment of the diseases caused by these agents.

Taking into account the huge financial investment associated with bringing a new antibiotic to the market and the limited lifetime of antibiotics, the design of drug delivery systems to enable the targeting of antibiotics inside the cells, to improve their activity in different intracellular niches at different pH and oxygen concentrations, and to achieve a reduced dosage and frequency of administration could represent a prudent choice [2]. This approach will allow reviving old antibiotics rendered useless by resistance or toxicity, rescuing the last line therapy antibiotics by increasing the therapeutic index, widening the antimicrobial spectrum of antibiotics scaffolds that failed due to membrane permeability problems, and thus reducing the gap between increasingly drug-resistant pathogens and the development of new antibiotics.

The purpose of this review is to present the limitations of each class of antibiotics in targeting intracellular pathogens and the main research directions for the development of drug delivery systems for the intracellular release of antibiotics.

## 2. Microbial adaptation to the intracellular lifestyle

Invasion (aggressiveness or invasiveness) represents the ability of pathogens to overcome epithelial barriers through specific mechanisms, to penetrate the host tissue, and to multiply, producing pathological effects [3]. Invasive microorganisms have the ability to penetrate into the host tissues or to stimulate the endocytic function of the substrate and to maintain their viability in the host cell [4].

Many pathogenic bacteria are capable of surviving inside eukaryotic, normally nonphagocytic cells (mucosal cells and blood vessel endothelial cells) [5, 6]. The intracellular medium offers protection to the microorganisms that could thereby multiply or persist [7].

Some pathogenic bacteria are facultative intracellular (e.g., *Mycobacterium* spp., *Listeria monocytogenes*, and *Salmonella* spp.) going through an intracellular phase during infectious cycle without being strictly dependent on the cellular medium, while others are obligate intracellular parasites (*Chlamydia* spp. and *Rickettsia* spp.), which do not survive in the extracellular medium of the host. They infect endothelial and epithelial cells and also monocytes.

Generally, invasive organisms adhere to the host cells using a class of molecules represented by proteins with adhesion function associated to the cell surface called invasins, which direct the entry of the bacteria into the cells [8]. The mechanisms of adherence trigger or promote cellular signals, which directly or indirectly facilitate the bacterial penetration [9].

After bacterial adherence, invasion is produced in two ways: (a) the “zipper” mechanism—after binding to the host cell, the adherent bacteria induce changes of the cytoskeleton, in particular, actin filaments, resulting in the embedding of the bacteria, and (b) internalization by a pathway independent of the membrane molecules that mediate adherence. In this case, the interaction of the bacteria with the host cell membrane produces localized intrusion (ruffling), followed by endocytosis [10].

Professional phagocytes express membrane receptors for conserved structures of the microbial pathogens called pathogen-associated microbial patterns (PAMP), which are missing from mammalian cells. The broad spectrum of microbial pathogens is therefore recognized by a limited number of receptor molecules of the host (pathogen recognition receptors [PRR]) belonging to the following groups: *receptors of TLR family (Toll-like receptors)*, which recognize different structures of the microorganisms—glycoproteins, lipoproteins, heat shock proteins, and flagellar proteins; *lectin-type receptors* with specificity for common carbohydrates expressed on the surface of bacteria, i.e.: (a) receptors for mannose (MBL) that could also recognize other carbohydrates (*N*-acetylglucosamine, glucose, and L-fucose), (b) receptors for galactose recognizing *N*-acetyl-galactosamine and galactose, (c) receptors for fucose and specific membrane molecules, such as CD14 with specificity for glycolipids (LPS) and for the lipoarabinomannans (LAM) of mycobacteria.

The fact that adhesion of bacteria to eukaryotic cells requires the recognition of specific oligosaccharides or glycoproteins [11] was demonstrated by the *in vitro* experimental results, showing that oligosaccharides are the most potent inhibitors of the interaction between the bacteria and the eukaryotic cell surface.

Invasion is an active event, sustained by normal cell functions [12], with the host cell cytoskeleton supporting the invasion and embedding process [13].

Pathogenic bacteria, such as *L. monocytogenes*, *Shigella* spp., and *Rickettsia* spp., possess mechanisms that induce cytoskeletal rearrangements (actin condensation with the formation of a propulsion actin comet behind the bacterial cells) of the host cell to assure their cytoplasmatic and intercellular transit [13].

Some bacterial strains could modulate the host cell apoptosis during the infectious cycle [14]. This proapoptotic effect could facilitate the endocytosis of the apoptotic bodies containing bacterial cells by the adjacent cells, without the occurrence of an inflammatory process, but bacteria could spread into the healthy tissues at the same time. The bacteria-induced apoptosis is mediated by the activation of caspases or Fas/FasL pathways correlated with the inactivation of antiapoptotic proteins (e.g., NFκB and MAP kinases). *Pseudomonas aeruginosa* could induce the lung epithelial cells apoptosis, a process by which the bacterial cells are cleared from the lung or other infected organs. However, *P. aeruginosa* could invade, survive, and multiply in the host cells and induce an antiapoptotic effect in order to maintain its host and protect itself from the immune response effectors [15].

By using microscopy evaluation and viable cells count assays, we have demonstrated that *P. aeruginosa* clinical strains could survive and multiply in nonphagocytic epithelial cells [5], inducing changes of cellular morphology (cytoplasm wrinkling, the formation of long, lamellar

pseudopodes). The respective *P. aeruginosa* strains were also able to modulate the apoptosis of the infected cells by increasing the expression of the proapoptotic caspase 3 and Bax genes and by decreasing the expression level of the antiapoptotic Bcl-2 and Mcl-1 genes [16].

Selective adherence to the microfold (M) cells is an effective way of invasion. Bacteria and viruses that use M cells transport pathways can infect the gastrointestinal mucosa and may disseminate systemically.

M cells, which cover the Peyer's patches, separate the epithelium-associated lymphoid follicles from the gut lumen. They are coated with a thin mucous layer, have short microvilli, but are very active in terms of pinocytosis compared with columnar epithelial cells. The Peyer's patches, consisting of aggregated lymphoid follicles, are the major component of the mucosal immune system and have a precise function: to exclude exogenous antigens, before they enter into the internal medium, and to avoid or minimize the exposure of the systemic immune apparatus to molecular antigens or cells that reach the internal medium. At the same time, mucosa-associated lymphoid tissue (MALT) should remain insensitive to normal mucosal microbiota. MALT is therefore a "control zone" of the body in contact with antigens and also has a regulatory role on the functionality of systemic immune response. This explains the fact that oral administration of an antigen in human or animals, in essence, does not produce a systemic immune response, but typically a mucosal immune response. The mechanism is unknown, but the mucosal immune system prevents an extensive immune response after the contact with a large number of intestinal antigens, especially with food origin. Bacterial or viral complex antigens can initiate a complex immune response through mucosal immune apparatus. MALT functional deficiencies expose the organism and systemic immune apparatus to a permanent state of activation, which exceeds the physiological limits, with the possible occurrence of autoimmune diseases [17].

M cells can uptake by pinocytosis soluble luminal material and transfer it to the underlying macrophages. Macrophages process the antigens and present them to the adjacent lymphocytes. They have few lysosomes, and the embedded materials are not submitted to degradation. M cells are carrying macromolecules, particles, and microorganisms directly into the cellular environment of the mucosal lymphoid follicles.

M cells have no receptors for polymeric immunoglobulins, indicating that they do not transfer IgA, which favors the access of the antigens to the mucosal surface. They are specialized for the transepithelial transport. The basolateral surface of M cells is deeply intrusive, presenting extensions of about 10- $\mu$ m dimension, which are forming a big intraepithelial "pocket" and extending in the underlying lymphoid tissue, in which transported macromolecules and particles are released. Below the epithelial M cells, there is a rich population of macrophages and dendritic cells in close spatial relationship with CD4 T cells harboring the  $\alpha\beta$  type receptor and B cells. Few lymphocytes are memory T cells or uncommitted (naive) cells. The folds of M cell are the site of interaction between T cells and antigen-presenting cells (B cells and macrophages).

Through follicular epithelium, microorganisms gain access to the lymphoid follicle structures. The consequence is beneficial because it initiates protective immune response against luminal

microorganisms. M cells are therefore regarded as an early warning system of the immune system. Although M cells have evolved as a strategic protective system, their functional properties are qualifying them as true gateways—the Achilles heel of the intestine, because the pathogenic bacteria could gain in this way access to deeper structures.

The bacterial cells interact with M cells, probably via carbohydrates [18]. M cells possess a wide range of glycoconjugates that modulate their capacity to uptake microorganisms [19]. Further, macrophages and dendritic are involved in the embedding pathogens transported by M cells, in processing and storing antigens [20].

Certain *Escherichia coli* pathogenic strains that colonize the intestinal mucosa could selectively adhere to the epithelial cells and interact with the M cells. The adherence to intestinal epithelial cells and to M cells induces the disintegration of the microvilli and M cells folds and also the appearance of some special structures called pedestals—a consequence of actin filaments reorganization at the adhesion site [21].

*Shigella* sp., a facultative intracellular pathogen induces severe damages of the small intestine and colon mucosa, accompanied by the loss of epithelial barrier function. *Shigella* sp. cells adhere to the cellular membrane, are phagocytosed and released into the cytoplasm after the degradation of the phagosome membrane, where they multiply, induce the assembly of a tail of actin filaments, and are eliminated in a vacuole with membranar origin, which is subsequently phagocytosed by the neighboring cells [22].

*In vitro* experiments with enterocytes have shown that *Shigella flexneri* does not invade the apical surface, if the epithelial tight junctions are intact. The invasion is possible only through the basolateral membrane. *In vivo*, *Shigella* invades the mucosa, first of all, through M cells, followed by the invasion of epithelial cells through the basolateral surface. Mucosal ulcerations have the highest frequency in the ileum and colon, where lymphoid follicles and M cells are more numerous. We have demonstrated that *S. flexneri* and *S. boydii* strains modulated the expression of different anti- and proinflammatory cytokines in HeLa cells, by decreasing the production of IL-1 $\beta$ , IL-6, TNF- $\alpha$ , and IL-17 [22, 23].

Studies on the relationship between viral and bacterial infections showed that the immunity of host organism is reduced temporarily in the context of viral infections, increasing the incidence of bacterial infections, probably by increasing the level of expression of epithelial cell receptors for bacterial adhesins. Virus-infected host cells could also undertake changes of the cytoskeleton [24], which may result in the increase/decrease of the bacterial invasion capacity. Therefore, we have investigated the influence of viral preinfection using vaccinia, measles, echovirus 32, and herpes simplex virus 1 strains on the ability of an enteroinvasive *E. coli* strain to colonize the HeLa cells, and we have demonstrated that the viral preinfection of the cellular substrate induced a decrease of the invasive ability, pleading for an increased incidence of infections with extracellular pathogenic organisms after viral infections [6].

In the small intestine, *Vibrio cholerae* expresses a group of pilliary adhesins used for the adherence to the enterocytes. The pilli maintain the vibriions adhered on the surface of the mucosa, and the cholera toxin induces the secretion of chloride ions from the intestinal cells into the lumen. *V. cholerae* also interacts closely with extensive areas of the apical membrane

of the M cells. The activating signal induces actin reorganization, and bacterial cell is phagocytosed, without the M cell damaging. However, bacteria embedding in the M cells does not cause the disease in this case [25], but on the contrary, the process activates a protective immune response of the mucosa, mediated by the secretion of anti-toxin and anti-LPS sIgA, which can prevent mucosal colonization by *V. cholerae* and by default, prevent diarrheal disease.

The ingestion of *Salmonella* cells induces the infection of Peyer's patches. *S. typhi* and *S. typhimurium* adhere rapidly and selectively to M cells and also directly invade through epithelium villi. *Salmonella* sp. cells are embedded in a large endocytic vacuole by a phagocytosis mechanism induced after apical microvilli disassembling and cytoskeleton reorganization.

The experiments with the ligated intestinal loops showed that after 30 min of injection, *Salmonella* sp. cells induce the growth of M cells volume; and a rapid incorporation of the bacteria was observed, followed by the degeneration of M cells and the access of the infectious cells to the mucosa structure.

*Yersinia* sp. cells penetrate the intestinal mucosa through M cells to which bacteria adhere preferentially, being embedded and crossing the cytoplasm by transcytosis.

A few bacterial species are able to force the entrance directly into the host cells, after adherence, by the local enzymatic digestion of the host cell membrane. For example, *Rickettsia prowazekii* secretes phospholipases that determine the localized and controlled degradation of the host cell membrane. Through the membrane lesions, the pathogen enters directly into the cytoplasm [26].

Most bacteria, including many pathogenic bacteria, are killed after their phagocytosis by macrophages or neutrophils (PMNN). Some other species have developed some strategies that allow them to survive and multiply inside phagocytes. *S. flexneri*, *L. monocytogenes*, and *Rickettsia* sp. dissolve the initial membrane vacuole and thus gain access to the cytoplasm rich in nutrients. *Salmonella* spp., *Mycobacterium* spp., and *Legionella* spp. could inhibit the fusion between phagosome and lysosome and thus escape phagocytosis.

The virulence factors that determine the bacterial resistance to lysosomal enzymes and increase the intracellular survival capacity are cell surface protective envelopes (capsule and LPS), bacterial enzymes that neutralize the toxic free radicals and reactive oxygen species, and proteolytic enzymes that degrade the lysosomal enzymes of the host [13].

### **3. Efficiency of different classes of antibiotics against intracellular pathogens**

Antibiotics are low molecular weight substances produced by microbial biosynthetic processes or by chemical synthesis, which can be used in low concentrations to specifically inhibit the proliferation or to kill microorganisms [27]. Because of their high specificity, antibiotics exhibit different efficiencies against various microbial species. Antimicrobial

drugs act by different mechanisms, such as inhibition of cell wall synthesis, inhibition of cell membrane functions, inhibition of protein synthesis at different stages (translation or transcription), inhibition of nucleic acid synthesis, and blockage of metabolic pathways by competitive inhibition (Figure 1) [28].

Depending on the number and diversity of affected microbial species, the activity spectrum of the antibiotics can be broad (i.e., the spectrum of tetracycline is represented by Gram-negative bacteria, including *Chlamydia* sp. and *Rickettsia* sp. and Gram-positive species; penicillins are active especially against Gram-positive species, and some Gram-negative bacteria, including *Chlamydia* sp., nitrofurans, rifampin, and sulfonamides are active on a large number of Gram-positive and Gram-negative bacteria species), narrow (novobiocin is active on Gram-positive bacteria, especially staphylococci, but also on Gram-negative species, such as *Haemophilus* sp. and *Pasteurella* sp., glycopeptides and bacitracin are active against Gram-positive bacteria), and limited (nitroimidazoles are active only against anaerobic microorganisms).

Even within the same microbial species, there can be large differences regarding the susceptibility of different strains to a particular antibiotic; thus, antibiotic treatment in the clinical setting requires the isolation of the microbial strain, which is the etiologic agent of a specific infection (especially if it belongs to genera and species with a high ability of acquiring clinical resistance) and determining its antibiotic susceptibility spectrum.

The *in vivo* antimicrobial activity is more complex, involving different host-related factors along with the impact of the antibiotic and the nature of the antimicrobial agent. Thus, in the host, a number of local factors (partial pressure of O<sub>2</sub>, pH etc.) could influence the activity of the antibiotic. On the other hand, antibiotics are absorbed within the intestinal tract and distributed unevenly in various tissues and body fluids, and very few reach active concentrations in the central nervous system (CNS) or inside most eukaryotic cells. It is also very difficult to maintain an active concentration of the antibiotic for a prolonged period of time, so the interval between doses should be rigorously respected. Some antibiotics have postantibiotic effects (such as observed in the case of carbapenems activity against the Gram-negative bacilli) and may modulate the inflammatory response by indirectly inducing the chronicity of inflammatory reactions due to the accumulation of bacterial fragments. The combination of two or more antimicrobials is recommended for the treatment of severe and chronic infections to avoid the appearance of resistant mutants (i.e., tuberculosis) and also in mixed infections, for obtaining a synergy of action and a strong bactericidal effect (i.e., beta lactams and aminoglycosides, trimethoprim and sulfamethoxazole, amphotericin and flucytosine, beta-lactamase inhibitors and beta-lactam antibiotics).

Some antibiotic classes, such as macrolides, fluoroquinolones, tetracyclines, and ansamycins, are known to be active against obligate intracellular and facultative intracellular organisms, while others, such as beta-lactams and aminoglycosides, show no or only a poor intracellular activity. However, these antibiotics are active against facultative intracellular organisms, including *Mycobacterium tuberculosis*.

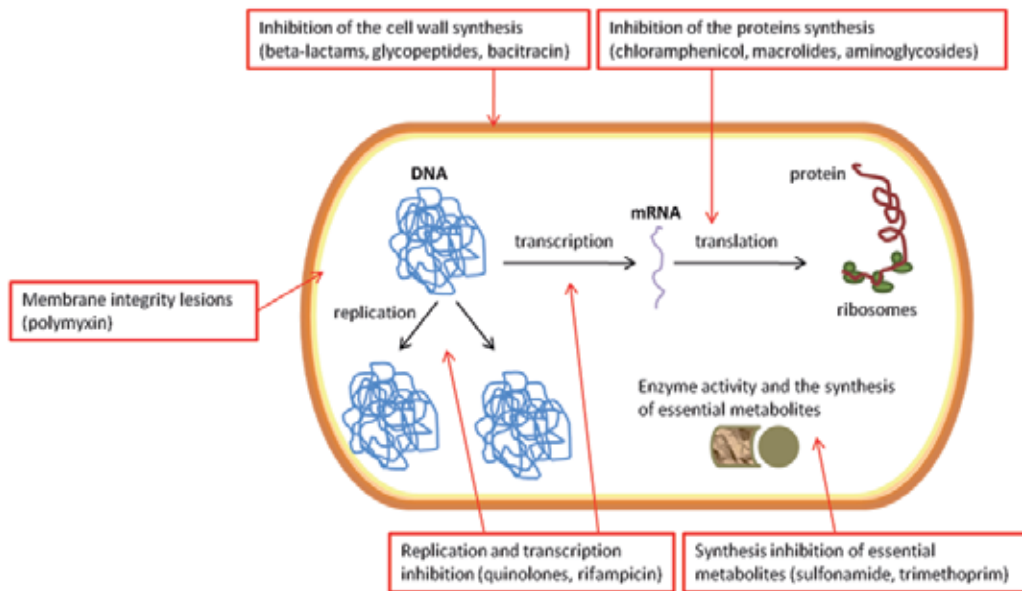


**Figure 1.** The main mechanisms of action and cellular targets of antibiotics within the bacterial cell.

### 3.1. Inhibition of cell wall synthesis

Peptidoglycan cell wall is a closed structure, composed by covalently linked units, which allow the sequential addition of new units on the external side of the cytoplasmic membrane, while the old units from the peptidoglycan's structure are shifted outward and released by the action of autolysins.

The synthesis of the peptidoglycan takes place in three stages: (i) low-molecular-weight-soluble precursors (GlcAc UDP and UDP-MurNAc-L-Ala-D-Glu-mezoDap-D-Ala-D-Ala) are synthesized in the cytoplasm; (ii) the nonnucleotide region of the previously synthesized molecular precursor (intermediate *N*-acetyl glucosamine and *N*-acetyl muramic acid-penta-peptide) is attached to a lipid carrier, integrated in the membrane and subsequently modified by adding GlcNAc and pentaglycine, resulting undecaprenol-pyrophosphate MurNAc (L-Ala-D-Gln [NH<sub>2</sub> [Gly5] L-Lys-D-Ala-D-Ala]-[beta1-4]-GlcNAc), that will be translocated across the plasma membrane and serves as a substrate for a transglycosylation reaction, polymerizing the bacterial glycan chains of the cell wall, to form a repetitive disaccharide (MurNAc-GlcNAc)<sub>n</sub>; and (iii) the subunits of the peptidoglycan are polymerized by their insertion in the preexisting cell wall, by the reaction of transpeptidation, which takes place at the terminal D-ala-D-ala residues.

The polymerization and cross-linking of the sugar tetrapeptide chains are catalyzed by penicillin-binding protein enzymes (PBP), located in the cytoplasmic membrane and the periplasmic space.

Some antibacterial agents interfere with the early steps of the cell wall synthesis (vancomycin, bacitracin, and cycloserine), while others ( $\beta$ -lactam antibiotics, penicillins, cephalosporins, monobactams, and carbapenems) inhibit the last steps of peptidoglycan synthesis, such as the formation of interpeptidic links, because these antibiotics have structural analogy with terminal D-ala-D-ala dipeptide [29].

Glycopeptides (vancomycin and teicoplanin) inhibit the early stage of the peptidoglycan synthesis by binding to the carboxy-terminal dipeptide D-Ala-D-Ala. It has been revealed that vancomycin shows a slow uptake and modest accumulation into macrophages, especially in the lysosomes compartment (up to eightfold in 24 h) [30, 31], while teicoplanin, a more lipophilic compound, shows a more extensive and faster intracellular accumulation (40- to 60-fold) [32, 33].

A newly investigated glycopeptide antibiotic called oritavancin (LY333328) proved to be avidly accumulated by J774 and THP-1 macrophages and rat fibroblasts and to a lesser extent by LLC-PK1 and Caco-2 cells. The intracellular pharmacokinetic and pharmacodynamic results demonstrated that the level of accumulation reached a plateau (at 370-fold the extracellular concentration) within 24 h, and the effect was partly defeated by a rise in serum protein levels [34].

Bacitracin (a cyclic peptide) prevents the dephosphorylation of the lipid carrier molecule, which transfers a newly synthesized peptidoglycan molecule to the cell membrane during the synthesis of the cell wall. This antibiotic is toxic to kidneys and is not systemically administered but is applied topically to treat skin and mucosa infections.

Cycloserine competitively inhibits the formation of D-ala from L-ala and thus stops the synthesis of the dipeptide D-ala-D-ala. This antibiotic is relatively toxic and is used for the treatment of *M. tuberculosis* infections resistant to other drugs.

Fosfomycin is a pyruvyl-transferase inhibitor, which blocks the synthesis of *N*-acetyl-muramic acid.

Cycloserine and fosfomycin act as peptidoglycan precursor analogues. They are very hydrophilic molecules and enter the cytoplasm following the path of transport systems usually utilized for some related metabolites; i.e., fosfomycin is structurally analogous to the phosphoenol-pyruvate and cycloserine is similar to D-alanine.

Beta-lactam antibiotics act as pseudosubstrates and perform the acylation of the active sites of the PBP transpeptidases, which are thus unable to catalyze the polymerization of the peptidoglycan. The acylation reaction of the PBP is very slowly reversible. PBP-deacylated enzymes are unable to catalyze the cross-linking of peptides (Figure 2). Antibiotic-PBP complexes stimulate the release of autolysins, which produce the degradation of the cell wall, leading to osmotic bacterial cell lysis.

The inhibitors of beta-lactamase enzymes, such as clavulanic acid, sulbactam, tazobactam, have a high affinity for the respective antibiotic-inactivating enzymes, inducing their acylation and formation of stable, unefficient complexes (Figure 3).

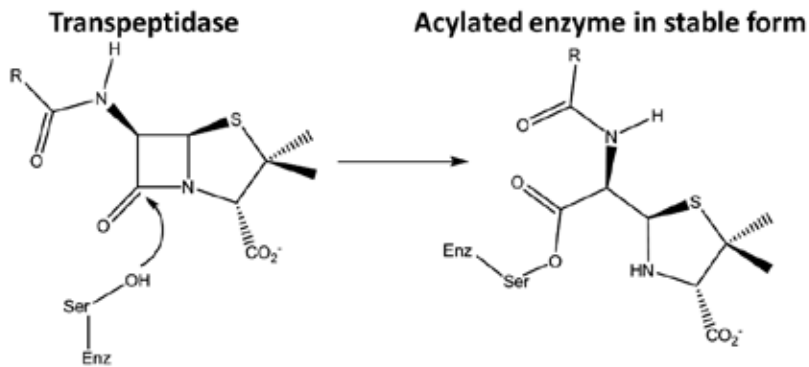


Figure 2. Beta-lactam antibiotics mediate the inactivation of PBP by the acylation reaction.

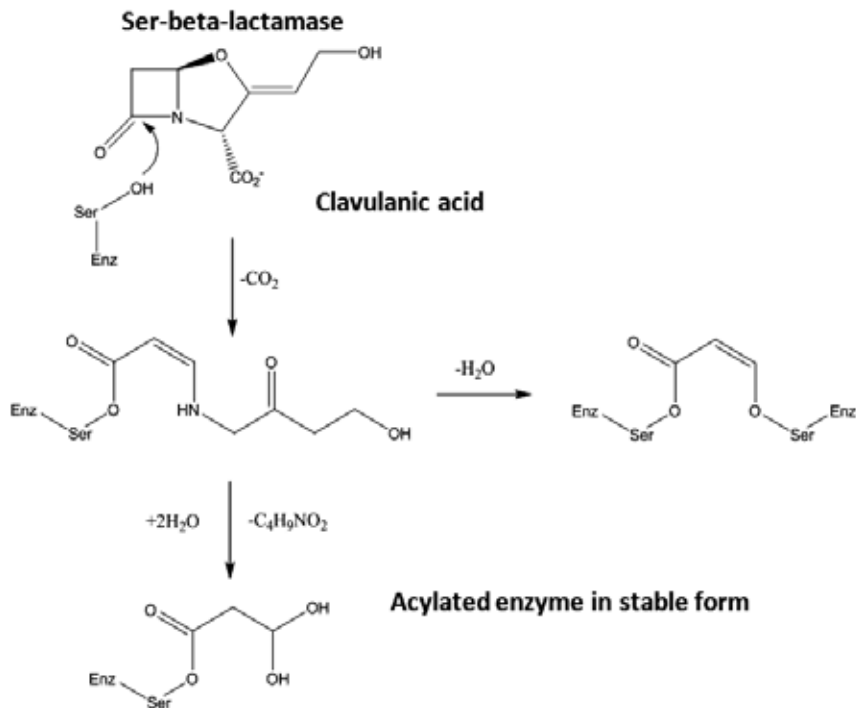


Figure 3. Beta-lactamase enzymes inactivation by acylation in the presence of clavulanic acid.

Penicillin G is the drug of choice for meningococcal and gonococcal intracellular infections. Third-generation cephalosporins (cefotaxime, ceftazidime, ceftriaxone, cefotetan, ceftizoxime, cefoperazone, and cefixime) may cross the blood–brain barrier; therefore, cefotaxime, ceftriaxone, and ceftizoxime are usually intravenously administered for the treatment of meningitis caused by Gram-negative bacteria. The intracellular concentration of beta-lactams is usually

lower than the extracellular amount, as revealed for both phagocytic and nonphagocytic cells [35, 36]. This could be explained by the weak acidic character of these molecules affecting their accumulation in acidic cytosol milieu [37].

### 3.2. Inhibition of the cytoplasmic membrane function

Cytoplasmic membrane acts as a selective permeability barrier for ions and nutrients and is also the headquartered structural transport system that controls the chemical composition of the cytoplasm. The disruption of structural integrity and/or functional parameters entails the amendment of ion-selective permeability and loss of ionic or macromolecular balance.

Bacteria and fungi have a slightly different cellular membrane as compared with the animal cells, this being injured faster by different therapeutic agents, which enables selective therapy. Biological membranes are comprised of a lipid matrix, wherein the randomly distributed globular proteins penetrate the lipid layer. Cationic, anionic, or neutral detergents may disrupt biological membranes. The effect of polymyxins is similar to the cationic detergents. Their molecule contains hydrophilic and hydrophobic groups. These antibiotics are positively charged at neutral pH and act similar with the cationic compounds, which are active against the polyanionic outer membrane of Gram-negative bacteria (the load offered by the lipopolysaccharide). Detergents (which are molecules containing lipophilic and hydrophilic group) act by disorganizing the double lipid layer leading to cell disruption.

Polymyxins are polypeptide antibiotics (octapeptides of high molecular weight) with specific chemical and biological properties. There are five known major chemically distinct polymyxins, designated as polymyxin A, B, C, D, and E. All polymyxins are synthesized by *Bacillus polymyxa* and have the same antibacterial spectrum. Polymyxins A and D are nephrotoxic and therefore cannot be used *in vivo*. The most representative are polymyxin B and colistin (or polymyxin E), which are also the less cytotoxic (in concentrations up to 5 µg/ml), being most active against Gram-negative bacteria, such as *Brucella* sp., *Yersinia* sp., *Salmonella* sp., *Shigella* sp.), probably due to their negative lipid charge.

Polymyxins are not absorbed from the intestine, and also they do not accumulate in active concentrations in soft tissues, being not efficient in the treatment of systemic or internal organs infections. In exchange, they can be used for the treatment of superficial, cutaneous, or mucosal infections (wounds, burns, intestinal tract mucosa, and pleural cavity infections), as well as for the prophylaxis of transplant or digestive tract surgery. Polymyxins are used with great effectiveness in the treatment of meningial, lung, and urinary tract infections. They are often associated with other antibiotics to extend the antimicrobial activity spectrum.

The fixation of the antibiotics within the membrane structure depends on the concentration of divalent environmental cations: their deficiency or excess inhibits the action of polymyxins. Also, the LPS composition, bacterial membrane phospholipids, and proteins influence the sensitivity or resistance of various bacterial species to the action of polymyxins.

Polymyxin and other polycationic molecules bind to the lipid A of LPS in a stoichiometric ratio and are inserted into the membrane structure. Such a molecular patchwork disorganizes the lipid layers so that the cell membrane does not function normally as effective osmotic barrier.

Due to structural deterioration of external and internal membranes, osmotic balance is disrupted by the loss of  $K^+$  ions. The permeability changes are associated with the loss of soluble cell constituents and viability. The mechanism is the same as that proposed for hemolysis by the action of ionic detergents. The hemolytic effect occurs due to the disruption of cholesterol–phospholipid–lipoprotein complex from the erythrocyte membrane. Other agents acting on the cytoplasmic membrane are amphotericin B, imidazoles, and triazoles.

### 3.3. Inhibition of the protein synthesis

Several classes of antibiotics are active specifically on the 70S ribosomes, thus blocking protein synthesis at different levels [38].

Aminoglycosides are low molecular weight cationic molecules, but very hydrophilic, which accumulate in the cell only through an energy-dependent transport process. Their accumulation in the bacterial cell occurs through two phases: Phase I is slow and depends on the transmembrane gradient of the electrical potential and thus the oxidative respiratory sinergon, and phase II is quick and translates into an important intracellular accumulation. Intracellular concentrations are approximately 100 times higher than those from the external environment. Slow accumulation causes a bacteriostatic antibiotic, while rapid accumulation produces bactericidal effects. The accumulation rate is conditioned by the size of the electric component ( $\Delta\psi$ ) and the proton-motive force. This explains why microorganisms with transportation systems deficiencies, such as anaerobes, are intrinsically resistant to aminoglycosides. For the same reason, enterococci and other facultative anaerobes are resistant to low concentrations of aminoglycosides [39].

An important role in the intracellular accumulation of aminoglycosides is attributed to the periplasmic proteins whose synthesis is induced by the antibiotic.

Aminoglycosides induce the pleiotropism phenomenon (i.e., simultaneous changes in the expression of many genes) and also produce mRNA reading errors.

Aminoglycosides are rapidly acting antibiotics with broad spectrum of action being active against strict and facultative Gram-positive and negative aerobic bacteria.

Aminoglycosides could slowly accumulate through endocytosis in the lysosomes of the eukaryotic cells to an apparent cellular-to-extracellular ratio of 2 to 4, excepting some tissues like kidney proximal tubular cells, exhibiting binding sites such as megalin and acidic phospholipids where the accumulation is faster [40–43].

Spectinomycin is an aminocyclitol antibiotic related to the aminoglycosides, manifesting bacteriostatic action, usually used for the treatment of gonorrhea produced by penicillin-resistant *Neisseria gonorrhoeae* strains.

The encapsulation of aminoglycosides in liposomes could increase the therapeutic index of the drug by reducing the level of drug delivered at the sites where the antibiotic is toxic to the therapeutic amounts necessary for the treatment of infection. This procedure also increases the aminoglycosides efficiency against intracellular bacteria.

Tetracyclines represent a family of antibiotics inhibitory for the protein synthesis through a mechanism of blocking the attachment of aminoacyl-tRNA complex to the ribosome acceptor site (site A) [44]. These antibiotics have a broad spectrum bacteriostatic effect, being active against Gram-positive Gram-negative bacteria and protozoa, but they also kill normal gut microbiota and produce gastrointestinal disorders.

Tetracyclines have the ability to accumulate in eukaryotic cells, including neutrophils [45].

Tetracyclines are strong chelating agents, their pharmacological properties being influenced by the presence of metal ions. Each of the rings of the tetracycline core can contain only linear carbon atoms in order to keep the antibiotic activity.

Atypical tetracyclines and some of their analogues disrupt the cytoplasmic membrane structure and manifest a bactericidal effect, which contrasts with the bacteriostatic effect of tetracyclines, reversibly inhibiting protein synthesis. Atypical effects of membrane disruption are likely a consequence of the lipophilic nature of the molecule. Because of many side effects derived from their nonspecific interaction with prokaryotic and eukaryotic cell membranes, atypical tetracyclines present no current therapeutic interest.

The use of this antibiotic during pregnancy or in the first 5 years of life results in the deformation of the fetus skull bones and permanent teeth staining due to their ability to bind  $\text{Ca}^{2+}$ .

In the 80s, before the emergence of resistant strains of *N. gonorrhoeae*, tetracycline was used to treat sexually transmitted infections and is currently used in the treatment of non gonococcal urethritis and chlamydial infections

Tetracycline resistance is widespread in Gram-positive cocci and is present also in *Mycoplasma* sp.

Although the main action of tetracycline is antibacterial, this antibiotic is also active against protozoan parasites, inhibiting *Giardia lamblia*, *Trichomonas vaginalis*, *Entamoeba histolytica*, and *Plasmodium falciparum*. The effectiveness of tetracycline derivatives to parasitic protozoa is correlated with the degree of penetration into the cell. The most effective are lipophilic compounds that cross quickly the cytoplasmic membrane (such as the tiotetracycline derivative).

Glicil-tetracyclines are represented by tigecycline, used to treat skin and abdominal infections. The structural feature of tigecycline is the substitution in the position 9 of the tetracycline with a glycine residue. These are broad-spectrum antibiotics against *N. gonorrhoeae*, *Legionella pneumophila*, and also for fast growing non tubercular mycobacteria.

They are active agents to be used for the prophylaxis of malaria and strains of *P. falciparum* resistant to specific chemotherapeutic agents.

Macrolides, lincosamides, and streptogramins (MLS) have a different chemical structure, but they act in a similar manner on a variety of intracellular bacteria (e.g., Gram-positive, Gram-negative cocci, *Chlamydia* spp., *Mycoplasma* spp., and *Legionella* spp.).

MLSs prevent bacterial ribosomes to translate the RNA in two different ways, either by the inhibition of translocation of peptidyl-tRNA from the acceptor site (A) and the peptidyl donor site (P) or by inhibiting the initial steps of the assembly of the 50S ribosomal subunit.

Macrolides have a marked intracellular accumulation in almost all cells, explained by their weak basic character favoring the accumulation in the acidic cytosol compartment, particularly in the lysosomal apparatus, with a rate depending on the derivative structure, lower for erythromycin and higher for those carrying two basic functions [46, 47].

Regarding their structure, macrolides are characterized by a multiunit lactone ring with 12, 14, 15, or 16 carbon atoms, with few double bonds, which contain attached 1–3 glucidic residues by glycosidic linkages.

Macrolides are active against Gram-positive and Gram-negative bacteria (*Mycobacterium* spp., *Treponema pallidum*, *Mycoplasma pneumoniae*, *Chlamydia* sp., *Rickettsia* sp.).

Novel molecules, such as azithromycin and clarithromycin, have a superior antibacterial activity as compared with erythromycin because they have higher coefficients of intracellular penetration and are more stable, being more easily absorbed and manifesting lower incidence gastrointestinal side effects. Azithromycin is active against *Mycoplasma* spp. and *Chlamydia* spp. Clarithromycin has significant antibacterial activity *in vitro* against mycobacteria.

Streptogramins are represented by two synergistic components (A and B). Similar with macrolides and lincosamides, the A and B compounds of the streptogramin set at the ribosomal subunit 50S, 23S, and to rRNA.

Lincomycin and clindamycin are macrolides, but many of their biological properties are similar to erythromycin. They consist of an amino acid linked to an amino-sugar. Ketolides (telithromycin) are new chemical entities, characterized by the replacement of L-cladinose in the erythronolide A ring, with a 3-keto function and the C11–C12 carbamate [48]. ABT 773 represents the latest generation of drugs, characterized by 3-keto group that substitutes the sugar rest of the 3-cladinose from erythromycin and clarithromycin [49].

Oxazolidinones (eperezolid and linezolid) represent a unique class of synthetic antimicrobial agents with a unique mechanism of action, which eliminates the risk of extending existing resistance to the available antimicrobial agents. The oxazolidinones are inhibitors of ribosomal protein synthesis in bacteria, preventing the formation of the 70S initiation complex comprising fMet RNA, mRNA, and the two ribosomal subunits.

Linezolid has a good *in vitro* activity against *N. gonorrhoeae*, *N. meningitidis*, and *M. tuberculosis*.

There are few studies showing the capacity of oxazolidinones (i.e., linezolid) to preferentially and rapidly accumulate intracellularly (in concentrations 1.2 times higher than the extracellular ones within 20 min), both in human phagocytic (PMNs) and in nonphagocytic (McCoy) cells. However, the efflux of the antibiotic is also very rapid, the great amount of the intracellular antibiotic being released in less than 2 min [50].

Sulfonamides are synthetic chemotherapeutic agents, very similar to sulfanilamide (para-amino-benzenesulfonamide). The bacteriostatic action of this antibiotic is due to the interference with the folic acid synthesis pathway.

The best known sulfonamides are sulfadiazine and sulfamethoxazole (cotrimoxazole). As sulfonamides, para-aminosalicylic acid (APAS) and dapsone obtained by chemical synthesis are competitive inhibitors for the para-aminobenzoic acid metabolism and inhibits the synthesis of folic acid, being active against *M. tuberculosis* and *Mycobacterium leprae*.

The family of the diaminopyrimidine derivatives includes trimethoprim and tetroxoprim.

Trimethoprim is an analog of dihydrofolic acid, which competitively inhibits dihydrofolate reductase, an enzyme that converts dihydrofolate to the active cofactor—tetrahydrofolic acid [51].

The blockage of the same biosynthetic pathways sequence under the action of sulfonamides and trimethoprim provides a high degree of synergistic activity against a broad spectrum of microorganisms.

### 3.4. Chemotherapeutic agents acting by inhibiting DNA replication and transcription

Quinolones (also known as 4-quinolones) are the first antimicrobials produced synthetically and form a family of compounds that resemble the core quinolinic existence.

Along with the  $\beta$ -lactam antibiotics and macrolide antibiotics, quinolones represent one of the three major families of antimicrobial agents used in human therapy [52]. Nalidixic acid is an intermediate for the synthesis of quinolones. Subsequently, quinolones have diversified by introducing a fluorine (F) in position 6 and position 7 of a heterocyclic ring (piperazine, pyrrolidine etc.), which generated fluoroquinolones.

Fluoroquinolones (norfloxacin, pefloxacin, ofloxacin, ciprofloxacin etc.) have a broad spectrum of activity against intracellular bacteria, including *Chlamydia* sp., *Rickettsia* sp. and mycobacteria. These molecules penetrate the bacterial cell by passive diffusion and act on specific targets represented by topoisomerases: DNA gyrase (topoisomerase II) and topoisomerase IV, probably inducing lethal effects such as bacterial DNA damage.

Rifampicin B is naturally synthesized, but in the recent years, the semisynthetic derivatives of rifampicin are the most extensively used. Rifampicin belongs to a group consisting of an aromatic chromophore, which is included in the aliphatic chain. It is associated with the B subunit of DNA-dependent RNA polymerase, thus blocking transcription and RNA synthesis initiation. The antibiotic is widely used in the combinatory therapy of tuberculosis.

It was demonstrated that quinone and hydroquinone forms of rifampin can accumulate in PMNs from normal and chronic granulomatous disease individuals and be active against intracellular staphylococci invading the chronic granulomatous disease PMN [53].

### 3.5. Other synthetic chemotherapeutic agents

Nicotinic acid hydrazide (isoniazid, INH), introduced in the clinic before 1950, together with rifampin, forms the basis of antituberculosis chemotherapy. Isoniazid is a nicotinamide derivative. The mechanism of action is not known, but it influences the synthesis of lipids, nucleic acids and mycolic acid from *M. tuberculosis*.

It is assumed that isoniazid is active by competing with pyridoxine (vitamin B6) necessary for the growth of *M. tuberculosis* cells or by inhibiting mycolic acid synthesis. It is bactericidal to the growing cells and has a bacteriostatic action against the cells that do not replicate. Together with PASA and dapson, isoniazid is used to treat infections with *Mycobacterium* sp.

Ethambutol, pyrazinamide, and ethionamide block the enzymatic reactions in the bacterial cell because they are similar but not identical to bacterial vitamins.

Ethambutol inhibits arabinosyl chloride-transferase enzyme involved in the biosynthesis of arabinogalactan and lipoarabinomannan. Other effects attributed to metabolic inhibition action of ethambutol are RNA and phospholipids synthesis, inhibiting the transfer of mycolic acids linked to arabinogalactans of the murine cell wall and also inhibiting the synthesis of spermidine at early stage conversion of glucose into monosaccharides used for the synthesis of parietal polysaccharides and peptidoglycan. It is a very specific and effective drug used in association with isoniazid for tuberculosis treatment. It has a good bacteriostatic effect [54].

Pyrazinamide is a synthetic derivative of nicotinamide, which is metabolized to the pyrazinoic acid, antibacterial active intermediary.

Ethionamide, a derivative of the isonicotinic acid, is active against *M. tuberculosis* and other mycobacteria, acting through inhibition of mycolic acid synthesis.

Despite the massive amount of literature on the intracellular activity of antibiotics and on its relation to cellular accumulation and disposition, the relationship between drug concentration (or dosing), time of exposure (or other pertinent pharmacokinetic parameters), and chemotherapeutic response (in terms of quantitative measurement of the variation in the bacterial population) is incompletely elucidated [55]. Clinical studies, in this context, are particularly difficult due to the complex extracellular and intracellular pharmacokinetic variables, microbial and host-response variables, and simultaneous presence of extracellular and intracellular foci of infection. Some classes of antibiotics, such as ansamycins, macrolides, tetracyclines, and fluoroquinolones, are generally considered as being active against intracellular pathogens, being already clinically used for the treatment of bacterial infections with obligate and facultative intracellular bacteria. Conversely, there is a consensus over the fact that beta-lactams and aminoglycosides show no or only a poor intracellular activity. However, beta-lactams could exhibit a time-dependent activity against intracellular bacteria when administered in prolonged treatments at the maximal dose to compensate for the lack of accumulation, whereas aminoglycosides, which are concentration-dependent, could be active at high concentrations [56]. For macrolides, activity is clearly observed against phagosomal organisms (phagosomes are neutral or only slightly acidic) at a sufficiently high concentration to cope with the loss of activity caused by low pH or binding to cell constituents. Although

some organisms, like *Chlamydia* sp. and *Legionella* sp., are quite sensitive, this may not be the case for others, such as *Staphylococcus aureus*.

The balance between influx and efflux, metabolism, and binding properties determines the intracellular concentration of free active drug; bacterial responsiveness, physico-chemical conditions prevailing at the site of infection, and degree of cooperation (or hindrance) with the host defenses are affecting the intracellular activity of antibiotics.

## 4. Antibiotics carriers for the intracellular delivery

Intracellular bacterial pathogens are hard to treat because of the inability of conventional antimicrobial agents belonging to widely used classes to penetrate the lipidic membrane. They accumulate in different compartments of the cells and face the limiting conditions of the phagocytic cells, such as the lysosomal acidic pH and inactivating enzymes, low oxygen pressure, etc. [57, 58], requiring the development of efficient delivery systems that could release the antimicrobial agent intracellularly in active concentrations, thus increasing its effectiveness while decreasing the required therapeutic doses, its systemic toxicity, and the probability of selecting resistance [59–61].

Different improved drug carriers have been developed for treating intracellular pathogens, including antibiotics loaded into liposomes and other lipid formulations, microspheres, polymeric carriers, fullerenes, dendrimers and nanoplexes [1, 61–63].

The advantages of using drug delivery systems are represented by the tunable surface/size/shape/functionalization properties, depending on the structure of the transported drug; evasion of the immune system; use of the same carrier to transport more than one drugs; improvement of the biodisponibility, biodistribution, and pharmacokinetics of the drugs; availability of drug carriers for different administration routes; and low probability of selecting resistance [64, 65].

This section will focus on drug delivery systems oriented toward treatment of intracellular infections.

### 4.1. Polymeric drug carriers

Polymeric (both natural and synthetic) biodegradable and/or biocompatible matrixes, such as poly ( $\epsilon$ -caprolactone) (PCL), poly(lactic acid) (PLA), poly(lactic-co-glycolic acid) (PLGA), poly( $\gamma$ -glutamic acid) (PGA), poly(L-lysine) alginate, gelatin, collagen, cellulose, albumin, fibrin, dextran, pectin, chitosan, agar, agarose, and carrageenans, could be used to embed/encapsulate/adsorb/conjugate a certain drug in order to protect it against enzymatic and hydrolytic degradation [66–79] to control the rate of drug release with an optimal maintenance of the biologically active drug level within therapeutic window [80, 81], to prevent toxicity, to target drugs to the site of action, and to improve absorption, bioavailability, and therapeutic efficacy [82, 83].

The polymeric carrier systems could be classified in four different categories: diffusion controlled (the drug is released by diffusion), chemically controlled (the drug molecules are linked to a polymeric backbone often by means of a spacer molecule, being released inside the host tissue by hydrolysis or by the enzymatic cleavage of the linkage between the polymer carrier and the drug, by polymer biodegradation or by bioerosion), solvent activated (controlled by swelling or osmosis allowing the drug inside the system to diffuse outward), and magnetically controlled (the polymer carrier is combined with magnetic microparticles of iron, cobalt, and nickel, which could be oriented inside the body by an externally applied magnetic field) [67, 84–87].

Responsive or smart polymers respond and modulate their properties in accordance with different external parameters (e.g., UV/visible light, electric charges, electromagnetic radiation, temperature, pH, ionic strength, ionic or metallic interactions), leading to degradation, drug release, dissolution/precipitation, swelling/collapsing, and formation of micelles and vesicles [88, 89].

Particulated micro- and nanospheres and capsules prepared from natural polymers have been synthesized by emulsion polymerization, solvent evaporation, ionic gelation, self-assembly, nanoprecipitation, and supercritical fluid technology for drug delivery [90–92].

While microparticles are likely to remain in time at the injection place and can be engulfed only by phagocytes, the smaller nanoparticles can diffuse from the injection place and cross biological barriers, including the cellular membrane of different cell types [93, 94].

Nanoparticle-based drug delivery systems were applied in the treatment of different infectious diseases with intracellular pathogens, such as acquired immune deficiency syndrome (AIDS), malaria, and tuberculosis [95, 96]. Polymeric nanoparticles represent also a promising solution for the local delivery of therapeutics to the central nervous system through the blood–brain barrier [96, 97].

The polymeric micelles consisting of a hydrophilic shell and a drug-containing core were used to incorporate extremely hydrophobic drugs, to assure prolonged drug circulation time, drug stability, and escape from the reticuloendothelial system due to their nanometer size [98]. Nanoparticles formulated using biodegradable polymers have been also shown to enhance the delivery of antibiotics intracellularly and to improve their effectiveness as revealed by the reduced microbial burden.

In comparison with other delivery systems, natural polymers are generally safer and more stable, easier to obtain, and offer better control over agent release [82, 99].

Dextran, a biodegradable, biocompatible, nonimmunogenic, and nonantigenic polymer of bacterial origin, composed essentially of  $\alpha$ -1,6-linked D-glucopyranose units [100], proved to improve the activity of polar molecules such as penicillins, aminoglycosides, rifampicines, and quinolones and to efficiently challenge the drug delivery into the infected cells in an active form, leaving the host cells intact [101]. Dextran microspheres could act as macromolecular carriers for the small molecules antibiotics and induce endocytosis of the drug by the target cell *via* a specific receptor, followed by the subcellular distribution of the drug to sites where the microbial cells are localized [102].

Chitosan-dextran sulfate (CD) nanocapsules were assessed for their efficiency in delivering ciprofloxacin or ceftriaxone drugs against *Salmonella* using a murine salmonellosis model. CD nanocapsules proved to efficiently target and kill the intracellular pathogen at a significantly lower dose, as compared to the free antibiotic, assuring also a more increased retention time of ciprofloxacin in the blood and organs [103].

Cyclodextrin, a cyclic oligosaccharide consisting of six to eight glucopyranose units joined by  $\alpha$ -(1  $\rightarrow$  4) glucosidic linkages, exhibits an internal lipophilic cavity, which can be complexed with hydrophobic agents [104], improving drug solubility, stability, and bioavailability [105, 106].

Hyaluronic acid, a linear anionic polysaccharide of animal or microbial origin, belonging to the glycosaminoglycans family, consisting of alternating units of *N*-acetyl-D-glucosamine and glucuronic acid, is a promising delivery vehicle for antibiotics [107].

Alginate nanoparticles increased the activity of rifampicin, isoniazid, pyrazinamide, and ethambutol against *M. tuberculosis* by assuring a higher drug payload and therapeutic efficacy as well as an improved pharmacokinetic [96].

Some pathogens can survive for a prolonged period of time in the first-line anti-infective defense cells represented by polymorphonuclear leukocytes (PMNs). The amorphous chitin nanoparticles with a size of  $350 \pm 50$  nm in diameter proved to achieve a sustained release of rifampin till 72 h and significantly enhanced the drug accumulation into the intracellular compartments of PMNs [108].

Synthetic polymers are preferentially used for the development of drug delivery systems due to their excellent and tailor-made properties (biocompatibility; water compatibility; lack of immunogenicity; optimal degradation time coinciding with their function; appropriate mechanical properties in terms of toughness, flexibility, and swelling; generation of nontoxic degradation products that can be easily resorbed or excreted; flexibility for chemical modification to get increased biocompatibility and to enlarge the variety of the loaded agent; they do not need to be removed from the body being able to be degraded and excreted or resorbed; the existence of FDA and European Medicine Agency approval for drug delivery systems for parenteral administration; and protection of the loaded agent from degradation, assuring its sustained and targeted release) [99, 109–114].

Amoxicillin-loaded PLGA microspheres successfully eliminated *L. monocytogenes* from vital organs (kidney, spleen, and brain) and also increased the survival rate of treated animals in comparison with the free antibiotic, suggesting the targeted delivery of the antibiotic to the infected macrophages, as well as its sustained release over an prolonged period of time [115].

The PLGA nanoparticles proved to be efficient in encapsulating and releasing the rifampicin drug, showing an initial burst followed by the sustained release of this primary tuberculostatic agent [116, 117]. Also, rifampicin-loaded polybutylcyanoacrylate nanoparticles potentiated the *in vitro* and *in vivo* activity of rifampin and ciprofloxacin against *Mycobacterium avium* due to an effective delivery of drugs to macrophages [118, 119].

Gentamicin-loaded PLGA nanoparticles have been obtained for the treatment of brucellosis, proving to achieve high intracellular bactericidal activity of the antibiotic [120].

The PLGA microparticles proved efficient for the delivery of the antibacterial phosphorylcholine and of the dietary antigen beta lactoglobulin in a mouse model, inducing protective mucosal immunity against intestinal infection by *S. typhimurium* [121].

PLGA nanoparticles have been shown to efficiently accumulate in inclusions in both acutely and persistently infected *Chlamydia*-infected cells, while the encapsulation of rifampin and azithromycin antibiotics in PLGA nanoparticles enhanced the effectiveness of the antibiotics in reducing microbial burden. The combination of rifampin and azithromycin was more effective than the individual drugs [122].

Gentamicin was ion-paired with the anionic AOT surfactant to obtain a hydrophobic complex (GEN-AOT) that was formulated as a particulated material either by the precipitation method or by encapsulation into PLGA nanoparticles. The *in vitro* studies against the intracellular bacteria *Brucella melitensis* demonstrated that the bactericidal activity of gentamicin was unmodified, proving their use for the treatment of infections caused by intracellular bacteria [123].

Rapamycin-loaded PLGA microparticles effectively released the active drug inside dendritic cells, under intra-phagosomal (pH 5) and extracellular (pH 7.4) conditions [124].

Amoxicillin-bearing human serum albumin and, more evident, amoxicillin-doped PLGA microparticles proved to be efficient in combating *L. monocytogenes* infection in a mouse experimental model, as revealed by the decreased bacterial burden in various organs and reduced viable counts, the results clearly demonstrating that the respective microparticles successfully target the infected macrophages [106].

Poly(isohexylcyanoacrylate) (PIHCA) nanospheres improved the activity of ampicillin against *S. typhimurium* and *L. monocytogenes*, but the particles themselves exhibited also antimicrobial activity [125, 126].

Ampicillin-encapsulated poly(isohexylcyanoacrylate) nanoparticles prove to be more efficient than the free antibiotic against *L. monocytogenes* infecting mouse peritoneal macrophage, as revealed by the more drastic decrease of viable cell counts. However, the nanoparticles acted on the intracellular bacteria after a lag period of 6–9 h, probably due to a required period for the degradation of the polymer [127].

Poly-lactide-co-glycolide (PLG) nanoparticles enhanced the bioavailability and pharmacodynamic properties of rifampicin, isoniazid, pyrazinamide, and ethambutol against *M. tuberculosis* [128].

Amphiphilic, cationic polymers with an amino moiety, a low molecular weight, and short alkyl chains designed to mimic the host secreted microbicidal peptides are considered promising candidates for potent and highly selective antimicrobial agents (acting on microbial walls or mitochondrial activity) with decreased risk to select resistance [129, 130].

The polyketal nanoparticles formulated from the hydrophobic polymer poly(1,4-phenyleneacetone dimethylene ketal) (PPADK) improved the activity of superoxide-dismutase to scavenge reactive oxygen species produced by macrophages [131, 132].

Poly-butyl cyanoacryle proved to increase the efficiency of the moxifloxacin fluoroquinolone against *M. tuberculosis* infecting the THP-1 cells [133].

Polyalkycyanoacrylate nanoparticles proved to improve the activity of ciprofloxacin and colistin against *S. typhimurium* at the early stages of the infection in mice and/or *in vitro* models. Ciprofloxacin-loaded nanoparticles induced a significant decrease of bacterial counts in the liver whatever the stage of infection and the form used. However, none of the treatments were able to sterilize the spleen or the liver. In the *in vitro* study, colistin was only active against bacteria recovered during the early phase of infection, whereas ciprofloxacin exerted its activity at all times postinfection [134].

Amphiphilic block copolymers could self-assemble, resulting in vesicles called polymersomes [135]. Polymersomes of (poly[2-[methacryloyloxy]ethyl phosphorylcholine] [PMPC]–poly[2-[diisopropylamino]ethyl methacrylate] [PDPA] block copolymers) proved to successfully deliver metronidazole and doxycycline in *Porphyromonas gingivalis*-infected oral keratinocytes significantly increasing their activity [136].

## 4.2. Liposomes

Liposomes are small spherical, uni- or multilamellar vesicles in which the central aqueous cavities are surrounded by amphipatic molecules, being thus able to entrap both hydrophilic and hydrophobic drugs [137]. After intravenous injections, liposomes are taken up by macrophages in the liver and in the spleen, representing thus a promising option for fighting infections due to facultative intracellular bacteria, parasites, or viruses [138].

The incorporation of different tuberculostatic agents in liposomes (such as ciprofloxacin) has shown good antibacterial efficacy both in both macrophage cell lines and in animal tuberculosis models [139, 140].

Streptomycin inclusion in phosphatidyl glycerol, phosphatidyl choline, and cholesterol-containing liposomes showed an increased antimicrobial activity against *Mycobacterium avium* [141].

The encapsulation of antibiotics in liposomes could represent a viable solution for the drug penetration into the systemic circulation through the alveolar-capillary barrier, followed by its accumulation in different organ tissues or for the direct administration to the lung [142].

Phosphatidylcholine, cholesterol, dicetylphosphate, *O*-steroyl amylopectin, and monosialogangliosides/distearylphosphatidylethanolamine-poly (ethylene glycol) 2000 liposomes have been shown to act as a promising targeted delivery systems for isoniazid and rifampicin to the lung in mice experimental model [143].

The liposomal encapsulation of membrane-impermeative antibiotics, like gentamicin is among the most used approaches to achieve intracellular antibiotic delivery and therefore increase the drug's therapeutic activity against intracellular pathogens.

Gentamicin, encapsulated in plurilamellar liposomal vesicles, proved to be active against intracellular *Brucella abortus* infecting murine monocytes [144].

Gentamicin entrapped within stable multilamellar liposomes was used to treat mice orally infected with *Salmonella dublin* and proved to achieve high and persistent (up to 10 days) concentrations of gentamicin in the spleen, while bacterial counts in the lymph nodes decreased. Also, gentamicin entrapped in liposomes was less toxic in mice than its free form [145]. Ciprofloxacin encapsulation in dipalmitoylphosphatidylcholine, dipalmitoylphosphatidylglycerol, and cholesterol containing liposomes also proved increased anti-*Salmonella dublin* activity demonstrated by the decreased mortality of animals and good distribution of liposomes to all areas of infection [145].

The encapsulation of ampicillin in liposomes reduced the *L. monocytogenes* viable counts in mice peritoneal macrophages [146]. The DOPE (dioleoylphosphatidylethanolamine) liposomes, sensitive to pH proved to be efficient in the ampicillin uptake by the macrophages infected with *L. monocytogenes*, correlated with an increase in the microbicidal activity. The efficiency of this drug delivery system was also proven in an *in vivo* mouse infection model, as revealed by the decrease of viable cell counts in the liver and spleen [147].

Liposomes, as well as nanoparticles coated with a lipid bilayer have been used to encapsulate drugs for the passive transport through the blood–brain barrier due to the enhanced lipophilic transport of drugs to the target tissues [148–150].

Streptomycin and doxycycline were entrapped into macromolecular nanoplexes with anionic homo- and block copolymers enabling the simultaneous binding of both antibiotics into the nanoplexes, which significantly reduced the *B. melitensis* load in the spleens and livers of the infected mice [151].

It was demonstrated that gentamicin can be easily introduced into membrane vesicles of Gram-negative pathogens that naturally bleb off the bacterium throughout its growth cycle and delivered directly not only to other Gram-positive and Gram-negative pathogens but also to mammalian cells [152].

#### 4.3. Niosomes

Niosomes or nonionic surfactant vesicles are microscopic, spherical, uni- or multilamellar, and polyhedral vesicles of 10–1000 nm formed by self-assembly of a mixture of cholesterol and a single alkyl chain nonionic and nontoxic surfactant with subsequent hydration [153]. Niosomes can be used for the delivery of hydrophilic, lipophilic, and amphiphilic drugs, irrespective of their degree of solubility [153]. Niosomes improve the activity of isoniazid and rifampicin against *M. tuberculosis* infecting the J774 macrophage cell line [154, 155].

#### 4.4. Solid Lipid Nanoparticles (SLN)

Solid lipid nanoparticles (SLN) (50 nm–1  $\mu$ m) are colloidal carriers for lipophilic and hydrophilic drugs, containing natural lipids dispersed in water or in the aqueous surfactant solution [156].

Mannose-conjugated SLNs were successfully used to selectively deliver rifabutin, isoniazid, and pyrazinamide to alveolar and lymphatic tissues [157]. Stearic acid SLN improved the activity of rifampicin, isoniazid, and pyrazinamide against *M. tuberculosis* by increasing the residence time and the drug bioavailability while decreasing the administration frequency [158].

Nanosuspensions could be used for nebulization procedures for delivering drugs poorly soluble in the lung secretions [159], as already proved by the antitubercular drugs (rifampicin, isoniazid, and pyrazinamide) incorporated into various formulations of solid lipid particles ranging from 1.1 to 2.1  $\mu\text{m}$  and nebulized to guinea pigs [160].

#### 4.5. Fullerenes

Fullerenes are a new form of carbon, with hollow sphere, ellipsoid, or tube size. The cationic fullerene derivatives bearing a substituted-quinazolin-4(3H)-one moiety as a side arm were reported to have a very good inhibitory potential on *M. tuberculosis* [161].

#### 4.6. Dendrimers

Mannosylated dendrimers proved to be an efficient drug delivery system for rifampicin in a rat alveolar macrophages, the sustained release taking place in a pH-dependent manner [162].

The mannosylated fifth-generation poly(propyleneimine) dendrimer nanocarriers proved to be very efficient for the intracellular uptake of lamivudine, a nucleoside/nucleotide reverse transcriptase inhibitor, and the reduction of the HIV-1 viral load in the infected MT2 cells [163].

Pegylated lysine-based copolymeric dendrimer improved the proved anti-*P. falciparum* of artemether drug, as revealed by the increased drug stability, enhanced solubility, and prolonged drug circulation half-life [164].

A fourth-generation hydroxyl-terminated poly(amidoamine) (PAMAM) dendrimer was used as the intracellular vehicle of azithromycin for the treatment of chlamydial inclusions, proving to be more efficient than the free drug with a sustained effect lasting for 24–48 h post-infection [165].

#### 4.7. Zeolites

Zeolites are crystalline materials with frameworks comprising Si, Al, and O [166]. The zeolites possess nanochannels and cages of regular dimensions [167]. The nanochannels (pores) of zeolites are open allowing the diffusion of therapeutic agents from the exterior to the interior of the zeolites. These networks exhibit a large specific surface area and a good stability in different environments [167].

Mesoporous silica nanoparticles proved to increase the efficiency of the rifampin and isoniazid against *M. tuberculosis* infecting the THP-1 cells [168].

The capability of porous sol-gel processed silica as a carrier for gentamicin has been demonstrated, showing a significantly higher rate of bacterial clearance from organs than did the free drug [169].

#### 4.8. Erythrocytes

Erythrocytes have a great the potential to provide an effective therapy against intracellular pathogens. Amikacin encapsulation in human carrier erythrocytes demonstrated a slow and sustained release from the loaded carrier till 48 h, suggesting the potential use of the erythrocytes as a slow release system for antibiotics [170].

### 5. Conclusion

In the last years, there was an important progress in improving the drug delivery systems for fighting intracellular bacterial infections. The proposed solutions led to decreased toxicity, improved bioavailability, and prolonged and sustained release associated with reduced frequency of administration and enhanced antimicrobial activity. However, the design of the optimal drug carrier for the intracellular release of different antibiotics should rely on the elucidation of the intracellular kinetics (accumulation, degradation, and distribution in different intracellular compartments and activities) of the respective drugs.

The most promising results have been obtained by using natural or synthetic polymers and liposomes and other lipid formulation carriers, whose efficiency has been demonstrated by *in vitro* and *in vivo* experimental studies, as well as in clinical trials, and which could therefore represent efficient strategies for fighting severe microbial infections produced by facultative or obligate intracellular microorganisms as well as for viral infections.

### Author details

Mariana Carmen Chifiriuc<sup>1,2</sup>, Alina Maria Holban<sup>1,2,3</sup>, Carmen Curutiu<sup>1,2</sup>, Lia-Mara Ditu<sup>1</sup>, Grigore Mihaescu<sup>1</sup>, Alexandra Elena Oprea<sup>3</sup>, Alexandru Mihai Grumezescu<sup>3\*</sup> and Veronica Lazar<sup>1</sup>

\*Address all correspondence to: grumezescu@yahoo.com

1 Microbiology Immunology Department, Faculty of Biology, University of Bucharest, Bucharest, Romania

2 Research Institute of the University of Bucharest–ICUB, Life, Environmental and Earth Sciences, Bucharest, Romania

3 Department of Science and Engineering of Oxide Materials and Nanomaterials, Faculty of Applied Chemistry and Material Science, University Politehnica of Bucharest, Bucharest, Romania

## References

- [1] Salouti M, Ahangari A. Nanoparticle Based Drug Delivery Systems for Treatment of Infectious Diseases. 2014. 2014-07-25.
- [2] Antibiotic Resistance: Implications for Global Health and Novel Intervention Strategies: Workshop Summary. Washington, DC: The National Academies Press. 2010. 496 p.
- [3] Todar K. Web Review of Todar's Online Textbook of Bacteriology. <http://wwwtextbookofbacteriology.net/Rickettsiahtml>. 2009.
- [4] Wilson JW, Schurr MJ, LeBlanc CL, Ramamurthy R, Buchanan KL, Nickerson CA. Mechanisms of bacterial pathogenicity. *Postgraduate Medical Journal*. 2002 April 1, 2002;78(918):216–24.
- [5] Chifiriuc MC, Lixandru M, Iordache C, Bleotu C, Larion C, Olguta D, et al. Internalization of *Staphylococcus aureus* and *Pseudomonas aeruginosa* bacterial cells by non-phagocytic, epithelial human cells. *Romanian Biotechnological Letters*. 2008;13(2).
- [6] Bleotu C, Chifiriuc MC, Dracea, O., Iordache C, Delcaru C, Lazar V. In vitro modulation of adherence and invasion ability of enteroinvasive *Escherichia Coli* by different viruses. *International Journal of Applied Biology and Pharmaceutical Technology*. 2010:1359–63.
- [7] Chifiriuc MC, Mihaescu G, Lazar V. *Medical Microbiology and Virology*. University of Bucharest Publishing House. 2011;ISBN 978-973-737-985-6579.61.
- [8] Mihaescu G, Chifiriuc C, Ditu L. *General microbiology* University of Bucharest Publishing House. 2007;ISBN-9789737372689:552.
- [9] Chifiriuc MC, Bleotu C, Pelinescu DR, Lazar V, Ditu LM, Vassu T, et al. Patterns of colonization and immune response elicited from interactions between enteropathogenic bacteria, epithelial cells and probiotic fractions. *International Journal of Medicine and Biomedical Research*. 2010;1(4):47–57.
- [10] Madigan M, Martinko J, J. P. Brock's *Biology of Microorganisms*. 8th edition. New Jersey: Prentice Hall. 1997.
- [11] Nizet V, Esko JD. *Bacterial and Viral Infections. Essentials of Glycobiology*. CSH Press. 2009.
- [12] Galan JE, Wolf-Watz H. Protein delivery into eukaryotic cells by type III secretion machines. *Nature*. 2006;444:567–73.
- [13] Chifiriuc MC, Bloetu C, Sokolov D, Mihaescu GLV. Host immune response to *Chlamydia* infection. In: Mares M, editor. *The Book Chlamydia*. Intech Open Access. 2011;ISBN 978-953-51-0470-4.

- [14] Weinrauch Y, Zychlinsky A. The induction of apoptosis by bacterial pathogens. *Annual Review of Microbiology*. 1999;53(1):155–87. PubMed PMID: 10547689.
- [15] Grassme H, Kirschnek S, Riethmueller J, Riehle A, von Kurthy G, Lang F, et al. CD95/CD95 ligand interactions on epithelial cells in host defense to *Pseudomonas aeruginosa*. *Science*. 2000 Oct 20;290(5491):527–30. PubMed PMID: 11039936. Epub 2000/10/20. eng.
- [16] Iordache C, Bleotu C, Holban A, Lixandru M, Cotar A, Lazar V, et al. Differential effects on caspase mediated apoptosis of hela cells induced by different *Pseudomonas aeruginosa* culture fractions. *International Journal of Applied Biology and Pharmaceutical Technology*. 2011;2(1):132–8.
- [17] Mihaescu G, Chifiriuc C, Ditu LM. *Imunobiology*. University of Bucharest Publication House. 2009;ISBN 978-973-737-734-0:572.
- [18] Reid CW, Fulton KM, Twine SM. Never take candy from a stranger: the role of the bacterial glycome in host-pathogen interactions. *Future Microbiology*. 2010 Feb;5(2):267–88. PubMed PMID: 20143949. Epub 2010/02/11. eng.
- [19] Vimr ER, Kalivoda KA, Deszo EL, Steenbergen SM. Diversity of microbial sialic acid metabolism. *Microbiology and Molecular Biology Reviews*. 2004;68(1):132–53. PubMed PMID: PMC362108.
- [20] Lazar V, Balotescu C, Cernat R, Bulai D, Stewart-Tull D. *Imunobiologie*. Ed Univ din Bucuresti. 2005;ISBN-973-73-7124-0:250.
- [21] Yatsuyanagi J, Saito S, Sato H, Miyajima Y, Amano K-I, Enomoto K. Characterization of enteropathogenic and enteroaggregative *Escherichia coli* isolated from diarrheal outbreaks. *Journal of Clinical Microbiology*. 2002 07/09/received 09/03/revised 10/21/accepted;40(1):294–7. PubMed PMID: PMC120118.
- [22] Chifiriuc MC, Bleotu C, Marutescu L, Cristea D, Lazar V. The modulation of HeLa cells secretory patterns by invasive *Shigella* spp. and enteroinvasive *E. coli* bacterial cells and their soluble components. *Roumanian Archives of Microbiology and Immunology*. 2010 Jul–Sep;69(3):139–44. PubMed PMID: 21434590. Epub 2011/03/26. eng.
- [23] Cristea D, Ceciu S, Chitoiu DT, Bleotu C, Lazar V, Chifiriuc MC. Comparative study of pathogenicity tests for *Shigella* spp. and enteroinvasive *Escherichia coli* strains. *Roumanian Archives of Microbiology and Immunology*. 2009 Jan–Mar;68(1):44–9. PubMed PMID: 19507627. Epub 2009/06/11. eng.
- [24] de la Torre JC, Borrow P. Chapter 22 Virus-induced alterations in cells. *Principles of Medical Biology*1998. p. 365–79.
- [25] Israil AM, Balotescu C, Alexandru A, Cojocar R, Bucurenci N, Chicu V, et al. Characterization of *V. cholerae* strain isolated in the Republic of Moldavia between 1995–1999. *Roumanian Biotechnological Letters*. 2005;10(6):2441–57.

- [26] Mihaescu G, Chifiriuc (Balotescu) MC. Toxins and other potentially toxic substances. Romanian Academy Publishing House. 2005;ISBN 973-27-1136-1:364.
- [27] Mihaescu G, Chifiriuc MC, L.M. D. Antibiotics and antimicrobial chemotherapeutic substances. Romanian Academy Publishing House. 2008;ISBN 978-973-27-1573-4.:358.
- [28] Brooks GF, Carroll KC, Butel JS, S.A. M. Jawetz, Melnick, & Adelberg's Medical Microbiology, 24th Edition. [www.accessmedicine.com](http://www.accessmedicine.com). 2007.
- [29] Collier L, Balows A, Sussman M. Topley and Wilson's Microbiology and Microbial Infections, Vol. I, II. 1998.
- [30] Beauchamp D, Gourde P, Simard M, Bergeron MG. Subcellular localization of tobramycin and vancomycin given alone and in combination in proximal tubular cells, determined by immunogold labeling. *Antimicrobial Agents and Chemotherapy*. 1992;36(10):2204–10. PubMed PMID: PMC245477.
- [31] Van Bambeke F, Snoeck A, Chanteux H, Mingeot-Leclercq M, Tulkens P. Is LY333328 glycopeptide a new cell-associated antibiotic? Comparative studies with vancomycin and azithromycin in a model of J774 mouse macrophages. 11th European Congress of Clinical Microbiology and Infectious Diseases Istanbul, Turkey, April 1–4, 2001. 2001.
- [32] Pascual A, Tsukayama D, Kovarik J, Gekker G, Peterson P. Uptake and activity of rifapentine in human peritoneal macrophages and polymorphonuclear leukocytes. *Antimicrobial Agents and Chemotherapy*. 1987 Apr;6(2):152–7. PubMed PMID: 2954817. Epub 1987/04/01. eng.
- [33] Maderazo EG, Breaux SP, Woronick CL, Quintiliani R, Nightingale CH. High teicoplanin uptake by human neutrophils. *Chemotherapy*. 1988;34(3):248–55. PubMed PMID: 2970950. Epub 1988/01/01. eng.
- [34] Van Bambeke F, Carryn S, Seral C, Chanteux H, Tyteca D, Mingeot-Leclercq MP, et al. Cellular pharmacokinetics and pharmacodynamics of the glycopeptide antibiotic oritavancin (LY333328) in a model of J774 mouse macrophages. *Antimicrobial Agents and Chemotherapy*. 2004 Aug;48(8):2853–60. PubMed PMID: 15273091. PubMed Central PMCID: PMC478544. Epub 2004/07/27. eng.
- [35] Jacobs RF, Thompson JW, Kiel DP, Johnson D. Cellular uptake and cell-associated activity of third generation cephalosporins. *Pediatric Research*. 1986 Sep;20(9):909–12. PubMed PMID: 3489219. Epub 1986/09/01. eng.
- [36] Carryn S, Van Bambeke F, Mingeot-Leclercq MP, Tulkens PM. Comparative intracellular (THP-1 macrophage) and extracellular activities of beta-lactams, azithromycin, gentamicin, and fluoroquinolones against *Listeria monocytogenes* at clinically relevant concentrations. *Antimicrobial Agents and Chemotherapy*. 2002 Jul;46(7):2095–103.

- PubMed PMID: 12069960. PubMed Central PMCID: PMC127291. Epub 2002/06/19. eng.
- [37] Wilkinson G. Pharmacokinetics: the dynamics of drugs absorption, distribution and elimination. In: Hardman JG, Limbird LL, editors. Goodman & Gilman's the Pharmacological Basis of Therapeutics. New York: McGraw Hill Medical Publishing Division. 2001:3–30.
- [38] Mingeot-Leclercq MP, Glupczynski Y, Tulkens PM. Aminoglycosides: activity and resistance. *Antimicrobial Agents and Chemotherapy*. 1999 Apr;43(4):727–37. PubMed PMID: 10103173. PubMed Central PMCID: PMC89199. Epub 1999/04/02. eng.
- [39] Vakulenko SB, Mobashery S. Versatility of aminoglycosides and prospects for their future. *Clinical Microbiology Reviews*. 2003;16(3):430–50. PubMed PMID: PMC164221.
- [40] Tulkens P, Trouet A. The uptake and intracellular accumulation of aminoglycoside antibiotics in lysosomes of cultured rat fibroblasts. *Biochemical Pharmacology*. 1978 Feb 15;27(4):415–24. PubMed PMID: 24449. Epub 1978/02/15. eng.
- [41] Just M, Erdmann G, Habermann E. The renal handling of polybasic drugs. 1. Gentamicin and aprotinin in intact animals. *Naunyn-Schmiedeberg's Archives of Pharmacology*. 1977 Oct;300(1):57–66. PubMed PMID: 304182. Epub 1977/10/25. eng.
- [42] Nagai J, Tanaka H, Nakanishi N, Murakami T, Takano M. Role of megalin in renal handling of aminoglycosides. *American Journal of Physiology. Renal Physiology*. 2001 Aug;281(2):F337–44. PubMed PMID: 11457726. Epub 2001/07/18. eng.
- [43] Sastrasin M, Knauss TC, Weinberg JM, Humes HD. Identification of the aminoglycoside binding site in rat renal brush border membranes. *Journal of Pharmacology and Experimental Therapeutics*. 1982 Aug;222(2):350–8. PubMed PMID: 7097555. Epub 1982/08/01. eng.
- [44] Chopra I, Roberts M. Tetracycline antibiotics: mode of action, applications, molecular biology, and epidemiology of bacterial resistance. *Microbiology and Molecular Biology Reviews*. 2001 Jun;65(2):232–60; second page, table of contents. PubMed PMID: 11381101. PubMed Central PMCID: PMC99026. Epub 2001/05/31. eng.
- [45] Coates TD, Torres M, Harman J, Williams V. Localization of chlorotetracycline fluorescence in human polymorphonuclear neutrophils. *Blood*. 1987 Apr;69(4):1146–52. PubMed PMID: 3828534. Epub 1987/04/01. eng.
- [46] Carlier MB, Garcia-Luque I, Montenez JP, Tulkens PM, Piret J. Accumulation, release and subcellular localization of azithromycin in phagocytic and non-phagocytic cells in culture. *International Journal of Tissue Reactions*. 1994;16(5–6):211–20. PubMed PMID: 7558665. Epub 1994/01/01. eng.
- [47] Van Bambeke F, Gerbaux C, Michot JM, d'Yvoire MB, Montenez JP, Tulkens PM. Lysosomal alterations induced in cultured rat fibroblasts by long-term exposure to low

- concentrations of azithromycin. *Journal of Antimicrobial Chemotherapy*. 1998 Dec; 42(6):761–7. PubMed PMID: 10052900. Epub 1999/03/03. eng.
- [48] Ackermann G, Tang YJ, Kueper R, Heisig P, Rodloff AC, Silva J, Jr., et al. Resistance to moxifloxacin in toxigenic *Clostridium difficile* isolates is associated with mutations in *gyrA*. *Antimicrobial Agents and Chemotherapy*. 2001 Aug;45(8):2348–53. PubMed PMID: 11451695. PubMed Central PMCID: PMC90652. Epub 2001/07/14. eng.
- [49] Vester B, Douthwaite S. Macrolide resistance conferred by base substitutions in 23S rRNA. *Antimicrobial Agents and Chemotherapy*. 2001;45(1):1–12. PubMed PMID: PMC90232.
- [50] Pascual A, Ballesta S, Garcia I, Perea EJ. Uptake and intracellular activity of linezolid in human phagocytes and nonphagocytic cells. *Antimicrobial Agents and Chemotherapy*. 2002 Dec;46(12):4013–5. PubMed PMID: 12435714. PubMed Central PMCID: PMC132792. Epub 2002/11/19. eng.
- [51] Wistreich AG. *Microbiology Laboratory Fundamentals and Applications (Hardcover)*. 1996.
- [52] Wolfson JS, Hooper DC. Fluoroquinolone antimicrobial agents. *Clinical Microbiology Reviews*. 1989;2(4):378–424. PubMed PMID: PMC358131.
- [53] Hoger PH, Vosbeck K, Seger R, Hitzig WH. Uptake, intracellular activity, and influence of rifampin on normal function of polymorphonuclear leukocytes. *Antimicrobial Agents and Chemotherapy*. 1985 Nov;28(5):667–74. PubMed PMID: 3004324. PubMed Central PMCID: PMC176354. Epub 1985/11/01. eng.
- [54] Musser JM. Antimicrobial agent resistance in mycobacteria: molecular genetic insights. *Clinical Microbiology Reviews*. 1995 Oct;8(4):496–514. PubMed PMID: 8665467. PubMed Central PMCID: PMC172873. Epub 1995/10/01. eng.
- [55] Carryn S, Chanteux H, Seral C, Mingeot-Leclercq MP, Van Bambeke F, Tulkens PM. Intracellular pharmacodynamics of antibiotics. *Infectious Disease Clinics of North America*. 2003 Sep;17(3):615–34. PubMed PMID: 14711080. Epub 2004/01/09. eng.
- [56] Dulhunty JM, Roberts JA, Davis JS, Webb SA, Bellomo R, Gomersall C, et al. Continuous infusion of beta-lactam antibiotics in severe sepsis: a multicenter double-blind, randomized controlled trial. *Clinical Infectious Diseases*. 2013 Jan;56(2):236–44. PubMed PMID: 23074313. Epub 2012/10/18. eng.
- [57] Seral C, Van Bambeke F, Tulkens PM. Quantitative analysis of gentamicin, azithromycin, telithromycin, ciprofloxacin, moxifloxacin, and oritavancin (LY333328) activities against intracellular *Staphylococcus aureus* in mouse J774 macrophages. *Antimicrobial Agents and Chemotherapy*. 2003 Jul;47(7):2283–92. PubMed PMID: 12821480. PubMed Central PMCID: PMC161849. Epub 2003/06/25. eng.

- [58] Abed N, Couvreur P. Nanocarriers for antibiotics: a promising solution to treat intracellular bacterial infections. *International Journal of Antimicrobial Agents*. 2014 Jun; 43(6):485–96. PubMed PMID: 24721232. Epub 2014/04/12. eng.
- [59] Singh R, Smitha MS, Singh SP. The role of nanotechnology in combating multi-drug resistant bacteria. *Journal of Nanoscience and Nanotechnology*. 2014 Jul;14(7):4745–56. PubMed PMID: 24757944. Epub 2014/04/25. eng.
- [60] Pelgrift RY, Friedman AJ. Nanotechnology as a therapeutic tool to combat microbial resistance. *Advanced Drug Delivery Reviews*. 2013 Nov;65(13–14):1803–15. PubMed PMID: 23892192. Epub 2013/07/31. eng.
- [61] Zhang L, Pornpattananangku D, Hu CM, Huang CM. Development of nanoparticles for antimicrobial drug delivery. *Current Medicinal Chemistry*. 2010;17(6):585–94. PubMed PMID: 20015030. Epub 2009/12/18. eng.
- [62] Pinto-Alphandary H, Andremont A, Couvreur P. Targeted delivery of antibiotics using liposomes and nanoparticles: research and applications. *International Journal of Antimicrobial Agents*. 2000 Jan;13(3):155–68. PubMed PMID: 10724019. Epub 2000/03/21. eng.
- [63] Briones E, Colino CI, Lanao JM. Delivery systems to increase the selectivity of antibiotics in phagocytic cells. *Journal of Controlled Release*. 2008 Feb 11;125(3):210–27. PubMed PMID: 18077047. Epub 2007/12/14. eng.
- [64] Huh AJ, Kwon YJ. “Nanoantibiotics”: a new paradigm for treating infectious diseases using nanomaterials in the antibiotics resistant era. *Journal of Controlled Release*. 2011 Dec 10;156(2):128–45. PubMed PMID: 21763369. Epub 2011/07/19. eng.
- [65] Rawat M, Singh D, Saraf S, Saraf S. Nanocarriers: promising vehicle for bioactive drugs. *Biological and Pharmaceutical Bulletin*. 2006 Sep;29(9):1790–8. PubMed PMID: 16946487. Epub 2006/09/02. eng.
- [66] Mahapatro A, Singh DK. Biodegradable nanoparticles are excellent vehicle for site directed in-vivo delivery of drugs and vaccines. *Journal of Nanobiotechnology*. 2011;9:55. PubMed PMID: 22123084. PubMed Central PMCID: PMC3238292. Epub 2011/11/30. eng.
- [67] Kumari A, Yadav SK, Yadav SC. Biodegradable polymeric nanoparticles based drug delivery systems. *Colloids and Surfaces B: Biointerfaces*. 2010 1/1;75(1):1–18.
- [68] Maham A, Tang Z, Wu H, Wang J, Lin Y. Protein-based nanomedicine platforms for drug delivery. *Small (Weinheim an der Bergstrasse, Germany)*. 2009 Aug 3;5(15):1706–21. PubMed PMID: 19572330. Epub 2009/07/03. eng.
- [69] Kanokpanont S, Damrongsakkul S, Ratanavaraporn J, Aramwit P. An innovative bilayered wound dressing made of silk and gelatin for accelerated wound healing. *International Journal of Pharmaceutics*. 2012 Oct 15;436(1–2):141–53. PubMed PMID: 22771972. Epub 2012/07/10. eng.

- [70] Kuehn C, Graf K, Mashaqi B, Pichlmaier M, Heuer W, Hilfiker A, et al. Prevention of early vascular graft infection using regional antibiotic release. *Journal of Surgical Research*. 2010 Nov;164(1):e185–91. PubMed PMID: 20828762. Epub 2010/09/11. eng.
- [71] Hou T, Xu J, Li Q, Feng J, Zen L. In vitro evaluation of a fibrin gel antibiotic delivery system containing mesenchymal stem cells and vancomycin alginate beads for treating bone infections and facilitating bone formation. *Tissue Engineering Part A*. 2008 Jul;14(7):1173–82. PubMed PMID: 18593356. Epub 2008/07/03. eng.
- [72] Portilla-Arias JA, Camargo B, Garcia-Alvarez M, de Ilarduya AM, Munoz-Guerra S. Nanoparticles made of microbial poly(gamma-glutamate)s for encapsulation and delivery of drugs and proteins. *Journal of Biomaterials Science, Polymer Edition*. 2009;20(7–8):1065–79. PubMed PMID: 19454169. Epub 2009/05/21. eng.
- [73] Okamoto S, Matsuura M, Akagi T, Akashi M, Tanimoto T, Ishikawa T, et al. Poly(gamma-glutamic acid) nano-particles combined with mucosal influenza virus hemagglutinin vaccine protects against influenza virus infection in mice. *Vaccine*. 2009 Sep 25;27(42):5896–905. PubMed PMID: 19647814. Epub 2009/08/04. eng.
- [74] Matsuo K, Ishii Y, Matsuo K, Yoshinaga T, Akashi M, Mukai Y, et al. The utility of poly(gamma-glutamic acid) nanoparticles as antigen delivery carriers in dendritic cell-based cancer immunotherapy. *Biological and Pharmaceutical Bulletin*. 2010;33(12):2003–7. PubMed PMID: 21139241. Epub 2010/12/09. eng.
- [75] Takehara M, Hibino A, Saimura M, Hirohara H. High-yield production of short chain length poly(epsilon-L-lysine) consisting of 5–20 residues by *Streptomyces aureofaciens*, and its antimicrobial activity. *Biotechnology Letters*. 2010 Sep;32(9):1299–303. PubMed PMID: 20464451. Epub 2010/05/14. eng.
- [76] Couffin-Hoarau AC, Aubertin AM, Boustta M, Schmidt S, Fehrentz JA, Martinez J, et al. Peptide-poly(L-lysine citramide) conjugates and their in vitro anti-HIV behavior. *Biomacromolecules*. 2009 Apr 13;10(4):865–76. PubMed PMID: 19296658. Epub 2009/03/20. eng.
- [77] Ravi Kumar MNV. A review of chitin and chitosan applications. *Reactive and Functional Polymers*. 2000 11//;46(1):1–27.
- [78] Hench LL. Biomaterials: a forecast for the future. *Biomaterials*. 1998 Aug;19(16):1419–23. PubMed PMID: 9794512. Epub 1998/10/30. eng.
- [79] Khoushab F, Yamabhai M. Chitin Research Revisited. *Marine Drugs*. 2010 06/28 05/02/received 05/24/revised 05/08/accepted;8(7):1988–2012. PubMed PMID: PMC2920538.
- [80] Jain KK. Drug delivery systems—an overview. *Methods in Molecular Biology (Clifton, NJ)*. 2008;437:1–50. PubMed PMID: 18369961. Epub 2008/03/29. eng.
- [81] Bajpai AK, Shukla SK, Bhanu S, Kankane S. Responsive polymers in controlled drug delivery. *Progress in Polymer Science*. 2008 11//;33(11):1088–118.

- [82] Chifiriuc MC, Grumezescu AM, Grumezescu V, Bezirtzoglou E, Lazar V, Bolocan A. Biomedical applications of natural polymers for drug delivery. *Current Organic Chemistry*. 2014;18(2):152–64.
- [83] Tiwari G, Tiwari R, Sriwastawa B, Bhati L, Pandey S, Pandey P, et al. Drug delivery systems: an updated review. *International Journal of Pharmaceutical Investigation*. 2012 Jan;2(1):2–11. PubMed PMID: 23071954. PubMed Central PMCID: PMC3465154. Epub 2012/10/17. eng.
- [84] Schmaljohann D. Thermo- and pH-responsive polymers in drug delivery. *Advanced Drug Delivery Reviews*. 2006 Dec 30;58(15):1655–70. PubMed PMID: 17125884. Epub 2006/11/28. eng.
- [85] von Burkersroda F, Schedl L, Gopferich A. Why degradable polymers undergo surface erosion or bulk erosion. *Biomaterials*. 2002 Nov;23(21):4221–31. PubMed PMID: 12194525. Epub 2002/08/27. eng.
- [86] Keraliya RA, Patel C, Patel P, Keraliya V, Soni TG, Patel RC, et al. Osmotic Drug Delivery System as a Part of Modified Release Dosage Form. *ISRN Pharmaceutics*. 2012 07/17 03/09/received 05/08/accepted;2012:528079. PubMed PMID: PMC3407637.
- [87] Urbina MC, Zinoveva S, Miller T, Sabliov CM, Monroe WT, Kumar CSSR. Investigation of magnetic nanoparticle–polymer composites for multiple-controlled drug delivery. *Journal of Physical Chemistry C*. 2008 2008/07/01;112(30):11102–8.
- [88] Mano JF. Stimuli-responsive polymeric systems for biomedical applications. *Advanced Engineering Materials*. 2008;10(6):515–27.
- [89] Qiu J, Charleux B, Matyjaszewski K. Controlled/living radical polymerization in aqueous media: homogeneous and heterogeneous systems. *Progress in Polymer Science*. 2001 12//;26(10):2083–134.
- [90] Kingsley JD, Dou H, Morehead J, Rabinow B, Gendelman HE, Destache CJ. Nanotechnology: a focus on nanoparticles as a drug delivery system. *Journal of Neuroimmune Pharmacology*. 2006 Sep;1(3):340–50. PubMed PMID: 18040810. Epub 2007/11/28. eng.
- [91] Pinto Reis C, Neufeld RJ, Ribeiro AJ, Veiga F. Nanoencapsulation I. Methods for preparation of drug-loaded polymeric nanoparticles. *Nanomedicine: Nanotechnology, Biology, and Medicine*. 2006 Mar;2(1):8–21. PubMed PMID: 17292111. Epub 2007/02/13. eng.
- [92] Lee LY, Wang CH, Smith KA. Supercritical antisolvent production of biodegradable micro- and nanoparticles for controlled delivery of paclitaxel. *Journal of Controlled Release*. 2008 Jan 22;125(2):96–106. PubMed PMID: 18054107. Epub 2007/12/07. eng.
- [93] Thiele L, Diederichs JE, Reszka R, Merkle HP, Walter E. Competitive adsorption of serum proteins at microparticles affects phagocytosis by dendritic cells. *Biomaterials*. 2003 Apr;24(8):1409–18. PubMed PMID: 12527282. Epub 2003/01/16. eng.

- [94] Ravi Kumar MN. Nano and microparticles as controlled drug delivery devices. *Journal of Pharmacy and Pharmaceutical Sciences*. 2000 May–Aug;3(2):234–58. PubMed PMID: 10994037. Epub 2000/09/20. eng.
- [95] Date AA, Joshi MD, Patravale VB. Parasitic diseases: liposomes and polymeric nanoparticles versus lipid nanoparticles. *Advanced Drug Delivery Reviews*. 2007 Jul 10;59(6):505–21. PubMed PMID: 17574295. Epub 2007/06/19. eng.
- [96] Ahmad Z, Pandey R, Sharma S, Khuller GK. Alginate nanoparticles as antituberculosis drug carriers: formulation development, pharmacokinetics and therapeutic potential. *Indian Journal of Chest Diseases and Allied Sciences*. 2006 Jul–Sep;48(3):171–6. PubMed PMID: 18610673. Epub 2008/07/10. eng.
- [97] Nagpal K, Singh SK, Mishra DN. Chitosan nanoparticles: a promising system in novel drug delivery. *Chemical and Pharmaceutical Bulletin*. 2010 Nov;58(11):1423–30. PubMed PMID: 21048331. Epub 2010/11/05. eng.
- [98] Huh KM, Lee SC, Cho YW, Lee J, Jeong JH, Park K. Hydrotropic polymer micelle system for delivery of paclitaxel. *Journal of Controlled Release*. 2005 Jan 3;101(1–3):59–68. PubMed PMID: 15588894. Epub 2004/12/14. eng.
- [99] Bertesteanu S, Chifiriuc MC, Grumezescu AM, Printza AG, Marie-Paule T, Grumezescu V, et al. Biomedical applications of synthetic, biodegradable polymers for the development of anti-infective strategies. *Current Medicinal Chemistry*. 2014;21(29):3383–90. PubMed PMID: 24606501. Epub 2014/03/13. eng.
- [100] Hornig S, Bunjes H, Heinze T. Preparation and characterization of nanoparticles based on dextran-drug conjugates. *Journal of Colloid and Interface Science*. 2009 Oct 1;338(1):56–62. PubMed PMID: 19635622. Epub 2009/07/29. eng.
- [101] Roseeuw E, Coessens V, Balazuc A-M, Lagranderie M, Chavarot P, Pessina A, et al. Synthesis, degradation, and antimicrobial properties of targeted macromolecular prodrugs of norfloxacin. *Antimicrobial Agents and Chemotherapy*. 2003 12/13/received 04/14/revised 08/11/accepted;47(11):3435–41. PubMed PMID: PMC253810.
- [102] Jiang D, Salem AK. Optimized dextran-polyethylenimine conjugates are efficient non-viral vectors with reduced cytotoxicity when used in serum containing environments. *International Journal of Pharmaceutics*. 2012 May 1;427(1):71–9. PubMed PMID: 22037445. PubMed Central PMCID: PMC3295901. Epub 2011/11/01. eng.
- [103] Gnanadhas DP, Ben Thomas M, Elango M, Raichur AM, Chakravorty D. Chitosan-dextran sulphate nanocapsule drug delivery system as an effective therapeutic against intraphagosomal pathogen *Salmonella*. *Journal of Antimicrobial Chemotherapy*. 2013 Nov;68(11):2576–86. PubMed PMID: 23798672. Epub 2013/06/27. eng.
- [104] De Paula EE, De Sousa FB, Da Silva JC, Fernandes FR, Melo MN, Frezard F, et al. Insights into the multi-equilibrium, superstructure system based on beta-cyclodextrin

- and a highly water soluble guest. *International Journal of Pharmaceutics*. 2012 Dec 15;439(1–2):207–15. PubMed PMID: 23022296. Epub 2012/10/02. eng.
- [105] Jain A, Gupta Y, Jain SK. Perspectives of biodegradable natural polysaccharides for site-specific drug delivery to the colon. *Journal of pharmacy & pharmaceutical sciences: a publication of the Canadian Society for Pharmaceutical Sciences, Societe Canadienne des Sciences Pharmaceutiques*. 2007;10(1):86–128. PubMed PMID: 17498397. Epub 2007/05/15. eng.
- [106] Farazuddin M, Chauhan A, Khan RM, Owais M. Amoxicillin-bearing microparticles: potential in the treatment of *Listeria monocytogenes* infection in Swiss albino mice. *Bio-science Reports*. 2011 Aug;31(4):265–72. PubMed PMID: 20687896. Epub 2010/08/07. eng.
- [107] Heijink A, Yaszemski MJ, Patel R, Rouse MS, Lewallen DG, Hanssen AD. Local antibiotic delivery with OsteoSet, DBX, and Collagraft. *Clinical Orthopaedics and Related Research*. 2006 Oct;451:29–33. PubMed PMID: 16906070. Epub 2006/08/15. eng.
- [108] Smitha KT, Nisha N, Maya S, Biswas R, Jayakumar R. Delivery of rifampicin-chitin nanoparticles into the intracellular compartment of polymorphonuclear leukocytes. *International Journal of Biological Macromolecules*. 2015 Mar;74:36–43. PubMed PMID: 25475841. Epub 2014/12/06. eng.
- [109] Puoci F, Cirillo G, Curcio M, Parisi OI, Iemma F, Picci N. Molecularly imprinted polymers in drug delivery: state of art and future perspectives. *Expert Opinion on Drug Delivery*. 2011 Oct;8(10):1379–93. PubMed PMID: 21933031. Epub 2011/09/22. eng.
- [110] Sah H, Thoma LA, Desu HR, Sah E, Wood GC. Concepts and practices used to develop functional PLGA-based nanoparticulate systems. *International Journal of Nanomedicine*. 2013;8:747–65. PubMed PMID: 23459088. PubMed Central PMCID: PMC3582541. Epub 2013/03/06. eng.
- [111] Kaditi E, Mountrichas G, Pispas S, Demetzos C. Block copolymers for drug delivery nano systems (DDnSs). *Current Medicinal Chemistry*. 2012;19(29):5088–100. PubMed PMID: 22963634. Epub 2012/09/12. eng.
- [112] Kluin OS, van der Mei HC, Busscher HJ, Neut D. Biodegradable vs non-biodegradable antibiotic delivery devices in the treatment of osteomyelitis. *Expert Opinion on Drug Delivery*. 2013 Mar;10(3):341–51. PubMed PMID: 23289645. Epub 2013/01/08. eng.
- [113] Ulery BD, Nair LS, Laurencin CT. Biomedical applications of biodegradable polymers. *Journal of Polymer Science Part B: Polymer Physics*. 2011;49(12):832–64.
- [114] Danhier F, Ansorena E, Silva JM, Coco R, Le Breton A, Preat V. PLGA-based nanoparticles: an overview of biomedical applications. *Journal of Controlled Release*. 2012 Jul 20;161(2):505–22. PubMed PMID: 22353619. Epub 2012/02/23. eng.
- [115] Farazuddin M, Alam M, Khan AA, Khan N, Parvez S, Dutt GU, et al. Efficacy of amoxicillin bearing microsphere formulation in treatment of *Listeria monocytogenes*

- infection in Swiss albino mice. *Journal of Drug Targeting*. 2010 Jan;18(1):45–52. PubMed PMID: 19624287. Epub 2009/07/25. eng.
- [116] Malathi S, Balasubramanian S. Synthesis of biodegradable polymeric nanoparticles and their controlled drug delivery for tuberculosis. *Journal of Biomedical Nanotechnology*. 2011 Feb;7(1):150–1. PubMed PMID: 21485846. Epub 2011/04/14. eng.
- [117] Pandey R, Sharma A, Zahoor A, Sharma S, Khuller GK, Prasad B. Poly (DL-lactide-co-glycolide) nanoparticle-based inhalable sustained drug delivery system for experimental tuberculosis. *Journal of Antimicrobial Chemotherapy*. 2003 Dec;52(6):981–6. PubMed PMID: 14613962. Epub 2003/11/14. eng.
- [118] Skidan IN, Gel'perina SE, Severin SE, Guliaev AE. [Enhanced activity of rifampicin loaded with polybutyl cyanoacrylate nanoparticles in relation to intracellularly localized bacteria]. *Antibiotiki i Khimioterapiia = Antibiotics and Chemotherapy [sic]/ Ministerstvo Meditsinskoi i Mikrobiologicheskoi Promyshlennosti SSSR*. 2003;48(1):23–6. PubMed PMID: 12741319. Epub 2003/05/14. Povyshenie aktivnosti rifampitsina, assotsirovannogo s nanochastitsami iz polibutirtsianoakrilata, v otnoshenii bakterii, lokalizovannykh vnutri kletok. rus.
- [119] Fawaz F, Bonini F, Maugein J, Lagueny AM. Ciprofloxacin-loaded polyisobutylcyanoacrylate nanoparticles: pharmacokinetics and in vitro antimicrobial activity. *International Journal of Pharmaceutics*. 1998 6/15;168(2):255–9.
- [120] Lecaroz C, Gamazo C, Renedo MJ, Blanco-Prieto MJ. Biodegradable micro- and nanoparticles as long-term delivery vehicles for gentamicin. *Journal of Microencapsulation*. 2006 Nov;23(7):782–92. PubMed PMID: 17123922. Epub 2006/11/25. eng.
- [121] Fattal E, Pecquet S, Couvreur P, Andremont A. Biodegradable microparticles for the mucosal delivery of antibacterial and dietary antigens. *International Journal of Pharmaceutics*. 2002 Aug 21;242(1–2):15–24. PubMed PMID: 12176221. Epub 2002/08/15. eng.
- [122] Toti US, Guru BR, Hali M, McPharlin CM, Wykes SM, Panyam J, et al. Targeted delivery of antibiotics to intracellular chlamydial infections using PLGA nanoparticles. *Biomaterials*. 2011 Sep;32(27):6606–13. PubMed PMID: 21652065. PubMed Central PMCID: PMC3133877. Epub 2011/06/10. eng.
- [123] Imbuluzqueta E, Elizondo E, Gamazo C, Moreno-Calvo E, Veciana J, Ventosa N, et al. Novel bioactive hydrophobic gentamicin carriers for the treatment of intracellular bacterial infections. *Acta Biomaterialia*. 2011 Apr;7(4):1599–608. PubMed PMID: 21115143. Epub 2010/12/01. eng.
- [124] Jhunjhunwala S, Raimondi G, Thomson AW, Little SR. Delivery of rapamycin to dendritic cells using degradable microparticles. *Journal of Controlled Release*. 2009 Feb 10;133(3):191–7. PubMed PMID: 19000726. PubMed Central PMCID: PMC2925512. Epub 2008/11/13. eng.

- [125] Gaspar R, Preat V, Opperdoes FR, Roland M. Macrophage activation by polymeric nanoparticles of polyalkylcyanoacrylates: activity against intracellular *Leishmania donovani* associated with hydrogen peroxide production. *Pharmaceutical Research*. 1992 Jun;9(6):782–7. PubMed PMID: 1409361. Epub 1992/06/01. eng.
- [126] Fattal E, Youssef M, Couvreur P, Andremont A. Treatment of experimental salmonellosis in mice with ampicillin-bound nanoparticles. *Antimicrobial Agents and Chemotherapy*. 1989;33(9):1540–3. PubMed PMID: PMC172698.
- [127] Forestier F, Gerrier P, Chaumard C, Quero AM, Couvreur P, Labarre C. Effect of nanoparticle-bound ampicillin on the survival of *Listeria monocytogenes* in mouse peritoneal macrophages. *Journal of Antimicrobial Chemotherapy*. 1992 Aug;30(2):173–9. PubMed PMID: 1399927. Epub 1992/08/01. eng.
- [128] Pandey R, Khuller GK. Oral nanoparticle-based antituberculosis drug delivery to the brain in an experimental model. *Journal of Antimicrobial Chemotherapy*. 2006 Jun;57(6):1146–52. PubMed PMID: 16597631. Epub 2006/04/07. eng.
- [129] Kuroda K, Caputo GA. Antimicrobial polymers as synthetic mimics of host-defense peptides. *Nanomedicine and Nanobiotechnology*. 2013 Jan–Feb;5(1):49–66. PubMed PMID: 23076870. Epub 2012/10/19. eng.
- [130] Palermo EF, Kuroda K. Structural determinants of antimicrobial activity in polymers which mimic host defense peptides. *Applied Microbiology and Biotechnology*. 2010 Aug;87(5):1605–15. PubMed PMID: 20563718. Epub 2010/06/22. eng.
- [131] Lee S, Yang SC, Heffernan MJ, Taylor WR, Murthy N. Polyketal microparticles: a new delivery vehicle for superoxide dismutase. *Bioconjugate Chemistry*. 2007 Jan–Feb;18(1):4–7. PubMed PMID: 17226951. Epub 2007/01/18. eng.
- [132] Seshadri G, Sy JC, Brown M, Dikalov S, Yang SC, Murthy N, et al. The delivery of superoxide dismutase encapsulated in polyketal microparticles to rat myocardium and protection from myocardial ischemia-reperfusion injury. *Biomaterials*. 2010 Feb;31(6):1372–9. PubMed PMID: 19889454. PubMed Central PMCID: PMC2813932. Epub 2009/11/06. eng.
- [133] Kalluru R, Fenaroli F, Westmoreland D, Ulanova L, Maleki A, Roos N, et al. Poly(lactide-co-glycolide)-rifampicin nanoparticles efficiently clear *Mycobacterium bovis* BCG infection in macrophages and remain membrane-bound in phago-lysosomes. *Journal of Cell Science*. 2013 Jul 15;126(Pt 14):3043–54. PubMed PMID: 23687375. Epub 2013/05/21. eng.
- [134] Page-Clisson ME, Pinto-Alphandary H, Chachaty E, Couvreur P, Andremont A. Drug targeting by polyalkylcyanoacrylate nanoparticles is not efficient against persistent *Salmonella*. *Pharmaceutical Research*. 1998 Apr;15(4):544–9. PubMed PMID: 9587949. Epub 1998/05/20. eng.

- [135] Discher BM, Won YY, Ege DS, Lee JC, Bates FS, Discher DE, et al. Polymersomes: tough vesicles made from diblock copolymers. *Science*. 1999 May 14;284(5417):1143–6. PubMed PMID: 10325219. Epub 1999/05/15. eng.
- [136] Wayakanon K, Thornhill MH, Douglas CW, Lewis AL, Warren NJ, Pinnock A, et al. Polymersome-mediated intracellular delivery of antibiotics to treat *Porphyromonas gingivalis*-infected oral epithelial cells. *FASEB Journal*. 2013 Nov;27(11):4455–65. PubMed PMID: 23921377. Epub 2013/08/08. eng.
- [137] Coune A. Liposomes as drug delivery system in the treatment of infectious diseases. Potential applications and clinical experience. *Infection*. 1988 May–Jun;16(3):141–7. PubMed PMID: 3042625. Epub 1988/05/01. eng.
- [138] Kelly C, Jefferies C, Cryan S-A. Targeted liposomal drug delivery to monocytes and macrophages. *Journal of Drug Delivery*. 2011;2011:11.
- [139] Khuller GK, Kapur M, Sharma S. Liposome technology for drug delivery against mycobacterial infections. *Current Pharmaceutical Design*. 2004;10(26):3263–74. PubMed PMID: 15544514. Epub 2004/11/17. eng.
- [140] Yanagihara K. Design of anti-bacterial drug and anti-mycobacterial drug for drug delivery system. *Current Pharmaceutical Design*. 2002;8(6):475–82. PubMed PMID: 12069384. Epub 2002/06/19. eng.
- [141] Gangadharam PR, Ashtekar DA, Ghorri N, Goldstein JA, Debs RJ, Duzgunes N. Chemotherapeutic potential of free and liposome encapsulated streptomycin against experimental *Mycobacterium avium* complex infections in beige mice. *Journal of Antimicrobial Chemotherapy*. 1991 Sep;28(3):425–35. PubMed PMID: 1960123. Epub 1991/09/01. eng.
- [142] Patton JS, Fishburn CS, Weers JG. The lungs as a portal of entry for systemic drug delivery. *Proceedings of the American Thoracic Society*. 2004;1(4):338–44. PubMed PMID: 16113455. Epub 2005/08/23. eng.
- [143] Deol P, Khuller GK. Lung specific stealth liposomes: stability, biodistribution and toxicity of liposomal antitubercular drugs in mice. *Biochimica et Biophysica Acta*. 1997 Mar 15;1334(2–3):161–72. PubMed PMID: 9101710. Epub 1997/03/15. eng.
- [144] Vitas AI, Díaz R, Gamazo C. Effect of composition and method of preparation of liposomes on their stability and interaction with murine monocytes infected with *Bruccella abortus*. *Antimicrobial Agents and Chemotherapy*. 1996;40(1):146–51. PubMed PMID: PMC163073.
- [145] Fierer J, Hatlen L, Lin JP, Estrella D, Mihalko P, Yau-Young A. Successful treatment using gentamicin liposomes of *Salmonella* dublin infections in mice. *Antimicrobial Agents and Chemotherapy*. 1990 Feb;34(2):343–8. PubMed PMID: 2327780. PubMed Central PMCID: PMC171584. Epub 1990/02/01. eng.
- [146] Bakker-Woudenberg IA, Lokerse AF, Roerdink FH. Effect of lipid composition on activity of liposome-entrapped ampicillin against intracellular *Listeria monocytogenes*.

- Antimicrobial Agents and Chemotherapy. 1988;32(10):1560–4. PubMed PMID: PMC175919.
- [147] Lutwyche P, Cordeiro C, Wiseman DJ, St-Louis M, Uh M, Hope MJ, et al. Intracellular delivery and antibacterial activity of gentamicin encapsulated in pH-sensitive liposomes. *Antimicrobial Agents and Chemotherapy*. 1998 Oct;42(10):2511–20. PubMed PMID: 9756749. PubMed Central PMCID: PMC105873. Epub 1998/10/03. eng.
- [148] Lockman PR, Mumper RJ, Khan MA, Allen DD. Nanoparticle technology for drug delivery across the blood–brain barrier. *Drug Development and Industrial Pharmacy*. 2002 Jan;28(1):1–13. PubMed PMID: 11858519. Epub 2002/02/23. eng.
- [149] Roney C, Kulkarni P, Arora V, Antich P, Bonte F, Wu A, et al. Targeted nanoparticles for drug delivery through the blood–brain barrier for Alzheimer’s disease. *Journal of Controlled Release*. 2005 Nov 28;108(2–3):193–214. PubMed PMID: 16246446. Epub 2005/10/26. eng.
- [150] Kreuter J. Nanoparticulate systems for brain delivery of drugs. *Advanced Drug Delivery Reviews*. 2001 Mar 23;47(1):65–81. PubMed PMID: 11251246. Epub 2001/03/17. eng.
- [151] Seleem MN, Jain N, Pothayee N, Ranjan A, Riffle JS, Sriranganathan N. Targeting *Brucella melitensis* with polymeric nanoparticles containing streptomycin and doxycycline. *FEMS Microbiology Letters*. 2009 May;294(1):24–31. PubMed PMID: 19493005. Epub 2009/06/06. eng.
- [152] Kadurugamuwa JL, Beveridge TJ. Delivery of the non-membrane-permeative antibiotic gentamicin into mammalian cells by using *Shigella flexneri* membrane vesicles. *Antimicrobial Agents and Chemotherapy*. 1998 Jun;42(6):1476–83. PubMed PMID: 9624497. PubMed Central PMCID: PMC105625. Epub 1998/06/13. eng.
- [153] Kamboj S, Saini V, Maggon N, Bala S, Jhawar V. Vesicular drug delivery systems: a novel approach for drug targeting. *International Journal of Drug Delivery*. 2013;5(2): 10. Epub 2013-09-17.
- [154] Singh G, Dwivedi H, Saraf S, Saraf S. Niosomal delivery of isoniazid: development and characterization. *Tropical Journal of Pharmaceutical Research*. 2011;10(2):203–10.
- [155] Jain C, Vyas S, VK. D. Niosomal system for delivery of rifampicin to lymphatics. *Indian Journal of Pharmaceutical Sciences*. 2006;68(5):575–8.
- [156] Mukherjee S, Ray S, Thakur RS. Solid lipid nanoparticles: a modern formulation approach in drug delivery system. *Indian Journal of Pharmaceutical Sciences*. 2009 Jul; 71(4):349–58. PubMed PMID: 20502539. PubMed Central PMCID: PMC2865805. Epub 2010/05/27. eng.
- [157] Nimje N, Agarwal A, Saraogi GK, Lariya N, Rai G, Agrawal H, et al. Mannosylated nanoparticulate carriers of rifabutin for alveolar targeting. *Journal of Drug Targeting*. 2009 Dec;17(10):777–87. PubMed PMID: 19938949. Epub 2009/11/27. eng.

- [158] Pandey R, Khuller GK. Solid lipid particle-based inhalable sustained drug delivery system against experimental tuberculosis. *Tuberculosis (Edinburgh, Scotland)*. 2005 Jul;85(4):227–34. PubMed PMID: 15922668. Epub 2005/06/01. eng.
- [159] Muller RH, Jacobs C. Buparvaquone mucoadhesive nanosuspension: preparation, optimisation and long-term stability. *International Journal of Pharmaceutics*. 2002 Apr 26;237(1–2):151–61. PubMed PMID: 11955813. Epub 2002/04/17. eng.
- [160] Aggarwal P, Hall JB, McLeland CB, Dobrovolskaia MA, McNeil SE. Nanoparticle interaction with plasma proteins as it relates to particle biodistribution, biocompatibility and therapeutic efficacy. *Advanced Drug Delivery Reviews*. 2009 Jun 21;61(6):428–37. PubMed PMID: 19376175. PubMed Central PMCID: PMC3683962. Epub 2009/04/21. eng.
- [161] Patel MB, Harikrishnan U, Valand NN, Modi NR, Menon SK. Novel cationic quinoxalin-4(3H)-one conjugated fullerene nanoparticles as antimycobacterial and antimicrobial agents. *Archiv der Pharmazie*. 2013 Mar;346(3):210–20. PubMed PMID: 23359525. Epub 2013/01/30. eng.
- [162] Kumar PV, Asthana A, Dutta T, Jain NK. Intracellular macrophage uptake of rifampicin loaded mannosylated dendrimers. *Journal of Drug Targeting*. 2006 Sep;14(8):546–56. PubMed PMID: 17050121. Epub 2006/10/20. eng.
- [163] Dutta T, Jain NK. Targeting potential and anti-HIV activity of lamivudine loaded mannosylated poly (propyleneimine) dendrimer. *Biochimica et Biophysica Acta*. 2007 Apr;1770(4):681–6. PubMed PMID: 17276009. Epub 2007/02/06. eng.
- [164] Bhadra D, Bhadra S, Jain NK. Pegylated lysine based copolymeric dendritic micelles for solubilization and delivery of artemether. *Journal of Pharmacy and Pharmaceutical Sciences*. 2005;8(3):467–82. PubMed PMID: 16401394. Epub 2006/01/13. eng.
- [165] Mishra MK, Kotta K, Hali M, Wykes S, Gerard HC, Hudson AP, et al. PAMAM dendrimer-azithromycin conjugate nanodevices for the treatment of *Chlamydia trachomatis* infections. *Nanomedicine: Nanotechnology, Biology, and Medicine*. 2011 Dec;7(6):935–44. PubMed PMID: 21658474. Epub 2011/06/11. eng.
- [166] Corma A, Garcia H. Supramolecular host–guest systems in zeolites prepared by ship-in-a-bottle synthesis. *European Journal of Inorganic Chemistry*. 2004;2004(6):1143–64.
- [167] Vilaça N, Amorim R, Machado AF, Parpot P, Pereira MFR, Sardo M, et al. Potentiation of 5-fluorouracil encapsulated in zeolites as drug delivery systems for in vitro models of colorectal carcinoma. *Colloids and Surfaces B: Biointerfaces*. 2013 12/1;112(0):237–44.
- [168] Clemens DL, Lee BY, Xue M, Thomas CR, Meng H, Ferris D, et al. Targeted intracellular delivery of antituberculosis drugs to *Mycobacterium tuberculosis*-infected macrophages via functionalized mesoporous silica nanoparticles. *Antimicrobial Agents*

and Chemotherapy. 2012 May;56(5):2535–45. PubMed PMID: 22354311. PubMed Central PMCID: PMC3346638. Epub 2012/02/23. eng.

- [169] Seleem MN, Munusamy P, Ranjan A, Alqublan H, Pickrell G, Sriranganathan N. Silica-antibiotic hybrid nanoparticles for targeting intracellular pathogens. *Antimicrobial Agents and Chemotherapy*. 2009 08/10 06/17/received 07/12/revised 08/03/accepted;53(10):4270–4. PubMed PMID: PMC2764215.
- [170] Gutierrez Millan C, Bax BE, Castaneda AZ, Marinero ML, Lanao JM. In vitro studies of amikacin-loaded human carrier erythrocytes. *Translational Research*. 2008 Aug; 152(2):59–66. PubMed PMID: 18674740. Epub 2008/08/05. eng.

---

# Device Integrity of Drug-eluting Depot Stent for Smart Drug Delivery

---

Hao-Ming Hsiao, Aichi Chien, Bor-Hann Huang, Dian-Ru Li, Hsin Chen and Chun-Yi Ko

Additional information is available at the end of the chapter

<http://dx.doi.org/10.5772/61790>

---

## Abstract

Atherosclerosis, or hardening of the arteries, is a condition in which plaque, made of cholesterol, fatty substances, cellular waste products, calcium, and fibrin, builds up inside the arteries. A metallic stent is a small mesh tube that is used to treat these narrowed arteries such as coronary artery diseases. The drug-eluting stent has a metallic stent platform coated with drug-polymer mix and has been shown to be superior to its metallic stent counterpart in reducing restenosis. In the past few years, a novel variation of the drug-eluting stent with micro-sized drug reservoirs (depot stent) has been introduced to the market. It allows smart programmable drug delivery with spatial/temporal control and has potential advantages over conventional stents. The drug-polymer mix compound can be altered from one reservoir to the next, allowing a highly-controlled release of different medications. For example, this depot stent concept can be applied in the renal indication for potential treatment of both renal artery stenosis (upstream) and its associated kidney diseases (downstream) simultaneously. However, the creation of such drug reservoirs on the stent struts inevitably compromises its mechanical integrity. In this study, the effects of these drug reservoirs on stent key clinical attributes were systematically investigated. We developed finite element models to predict the mechanical integrity of a balloon-expandable stent at various stages of its function life such as manufacturing and acute deployment, as well as the stent radial strength and chronic fatigue life. Simulation results show that (1) creating drug reservoirs on a stent strut could impact the stent fatigue resistance to certain degrees; (2) drug reservoirs on the high stress concentration regions led to much greater loss in all key clinical attributes than reservoirs on other locations; (3) reservoir shape change resulted in little differences in all key clinical attributes; and (4) for the same drug loading capacity, larger and fewer reservoirs yielded

higher fatigue safety factor. These results can help future stent designers to achieve the optimal balance of stent mechanical integrity and smart drug delivery, thereby opening up a wide variety of new opportunities for disease treatments. We also proposed an optimized depot stent with tripled drug capacity and acceptable marginal trade-off in key clinical attributes when compared to the current drug-eluting stents. This depot stent prototype was manufactured for the demonstration of our design concept.

**Keywords:** Drug-eluting stent, Drug reservoir, Depot stent, Mechanical integrity, Smart drug delivery

---

## 1. Introduction

Percutaneous coronary intervention (PCI), also known as angioplasty, has been the current standard for the treatment of coronary artery diseases. A metallic stent is a tiny, coiled wire-mesh tube that can be deployed into an artery and expanded using a catheter during angioplasty to open a narrowed artery. However, intimal cells can proliferate due to the artery injury during stenting, often leading to in-stent restenosis of the artery. Restenosis, the re-narrowing of the artery after the intervention, is the most common occurrence after angioplasty procedures in early days [1-3].

In the past decade, stent technology has evolved from the metallic stent to the so-called drug-eluting stent (DES). A drug-eluting stent has a metallic stent platform coated with an anti-proliferative drug (e.g., Sirolimus or Everolimus) that is known to interfere with the restenosis process. The drug is typically mixed with a polymer compound (durable or biodegradable) to precisely control its release rate and timing to the artery wall. The adoption of the drug-eluting stent has resulted in a dramatic lowering in restenosis rates from 20 to 30% for the metallic stent to the single digit now [4, 5], leading to a worldwide embrace of this new technology in healthcare. Since the introduction of the drug-eluting stent, restenosis has become less of an issue for the treatment of coronary artery diseases. The drug-eluting stent has thus become the gold standard for PCI procedures since then.

Although the drug-eluting stent has been hugely successful in lowering restenosis, the stenting technology continues to evolve in a quest for better solutions. The biodegradable vascular scaffold (BVS) presents the next frontier. Biodegradable stents stay in the blood vessel for a limited period of time, give mechanical support, and then degrade to non-toxic substances. Potential advantages of having the stent disappear from the treated site include reduced late stent thrombosis, facilitation of repeat treatments to the same site, and freedom from fracture-induced restenosis. The biodegradable stents with poly lactic acid (PLA) have good physical properties such as high strength and processability; and in a suitable disposal site it will degrade to natural products [6-8]. BVS has the potential to act as local drug delivery systems. Therefore, it is possible to design a BVS, not only offering a physical support to the vessel wall, but also presenting a pharmacological approach in the prevention of thrombus formation and intimal proliferation [9-11].

In recent years, another novel concept in smart drug delivery is the emergence of the depot stent: a metallic stent laser-drilled with micro-sized holes, or called "reservoirs," that can be loaded with single or multiple drugs, potentially in various doses or formulations [12, 13]. The drug-polymer mix can be varied from one reservoir to the next, allowing a high flexibility of controlled release of different drugs. For example, on the outer side of the reservoirs close to the artery wall, drugs preventing neointimal proliferation can be filled, while on the inner side of the reservoirs close to the blood stream, thrombocyte inhibitors can be filled to prevent stent thrombosis (Figure 1). In addition, it is believed that this stent concept could become even more powerful in some cases such as the renal indication for potential treatment of both renal artery stenosis (RAS) and its associated kidney diseases at the same time, as renal artery stenosis is usually related to progressive hypertension, renal insufficiency, or kidney failure reciprocally. For example, drugs preventing neointimal proliferation can be applied on the outside portion of the reservoirs closer to the artery wall, whereas on the inside portion of the reservoirs, drugs for kidney diseases can be loaded and carried by the blood stream to the distal kidney organ for direct target therapy. This proposed method could potentially help to treat two problems in one attempt. Figure 2 shows that different types of drugs can be administered independently at each stage after intervention.

The depot stent has other advantages. Unlike drug-eluting stents, the depot stent does not need to be surface-coated. Therefore, it is free of surface coating layers, thereby reducing direct contact between the artery wall and the polymer compound. Such contact is believed to increase the potential risk of chronic inflammation or late stent thrombosis. Another advantage is the decrease of the overall stent profile due to the absence of surface coating layers. Lower stent profile allows a stent to access narrower lesion sites and offers physicians easier deliverability. Given these potential advantages, however, creating reservoirs on the stent struts inevitably weaken the stent structure and compromise its mechanical integrity, namely, its abilities to sustain various loading conditions including crimping onto a balloon catheter during manufacturing, stent expansion during deployment, radial resistance to blood vessels from collapsing inward, and long-term fatigue resistance to systolic/diastolic pressure loadings. Therefore, the objective of this paper is to investigate the impact of the micro-sized reservoirs on the overall mechanical integrity of the depot stent.

Computational modeling has emerged as a powerful tool for optimization of stent designs and can be used along with bench testing to improve stent clinical performance [14-18]. Such computational tools could provide valuable insights to various aspects of stent design tactics which may consequently reduce the potential risk of vascular injury and restenosis. It also gives extensive information under a highly-controlled environment, making it feasible to screen numerous design iterations prior to costly prototyping. Therefore, in this study, computational models were developed to assess key clinical attributes of the depot stent using finite element analysis (FEA). Based on these findings, we propose an optimal depot stent design in an effort to increase the drug capacity without significantly comprising its mechanical integrity.

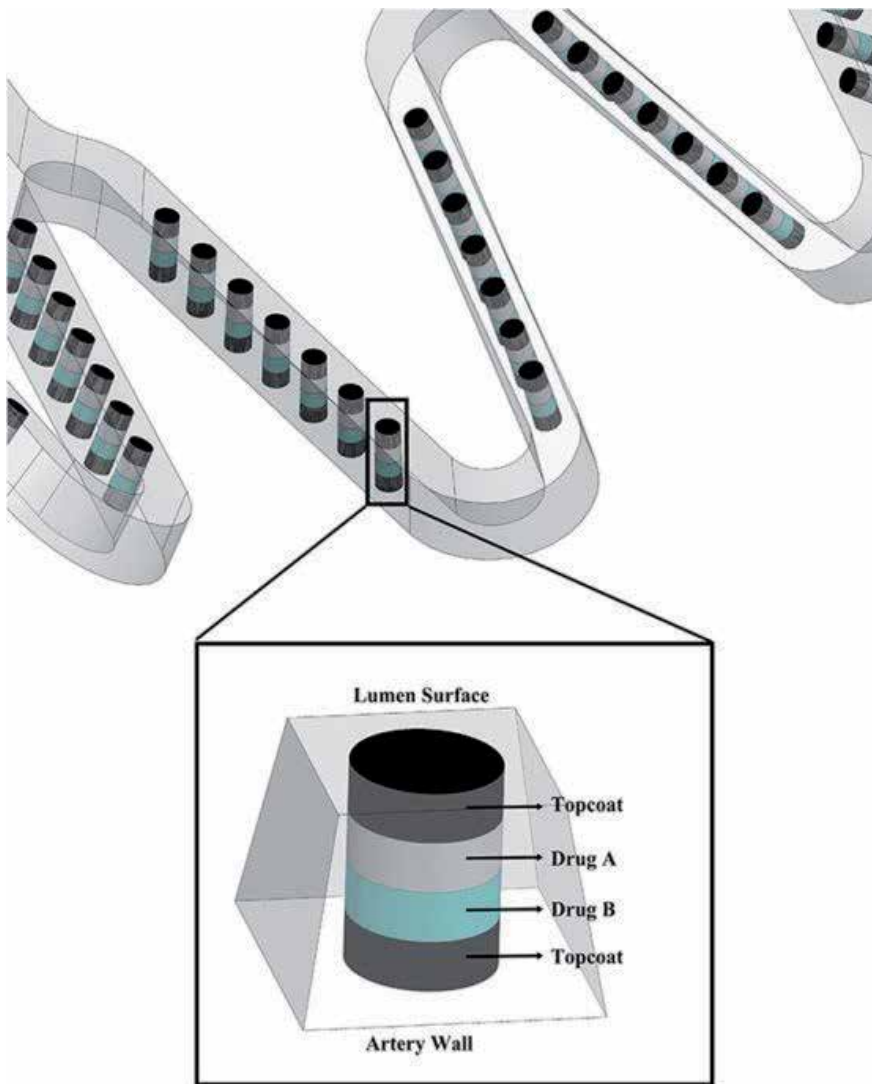


**Figure 1.** Depot stent concept with different types of drugs and release rates administered independently of opposite sides of the stent.

## 2. Depot stent configuration

An L-605 cobalt–chromium balloon-expandable stent was used as the “standard” stent for baseline in this study. Micro-sized drug reservoirs were created on this standard stent struts in order to investigate their effects on the stent mechanical integrity. The stent was designed to form a series of nested rings interconnected with bridging connectors (CO). The design parameters such as crown radius (CR) and strut dimension were tailored to optimize the overall stent performance.

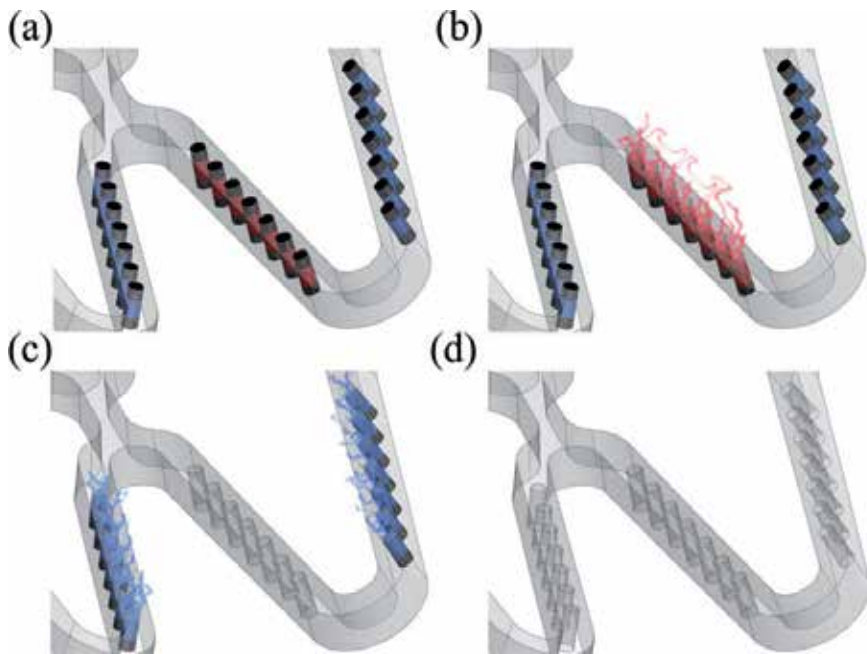


**Figure 2.** Schematic of sequential release of multiple drugs for each period after intervention.

The standard stent, which has exactly the same geometry as the investigated depot stents but without drug reservoirs, was first evaluated to establish the baseline information. The FEA simulation was then conducted to investigate the effects of reservoir location on the mechanical integrity of the depot stent. Five equally spaced circular (cylindrical if considering depth) reservoirs were created on three major locations of the depot stent, namely, connectors, bar arms (BA), and crowns (Figure 3). The diameter of each circular reservoir was 50% of the strut width, whereas the reservoir depth was varied for evaluation. The spacing between two adjacent reservoirs was 0.15 mm, as defined by the length between two reservoir centers along the strut centerline. The choice of the reservoir number and size was based on the condition that the total reservoir capacity of the drug-polymer mix inside the reservoirs of the depot stent was able to fully replace the total volume of surface coating layers on a typical drug-eluting stent with an average coating thickness of  $5\mu\text{m}$  [4].

Since adding more reservoirs increases the total drug capacity, investigation was also carried out on the depot stent with reservoirs uniformly spread on the entire stent to understand whether the mechanical integrity of such a depot stent is further compromised or not (Figure 3(d)). In this special case, the entire stent was covered by reservoirs with the same circular diameter and depth aforementioned. Another method of increasing the total drug capacity is by drilling through-holes instead of blind-holes into the stent struts. Therefore, FEA simulation was also conducted to investigate the effects of reservoir depth on the mechanical integrity. Further studies were conducted on the depot stent to investigate whether the reservoir shape, size, and number affect the stent mechanical integrity or not.

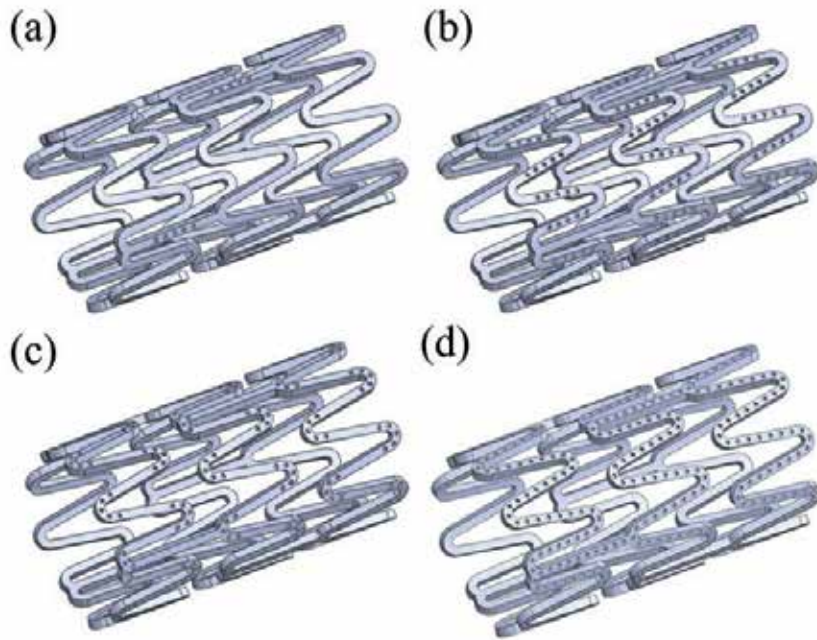


**Figure 3.** Depot stent with reservoirs on (a) connectors, (b) bar arms, (c) crowns, and (d) entire stent surfaces.

### 3. Computational model development

#### 3.1. Stent mechanical integrity assessment

On 18 April 2010, the US Food and Drug Administration (FDA) published an official document, “Non-Clinical Engineering Tests and Recommended Labeling for Intravascular Stents and Associated Delivery Systems,” to serve as a guide for the medical device industry. In addition to the routine stent dimensional tests such as dimensional verification, percent surface area, foreshortening, and recoil, this document lists several key clinical relevant functional attributes in which the FDA is interested when reviewing future new stent submissions. For the balloon-expandable stent, these key clinical attributes include radial strength, stresses–strains, and fatigue resistance. Each of these properties can serve as an indicator with respect to various aspects of the stent integrity. In this study, three key clinical attributes were used to assess the mechanical integrity of the depot stent.

##### 3.1.1. Radial Strength (RS)

One of the most important functions of the stent is to create a scaffolding structure in the artery and exert radial force against the artery wall to prevent its reclosure. Radial strength represents the ability of a stent to resist radial collapse under external pressure loadings exerted by the artery wall. It is defined as the maximum pressure at which the stent experiences irreversible deformation.

### 3.1.2. Equivalent plastic strain (PEEQ)

Since the in vivo deployment of a balloon-expandable stent involves large plastic deformation, the equivalent plastic stresses and strains have to be calculated throughout the stent. This stress analysis provides a risk assessment of acute device failure. The stress or strain contour plots provide the overall distribution of plastic stresses or strains and identify the most fracture-prone locations of a stent. Stent fracture may cause loss of the radial strength or perforation of the blood vessel by the fractured stent struts.

### 3.1.3. Fatigue Safety Factor (FSF)

Stent fracture due to long-term pulsatile fatigue loading may result in loss of the radial strength, thrombus formation, focal restenosis, or perforation of the blood vessel by the fractured stent struts. FDA recommends using a Goodman life analysis to determine the fatigue resistance of a stent to clinically relevant pressure loadings up to  $4 \times 10^8$  cycles. The Goodman life analysis, combined with the stress analysis aforementioned and accelerated fatigue bench testing, provides a comprehensive risk assessment of long-term stent durability. The resulting fatigue safety factor shows how safe a stent is from fatigue failure based on the Goodman life analysis.

## 3.2. Finite element analysis

### 3.2.1. Finite element model

A stent deployed in the vasculature system is subjected to various loading modes which may consequently compromise the stent mechanical integrity during its service life. In this study, finite element models were developed to evaluate the mechanical integrity and fatigue resistance of a stent to various loading conditions involved in manufacturing and deploying a stent consistent with the current practice. The entire stress-strain history of the stent in each loading step was considered to incorporate the effects of accumulated residual stress-strains throughout the procedures. It includes manufacturing (crimped onto a balloon catheter), in vivo deployment (expanded into an artery), and their corresponding recoil and pulsatile loading subjected to systolic/diastolic pressures. The FEA simulation determines the distribution of stress and strain, fatigue safety factor, and radial strength imposed by the following steps:

**Step 1.** Crimping a stent from 2.54 mm to 2 mm OD (crimp).

**Step 2.** Removing outer constraint to allow stent recoil after crimping (crimp-recoil).

**Step 3.** Expanding a stent to 6.0 mm ID (expansion).

**Step 4.** Removing inner constraint to allow stent recoil after expansion (expansion-recoil).

**Step 5.** Applying 180/80 mmHg systolic/diastolic pressures for stent fatigue assessment (or applying external pressure for radial strength assessment).

It should be noted that step 5 can be used to calculate either the fatigue safety factor or radial strength of a stent.

### 3.2.2. Stent geometry and meshing

The ABAQUS/standard finite element solver (Dassault Systemes Simulia Corp., Providence, RI, USA) was used to perform the stent FEA analysis. Since a stent has repeated patterns in its axial and circumferential directions, three representative rings instead of the entire stent were modeled to save computational time (Figure 3). In order to simulate the manufacturing (crimp onto a balloon catheter) and in-vivo deployment (expansion inside an artery) steps, two rigid cylinders with diameters of 2.54 and 1.12 mm were incorporated into the stent model with one cylinder inside the stent and the other one outside the stent. Gervaso et al. and De Beule et al. demonstrated that using the displacement-control expansion of a rigid cylinder for simulation of a balloon expansion could provide reliable and accurate information regarding the stent shape, stress–strain behavior, etc., when reaching the stent nominal diameter [19, 20]. Therefore, the displacement-control simplification was used in this study, as it is computationally less expensive than simulations involving balloon-driven expansion. Our goal is to assess the impact of drug reservoirs to the “standard” stent on a relative scale, so the displacement-control expansion serves that purpose well.

The stent model was meshed with the eight-node linear brick element in incompatible mode (C3D8I) with the element size of one-sixth of the strut width and one-third of strut thickness. This specific mesh size was chosen after a mesh sensitivity study to ensure that stress–strain variation on the stent was adequately captured. The inside and outside rigid cylinders were meshed with the four-node quadrilateral surface element (SFM3D4).

### 3.2.3. Material properties and boundary conditions

The material properties of L-605 cobalt–chromium alloy along with the ABAQUS von Mises plasticity model with isotropic hardening for large deformation analysis were used. Its Young’s modulus, Poisson ratio, yield stress, ultimate stress, ultimate strain, and fatigue endurance limit are 203 GPa, 0.3, 590 MPa, 1689 MPa, 60%, and 483 MPa, respectively.

A frictionless contact was used to prevent penetration between two surfaces of the model during crimping and expansion, with the following contact pairs implemented:

1. The first contact pair was defined as the surface contact between the inner surface of the outer rigid cylinder and the outer surface of the stent.
2. The second contact pair was defined as the surface contact between the outer surface of the inner rigid cylinder and the inner surface of the stent.
3. The third contact pair was defined as the side contact between any two stent struts during crimping.

### 3.2.4. Stent stress–strain analysis

In step 1, stress–strain analysis was conducted to simulate the crimping of a stent onto a balloon catheter. The outer rigid cylinder was compressed in the radial direction with the displacement control, forcing the stent to collapse inward. In step 2, stent recoil after crimping due to elastic

strain energy was modeled by removing the outer rigid cylinder to allow for the stent recovery. In step 3, to simulate the in-vivo deployment, the inner rigid cylinder was expanded in the radial direction with the displacement control to simulate the stent deployment to the target size. In the final step, stent recoil after expansion due to elastic strain energy was modeled by removing the inner rigid cylinder to allow for the stent recovery. Figure 4 demonstrates the configuration of the stent and rigid cylinders at each step of the modeling scheme.

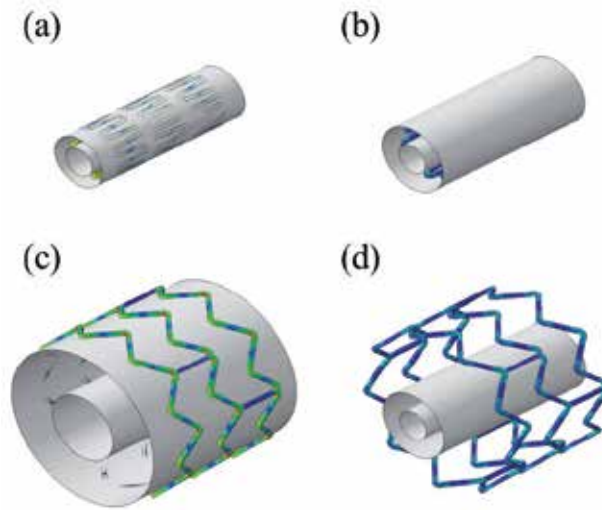


**Figure 4.** Configuration of the stent/cylindrical surfaces at each stage of the loading scheme: (a) crimp, (b) crimp-recoil, (c) expansion, and (d) expansion-recoil.

### 3.2.5. Stent Goodman life analysis

Following the previous four steps, systolic/diastolic arterial blood pressures of 180/80 mmHg were applied to simulate the pulsatile fatigue loading. In order to account for the external loading exerted by the arterial wall, an arterial pressure loading corresponding to the interaction between the stent and the artery was also imposed on the stent. The Goodman life analysis was performed using the multi-axial stress state experienced during the pulsatile fatigue loading to determine the fatigue resistance of a stent after implant [14]. It states that fatigue failure will occur if the stress state satisfies the following relationship:

$$\left(\frac{\sigma_a}{\sigma_e}\right) + \left(\frac{\sigma_m}{\sigma_u}\right) \geq 1 \quad (1)$$

where  $\sigma_a$  is the stress amplitude applied to the stent,  $\sigma_e$  is the modified material endurance limit for nonzero mean stress,  $\sigma_m$  is the mean stress applied to the stent, and  $\sigma_u$  is the material ultimate strength.

The Goodman diagram is a plot of the normalized stress amplitude  $\sigma_a/\sigma_e$  (on the y-axis) versus the normalized mean stress  $\sigma_m/\sigma_u$  (on the x-axis). The equation  $(\sigma_a/\sigma_e) + (\sigma_m/\sigma_u) = 1$  represents the failure line on the Goodman diagram for nonzero mean stress with the modified endurance limit defined as:

$$\sigma_e = \sigma_{e0} \left( 1 - \frac{\sigma_m}{\sigma_u} \right) \quad (2)$$

where  $\sigma_{e0}$  is the material endurance limit for zero mean stress. The fatigue safety factor (FSF) is defined as the ratio of the modified endurance limit divided by the stress amplitude. An FSF smaller than 1.0 indicates the fatigue failure:

$$FSF = \frac{\sigma_e}{\sigma_a} \quad (3)$$

## 4. Depot stent manufacturing

### 4.1. Laser cutting by integrated laser module

When making a stent, a design drawing is first sketched on the 2D plane, wrapped around a target cylinder, and coded into the 3D cylindrical coordinate using the CAD/CAM software. The coded stent geometry is then input into the laser cutting machine and the design pattern is cut onto a seamless hypotube of 1–2 mm. During the laser cutting process, the hypotube was rotated and translated in the axial direction by the motor stage while the laser source remained stationary.

In this study, a laser module consisting of a 100W Yb-doped pulsed fiber laser (Rofin-Baasel Taiwan Ltd.), a linear X-Y motor stage (Aerotech, Inc.), and a Z-direction server motor was assembled and integrated (Figure 5). The precision motor stage provides linear motion and rotation of the hypotube, whereas the Z-direction server motor controls the distance between the laser source and hypotube surface for the optimal focal position (Figure 6). The X-Y motor stage accuracy is  $\pm 2 \mu\text{m}$  and  $\pm 25$  arc-second in the axial and circumstantial direction, respectively; on the other hand, the linear encoder resolution for the Z-direction server motor is up to  $0.5 \mu\text{m}$ . Position synchronized output (PSO), a control algorithm that greatly enhances the efficiency and quality of the laser cutting, was used to coordinate the linear X-Y motor stage with the timing of laser firing. It can minimize the heat-affected zone (HAZ) during the laser cutting process. A3200 controller (Aerotech, Inc.) allows us to perform up to 32 axes of synchronized motion control and therefore could accomplish very sophisticated laser cutting patterns effortlessly.

The principles of laser cutting and drilling are based on fusion cutting, which involves a melting mechanism where the heated materials transformed into a molten state are expelled

from the cut kerf by a high pressure assisted gas such as nitrogen or argon. Laser cutting quality is typically controlled by several input laser parameters such as focal position, average laser power, pulse repetition rate, assisted gas pressure, etc. An appropriate position of the laser focal spot significantly improves the cutting outcome. The focal position of our laser module was assessed by measuring the kerf width on the hypotube while adjusting the distance between the laser source and hypotube surface. The smallest kerf width can be achieved by precisely focusing the laser sweet spot on the hypotube surface. A proper selection of laser power is crucial to the outcome as well, as excessive laser power results in a wider kerf and a thicker recast layer. On the other hand, insufficient laser power produces dross due to incomplete melting [21, 22]. Pulse repetition rate is another important laser parameter related to surface roughness and material removal. A higher pulse repetition rate corresponds to a better cutting surface and more effective material removal. Inert gas is a favorable assisted gas since it can avoid oxidation of the materials. High pressure inert gas was used during the cutting process to enhance drag forces and achieve high cutting quality [23].



**Figure 5.** Integrated laser module with a magnified view of the linear X-Y motor stage and laser source in the right window.



**Figure 6.** Stent design pattern cut onto a seamless hypotube by laser.

## 4.2. Surface finishing by electro-polishing

The laser cutting process inevitably generates dross, heat-affected zone, and other defects at stent surface. To achieve high quality of mirror-like surface, electro-polishing was performed on laser-cut depot stent prototypes. A 100 ml glass beaker was used as a bath. The experiment setup used for electro-polishing is illustrated in Figure 7. The stent was used as an anode, whereas the cathode was made of a thin lead sheet. The electrolyte consisted of 60 wt% phosphoric acid ( $H_3PO_4$ ), 20 wt% sulfuric acid ( $H_2SO_4$ ), and 20 wt% distilled water. Electro-polishing process was performed with continuous stirring of electrolyte to prevent oxygen bubbles from adhering to stent surface. Furthermore, several important polishing parameters including bath temperature, current, and time were determined through experiments to find the optimal conditions for electro-polishing of depot stents. The stents were then cleaned ultrasonically using distilled water for 5 minutes and were dried by air blowing as the final step.

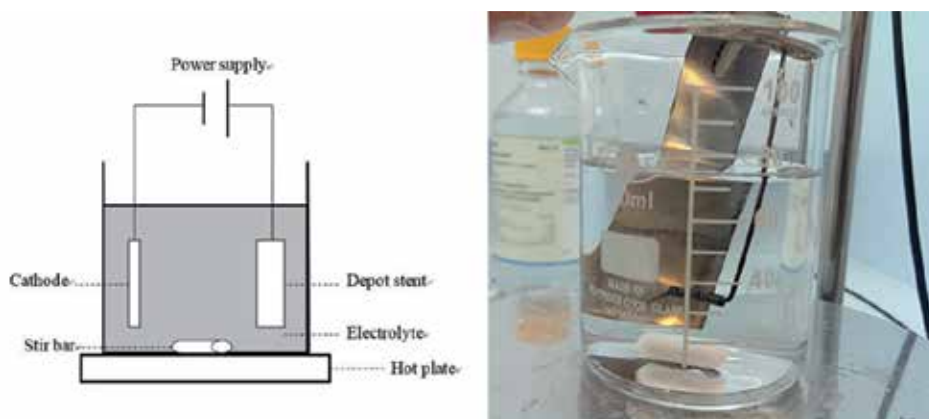


Figure 7. Experimental setup for electro-polishing of depot stent prototypes.

## 5. Results and discussion

### 5.1. Effects of reservoir location on stent mechanical integrity

The “standard” stent was first evaluated to establish the baseline information for this study. The FEA simulation was then conducted to investigate the impact of reservoir location on the mechanical integrity of the depot stent (e.g., equivalent plastic strain, radial strength, and fatigue safety factor). Five equally spaced circular (cylindrical if considering depth) and blind-hole reservoirs were cut on three major locations of the depot stent, namely, connectors, bar arms, and crowns (Figure 3).

From Table 1, it is clear that the creation of blind-hole reservoirs on either bar arms or connectors resulted in little or no change in equivalent plastic strain and radial strength. However,

the degradation in the fatigue safety factor was the most significant among major clinical attributes investigated, with a 16–18% reduction compared to the “standard” stent. This indicates that the depot stent with reservoirs on the bar arms or connectors is resistant to vessel collapse or acute stent fracture but susceptible to long-term stent fatigue failure. In other words, the depot stent is more sensitive to dynamic loading than static loading.

However, the depot stent with blind-hole reservoirs on the crowns led to noticeable changes in equivalent plastic strain (+12%) and radial strength (–8%). Its fatigue safety factor declined further from the standard case of 3.05 to 2.33, a significant 24% reduction. By comparing these three reservoir locations, it is clear that cutting reservoirs on the stent crowns has the most significant impact among the three major locations investigated. This is not surprising considering the standard case that the maximum von Mises stress and maximum equivalent plastic strain always occur on the inner surface of the curved crowns, whereas the connectors and the bar arms are mostly under elastic deformation.

Model	RS (N/mm)	Variation (%)	PEEQ (%Strain)	Variation (%)	FSF	Variation (%)
Standard	3.78	-	40.5	-	3.05	-
Hole- CO	3.77	-0.26	40.2	-0.74	2.56	-16.07
Hole- BA	3.66	-3.17	39.7	-1.98	2.49	-18.36
Hole- CR	3.49	-7.67	45.2	11.6	2.33	-23.61
Hole- All	3.45	-8.73	45.1	11.36	2.17	-28.85

**Table 1.** Effects of reservoir location on stent mechanical integrity (blind-hole reservoirs).

Adding the number of reservoirs increases the total drug capacity of the depot stent. Therefore, investigation was also conducted for reservoirs evenly spread on the entire stent to understand whether the mechanical integrity of such a stent is further compromised or not (Figure 3(d)). Simulation results show that this specific depot stent followed a similar trend to the previous case (blind-hole reservoirs on the crowns only). Their equivalent plastic strain and radial strength were almost identical, whereas the fatigue safety factor continued to decline further, with a 29% reduction compared to the “standard” stent. This again demonstrates that the mechanical integrity of the depot stent is mainly dominated by the reservoirs located on the stent crowns.

## 5.2. Effects of reservoirs depth on stent mechanical integrity

Another method of increasing the total drug capacity is to cut through-holes instead of blind-holes into the stent struts. The through-hole reservoir design also allows different types of drugs with different release rates to be administered independently on opposite sides of the stent. Since this dual-side drug delivery concept is quite interesting, simulation was then carried out to investigate the effects of reservoir depth on the mechanical integrity of the depot

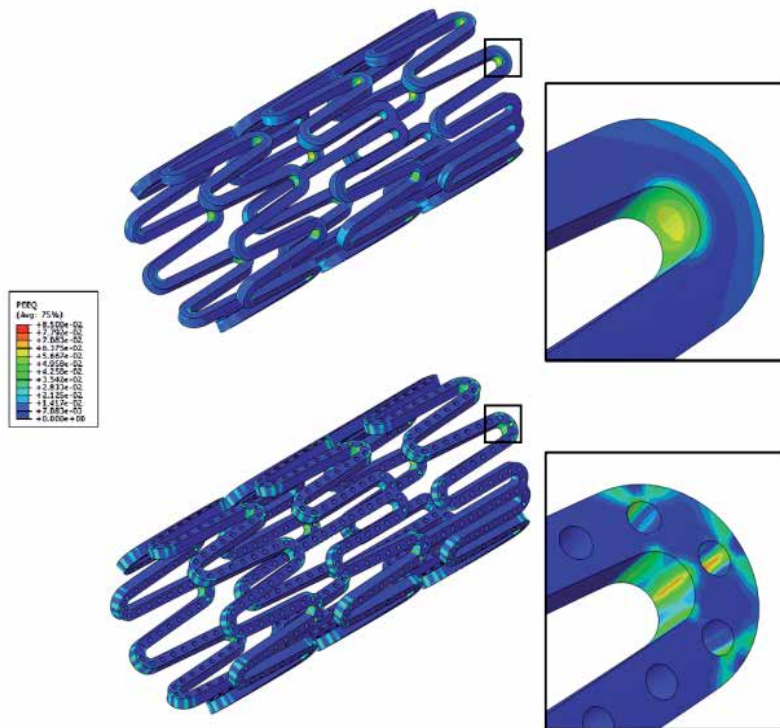
stent. The depth of the reservoirs was increased from 50% to 75% and 100% of the strut thickness, with the last case equivalent to the through-hole scenario.

Table 2 summarizes the effects of reservoir depth on the key stent attributes for the case of depot reservoirs evenly spread on the entire stent. Figures 8 and 9 show the contour plot comparisons of the equivalent plastic strain developed during different stages of the loading process (crimping and expansion, respectively) between the standard case and the depot stent with through-hole reservoirs on the entire stent. It shows again that the maximum equivalent plastic strain occurred on the inner surface of the most critical region of the stent, the curved crowns. The maximum equivalent plastic strain was increased by 16%, and its strain distribution, as indicated by the colors, changed significantly due to the appearance of the through-hole reservoirs on the stent crowns. It was more evenly spread along the crown arc for the standard case but became non-uniform when the maximum stress-strain occurred at the 6 o'clock location of each reservoir.

Model	RS (N/mm)	Variation (%)	PEEQ (%Strain)	Variation (%)	FSF	Variation (%)
Standard	3.78	-	40.5	-	3.05	-
Hole- All (50%)	3.45	-8.73	45.1	11.36	2.17	-28.85
Hole- All (75%)	3.33	-11.9	46.8	15.56	2.06	-32.46
Hole- All (100%)	3.08	-18.52	46.8	15.56	2.02	-33.77

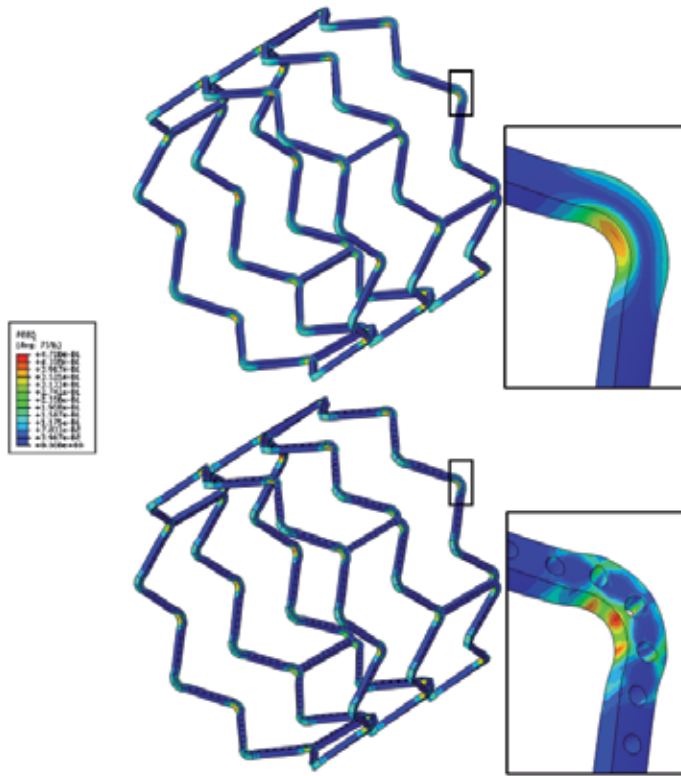
**Table 2.** Effects of reservoir location on stent mechanical integrity (blind-hole reservoirs).

Figure 10 shows the radial strength comparison between the “standard” stent and the depot stent with through-hole reservoirs on the entire stent. The radial strength dropped by 19% in this case, and its peak value shifted toward the right by 0.1 mm when compared to the “standard” stent. This suggests that the through-hole depot stent is not as strong as its standard counterpart and could be collapsed by the arterial pressure at an earlier stage. Figure 11 shows the Goodman diagram comparison of the pulsatile fatigue loading between the “standard” stent and the depot stent with through-hole reservoirs on the entire stent. Simulation data of the “standard” stent were far below the Goodman diagram failure line, indicating that the “standard” stent is able to pass the fatigue life of  $4 \times 10^8$  cycles with ease under pulsatile fatigue loading. Comparing Figure 11 (top) with Figure 11 (bottom), wherein the same stent but with through-hole reservoirs was evaluated for pulsatile fatigue loading, shows that the simulation data of the depot stent migrated toward the Goodman diagram failure line, indicating a significant drop of 34% in FSF and thus much lower fatigue resistance to systolic/diastolic blood pressures in this specific case.



**Figure 8.** Contour plot of the PEEQ of the standard stent (top) and the depot stent with through-hole reservoirs (bottom) at crimping with a magnified view of the stent crown in the right window.

Figure 12 shows the effects of reservoir depth on the key stent attributes of the depot stent with the reservoir depth ranging from 50%, 75% to 100% of the strut thickness on the entire stent. It is shown that the radial strength decayed almost linearly with the reservoir depth. The loss in radial strength reached the maximum, a 19% reduction compared to the standard case, when the reservoirs were completely cut through. The equivalent plastic strain rose moderately with the reservoir depth but eventually reached a plateau for an approximately 15–20% gain. The fatigue safety factor remained the most critical factor among these key stent attributes. According to the chart, it fell significantly right from the beginning, even with shallow blind holes, but eventually reached a plateau and settled with an approximately 30–35% loss when compared to the standard case. Since the major stent clinical attributes suffered significant losses, it is not a good idea to pursue this specific design with through-hole reservoirs spread all over the entire stent. Given the fact that the crown is a critical region in a stent, we propose that an optimal depot stent should have through-hole reservoirs on the stent bar arms and/or connectors for the maximum drug capacity without compromising its mechanical integrity significantly. It should be noted that although the depot stent has the wonderful feature of precise and programmable drug release control, it was found that its fatigue safety factor could be compromised to certain degrees for all various forms of the depot stent.



**Figure 9.** Contour plot of the PEEQ of the standard stent (top) and the depot stent with through-hole reservoirs (bottom) at expansion with a magnified view of the stent crown in the right window.

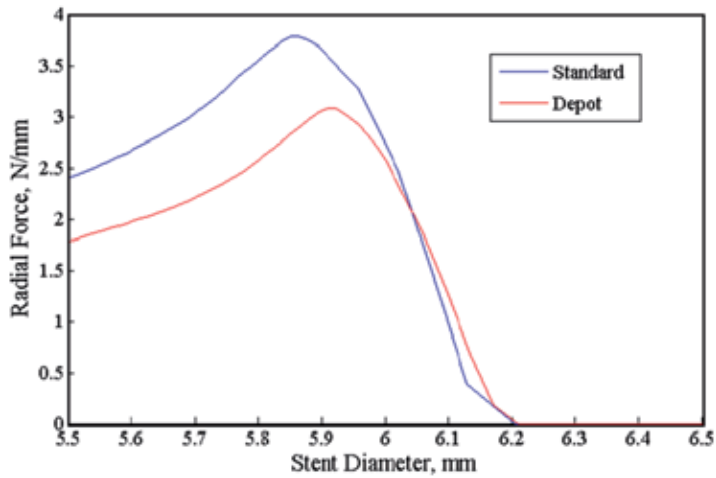


**Figure 10.** Radial strength comparison of the standard stent and the depot stent with through-hole reservoirs.

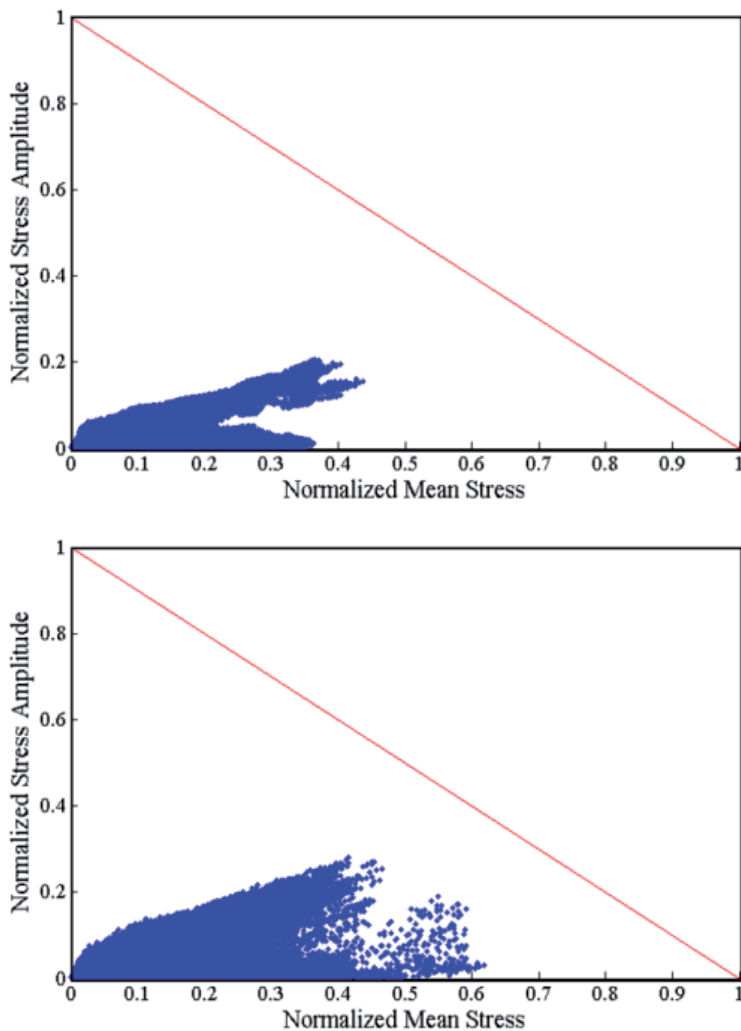


**Figure 11.** Goodman diagram comparison of the standard stent (top) and the depot stent with through-hole reservoirs (bottom).

### 5.3. Depot stent drug capacity

A typical DES (3-ring model) with a 5  $\mu\text{m}$  coating thickness carries a total drug-polymer volume of 0.0535  $\text{mm}^3$  (Table 3). For the depot stent, our chosen reservoir size is 50% of the strut width and 100% completely through the strut thickness. Such a design is able to carry approximately 0.0004  $\text{mm}^3$  of drug-polymer mix per reservoir. Therefore, by creating 135 through-hole reservoirs on the 3-ring depot stent model, its total reservoir capacity is enough to fully replace the surface coating layers of 0.0535  $\text{mm}^3$  on a typical drug-eluting stent. This helps to completely eliminate the surface coating layers and thus reduce the overall stent profile.

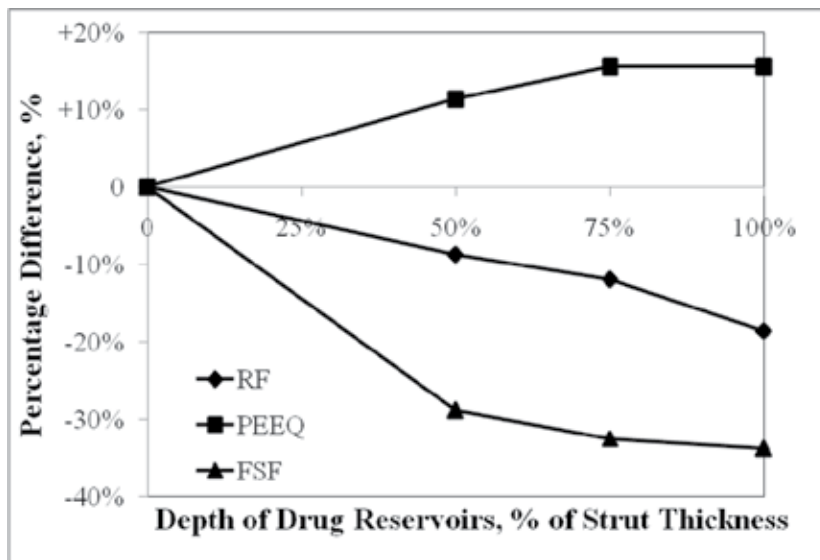


**Figure 12.** Variation of key clinically relevant functional attributes versus drug reservoir depth.

The density and size of the reservoirs could be changed to increase the total drug capacity of the depot stent. For example, the total volume of the drug-polymer mix can be quadrupled to  $0.221 \text{ mm}^3$  when the through-hole reservoirs are evenly distributed on the entire stent, as shown in Figure 3(d). Our proposed depot stent in the next section, same stent as the one in Figure 3(d) without reservoirs on the crowns, also triples the total volume to  $0.149 \text{ mm}^3$ .

Model	Number of reservoirs	Drug-polymer compound carried ( $\text{mm}^3$ )
5- $\mu\text{m}$ thickness coating on stent surface	-	0.0535
Through-hole reservoir (per reservoir)	-	0.0004
Through-hole reservoirs on CO	30	0.012
Through-hole reservoirs on BA	270	0.108
Through-hole reservoirs on CR	270	0.108
Through-hole reservoirs on entire stent	552	0.221
Proposed depot stent	372	0.149

**Table 3.** Estimated drug capacity of a depot stent (3-ring model).

## 5.4. Proposed depot stent and its variations

### 5.4.1. Proposed depot stent

We propose an optimal depot stent, with reservoirs uniformly distributed on the entire stent except the crown region, to increase the total drug capacity without comprising its mechanical

integrity significantly (Figure 13). This depot stent has eight reservoirs on the connectors and six reservoirs on the bar arms, with the spacing of approximately 0.15 mm between two reservoirs. Simulation results on the variations of major clinical attributes are listed in Tables 4 along with those on other stents for comparison. Figure 14 shows the contour plot comparison of the equivalent plastic strain developed at the expansion stage among the standard case, the depot stent with through-hole reservoirs on the entire stent, and the proposed depot stent. For the proposed depot stent, the maximum equivalent plastic strain was actually reduced by 9% and the strain distribution was spread out even more uniformly than the standard case. This was attributed to the creation of through-hole reservoirs on the bar arms, effectively shifting the stress–strains away from the crown reservoirs and re-distributing them along the crown arcs. The radial strength only dropped by 10%. The fatigue safety factor was reduced marginally by 13% when compared to the standard case, whereas the very same stent but with through-hole reservoirs on the entire stent showed a staggering 34% reduction. This significant gain in fatigue safety factor was partially due to the removal of through-hole reservoirs on the crowns and partially due to the stress–strain redistribution mentioned above.

To sum up, the total drug capacity of our proposed depot stent could be tripled, with only marginal trade-off in major clinical attributes: its radial strength and the fatigue safety factor were reduced by only 10% and 13%, respectively. Therefore, this depot stent could carry more drugs and deliver them more smartly than the modern drug-eluting stents, thereby opening up a wide variety of new treatment opportunities such as the renal disease or cancer target therapy.

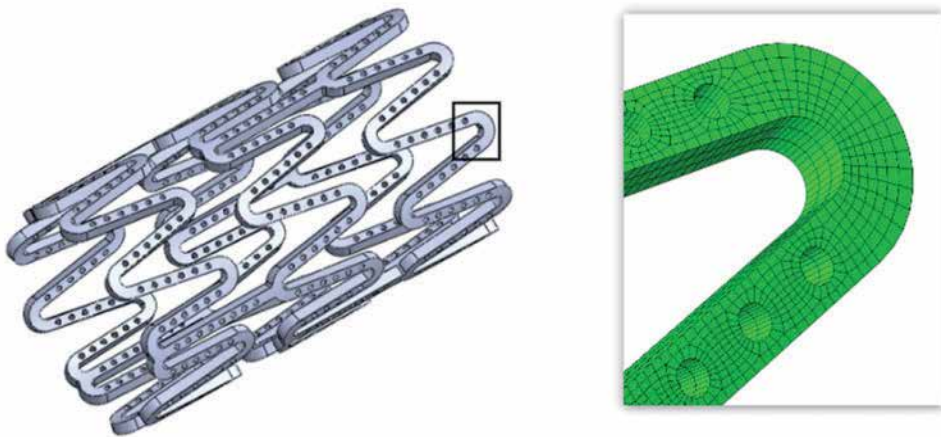


**Figure 13.** Proposed depot stent with a magnified view of the stent mesh in the right window.

#### 5.4.2. Effects of reservoir shape

Besides the circular (cylindrical if considering depth) reservoirs aforementioned, other reservoir shapes were also investigated, for example, hexagonal and square reservoirs (Figure

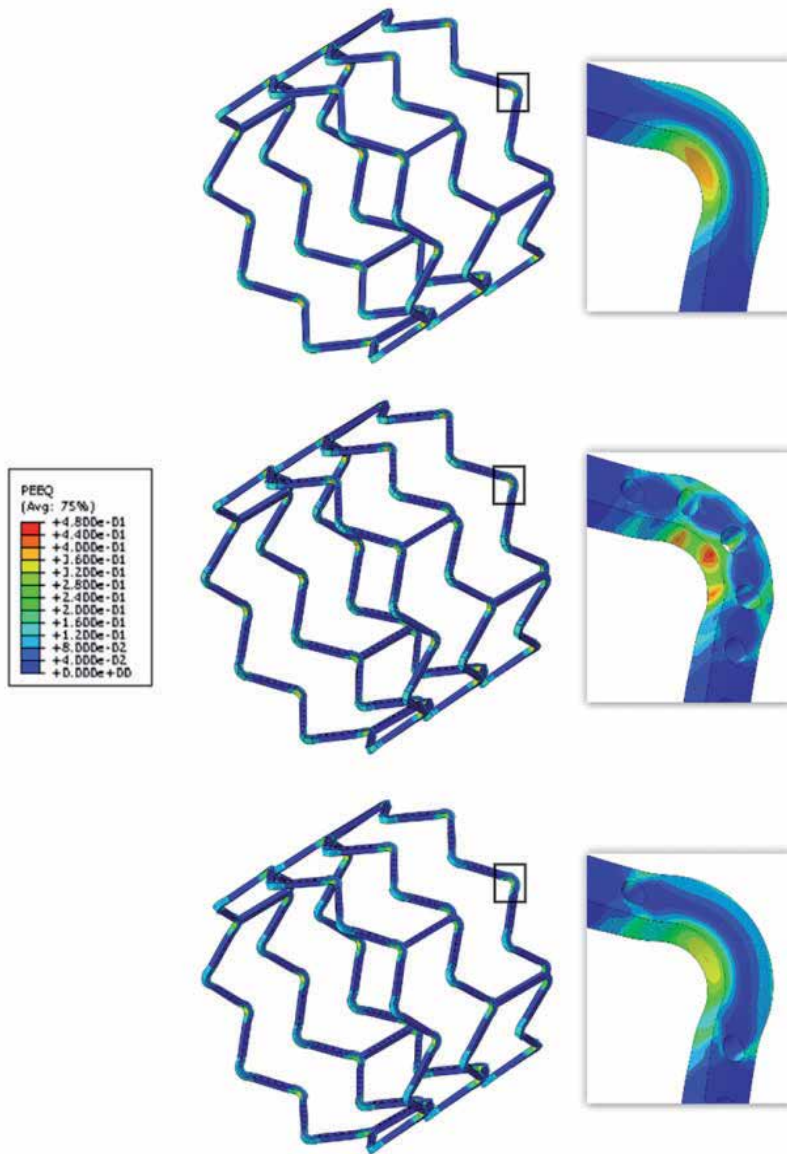


**Figure 14.** Contour plot of the equivalent plastic strain of the standard stent (top), the depot stent with reservoirs on the entire stent (middle), and the proposed depot stent (bottom) at expansion with a magnified view of the stent crown in the right window.

15). The length on each side of the hexagonal and square reservoirs (0.0349 mm and 0.0563 mm, respectively) was determined in a way that each reservoir capacity was identical to that of a circular reservoir. The location of the reservoir center remained unchanged.

Table 4 lists the mechanical integrity of the depot stent as a function of the reservoir shape. Simulation results show that the changes in the reservoir shape caused little differences in

equivalent plastic strain and radial strength, with approximately 10% across-the-board reductions when compared to the “standard” stent. In terms of the fatigue safety factor, the hexagonal reservoir had a slight 5% advantage over the circular and square reservoirs. This could be attributed to the stress re-distribution within the stent and the hexagonal reservoir makes a bigger impact than reservoirs with other shapes.

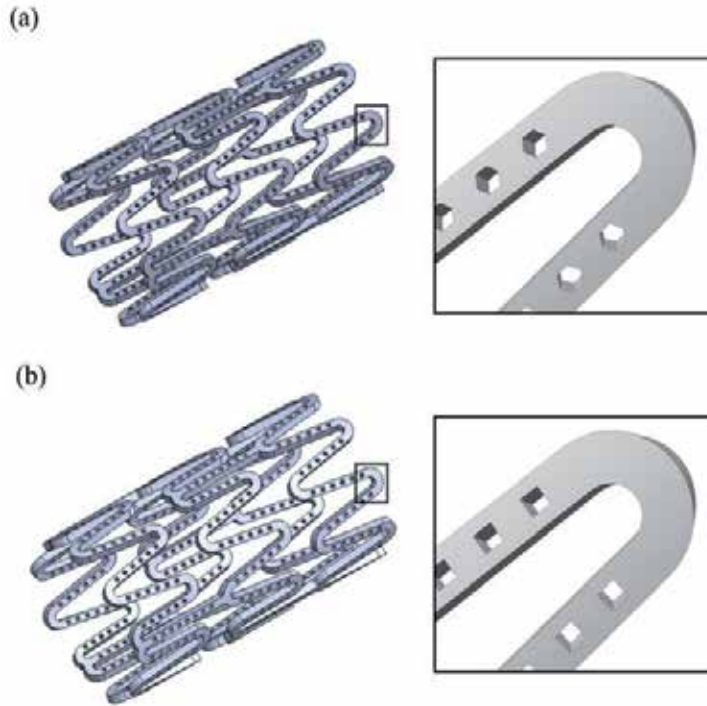


**Figure 15.** Depot stent with (a) hexagonal and (b) square reservoirs.

Model	RS (N/mm)	Variation (%)	PEEQ (%Strain)	Variation (%)	FSF	Variation (%)
Standard	3.78	-	40.5	-	3.05	-
Proposed depot stent	3.41	-9.79	36.7	-9.38	2.66	-12.79
Hexagonal reservoir	3.43	-9.26	36.4	-10.12	2.80	-8.20
Square reservoir	3.38	-10.58	36.1	-10.86	2.65	-13.11

**Table 4.** Effects of reservoir shape on stent mechanical integrity.

#### 5.4.3. Effects of reservoir size and number

Effects of the reservoir size and number of the depot stent were also investigated (Figure 16). The total drug loading capacity on each bar arm/connector was intended to maintain the same,

whereas the size and number of the reservoirs were adjusted accordingly. Stent variation #1 had smaller but more reservoirs, with 8 reservoirs on the bar arms and 10 reservoirs on the connectors; on the other hand, stent variation #2 had larger but fewer reservoirs, with four reservoirs on the bar arms and six reservoirs on the connectors. In all cases, the total length between the farther edges of two end reservoirs remained unchanged.

Table 5 lists the mechanical integrity of the depot stent as a function of the reservoir size and number. Simulation results show that, for the same drug loading capacity, stent variation #2 with larger and fewer reservoirs yielded lower radial strength, but smaller equivalent plastic strain and thus higher fatigue safety factor. In addition, the fatigue safety factor seems to be more sensitive than the equivalent plastic strain and radial strength in this case. Its value increased from 2.36 to 2.88, a 17% jump from stent variation #1 to #2, which is consistent with the earlier observation. Therefore, stent variation #2 of larger and fewer reservoirs is a better candidate for drug delivery; its total drug capacity could be tripled with marginal trade-off in its major clinical attributes: the radial strength and fatigue safety factor were reduced by only 11% and 6%, respectively.

Model	RS (N/mm)	Variation (%)	PEEQ (%Strain)	Variation (%)	FSF	Variation (%)
Standard	3.78	-	40.5	-	3.05	-
Proposed depot stent	3.41	-9.79	36.7	-9.38	2.66	-12.79
Variation #1	3.48	-7.94	37.6	-7.16	2.36	-22.62
Variation #2	3.38	-10.58	34.8	-14.70	2.88	-5.57

**Table 5.** Effects of reservoir size and number on stent mechanical integrity.

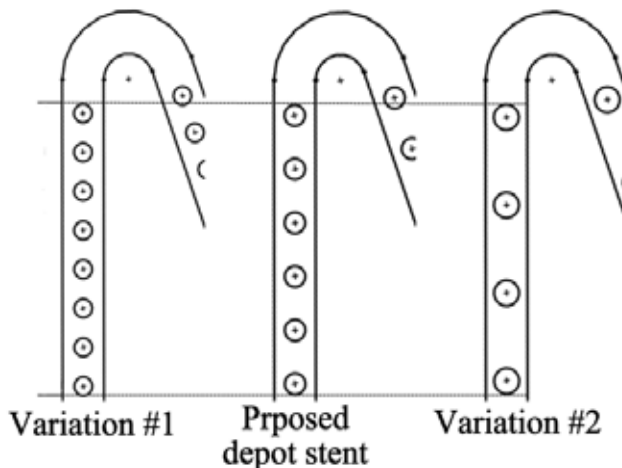


**Figure 16.** Proposed depot stent and its variation #1 and #2.

### 5.5. Depot stent prototyping

In this study, the input laser parameters used for cutting stents are listed as follows: average power 37.5 W, pulse repetition rate 80 KHz, cutting speed 5 mm/s, and Argon pressure 12 bar. Optical microscopy was used to measure the kerf width and observe the surface conditions of each stent.

Figure 17 shows the relationship of the average kerf width vs. the distance between the laser source and hypotube surface. The kerf width had the minimum value of 23.2  $\mu\text{m}$  at the distance of 0.37 mm. When the distance was between 0.27 mm and 0.51 mm, the laser beam was able to penetrate through the hypotube, resulting in successful cutting within a focal-depth range of 0.24 mm. Figure 6 is the depot stent design pattern cut onto a seamless hypotube by laser prior to material removal and electro-polishing.

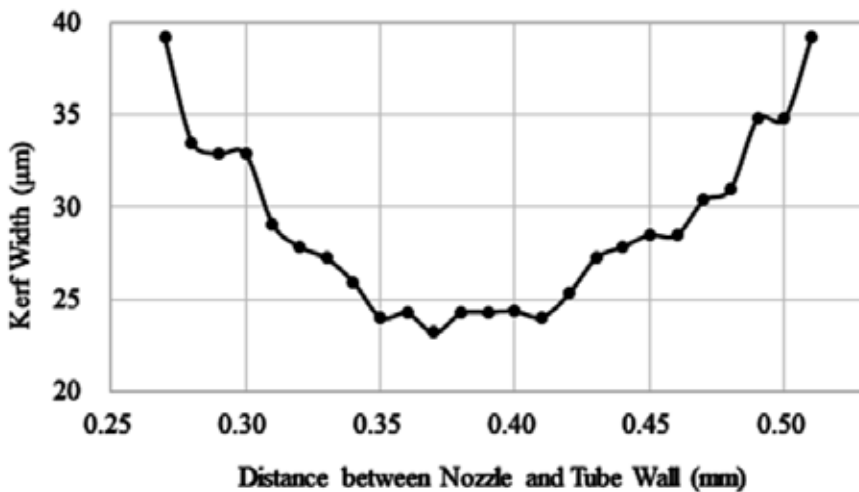
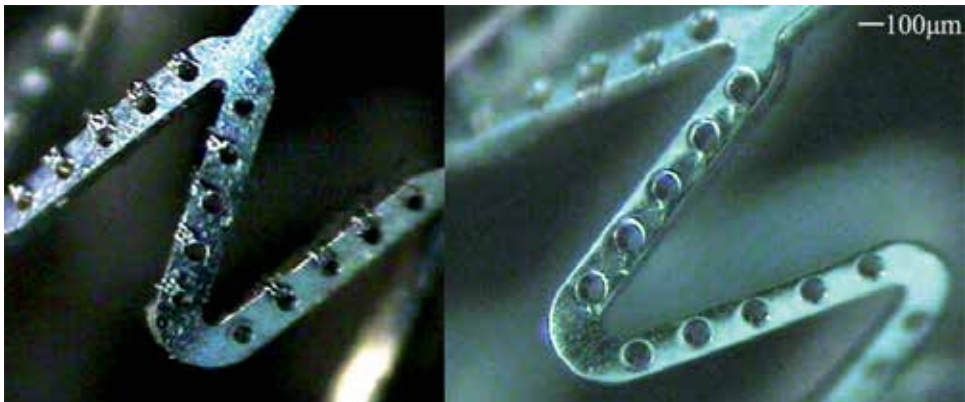


Figure 17. Average kerf width vs. distance between laser source and hypotube surface.

The polishing conditions for surface finishing of depot stent prototypes are listed in Table 6. Figure 18 shows the depot stent prototype before and after electro-polishing. These stents were able to achieve high quality of mirror-like surface finishing after polishing. Figure 19 is the prototype of our proposed depot stent of 2 mm diameter and 22 mm long for demonstration of our design concept.

Stirring speed (RPM)	Current (A)	Time (sec)	Temperature ( $^{\circ}\text{C}$ )
500–550	0.242	105–135	50–55

Table 6. Electro-polishing conditions for surface finishing of depot stents.



**Figure 18.** Surface conditions of manufactured depot stents before (left) and after (right) electro-polishing.

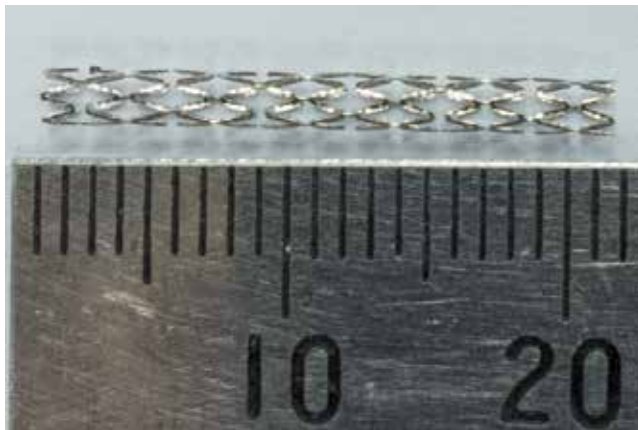


**Figure 19.** Prototype of our proposed depot stent.

## 6. Conclusion

The depot stent with micro-sized drug reservoirs is a novel concept for smart drug delivery and provides a promising future for highly controlled release of different medications with programmable spatial/temporal control. However, creating such drug reservoirs on the stent struts inevitably weaken the stent scaffolding and compromise its mechanical integrity. The impact of these drug reservoirs on major clinical attributes of the depot stent was systematically investigated. Several conclusions were drawn from this study:

- i. The reservoirs on either bar arms or connectors had little effects in equivalent plastic strain and radial strength when compared to the “standard” drug-eluting stent. However, the fatigue safety factor was reduced more significantly, suggesting that

the depot stent is resistant to acute stent fracture or vessel collapse but susceptible to long-term stent fatigue failure.

- ii. Creating reservoirs on the crown region of the depot stent has the most significant impact among all major locations.
- iii. The degradation in mechanical integrity is more sensitive to reservoir location than reservoir depth.
- iv. The hexagonal reservoirs resulted in a marginal increase in fatigue resistance when compared to the circular and square reservoirs.
- v. For the same drug loading capacity, larger and fewer reservoirs resulted in a noticeable increase in the fatigue resistance over smaller and more reservoirs.
- vi. Our proposed depot stent was proven to be a feasible design. Its total drug capacity could be tripled with acceptable/marginal trade-off in major clinical attributes: the radial strength and the fatigue safety factor of our proposed depot stent were reduced by only 10% and 13%, respectively.
- vii. A prototype of our proposed depot stent (2 mm diameter and 22 mm long) was manufactured for the feasibility demonstration of our design concept.

This study can serve as a guideline to help future depot stent designs to achieve the best combination of stent mechanical integrity and smart drug delivery.

## Acknowledgements

This research was supported by the Ministry of Science and Technology in Taiwan through Grants MOST-103-2622-E-002-010-CC1 and NSC-102-2221-E-002-130-MY3. The authors are grateful for the support and help.

## Author details

Hao-Ming Hsiao<sup>1\*</sup>, Aichi Chien<sup>2</sup>, Bor-Hann Huang<sup>1</sup>, Dian-Ru Li<sup>3</sup>, Hsin Chen<sup>4</sup> and Chun-Yi Ko<sup>1</sup>

\*Address all correspondence to: [hmhsiao@ntu.edu.tw](mailto:hmhsiao@ntu.edu.tw)

1 Department of Mechanical Engineering, National Taiwan University, Taipei, Taiwan

2 Department of Radiology, University of California, Los Angeles, CA, USA

3 Department of Mechanical Engineering, University of Michigan, Ann Arbor, MI, USA

4 Department of Mechanical Engineering, Stanford University, Stanford, CA, USA

## References

- [1] M. R. Bell, P. B. Berger, J. F. Bresnahan, G. S. Reeder, K. R. Bailey, and D. Holmes, "Initial and long-term outcome of 354 patients after coronary balloon angioplasty of total coronary artery occlusions," *Circulation*, vol. 85, pp. 1003-1011, 1992.
- [2] C. Landau, R. A. Lange, and L. D. Hillis, "Percutaneous transluminal coronary angioplasty," *New England Journal of Medicine*, vol. 330, pp. 981-993, 1994.
- [3] B. L. Van der Hoeven, N. M. Pires, H. M. Warda, P. V. Oemrawsingh, B. J. van Vlijmen, P. H. Quax, *et al.*, "Drug-eluting stents: results, promises and problems," *International Journal of Cardiology*, vol. 99, pp. 9-17, 2005.
- [4] M.-C. Morice, P. W. Serruys, J. E. Sousa, J. Fajadet, E. Ban Hayashi, M. Perin, *et al.*, "A randomized comparison of a sirolimus-eluting stent with a standard stent for coronary revascularization," *New England Journal of Medicine*, vol. 346, pp. 1773-1780, 2002.
- [5] J. W. Moses, M. B. Leon, J. J. Popma, P. J. Fitzgerald, D. R. Holmes, C. O'Shaughnessy, *et al.*, "Sirolimus-eluting stents versus standard stents in patients with stenosis in a native coronary artery," *New England Journal of Medicine*, vol. 349, pp. 1315-1323, 2003.
- [6] A. Colombo and E. Karvouni, "Biodegradable stents "fulfilling the mission and stepping away", " *Circulation*, vol. 102, pp. 371-373, 2000.
- [7] H. R. Kricheldorf, I. Kreiser-Saunders, C. Jürgens, and D. Wolter, "Polylactides-synthesis, characterization and medical application," *Macromolecular Symposia*, pp. 85-102, 1996.
- [8] J. A. Ormiston and P. W. Serruys, "Bioabsorbable coronary stents," *Circulation: Cardiovascular Interventions*, vol. 2, pp. 255-260, 2009.
- [9] T. Tsuji, H. Tamai, K. Igaki, E. Kyo, K. Kosuga, T. Hata, *et al.*, "Biodegradable stents as a platform to drug loading," *International Journal of Cardiovascular Interventions*, vol. 5, pp. 13-16, 2003.
- [10] R. Waksman, "Biodegradable stents: they do their job and disappear," *The Journal of Invasive Cardiology*, vol. 18, pp. 70-74, 2006.
- [11] R. Blindt, K. Hoffmeister, H. Bienert, G. Bartsch, H. Thissen, D. Klee, *et al.*, "Development of a new biodegradable intravascular polymer stent with simultaneous incorporation of bioactive substances," *The International Journal of Artificial Organs*, vol. 22, pp. 843-853, 1999.
- [12] P. W. Serruys, G. Sianos, A. Abizaid, J. Aoki, P. den Heijer, H. Bonnier, *et al.*, "The effect of variable dose and release kinetics on neointimal hyperplasia using a novel

- paclitaxel-eluting stent platform: the Paclitaxel In-Stent Controlled Elution Study (PISCES)," *Journal of the American College of Cardiology*, vol. 46, pp. 253-260, 2005.
- [13] A. Finkelstein, D. McClean, S. Kar, K. Takizawa, K. Varghese, N. Baek, *et al.*, "Local drug delivery via a coronary stent with programmable release pharmacokinetics," *Circulation*, vol. 107, pp. 777-784, 2003.
- [14] H.-M. Hsiao, Y.-H. Chiu, K.-H. Lee, and C.-H. Lin, "Computational modeling of effects of intravascular stent design on key mechanical and hemodynamic behavior," *Computer-Aided Design*, vol. 44, pp. 757-765, 2012.
- [15] H.-M. Hsiao, C.-T. Yeh, C. Wang, L.-H. Chao, and D.-R. Li, "Effects of stent design on new clinical issue of longitudinal stent compression in interventional cardiology," *Biomedical Microdevices*, vol. 16, pp. 599-607, 2014.
- [16] H.-M. Hsiao, Y.-H. Chiu, T.-Y. Wu, J.-K. Shen, and T.-Y. Lee, "Effects of through-hole drug reservoirs on key clinical attributes for drug-eluting depot stent," *Medical Engineering & Physics*, vol. 35, pp. 884-897, 2013.
- [17] H.-M. Hsiao and M.-T. Yin, "An intriguing design concept to enhance the pulsatile fatigue life of self-expanding stents," *Biomedical Microdevices*, vol. 16, pp. 133-141, 2014.
- [18] H. M. Hsiao, A. Nikanorov, S. Prabhu, and M. K. Razavi, "Respiration-induced kidney motion on cobalt-chromium stent fatigue resistance," *Journal of Biomedical Materials Research Part B: Applied Biomaterials*, vol. 91, pp. 508-516, 2009.
- [19] M. De Beule, P. Mortier, S. G. Carlier, B. Verhegghe, R. Van Impe, and P. Verdonck, "Realistic finite element-based stent design: the impact of balloon folding," *Journal of Biomechanics*, vol. 41, pp. 383-389, 2008.
- [20] F. Gervaso, C. Capelli, L. Petrini, S. Lattanzio, L. Di Virgilio, and F. Migliavacca, "On the effects of different strategies in modelling balloon-expandable stenting by means of finite element method," *Journal of Biomechanics*, vol. 41, pp. 1206-1212, 2008.
- [21] L. Shanjin and W. Yang, "An investigation of pulsed laser cutting of titanium alloy sheet," *Optics and Lasers in Engineering*, vol. 44, pp. 1067-1077, 2006.
- [22] C. Wandera, "Laser cutting of austenitic stainless steel with a high quality laser beam," LAPPEENRANTA UNIVERSITY OF TECHNOLOGY, 2006.
- [23] W. Steen, K. G. Watkins, and J. Mazumder, *Laser material processing*: Springer Science & Business Media, 2010.



---

# Diabetic Neuropathy and Treatment Strategy – New Challenges and Applications

---

Emine Hande Bayram, Ali Demir Sezer and Hatice Kübra Elçioğlu

Additional information is available at the end of the chapter

<http://dx.doi.org/10.5772/62221>

---

## Abstract

Smart drug delivery systems are very popular drug delivery systems for treatment to common disease such as gene therapy, heart disease, cancer therapy, and neuropathy. Neuropathy is the most common chronic complication of diabetes that is associated with especially loss of peripheral nerve fibers. Hyperglycemia, insulin deficiency and dyslipidemia largely affect the development and progression of diabetic neuropathy. Several metabolic disruptions including altered protein kinase C, elevated polyol pathway activity, oxidative stress, the formation of advanced glycation and lipoxidation end products, and various pro-inflammatory changes directly affect neural tissue and cause neurodegenerative changes in diabetes. The therapeutic interventions of these metabolic pathways have a limited success to relieve the symptoms of diabetic neuropathy. This review emphasizes on the pathogenesis of neurovascular changes, presently available therapeutic approaches future directions for the management of diabetic neuropathy and related new drug delivery systems.

**Keywords:** Diabet, Diabetic neuropathy, Treatment

---

## 1. Introduction

Diabetes mellitus (DM) is the most common disease, causing neuropathy worldwide. In the last century, although we have more information about clinical forms of diabetic neuropathy, sufficient knowledge about the pathophysiology of neuropathy could not be reached.

Diabetic neuropathy is defined as a peripheral neuropathy that may occur in clinical and subclinical levels and develops in the DM ground in the absence of other peripheral neuropathy factors.

---

While neuropathy is present at the time of diagnosis in 10% of diabetic patients, this rate reaches to 50% at the end of 20 years. There are studies, which demonstrate that neuropathy starts within 9 years after the diagnosis of Type 2 diabetes. It may include manifestations associated with somatic and/or autonomic parts of peripheral nervous system.

The relationship between DM and neuropathy is known for over 100 years. The classification was first suggested by Leyden in 1893 with hyperesthetic (painful), paralytic (motor), and ataxic forms. Large sensory, small sensory, autonomic, and motor fibers may be affected by neuropathy. The findings may be symmetrical or asymmetrical. The most common form of neuropathy is distal sensorimotor polyneuropathy. The most common mononeuropathy is carpal tunnel syndrome (CTS). However, the recognition of some rare types such as diabetic lumbosacral radiculoplexus neuropathy that may cause pain and weakness is important for the reduction of morbidity.

The annual incidence of neuropathy is closely associated with the known duration of diabetes. Height, maximum body mass index, smoking, systolic and diastolic blood pressures, estradiol level, and cholesterol level were not found different in those with neuropathy and without neuropathy.

Given that diabetes is estimated to affect about 246 million people worldwide, it may be calculated that there are 20–30 million people suffering from symptomatic diabetic neuropathy. This number is thought to double by 2030 [1].

The contribution of neuropathy to mortality is very low. Disability was reported to be in 44% of the patients with Type 1 DM and definite neuropathy, and partial restriction was reported to be in activity in 74% of those with Type 2 DM and sensory neuropathy [2,3]. Hypertension, independent of duration of diabetes, has been shown to be the most important factor in the development of neuropathy in a study of Pittsburg Epidemiology of Diabetes Complications (EDC) about the effects of hypertension, height, and smoking on the incidence of distal symmetric polyneuropathy in long-lasting and poorly controlled diabetic patients [4].

Diabetic cardiac autonomic neuropathy is a serious complication seen in one fourth of Types 1 and 2 diabetic patients. It results in high mortality and silent myocardial ischemia. Autonomic dysfunction has been shown as the reason for having the risk of cardiovascular disease and sudden death in patients with Type 2 diabetes. The activation of cytokines is the indicator of the inflammation in patients with diabetes. These changes have been associated with the sympathetic–vagal balance disorders. Patients have complaints of orthostatic hypotension, exercise intolerance, lack of enhanced stability during surgery, silent myocardial infarction, and ischemia. The use of heart rate change (HRV) and Valsalva maneuver has been reported in the diagnosis of cardiac autonomic neuropathy [5]. An over activation of the sympathetic system and the activation of inflammatory cascade were observed with hyperleptinemia and lack of adiponectin in case of sleep apnea that is common in diabetes and metabolic syndrome. Ultimately, negative effects seen in the autonomic nervous system as a result of cardiovascular function impairment give rise to higher morbidity and mortality in diabetic patients [6].

## 2. Pathogenesis of diabetic neuropathy

Diabetic neuropathy develops as a result of involvement of different nerves in varying degrees in different individuals. The actual lesions were observed to be in peripheral nerve axons in histopathological studies conducted in patients with diabetic neuropathy. *Schwann* cells, perineural cells, and endoneurial vascular structures are also affected by neuropathies. *Wallerian* degeneration, segmental and paranodal demyelination, and endoneurial connective tissue proliferation occurred with the loss and damage of thick and thin myelinated nerve fibers. Severe axonal atrophy, widespread fiber loss, and nodal and paranodal changes develop in Type 1 diabetes. Structural changes in Type 2 diabetes are milder. Mild axonal atrophy, localized fiber loss, segmental demyelination, and *Wallerian* degeneration are observed. Primary axonal changes are more evident in Type 1 diabetes, and primer *Schwann* cell pathology is more evident in Type 2 diabetes.

There is a close relationship between the degree and duration of hyperglycemia and the development of diabetic neuropathy. Development of neuropathy can be delayed or prevented through good metabolic control. The development of clinical diabetic neuropathy was observed to be decreased by 69% in the primary prevention group and 57% in the secondary intervention group after 5 years of intensive diabetes treatment in those with Type 1 diabetes in a study. Six separate factors associated with each other are thought to have an important role in the pathogenesis of DM.

Several mechanisms have been suggested in the pathogenesis of diabetic neuropathy. These are metabolic processes which involve direct nerve damage, endoneurial microvascular damage, autoimmune inflammation, and reduced neurotrophic support.

Epidemiological studies showed that the duration and severity of hyperglycemia are major risks in the development of neuropathy in patients with Types 1 and 2 DM [7]. Common opinion on the development of DSP (diabetic symmetric polyneuropathy) is that starting of the early nerve damage from the short, thin, myelinated A-delta fibers and unmyelinated C type of nerve fibers. The gold standard to assess the morphological changes in the short nerve fibers is a skin biopsy. However, not providing information about the nerve function, cost, and superficiality and being of no use in all patients with Type 1 diabetes limit this technique. The presence of a valid clinical practice, which identifies early short fiber disorder by using imaging techniques, was reported recently [8].

### 2.1. Metabolic factors

#### 2.1.1. Increased glycosylation end products

The glycosylation of the plasma and tissue proteins plays a major role in diabetic microvascular complications by causing the formation of advanced glycation end products (AGEs). Excess glucose combines with amino acids on circulating and tissue proteins in the presence of chronic hyperglycemia. This non-enzymatic process initially leads to the formation of reversible early glycosylation end products and, later, to irreversible advanced glycosylation end products.

Advanced glycosylation products change their function by modifying intracellular proteins and extracellular matrix proteins that interact with extracellular integrins. AGE precursors modify plasma proteins by binding IGF1 receptors RAGE (receptor of advanced glycation end products) in mesangial endothelial cells, microglia, and macrophages. Thus, they initiate the production of reactive oxygen species (ROS). The activation of NF- $\kappa$ B initiates proinflammatory gene expression. Cytokines and growth factors are expressed by macrophages and mesangial cells [9]. Significantly increased serum concentrations of AGEs have been reported to lead to the development of diabetic complications by their proinflammatory effect in diabetic patients. The other effects of AGEs are increasing in vascular permeability, procoagulant activity, adhesion molecule expression, and monocyte invasion [10].

*Sorbitol:* Glucose, which enters into the cell, is metabolized to sorbitol by the enzyme aldose reductase. Glucose is converted to sorbitol and fructose by the enzyme aldose reductase due to excessive activation of this pathway owing to hyperglycemia. The accumulation of sorbitol in the cell results in the reduction of myoinositol and taurine, and this leads to decrease in Na-K adenosine triphosphatase (ATPase) activity and reduction of nerve conduction velocity. As a result of the accumulation of sorbitol in the cell, nicotinamide adenine dinucleotide phosphate (NADPH) associates with reduced cell metabolism, increased cell osmolarity, and decreased intracellular myoinositol, and the cell has a tendency to oxidative stress. Hyperglycemia may cause an increase in glucose in some intracellular tissues (such as nerves, lenses, kidneys, and blood vessels) that do not require insulin for glucose transport. Sorbitol and fructose that increase in these tissues cause two undesirable effects. First, accumulated sorbitol and fructose lead to an influx of water and eventually to osmotic cell injury by increasing intracellular osmolarity. Second, sorbitol accumulation results in reduction in the myoinositol content and impairment of Na-K ATPase. This mechanism may be responsible for the damage in Schwann cells and retinal capillary pericytes and causes peripheral neuropathy and microaneurysms. Although the relationship between oxidative stress and diabetic retinopathy, nephropathy, and neuropathy is well known, the therapeutic efficacy of many antioxidants (including aldose reductase inhibitors, vitamins C and E) tested in clinical trials has not yet been established.

*Hexosamine:* Uridine diphosphate-*N*-acetyl glucosamine (UDPGlcNAc), which regulates transcription factors needed for normal cell functions, is produced in hexosamine pathway. Excess glucose is replaced with glycolytic mediators in hexosamine pathway, and thus, glucose flux to hexosamine pathway results in cell injury and increased oxidative stress. The effects of aldose reductase inhibitors in animal models were found to be more effective than clinical trials. One of the reasons is being lower dose used in clinical trials compared with dose used in animal studies.

*Protein kinase C:* Excess glucose is converted to diacylglycerol that activates protein kinase C. The activation of protein kinase C increases in contractility, permeability, and vascular cell proliferation and enhances the production of extracellular matrix and cytokines. Thus, vasoconstriction and nerve ischemia occur. These neurovascular changes also contribute to diabetic neuropathy. Diacylglycerol-protein kinase C activation was also shown to be associated with many vascular abnormalities in retinal, renal, and cardiovascular tissues in diabetes

and insulin resistance period. High glucose enhances ROS formation by causing NF- $\kappa$ B activation in endothelial cells. This condition may be prevented by PKC (protein kinase C) inhibitors [9].

*Poly (ADP-ribose) polymerase:* Nuclear enzyme poly (ADP-ribose) polymerase (PARP) becomes activated in response to high glucose. This enzyme helps to repair DNA by separating nicotinamide adenine dinucleotide (NAD<sup>+</sup>) into the remains of nicotinamide and adenine ribose. Over activation of PARP results in increased free radical formation, harmful changes in gene transcription, protein kinase C activation, and increased AGEs.

## 2.2. Oxidative stress

As mentioned above, hyperglycemia causes accumulation of ROS and oxidative stress eventually by interacting with many different ways. The free radical is a chemical species usually having very reactive unpaired electron in the molecular or atomic orbit. Although free radical reactions are necessary for defense mechanisms of immune system cells including neutrophils and macrophage, the overproduction of free radicals results in tissue injury and cell death. Free radicals affect all essential components of cells such as lipids, proteins, DNA, and carbohydrates and lead to the deterioration of their structure. The formation and elimination rates of free radicals are in balance in the organism, which are known as oxidative balance. The organism is not affected by free radicals as long as oxidative stability is provided. Studies in which the relationship between diabetes and diabetes complications and the ROS are shown, it is highlighted that tissue injury due to non-enzymatic glycation, metabolic stress caused by changes in energy metabolism, sorbitol path activity, hypoxia, and ischemia-reperfusion, increases the production of free radical and alters the antioxidant defense system. There are studies, which support that the formation of free radical is a direct result of hyperglycemia, as well as experimental trials that show that the formation of free radical starts when the endothelial and smooth muscle cells were incubated in the medium containing high concentrations of glucose. Hyperglycemia-mediated ROS production occurs via three mechanisms. The first mechanism is the auto-oxidation of glucose and superoxide production. Glucose is converted to reactive keto aldehydes and superoxide anion in the presence of a transition element. The chain of reactions results in the transformation of superoxide radical into extremely reactive hydroxyl radical via hydrogen peroxide. The intracellular glucose oxidation leads to the release of NADH. NADH is used for providing needed energy for ATP production by the oxidative phosphorylation way in the respiratory chain. Superoxide radical is released during this reaction in the respiratory chain. The production of superoxide radicals increases in this way in the presence of high glucose concentration. Mitochondrial respiratory chain is the main intracellular source of ROS production. It is considered that superoxide radical occurs continuously during normal respiration chain of events. Recent studies showed that much pathology in diabetes was associated with increased mitochondrial ROS production. The second mechanism in the hyperglycemia-mediated ROS production is the glycation of proteins and the formation of AGE products. When the proteins exposed to high glucose concentrations, glucose leads to uncontrolled glycation reactions by binding to protein without requiring the mediation of an enzyme. The glycated protein causes the formation of ROS by

donating an electron to molecular oxygen. AGE products are formed after this non-enzymatic reaction. Advanced glycosylation products lead to endothelial damage by increasing vasoconstriction via endothelin-1 and have the capacity to generate free radicals through complex biochemical mechanisms. Toxic effects of AGEs also include being able to change the structure and function of proteins and to induce oxidative stress with its receptors. The third mechanism of ROS production is polyol pathway. High glucose concentration causes the sorbitol production by polyol pathway. As NADH is used for the activity of enzyme aldose reductase in this pathway, intracellular NADH is consumed. NADH is required for converting oxidized glutathione to reduced form and nitric oxide (NO) synthesis. Therefore, being active of the sorbitol way and the absence of NADPH ultimately mean a limitation of cell's antioxidant capacity. The decrease in reduced glutathione and NO synthesis that has a function in vasodilatation leads to the reduction of endoneurial blood flow, consequently endoneurial hypoxia or ischemia. Due to this event, the damage occurs in neuronal cells, Schwann cells.

### **2.3. Vascular hypotheses**

Swellings of the capillary vascular endothelial cells, thickening of the blood vessel wall, and undergoing aggregation or fibrin and occlusion with platelets of capillary lumen were shown in various studies. The sudden onset of clinical signs of focal neuropathies in diabetes supports the vascular cause. Decrease in NO production, abnormalities in eicosanoid production, and an increase in oxidative pathway lead to vasoconstriction in endoneurial microvascularization and nerve hypoxia.

### **2.4. Immunological mechanisms**

Autoantibodies against the sympathetic ganglia develop in patients with insulin-dependent diabetes. Endoneurial or epineural lymphocytic infiltration has been displayed in the sural nerve biopsy of diabetic patients. Coexistence of diabetic neuropathy and chronic inflammatory demyelinating polyneuropathy is also a suggestive finding of immune or cytotoxic factors [11].

### **2.5. Neurotrophic factors**

Neurotrophins are proteins that ensure the growth, permanence, survival, and differentiation into different specific populations of the neurons. There are studies, which show that impaired neurotrophic support is involved in the pathogenesis of diabetic polyneuropathy. Since nerve growth factor (NGF), a typical growth factor for the nerve, is needed for the survival and the continuity of sympathetic and thin sensory nerve fibers, it was examined particularly well. NGF also regulates the expression of the neuropeptides including calcium gene-related peptide and substance P in sympathetic nerves and sensory neurons of dorsal root ganglion. Retrograde axonal transport from target tissue to neuronal cell body is impaired in diabetes. There is evidence, which shows that NGF expression is decreased in the skin, submandibular glands, and the sympathetic ganglia in experimental diabetic neuropathy. NGF, when administered to rats with streptozotocin-induced diabetes, prevented the protection of the response to thermal painful stimuli (tail flick threshold) and the decrease in levels of neuro-

peptides including calcitonin gene-related peptide and substance P measured in the cervical dorsal root ganglia. In diabetic autonomic neuropathy model, dystrophic changes in sympathetic ganglia following the administration of NGF indicate that there may be a different dosing effect. Neurotrophin-3 (NT-3) supports the differentiation and survival of sensory neurons. Decreased messenger RNA (mRNA) was shown in the leg muscle of NT-3 diabetic mice. Due to their neurotrophic effect in the treatment of diabetic neuropathy in recent years, glucagon-like peptide-1 (GLP-1) analogues (exendin-4) and peptides such as ghrelin were also found to give successful results in animal models [12].

### 3. Diagnosis

Symptoms and physical examination findings should be evaluated together for an accurate diagnosis of diabetic peripheral neuropathy (DPN). Standardization and easy application of diagnostic methods are of great importance in terms of widespread availability. There is no gold standard in the detection of presence of diabetic neuropathy. The San Antonio consensus panel recommends performing at least one measurement in five different diagnostic categories. These are symptom scoring, physical examination scoring, QST, cAFT, and EDS. The neurological examinations of the patients often reveal gloves socks style sensory deficit, hyporeflexia or areflexia, increase in vibration sense perception threshold, and moderate atrophy and weakness particularly in intrinsic foot muscles.

Neuropathic pain is one of the most common symptoms that are ignored by both the patient and the physician. Of the patients, 12.5% with painful DPN stated that they had never mentioned the pain to the physicians before and 40% expressed that they had received no treatment for pain. There are several questioning methods to query pain due to diabetic polyneuropathy, but none of these methods have been accepted as the gold standard.

Visual Analog Scale (VAS) is an easy method applied by grading the pain on a scale of 1–10 by the patient. Another method of pain assessment is “The Leeds Assessment of Neuropathic Symptoms and Signs” (LANSS) pain inquiry. Having a LANSS score of 12 or more is diagnostic for neuropathic pain. The Michigan Neuropathy Screening Instrument is one of the other commonly used interrogation methods, which is used in the diagnosis of neuropathic pain. Neuropathy Disability Score (NDS), which was first developed by Dick for the standardization of examination findings and correct interpretation of the findings and was simplified and modified in the following years, is regarded as a reliable and easy method that does not require experience in neurology. NDS = 0 is considered normal, NDS = 10 indicates maximum deficits, and NDS = 6 or more indicates the risk of developing diabetic foot ulcers. Touch pressure, vibration, hot–cold sensation, thermal pain, cold pain, and mechanical pain detection thresholds are tested in quantitative sensory testing.

The tests related to the vasomotor control, baroreceptor reflex, sudomotor function, pupil, bladder, and bowel innervation are used in autonomic function tests. Electrodiagnostic studies are one of the most common and objective methods used in the diagnosis of DPN. Weakness of electrodiagnostic studies is not showing the early stages of thin fiber damage. Unmyelinated

C fiber injury, the most common cause of painful DPN, does not provide any electrophysiological findings, but thick myelinated A $\alpha$  and A $\beta$  fiber involvements have EDS findings.

Staining of a 3-mm skin sample using protein gene product-9.5 allows the assessment of intraepidermal thin fibers and early diagnosis of neuropathic damage. Although its sensitivity is high, its use is limited because it is an invasive procedure [13].

## 4. Treatment in diabetic neuropathy

The prevention of occurrence of diabetic polyneuropathy or its definitive treatment is impossible. However, some measures that slow down the development of neuropathy, reduce the severity of symptoms, and prevent the complications of neuropathy may be taken. Normal or nearly normal blood glucose control of the patients should be provided. Keeping HGBA1C below 7, cholesterol control, smoking cessation, alcohol reduction, avoiding obesity, and having foot care delay the progression of neuropathy. When the structural link between membrane ion channel dysfunction and axonal loss is assessed, neuropathy can be diagnosed at an early stage with the detection of clinical biomarkers (biomarkers) that may identify the presence of early changes in ion channel. Therefore, the opportunity arises to start treatment without irreversible nerve damage [14].

### 4.1. Metabolic control

The most important treatment for the prevention of diabetic PNP (peripheral neuropathy) is to control blood glucose. According to Diabetes Control and Complications Center (DCTT) data, the reduction of neuropathy by 57% has been shown in Type 1 DM after 5 years of tight blood glucose control.

### 4.2. Myoinositol

The addition of myoinositol to the diet was shown to improve nerve Na–K ATPase activity and nerve conduction values in laboratory studies; however, no improvement was found in electrophysiological parameters in humans. Their potential benefits are being able to inhibit nerve damage. Thus, its administration is recommended at an early stage.

### 4.3. Vitamin addition

Vitamin treatment is often a non-specific therapy in neuropathy. Controlled studies show that receiving thiamine, vitamin B12, pyridoxine, or pantothenic acid in diabetic neuropathy is of no use [2,15].

### 4.4. ROS inhibitors

*Alpha lipoic acid:* High doses of alpha-lipoic acid were shown to have therapeutic efficacy in the treatment of diabetic polyneuropathy and insulin resistance in experimental and clinical

trials [2,9]. The patients (with symptomatic diabetic neuropathy) were given randomized IV ALA 5 days a week (600 mg) or placebo in Sydney trials. After this treatment, a significant improvement was noted in TSS of the patients treated with ALA compared to those given placebo (5.7 vs. 1.8 points  $p \leq 0.001$ ) [16].

*Nicotinamide*: It inhibits oxidative stress–PARP activation cascade.

*Resveratrol*: It regulates NCV, diabetic neuropathic pain and inhibits NF- $\kappa$ B.

*Routine*: It prevents protein glycosylation.

*Taurine*: It reduces oxidative and nitrosative stress in Schwann cells. It reverses neurovascular insufficiency and reduces increased pain sensitivity [9,17,18].

*NO agonist*: NO is one of the factors that play a role in the pathogenesis of DPN and l-arginine, a NO agonist, was shown to increase Na–K ATPase activity [9].

*Aldose reductase inhibitors*: Many aldose reductase inhibitor drugs that are effective through the polyol pathway were reported in the DPN treatment. Sorbinil, an aldose reductase inhibitor, prevents sorbitol accumulation by inhibiting the enzyme aldose reductase in those with diabetes and corrects neuronal dysfunction due to the change in the myoinositol content. It leads to increase in NCV. Tolrestat is the other aldose reductase inhibitors and repairs impaired NCV. Ponalrestat is effective in the delayed treatment of DPN. It normalizes NCV and prevents the impaired neural induction of ornithine decarboxylase. Fidarestat induces the maturation of the nerve fibers, stimulates the repair of nerve fibers, and stops the destruction of nerve fibers. Epalrestat prevents the progression of MNCV, regulates the polyol pathway, and suppresses the production of IGU [9].

*PKC inhibitors*: Ruboxistaurin, a PKC- $\beta$  inhibitor, was found to be successful in treating neuropathic sensory symptoms. It improves nerve fiber functions and microvascular blood flow and increases life quality in those with DPN [9,19,20].

*Immunosuppressive therapy*: Inflammatory vasculopathy is thought to be important in the pathogenesis of cases in which proximal diabetic neuropathy or amyotrophy was detected. The treatment that is appropriate to the natural progress of diabetic amyotrophy and whose validity was accepted is the treatment with immunomodulatory agents including IVIG or corticosteroid. Better response is achieved with corticosteroid therapy and its cost of treatment is less compared to IVIG. However, blood glucose regulation may be difficult with corticosteroid. Starting with the dose of 0.75 mg/kg/day 3–4 times a week and discontinuing gradually are recommended [21].

*Pain treatment in diabetic neuropathy*: Antidepressants, particularly tricyclic drugs, are the most frequently used. Amitriptyline, imipramine, and nortriptyline may be used. Anticonvulsants such as carbamazepine, gabapentin, pregabalin, and lamotrigine are among the treatment options. Antiarrhythmics, mexiletine, and lidocaine are other pharmacological agents that are used in case of unresponsiveness to other drugs. Capsaicin derived from paprika may be preferred to as a topical agent for treating pain [21].

*Tricyclic antidepressants:* A great percentage of patients were given at an average dose of 105 mg of amitriptyline or at an average dose of 111 mg desipramine in a double-blind, randomized, placebo-controlled trial of the patients with painful diabetic peripheral neuropathy (PDPN). Decrease in pain by 74%, 61%, and 41% was observed in patients who received amitriptyline, desipramine, and placebo, respectively. Number needed to treat (NNT) is 2.1 (1.9–2.6) and number needed to harm (NNH) value is 2.8 for minor adverse events and 19 for major adverse events. TCAs may promote orthostatic hypotension and may prolong QT (**Q wave** and **T wave**) interval. An increase in the risk of sudden death has been reported with TCAs by taking more than 100 mg amitriptyline or its equivalent [22].

*Selective serotonin reuptake inhibitors (SSRIs):* Alternatively, the patients are treated with SSRIs because of many side effects of TCAs. These agents inhibit the presynaptic serotonin reuptake selectively [9]. Unlike the tricyclics, SSRIs lack the postsynaptic receptor-blocking effect. NNT to achieve 50% pain relief is 6.8 (3.4–441), and NNH is not known. While the benefit was observed with paroxetine and citalopram, no benefit was obtained with fluoxetine [22].

*Serotonin-norepinephrine reuptake inhibitors (SNRIs):* The direction of the treatment of DPN was shifted toward SNRIs because SSRIs are less effective in the treatment than TCAs and SNRIs inhibit both serotonin and norepinephrine reuptake. Duloxetine and venlafaxine are examples of SNRIs. Venlafaxine was argued to decrease the pain, and the effect on norepinephrine is presumed to be more specific in a study in which high dose of venlafaxine was used. Duloxetine is more effective in terms of the affinity in noradrenergic and serotonergic reuptake inhibition. Many people were given duloxetine in the randomized, placebo-controlled studies and 60 mg and 120 mg daily doses were reported to be effective in DPN [9,23,24].

*Anticonvulsants:* Antiepileptic drugs act by blocking sodium channels (felbamate, lamotrigine, oxcarbazepine, topiramate, and zonisamide), potentiating the activity of GABA (tiagabine and topiramate), blocking calcium channel (felbamate, lamotrigine, topiramate, and zonisamide), antagonizing glutamate at *N*-methyl-d-aspartate (NMDA)  $\alpha$ -receptors (felbamate), and behaving as the antagonist of AMPA (a-amino-3-hydroxy-5-methyl-4-isoxazole) receptors (felbamate and topiramate). Rational polytherapy by which we can obtain a synergistic effect comes to the fore through understanding the mechanisms of these drugs. For example, lamotrigine can be given for sodium channel blocking and felbamate may be added to antagonize glutamate receptors or different mechanisms can be targeted with a single medication, for instance, topiramate, and chance of success may be increased. It was reported that a patient who was unresponsive to one of the antiepileptic drugs will respond to another drug or combination treatment consisted of two or more drugs [25,26].

*Topical capsaicin (capsaicin = 8-methyl-N-vanillyl-trans-6-nonenamide):* C fibers use neuropeptide P as a neurotransmitter, the reduction of axonal substance P causes pain relief. Storage of substance P, which is released from sensory nerve terminals, finishes with the application of capsaicin. Thus, the transmission of painful stimulus from peripheral nerve terminals is reduced or completely eliminated. A significant improvement was observed in patients with painful neuropathy treated with Capsaicin cream (0.075%) for 8 weeks. The treatment with capsaicin should be limited to 8 weeks, because it is noted that adverse event may be observed in sensory nerves at the end of this period. Eight percent capsaicin patch may be used in

postherpetic neuralgia; however, it is contraindicated in diabetic neuropathy, because it desensitizes the nociceptive sensory nerve endings, so it is reported that the risk of development of diabetic foot ulcers may be increased [25,27].

*Topical lidocaine:* Use of topical lidocaine in painful neuropathy is associated with postherpetic neuralgia [16]. Lidocaine has been shown to be as effective as pregabalin in reducing pain without causing the side effects in a multicenter, randomized, open-label, parallel group study conducted by treating a group ( $n = 99$ ) with 5% lidocaine for 2 weeks and treating another group ( $n = 94$ ) with pregabalin for 4 weeks. This therapy may be continued with oral mexiletine in order to succeed. Relief of superficial pain caused by overstimulation is targeted with oral mexiletine [25].

*Acetyl-L-carnitine:* It was reported that the pain and the slowed nerve conduction velocity were improved, and nerve regeneration was increased with acetyl-L-carnitine in rats with streptozotocin-induced diabetic neuropathy. It was reported that the pain disappeared with acetyl-L-carnitine, and the pain was resolved by prophylactic treatment in paclitaxel-treated rats [28].

## 5. Current therapeutic strategies in diabetic neuropathy

DPN is one of the most common symptoms of chronic neuropathic pain in clinical practice. Various treatment methods are tried in patients with diabetic neuropathy. Tramadol, an opioid, is a weak opioid analgesic used for reducing severe pain. It was reported that randomized controlled trials for a period of 6 weeks were better than the placebo and symptomatic relief continued for at least 6 months. The likelihood of side effects, as other opioid-like drugs, is common. However, the development of drug tolerance and the development of addiction with long-term therapy with tramadol are not common. NMDA receptors play a key role in the sensitization of the neuropathic pain, but the use of these drugs is not widespread because of their dose-limiting side effects [25]. NMDA receptor antagonists are used for modulation of excitatory transmission in the primary afferent spinothalamic neuron synapses in recent years. The pain ceases with the blockade of excitatory glutamatergic NMDA receptors in the spinal cord. Dextromethorphan is one example of such painkiller medications. NMDA receptor antagonists have been shown to be as effective as opioid analgesics for chronic pain conditions. The diagnosis of diabetic neuropathy was made by a clinical evaluation (medical history, motor, sensory, and reflex examination) and electrophysiological tests for 24 patients with Type 2 diabetes and diabetic neuropathy. Pain complaints of the patients were assessed with a VAS before and after the treatment. While a significant improvement in VAS scores was observed in both treatment groups compared to the control group, the difference between treatment groups was found to be significant. In conclusion, Memantine (NMDA receptor antagonist) treatment provides an improvement in the treatment of neuropathic pain in diabetic polyneuropathy [29].

Flavonoids, which many positive effects on human health were determined, have antioxidant, anti-inflammatory, cholesterol lowering, antibacterial, antihyperglycemic, and antiallergic features. It may be called P factor or P vitamin considering its capillary circulation regulating

blood pressure lowering effects. The main one of these flavonoids is proanthocyanidin found in grape seeds. The grape seed extract was given at the dose of 25 mg/kg and 50 mg/kg by oral gavage for 6 weeks in a study in which diabetes was induced in BALB/C mice. The pain threshold was measured using the Hot Plate Test, a thermal pain model, in these animals at the end of second and sixth weeks. When the sciatic nerve and abdominal aorta tissue from animals were examined histologically at the end of the study, hot plate measurements of the groups received grape seed extract and the measurements between other groups were considered significant. UCE (was seen to decrease damage in diabetes-induced micro and macrovascular complications in histological evaluations [30].

### 5.1. DPP-4 inhibitors

Dipeptidyl peptidase-4 incretin hormones are secreted from intestinal endocrine cells. It plays a key role in regulating blood glucose levels by stimulating glucose-dependent insulin secretion, decreasing glucagon secretion, and slowing gastric emptying. DPP-4 inactivates GLP-1 and glucose-dependent insulin tropical polypeptides (GIP) in vivo by destroying them. These peptides are short lived in the circulation because they are destroyed by DPP-4. Alogliptin is a DPP-4 inhibitor. The effects of this medication on vascular and neural complications were evaluated in male Sprague–Dawley rats with STZ-induced diabetes. Alogliptin was observed to regulate MNCV and thermal response latency after a 12-week treatment. No improvement in the decrease in intraepidermal nerve fiber density was detected while SNCVs of the mice were regulating. PKF 275-055, new analog of Vildagliptin, was given to STZ-induced diabetic rats in the study of Bianchi et al., and it was found that it displays an anabolic effect by preventing changes in nociceptive threshold, Na–K ATPase, and NCP. DPP-4 inhibitors were stated to prevent some neural and vascular complications associated with diabetes in the studies conducted [9,31,32,33].

### 5.2. Cannabinoid CB1 receptor antagonists

Nabilone is a CB1 predominant receptor agonist. It was used in neuropathic pain based on the anecdotal evidence and uncontrolled case series [34]. Pain reduction has been reported to occur in 30% of the patients in a single center, randomized, double-blind, placebo-controlled, flexible 5-week study conducted by administering a dose ranges from 1 to 4 mg per day or placebo. DPN symptoms disappeared, and their impaired sleep and standard of living were improved in those received flexible dose. Nabilone is a well tolerated and successful adjuvant in patients with DPN. Rimonabant is a CB1 receptor antagonist; it accelerates skin blood flow and decreases TNF- $\alpha$  level in diabetic rats. It was stated that Rimonabant may be beneficial in the treatment of DPN due to its micro and macro blood vessel protection and inflammatory effects [9,34,35].

### 5.3. Natural products

*Metanx*: It is a product, used for the endothelial function disorder, containing l-methyl folate, pyridoxal 5' phosphate and methylcobalamin. It prevents endothelial NO synthesis, oxidative stress in endothelium, and peripheral nerves. A significant improvement was noted in numbness, tingling, pain, burning, sharp pain, and allodynia by giving *Metanx* to placebo-

controlled diabetic neuropathy patients for 24 weeks. An increased emotional, social functions, and vitality components of mental health were also detected. Side effects at less than 2% were seen along this response. Generally, the side effects were rash and gastrointestinal disorders and were no greater than the side effects seen with placebo [25].

*Botulinum toxin*: It was tried in trigeminal neuralgia and was reported that it has a long-term antinociceptive effect in CTS without having electrophysiological repair [25].

## Author details

Emine Hande Bayram<sup>1</sup>, Ali Demir Sezer<sup>2</sup> and Hatice Kübra Elçioğlu<sup>1\*</sup>

\*Address all correspondence to: kubra.elcioglu@marmara.edu.tr

1 Department of Pharmacology, Faculty of Pharmacy, Marmara University, Haydarpaşa, Istanbul, Turkey

2 Department of Pharmaceutical Biotechnology, Faculty of Pharmacy, Marmara University, Haydarpaşa, Istanbul, Turkey

## References

- [1] Satılmış, I. Diyabetes Mellitusda İnsülin Tedavisinin Periferik Sinir Sistemine Etkileri: Klinik ve Elektrofozyolojik Değerlendirme, Sağlık Bakanlığı Şişli Etfal Eğitim ve Araştırma Hastanesi 2. Nöroloji Kliniği, Uzmanlık Tezi, İstanbul, 2007.
- [2] Terzi M, Cengiz N, Onar MK. Diyabetik Nöropati. OMÜ Tıp Dergisi. 2004;21(1):39–49.
- [3] Jennifer AT, James BD. The Spectrum of Diabetic Neuropathies. Phys Med Rehabil Clin N Am. 2008;19(1):1–26.
- [4] Habib AA, Brannapan 3 TH. Therapeutic Strategies for Diabetic Neuropathy, Springer Science + Business media, LLC, 2010.
- [5] Vinik AI, Erbas T, Casellini CM, Diabetic Cardiac Autonomic Neuropathy, İnflammation and Cardiovascular Disease, J Diabet. 2013;4(1):4-18.
- [6] Vinik AI, Maser RE, Ziegler D. Autonomic İmbalance; Prophet of Doom or Scope for Hope? Diabet Med. 2011;28:643–651.
- [7] Şahin C. Diyabetik Sıçanlarda Meydana Gelen Sinir Yaralanmaları Onarımında Perinörotomi Uygulamasının Etkisi, Genelkurmay Başkanlığı Gata Haydarpaşa Eğitim Hastanesi Plastik VE Rekonstrüktif Cerrahi Servis Şefliği, Tıpta Uzmanlık Tezi, 2011.

- [8] Nouri MN, Ahmed A, Brill V, Orszag A, Ng E, Nwe P, Perkins BA. Diabetic Neuropathy and Axon Reflex Mediated Neurogenic Vasodilatation in Type 1 Diabetes. *PLoS ONE* 2012;7(4):e34807. doi:10.371/journal.Done.0034807
- [9] Sing R, Kishore L, Kaur N. Diabetic Peripheral Neuropathy: Current Perspective and Future Directions. *Pharmacolog Res.* 2014;80:21–35.
- [10] Singh R, Barden A, Mori T, Beilin L. Advanced Glycation End-Products: A Review. *Diabetologia.* 2001;44(2):129–146.
- [11] Kılıç E, Fisetin ve Alfa Lipoik Asidin Ağrılı Diyabetik Nöropati Üzerine Etkilerinin İncelenmesi: Fare Modelinde İn Vivo Davranışsal Çalışma, Ondokuz Mayıs Üniversitesi Tıp Fakültesi İç Hastalıkları Anabilim Dalı Endokrinoloji Bilim Dalı, Uzmanlık Tezi, Samsun, 2013.
- [12] Erbaş O. Diyabetik Nöropatili Sıçanlarda Oksitosin, Mesna ve Glutamin' in, Nöropati Üzerine Etkilerinin Elektrofizyolojik (EMG) ve Histolojik Yöntemlerle Araştırılması, Ege Üniversitesi Tıp Fakültesi Fizyoloji Anabilim Dalı Tıpta Uzmanlık Tezi, İzmir, 2012.
- [13] Cengizhan E. Diyabetik Hastalarda Michigan Nöropati Tarama Enstrümanı Bulgularının Elektrofizyolojik Bulgularla Bağlıntısı, Süleyman Demirel Üniversitesi Tıp Fakültesi Nöroloji Anabilim Dalı Tıpta Uzmanlık Tezi, Isparta, 2010.
- [14] Kiernan MC. Emergence of a Predictive Clinical Biomarker for Diabetic Neuropathy. *Diabetes* 2012;61:1346-1347.
- [15] Ağırman M. Diyabetik Hastalarda Polinöropati ve Karpal Tünel Sendromu Tanısında Ultrasonun Elektrofizyolojiye Göre Tanıdaki Yerinin Araştırılması, Marmara Üniversitesi Tıp Fakültesi Fiziksel Tıp ve Rehabilitasyon Anabilim Dalı, Uzmanlık Tezi, İstanbul, 2012.
- [16] Dam PSV, Cotter MA, Bravenboer B, Cameron NE. Pathogenesis of Diabetic Neuropathy: Focus on Neurovascular Mechanisms. *Eur J Pharmacol.* 2013;719:180–186.
- [17] Sharma SS, Kumar A, Arora M, Kaundal RK. Neuroprotective Potential of Combination of Resveratrol and 4-Amino 1,8 Naphthalimide in Experimental Diabetic Neuropathy: Focus on Functional, Sensorimotor and Biochemical Changes. *Free Radic Res.* 2009;43:400–408.
- [18] Li F, Obrosova IG, Abatan O, Tian D, Larkin D, Stuenkel EL, et al. Taurine Replacement Attenuates Hyperalgesia and Abnormal Calcium Signaling in Sensoryneurons of STZ-D Rats. *Am J Physiol Endocrinol Metab* 2005;288:E29–E36.
- [19] Hotta N, Toyota T, Matsuoka K, Shigeta Y, Kikkawa R, Kaneko T, et al. Clinical efficacy of fidarestat, a novel aldose reductase inhibitor, for diabetic peripheral neuropathy: a 52-week multicenter placebo-controlled double-blind parallel group study. *Diabet Care* 2001;24:1776–82.

- [20] Hotta N, Akanuma Y, Kawamori R, Matsuoka K, Oka Y, Shichiri M, et al. Long-Term Clinical Effects of Epalrestat, an Aldose Reductase Inhibitor, on Diabetic Peripheral Neuropathy: The 3-Year, Multicenter, Comparativealdose Reductase Inhibitor-Diabetes Complications Trial. *Diabet Care*. 2006;29:1538–1544.
- [21] Said G. Focal and Multifocal Diabetic Neuropathies. *Arq Neuropsiquiatr*. 2007;65(4):1272–1278.
- [22] Tahrani AA, Aswith T, Stevens MJ. Emerging Drugs for Diabetic Neuropathy. *Expert Opin Emerg Drugs* 2010;15(4):661–683.
- [23] Rowbotham MC, Goli V, Kunz NR, Lei D. Venlafaxine Extended Release in the Treatment of Painful Diabetic Neuropathy: A Double-Blind, Placebo-Controlled Study. *Pain* 2004;110:697–706.
- [24] Sultan A, Gaskell H, Derry S, Moore RA. Duloxetine for Painful Diabetic Neuropathy and Fibromyalgia Pain: Systematic Review of Randomised Trials. *BMC Neurol*. 2008;8:29.
- [25] Vinik AI, Nevoret ML, Casellini C, Parson H. Diabetic Neuropathy. *Endocrinal Metab Clin N Am* 2013;42:747–787.
- [26] Raskin P, Donofrio PD, Rosenthal NR, et al. Topiramate vs Placebo in Painful Diabetic Neuropathy: Analgesic and Metabolic Effects. *Neurol*. 2004;63:865–873.
- [27] Mason L, Moore RA, Derry S, et al. Systematic Review of Topical Capsaicin for the Treatment of Chronic Pain. *BMJ* 2004;328:991.
- [28] Bennett GJ, Doyle T, Salvemini D. Mitotoxicity in Distal Symmetrical Sensory Peripheral Neuropathies. *Nat Rev Neurol*. 2014;10:326–336.
- [29] Gökçe F. Diyabetik Polinöropatik Hastalarda Memantinin Ağrı Üzerine Etkinliği. *Orjinal Araştırma* 2014;36:474–478.
- [30] Yurt A. Streptozosinle Diyabet Oluşturulan Farelerde Üzüm Çekirdeği Ektresinin Nöropatik Ağrı Üzerine Etkiler, İnönü Üniversitesi Sağlık Bilimleri Enstitüsü Yüksek Lisans Tezi, Malatya, 2015.
- [31] Neumiller JJ, Wood L, Campbell RK. Dipeptidyl Peptidase-4 Inhibitors for the Treatment of Type 2 Diabetes Mellitus. *Pharmacother*. 2010;30:463–484.
- [32] Lam S, Saad M. Saxagliptin: A New Dipeptidyl Peptidase-4 Inhibitor for Type 2 diabetes. *Cardiol Rev*. 2010;18:213–217.
- [33] Davidson EP, Coppey LJ, Dake B, Yorek MA. Treatment of Streptozotocin-Induced Diabetic Rats with Alogliptin: Effect on Vascular and Neural complications. *Exp Diabet Res*. 2011;8104–8169.
- [34] Toth C, Mawani S, Brady S, Chan C, Liu C, Mehina E, et al. Anenriched-Enrolment, Randomized Withdrawal, Flexible-Dose, Double-Blindplacebo-Controlled, Parallel

Assignment Efficacy Study of Nabilone As Adjuvant in the Treatment of Diabetic Peripheral Neuropathic Pain. *Pain*. 2012;153:2073–2082.

- [35] Liu WJ, Jin HY, Park JH, Baek HS, Park TS. Effect of Rimonabant, the Cannabinoid CB1 Receptor Antagonist, on Peripheral Nerve in Streptozotocin-Induced Diabetic Rat. *Eur J Pharmacol*. 2010;637:70–76.





*Edited by Ali Demir Sezer*

This contribution book collects reviews and original articles from eminent experts working in the interdisciplinary arena of novel drug delivery systems and their uses. From their direct and recent experience, the readers can achieve a wide vision on the new and ongoing potentialities of different smart drug delivery systems. Since the advent of analytical techniques and capabilities to measure particle sizes in nanometer ranges, there has been tremendous interest in the use of nanoparticles for more efficient methods of drug delivery. On the other hand, this reference discusses advances in the design, optimization, and adaptation of gene delivery systems for the treatment of cancer, cardiovascular, diabetic, genetic, and infectious diseases, and considers assessment and review procedures involved in the development of gene-based pharmaceuticals.

Photo by agsandrew / DollarPhoto

**IntechOpen**

